Development of culture and imaging techniques to investigate human follicle development

Bríet Dögg Bjarkadóttir

St Cross College

Nuffield Department of Women's and Reproductive Health

University of Oxford

Thesis submitted for the degree of

Doctor of Philosophy

Trinity term 2021

Abstract

The number of young cancer survivors is growing, as both the incidence and survival rates for cancer increases. Cancer treatment can cause damage to the ovaries, which can cause infertility. Although there are ways of preserving the fertility of girls and women undergoing cancer treatment, these methods are invasive and some do not restore ovarian function. In recent years, there has been growing interest in developing non-invasive pharmacological methods of fertility preservation, including administrating drugs to protect the ovaries from the damaging effects of chemotherapy. However, the mechanisms of chemotherapy-induced follicle loss remain poorly understood, hampering progress in the field. The aim of this thesis was to address the knowledge gaps by developing culture and imaging techniques to investigate human follicle development *in vitro*. The effect of different culture conditions on follicle health and development in cryopreserved human ovarian tissue was investigated, revealing that culture in a low volume of αMEM medium improved follicle health. Experiments investigating different thawing protocols on ovarian stromal health highlighted that cryopreservation causes damage to both follicles and stroma and therefore fresh ovarian tissue was used in the remaining experiments. A technique to allow three-dimensional visualisation of follicles was developed using whole-mount immunolabelling and tissue clearing and was used to investigate follicle activation of fresh ovarian tissue *in vitro.* This study revealed that three-dimensional analysis was necessary to accurately distinguish between primordial and transitional follicles and that a large proportion of follicles were disc-shaped rather than spherical. No apparent increase in follicle activation was observed within 48 h of culture, however low sample numbers limited this study. A final set of experiments was planned, investigating the effects of chemotherapy drugs on human primordial follicles *in vitro,* however this could not be performed due to the coronavirus disease of 2019 (COVID-19) pandemic. The work presented in this thesis highlights the need to consider the heterogeneity and the three-dimensional structure of follicles within the human ovary.

Impact of coronavirus disease of 2019 (COVID-19) on this thesis

The COVID-19 pandemic significantly disrupted a portion of the work presented in this thesis. Prior to the pandemic I was on track to complete my thesis by October 2020. The experiments described in Chapters 3-5 had been completed and experimental work for Chapters 6 and 7 was ongoing in early 2020. In response to the pandemic, the department shut down on 25 March 2020 and remained closed until 23 September 2020, therefore no laboratory work could be performed during this 6-month period. Once the department re-opened with limited access, experimental work for Chapters 6 and 7 could resume, however access to the confocal imaging facilities at the Weatherall Institute of Molecular Medicine remained restricted until December 2020. Due to a combination of COVID-19-related restrictions and personal circumstances compounded by the pandemic, analysis for Chapter 7 was not completed until May 2021.

A final experiment was planned for this thesis investigating the effects of chemotherapy drugs on human primordial follicles *in vitro*. However, the experimental design for this study relied on the outcome of the study described in Chapter 7, which had been significantly delayed and compromised as described above. Therefore, I decided in consultation with my supervisor not to carry out this final experiment and instead focus on completing and analysing the experiments that had already been completed.

Publication arising from this work

Bjarkadottir BD*, Walker CA*, Fatum M, Lane S, Williams SA

Analysing culture methods of frozen human ovarian tissue to improve follicle survival

Reproduction and Fertility. 2021. **2** 59-68

doi: 10.1530/raf-20-0058

*equal contribution to work

(See Appendix B)

Abstracts for poster presentations arising from this work

Bjarkadottir BD, Boskovic N, Adeniran BV, Lane S, Williams SA. *Effect of post-thaw processing conditions on human ovarian stroma.* Fertility Conference 2020. Edinburgh, UK.

Bjarkadottir BD, Boskovic N, Adeniran BV, Lane S, Williams SA. *Effect of post-thaw processing conditions on human ovarian stroma*. International Society for Fertility Preservation 2019. New York, USA.

Bjarkadottir BD, Walker CA, Lane S, Williams SA. *Does in vitro environment of cultured human cryopreserved ovarian tissue affect follicle development and health?* Fertility Conference 2019. Birmingham, UK.

Bjarkadottir BD, Walker CA, Lane S, Williams SA. *Does in vitro environment of cultured human cryopreserved ovarian tissue affect follicle development and health?* 2018. 2nd UK Fertility Preservation Conference. Oxford, UK.

Assistance given throughout this investigation

All work detailed throughout this thesis was conducted by me with the following exceptions:

- **Chapter 4:** Charlotte Walker and I contributed equally to tissue processing, culture, embedding, sectioning, staining and imaging.
- **Chapter 5:** Babatomisin Adeniran and I contributed equally to tissue processing and culture. Nina Boskovic (MSc student) carried out histological processing (embedding and sectioning), staining (Masson's trichrome staining and TUNEL labelling) and data acquisition under my supervision.

Acknowledgements

First, I would like to thank my supervisors, Prof Suzannah Williams and Dr Sheila Lane. To Suzannah I express my sincere gratitude for her supervision and support over the past four years. She has provided me with both mentorship and friendship and helped steer me in the right direction while also giving me the space and freedom to explore my own ideas and grow as a researcher. I would like to warmly thank Sheila for her offering her time, guidance and clinical expertise, particularly around the major milestones of my DPhil.

I would like to thank my funding bodies, the Oxford-MRC Doctoral Training Programme and Scatchered European Scholarship, as well as The Iceland Cancer Society (Krabbameinsfélag Íslands). Without their financial support I would not have been able to accept my place at Oxford or pursue this research. I would also like to thank the Medical Science Division for offering me a COVID-related funding extension to help me complete this work.

Thanks to the staff at the Oxford Cell and Tissue Biobank (Emma, Jill, Gemma, Faz, Martha and Agnes) for their time in providing me with samples to use in my research. Thanks also to Dr Chris Largerholm and Dr Jana Koth at the Wolfson Imaging Facility for technical advice and access to equipment. I am grateful to the late Dr Dan Lunn (Department of Statistics) for being a springboard into the world of statistical modelling.

I am also grateful to our collaborator at the University of Edinburgh, Prof Norah Spears, and her research group. I offer my sincere appreciation and thanks to Norah for not only welcoming me to her research group but also to her home (and local Pilates class!) during my visit. I'm also grateful to the members of her group and department (Caroline, Agnes, Federica and Vivian) for their warm welcome and for being friendly faces at conferences.

I am lucky to have been a member of a fantastic research group and am grateful to the other members of the Williams lab, both past and present (Sairah, Charlotte, Xi, Eleni, Tomi, Ruth and Aleona) as well as the MSc students I had the pleasure of co-supervising (Mila, Nina and Lorelí).

Members of the NDWRH have also offered me an enormous amount of support during my DPhil, both technical and personal. I would like to thank Dr Karin Hellner, Dr Jane Hirst, Prof Christian Becker and Prof Anne Goriely for acting as examiners at various stages of my DPhil and for providing constructive criticism and useful discussion on my project. Within the wider department I am grateful to Karl, Tiff, Judith, Sarah, Jen and Gavin who also welcomed me into their unofficial lunch and quiz club. Thanks also to the other DPhil students and End Office members, particularly Mira, Magda, Neva and Carolina.

I am grateful to my family and friends back home for their constant support and encouragement. This DPhil has involved both highs and lows but has always included the unwavering love and support of my fiancé Sigurgeir to whom I am so thankful.

Finally, I would like to thank the patients who donated their tissue to research. Without them these pages would be empty.

Table of contents

List of tables

List of figures

Abbreviations

4EBP1	Eukaryotic translation initiation factor 4E-binding protein 1
Akt	Protein kinase B
AMH	Anti-Müllerian hormone
BIRC	Baculoviral IAP repeat containing
bpV(HOpic)	Dipotassion bisperoxo(5-hydroxypyridine-2-carboxyl)oxovanadate
BSA	Bovine serum albumin
CAM	Chorioallantoic membrane
cAMP	Cyclic adenosine monophosphate
CC3	Cleaved caspase 3
CC7	Cleaved caspase 7
CCN2	Connective tissue growth factor
CDC42	Cell division cycle 42
COVID-19	Coronavirus disease of 2019
CREB	cAMP response element-binding protein
DAB	3,3'-diaminobenzidine
DAPI	4′,6-diamidino-2-phenylindole
DMEM	Dulbecco's modified Eagle medium
DMSO	Dimethylsulfoxide
EBSS	Earle's balanced salt solution
ECM	Extracellular matrix
EGF	Epithelial growth factor
eIF3	Eukaryotic initiation factor 3
eIF4E	Eukaryotic translation initiation factor 4E
FOXL2	Forkhead box transcription factor L2
FOXO1	Forkhead box transcription factor 1
FOXO3	Forkhead box transcription factor 3
FOXO4	Forkhead box transcription factor 4
FrOC	Fragmented ovary culture
FSH	Follicle stimulating hormone
GFP	Green fluorescent protein
GnRH	Gonadotropin-releasing hormone
hFrOC	Human fragmented ovary culture
HSA	Human serum albumin
IGF1	Insulin growth factor 1
IHC	Immunohistochemistry
ITS	Insulin, transferrin and selenium
JNK-1	c-Jun N-terminal kinase 1
KL	Kit ligand
L-15	Leibovitz’s 15 medium
LATS1/2	Large tumour suppressor homolog 1/2
LH	Luteinising hormone
LIF	Leukaemia inhibitory factor
MAPK3/1	Mitogen-activated protein kinase 3/1
mFrOC	Mouse fragmented ovary culture

MOB1	MOB kinase activator 1
MST1/2	Mammalian Ste-20-like kinase 1/2
mTOR	Mammalian target of rapamycin
mTORC1	Mammalian target of rapamycin complex 1
NA	Numerical aperture
NBF	Neutral buffered formalin
NR	Neutral red
OCTB	Oxford Cell and Tissue Biobank
OTC	Ovarian tissue cryopreservation
p27	Cyclin-dependent kinase inhibitor 1B
PBS	Phosphate buffered saline
PBST	Phosphate buffered saline with Tween 20 or TritonX-100
PDK1	Phosphoinositide-dependent-kinase-1
PI3K	Phosphatidylinositol 3 kinase
PIP2	Phosphatidylinositol-4,5-bisphosphate
PIP3	Phosphatidylinositol-3,4,5-triphosphate
PKA	Protein kinase A
POI	Premature ovarian insufficiency
PTEN	Phosphatase and tensin homologue deleted on chromosome 10
RT	Room temperature
S6K1	Ribosomal protein S6 kinase beta-1
SAV1	Salvador
SIRT1	Sirtuin 1
TAZ	Transcriptional coactivators PDZ-binding motif
TBS	Tris buffered saline
TBST	Tris buffered saline with Tween 20 or TritonX-100
TdT	Terminal deoxynucleotidyl transferase
TGFβ	Transforming growth factor beta
TSC1/2	Tuberous sclerosis complex 1/2
TUNEL	Terminal deoxynucleotidyl transferase dUTP nick end labeling
VEGF	Vascular endothelial growth factor
VIP	Vasoactive intestinal peptide
WIMM	Weatherall Institute of Molecular Medicine
YAP	Yes-associated protein
αMEM	Minimum essential medium alpha

Chapter 1

Introduction

1.1 Cancer and fertility

It is estimated that one in two people will be diagnosed with cancer in their lifetime and cancer remains one of the leading causes of death in the UK. According to the most recent data, there were around 367,000 new cancer cases in the UK every year between 2015-2017 (Cancer Research UK, 2020). While cancer mostly affects people aged 50 or above, adults aged 25-49 contribute to around 10% of all new cancer cases (Office For National Statistics, 2020a). Cancer incidence increases with age; approximately 2,300 women aged 20-29 were diagnosed with cancer annually in England compared to over 6,000 women aged 30-39 years (Office For National Statistics, 2020a). The number of young people diagnosed with cancer is also not insignificant, as on average over 1,700 girls and young women (aged <25 years) received a cancer diagnosis each year between 1997-2016 (Public Health England, 2021). While the incidence of cancer has increased in recent years, particularly in those aged 0-24, survival rates have doubled in the last 40 years (Cancer Research UK, 2014). The 5-year survival rate of women of all ages is 59% and over 80% for those under the age of 25 (Cancer Research UK, 2014; Public Health England, 2021). As the number of young cancer survivors increases, improving the quality of life for these individuals is becoming a greater priority.

Cancer treatment, which includes surgery, radiotherapy, chemotherapy in addition to endocrine- and immunotherapy, may have short and long-term effects on fertility in both males and females. One significant long-term effect of cancer treatment faced by many female cancer survivors is infertility, defined as the inability to conceive after one year of unprotected intercourse. This is

due to chemotherapy and radiotherapy causing irreversible loss of germ cells within the ovaries and/or damage to other reproductive organs. Childhood cancer survivor studies revealed that 6.3% of survivors developed loss of ovarian function within 5 years of diagnosis (acute ovarian failure), while 10.9% of survivors underwent premature ovarian insufficiency (POI), defined by persistent amenorrhea before the age of 40 (Chemaitilly *et al.*, 2006, 2017). Female childhood cancer survivors have also been demonstrated to have an increased time to pregnancy, lower pregnancy rates and an increased risk of infertility compared to female siblings (Barton *et al.*, 2013). Children or adolescents diagnosed with cancer may not comprehend the implications of cancer on their future fertility and are unlikely to have considered their desire to have children in the future. Therefore, they should be carefully counselled prior to treatment along with their legal guardians, as POI and/or infertility may affect their quality of life long-term. Furthermore, women aged 30-39 at the time of cancer diagnosis were ~50% less likely to achieve pregnancy after diagnosis compared to the general population (Anderson *et al.*, 2018). Considering that the average age for first time mothers in the UK is now over 30 years (Office For National Statistics, 2020b), these women may not have started, or completed, their families at the time of cancer diagnosis and therefore POI may be a particularly distressing experience for these patients. The effects of cancer treatment on reproduction are not solely related to fertility or a wish for pregnancy; impaired ovarian function resulting in disrupted hormone levels and amenorrhea can lead to other long-term health consequences such as low bone density, cardiovascular disease and neurological disorders (Faubion *et al.*, 2015; Hamoda and British Menopause Society and Women's Health Concern, 2017).

The degree of damage to ovarian function caused by cancer treatment depends on several factors including patient age and ovarian reserve prior to treatment, as well as the type, dose and duration of chemotherapy and/or radiotherapy treatment they receive (Table 1-1; Meirow *et al.*, 2010; van den Berg *et al.*, 2021). The human oocyte is extremely sensitive to radiation, with low doses of 2 Gy being sufficient to reduce the ovarian reserve by 50% (LD50) and doses of over 14 Gy causing ovarian failure, depending on patient age (Wallace *et al.*, 2003; Anderson *et al.*, 2015).

Over 90% of patients exposed to total body or pelvic radiation will experience ovarian failure (Shalet *et al.*, 1976; Meirow *et al.*, 2010). Chemotherapy drugs in the class of alkylating agents are highly toxic, carrying an odds ratio of 4.0 for causing ovarian failure, while platinum derivatives have an odds ratio of 1.8 (Meirow *et al.*, 2010). In almost all cases, patients will receive a combination of different chemotherapy drugs and/or radiation and therefore it is difficult to calculate the risk of ovarian failure from one particular drug.

Table 1-1 Risk of subfertility after treatment for common cancers in childhood and adolescence (Sonmezer and Oktay, 2004; Wallace *et al.*, 2005)

High risk (>80%)	Medium risk	Low risk (<20%)
Hodgkin's disease (treatment with alkylating drugs)	Acute myeloblastic leukaemia	Acute lymphoblastic leukaemia
Soft-tissue sarcoma: stage IV (metastatic)	Hepatoblastoma	Wilms' tumour
Ewing's sarcoma (metastatic)	Osteosarcoma	Soft-tissue sarcoma (stage I)
	Ewing's sarcoma (non-metastatic)	Germ-cell tumours (with gonadal preservation and no radiotherapy)
	Soft-tissue sarcoma (stage II or III)	Retinoblastoma
	Neuroblastoma	Brain tumour (surgery only, cranial irradiation <24 Gy)
	Non-Hodgkin lymphoma	
	Hodgkin's disease	
	Brain tumour (craniospinal radiotherapy, cranial irradiation >24 Gy)	

1.1.1 Fertility preservation for female cancer patients

Currently there are several options for fertility preservation available to girls and women undergoing cancer treatment. The most commonly used methods of female fertility preservation are cryopreservation of oocytes or embryos (Yasmin *et al.*, 2018). This involves the patient undergoing controlled ovarian hyperstimulation to produce a large number of mature eggs which

can be collected and cryopreserved, or fertilised with donor or partner sperm, cultured to the blastocyst stage and then cryopreserved. Oocyte and embryo cryopreservation have similar live birth rates in cancer patients (Table 1-2). While this method offers the patient a chance of pregnancy it does not prevent ovarian failure or restore ovarian function. In addition, chemotherapy must be delayed by at least 10 to 12 days to allow time for ovarian stimulation (Donnez and Dolmans, 2013; De Vos *et al.*, 2014; Cobo *et al.*, 2016). The patient must also be both physically and emotionally developed enough to undergo controlled ovarian hyperstimulation and egg retrieval, therefore this method is not available to many young patients (Wallace *et al.*, 2005, 2016; Jadoul *et al.*, 2010; Donnez and Dolmans, 2013).

Table 1-2. Overview of fertility preservation methods and live birth rates for reproductive-aged female cancer survivors

Method	Restores ovarian function?	Reported live birth rates
Oocyte cryopreservation	No	41-44% per embryo transfer (Druckenmiller *et al.*, 2016; Cobo *et al.*, 2018)
Embryo cryopreservation	No	20-31% per embryo transfer (Barcroft *et al.*, 2013; Dolmans *et al.*, 2015; Creux *et al.*, 2018)
Ovarian tissue cryopreservation	Yes	23-42% per transplantation (Donnez and Dolmans, 2015; Donnez *et al.*, 2015a, b; Van der Ven *et al.*, 2016; Shapira *et al.*, 2020)

Some fertility preservation methods can prevent or reduce damage to the ovaries. These include ovarian transposition, where the ovaries are surgically moved out of the field of irradiation, and ovarian shielding where exposure to the ovaries is minimised using external blocks, however this latter method is of limited use and neither method protects the ovaries from chemotherapy-induced damage (McCall *et al.*, 1958; Al-Asari and Abduljabbar, 2012; Fawcett *et al.*, 2012). Furthermore, the patient may still be exposed to pelvic irradiation which may impact the uterus and reduce the chances of successful pregnancy (Critchley and Wallace, 2005; Wallace *et al.*,

2005). Ovarian tissue cryopreservation and reimplantation is far more effective and is becoming increasingly available as it can restore ovarian function to the patient following treatment, can be offered to young girls and has a similar live birth rate (per transplantation) to oocyte and embryo cryopreservation (Table 1-2), although the data is still limited compared to egg freezing.

Ovarian tissue cryopreservation involves the surgical removal of either a portion or a whole ovary, followed by isolation and cryopreservation of the outermost layer of the ovary, which contains the ovarian reserve. This tissue can then be transplanted back to the patient either orthotopically (within the pelvic cavity) or heterotopically (e.g. abdominal wall or arm) following treatment and once the patient wishes to become pregnant or restore their menstrual cycles. For orthotopic transplantation, endocrine function, measured by the resumption of menstrual cycles, is restored in over 95% of cases and remains functional for two to five years on average (Donnez and Dolmans, 2015; Gellert *et al.*, 2018; Shapira *et al.*, 2020). Additional transplantations may be required. The first pregnancy following ovarian tissue cryopreservation and transplantation was reported in 2004 and since then over 130 live births have been reported (Donnez *et al.*, 2015b; Dunlop *et al.*, 2016; Meirow *et al.*, 2016; Rodriguez-Wallberg *et al.*, 2016; Van der Ven *et al.*, 2016; Donnez and Dolmans, 2017; Jensen *et al.*, 2017; Gellert *et al.*, 2018). Two live births have been reported following transplantation of pre-menarcheal paediatric ovarian tissue (Demeestere *et al.*, 2015; Matthews *et al.*, 2018). Despite its many benefits, ovarian tissue cryopreservation is an invasive procedure, requiring at least two surgeries which carry their own risks, in addition to the possible risk of reintroducing malignant disease, particularly for leukaemia (Bastings *et al.*, 2013; Gellert *et al.*, 2018).

In recent years there has been increased interest in developing non-invasive pharmacological methods of fertility preservation. Once developed, these could involve administration of a pharmacological agent alongside cancer treatment, which would protect the ovaries from the damaging effects of chemotherapy. Following cancer treatment, the patient would suspend the use of the agent and resume normal ovarian function and fertility. The only pharmacological method currently in use is suppression of ovarian function by administration of gonadotropin-

releasing hormone (GnRH) agonists. GnRH agonists suppress follicle stimulating hormone (FSH) which in turn suppresses ovarian function, reducing damage to the ovary. Despite a number of studies being performed using GnRH agonists, mostly in patients with breast cancer, the effectiveness of this treatment remains controversial and hotly debated (Blumenfeld, 2008; Lambertini *et al.*, 2015; Taylan and Oktay, 2017).

1.2 Ovarian physiology

1.2.1 Formation and structure of the ovary

The human ovary is a dynamic oval-shaped organ, approximately 3-5 cm long in adults, located on either side of the uterus in the pelvic cavity (Figure 1-1). The ovaries serve two main functions: they develop the female germ cells and produce hormones to support the female phenotype and reproduction. The ovaries begin to form during foetal life when the primordial germ cells migrate from the yolk sac into the indifferent gonad by the seventh week of gestation, where they undergo proliferation (Sarraj and Drummond, 2012). The total number of germ cells reaches a peak of about seven million at 20 weeks gestation, after which their number declines to approximately 1 million at birth and 300,000-400,000 at menarche (Faddy *et al.*, 1992; Te Velde *et al.*, 1998). The formation of the human ovary is completed shortly after birth, at which time it consists of an inner medulla and an outer cortex, which is enclosed by the tunica albuginea.

Follicles are the functional unit of the ovary. Each follicle consists of a single oocyte surrounded by somatic cells which support its development and maturation (discussed in the next section). The majority of follicles are located in the cortex which is enriched in a dense extracellular matrix which provides structural support and plays an important role in follicle development and function (Woodruff and Shea, 2007). In addition to follicular cells, the cortex also contains immune cells, endothelial cells, perivascular cells and stromal cells (Fan *et al.*, 2019; Wagner *et al.*, 2020). The medulla is less dense than the cortex, harbouring follicles in advanced stages of development, and is enriched with blood vessels (Blaustein, 1982).

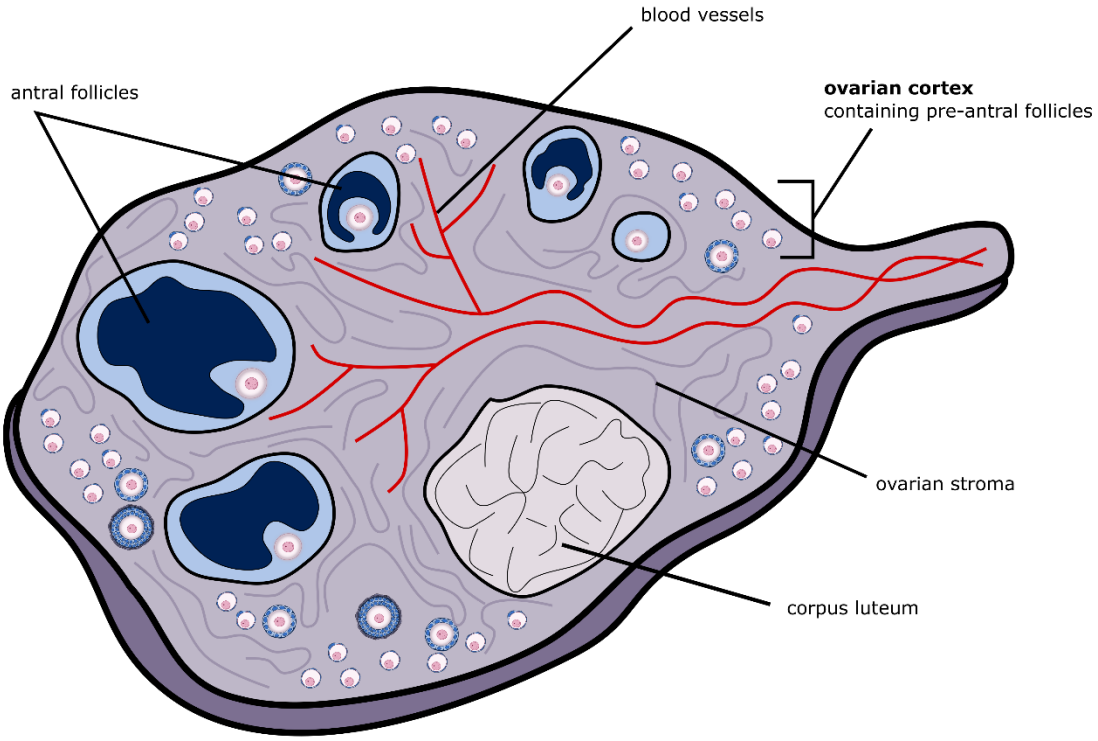

Figure 1-1. Structure of the human ovary. The human ovary is an oval-shaped organ, approximately 3-5 cm in length in adults. Primordial and early growing follicles are located in the ovarian cortex, the outermost area of the ovary. The medulla is the inner section of the ovary, enriched in blood vessels and containing growing follicles. The ovarian stroma contains stromal cells, immune cells, endothelial cells, perivascular cells and is enriched in a dense extracellular matrix. Follicles at various stages of development (pre-antral and antral) are depicted, in addition to a corpus luteum.

1.2.2 Follicle development

The dominant population of follicles in the human ovary is classically considered to be primordial follicles and these represent the ovarian reserve. Primordial follicles consist of a single oocyte, arrested in the diplotene stage of prophase I, surrounded by a single layer of flattened pre-granulosa cells and a basement lamina (Smitz and Cortvrindt, 2002). Each follicle is destined to either undergo atresia or begin the process of follicle development, which ultimately leads to either atresia or the release of a mature egg ready for fertilisation (Figure 1-2). A follicle may remain in a dormant state for years or even decades but once it receives the signal(s) to undergo activation (see Section 1.4) the pre-granulosa cells divide and undergo a squamous-to-cuboidal transition. In mice, granulosa cells have been observe to 'zip up' as two neighbouring cells lengthen on the adjacent side (Hardy *et al.*, 2018). Follicles that contain a mixture of flattened pre-granulosa cells and cuboidal granulosa cells are termed transitional follicles (also known as

transitory or intermediary follicles; (Gougeon, 1996)). Although transitional follicles have undergone morphological changes and may therefore be thought to be activated, many consider them to belong to the resting follicle pool (Gougeon, 1996; de Bruin *et al.*, 2002; Smitz and Cortvrindt, 2002). This is because transitional follicles have been found to be an equal or larger proportion of the total follicle pool to primordial follicles and exhibit slow growth (Gougeon and Chainy, 1987; Gougeon, 1996; de Bruin *et al.*, 2002). In fact, in bovine ovaries, primordial follicles are considered to have a mixture of flattened and cuboidal (pre-)granulosa cells (van Wezel and Rodgers, 1996). Primordial follicle activation is an irreversible process that occurs continuously beginning during foetal life until menopause.

Once the oocyte is surrounded by a single layer of cuboidal granulosa cells (primary follicle) it begins to increase in volume and the zona pellucida is formed. The transition from the primordial to the primary stage occurs very slowly over a span of around 150 days (Gougeon, 1986). Active follicle growth begins once the oocyte nucleus has reached a diameter of ~19 μm and when approximately 15 granulosa cells are present at the largest cross-section (Gougeon and Chainy, 1987). The oocyte continues to grow in size and the granulosa cells proliferate, forming first two layers (secondary follicle), and then multiple layers (pre-antral follicle). During the secondary follicle stage, stromal cells surrounding the basal lamina are recruited by the follicle to form theca cells as the follicle grows (Gougeon, 1996). Primordial to primary follicles lack a direct blood supply, however blood vessels are incorporated into the outermost area of the follicle, remaining outside the basal lamina, during the secondary follicle stage and thus the follicle becomes directly exposed to circulating blood (Bassett, 1943).

Small fluid-filled cavities of ~40 μm in diameter begin to form between the granulosa cells and merge together to form the antrum. At this point the antral follicle is approximately 200 μm in diameter and over 270 days have passed since the follicle underwent activation (Gougeon, 1986). Although the oocyte has already reached a terminal size of ~120 μm by this point, a follicle destined for ovulation will increase its diameter by two orders of magnitude as the antrum increases in volume, and granulosa and theca cells continue to proliferate. Once follicles have

reached a diameter of 2-5 mm they can be selected in response to a rise in FSH during the late luteal phase to prepare for ovulation in the subsequent cycle (Gougeon and Lefevre, 1983; McNatty *et al.*, 1983). In the absence of FSH, e.g. prior to puberty or during pregnancy, follicles do not develop beyond this stage and undergo atresia (see Section 1.5.1.1). Out of approximately 10 to 20 follicles that are selected for pre-ovulatory growth, only one follicle (or in rare cases multiple) gains dominance and supresses the growth of the other follicles (Fauser and Van Heusden, 1997; McGee and Hsueh, 2000). In response to a mid-cycle surge in luteinising hormone (LH), the oocyte resumes meiosis up to metaphase II and the follicle ruptures to release the mature egg into the Fallopian tube. The remaining granulosa and theca cells undergo differentiation to become the cells of the corpus luteum.

The follicle is a hormone-producing unit and has two main functions. First, it supports the growth and maturation of the oocyte through the production of androgens and oestrogen, resulting in the release of a fertilisable oocyte Second, it releases progesterone following ovulation to support early pregnancy. Androgens (androstenedione and testosterone) are produced by theca cells in response to LH and are transported to the granulosa cells where FSH triggers their conversion to oestrogens; this is referred to as the 'two cell, two gonadotrophin' theory (Gougeon, 1996). Once the corpus luteum has formed, the luteal cells begin to produce progesterone in place of oestrogen to support early pregnancy until the point where the placenta takes over progesterone production.

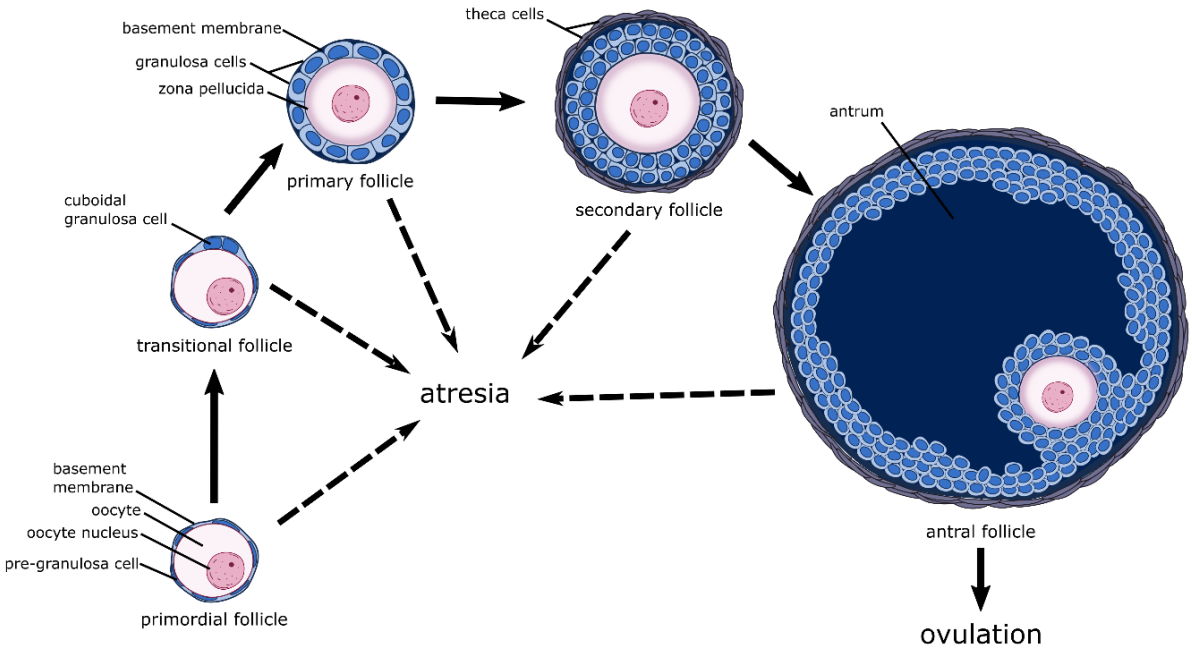

Figure 1-2. Overview of follicle development. Follicles at the earliest stage of development are termed primordial follicles. They consist of a single oocyte surrounded by a single layer of flattened pre-granulosa cells. Upon follicle activation, the pre-granulosa cells divide and become cuboidal granulosa cells; transitional follicles contain a mixture of flattened and cuboidal cells. The granulosa cells continue to divide as the follicle develops to the primary and secondary stage, with one and two layers of granulosa cells, respectively. The oocyte begins to form the zona pellucida, an outer glycoprotein layer, during the primary stage. The theca layer forms at the secondary follicle stage. The follicle continues to grow as the granulosa cells divide to form several layers and the oocyte increases in size. Small fluid-filled cavities form between the granulosa cells and merge together to form the antrum. All follicles prior to this can be grouped and termed pre-antral. Although the oocyte reaches a terminal size of 120 µm at the antral stage, the follicle continues to grow and reaches a final size of ~20 mm before ovulation. Only one follicle is ovulated in each menstrual cycle, the remaining follicles undergo atresia at various points in the developmental process. Image not to scale.

1.3 Strategies to investigate human ovarian follicles

In order to directly investigate the human ovary and the follicles contained within it, the ovary (or a portion of it) must first be surgically removed from the body at which point it can be preserved, for example by fixation or cryopreservation, for subsequent analysis. Analysis of human ovaries has shed light on the structure of the ovary and follicles and allowed for the classification of follicle development as described in Section 1.2. However, in order to gain a deeper understanding of ovarian and follicle function, treatment with various drugs and/or repeated sampling of the ovary would be needed, however this is extremely unethical to perform

in humans. To overcome this dilemma, scientists have developed various experimental systems to replicate follicle development that occurs *in vivo*. These methods include grafting a portion of ovarian tissue into an experimental animal (most commonly immunocompromised mice) or *in vitro* methods such as culture of ovarian tissue or isolated follicles. These methods are discussed in the following sections, with an emphasis on *in vitro* techniques, in addition to the most common techniques used to analyse human ovarian tissue, and their limitations.

1.3.1 Methods of investigating human follicle development *in vivo*

Ovarian tissue xenotransplantation involves the grafting of ovarian tissue into an immunosuppressed host animal, most commonly mice with severe combined immunodeficiency (SCID strain), and allows for long-term evaluation of follicle development, as grafts/mice can be easily maintained for several months. Xenotransplantation is a useful model for investigating ovarian physiology, including follicle viability and development, and it is the experimental system which most closely resembles the natural state of the human ovary (Gosden *et al.*, 1994a). Following the grafting procedure, the transplanted tissue becomes connected to the host's bloodstream through neovascularisation and thus the tissue is exposed to endogenous gonadotrophins (or administered exogenous gonadotrophins), assuming that the host is not deficient in pituitary gonadotrophins, due to mutation (such as in hypogonadal (*hpg*) mice (Mason *et al.*, 1986)).

Xenotransplantation of human ovarian tissue has been performed for several decades, using both fresh and cryopreserved tissue from patients of all ages with the duration of transplantation ranging from a few weeks to several months, demonstrating that it can support follicle development up to the antral stage, with mature eggs having been obtained in several instances (Oktay *et al.*, 1998; Nisolle *et al.*, 2000; Gook *et al.*, 2001, 2003; Kim *et al.*, 2002, 2005; Hernandez-Fonseca *et al.*, 2004; Nottola *et al.*, 2008; Terada *et al.*, 2008; Dath *et al.*, 2010; Soleimani *et al.*, 2010; David *et al.*, 2012; Luyckx *et al.*, 2013a; Lotz *et al.*, 2014; Raffel *et al.*, 2017). There is even one report of xenotransplantation supporting full and repetitive follicle development, with mature eggs being aspirated from antral follicles 37 days apart after an initial four months of

xenotransplantation (Lotz *et al.*, 2014; Raffel *et al.*, 2017). Another benefit of using xenotransplantation to study follicle development is that it allows for a more physiological study on the effects of various drugs or compounds, as drugs can be administered to the ovarian tissue via the bloodstream, instead of the tissue being in direct contact with high concentrations of the drugs as is the case for *in vitro* culture.

Ovarian tissue can be grafted to any number of sites within the mouse, with the main limitation being the size of the graft itself. Several different sites have been reported in the literature, with the most common ones being the subcutaneous space (Nisolle *et al.*, 2000; Kim *et al.*, 2002, 2005; Hernandez-Fonseca *et al.*, 2004; Terada *et al.*, 2008; Dath *et al.*, 2010), kidney capsule (Oktay *et al.*, 1998; Gook *et al.*, 2001, 2003; Hernandez-Fonseca *et al.*, 2004; Terada *et al.*, 2008; Soleimani *et al.*, 2010) and ovarian bursa (Terada *et al.*, 2008; Dath *et al.*, 2010). Several studies have compared different transplantation sites, and while they indicate that follicle development may be influenced by transplantation site, the results remain inconclusive (Hernandez-Fonseca *et al.*, 2004; Terada *et al.*, 2008; Dath *et al.*, 2010). Experiments within our own research group have found that tissue grafted to the ovarian bursa and kidney capsule had low follicle numbers, while follicles were found in all subcutaneous grafts, following six-week xenotransplantation (Wei, 2018). Transplantation to the subcutaneous space is a less complicated procedure which also allows the graft to be monitored from the outside, which is useful to enable assessment of the development of large follicles.

Despite xenotransplantation providing an environment that most closely resembles that of the human ovary *in situ*, there are some limitations and follicle development may not be fully physiological. Xenotransplantation may not be an adequate model to study late follicle development, as follicle growth in ovarian grafts does not correlate fully with normal follicle development. Follicles grown in xenografts do not reach a terminal size equal to that *in situ* (maximum reported size in xenografts is 6 mm, while in humans follicles reach a size of up to 20 mm (Gougeon, 1986)) and low maturation rates have been reported for oocytes aspirated from antral follicles (Kim *et al.*, 2005). Single-cell RNA sequencing recently revealed that many genes

are differentially expressed in granulosa cells from antral follicles derived from *in situ* human ovaries and xenografted ovarian tissue (Man *et al.*, 2020). Unusual characteristics of pre-antral follicles have also been reported following xenotransplantation (Nottola *et al.*, 2008; David *et al.*, 2012).

Although xenotransplantation allows the study of ovarian follicles in a physiological environment like that of the human ovary, it requires the use of experimental animals which calls for considerations regarding animal welfare, ethics and cost. Public opinion and governing bodies in some countries have placed great emphasis on the principles of the 3Rs (reduction, refinement and replacement) for the use of laboratory animals for research. Therefore, in some cases *in vitro* culture methods may be more suitable as a model to study follicle function and development, for instance for the study of more basic investigations of follicle development, drug screening or as pilot studies prior to advancing to xenotransplantation.

1.3.2 Methods of investigating human follicle development *in vitro*

In vitro follicle growth (IVFG) is the technique of supporting ovarian follicles derived from a living organism in an external culture environment. This strategy can offer a more controlled setting to study follicles compared to *in vivo* methods and can be used to study the mechanisms involved in follicle activation and development (Carlsson *et al.*, 2006a; Grosbois and Demeestere, 2018), as a toxicity assay (Cortvrindt and Smitz, 2002) or to study the effects of drugs and chemicals (Hao *et al.*, 2017; Lopes *et al.*, 2020). IVFG is also being investigated as a possible means of fertility preservation for patients for whom other methods are unavailable or contraindicated, for example in the case of ovarian tissue transplantation for patients with leukaemia or metastatic disease where there may be a risk of reintroducing malignant cells present in the cryopreserved tissue (Anderson *et al.*, 2017). An alternative fertility preservation method for these patients could involve complete IVFG followed by *in vitro* maturation (IVM) of oocytes that can then be frozen and/or fertilised for future use (Salama *et al.*, 2019). Alternatively, it has been proposed that isolated follicles, which are enclosed in a basement membrane and therefore not in direct contact with white blood cells or capillaries (Rodgers *et al.*, 2003), could be seeded into a scaffold

to create an 'artificial ovary' which could be transplanted back to the patient (Luyckx *et al.*, 2013b; Laronda *et al.*, 2017).

In light of the different applications of IVFG, a number of different culture systems have been developed using follicles from a range of species such as mice (Xu *et al.*, 2006a, 2009a; Hornick *et al.*, 2013), domestic animals (e.g. sheep: Muruvi *et al.*, 2005, and goats: Silva *et al.*, 2015) and humans (Xiao *et al.*, 2015; McLaughlin *et al.*, 2018; Hao *et al.*, 2020; Xu *et al.*, 2021). These methods range from the culture of isolated preantral follicles to those that support complete follicle development, starting with primordial follicles and resulting in mature fertilisable oocytes, even leading to the birth of live offspring (Eppig and O'Brien, 1996).

There are two main strategies available to support IVFG: culture of isolated follicles or culture of follicles within ovarian tissue (hereafter referred to as 'ovarian tissue culture'). Several different protocols have been developed for each of these techniques; this section will discuss these different strategies, with a focus on those developed for studying human ovarian follicles.

1.3.2.1 IVFG using isolated follicle culture

Culture systems using isolated murine follicles were first described in 1977 (Eppig, 1977) and have since been established in multiple species (Simon *et al.*, 2020). The majority of these systems have been developed using rodent models, and to date only live births have been achieved from gametes originating from murine follicle culture (Eppig and Schroeder, 1989; Xu *et al.*, 2006b). However, mature oocytes and/or embryos have been obtained in follicles from other species, including sheep (Arunakumari *et al.*, 2010) and rhesus macaque (Peluffo *et al.*, 2012). Due to ethical restrictions, only meiotically competent MII oocytes have been obtained from *in vitro* grown human follicles (Xiao *et al.*, 2015). Most animal studies have been carried out using follicles from reproductively young or even prepubertal animals, as the ovaries from these animals contain higher follicle numbers. In the case of larger animals such as sheep and humans the ovarian cortex is softer and easier to work with in younger individuals, facilitating follicle isolation (Simon *et al.*, 2020). However, due to sample limitations, studies on human follicles are

more often performed using samples from adults undergoing treatment for benign gynaecological conditions or caesarean sections.

In order to culture individual preantral follicles *in vitro*, the follicles must first be isolated from the ovarian cortex and must remain morphologically intact so as to support further development (Demeestere *et al.*, 2002). Ovarian follicle isolation methods can be categorised as mechanical or enzymatic, though often a combination of both methods is used (Simon *et al.*, 2020). For mechanical isolation, follicles are individually isolated from the ovarian tissue using tools such as tissue choppers, scalpel blades, insulin needles or watchmakers forceps (Abir *et al.*, 1997). In contrast, enzymatic isolation involves the digestion of the extracellular matrix with enzymes (either single enzymes such as collagenase or enzyme cocktails), allowing the follicles to be collected from the digested mixture (Roy and Treacy, 1993; Abir *et al.*, 1999; Dolmans *et al.*, 2006; Schmidt *et al.*, 2018). Although enzymatic isolation can be more easily scaled up and is less time consuming it can cause damage to the follicle basement membrane and compromise follicle growth (Abir *et al.*, 1999). Due to the dense and fibrous nature of the human ovary, a combination of mechanical and enzymatic isolation has been found to be favourable to isolate human follicles (Dolmans *et al.*, 2006; Kristensen *et al.*, 2011; Vanacker *et al.*, 2011).

Once the follicles have been isolated, they must be placed in a culture environment capable of supporting further development. Many culture systems have been developed for this purpose and these are commonly categorised as attached (two-dimensional) or suspended (three-dimensional) culture systems. Attached culture systems were the first culture systems developed for isolated follicle culture and involve culturing follicles directly on the surface of a culture dish or on surfaces coated with extracellular matrix components. The first studies of human preantral follicle culture were performed using attached culture systems and were shown to be dependent on FSH (Roy and Treacy, 1993; Abir *et al.*, 1997). Although these studies demonstrated follicle growth, attached culture systems are not able to support full follicle development as the proliferating granulosa cells eventually break through the basement membrane and attach to the culture surface, disrupting the follicle structure (Cortvrindt *et al.*, 1996; West *et al.*, 2007). They

are therefore only suitable for short-term culture, or as part of a multi-step culture system (discussed below).

In the ovary, follicles are in uniform and direct contact with the ovarian stroma. Suspended culture systems prevent the follicle from attaching to the culture plate and are therefore better able to maintain follicle integrity and support normal cell-cell interactions, for example through rotation or orbiting of the culture system (Rowghani *et al.*, 2004), with the use of inverted drops (Wycherley *et al.*, 2004), or encapsulation in a biomaterial (Torrance *et al.*, 1989). Biomaterials may also offer additional support to the follicle by providing a more structured environment similar to that *in vivo* (West *et al.*, 2007). In the case of encapsulation, the biomaterial must be strong enough to support the structure of the follicle, but not so rigid that it restricts its growth and expansion (Shea *et al.*, 2014). It must also be permeable to the surrounding media, to allow the diffusion of nutrients, proteins and hormones to the follicle (Chan and Leong, 2008). Suspended culture of human follicles was found to be superior to attached culture, with follicle growth being observed in follicles isolated from fresh and cryopreserved tissue and encapsulated in a collagen gel, while no follicle growth was observed in follicles cultured on a layer of ECM in a 24-hour culture period (Abir *et al.*, 2001). However this system did not support follicle growth beyond 24 h (Abir *et al.*, 1999). Notably, only fully isolated follicles grew in culture, while partially isolated follicles detached from the collagen gel and died (Hovatta *et al.*, 1999; Abir *et al.*, 2001).

Encapsulated follicle culture systems have proven very successful, with most systems using hydrogels as the encapsulating biomaterial. Hydrogels are formed by ionic or covalent cross-linking of water-soluble polymers. The most commonly used hydrogel for follicle culture is alginate, or a combination of fibrin and alginate, though other hydrogels have also been investigated such as hyaluronic acid and polyethylene glycol (Drury and Mooney, 2003; Chan and Leong, 2008). Alginate hydrogels have been successfully used to culture mouse preantral follicles to the antral stage, the oocytes of which were matured and fertilised resulting in healthy, fertile offspring (Xu *et al.*, 2006b). Culture in alginate (or fibrin-alginate) hydrogels can also support human follicle development (Xu *et al.*, 2009b; Xiao *et al.*, 2015). Preantral follicles (approximately

170 μm) isolated from fresh human ovarian tissue were encapsulated with alginate and cultured for up to 30 days. The follicles grew to the antral stage and reached a terminal diameter of up to 1 mm (oocyte diameter 110 μm) (Xu *et al.*, 2009b). This method was later refined by releasing the follicles from the alginate once they had reached the antral stage and continuing the culture in low-attachment plates for up to 40 days. This resulted in meiotically competent metaphase II oocytes after IVM though the follicles did not reach a terminal size equivalent to that observed *in vivo* (Xiao *et al.*, 2015).

Although complete follicle development has been obtained from the culture of isolated preantral follicles, culture starting with isolated *primordial* follicles has not been achieved in humans. Isolation of human primordial follicles has proven challenging due to the dense and heterogeneous nature of the human ovarian cortex, as demonstrated by the variation between patients in collagen density in areas containing follicles (Laronda *et al.*, 2014). This makes it difficult to design follicle isolation protocols and requires bespoke protocols to be used. Indeed, even when adjusting the digestion protocol on a case-by-case basis for 12 patients aged 14-39, the number of isolated primordial follicles ranged from zero to 300 and many of the isolated follicles had lost integrity (Laronda *et al.*, 2014). The remaining intact follicles were encapsulated in 2% alginate, however after three days of culture, all follicles had dissociated and none survived, suggesting that culture of isolated human primordial follicles may not be feasible or requires considerable optimisation. All primordial follicles isolated from ovarian medulla tissue and encapsulated in 0.3% or 0.5% alginate underwent atresia within seven days in culture, compared to higher survival rates in isolated primary (38%) and secondary follicles (70%; Yin *et al.*, 2016).

Transitional follicles represent a large portion of the ovarian follicle pool and isolation of these follicles may be more successful than primordial. Amorim *et al.* successfully isolated 'small pre-antral' follicles from cryopreserved tissue and cultured in alginate hydrogen beads for up to seven days. Based on the representative images, these follicles appeared to be at the transitional stage (~40 μm in diameter with a mixture of flattened and cuboidal (pre-)granulosa cells); after culture they had grown to up to ~55 μm in diameter with a 90% survival rate (Amorim *et al.*, 2009).

The inability to isolate and culture primordial follicles is a considerable limitation if ovarian culture is to be used for fertility preservation, as the dominant population of follicles in the ovary are at the primordial stage. In addition, it is currently not possible to study complete follicle development using isolated primordial follicles. Many research groups have therefore determined that IVFG of human follicles requires a multi-step culture system, beginning with culture of primordial follicles within the ovarian tissue, followed by isolation of preantral follicles and further culture (Telfer *et al.*, 2008; Laronda *et al.*, 2014; Salama and Woodruff, 2019; Xu *et al.*, 2021). The development of human ovarian tissue culture protocols and these multi-step protocols is discussed in the next section.

1.3.2.2 IVFG using ovarian tissue culture

Culture of human follicles within ovarian tissue (ovarian tissue culture) began in the 1990s. These early studies focused on determining which culture conditions best supported follicle growth, investigating different culture media, sources of albumin and addition of factors such as FSH and insulin, transferrin and selenium (ITS; Hovatta *et al.*, 1997; Wright *et al.*, 1999). Hovatta *et al.* compared culture of fresh human ovarian tissue from 20 patients (mean 35 years) in minimum essential medium alpha (αMEM) medium or Earle's balanced salt solution (EBSS) supplemented with pyruvate (Hovatta *et al.*, 1997). They also compared culture on Millicell inserts alone or coated with extracellular matrix (Matrigel). Before culture, over 90% of follicles in tissue were viable, however the number of atretic follicles increased throughout the culture period (up to 21 days). Culture in EBSS resulted in a higher proportion of viable follicles (77%, n=136 follicles) after 4-11 days compared to αMEM (38%, n=63), though there was no difference between the groups after 14-21 days. The proportion of viable follicles was also higher after 10-15 days in culture in tissue cultured with extracellular matrix (85%, n=21) compared to without (19%, n=20), however there was no difference at the other time points (4-9 days and 18-21 days). It should be noted that although ovarian tissue from 20 patients were used in this study, they were not matched across the different conditions due to small biopsy size and the total number of follicles analysed per group varied. In a later study the same research group again compared

culture in αMEM and EBSS, in addition to Waymouth's medium (Wright *et al.*, 1999). They also investigated culture supplements such as FSH and the use of serum-free medium, using human serum albumin (HSA) and ITS in place of inactivated human serum. In this study, culture in αMEM resulted in the highest rate of development compared to the other media used and was the only condition that supported development to the pre-antral stage. FSH reduced the proportion of atretic follicles and increased the proportion of secondary follicles after 15 days in culture. In addition, replacement of serum with HSA+ITS reduced the number of atretic follicles and increased follicle growth after five days (Wright *et al.*, 1999).

Based on these studies, serum-free complex medium such as αMEM is most commonly used for the culture of human ovarian tissue, although other media such as McCoy's 5A and Dulbecco's Modified Eagle Medium (DMEM) are also used (Telfer *et al.*, 2008; Guzel *et al.*, 2018a; Lopes *et al.*, 2020). Aside from antibiotics (most commonly penicillin and streptomycin), common supplements include human serum albumin (HSA), L-glutamine, FSH, insulin, transferrin and selenium (ITS) and ascorbic acid. The use of serum-free medium allows more control over the culture system and allows the study of various growth factors.

Growth differentiation factor 9 (GDF9), an oocyte-secreted growth factor belonging to the Transforming growth factor beta (TGFβ) superfamily, was found to promote the growth, development and survival of follicles in human ovarian tissue culture, confirming its important role in follicle development (Hreinsson *et al.*, 2002). There was a higher proportion of secondary follicles after seven-day culture with 200 ng/mL recombinant GDF9 compared to no GDF9 supplementation, however after 14 days the difference was not significant. Furthermore, this effect was only seen in cultures supplemented with HSA with no difference in tissue cultured with foetal bovine serum. However, GDF9 supplementation did have a positive effect on follicle viability. Despite these findings, GDF9 is not commonly used in human ovarian tissue cultures, likely due production difficulties and expense. In contrast, insulin is a standard supplement, usually added in combination with transferrin (an iron carrier) and selenium (an antioxidant) in the form of ITS. Insulin and insulin-like growth factors I and II (IGF-I and IGF-II) were all found to

act as survival factors in human ovarian tissue culture (containing serum), resulting in increased follicle growth and reduced atresia after 14-day culture (Louhio *et al.*, 2000). These observations were made using only 33 ng/mL insulin, whereas most current culture systems use insulin (in the form of ITS) at a concentration of 10 µg/mL, a 300-fold higher concentration than that used by Louhio *et al.* Insulin causes stimulation of oestradiol production in granulosa cells (Erickson *et al.*, 1990). Activin A, which is produced by granulosa cells and promotes proliferation, supports ovine, caprine and rodent pre-antral follicle growth *in vitro* (McGee *et al.*, 2001; Thomas *et al.*, 2003; Silva *et al.*, 2006). However, activin was found to inhibit follicle activation *in vitro* in human ovarian tissue (Ding *et al.*, 2010). No effect was observed on follicle health or survival. Therefore, activin is not routinely used in ovarian tissue culture but is used in a multistep culture system, following isolation of pre-antral follicles (Telfer *et al.*, 2008; McLaughlin *et al.*, 2018). Since these early studies were performed, a number of different culture protocols have been developed by different research groups (Schmidt *et al.*, 2005; Webber *et al.*, 2007; Asadi Azarbaijani *et al.*, 2015; Guzel *et al.*, 2018b; McLaughlin *et al.*, 2018; Talevi *et al.*, 2018).

There have been two successful reports of complete IVFG in humans resulting in mature oocytes (McLaughlin *et al.*, 2018; Xu *et al.*, 2021). Both studied used fresh human ovarian tissue and a multi-step culture system. In the study by McLaughlin *et al.*, human ovarian tissue was cultured for eight days to support development from the primordial to the pre-antral stage (step 1), after which growing follicles were isolated and cultured individually for a further eight days (step 2; Telfer *et al.*, 2008). Cumulus-oocyte-complexes (COCs) were then isolated from healthy antral follicles and cultured for a further four days (step 3) and the oocytes then matured *in vitro* (step 4; McLaughlin *et al.*, 2018). This method was considerably limited by the low follicle numbers retrieved at each stage. Out of 24 cultured ovarian fragments, only 87 preantral multilaminar follicles were successfully isolated for further culture. Out of these, 54 remained intact following step 2 of culture (16 days total in culture) and had reached the early-mid antral stage. From these follicles, 48 oocyte-granulosa cell complexes were isolated and carried over to step 3. Thirty-two of these complexes showed significant oocyte growth and underwent IVM but only 9 oocytes went

on to emit polar bodies. This represents a 40-60% loss of follicles between steps, due to atresia or developmental failure and highlights the need to further develop this system. Furthermore, although nine MII oocytes were obtained (28% maturation rate), all of these looked severely abnormal with enlarged polar bodies and abnormal spindle formation calling into question the developmental capability of these oocytes.

McLaughlin and colleagues were able to recapitulate full human follicle development *in vitro* within three weeks, however *in vivo* this process takes several months (Gougeon, 1996). Recently, Xu *et al.* reported the successful development of human metaphase II oocytes from unilaminar follicles using a multi-step culture system spanning nine weeks (Xu *et al.*, 2021). Small ovarian tissue fragments were cultured for three weeks, after which growing follicles were mechanically isolated and cultured either individually or in groups of 3-5 for six weeks. Individually grown follicles were supplemented with AMH during weeks 0-3, which resulted in larger antral follicles though follicle survival or antrum formation rates were not changed. IVM was performed on individual COCs of group-cultured follicles and oocyte meiotic status determined. As follicle development during the culture period was not quantified, it is difficult to fully assess the success of this method. However, interestingly, the authors demonstrated the presence of theca cells in the *in vitro* grown antral follicles through steroidogenesis and 17a-hydroxylase/17,20-lyase (CYP17A1) immunolabelling. Impaired theca cell development has been reported for *in vitro* grown murine follicles (Eppig and O'Brien, 1996; Lo *et al.*, 2019) and cryopreserved xenografted human ovarian tissue (Amorim *et al.*, 2011) and the results of this study are therefore promising. Furthermore, out of 14 COCs, three oocytes matured to the MII stage (21% maturation rate), and all had morphologically normal first polar bodies and spindles, suggesting developmental competence.

1.3.2.3 Challenges of IVFG

Complete follicle development is a process that takes several months *in vivo* and therefore follicle development is expedited in follicles grown *in vitro* as mature oocytes have been obtained within three weeks. It is unclear what effects *in vitro* culture may have on the quality or genomic stability

of the oocytes that are produced. Indeed, murine oocytes grown *in vitro* are not equivalent to their *in vivo* counterparts with regards to frequency of maturation to metaphase II, completion of the two-cell stage to blastocyst transition or development to term (O'Brien *et al.*, 2003). Although live offspring have been obtained in mice following IVFG, the first of these, Eggbert, encountered late-onset health problems including obesity and neurological abnormalities (Eppig and O'Brien, 1998). There are also challenges involved in maintaining adequate nutrient supply, gas exchange and providing the necessary hormones and growth factors over extended culture periods. While mouse follicles reach a terminal size of less than 500 µm, human pre-ovulatory follicles can be almost two centimetres in diameter (Gougeon, 1986), though human follicles grown *in vitro* have not grown beyond 600-700 µm, after which the oocytes are released for further culture and maturation (Xiao *et al.*, 2015; McLaughlin *et al.*, 2018). However, it may not be necessary for follicles to reach such a large terminal size, as human oocytes retrieved from antral follicles <6 mm have produced blastocysts and live births (Guzman *et al.*, 2012). Mature human oocytes are approximately 120 µm in diameter, while those obtained from IVFG have been reported to be approximately 100-120 µm (Table 1-3; Xiao *et al.*, 2015; McLaughlin *et al.*, 2018; Xu *et al.*, 2021).

Table 1-3. Comparison of antral follicle size and oocyte size between human *in vivo* and *in vitro* grown follicles.

Parameter	***In vivo***	***In vitro***
Antral follicle diameter	200 µm - 20 mm	• 600-700 µm (Xiao *et al.*, 2015) • 248 ± 4.5 µm (McLaughlin *et al.*, 2018) • 676 ± 21 µm (Xu *et al.*, 2021)
Oocyte diameter (MII)	120 µm	• 111.4 ± 2.1 µm (Xiao *et al.*, 2015) • >100 µm prior to IVM (McLaughlin *et al.*, 2018) • 119 ± 3.3 µm (Xu *et al.*, 2021)

IVFG has mostly been performed using fresh ovarian tissue from healthy adults or cryopreserved tissue from cancer patients (Table 1-4). A limited number of studies have been performed using tissue from young cancer patients and only one group has cultured tissue from patients previously exposed to chemotherapy (Asadi Azarbaijani *et al.*, 2015; Pampanini *et al.*, 2019).

Cryopreservation is known to damage ovarian tissue and cryopreserved tissue may require different medium or supplements to support follicle development *in vitro,* as has been demonstrated in animal models (Ting *et al.*, 2011; Castro *et al.*, 2014). Chemotherapy treatment may also compromise follicle development *in vitro*, however only two studies exist and data are confounded by differences in the age between control and treated groups (Asadi Azarbaijani *et al.*, 2015; Pampanini *et al.*, 2019). Patient age may also influence the success of IVFG, as ovaries from prepubertal girls have been shown to contain a high proportion of abnormal primordial follicles, characterised by indistinct germinal vesicle membrane and absent nucleolus (Anderson *et al.*, 2014). In addition, very few follicles from these patients developed to the secondary stage and showed limited growth following isolation and further culture with no change in oocyte diameter. Follicles from pubertal ovaries did grow *in vitro*, though to a lesser extent to follicles from adults, with oocyte growth being proportionate to follicle size (Anderson *et al.*, 2014). In addition, IVM of oocytes collected from ovarian biopsies of pre-pubertal girls is less successful than in pubertal or adult patients (Karavani *et al.*, 2019). This suggests that oocytes from pubertal ovaries may lack meiotic competence, however perhaps this can be acquired via supplementation during IVFG. Where the aim is to develop IVFG as a fertility preservation method for girls and women undergoing gonadotoxic treatment, culture systems must be optimised to support the culture of ovarian tissue that has been exposed to chemotherapeutic agents and/or cryopreservation and tissue procured from young girls.

Table 1-4 Studies investigating *in vitro* follicle development using human ovarian tissue. Studies that have investigated *in vitro* growth of human ovarian tissue, grouped by tissue type (fresh or cryopreserved) and patient population (indication and age). Some studies are duplicated as they contained patient samples from multiple groups (i.e. fresh and frozen tissue or tissue from adults and young people). Only studies that included follicle development as an outcome measure were included.

Tissue type	Indication	Age	Studies	References
Fresh	Cancer or haematological disease	<15 years	3	(Anderson *et al.*, 2014; Laronda *et al.*, 2014; McLaughlin *et al.*, 2017)
		>15 years	4	(Liebenthron *et al.*, 2013; Laronda *et al.*, 2014; Ikeda *et al.*, 2016; McLaughlin *et al.*, 2017)
	Healthy or benign	<15 years	None	
		>15 years	27	(Hovatta *et al.*, 1997, 1999; Wright *et al.*, 1999; Rahimi *et al.*, 2001; Otala *et al.*, 2002, 2004; Hreinsson *et al.*, 2002; Scott *et al.*, 2004b, a; Zhang *et al.*, 2004; Carlsson *et al.*, 2006a, b; Morimoto *et al.*, 2007; Webber *et al.*, 2007; Telfer *et al.*, 2008; Ding *et al.*, 2010; Stubbs *et al.*, 2013; McLaughlin *et al.*, 2014, 2018; Bildik *et al.*, 2018; Talevi *et al.*, 2018; Yan *et al.*, 2018; Guzel *et al.*, 2018a; Vatansever *et al.*, 2020; Hao *et al.*, 2020; Lopes *et al.*, 2020; Xu *et al.*, 2021)
Cryopreserved	Cancer or haematological disease	<15 years	10	(Schmidt *et al.*, 2005; Sadeu and Smitz, 2008; Garor *et al.*, 2009; Kedem *et al.*, 2011a, b; Lerer-Serfaty *et al.*, 2013; Anderson *et al.*, 2014; Asadi Azarbaijani *et al.*, 2015; McLaughlin *et al.*, 2017)
		>15 years	17	(Schmidt *et al.*, 2005; Fabbri *et al.*, 2007; Sadeu and Smitz, 2008; Garor *et al.*, 2009; Kedem *et al.*, 2011b, a; Lerer-Serfaty *et al.*, 2013; Asadi Azarbaijani *et al.*, 2015; McLaughlin *et al.*, 2017; Grosbois and Demeestere, 2018; Grosbois *et al.*, 2019; De Roo *et al.*, 2020; Bjarkadottir *et al.*, 2021; Olesen *et al.*, 2021; Walker *et al.*, 2021; Cheng *et al.*, 2021)
	Healthy or benign	<15 years	None	
		>15 years	5	(Hovatta *et al.*, 1997; Oktem *et al.*, 2011; Sanfilippo *et al.*, 2013; De Roo *et al.*, 2020; Ghezelayagh *et al.*, 2020, 2021)

1.3.3 Challenges in human follicle analysis

The human ovary is a dynamic and heterogeneous organ containing a variety of different cell types, ranging from endothelial cells to immune cells, and of course germ cells, as described in Section 1.2. Within the ovarian cortex, which is the tissue material most commonly used for the investigation of human ovarian follicles, six main cell types have been characterised: oocytes, granulosa cells, immune cells, endothelial cells, perivascular cells and stromal cells (Wagner *et al.*, 2020). This presents some challenges when it comes to analysing human ovarian tissue, as generally only a subset of these cells is of interest, namely the oocyte and somatic cells (granulosa and theca) within the follicle. Therefore, methods which involve tissue homogenisation, such as western blot and qPCR are often inappropriate for ovarian follicle analysis as it is impossible to identify the cells responsible for the signal observed, unless cell- or organelle-specific controls are used (Lopes *et al.*, 2014). Alternatively, follicles can first be isolated using enzymatic digestion or laser-capture dissection to ensure that only the cells of interest are analysed (Ernst *et al.*, 2017; Talevi *et al.*, 2018; Titus *et al.*, 2021). Moreover, it is often necessary to analyse follicles individually to characterise and/or quantify morphological or molecular markers of interest, which further increases the workload involved in follicle analysis.

Considering these limitations, the most widely used methods of ovarian tissue analysis are histology and immunohistochemistry. This generally involves fixing the tissue, embedding it in paraffin wax and producing thin serial sections which can then be stained and analysed. Commonly used fixative agents include Bouin's solution, neutral buffered formalin and paraformaldehyde, each having their own set of advantages and disadvantages. We recently developed a novel fixative consisting of neutral buffered formalin with 5% acetic acid (termed form-acetic) which maintains ovarian morphology to a high standard while also allowing for molecular analysis such as immunohistochemistry (Adeniran *et al.*, 2021). While histological analysis allows for detailed analysis of individual follicles, it is an extremely time-consuming process, particularly for the analysis of human ovaries and other large mammalian species due to the heterogeneity of follicle distribution. The follicle density of human ovaries can vary by more

than 20-fold (Schmidt *et al.*, 2003; Wallace and Kelsey, 2010; McLaughlin *et al.*, 2015; Walker *et al.*, 2021). In contrast, follicle density in mouse ovaries is uniform, allowing a subset of the ovary to be analysed and total follicle numbers estimated by multiplying by the fraction of sections counted and a correction factor to adjust for duplicate counts (Abercrombie, 1946; Lo *et al.*, 2019). Due to the heterogeneity of human ovaries, this method cannot be used to accurately estimate human follicle density. Therefore, when calculating follicle density, the entire piece of tissue should be visualised and every follicle analysed, wherever possible.

Another limitation in the analysis of human ovarian tissue is that by the nature of the tissue processing required the follicle is in fact destroyed (i.e. fixed and stained or homogenised). This means that follicles cannot be followed throughout the study period and changes within the same follicle characterised. Instead, a population of follicles must be analysed at the start of the experiment and compared to another population that has undergone some intervention (for example cryopreservation, drug exposure or culture). This poses difficulties during statistical analysis as most statistical tests do not account for the intrinsic variability within or between these populations and the inappropriate use of such test may skew the results. This calls for the use of complex statistics to account for such variability, however this is not yet common practice in the field. In fact, most studies pool together all follicles analysed in the experiment and do not take into account (a) the fact that follicles derived from one patient may differ slightly from those derived from another, and (b) that the number of follicles analysed for each patient may differ significantly (sometimes even by an order of magnitude) and therefore the results may be heavily skewed. This line of thought is explored in more detail in Chapter 4 of this thesis.

Finally, a major limitation of follicle analysis perhaps reflects a more widespread problem within the field. Histological analysis results in cross-sections of ovarian tissue and the subsequent microscopy imaging leads to two-dimensional analysis of ovarian tissue and follicles. However, it is critical to remember the native structure of the tissue and the fact that follicles are three-dimensional, spherical structures. Processing these structures at a two-dimensional level poses two problems. First, as follicles are larger than 5 μm (indeed, they are at least 30 μm), it is

impossible to capture an entire follicle within a histological section and as a result, only a portion of cells within that follicle are analysed. Due to the large size of the oocyte, this mainly affects analysis of granulosa and theca cells. However, the limitations of analysing only a portion of a follicle's granulosa cells should be emphasised. The second problem is more specific to staging of follicles. During follicle staging, it is considered best practice to analyse each follicle only at the largest cross section, where the oocyte nucleus is clearly defined and visible. This both avoids double counting of follicles and ensures that the shape of the surrounding granulosa cells is correctly assessed. However, it is easy to imagine that the cross-sectional view of a follicle is determined by the angle at which it is sectioned, something that is impossible to control. This is not a problem in most cases, however it is an important consideration when staging early developing follicles, as a follicle surrounded by flattened pre-granulosa cells at the largest cross-section will be classified as being primordial, when there may in fact be one or more cuboidal granulosa cells at either end of the follicle which have not been observed, making this method prone to inaccuracy. In fact, perhaps shedding light on a larger issue within the field, many researchers do not distinguish between primordial and transitional follicles or classify transitional follicles arbitrarily with primordial or primary follicles. This topic is further explored in Chapter 7 of this thesis. These factors are a major limitation within the field of ovarian biology, and rather strangely are rarely discussed. However, currently there are no other methods available that enable more accurate analysis and therefore histological analysis remains the gold-standard in the field. Nevertheless, it is important to be aware of these limitations and take steps to mitigate their negative effects.

1.4 Initiation of follicle growth and maintenance of ovarian reserve

Each primordial follicle is subject to one of four fates: (1) to remain dormant, (2) to undergo atresia, (3) to activate but undergo atresia at some stage of development or, for a select few, (4) to activate, develop, mature and ovulate. The factors that determine the destiny of each follicle remain to be fully elucidated. As the primordial follicle pool is established before birth in humans, some primordial follicles can remain in a dormant state for several decades. However, evidence

in mice suggests that these follicles are not fully inactive as both gene transcription and protein synthesis have been demonstrated to occur in murine primordial follicles (Lintern-Moore and Moore, 1979). Follicle activation is a tightly controlled and regulated process that involves communication between the oocyte and surrounding granulosa cells, as well as the follicle's surrounding environment. The next sections will give an overview of the factors involved in maintaining follicle dormancy and the pathways involved in follicle activation.

1.4.1 Maintenance of primordial follicle dormancy

Primordial follicle dormancy is maintained through both intracellular signalling pathways within the follicle, and extracellular signals from the follicular environment, which dictate when the follicle should activate. Early culture experiments revealed that murine primordial follicles underwent activation during whole ovary culture, demonstrating that follicle activation was independent of pituitary hormones (Eppig and O'Brien, 1996). Foetal bovine and baboon primordial follicles were found to undergo rapid activation after *in vitro* tissue culture (Wandji *et al.*, 1996, 1997). This suggested the existence of inhibitory substances in the ovary, the removal of which during ovarian explant and culture, triggered activation. Interestingly, when foetal bovine cortical tissue was grafted beneath the chorioallantoic membrane (CAM) of developing chick embryos, follicle activation did not occur (Fortune *et al.*, 2000). The authors suggested that either this unknown ovarian inhibitory substance was also present in developing chick embryos, or that large scale follicle activation *in vitro* occurred due to the *in vitro* environment being richer in oxygen and nutrients than their natural *in vivo* environment. An inhibitory factor present in the CAM of chick embryos was later identified as anti-Müllerian hormone (discussed in Section 1.4.1.1). It should be noted that it was later thought that follicle activation *in vitro* occurred due to high levels of insulin used in the culture media, as insulin was found to increase follicle activation in human ovarian tissue *in vitro* (Wright *et al.*, 1999; Louhio *et al.*, 2000).

Since these observations were first made many studies have investigated the factors maintaining primordial follicle activation and the process of follicle activation, and it is now understood to be controlled by a balance of inhibitory and stimulatory factors, some of which remain unidentified.

The genes and proteins involved have mainly been elucidated from mouse models, particularly using genetically modified mice, however there might be some species-specific differences. Studies performed in other animal models or in humans will therefore be highlighted in the text. This section will give an overview of factors expressed within or acting upon primordial follicles to maintain their dormant state (Figure 1-3). The process of follicle activation will then be discussed in the next section.

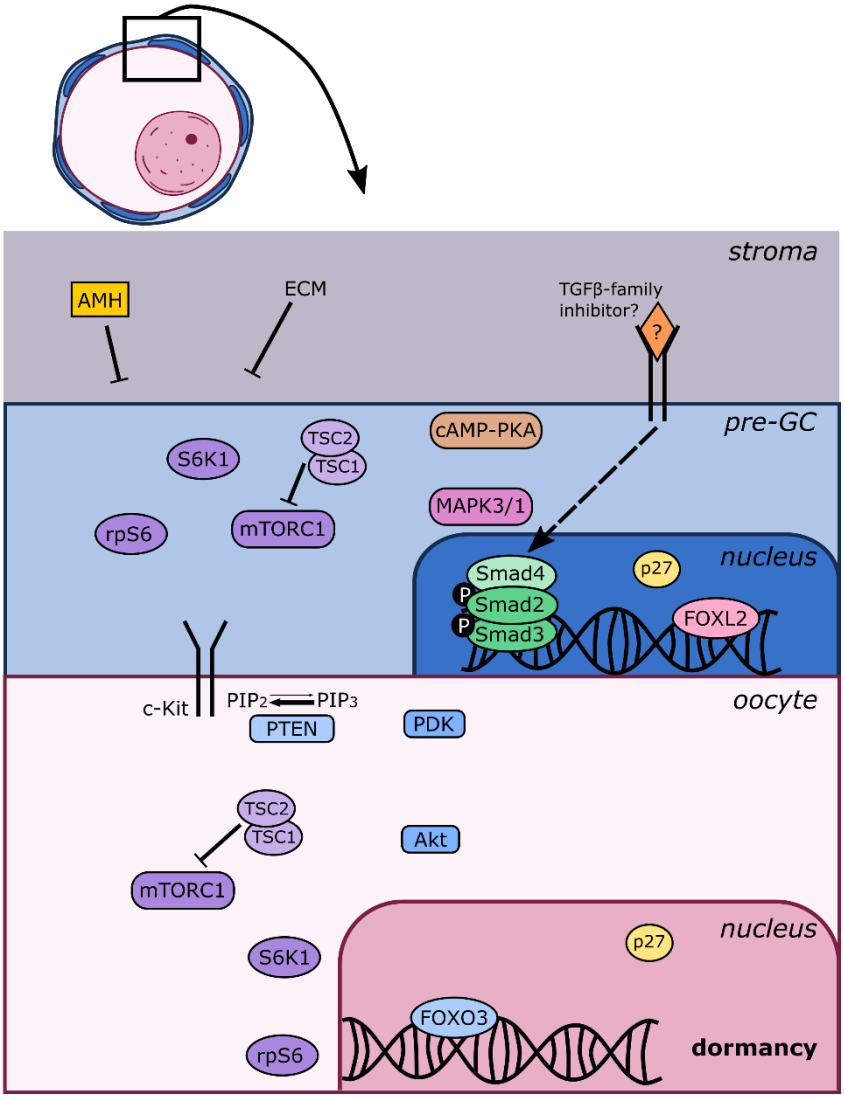

Figure 1-3 Factors maintaining follicle dormancy. Primordial follicles are maintained in a dormant state by a combination of external and intrinsic factors. Extra-follicular factors that maintain dormancy include the extracellular matrix, AMH secreted by growing follicles and other unidentified inhibitory factors, possibly released by neighbouring primordial follicles. The mTOR pathway (purple) remains inactive in both pre-granulosa cells (pre-GCs) and oocytes of primordial follicles. Recent research in mice suggests that an unidentified inhibitor, possibly belonging to the TGFβ-superfamily binds to pre-GCs and activates Smad2/3 which is transported to the nucleus by Smad4. Other nuclear factors in pre-GCs that maintain dormancy are transcription factor FOXL2 and cell cycle inhibitor p27, which is also active in the oocyte nucleus. In oocytes, the PI3K pathway (blue) is inactive due to inhibition by PTEN. Transcription factor FOXO3 (and/or possibly FOXO1 in humans) maintains dormancy. Please see main text for further details and references.

1.4.1.1 Extra-follicular factors and pathways

Although much of the research on follicle development has focused on the follicles themselves, recently there has been increased interest in investigating the role of the follicle microenvironment: the stroma and extracellular matrix. Advances in culture of isolated follicles

in hydrogel systems revealed that the rigidity of the alginate hydrogel influenced follicle growth and affected oocyte gene expression in mice (Jiao and Woodruff, 2013; Vanacker and Amorim, 2017).

As previously discussed, the ovary is a dynamic, heterogenous organ with a central vascularised medulla and a rigid outer cortex. During the dormant primordial stage, follicles are located around the periphery of the ovary in the collagen-rich cortex but move into the more pliant medulla as they grow, suggesting a role for the ovarian structure in follicle development. Two distinct populations of primordial follicles have been characterised in the mouse ovary, the first wave of primordial follicles is located in the medulla and these follicles are activated after birth, contributing to the onset of puberty and fertility in young adulthood. In contrast, the second wave is located in the cortex and its follicles are initially dormant, gradually replacing the first wave until the end of reproductive life (Zheng *et al.*, 2014a, b). It is not known whether similar distinct populations exist in human ovaries or other species.

The extracellular matrix has been shown to be a key component in maintaining primordial follicles in a dormant state. *In vitro* treatment of mouse ovaries with an enzymatic solution to partially digest the extracellular matrix induces follicle activation while dormancy is maintained in response to exogenous pressure (Nagamatsu *et al.*, 2019). Interestingly, the nuclei of primordial follicle oocytes were observed to rotate in response to mechanical stress. Pausing the rotation by inhibiting dynein, a motor protein, triggered follicle activation.

The role of anti-Müllerian hormone (AMH, also known as Müllerian inhibitory substance) in maintaining the ovarian reserve has been well characterised. AMH is a member of the Transforming Growth Factor beta (TGFβ) superfamily and is secreted by the granulosa cells of growing follicles (Vigier *et al.*, 1984; Takahashi *et al.*, 1986; Hirobe *et al.*, 1992; Baarends *et al.*, 1995; Durlinger *et al.*, 2002; Weenen *et al.*, 2004). The glycoprotein signals via a type I and type II receptor serine-threonine kinase receptor complex. Downstream signalling occurs via effector proteins Smad1, 5 and 8 (Moustakas *et al.*, 2001). Fortune and colleagues identified AMH as being

a contributing factor for maintaining primordial follicle dormancy in neonatal mouse and foetal bovine tissue transplanted under the CAM of chick embryos, which have high circulating levels of AMH (Gigli *et al.*, 2005). AMH-null mice undergo partial depletion of the primordial follicle pool by four months of age due to premature activation (Durlinger, 1999) and follicle activation is inhibited in mouse ovaries cultured with AMH (Durlinger *et al.*, 2002). The role of AMH in monovulatory species is less clearly defined. Rat recombinant AMH at 100 ng/mL was found to inhibit follicle activation of fresh human ovarian tissue cultured for seven days (Carlsson *et al.*, 2006b) while 300 ng/mL of human recombinant AMH *promoted* follicle activation in cryopreserved-thawed human ovarian tissue cultured for four weeks (Schmidt *et al.*, 2005).

1.4.1.2 Intra-follicular factors and pathways

Forkhead box transcription factors

Several forkhead box (FOX) transcription factors are expressed in the follicle where they play a role in maintaining follicle dormancy (Figure 1-3). The role of FOXL2 in pre-granulosa cells was demonstrated in *Foxl2*-knockout mice (Schmidt *et al.*, 2004; Uda *et al.*, 2004). In these *Foxl2* null mice, follicle activation occurs prematurely by two weeks of age but is functionally disrupted; although the oocytes grow in size, the pre-granulosa cells fail to divide and differentiate into cuboidal granulosa cells. As a transcription factor, FOXL2 likely regulates transcription of key inhibitory factors in pre-granulosa cells. FOXL2 is expressed in oocytes and (pre-)granulosa cells in human follicles, with protein levels in granulosa cells increasing as the follicle develops to the primary stage (Ernst *et al.*, 2018). In humans, haploinsufficiency of FOXL2 causes blepharophimosis/ptosis/epicanthus inversus syndrome (BPES), a rare developmental disorder that affects the eyelid and can cause POI (Crisponi *et al.*, 2001).

A number of FOX transcription factors are also expressed in the oocyte, including FOXO1 (FKHR), FOXO3 (FKHRL1) and FOXO4 (AFX; Brunet *et al.*, 1999; Accili and Arden, 2004). These proteins promote the transcription of pro-apoptotic genes and dormancy factors, maintaining the oocyte in a dormant state (Brunet *et al.*, 1999; Burgering and Medema, 2003). *Foxo3* KO mice exhibited

premature follicle activation at puberty, resulting in POI (Castrillon *et al.*, 2003). Conversely, in mice expressing a constitutively active form of *Foxo3*, follicle activation was inhibited, demonstrating the role of FOXO3 in suppressing follicle development (Liu *et al.*, 2007). FOXO1 knockout results in an embryonically lethal phenotype, while FOXO4 knockout has no phenotypic effect (Hosaka *et al.*, 2004). No studies have performed oocyte-specific knockout of FOXO1. While there is considerable evidence that FOXO3 is the key FOX protein involved in maintaining primordial follicle dormancy in mice, the role of FOX proteins in human follicle activation is less clear, with studies reporting contradictory results.

The phenotype exhibited by *Foxo3* null mice is similar to that of women with POI. However, *FOXO3* or *FOXO1* mutations or single-nucleotide polymorphisms (SNPs) are not a common cause for POI or idiopathic primary amenorrhea in humans (Watkins *et al.*, 2006; Gallardo *et al.*, 2008; Wang *et al.*, 2010). *FOXO3* has been shown to be expressed in human ovarian tissue and women with POI had lower levels of ovarian *FOXO3* mRNA compared to controls (Thanatsis *et al.*, 2019), however this is likely due to the fact that no follicular structures were observed in the POI samples, suggesting that the lack of *FOXO3* was a consequence, rather than a cause, of POI. Another recent study which characterised *FOXO3* expression in the human ovary, from foetal to adult age, found that FOXO3 was not universally present in all follicles (Albamonte *et al.*, 2020). While ovarian *FOXO3* mRNA levels did not change with age, the population of FOXO3-positive primordial follicles did, suggesting that *FOXO3* expression in the ovary may not be limited to follicles. FOXO3 was not detected in foetal primordial follicles, while there was a variable number of FOXO3-positive follicles in infant, pubertal and adult ovaries. This is an opposite pattern to that observed in rhesus macaque ovaries, where the prevalence of FOXO3 was highest in germ cells prior to follicle assembly, decreasing with age and disappearing in adult monkey ovaries (Ting and Zelinski, 2017). Ernst *et al.* performed transcriptomic analysis of human oocytes from primordial and primary follicles and found *FOXO3* to be expressed only in oocytes from primary follicles, not primordial follicles. Interestingly, the expression of *FOXO1* was down-regulated in oocytes during the primordial-to-primary transition (Ernst *et al.*, 2017). The authors claimed that

FOXO1 was present in the nucleus of primordial follicles while a diffuse signal restricted to the cytoplasm was reported in primary follicles; however, it should be noted that out of the two representative follicles shown in the paper (one 'primordial' and one 'primary'), neither of the sections appeared to contain the oocyte nucleus based on DAPI staining and as FOXO1 is a transcription factor, the results should be interpreted with caution. The authors suggested that FOXO1 functions in parallel with FOXO3 in human follicles (Ernst *et al.*, 2017).

Tarnawa *et al.* reported that FOXO3 was present in primordial follicles of rodents only, and was undetectable in larger mammals including cow, primate and human (Tarnawa *et al.*, 2013), suggesting that FOXO3 did not have a role in follicle activation in these species. However, FOXO1 was detected in oocytes of bovine primordial and primary follicles. This study has several limitations, including the methodology (same immunohistochemistry protocol for all species/samples, incubation of primary antibody was only one hour, same antibody concentration used for all samples) and only a single ovary was used for many of the large mammal species (for example, one ovary from a 38-year-old human donor). Indeed, others have detected FOXO3 in bovine follicles (Bao *et al.*, 2011; Maidarti *et al.*, 2018) and knockdown of FOXO3 with small interfering RNAs (siRNAs) accelerated follicle development after 2-month xenografting (Bao *et al.*, 2011). Studies using human ovarian tissue have demonstrated the presence of both FOXO1 (Ernst *et al.*, 2017; Masciangelo *et al.*, 2020) and FOXO3 (McLaughlin *et al.*, 2014; Takeuchi *et al.*, 2019) in oocytes, with both transcription factors reportedly displaying the characteristic pattern of nuclear-to-cytoplasmic translocation as the follicle develops from the primordial to the primary stage. However, only three studies have quantified the nuclear export of FOXO1/3, two using FOXO3 in bovine (Maidarti *et al.*, 2018) and human (McLaughlin *et al.*, 2014) ovaries and one using FOXO1 in human ovaries (Masciangelo *et al.*, 2020). No studies have compared the presence of FOXO1 and 3 in human ovarian follicles. Therefore, the precise role of the FOX family of transcription factors in maintaining primordial follicle dormancy in humans remains to be elucidated.

PTEN

The phosphatidylinositol 3 kinase (PI3K) pathway is a key signalling pathway within cells, controlling processes such as growth, proliferation, metabolism and the maintenance of genomic integrity (Figure 1-3; Engelman *et al.*, 2006; Hemmings and Restuccia, 2012). Phosphatase and tensin homologue deleted on chromosome 10 (PTEN) negatively regulates PI3K by converting phosphatidylinositol-3,4,5-triphosphate (PIP3) to phosphatidylinositol-4,5-bisphosphate (PIP2) at the intracellular membrane, preventing the increase in PIP3 which would otherwise trigger the PI3K pathway (Robertson, 2005; Salmena *et al.*, 2008; Chen *et al.*, 2018). Oocyte-specific deletion of *Pten* results in mass activation of primordial follicles and follicle depletion in mice (John *et al.*, 2008; Reddy *et al.*, 2008).

Interestingly, one study reported that PTEN was not detected by immunohistochemistry in follicles of foetal, infant, pubertal or adult human ovaries (age range 8 weeks post-conception to 52 years) and there was no difference in *PTEN* mRNA levels between age groups (Gallardo *et al.*, 2018). However, the functionality of PTEN in human ovarian tissue has been clearly demonstrated in other studies. Inhibition of PTEN in human ovarian tissue *in vitro* using dipotassion bisperoxo(5-hydroxypyridine-2-carboxyl)oxovanadate (bpV(HOpic)) resulted in increased activation of primordial follicles (McLaughlin *et al.*, 2014). This PTEN inhibitor has also been used clinically to restore fertility in patients with POI (Suzuki *et al.*, 2015). PTEN is therefore a key regulator for maintaining primordial follicle dormancy.

TSC 1 and 2

The mammalian target of rapamycin (mTOR) pathway is another key pathway in follicle activation which is partly regulated by the PI3K pathway (discussed in Section 1.4.2). The mTOR pathway is negatively regulated by two proteins, tuberous sclerosis complex (TSC) 1 and 2. TSC1 and TSC2 form a heterodimeric complex which supresses the activation of mammalian target of rapamycin complex 1 (mTORC1; Figure 1-3; Chong-Kopera *et al.*, 2006). Mice with an oocyte-specific *Tsc1* or *Tsc2* deletion (linked to the *Gdf9* promoter) exhibited global activation of

primordial follicles at puberty, which led to premature follicle depletion in early adulthood (Adhikari *et al.*, 2009a, b). These studies also demonstrated the synergistic role of TSC and PTEN, as both are required to maintain the quiescence of primordial follicles. Ribosomal protein S6 kinase beta-1 (S6K1) phosphorylates several target proteins linked to protein translation. S6K1 remains inactive in primordial follicles until it is phosphorylated at two sites, threonine 229 (T229) and 389 (T389). Phosphorylation at T229 is inhibited by PTEN (Reddy *et al.*, 2009), while TSC1/2 inhibits phosphorylation at T389 (Adhikari *et al.*, 2009a, b). In mice lacking both Pten and Tsc1 in oocytes, the rate of oocyte growth was even greater than in single mutants, demonstrating that these pathways act in parallel to maintain primordial follicle dormancy (Adhikari *et al.*, 2009b). Expression of TSC1 has been demonstrated both in human ovarian tissue lysates and in isolated oocytes (Ernst *et al.*, 2017; Grosbois and Demeestere, 2018).

p27

Cyclin-dependent kinase inhibitor 1B (p27) is a suppressor of cell cycle progression (Figure 1-3; Kaldis, 2007). The protein is present in oocytes of primordial and primary murine follicles but decreases as the follicle develops. It is also present in pre-granulosa and granulosa cells (Rajareddy *et al.*, 2007). Mice lacking p27 have a larger ovarian reserve and undergo global follicle activation at puberty, leading to POI in adulthood and knockdown of p27 in mouse ovaries causes increased activation (Rajareddy *et al.*, 2007; Hirashima *et al.*, 2011). Interestingly, this pathway was shown to be independent of FOXO3 (Rajareddy *et al.*, 2007). FOXO3 has been demonstrated to modulate transcriptional regulation of p27 in a murine pre-B-cell line treated with interleukin-3 (Dijkers *et al.*, 2000).

1.4.2 Primordial follicle activation

Early studies investigating follicle activation revealed that the first morphological change to occur in primordial follicles was proliferation and differentiation of the pre-granulosa cells, followed by oocyte growth (Lintern-Moore and Moore, 1979; Hirshfield AN, 1991). Despite these observations, early studies on follicle activation focused their attention on changes in the oocyte,

and proof that activation begins in the pre-granulosa cells was not acquired until more recently (Zhang *et al.*, 2014). Primordial follicle activation involves proliferation of the pre-granulosa cells coupled with their transition from a squamous to cuboidal shape – after which they are termed granulosa cells (Figure 1-2). The oocyte grows in size and secretes glycoproteins which form the zona pellucida, a layer of glycoproteins surrounding the oolemma (Kierzenbaum, 2007). Interestingly, while mouse oocyte growth begins at the transitional stage, the size of human oocytes remains unchanged until the secondary stage (Gougeon and Chainy, 1987). Figure 1-4 provides an overview of the key pathways involved in follicle activation, which will be discussed in detail below. The pathways involved in primordial follicle activation were predominantly elucidated using transgenic mouse models (Adhikari *et al.*, 2009b; Zhang *et al.*, 2014), however studies in humans will be highlighted where available.

As discussed in the previous section, primordial follicles are kept in a state of quiescence by inhibitory signals secreted from the surrounding ovary. The inhibitory effects of AMH have already been described, however additional studies suggest that the primordial follicles themselves may release an inhibitory signal which acts in an autocrine or a paracrine manner (Da Silva-Buttkus *et al.*, 2009). When the levels of this inhibitor, which remains to be identified, are reduced, follicle activation is thought to occur. This inhibitor is thought to belong to the TGFβ superfamily of growth factors. This is because the TGFβ signalling pathway has a role in maintaining a cytostatic phenotype in epithelial cells, which have some qualities in common with pre-granulosa cells, namely low proliferation rates and attachment to a basal lamina (Da Silva-Buttkus *et al.*, 2008; Mora *et al.*, 2012; Hardy *et al.*, 2018). While the identity of this putative inhibitor remains unknown, many of the downstream signalling pathways have been identified and will be discussed in the following sections. Follicle activation may also be triggered by an unidentified activation signal.

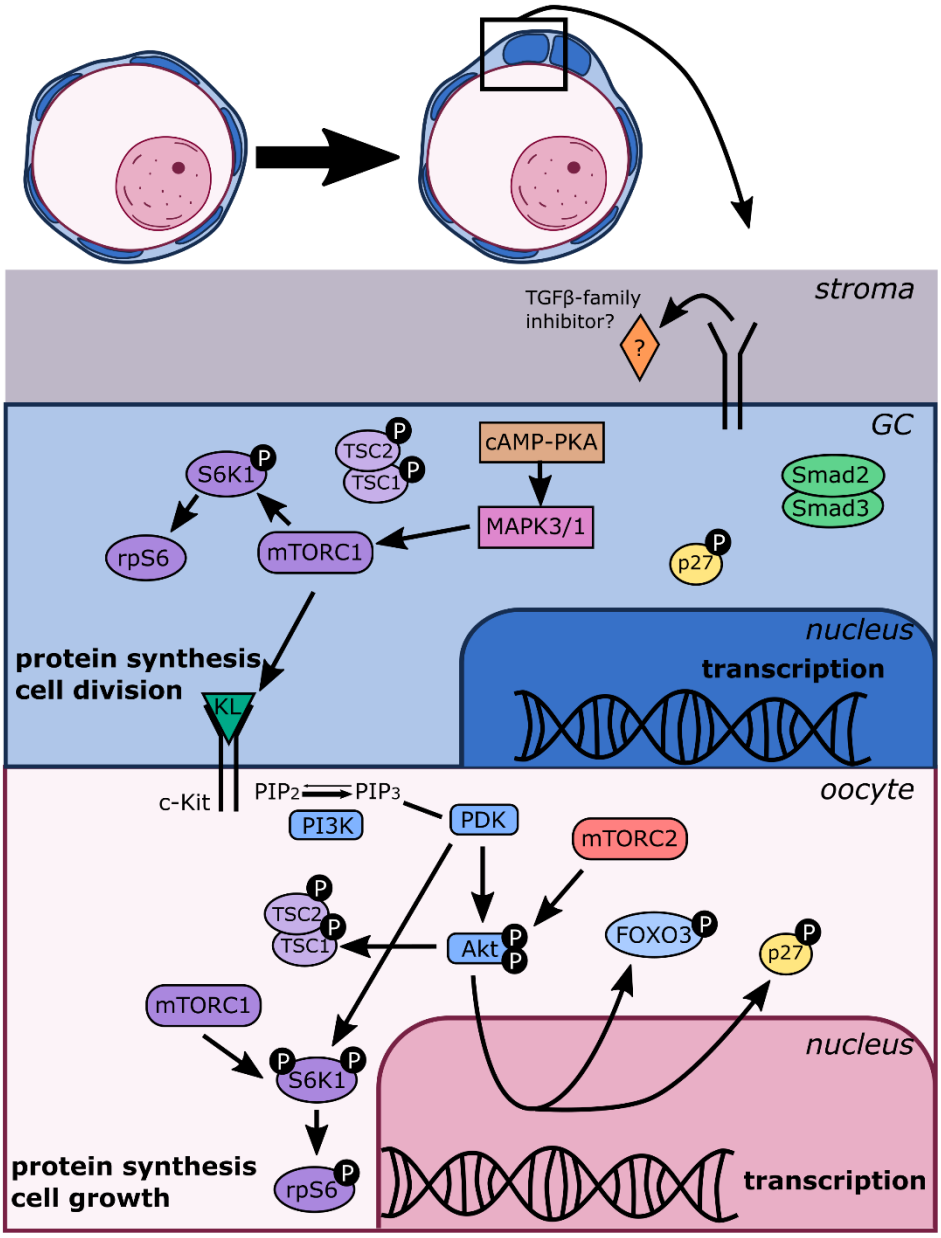

Figure 1-4. Overview of follicle activation. Follicle activation begins in the pre-granulosa cells and may be triggered by the loss of an unknown inhibitory factor, possibly a member of the TGFβ superfamily, or by an activation signal. This causes Smad2/3 to become inactivated and translocated from the nucleus, removing cell cycle inhibition, for example by p27. This leads to activation of the mTOR pathway (purple) via the cAMP/PKA and MAPK3/1 pathways, resulting in cell proliferation and squamous-to-cuboidal-transformation. Kit ligand (KL) is produced by the granulosa cells (GCs) and transported to the oocyte where it binds to c-Kit and activates the PI3K pathway (blue). This leads to activation of Akt, which is also activated by mTORC2. Akt causes the translocation of FOXO3 (or possibly FOXO1 in humans) from the nucleus and the release of oocyte dormancy. Akt also inactivates p27 and regulates the mTOR pathway in the oocyte which leads to gene transcription, protein synthesis and oocyte growth. See main text for further details and references.

1.4.2.1 Smad proteins

The Smad proteins are a family of eight signal transducers that belong to the TGFβ superfamily. Smads transmit TGFβ signals from the cell surface to the cell nucleus and are therefore critical for the regulation of cell growth and differentiation. Smad2 and -3 (Smad2/3) transduce the signal of Activins, TGFβ1-3 and growth differentiation factor 9 (GDF9) while anti-Mullerian hormone (AMH) and bone morphogenic protein (BMP) act via Smad1/5/8 (sometimes referred to as Smad1/5/9; Kaivo-Oja *et al.*, 2006). Smad2 and -3 are similar both structurally and functionally, with the exception that only Smad3 can bind DNA directly; Smad2 is unable to bind DNA due to its structure blocking the DNA-binding domain (McGee and Raj, 2015). Inactive Smad2/3 and Smad1/5/8 are predominantly located in the cell cytoplasm, however once activated, these Smads form complexes with Smad4 and are translocated into the nucleus where they regulate gene expression. In contrast, Smad6/7 inhibits the activation of receptor-activated Smads, by competitive binding to receptors or Smad4 (Moustakas *et al.*, 2001; Attisano, 2002; Shi and Massagué, 2003). Smad proteins can also interact with proteins outside of the TGFβ superfamily, for instance mitogen-activated protein kinases (MAPKs), which can modify TGFβ signals (Attisano, 2002). In addition, TSC1 has been shown to regulate Smad2/3 phosphorylation to target gene expression and control TGFβ-induced growth arrest and epithelial-to-mesenchymal transition, demonstrating a connection between the TGFβ superfamily pathways and the mTOR pathways (Thien *et al.*, 2015).

Most of our understanding of the function of Smads in ovaries results from studies performed in rodent models, predominantly transgenic mice. *Smad3* knockout mice display reduced fertility through dysregulation of follicle development (Tomic *et al.*, 2002). Conditional knockout (cKO) models, using granulosa cell-specific disruption of *Smad2, -3* or both, coupled to the AMH receptor type 2 gene (*Amhr2*), revealed that these proteins have an overlapping function, as *Smad2* or *Smad3* cKO mice displayed minimal fertility changes with minimal changes in ovarian histology (Li *et al.*, 2008). In contrast, double cKO of *Smad2/3* resulted in females with dramatically reduced fertility, with substantially reduced litter sizes and infertility after 4 months of breeding, and with

reduced numbers of antral follicles and signs of increased follicle atresia (Li *et al.*, 2008). Similar cKO of *Smad1/5* or *Smad1/5/8* resulted in ovarian tumours and infertility in mice, though individual cKO of these genes had no effect (Pangas *et al.*, 2008).

The temporal and localisation pattern of Smads has been extensively studied in mice, revealing both a spatial and stage-specific pattern of Smad activity. Smad2/3 has been shown to be present in oocytes and granulosa cells of early follicles (primordial, transitional and primary), located around the outer cortex of the mouse ovary (Xu *et al.*, 2002). As follicles develop to the secondary stage, both Smad2/3 and Smad1/5/8 can be detected, while Smad1/5/8 are predominantly present in large preantral and antral follicles, located in the inner medulla of the ovary (Xu *et al.*, 2002; Fenwick *et al.*, 2013). There is limited data available on Smad expression in non-human primate or human ovaries. Smad2/3 and -4 were detected in baboon foetal ovaries, with both Smad types being localised to the oocyte and (pre-)granulosa cells of primordial to antral follicles (Billiar *et al.*, 2004). Smad2 and -4 were detected in granulosa cells of both aromatizing and non-aromatizing antral follicles in humans, in addition to Smad4 being detected in oocytes, granulosa cells and theca cells of preantral follicles, with low Smad2 detection (Pangas *et al.*, 2002).

Recent studies have suggested that Smad2/3 is involved in maintaining primordial follicle quiescence (Figure 1-3). Smad2/3 was shown to be predominantly localised in the nucleus of murine pre-granulosa cells but is translocated to the cytoplasm in early growing follicles (Hardy *et al.*, 2018). This translocation was coupled with expression of Ki67 in granulosa cell nuclei lacking Smad2/3, suggestive of cell proliferation. The changes in Smad2/3 localisation preceded changes in the oocyte, namely nuclear translocation of FOXO3, highlighting that follicle activation begins in the pre-granulosa cells (Hardy *et al.*, 2018). These findings suggest that the Smad2/3 pathway is active in pre-granulosa cells of primordial follicles, which indicates that there is a yet-unidentified ligand, likely belonging to the TGFβ superfamily, that has a role in maintaining primordial follicle quiescence and that this inhibition is somehow lifted as follicles activate (Hardy *et al.*, 2018). In a subsequent study, the same researchers demonstrated that Smad3 is responsible for the differential localisation described above, as Smad2 is weakly detected and

expressed in (pre-)granulosa cells of all stages. Furthermore, Smad3 directly regulates *Ccnd2* and *Myc* expression in primordial follicles, promoting the expression of the former and repressing the latter (Granados-Aparici *et al.*, 2019). Cyclin D2 (CCND2) regulates cyclin-dependent kinases, which are involved in regulating the cell cycle, while Myc is a transcription factor that activates the expression of pro-proliferative genes. Therefore, Smad3 signalling appears to play a role in maintaining dormancy in primordial follicles in mice. The loss of nuclear Smad3 coincides with elevated levels of rpS6, an mTOR signalling protein, providing a possible link between the two pathways.

The mechanism of Smad2/3 signalling in the human ovary has not been reported, however one study investigated the role Gremlin-2, an endogenous BMP4 inhibitor that acts via Smad1/5/8 (Ikeda *et al.*, 2016). Ikeda *et al.* demonstrated that Gremlin-2 suppresses primordial follicle activation in a human ovarian culture system, likely by down-regulating the Smad1/5/8 signalling pathway, as demonstrated by reduced phosphorylated-Smad1/5/8 signal (detected by IHC) after culture with Gremlin-2 (Ikeda *et al.*, 2016).

1.4.2.2 mTOR pathway

The discovery of the mTOR pathway in pre-granulosa cells gave the first indication that follicle activation begins in the somatic cells – until this point studies on follicle activation had focused on the oocyte (Zhang *et al.*, 2014). mTOR is a serine/threonine kinase that regulates cell growth, metabolism, survival and modulates processes such as protein synthesis and autophagy. As discussed in Section 1.4.1, mTOR is negatively regulated by TSC1 and TSC2 (Figure 1-3). In mice with conditional knockout of mTORC1 component *Rptor*, in pre-granulosa cells, follicle activation was impaired due to failure of the pre-granulosa cells to divide and differentiate (Zhang *et al.*, 2014). In contrast, deletion of *Tsc1*, which normally inhibits mTORC1 led to overactivation of follicles. This demonstrated that the mTOR pathway is a key pathway in follicle activation and one of the first pathways to be initiated, occurring upstream to activation of the oocyte (Figure 1-4).

Recent studies have elucidated some of the pathways that lie upstream of mTOR, in particular, the cyclic adenosine monophosphate protein (cAMP) protein kinase A (PKA) and mitogen-activated protein kinase 3/1 (MAPK3/1; also known as extracellular signal-regulated kinase 1 and 2 (ERK1/2)) pathways (Figure 1-4). Vasoactive intestinal peptide (VIP) is a peptide hormone that activates the cAMP-PKA signalling pathway. VIP and its receptors are expressed in (pre-)granulosa cells and oocytes of primordial and early growing follicles. Culture of neonatal rat ovaries with VIP caused wide-spread follicle activation which was shown to occur via the MAPK3/1-mTOR pathway (Li *et al.*, 2019). Activation of the cAMP/PKA pathway leads to phosphorylation of transcription factors such as cAMP response element-binding protein (CREB; Delgado and Ganea, 2013). This transcription factor is mainly expressed in pre-granulosa cells in mice and knockdown of CREB significantly suppresses primordial follicle activation and increases apoptosis (Li *et al.*, 2020). Activation of CREB increases expression of Kit ligand in the pre-granulosa cells (Li *et al.*, 2020). MAPK3/1 acts downstream of the cAMP-PKA signalling pathway and is expressed in some mouse primordial follicles and all growing follicles. Inhibition of MAPK3/1 and other members of the family such as c-Jun *in vitro* also reduces follicle activation and increases apoptosis (Bertoldo *et al.*, 2016; Zhao *et al.*, 2018). Taken together, these studies demonstrate that the cAMP/PKA and MAPK3/1 signalling pathways act upstream of mTOR signalling and are key pathways in the activation of pre-granulosa cells.

1.4.2.3 c-Kit/Kit ligand signalling

One of the first signalling pathways to be identified as being involved in primordial follicle activation was c-Kit/Kit ligand signalling, a pathway which highlights the close relationship between oocytes and granulosa cells. The c-Kit receptor is a transmembrane tyrosine kinase receptor located on the oocyte membrane. The ligand for c-Kit is Kit ligand (KL), also known as stem cell factor (SCF; Liang *et al.*, 2013). In mice, KL is expressed in granulosa cells while c-Kit is found only in oocytes and theca interna cells (Manova *et al.*, 1990, 1993; Horie *et al.*, 1991; Keshet *et al.*, 1991; Motro *et al.*, 1991; Motro and Bernstein, 1993). In humans, KL is expressed in granulosa cells at all stages, while c-Kit is expressed in both oocytes and granulosa cells

primordial, primary and pre-antral follicles (Horie *et al.*, 1993; Tanikawa *et al.*, 1998; Robinson *et al.*, 2001; Høyer *et al.*, 2005; Stoop *et al.*, 2005; Carlsson *et al.*, 2006a; David *et al.*, 2011; Tuck *et al.*, 2015).

KL is released from the granulosa cell, downstream of the mTOR pathway, where it binds to c-Kit on the oocyte membrane and activates the PI3K pathway (discussed in the next section), leading to activation of the oocyte (Figure 1-4; Saatcioglu *et al.*, 2016). Mice with constitutive c-Kit activity display global primordial follicle activation, while a total lack of follicle activation was observed in mice lacking functional c-Kit in oocytes (Saatcioglu *et al.*, 2016). KL promotes primordial germ cell survival in mice in combination with leukaemia inhibitory factor (LIF) and initiates growth of oocytes in foetal mouse ovarian tissue (Dolci *et al.*, 1991; Godin *et al.*, 1991; Matsui *et al.*, 1991; Pesce *et al.*, 1993; Morita *et al.*, 1999). Follicles from mice lacking sufficient KL are unable to progress beyond the primary stage (Huang *et al.*, 1993) and blocking of c-Kit with an anti-c-Kit antibody, ACK2, causes a similar phenotype (Yoshida *et al.*, 1997). C-Kit/KL signalling is also necessary for follicle survival *in vitro* as blocking of the c-Kit receptor induces follicle atresia in cultured human ovarian tissue (Carlsson *et al.*, 2006a). However, blocking c-Kit had no effect on mouse primordial follicle survival *in vivo* (Yoshida *et al.*, 1997). KL upregulates the expression of anti-apoptotic proteins Bcl-2 and Bcl-cL in cultured rat ovaries, while downregulating pro-apoptotic factor Bax via the PI3K pathway (Jin *et al.*, 2005).

1.4.2.4 PI3K signalling

Once activated by KL, c-Kit directly activates PI3K, which is a lipid kinase that converts PIP2 to PIP3 at the intracellular membrane (Figure 1-4). PI3K can also be activated by other compounds such as insulin, insulin growth factor 1 (IGF1) and epithelial growth factor (EGF) (Grosbois *et al.*, 2020; Zhang *et al.*, 2020). The PI3K pathway is one of the most studied pathways of follicle activation and is a key mediator of oocyte activation and growth. As discussed in Section 1.4.1, PI3K activity is negatively regulated by PTEN. Cell division cycle 42 (CDC42) binds to PI3K and regulates PTEN expression in mouse ovaries. Inhibition of CDC42 activity or knockdown of *Cdc42*

supresses follicle activation, while overexpression of *Cdc42* increases activation and growth (Yan *et al.*, 2018).

PIP3 accumulates in the oocyte and binds to phosphoinositide-dependent-kinase-1 (PDK1) which phosphorylates the serine/threonine protein kinase Akt. Akt is further phosphorylated by mTORC2 and transported to the oocyte nucleus where it phosphorylates FOXO3 (or possibly FOXO1 in humans as discussed in Section 1.4.1.2; Kim and Kurita, 2018). As discussed above, FOXO3 is a transcription factor which maintains oocyte dormancy, but once phosphorylated it is rendered inactive and translocated from the nucleus into the cytoplasm (Castrillon *et al.*, 2003; John *et al.*, 2008). This event is one of the hallmarks of follicle activation and can be clearly visualised in mouse ovaries using immunohistochemistry.

The PI3K pathway also activates the mTOR pathway in the oocyte. Akt phosphorylates TSC1/2 which leads to activation of mTORC1. mTORC1 binds to eukaryotic initiation factor 3 (eIF3) and phosphorylates S6K1 (at T389) and eukaryotic translation initiation factor 4E (eIF4E)-binding protein 1 (4EBP1). S6K1 must also be phosphorylated at T229 by PDK1 to become active, at which point it promotes cell growth via activation of rpS6 leading to enhanced protein translation and ribosome biogenesis (Yang and Guan, 2007; Adhikari and Liu, 2009). Normally the phosphorylation sites on S6K1 are inhibited by TSC1 and PTEN, respectively, discussed above. Activation of 4EBP1 releases it from eIF4E and allows it to stimulate translation initiation.

In summary, a cascade of pathways is activated beginning in the pre-granulosa cells with activation of the cAMP-PKA, MAPK3/1 and mTOR, pathways, which leads to cell division, transition to a cuboidal shape and production of KL. KL acts via c-Kit to activate the PI3K pathway in the oocyte, leading to translocation of FOXO3 from the nucleus and the release of its inhibitory effects. The PI3K pathway also activates mTOR pathway in the oocyte, leading to transcription initiation, protein translation and cell growth. While this series of events represents our current understand of follicle activation, many questions remain unanswered, in particular what the initial trigger that causes follicle activation is and how it is regulated. In addition, several

environmental and non-physiological factors can affect follicle activation; these will be discussed in the following section.

1.4.3 Other factors that control follicle activation

1.4.3.1 Hippo pathway

The Hippo pathway is involved in regulating cell growth and maintaining organ size via growth inhibition (Lee *et al.*, 2010; Xin *et al.*, 2013). Under physiological conditions, mammalian Ste-20-like kinase 1/2 (MST1/2) and Salvador (SAV1) form a complex that activates large tumour suppressor homolog 1/2 (LATS1/2) and MOB kinase activator 1 (MOB1). The LATS1/2-MOB1 complex phosphorylates two key effectors: Yes-associated protein (YAP) and transcriptional coactivators PDZ-binding motif (TAZ), which are not able to enter the nucleus. Once stimulated, YAP/TAZ enter the nucleus where they interact with the TEAD transcription factors to induce the transcription of target genes such as connective tissue growth factor (CCN2), baculoviral IAP repeat containing (BIRC) and the cell cycle regulator c-Myc. Activation of these genes leads to cell proliferation and differentiation (Kawashima and Kawamura, 2018).

The Hippo pathway is active in the ovaries, as in many organs, and may play a role in regulating the size of the organ, as indicated by aberrant Hippo signalling in polycystic ovaries, which is characterised by increased ovarian volume (Maas *et al.*, 2018). Mice lacking LATS1 or TAZ experience massive follicle activation and POI (St John *et al.*, 1999; Hossain *et al.*, 2007) while deletion of CCN2 in granulosa cells is associated with impaired follicle development (Nagashima *et al.*, 2011). However, the role of the Hippo pathway in follicle activation under physiological conditions remains unclear. It is possible that structural changes in the ovarian environment as follicles grow during the menstrual cycle may activate the Hippo pathway, triggering activation in neighbouring follicles (Bernabé *et al.*, 2020).

Fragmentation of ovarian tissue triggers follicle activation via the Hippo pathway, causing nuclear exclusion of YAP in pre-granulosa cells and increased expression of *BIRC1* and *CCN2* (Kawamura *et al.*, 2013; Grosbois and Demeestere, 2018; De Roo *et al.*, 2020). This is also associated with

activation of the PI3K pathway, but it remains unclear whether the pathways interact or act in parallel (Cheng *et al.*, 2015; Devos *et al.*, 2020; Masciangelo *et al.*, 2020).

1.4.3.2 Blood vessels

A recent study suggested that the cue for follicle activation could come from blood vessels (Komatsu and Masubuchi, 2020). Activated follicles were observed to be in contact with blood vessels in adult mouse ovaries and activation could be promoted by either inducing angiogenesis *in vivo* using biodegradable gels transplanted to the ovarian bursa that released recombinant vascular endothelial growth factor (VEGF), and *in vitro* by increasing the foetal bovine serum concentration (Komatsu and Masubuchi, 2020). VEGF is known to be able to initiate follicle activation, however Komatsu *et al.* reported no activation after culture with VEGF, though at considerably lower doses than were present in the gels.

The hypothesis that the follicle activation signal may come from the blood supply is an interesting one, as primordial follicles are generally thought to have limited access to the blood supply and it is generally believed that follicle activation occurs independently of cyclic pituitary hormones. Indeed, the widespread follicle activation that is observed following grafting of ovarian tissue is generally thought to be due to ischemia (Gosden *et al.*, 1994b; Donnez, 2006), and several recent studies have investigated methods to promote rapid neovascularisation in the grafts to prevent follicle loss (Gao *et al.*, 2015; Xia *et al.*, 2015; Tavana *et al.*, 2016; Manavella *et al.*, 2018). Further studies into this subject area are necessary to better understand the mechanisms involved.

1.4.3.3 Other factors

Environmental factors such as nutrition or chronic stress may also influence the dynamics of follicle activation. Protein intake was demonstrated to affect follicle activation, with a low protein diet reducing activation while activation was accelerated by excessive protein intake in mice (Zhuo *et al.*, 2019). Obesity following a high-fat diet has similarly been implicated with accelerated follicle activation, while caloric restriction extends ovarian lifespan (Wang *et al.*, 2014). Both these processes appear to be mediated through the mTOR pathway. In humans,

obesity and caloric restriction are known to disrupt reproductive function (Seli *et al.*, 2014). Chronic stress also leads to excessive recruitment of primordial follicles in mice, with increased expression of KL and c-Kit leading to overactivation of the PI3K pathway (Xu *et al.*, 2018).

1.5 Effect of chemotherapy on follicles

The aim of chemotherapy treatment is to destroy cancer cells, while preserving normal cells. However, most chemotherapeutic agents act broadly and can have off-target damaging effects on the patient's normal cells. Chemotherapy drugs can be classified based on their origin or mechanism of action and carry different risks of gonadotoxicity (Table 1-5). Alkylating agents act directly on DNA strands by forming cross-links, causing abnormal base pairing or DNA strand breaks, ultimately preventing the cell from dividing (Colvin, 2003). Alkylating agents can affect cells in any phase of the cell cycle and can therefore destroy non-growing cells. Platinum derivatives are sometimes classed as alkylating agents as they also act by cross-linking. They contain a central platinum atom which reacts directly with DNA to form adducts or nuclear lesions, distorting the structure of the DNA preventing cell division (Eastman, 1987). Anti-tumour antibiotics include anthracyclines which target cells in the synthesis (S) and Gap2/Mitotic (G2/M) phase (Ling *et al.*, 1996). Anthracyclines act by intercalating into double-stranded DNA, causing structural changes that interfere with DNA synthesis and transcription (Rubin and Hait, 2003). They also generate reactive oxygen species that damage DNA, mRNA, proteins and lipids.

Taxanes and vinca alkaloids are categorised as mitotic inhibitors or plant alkaloids due to being derived from certain species of plants. Both act on microtubules, though their mechanism of action differs slightly. Taxanes stabilise microtubules, preventing microtubule dissociation and causing mitotic arrest and cell death (Rowinsky, 2003). Vinca alkaloids also affect microtubule integrity through different binding sites to taxanes, disrupting the mitotic spindle and leading to metaphase arrest. Anti-metabolites are cell-cycle specific and are incorporated into the cellular metabolism, ultimately leading to cell-cycle arrest as the cell is unable to divide. They are

classified according to the substances with which they interfere: folate antagonists, pyrimidine analogues and purine analogues (Kamen *et al.*, 2003; Pizzorno *et al.*, 2003).

Table 1-5. Risk of gonadotoxicity of different chemotherapeutic agents.

Risk of gonadotoxicity	Drug class	Agents
High	Alkylating agents	Cyclophosphamide, busulphan, chlorambucil, procarbazine, melphalan, ifosfamide, chlormethamine
Medium	Platinum derivatives	Cisplatin, carboplatin
	Anti-tumour antibiotics (anthracyclines)	Doxorubicin
	Taxanes	Doxetaxel, pacitaxel
Low	Vinca alkaloids	Vincristine, vinblastine
	Anti-tumour antibiotics	Bleomycin
	Anti-metabolites	Methotrexate, 5-fluorouracil, mercaptopurine

The effects of chemotherapy treatment on female fertility first began to be elucidated in the 1970s, with cyclophosphamide reported to cause amenorrhea, ovarian failure and follicle destruction (Miller *et al.*, 1971; Fries *et al.*, 1973; Koyama *et al.*, 1977). Alkylating agents have since been found to carry the highest risk of ovarian toxicity, while platinum derivatives and anthracycline antibiotics are also closely linked to adverse effects on female fertility (Meirow and Nugent, 2001; Green *et al.*, 2009; Bedoschi *et al.*, 2016, 2019; Chow *et al.*, 2016; Van Dorp *et al.*, 2018). Patients are routinely treated with combinations of several chemotherapy drugs of different classes and therefore understanding the effects of individual drugs is extremely challenging. Most *in vitro* human studies or animal studies have focused on the effects of cyclophosphamide, cisplatin or doxorubicin, as these carry a medium-to-high risk of gonadotoxicity and are commonly used to treat different types of cancers. This section will give an overview of that key pathways involved in follicle damage and death and outline our current

understanding of the effects of chemotherapy drugs on ovaries, with a focus on studies performed using human ovarian tissue, however animal studies will be highlighted where appropriate.

1.5.1 Mechanisms of follicle damage and death

1.5.1.1 Hallmarks of follicle atresia

At the time of birth, over six million follicles have already been lost and out of the 300-400,000 follicles present at menarche, less than 1% will reach ovulation. Thus over 99% of follicles undergo atresia, the degenerative process by which follicles are eliminated (Gougeon, 1986). Follicle atresia can occur at any stage of follicle development but the highest rates after birth are observed at the antral stage (Gougeon *et al.*, 1994). Antral follicle atresia is thought to occur through apoptosis of the granulosa cells, which is characterised by morphological changes including condensation (pyknosis) and fragmentation (karyorrhexis) of nuclear material, and shrinkage and blebbing of the plasma membrane (Kaipia and Hsueh, 1997; Mariño *et al.*, 2014). Atresia of pre-antral follicles occurs rarely under physiological conditions, but is more commonly characterised by degeneration of the oocyte, while granulosa cells remain intact (Spanel-Borowski, 1981; Teerds and Dorrington, 1993). Atresia of pre-antral follicles was recently shown to be mediated mainly by granulosa cell autophagy, rather than apoptosis, under physiological conditions (Meng *et al.*, 2018). However, pre-antral follicles are capable of undergoing apoptosis in response to external insults such as gamma-irradiation and chemotherapy treatment, as discussed in Section 1.5.3.

1.5.2 Key pathways for cell damage and death

1.5.2.1 Apoptosis

When a cell suffers irreparable DNA damage or cellular stress, it undergoes apoptosis. Apoptosis is triggered by proteases called caspases, which can be classified into initiator caspases (caspases 2, 8 and 9) and executioner caspases (caspases 3, 6 and 7), and remain in their inactive precursor form until they are activated during apoptosis (Kumar, 2007). Initiator caspases are triggered by apoptotic signals to form active dimers which cleave and activate the executioner caspases. These then catalyse the widespread irreversible protein cleavage events that kill the cell. Proteins that

are cleaved by executioner caspases include cell-cell adhesion proteins, DNA endonuclease inhibitor proteins, nuclear lamins and components of the cytoskeleton. Cleavage of these proteins leads to cell detachment, DNA fragmentation and breakdown of the nuclear and cellular structure (Alberts *et al.*, 2015). Apoptosis can occur through either extrinsic or intrinsic pathways. The extrinsic pathway is triggered when extracellular signal proteins, such as lymphocyte Fas ligand, bind to cell-surface death receptors, such as tumour necrosis factor (TNF) receptor family protein Fas. Activated death receptors bind adaptor proteins which form a death-inducing signalling complex (DISC) with initiator caspases, activating downstream executioner caspases to induce apoptosis (Alberts *et al.*, 2015).

The intrinsic, or mitochondrial, pathway of apoptosis is triggered in response to harmful conditions within the cell, such as DNA damage. The intrinsic pathway is regulated by several proteins such as the Bcl2 protein family which control the release of cytochrome c from the mitochondria. Cytochrome c is a component of the mitochondrial electron-transport chain, but when released into the cytosol it binds to adaptor protein Apaf1 (apoptotic protease activating factor-1). Apaf1 oligomerises into an apoptosome which recruits initiator caspase-9 proteins which cleaves downstream executioner caspase 3 (Kumar, 2007). Bcl2 family proteins consist of both pro- and anti-apoptotic proteins and it is the balance between these two functional classes that largely determines the fate of a cell. Anti-apoptotic Bcl2 family proteins includes Bcl2, while pro-apoptotic proteins include Bax, Bak, PUMA and NOXA. Bcl2 and other anti-apoptotic proteins are located on the cytosolic surface of the outer mitochondrial membrane where they prevent the inappropriate release of cytochrome c. Transcription of PUMA and NOXA, which belong to the BG3-only subclass of the Bcl2 family proteins, is activated by accumulation of p53 in response to irreparable levels of DNA damage. P53 regulates the cell cycle by controlling the G1-S and G2-M checkpoints, allowing the cell to invoke cell cycle arrest and DNA repair, however apoptosis is triggered when DNA damage levels overwhelm a critical threshold. PUMA and NOXA function mainly by binding and inhibiting the anti-apoptotic Bcl2 family proteins in response to apoptotic stimuli (Kuwana *et al.*, 2005). This enables other pro-apoptotic proteins Bax and Bak to aggregate

on the surface of mitochondria, triggering the release of cytochrome c and downstream events leading to cell death.

1.5.2.2 Autophagy

Autophagy is a process whereby damaged proteins and organelles are degraded, recycled and prepared for reuse by the cell and is essential for normal cellular function. There are three types of autophagy: macro-autophagy, micro-autophagy and chaperone-mediated autophagy, all of which involve the degradation of cellular components at the lysosome. Macro-autophagy (hereafter referred to as autophagy) is the classic mechanism wherein cellular cargo is delivered to the lysosome in an autophagosome, a double membrane-bound vesicle. Other types of autophagy include micro-autophagy, where components are taken up directly by the lysosome itself through invagination of the lysosomal membrane, and chaperone-mediated autophagy where proteins are targeted and translocated across the lysosomal membrane in a complex with chaperone proteins (Glick *et al.*, 2010). Autophagy occurs constitutively under physiological circumstances as part of the natural turn-over of organelles, but can be initiated during episodes of cellular stress, such as starvation, hypoxia, oxidative stress or endoplasmic reticulum stress (Loos *et al.*, 2013). Initiation of autophagy results in the recruitment of autophagy-related proteins (ATGs) to the phagophore assembly site and formation of the cup-shaped phagophore. The phagophore elongates and eventually surrounds the cytosolic material and seals into a double-membraned vesicle, the autophagosome. The autophagosome is transported along microtubules to the lysosome where it fuses and releases its cargo which is degraded and released back into the cytoplasm to be reused by the cell (Dikic and Elazar, 2018).

Interestingly, regulation of autophagy is maintained through many pathways which overlap with follicle activation, including the PI3K and mTOR pathways (Zhou *et al.*, 2019). Microtubule-associated light-chain protein 3 (LC3) and ATG7, early markers for autophagy, were present in atretic pre-antral follicles, while cleaved-caspase 3, a marker for apoptosis, was negligible, suggesting that the favoured cell-death pathway in pre-antral follicles is autophagy (Meng *et al.*, 2018). Autophagy is the dominant form of follicle atresia during the mouse neonatal period, when

massive loss of primordial and primary follicles occurs (Hułas-Stasiak and Gawron, 2011). Cultured human granulosa cells have also been found to destroy apoptotic immature oocytes via autophagy (Yefimova *et al.*, 2020).

1.5.2.3 Endoplasmic reticulum stress

The rough endoplasmic reticulum (ER) is the site of post-translational modification of proteins and protein folding. Proteins are transported directly into the ER lumen following translation, where they undergo folding and other modifications. For this process to be successful, the environmental conditions of the ER lumen must be maintained. The ER lumen is oxidative in order to allow the formation of disulphide bonds (Frand *et al.*, 2000) and the intraluminal calcium concentration is high to enable the correct function of chaperone proteins (Burton *et al.*, 2009). If these conditions are disrupted, protein folding cannot occur and misfolded proteins accumulate within the lumen, causing ER stress and triggering the unfolded protein response (UPR).

The UPR consists of three main pathways that aim to restore homeostatic balance within the ER lumen so that normal function may resume, or, if this is not possible, signal the cell to undergo apoptosis. These pathways are initiated by the activation of three ER membrane-bound proteins that are bound by the chaperone protein immunoglobin binding protein (BiP, also known as glucose regulated protein 78 or GRP78) and thus held in an inactive state. These proteins are PKR-like endoplasmic reticulum kinase (PERK), inositol-requiring enzyme 1 (IRE1) and activating transcription factor 6 (ATF6). The rise of misfolded proteins causes BiP to dissociate from these proteins due to competitive binding to misfolded proteins, resulting in their activation. In its active form PERK phosphorylates eukaryotic initiation factor 2 subunit α (eIF2α), causing protein translation attenuation and reducing the accumulation of misfolded proteins (Harding *et al.*, 1999). Ire1 and ATF6 promote that transcription of chaperone proteins which mediate ER-associated degradation (ERAD) of misfolded proteins (Yoshida *et al.*, 2001). In cases of irreversible ER stress, PERK and ATF6 promote the activation of apoptotic pathways through expression of pro-apoptotic protein C/EBP homologous protein (CHOP; Oslowski and Urano, 2011).

ER stress and UPR occurs in the ovary under both physiological and pathological conditions and ER stress is involved in follicle atresia (Huang *et al.*, 2017). Cultured atretic follicles have a higher ER surface area (Henderson *et al.*, 1987). ER stress has been demonstrated during follicle growth and maturation through the expression of XPB1 and heat shock 70 kDa protein 5 (HSPA5) and activation of IRE1 and PERK (Harada *et al.*, 2015). Murine and caprine follicles exhibit signs of ER stress during atresia through ATF6 and PERK signalling (Lin *et al.*, 2012; Yang *et al.*, 2013). Expression of apoptosis-inducing factor (AIF), which mediates caspase-independent apoptosis, is also increased during follicle atresia in goats (Yang *et al.*, 2017).

1.5.2.4 Oxidative stress

Reactive oxygen species (ROS) are highly reactive molecules, including peroxides, superoxide and hydroxyl radical, that form naturally as a by-product of cell division and metabolism. Antioxidants are responsible for neutralising these compounds; however, accumulation of ROS can lead to oxidative stress and damage to cells or tissues. Although the role of ROS on follicle development is not well characterised, there may be some interaction between the two pathways. c-Jun N-terminal kinase 1 (JNK-1) is activated under oxidative stress and activates FOX proteins and other transcription factors to promote the expression of autophagy-related genes (Hansen *et al.*, 2008). Oxidative stress also increases PUMA expression, which is regulated by FOXO1, and induces apoptosis in mouse granulosa cells (Liu *et al.*, 2015). Sirtuin 1 (SIRT1), an NAD^+-dependent deacetylase is an sensor of oxidative stress and regulates cellular defence and cell fate and may be able to reduce the effects of oxidative stress in mouse ovaries (Di Emidio *et al.*, 2017, 2019).

1.5.2.5 TAp63 – a key mediator of oocyte apoptosis

Whereas p53 is a key mediator in regulating somatic cell apoptosis, it is not required for germ cell apoptosis (De Felici *et al.*, 2004). The p53 protein family consists of three tumour suppressor proteins: p53, p63 and p73 (also referred to as TAp53, TAp63 and TAp73 respectively), with several isoforms of p63 and p73 having been described (Kaghad *et al.*, 1997; Yang *et al.*, 1998). Despite their high sequence similarity, all three proteins serve different biological functions, as highlighted by studies using knock-out mice (Donehower *et al.*, 1991; Jacks *et al.*, 1994; Yang *et*

al., 1999, 2000). In contrast to p53, p63 is highly expressed in oocytes of neonatal mouse primordial follicles, in addition to p73 (Suh et al 2006, Livera et al 2008). Specifically, p63 expression is initiated in the diplotene stage of prophase I in oocytes. TAp63α is the main p63 isoform expressed in oocytes from primordial and primary follicles with expression being lost in more advanced follicles (Suh *et al.*, 2006; Livera *et al.*, 2008). Expression of p63 has also been described in female foetal primordial germ cells, though most cells were negative (Kurita *et al.*, 2005). TAp63 has been shown to be present in human ovarian tissue lysates and is activated in response to cisplatin exposure (Bildik *et al.*, 2018). Immature human oocytes exposed to cisplatin also display active TAp63 (Bildik *et al.*, 2018). TAp63 expression has not been described in large mammalian species or non-human primates.

TAp63 can be activated by several kinases, including checkpoint kinases 1 and 2 (CHK1 and CHK2) which are mediated by Ataxia Telangiectasia and Rad3-related (ATR) and Ataxia telangiectasia mutated (ATM), respectively. ATR is preferentially activated by DNA-adducts, caused for example by chemotherapy drugs, while ATM is activated in response to double-stranded DNA breaks, caused for example by gamma-irradiation (Bolcun-Filas *et al.*, 2014; Kim *et al.*, 2018; Luan *et al.*, 2019). TAp63 can also be activated by c-Abl tyrosine kinase, as demonstrated in mice treated with cisplatin (Gonfloni *et al.*, 2009). Activation of TAp63 leads to the expression of PUMA and NOXA which trigger the induction of apoptosis via Bax/Bak as described above (Kerr *et al.*, 2012a; Coutandin *et al.*, 2016). Interestingly, gamma-irradiation of mice lacking *Puma*, with or without *Noxa*, did not result in total primordial follicle loss; a portion of the follicles were protected from apoptosis and remarkably the mice went on to produce healthy offspring (Kerr *et al.*, 2012b). This effect has also been demonstrated in *Puma*$^{-/-}$ mice exposed to cyclophosphamide or cisplatin, which cause DNA adducts in primordial follicle oocytes (Nguyen *et al.*, 2018). This indicates that the oocyte is capable of efficient DNA repair and subsequent normal function, if given time and not directed down the apoptosis pathway. However, the upper limit of damage that the oocyte can tolerate before it is beyond repair is not known; this is critical to avoid passing harmful mutations down to offspring.

Unlike somatic cells, the quiescent oocyte already contains all factors (kinases) required for activation of DNA-damage-induced apoptosis, without the need for protein synthesis (Coutandin *et al.*, 2016; Gebel *et al.*, 2017). This may explain why oocytes are more sensitive to DNA damage than the surrounding somatic cells. Indeed, as oocytes represent the germline that is passed down generations, it is critical that oocyte genomic integrity is under constant surveillance and that adequate response mechanisms are in place to prevent damaging mutations being introduced into the germline.

1.5.3 Chemotherapy-induced ovarian damage

As discussed previously in Section 1.2, the ovary is a dynamic organ containing several different cell types. Therefore, there are many potential targets in the ovary that chemotherapy drugs could act on that would lead to ovarian failure. In addition, as described above (Section 1.5), different chemotherapy drugs act via different mechanisms and could therefore target different cell types. Chemotherapy-induced ovarian failure occurs due to depletion of the primordial follicle pool. Therefore, understanding the effects of chemotherapy drugs on primordial follicles is critical. Primordial follicles could theoretically be lost through three different, though perhaps interconnected, pathways. First, primordial follicles could be directly destroyed by chemotherapy drugs, leading to follicle loss. Second, chemotherapy drugs could damage growing follicles, which would lead to a loss in inhibitory signals (see Section 1.4.1) and cause follicle activation; continued treatment would result in this cycle repeating itself, leading to depletion of the primordial follicle pool ('burn-out'). Finally, the ovarian stroma and/or blood vessels could be damaged by chemotherapeutic agents, damaging the follicle microenvironment and leading to disrupted follicle development or follicle loss. These role of each of these mechanisms is much debated, with some research groups favouring one theory above the other. These next sections will discuss the effects of chemotherapy on ovarian tissue and present the available evidence for each mechanism that may contribute to primordial follicle loss.

1.5.4 Characteristics of human ovarian tissue following chemotherapy treatment

Several studies have assessed ovarian tissue samples from patients who have undergone prior chemotherapy treatment. Primordial follicle density was found to be reduced by approximately 54% in fresh ovarian samples from patients who had received prior chemotherapy (n=10) compared to control (n=13), and between age-matched patients (Oktem and Oktay, 2007a). Within the chemotherapy-treated group, primordial follicle density was significantly lower in patients who were treated with alkylating agents compared to those who had not received alkylating agents. Other studies have also reported reduced primordial follicle densities or numbers (Familiari *et al.*, 1993; Poirot *et al.*, 2019; Shai *et al.*, 2021), however some have found no difference in density (El Issaoui *et al.*, 2016), though in the latter study ovarian volume and surface area was reduced by 10-30% in patients who had received treatment and therefore the total number of follicles may have been reduced. Interestingly, one study found that patients with Hodgkin lymphoma and treated with a non-alkylating treatment of adriamycin (doxorubicin), bleomycin, vinblastine and dacarbazine (ABVD, aged 16-29 years, n=8) had a *higher* density of non-growing follicles compared to healthy women (aged 23-39 years, n=12; McLaughlin *et al.*, 2017). However, the controls used in this study may have been unsuitable due to a difference in age between the two populations. Though not reported in the study, the mean ages were 22.6 ± 3.7 years (AVBD group) and 31.1 ± 5.2 years (control) and these were significantly different ($P<0.001$) according to an unpaired, two-tailed t-test I performed based on the published data (McLaughlin *et al.*, 2017). The study also found that AVBD-treated patients had a higher observed mean follicle density than predicted according to a validated age-related model by the same group, however this model was created using data from healthy patients aged 27.7 ± 5.7 years (range 16-37 years) and externally validated using data from cancer patients aged 30.9 ± 6.9 years (range 13-39 years) and therefore the model may not be accurate for younger patients (Schmidt *et al.*, 2003; McLaughlin *et al.*, 2015, 2017). A recent study with a larger patient cohort and age-matched controls found no difference in primordial follicle density in patients treated

with ABVD compared to cancer patients with no previous chemotherapy treatment (Shai *et al.*, 2021).

Chemotherapy has also been found to affect follicle health. Prior chemotherapy treatment resulted in a higher proportion of morphologically abnormal primordial and transitional follicles (Asadi Azarbaijani *et al.*, 2015; Pampanini *et al.*, 2019) and follicles at other stages (Abir *et al.*, 2008). Treatment regimens including alkylating agents are particularly associated with abnormal oocytes (McLaughlin *et al.*, 2017). Several studies have found evidence for damage to the ovarian stroma following chemotherapy, with increased fibrosis or DNA fragmentation (Marcello *et al.*, 1990; Meirow *et al.*, 2007; Oktem and Oktay, 2007a; Pampanini *et al.*, 2019; Shai *et al.*, 2021). Ovarian tissue exposed to chemotherapy produces less steroid hormones *in vitro*, due to either damage to growing follicles or the ovarian stroma (Oktem and Oktay, 2007a; Pampanini *et al.*, 2019).

These studies are limited by the fact that the patient groups are often not homogenous in terms of age, treatment regimens and time from treatment to ovary procurement. In particular, in two studies reporting a higher proportion or density of atretic primordial follicles following chemotherapy treatment, the treatment group is significantly younger than the non-treated cancer patients (Asadi Azarbaijani *et al.*, 2015; Pampanini *et al.*, 2019). Ovaries from young individuals have been shown to have a higher proportion of morphologically abnormal follicles which may affect these results (Anderson *et al.*, 2014). This is an intrinsic limitation in the study of human ovarian tissue and highlights the need for suitable controls and rigorous statistics.

Although there is considerable evidence that the ovaries are damaged by chemotherapy treatment, exposure to low-dose or first-line chemotherapy treatment may still be possible prior to fertility preservation by ovarian tissue cryopreservation, in cases where this is deemed clinically necessary. Exposure to chemotherapy prior to ovarian tissue cryopreservation is not associated with inferior pregnancy outcomes following transplantation (Meirow *et al.*, 2016; Poirot *et al.*, 2019), although graft survival time may be reduced in patients exposed to

bifunctional alkylating agents (cyclophosphamide, procarbazine, busulfan and ifosfamide; Poirot *et al.*, 2019).

1.5.5 Direct damage to oocytes

Chemotherapy treatment has been consistently demonstrated to cause a significant reduction in the number of primordial follicles in mice, both *in vitro* and *in vivo*, following treatment with cyclophosphamide, cisplatin or doxorubicin (Desmeules and Devine, 2006; Roti Roti *et al.*, 2012; Kalich-Philosoph *et al.*, 2013; Morgan *et al.*, 2013; Chen *et al.*, 2016; Goldman *et al.*, 2017; Luan *et al.*, 2019; Nguyen *et al.*, 2019; Wang *et al.*, 2019). However, the mechanism by which these follicles were lost remained unclear as it was not associated with primordial follicle apoptosis as determined by labelling of cleaved-caspase 3 or DNA fragmentation (Kalich-Philosoph *et al.*, 2013; Chen *et al.*, 2016; Goldman *et al.*, 2017). Recently, Nguyen *et al.* demonstrated that ovaries from mice treated with a single dose of cisplatin (5 mg/kg) or cyclophosphamide (300 mg/kg) exhibited signs of double-stranded DNA breaks in follicles at all stages, including oocytes of primordial follicles, within eight hours of treatment (Nguyen *et al.*, 2019). This effect was resolved within 24 hours, indicating that affected follicles had either undergone apoptosis or initiated repair. As the primordial follicle population was reduced by 66% and 73% following treatment with cyclophosphamide and cisplatin, respectively, apoptosis is likely the dominating pathway following activation of the DNA damage response, this was confirmed by the detection of increased *Puma* mRNA within 8 hours of treatment and TUNEL-positive primordial follicle oocytes at both 8 and 24 hours (Nguyen *et al.*, 2019). Similar findings have also recently been demonstrated by other groups (Alexandri *et al.*, 2019; Luan *et al.*, 2019; Eldani *et al.*, 2020). Cisplatin and doxorubicin have also been found to activate the apoptotic pathway in mouse primordial follicle oocytes *in vitro* by inducing double-stranded DNA breaks and activation of TAp63α (Rossi *et al.*, 2017; Tuppi *et al.*, 2018).

While there is growing and robust evidence that primordial follicles are directly damaged by chemotherapeutic agents in mice *in vivo,* investigating these effects in human ovarian tissue remains challenging as it is impossible to perform *in vivo* experiments on human subjects.

Therefore, we must rely on human xenografts (Section 1.3.1) and *in vitro* culture of human ovarian tissue (Section 1.3.2). Oktay and colleagues developed a xenograft model to investigate the effect of cyclophosphamide and doxorubicin on human ovarian tissue, and all the evidence for direct damage to human primordial follicles comes from these studies, described below.

Human foetal ovarian tissue xenografts demonstrated significant primordial follicle apoptosis after a single dose of cyclophosphamide (Oktem and Oktay, 2007b). Tissue from foetuses at 24-weeks' gestation was xenografted subcutaneously for two weeks and then exposed to a single dose of 200 mg/kg cyclophosphamide. Primordial follicle density was reduced by 12% at 12 h compared to vehicle-treated controls and reached a nadir of 93% by 48 h; DNA fragmentation was also demonstrated to peak by 12 h. The authors justified the suitability of foetal ovarian tissue by the fact that at 24 weeks gestational age all follicles are at the primordial stage, however preantral follicle development occurs at the foetal stage (Cole *et al.*, 2006). Therefore, some of the follicles analysed may have been at the transitional stage – this was not clearly stated in the paper.

Cyclophosphamide triggered primordial follicle apoptosis (measured using cleaved-caspase 3 labelling) within 72 h after administration in a xenograft model from patients aged 16-37 (Li *et al.*, 2014). A more recent study from the same group demonstrated that human primordial follicle oocytes are the direct target of cyclophosphamide (Titus *et al.*, 2021). Using cryopreserved-thawed human ovarian tissue that had been xenotransplanted subcutaneously for 10 days to allow revascularisation, followed by a single dose of cyclophosphamide (75 mg/kg) and retrieval 12 h later, the authors performed single-cell RNA sequencing of primordial follicle oocytes. A total of 190 genes were differentially expressed between the cyclophosphamide and vehicle-treated groups, demonstrating that cyclophosphamide triggered apoptotic pathways but did not cause transcriptomic activation of PI3K/PTEN/Akt pathway genes, which are involved in follicle activation. However, only two primordial follicle oocytes were analysed per condition from each of the two different donor ovaries. While there was no significant increase in the expression of pro-apoptotic *Bcl2* and *BAD*, there was a significant increased colocalization of BAD and BCL2 proteins in primordial follicles. Moreover, there was a significant increase in damaged and

apoptotic primordial follicles following cyclophosphamide treatment as assessed by γH2AX and cleaved-caspase 3 labelling, respectively.

Doxorubicin has also been found to result in accumulation of γH2AX in human primordial follicles within 24 h in a xenograft model (treated with 10 mg/kg doxorubicin), indicating double-stranded DNA breaks, in addition to oocytes and granulosa cells of growing follicles (Soleimani *et al.*, 2011). Follicle apoptosis is also increased 72 h following doxorubicin administration, as assessed by cleaved-caspase 3 labelling, though the authors did not specify how primordial follicles were defined (Li *et al.*, 2014). Culture of human ovarian tissue with doxorubicin also resulted in an accumulation of γH2AX in primordial follicle oocytes within 24 to 72 h in a dose-dependent manner. Doxorubicin also triggered apoptosis in primordial follicles, measured with cleaved-caspase 3 labelling, at the highest dose (100 μg/mL; Soleimani *et al.*, 2011a). This effect was also observed in the xenografts.

A major limitation of these four studies is lack of clarity as to how primordial follicles were classified. Only one study includes information on this classification: Titus *et al.* defined primordial follicles as *'an oocyte surrounded by a single layer of flattened, squamous follicular cells'*. Follicles with a single layer of cuboidal granulosa cells were classified as primary, however there is no mention of follicles with a mixture of flattened and cuboidal (pre-)granulosa cells, i.e. transitional follicles. This is surprising, as transitional follicles make up a considerable proportion of the total follicle population (Gougeon and Chainy, 1987) It is therefore impossible to know whether the 'primordial follicles' reported in the studies by the Oktay group is a clean population of only primordial follicles, or if it also contains transitional follicles.

1.5.6 Accelerated follicle activation and 'burn-out'

The follicle 'burn-out' theory was first proposed by Prof Meirow and colleagues (Kalich-Philosoph *et al.*, 2013). Cyclophosphamide was administered to eight-week-old mice as a single dose of 75 mg/kg to 150 mg/kg or as four weekly doses of 75 mg/kg. Cyclophosphamide was found to cause a loss of primordial follicles at all doses after one week of treatment and with increasing doses

there was an increasingly high ratio of early growing (primary and secondary) versus primordial follicles (Kalich-Philosoph *et al.*, 2013). While extensive cleaved-caspase 3 and TUNEL labelling was observed in granulosa cells of growing follicles, no apoptosis was detected in primordial follicles 4, 12 or 24 h after treatment. Five-day-old mice treated with a single dose of 150 mg/kg cyclophosphamide showed the same pattern of a loss of primordial follicles and an increase in growing follicles a week after treatment that was not observed in the control, suggesting that cyclophosphamide triggered follicle activation. Furthermore, the authors found that key proteins involved in follicle activation, Akt, mTOR, rpS6 and FOXO3, were activated within 24 h of cyclophosphamide administration. Other groups substantiated these findings and cisplatin was also found to have a similar effect (Chang *et al.*, 2015; Goldman *et al.*, 2017; Xie *et al.*, 2020).

Many of the studies reporting accelerated activation following chemotherapy treatment utilise the ratio of growing to primordial follicles. However, an increase in this ratio could also be explained by a loss of primordial follicles due to direct damage, without an increase in growing follicles. Indeed, in the study by Kalich-Philosoph *et al.* while there was a decrease in the number of primordial follicles 1, 3 and 7 days after treatment with 150 mg/kg cyclophosphamide, the number of primary and secondary follicles did not increase, with the exception of an approximate 40% increase 3 days after treatment (Kalich-Philosoph *et al.*, 2013). In addition, quantification of proteins involved in follicle activation were performed on ovarian lysates and therefore were not specific to the germ cell population and are not representative of primordial follicles (Kalich-Philosoph *et al.*, 2013; Goldman *et al.*, 2017; Xie *et al.*, 2020).

Two studies have reported evidence of accelerated activation caused by chemotherapeutic agents in human ovarian tissue (Lande *et al.*, 2017; Shai *et al.*, 2021). In the first study, cryopreserved-thawed human ovarian tissue was cultured with cyclophosphamide (3 or 10 μM) for 24 to 48 h. The authors reported that there was a decrease in the proportion of primordial follicles following treatment with cyclophosphamide, and an increase in growing follicles (Lande *et al.*, 2017). In addition, no apoptosis was detected it any of the samples (evaluated using the TUNEL assay) and there was an increase in the production of AMH and oestradiol in cyclophosphamide-treated

samples compared to untreated. However, the integrity of the data is questionable, as the proportion of primordial and growing follicles presented for each group does not add up to 100%, the data should have been more accurately analysed using follicle counts or densities. Moreover, the authors state that positive AMH signal was observed in the samples, however this signal appeared to be located in the oocyte, whereas AMH is a product of granulosa cells, again drawing into question the validity of the data presented.

In a recent study, Shai *et al.* compared fresh ovarian tissue collected from cancer patients exposed to chemotherapy (alkylating agents, AA, n=24, non-alkylating agents, non-AA, n=24) within 6 months prior to ovarian tissue procurement and compared to age-matched cancer patients who had not received chemotherapy (n=48). Ovaries from the AA group had significantly fewer primordial follicles per section and significantly more growing follicles per section compared to control, suggesting increased follicle activation following treatment with alkylating agents. There was no difference in primordial or growing follicle numbers in the non-AA group compared to control. Immunohistochemistry to detect FOXO3 and cleaved caspase 3 was performed on tissue from patients who had received chemotherapy only 4-12 days before ovary procurement (n=4 per treatment group, age-matched). Nuclear FOXO3 was detected in 7 out of 15 primordial follicles (43%) from the AA-group, compared to 53 out of 69 follicles (77%) in controls and 25 out of 31 (80%) in the non-AA group. However, ovaries with no nuclear FOXO3 did not have cytoplasmic FOXO3, so it is unclear whether it can be assumed that these follicles had undergone activation. Variability in FOXO3-positivity between follicles has been previously reported (Albamonte *et al.*, 2020). The study further reported no increase in cleaved-caspase 3 detection in primordial follicles in the AA-group compared to control, while there was an increase in cleaved-caspase 3 in growing follicles. No statistical analysis was performed for either FOXO3 or cleaved-caspase 3 detection. These studies do not provide robust evidence that chemotherapy causes increased follicle activation and burn-out in humans and further studies are needed, ideally investigating multiple markers within the follicle activation and apoptotic pathways.

While there is a growing body of evidence for chemotherapy drugs causing direct damage to primordial follicles, a recent study in mice determined that doxorubicin damages mouse ovarian follicles through both primordial follicle atresia and accelerated activation (Wang *et al.*, 2019). Mice treated with a single dose of doxorubicin (10 mg/kg) demonstrated massive primordial follicle loss within 4 days of treatment. Doxorubicin induced apoptosis (assessed by TUNEL labelling) in primordial follicle oocytes and granulosa cells of growing follicles within one day of treatment. There was also an increase in γH2AX in primordial follicle oocytes within 6 hours of treatment, resulting in activation of TAp63 and cleaved caspase 3. An increased number of primary follicles from day 1 to day 4 after doxorubicin treatment suggested accelerated activation. The authors also noted an increased number of 'early-growing primordial follicles', follicles with an enlarged oocyte and yet a single layer of flattened pre-granulosa cells. However, this is not consistent with our current understanding of normal follicle activation, as oocyte growth is preceded by flattened-to-cuboidal granulosa cell transition. Therefore, these follicles may represented an unhealthy cohort and indeed they appeared to exhibit aberrant follicle growth at later stages (Wang *et al.*, 2019). While there was a decrease in primary follicle numbers from day 1 to day 3 in the control group, this decrease was not observed in the doxorubicin-treated group, suggesting that some primordial follicles may have become activated and progressed to the primary stage in this time. Activation of Akt and FOXO3 in oocytes was also observed in the doxorubicin-treated group. In summary, this paper found clear evidence for direct damage to primordial follicles, with some suggestion that accelerated activation may also contribute to primordial follicle loss to some degree.

1.5.7 Stromal and vascular damage

As discussed above, several histological studies on ovarian tissue from patients previously treated with chemotherapy have demonstrated damage to the ovarian stroma and vasculature. Ovaries exposed to chemotherapy drugs exhibit signs of fibrosis, increased collagen deposition, in the stroma and damage to the blood vessels (Marcello *et al.*, 1990; Meirow *et al.*, 2007; Oktem and Oktay, 2007a). Injury to the ovarian vasculature can cause local ischemia, causing a loss of

primordial follicles (Meirow *et al.*, 2007). Ischemia may also lead to hypoxia, exacerbating the production of reactive oxygen species and causing ovarian damage (Yadav *et al.*, 2019). Cyclophosphamide was found to cause vascular injury in mice within two weeks of a single dose of 75 mg/kg (Pascuali *et al.*, 2018). Doxorubicin is known to cause damage to the ovarian vasculature and stroma in human ovarian tissue (Soleimani *et al.*, 2011) and *in vivo* administration of doxorubicin causes a reduction in ovarian blood flow and disintegration of the vessel wall (Ben-Aharon *et al.*, 2010; Bar-Joseph *et al.*, 2011). Human ovarian tissue exposed to doxorubicin and/or cisplatin *in vitro* exhibited increased stromal apoptosis and decreased cell proliferation (Lopes *et al.*, 2020).

1.6 Thesis scope and aims

When I began my DPhil project, I initially set out to investigate novel non-invasive pharmacological methods to prevent chemotherapy-induced follicle damage. However, when studying the literature and preparing my research plan it became apparent that there were several gaps of knowledge that needed to be filled before this research could begin, which have been alluded to in the text above. Firstly, the exact mechanisms involved in chemotherapy-induced follicle damage in humans remains poorly understood and hotly debated. Secondly, the methods used to grow human ovarian tissue *in vitro* to test chemotherapy drugs or assess molecular mechanisms, particularly using cryopreserved tissue, required optimisation to improve follicle health and development. Finally, there appeared to be a fundamental problem in the way follicle analysis was performed, both on a basic and statistical level. Therefore, in order to fill in these gaps of knowledge to progress the field and hopefully lead to better understanding of these processes, the aims of my DPhil project were as follows:

1. To determine if a technique that enables real-time observation of follicle development in mice could be adapted for human ovarian tissue culture (Chapter 3)

2. To improve the *in vitro* development of cryopreserved-thawed human ovarian tissue by investigating different culture methods (Chapter 4) and thawing protocols (Chapter 5)
3. To develop a novel analysis method for human ovarian tissue allowing three-dimensional visualisation of follicles and identification of primordial follicles (Chapter 6)
4. To investigate primordial follicle activation *in vitro* in fresh ovarian tissue (Chapter 7)

A final aim was also planned for my DPhil (to investigate the effect of chemotherapy drugs on primordial follicles *in vitro*), however this could not be achieved due to the COVID-19 pandemic.

Chapter 2

Materials and methods

2.1 Ethics

The use of human ovarian tissue was approved by the Health Research Authority South Central – Oxford B Research Ethics Committee under two REC licences (REC references 14/SC/0041 and 19/NW/0526, R&D reference 8825, Table 2-1). Tissue was collected from the Oxford Cell and Tissue Biobank (OCTB) located at the John Radcliffe Hospital, Oxford, UK. All patients, or their legal guardians, provided informed consent prior to collection of ovarian tissue.

2.2 Human ovarian tissue samples

Ovarian tissue was donated by patients undergoing unilateral oophorectomy and ovarian tissue cryopreservation due to gonadotoxic treatment, or by patients undergoing oophorectomy (total or unilateral) for benign disease. In one case, ovaries were donated post-mortem by the family of a terminally ill patient. Patients undergoing ovarian tissue cryopreservation could elect to donate up to 10% of their cortical tissue to research. Patients undergoing total oophorectomy due to benign disease and not for fertility preservation could elect to donate whole ovaries to research. Information on all patient samples included in this thesis, include patient details and ethical approval, can be seen in Table 2-1.

Table 2-1. Details on patient samples used in this thesis. Patients are represented by a non-identifiable ID, organised by the order of appearance in the thesis. Patient age and diagnosis are indicated in addition to whether tissue was fresh or frozen, cortical strips or whole ovaries. As this work was undertaken under two ethical approval licences, the appropriate licence number is indicated for each patient. None of the patients had received prior chemotherapy.

Patient	Age (years)	Diagnosis	Fresh or frozen	Type of donation	Ethical approval	Chapter
A	13	Ewing's sarcoma	Frozen	Cortical strips	14/SC/0041	3, 6
B	53	Benign gynaecological disease	Fresh	Whole ovary	14/SC/0041	3
C	0.2	Type 1 spinal muscular atrophy	Fresh	Whole ovary	14/SC/0041	3, 6
D	25	Cervical cancer	Frozen	Cortical strips	14/SC/0041	4
E	17	Ewing's sarcoma	Frozen	Cortical strips	14/SC/0041	4
F	22	Atypical teratoid rhabdoid tumour	Frozen	Cortical strips	14/SC/0041	4
G	18	Hilar cholangiocarcinoma	Frozen	Cortical strips	14/SC/0041	5, 6
H	21	Small round blue cell of distal fibula	Frozen	Cortical strips	14/SC/0041	5
I	30	Medulloblastoma	Frozen	Cortical strips	14/SC/0041	5
K	31	Medulloblastoma	Frozen	Cortical strips	14/SC/0041	5
L	15	Bone tumour of tibia and femur with lung metastases	Frozen	Cortical strips	14/SC/0041	6
M	10	Severe congenital neutropenia	Frozen	Cortical strips	14/SC/0041	6
N	6	Sickle cell disease	Frozen	Cortical strips	14/SC/0041	6
O	12	Aplastic anaemia	Frozen	Cortical strips	14/SC/0041	6
R	9	Osteosarcoma	Fresh	Cortical strips	19/NW/0526	7
S	11	Sickle cell disease	Fresh	Cortical strips	19/NW/0526	7
T	12	Localised synovial sarcoma	Fresh	Cortical strips	19/NW/0526	7

2.2.1 Ovary procurement and cryopreservation of cortical strips

Ovary procurement and cryopreservation was performed by OCTB staff. Briefly, ovaries were collected from surgery and transported to the OTCB in chilled Leibovitz's L-15 (L-15) medium and stored at 4°C until the time of dissection, or collection in the case of whole ovary donation. Ovary dissection by the OCTB was performed as soon as possible after procurement and within 48 h. Dissection was performed by specialised technicians at the OCTB under aseptic conditions in a clean room. The ovary was bivalved and medulla gently removed using a scalpel and curved scissors, this being performed in L-15 medium on a *Medicool* ice block. The remaining cortex, approximately 1 mm in thickness, was cut into strips approximately 1 x 2 x 5 mm in size. Strips were placed into cryovials containing 1 mL of cryoprotectant (1.5 M ethylene glycol, 0.1 M sucrose and 10% v/v serum substitute supplement in L-15 medium). Vials were incubated at 4°C for 1 h before being cryopreserved using a controlled rate freezer (IceCube 14S, SY-LAB, Sweden). The following cryopreservation programme was used: start temperature: 4°C; cooling rate I: -2°C/min to -9°C; cooling rate II: -0.3°C/min to -40°C; cooling rate III: -10°C/min to -140°C. Manual or automatic seeding was performed at -9°C and after freezing, samples were stored in vapour phase liquid nitrogen. Samples collected from the OCTB were kept either in vapour phase liquid nitrogen (cryopreserved samples) or at 4°C (fresh samples) prior to use. Fresh samples were used within 1 h of collection while frozen samples were used within 1-7 days.

2.2.2 Thawing of cortical strips

Cryovials containing frozen ovarian strips were removed from liquid nitrogen, held at room temperature for approximately 1 min and immersed in a 30°C water bath for up to 3 minutes or until the cryoprotectant had melted. Cortical strips were removed from the cryovials and washed in three thawing solutions for 5 min each at room temperature with gentle agitation to remove the cryoprotectant. The thawing solutions contained a reversed ethylene glycol gradient (1 M, 0.5 M and 0 M; 324558, Sigma-Aldrich, Poole, UK), 0.1 M sucrose (S7903, Sigma-Aldrich) and 3

mg/mL human serum albumin (HSA; AI653, Sigma-Aldrich) in L-15 medium[1]. Following the final wash step, cortical strips were transferred to a petri dish containing dissection medium. The dissection medium consisted of 3 mg/mL HSA, 100 U/mL penicillin, 100 µg/mL streptomycin (Penicillin-Streptomycin; P0781, Sigma-Aldrich), 2 mM L-glutamine (25030024, Life Technologies, Renfrew, UK) and 2 mM sodium pyruvate (S8636, Sigma-Aldrich) in L-15 medium.

2.3 Human cortical strip processing

Whole ovaries were processed into cortical strips in dissection medium using the same methods described in Section 2.2.1. Fresh or thawed cortical strips were processed manually on a heated stage at 37°C using scalpel blades (no. 15, 233-5366, and no. 24, 233-5529, VWR International, Lutterworth, UK) under a dissection microscope.

Processed fragments were stained with neutral red to identify pieces containing viable follicles. Optimisation of the use of neutral red with *in vitro* culture had been previously developed and optimised in our group (Walker *et al.*, 2021). Processed fragments were incubated in 25 or 50 µg/mL neutral red for at least 1 h or up to 4 h at 37°C. Neutral red was made up either using L-15-based dissection medium as described above (incubation performed in a warming oven with atmospheric CO_2) or αMEM-based dissection medium with the same supplements (incubation performed in a humified incubator with 5% CO_2). Fragments were visualised under a dissection microscope (dark-field) and fragments containing visible, red-stained follicles (neutral red positive) were preferentially selected for culture before those with no staining. Tissue pieces were washed briefly in dissection medium before being placed in culture or fixed as non-cultured control.

[1] Two different formulations of L-15 were used in this thesis. Leibovitz's L-15 medium from Gibco™ (11415049, Life Technologies, Renfrew, UK) containing L-glutamine was used in Chapter 4, while L-15 medium from Sigma (L5520, Sigma-Aldrich) without L-glutamine was used in all other chapters, to maintain consistency with OTCB procedures.

2.4 Human cortical strip culture

Tissue pieces were cultured individually in Corning Costar 24-well culture plates (3526, Scientific Laboratory Supplies, Nottingham, UK). The group's culture system was developed by a previous DPhil student (Dr Charlotte Walker) based on the technique used by Prof Spears's group (University of Edinburgh; Lopes *et al.*, 2020; Walker *et al.*, 2021). The method was further optimised as described in Chapter 4 of this thesis. Using the optimised culture system developed in Chapter 4, tissue fragments were cultured in 300 µL culture medium, consisting of minimal essential medium alpha (αMEM; 22561021, Thermo Fisher) supplemented with 1 mg/mL HSA, 100 U/mL penicillin, 100 µg/mL streptomycin, 2 mM L-glutamine (25030024, Thermo Fisher), 10 µg/mL insulin, 5.5 µg/mL transferrin, 5 ng/mL selenium, (ITS liquid media supplement; I3145, Sigma-Aldrich) 50 µg/mL ascorbic acid (10012011, Thermo Fisher) and 12.5 IU/L recombinant human FSH (Gonal-F; Z1540, Merck Serono, Feltham, UK). Sterile water supplemented with 100 U/mL penicillin and 100 µg/mL streptomycin was added to the inter-well space to prevent medium evaporation. Tissue pieces were cultured for six days. Medium was changed every second day, with half the medium being removed and replaced with fresh medium. All culture medium was equilibrated for at least 1 h in an incubator before use.

2.5 Histological processing

2.5.1 Fixation

Tissue samples were fixed by immersive fixation using a volume of fixative at least tenfold the volume of tissue. Fixation was performed using either 10% neutral buffered formalin (NBF), Bouin's solution or Form-Acetic, a novel fixative developed by our group consisting of NBF with 5% acetic acid (Adeniran *et al.*, 2021). Tissue was fixed at room temperature (RT) on a rocker for up to 24 hours after which samples were transferred to 70% ethanol and stored at 4°C until processing.

2.5.2 Embedding

Fixed tissue samples were dehydrated in a series of ethanol (70%, 80%, 95% and 3x 100%) for 15 min each at RT. Samples were subsequently cleared in three washes of xylene for 20 min each at RT. The volume of ethanol or xylene used was at least tenfold that of the tissue. After clearing, samples were embedded in paraffin wax (heated to 62°C) for three hours. Wax blocks were stored at room temperature.

2.5.3 Sectioning

Sectioning of paraffin-embedded samples was performed using a RM2245 semi-motorized rotary microtome (Leica Biosystems, Milton Keynes, UK). Sectioned ribbons were floated on a water bath heated to 38-42°C before being mounted on positively charged glass slides (Superfrost, 631-0108, VWR International). Samples that were to be stained with haematoxylin and eosin were sectioned to completion with serial sections mounted onto slides. Samples that were used for molecular labelling were mounted three per slide, with either every 4th or every 10th section mounted on separate slides. These slides were stained with haematoxylin and eosin so that sections containing follicles could be identified and adjacent slides preferentially selected for molecular labelling. After sectioning, slides were baked at 62°C for one hour to melt residual wax and ensure tissue adhesion to the slides.

2.6 Histological staining

2.6.1 Haematoxylin and eosin staining

Details for the haematoxylin and eosin staining procedure are presented in Table 2-2. Slides were deparaffinised in three washes of xylene and rehydrated in a graded series of ethanol (100%-50%) and water. Slides were stained with haematoxylin (Gills no. 2 haematoxylin, GHS232, Sigma-Aldrich) and excess staining removed using acid alcohol (1% HCl in 70% ethanol). Slides were then stained with eosin Y solution (HT110333, Sigma-Aldrich) before being dehydrated in a graded series of ethanol and xylene. Finally, slides were mounted with coverslips (no. 1.5, 630-1845 VWR International) using DPX (06522 Sigma-Aldrich) and left to dry overnight. This

staining resulted in nuclei being stained purple and cytoplasm and extracellular matrix being stained pink.

Table 2-2. Haematoxylin and eosin staining procedure. All steps were performed at RT.

Step	Chemical or reagent	Incubation time
Deparaffinisation	Xylene I	8 min
	Xylene II	4 min
	Xylene III	4 min
Rehydration	100% ethanol I	3 min
	100% ethanol I	3 min
	90% ethanol	2 min
	70% ethanol	2 min
	50% ethanol	3 min
	Tap water	3 min
Staining	Haematoxylin, Gill no. 2	2 min
	Running tap water	5 min
	Acid alcohol (1% HCl in 70% ethanol)	5 s
	Running tap water	5 min
	80% ethanol	1 min
	Eosin Y	2 s
Dehydration	95% ethanol	30 s
	100% ethanol I	45 s
	100% ethanol II	1 min
	100% ethanol III	2 min
	Xylene I	8 min
	Xylene II	8 min

2.6.2 Masson's trichrome staining

Masson's trichrome staining was performed using a Trichrome stain kit (ab150686, Abcam, Cambridge, UK). Details of the staining procedure are presented in Table 2-3. Following deparaffinisation and rehydration, samples were re-fixed in Bouin's solution at 56°C in a water bath for 1 h. After cooling, samples were stained in Weigert's iron haematoxylin working solution (equal parts of stock solution A and B) for 5 min. Slides were rinsed and transferred to Biebrich scarlet-acid fuchsin solution for 15 min, followed by differentiation in phosphomolybdic-phosphotungstic acid solution for 14 min, until the collagen was no longer red. Slides were transferred directly to aniline blue solution for 9 min, then rinsed and differentiated in 1% acetic acid solution for 5 min. Finally, slides were dehydrated in ethanol and xylene and mounted using DPX. This staining procedure resulted in collagen being stained blue, nuclei black and muscle and cytoplasm red.

Table 2-3. Masson's trichrome staining procedure. All steps were performed at RT unless otherwise indicated.

Step	Chemical or reagent	Incubation time
Deparaffinisation and rehydration	See Table 2-2	
Re-fixing	Bouin's solution	1 h at 56°C followed by 10 min at RT
	Running tap water	Until sections are no longer yellow
	Distilled water	Quick rinse
Staining	Working Weigert's iron haematoxylin (A+B)	5 min
	Biebrich scarlet-acid fuchsin solution	15 min
	Distilled water I	3 min
	Distilled water II	3 min
	Phosphomolybdic-phosphotungstic acid solution	14 min
	Aniline blue solution	9 min
	Distilled water I	3 min
	Distilled water II	3 min
	Acetic acid (1% solution)	5 min
Dehydration	95% ethanol I	Quick rinse
	95% ethanol II	Quick rinse
	100% ethanol I	30 s
	100% ethanol II	30 s
	Xylene I	8 min
	Xylene II	8 min

2.6.3 Assessment of follicle development and health

2.6.3.1 Follicle classification

Only follicles with a single oocyte were analysed. All analysis was performed on the largest cross-section of the follicle, where the oocyte nucleolus or nuclear membrane was clearly visible. Follicles were tracked through neighbouring sections to avoid double counting. Follicle classification was based on Gougeon (1996) and follicles were classed as primordial, transitional (also known as intermediary), primary or multilayer (including both secondary and pre-antral follicles; (Figure 2-1). Primordial follicles had an oocyte surrounded by a single layer of flattened pre-granulosa cells (Figure 2-1A), while transitional follicles had a mixture of flattened pre-granulosa cells and cuboidal granulosa cells (Figure 2-1B). Primary follicles had a single layer of cuboidal granulosa cells (Figure 2-1C), while follicles were classed as multilayer if more than one layer was observed (Figure 2-1D).

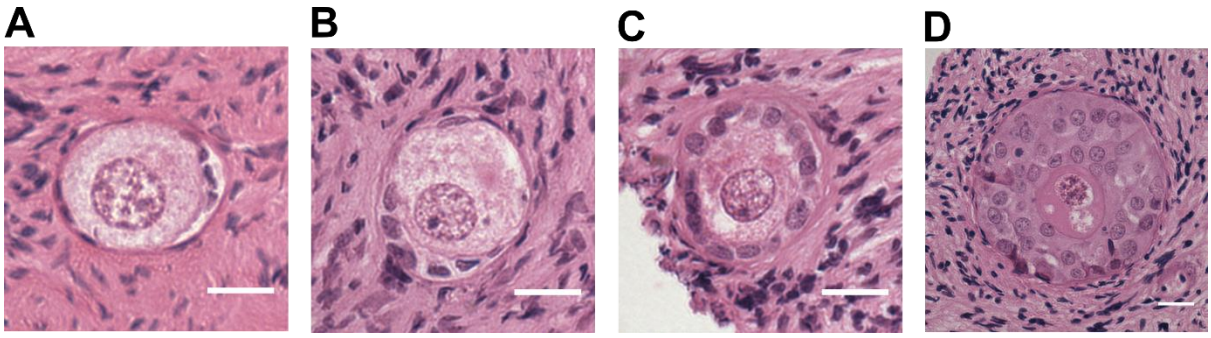

Figure 2-1. Classification of early follicle development. Representative images of cryopreserved, thawed follicles stained with haematoxylin and eosin. Follicles were classified as (A) primordial with a single layer of flattened pre-granulosa cells, (B) transitional with a single granulosa cell layer and at least one cuboidal granulosa cell, (C) primary with a single complete layer of cuboidal granulosa cells, or (D) multilayer with at least one additional partial or complete layer of granulosa cells. Scale bar: 20 μm.

2.6.3.2 Follicle morphology

Follicle morphology was assessed and follicles graded according to health based on the presence of pyknotic nuclei (granulosa cells or oocyte), and shrinkage of the ooplasm (Figure 2-2; Gougeon, 1996). These markers were selected based on the existing literature and the ability to detect them in a non-biased manner. Other morphological markers, such as dense chromatin, eosinophilia and vacuoles, were considered but these were found to be prone to bias or were affected by sample

processing. Normal follicles were defined as having a non-pyknotic non-shrunken oocyte with non-pyknotic granulosa cells (Figure 2-2A), degenerating follicles had one of the above factors (Figure 2-2B), while follicles were classified as atretic if they had both an oocyte with a pyknotic nucleus and pyknotic granulosa cells (Figure 2-2C).

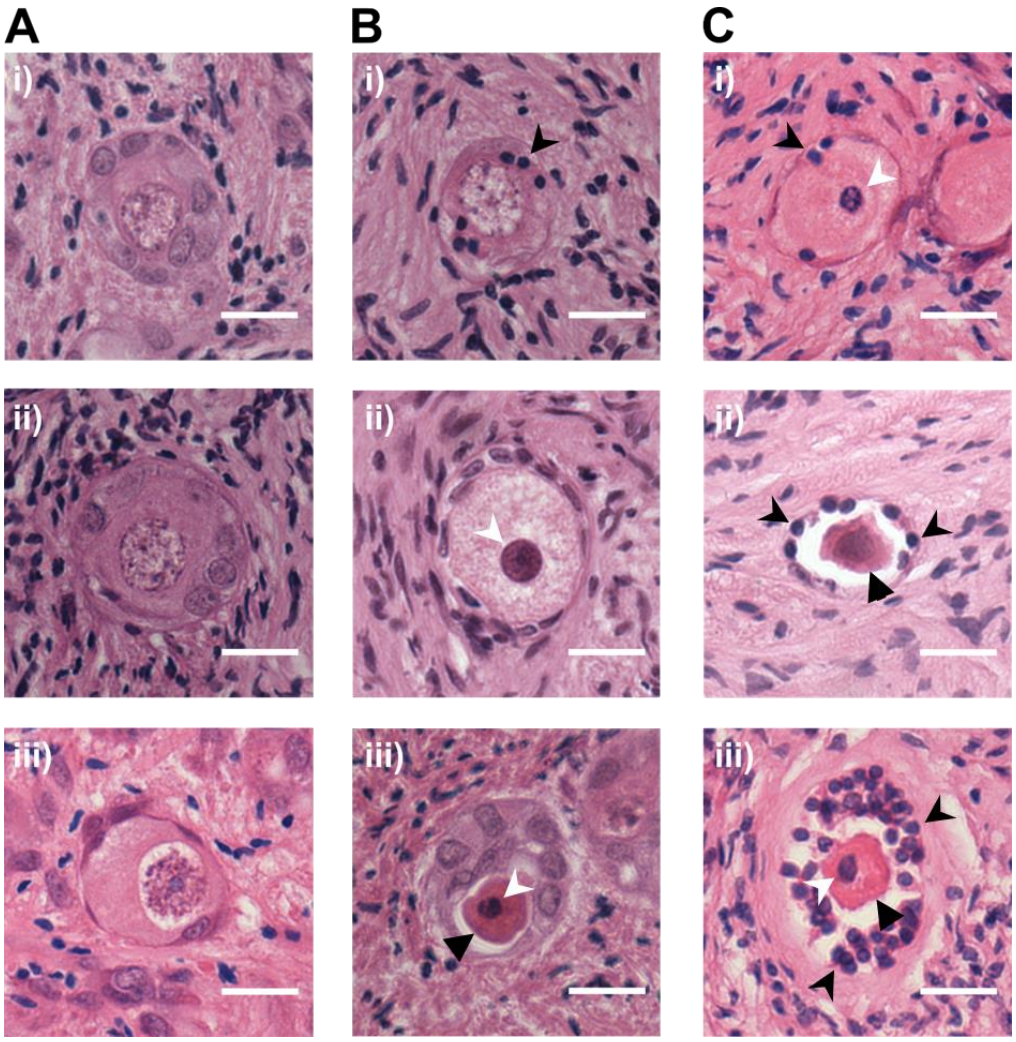

Figure 2-2. Classification of follicle morphological health. Representative images of cryopreserved, thawed follicles stained with haematoxylin and eosin. Follicle health was assessed based on the presence of pyknotic granulosa cells (black arrowhead), a pyknotic oocyte (white arrowhead) or a shrunken ooplasm (black triangle). A) Healthy follicles had non-pyknotic granulosa cells and a non-pyknotic and non-shrunken oocyte (i-iii). B) Degenerating follicles had either pyknotic granulosa cells (i) or a pyknotic oocyte (ii) and could have non-shrunken (ii) or shrunken (iii) ooplasm. C) Atretic follicles had both pyknotic granulosa cells and a pyknotic oocyte, with (ii-iii) or without (i) a shrunken ooplasm. Scale bar: 20 µm.

2.6.3.3 Calculation of follicle density

In order to calculate follicle density, the area of every 12th section was measured using the freehand measuring tool in ImageJ Fiji (Version 1.45r or later; National Institutes of Health,

Bethesda, MD, USA; Schindelin *et al.*, 2012; Schneider *et al.*, 2012; Rueden *et al.*, 2017). Area measurements were used to calculate the volume of each tissue piece (V) using Equation 2-1.

$$V = \bar{A} \cdot N_s \cdot t \qquad \text{Equation 2-1}$$

where $\bar{A}$ denotes the average area, N_s is the total number of tissue sections and t the section thickness (5 μm). Follicle density was then determined by dividing the total number of follicles counted in a tissue sample by the tissue volume.

2.6.4 Assessment of ovarian tissue fibrosis

Collagen fibres were quantified using a method adapted from Chen *et al.* (2017) using the colour deconvolution plugin in ImageJ (Ruifrok and Johnston, 2001). Images were deconvoluted to isolate the red, green and blue components. The area of blue staining (A_{blue}; containing both collagen and cell nuclei) was measured by thresholding, with the same threshold value being used for all images. A second threshold was applied to an RGB stack of the image to measure the area of cell nuclei (A_{nuclei}), again applying the same threshold to all images. This value was subtracted from the first to obtain the collagen area ($A_{collagen}$; Equation 2-2). Finally, the total section area (A_{total}) was measured by applying a threshold to the RGB stack to cover the entire section. The proportion of collagen-enriched area ($P_{collagen}$) was then calculated (Equation 2-3).

$$A_{collagen} = A_{blue} - A_{nuclei} \qquad \text{Equation 2-2}$$

$$P_{collagen} = \frac{A_{collagen}}{A_{total}} \qquad \text{Equation 2-3}$$

2.7 Molecular analysis

2.7.1 TUNEL assay

Cells containing double-stranded DNA breaks, a hallmark of cell death, were visualised using the TUNEL assay (Apoptag peroxidase *in situ* apoptosis detection kit; S7100, Merck Millipore, Watford, UK). Samples were deparaffinised and rehydrated in xylene and ethanol (Table 2-4). Antigen retrieval was performed with sodium citrate (10 mM, pH 6.0) and microwave heating

(700W for 1 min, 70W for 20 min followed by 20 min cooling). The remaining protocol was performed following the manufacturer's instructions, with the exception that Tris-buffered saline (TBS; 20 mM Tris, 140 mM NaCl, pH 7.6) was used in place of phosphate buffered saline (PBS; 20 mM phosphate, 150 mM NaCl, pH 7.4) as this was found to give lower background signal. Briefly, after blocking endogenous peroxidase activity with 3% hydrogen peroxide, DNA strand breaks were detected by enzymatically labelling the free 3'-OH termini with nucleotides (some of which were labelled with digoxigenin) using terminal deoxynucleotidyl transferase (TdT) with incubation at 37°C for 1 h. Samples were then incubated with anti-digoxigenin antibody conjugated to a peroxidase reporter molecule for 30 min. Signal was visualised with 3,3'-diaminobenzidine (DAB; SK-4100, Vector Laboratories, Peterborough, UK) as a brown stain. The same DAB exposure time was used for all samples within an experiment or group. Slides were counterstained with haematoxylin, dehydrated and mounted with coverslips (

Table 2-5).

Table 2-4. Deparaffinisation and rehydration of samples prior to molecular analysis.

Step	Chemical	Duration
Deparaffinisation	Xylene I	4 min
	Xylene II	3 min
	Xylene III	3 min
Rehydration	100% ethanol I	1 min
	100% ethanol II	1 min
	90% ethanol	1 min
	80% ethanol	1 min
	70% ethanol	1 min
	Distilled water	1 min
	Distilled water	1 min
	Distilled water	1 min

Table 2-5. Counterstaining and dehydration of samples following molecular analysis.

Step	Chemical	Duration
Counterstaining	Haematoxylin, Gill no. 2	2 min
	Running tap water	5 min
Dehydration	50% ethanol	1 min
	70% ethanol	1 min
	90% ethanol	1 min
	100% ethanol I	1 min
	100% ethanol II	1 min
	Xylene I	3 min
	Xylene II	3 min
	Xylene III	4 min

2.7.2 Immunohistochemistry

The following general protocol was used for immunohistochemistry. In some cases the protocol was slightly altered, for example where TBS was used in place of PBS. This is indicated in the methods section of the relevant chapters. Slides were first deparaffinised and rehydrated according to Table 2-4. Antigen retrieval was performed using sodium citrate (10 mM, pH 6.0) and microwave heating (700W for 1 min, 70W for 20 min followed by 20 min cooling) unless otherwise stated. Where DAB was used for visualisation, endogenous peroxidase was quenched using 3% H_2O_2 for 5 min. After washing in PBS sections were isolated using a hydrophobic barrier pen (ImmEdge, H-4000, Vector Laboratories) and blocked with 20% normal serum and 5% bovine serum albumin (BSA; BPE1600, Fisher Scientific) in PBST (PBS with 0.1% TritonX-100; T-8787, Sigma) for 1 h at RT to prevent non-specific secondary antibody binding. The normal serum used matched that of the host species of the secondary antibody used. Antibodies were diluted to the desired concentration in 10% normal serum and 5% BSA in PBST and incubated overnight at

4°C. The following day, slides were allowed to reach room temperature and washed twice in PBST before the secondary antibody was added, diluted in 10% normal serum with 5% BSA in PBST, and incubated for 1 h at RT.

For DAB visualisation, biotinylated secondary antibodies were used. After secondary antibody incubation, antigen signal amplification was performed using an avidin-peroxidase complex (Vectastain ABC Elite, PK6101, Vector Laboratories) for 30 min at RT after which samples were washed 3 times for 5 min with PBST before being visualised with DAB (see Section 2.7.1) and counterstained with haematoxylin.

For fluorescence detection, secondary antibodies conjugated to an Alexa Fluor fluorophore were used. In some cases, a biotinylated secondary antibody was used, followed by signal amplification using a streptavidin-conjugated fluorophore. Secondary antibody incubation and all subsequent steps were performed in light-sealed vessels and care was taken to avoid exposing samples to light. Slides were washed twice for 5 min in PBST and counterstained with 5 µg/mL 4′,6-diamidino-2-phenylindole (DAPI, D9542, Sigma-Aldrich) for 10 min before being washed twice with PBST and mounted with either aqueous (Vectashield® Antifade mounting medium, H-1000-10, Vector Laboratories) or hardset (Vectashield® Hardset™ Antifade mounting medium; H-1400, Vector Laboratories) mounting medium. Slides were stored at 4°C in the dark.

2.8 Whole-mount immunolabelling and tissue clearing

A protocol was developed to allow visualisation of human ovarian tissue fragments using a commercially available Tissue Clearing Kit (ab243298, Abcam), as described in full in Chapter 6. The final optimised protocol is described here.

2.8.1 Whole-mount immunolabelling

Washing and permeabilisation was performed in 2 mL microcentrifuge tubes with 1.8 mL solution. All incubation steps were performed at 4°C with gentle agitation unless otherwise indicated. Fixed tissue fragments were first washed in PBS and then permeabilised in dimethylsulfoxide (DMSO; D8418, Sigma) and methanol (Table 2-6). Samples were then

incubated in a penetration buffer (PBS with 0.2% TritonX-100, 0.3 M glycine and 20% DMSO) overnight at RT with gentle agitation. The next day, samples were transferred to a 400 µL blocking solution (PBS with 0.2% TritonX-100, 6% donkey serum and 10% DMSO) and incubated overnight. Samples were then incubated in the required primary antibody, diluted in antibody buffer (PBS with 0.2% Tween, heparin, 3% donkey serum and 5% DMSO, total volume 400 µL) for seven days. Following primary antibody incubation, samples were washed five times for 20 min in washing buffer (PBS with 0.2% Tween and heparin) after which they were transferred to 400 µL secondary antibody solution (secondary antibody at 1:100 with 5 µg/mL DAPI in antibody buffer). Samples were incubated for seven days, protected from light.

Table 2-6. Washing and permeabilisation protocol prior to whole-mount immunolabelling.

Step	Chemical	Duration
Dehydration	PBS	15 min
	PBS	15 min
	50% methanol/PBS	15 min
	80% methanol	15 min
	100% methanol	15 min
Permeabilisation	20% DMSO/methanol	15 min
Rehydration	80% methanol	15 min
	50% methanol/PBS	15 min
	PBS	15 min
	0.2% TritonX-100 in PBS	15 min

2.8.2 Tissue clearing

All following steps were performed while protecting samples from light. Following immunolabelling, samples were washed 10 times in washing buffer for 10 min at RT with gentle agitation, protected from light. Samples were then dehydrated by washing in 50% methanol/PBS, 80% methanol and three washes of 100% methanol for 15 min at RT with gentle agitation.

Samples were removed from methanol and carefully dried (using lens paper and allowing the methanol to evaporate) before being transferred to a glass embryo-dish containing 1 mL Tissue Clearing Reagent 1 (refractive index of 1.50) and incubated for one hour at RT with gentle agitation. Samples were mounted in a prepared silicone isolator (approx. 13 mm diameter, 0.25 mm deep) on a glass coverslip (22 x 50 mm, #1.5) filled with Tissue Clearing Reagent 2 (refractive index 1.50). Samples were placed in the middle of the well and sealed with a square coverslip (22 x 22 mm, #1.5). Samples were stored at 4°C away from light. Tissue clearing could be reversed by incubating cleared samples in 100% ethanol at RT until sample opacity was restored. Samples could then be processed for histology as described in Section 2.5.

2.9 Imaging

2.9.1 Brightfield microscopy

Ovarian tissue dissection was performed under one of two stereomicroscopes, the MZ8 and M125 (both Leica Microsystems, Milton Keynes UK). The M125 camera was fitted with a Lumenera 5-3 camera (Teledyne Photometrics, Birmingham, UK) running Infinity Analyse software (Teledyne Photometrics). Sectioned samples stained with chromogenic labels or dyes were imaged using a light microscope (DM2500, Leica Microsystems). Three different cameras were used throughout the time of this thesis, the Micropublisher 5.0 RTV, Lumenera 5-5 and Micropublisher 6 (all Teledyne Photometrics). The Micropublisher 5.0 camera was used with QCapture Pro 7 software, the Lumenera with Infinity Analyse software and the Micropublisher 6 with Ocular software. Light intensity and exposure were adjusted as appropriate within each imaging session.

2.9.2 Fluorescence microscopy

Samples labelled with a fluorescent marker were imaged using an upright fluorescence microscope (DMRBE, Leica Microsystems) with LED illumination and DAPI-FITC-TRITC filters. Images were captured using the QImaging Retiga R3 camera (Teledyne Photometrics) and Volocity software (version 6.3.1.; Quorum Technologies, Lewes, UK). All sections within an experiment or group were imaged using the same acquisition settings (LED light strength, gain

and exposure). Care was taken to expose images minimally to mitigate photobleaching. Post-imaging processing was performed as described in Section 2.9.5.

2.9.3 Confocal microscopy

Confocal microscopy was performed at the Wolfson Imaging Centre at the Weatherall Institute of Molecular Medicine (WIMM; Oxford, UK). Images were collected using a Zeiss 780 upright confocal microscope (Zeiss Cambridge, UK) with a x10/0.45 numerical aperture (NA) objective (working distance 2 mm) or a x25/0.8 NA oil immersion objective (working distance 570 µm). DAPI was excited using a 405 nm laser detected at 380-480 nm. Alexa Fluor 488 was detected using a 488 nm laser and a 490-555 nm emission. Alexa Fluor 568 and 594 were excited using a 594 nm laser and detected at 580-630 nm. Optimal pinhole size and gain settings were determined for each channel and the settings were kept constant for each experiment.

Z-stacks were obtained by identifying the top and bottom of the sample. Samples were first imaged from one side and then flipped over and imaged from the other side to overcome imaging resolution limitations. Where appropriate, z-compensation with extrapolation was used to adjust for decreasing signal brightness at greater z-depths.

2.9.4 Assessment of DAB signal

DAB signal could be observed as brown staining, with DAB-negative cells having no or very faint staining. In samples that had been counterstained with haematoxylin, DAB-positive cells appeared brown-black while DAB-negative cells appeared blue (nuclei) or clear (cytoplasm). DAB signal does not follow the Beer-Lambert law and is not linear to the quantity of the antigen, therefore DAB signal intensity should not be analysed. However, the number or proportion of DAB-positive cells can be quantified.

For TUNEL-labelled samples, each sample was imaged using a 40x objective at two different locations of the ovarian cortex. For detection of stromal cell death, only stromal cells were analysed and follicles were excluded. The proportion of TUNEL-positive stromal cells was measured using the ImmunoRatio plugin in ImageJ (Tuominen *et al.*, 2010). After controlling for

background and setting the scale, the proportion of TUNEL-positive nuclei was automatically calculated, with TUNEL-positive nuclei highlighted in orange while negative cells were highlighted in blue. All analysis was performed in a blinded manner.

2.9.5 Assessment of fluorescence signal

Post-imaging processing was performed using ImageJ Fiji to enhance qualitative aspects (brightness and contrast) of each channel (blue, green, red) to allow for increased visibility of figures in print. All adjustments were made following best-practice guidelines (Lee and Kitaoka, 2018), with all images (control and experimental across all groups) treated and adjusted identically and with adjustments applied uniformly to whole images. Imaging processing steps involved adjusting the upper and lower limits of the display range by modifying the minimum and maximum settings of the image. The optimal range was first determined using the sample group with the lowest level of observed signal and the corresponding negative control to ensure high signal visibility with minimal background. The same settings were then applied to all other sample groups.

Unlike DAB, the intensity of fluorescent antibodies is directly proportional to fluorophore concentration and therefore the fluorescence signal can be quantified as a measure of antigen levels. Intensity measurements were performed by using the freehand selection tool to select the area of interest, which could then be measured as intensity (arbitrary intensity units). This could be performed for entire cells, or only the cytoplasmic or nuclear region of the cell, depending on the antigen being studied. The ratio of nuclear to cytoplasmic signal could be calculated as the proportion of nuclear to cytoplasmic (or total cell) signal.

2.9.6 Three-dimensional reconstruction

Images of cleared tissue samples were analysed using ImageJ Fiji and Imaris (version 9.7.0. Measurements across the xy, xz or yz planes were performed in ImageJ Fiji using orthogonal views and the measurement tools. Three-dimensional tissue or follicle reconstructions were

created manually using the Surface tool in Imaris. For spatial analysis, follicles were labelled using the spot tool and measurements obtained from the Imaris software.

Chapter 3

Development of a fragmented ovary culture method for human ovarian tissue

3.1 Background

In vitro culture of ovarian tissue is a useful technique to study early follicle development. However, as described in Section 1.3.3, there are some limitations to this method, namely that as follicles are enclosed in the ovarian tissue, they cannot be observed directly throughout the culture period. Histological analysis, which is routinely used to analyse ovarian tissue, involves destruction of the tissue as it requires fixation and sectioning and therefore each piece of tissue can only be analysed once. Thus, the same follicle cannot be observed throughout the experimental period and instead each tissue sample must be representative for the group. This presents some difficulty when working with human ovarian tissue, as the density and morphology of follicles can vary considerably due to the heterogeneity of the tissue (discussed further in Chapter 4; Qu *et al.*, 2000; Poirot *et al.*, 2002; Schmidt *et al.*, 2003). Furthermore, the methods required to process and analyse the tissue samples are time consuming and labour intensive. There would therefore be a great benefit in developing a culture method that would lessen the workload required to obtain equivalent data on follicle development and health, and that would enable the tissue to be observed and analysed in real-time throughout the culture period.

Maiani *et al.* (2012) developed a mouse ovary culture method which allows oocytes to be directly observed during culture. This fragmented ovary culture (FrOC) method involves ovaries from new-born mice (postnatal day 4) being sliced into small fragments which, when placed in culture,

form rounded 'mushroom-like' structures, allowing follicles to be visualised under a microscope. The group used transgenic mice with expression of green fluorescent protein (GFP) linked to the c-Kit oocyte-specific promoter, which allowed visualisation of oocytes (Figure 3-1A). Oocytes can be visualised and counted at the start of the culture experiment, and changes in numbers observed throughout the culture period. The FrOC method has been used to demonstrate that cisplatin-induced follicle damage can be prevented by LH (Rossi *et al.*, 2017). Brightfield microscopy can also be used to visualise the samples, allowing non-transgenic mice to be used (Figure 3-1B). Follicle viability can be assessed using Trypan blue staining, a vital stain that stains dead cells blue, and therefore this method can also be used to study the effects of chemotherapeutic agents on follicles (Prof Spears, personal communication).

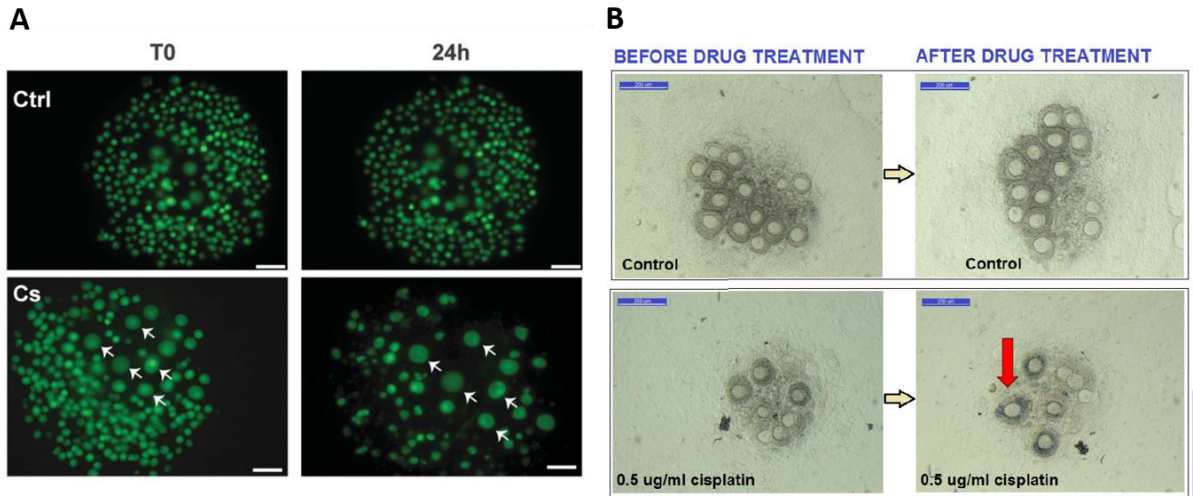

Figure 3-1. Mouse fragmented ovary culture. Ovaries from new-born mice are fragmented into eight pieces and cultured until they have attached to the culture surface and formed mushroom-like structures. At this point, drugs such as cisplatin (Cs) can be introduced to the culture system. This technique can be used using **(A)** transgenic mice expressing c-Kit-linked green fluorescent protein or **(B)** non-transgenic mice with trypan blue staining to assess viability. A from Rossi *et al.* (2017), licenced under a Creative Commons Attribution-NonCommercial-NoDerivatives 4.0 International Licence, B from poster by Kirkwood *et al.*, courtesy of Prof Spears. Scale bar: 75 µm.

3.1.1 Chapter aims

The aim of this chapter was to adapt the mouse fragmented ovary culture (mFrOC) method to enable visualisation of oocytes in human ovarian tissue, (hFrOC). This was done in collaboration with Prof Spears (University of Edinburgh), as this group had established the mFROC method and adapted it to be used with brightfield microscopy. The specific aims of this chapter were:

(i) to become proficient in the mFROC method;

(ii) to adapt the mFROC method to culture human ovarian tissue to allowing real-time observation of follicles in cultured human ovarian tissue.

The following objectives were identified to adapt the mFROC method to human ovarian tissue:

- to compare different processing methods (manual dissection and enzymatic digestion) to obtain human ovarian tissue fragments (experiments 1 and 4),
- to compare tissue attachment factors to promote the attachment of human ovarian tissue fragments (experiments 3 and 5),
- to determine whether patient age or ovarian tissue cryopreservation performed differently, by culturing cryopreserved tissue (experiments 1-5), or fresh tissue from a young (experiment 6) and old patient (experiment 7),
- to assess the suitability of viability stains (trypan blue and neutral red) to visualise dead and living cells, respectively.

3.2 Materials and methods

3.2.1 Mouse fragmented ovary culture

3.2.1.1 Animals

Wild-type C57BL/6 female mouse pups (postnatal day 4-5) were collected and sacrificed by cervical dislocation by a trained and qualified member of the Williams group. Mice were transported to the laboratory within 30 min for dissection.

3.2.1.2 Dissection and culture

A total of six pups (postnatal day 4-5) were used over three experiments to carry out new-born ovary dissection and fragmented ovary culture. Ovary dissection was performed by laying the pup on its front, pulling up the skin on the lower back and making a cut across the lower back, pulling the skin back to expose the internal organs. The kidneys were visualised and a pocket created by carefully cutting the peritoneum along the bottom of the kidney. The ovary was

identified just below the kidney, dissected using fine forceps and scissors and placed in a glass embryo dish containing pre-warmed sterile dissection medium (L-15 medium with 3 mg/mL BSA) . These steps were repeated until the ovaries from all mice in each experiment had been collected.

Dissected ovaries were transferred to a biosafety cabinet and cleaned using forceps and insulin needles (1 mL syringe with fixed 27G x ½" needle, Merck, UK) to remove any fatty tissue, oviducts and ovarian bursa. Cleaned ovaries were moved to a dish containing fresh dissection medium. Using a combination of acupuncture needles (30 mm x 0.25, Accumedic) and insulin needles, each ovary was carefully cut into eight fragments by halving each piece three times. Using a curved glass Pasteur pipette with wide bore end, the ovary fragments were transferred to a 24-well plate. Culture medium consisted of 10% FBS (FB-1090/500, BioSera, Nuaille, France), 2 mM L-glutamine, 100 U/mL penicillin, 100 µg/mL streptomycin, 0.25 mM sodium pyruvate, 0.2 mg/mL N-acetyl-L-cysteine (A-8199, Sigma), 10 µg/mL insulin, 5.5 µg/mL transferrin, 5 ng/mL selenium, in αMEM. The fragments were first washed briefly in a well containing culture medium before being placed in groups of 4-5 fragments into wells containing 1 mL of culture medium. Care was taken to place the fragments close together without touching. Medium was changed on day 3 (day of dissection was defined as day 0) by removing half the culture medium and replacing with freshly prepared, pre-warmed medium. Cultures were assessed on day 4 to check for attachment and to see whether the fragments had formed a mushroom-like shape. Cultures were stained with either neutral red or trypan blue (see below) and imaged on day 4. Fragments were discarded at the end of the culture period.

3.2.2 Human fragmented ovary culture

3.2.2.1 Patient details

See Section 2.1-2.2 for details on ethical approval and tissue procurement. To test the FrOC method for cryopreserved-thawed ovarian tissue, samples from a 13-year-old patient with Ewing's sarcoma were used (Experiments 1-5). For experiments using fresh ovarian tissue, two patient samples were obtained. The first was from a 53-year-old patient and the second sample

from a terminally ill 13-week-old donor with type 1 spinal muscular atrophy. All patients, or their legal guardians, provided informed consent to donate their tissue to research.

3.2.2.2 Sample processing and culture

Cryopreserved samples were thawed as described in Section 2.2.2. After thawing, tissue was processed into small pieces using either a tissue chopper or manual dissection with scalpels and needles, or a combination. Processing was performed in dissection medium (L-15 supplemented with 3 mg/mL HSA, 100 U/mL penicillin, 100 µg/mL streptomycin, 2 mM L-glutamine and 2 mM sodium pyruvate). Tissue was processed into fragments of varying sizes (all under 0.5 x 0.5 x 0.25 mm) for comparison. Where enzymatic digestion was used (Experiment 1), samples were incubated in 1 mg/mL collagenase (C0130; Sigma) or 0.5 mg/mL and trypsin (25300054, Thermo Fisher) for 15 minutes at 37°C and then washed in culture medium.

For Experiment 1, both serum and serum-free culture media were used, in each case 1 mL of medium was used per well. Serum medium was supplemented with 10% FBS, 2 mM L-glutamine, 100 U/mL penicillin, 100 µg/mL streptomycin, 0.25 mM sodium pyruvate, 0.2 mg/mL N-acetyl-L-cysteine, 10 µg/mL insulin, 5.5 µg/mL transferrin, 5 ng/mL selenium, in αMEM. Serum-free medium contained 1 mg/mL HSA, 100 U/mL penicillin, 100 µg/mL streptomycin, 2 mM L-glutamine, 10 µg/mL insulin, 5.5 µg/mL transferrin, 5 ng/mL selenium, 50 µg/mL ascorbic acid and 12.5 IU/L recombinant human FSH, in αMEM. Serum-free medium was used for all other experiments.

For Experiment 3, culture plates were coated with various extracellular matrix agents. Collagen IV (0.1 and 0.2 mg/mL; C0543, Sigma) was prepared from 2 mg/mL stock solution with 0.25% acetic acid. Gelatin (1 mg/mL and 5 mg/mL; G1393, Sigma) was prepared from 2% stock with sterile PBS. Plates were coated with 100 µL collagen IV, gelatin or extracellular matrix (ECM) solution (4-6 mg/mL; E1270, Sigma) and left to dry overnight. In Experiment 5, plates were coated with 200 µL of 0.1 mg/mL poly-lysine (gift from Dr T Lodge) for five minutes before the

solution was removed and plates rinsed with sterile water and allowed to dry before culture. All samples were discarded at the end of the culture period.

3.2.3 Assessment of tissue viability

3.2.3.1 Neutral red staining

Prior to culture, human samples were stained with 25 μg/mL neutral red in serum-free medium (αMEM supplemented with 3 mg/mL HSA, 100 U/mL penicillin, 100 μg/mL streptomycin, 2 mM L-glutamine and 2 mM sodium pyruvate) for at least one hour in an incubator. Samples were transferred to fresh dissection medium for visualisation. Mouse fragmented ovaries were stained with 25 μg/mL neutral red following culture using the same protocol.

3.2.3.2 Trypan blue staining

Mouse and human samples that had been cultured in medium containing serum were first washed twice for three minutes in serum-free medium. Trypan blue (0.4%, T8154, Sigma) was diluted 1:5 in serum-free medium and 0.5 mL solution was added to each well. Samples were incubated twice for two minutes to allow staining and then washed twice for three minutes in serum-free medium to remove excess dye. Fresh medium was added for observation under the microscope.

3.3 Results

3.3.1 Mouse fragmented ovary culture

Establishing the method of mFrOC was successfully achieved. Fragments were observed to attach to the culture surface and form raise mushroom-like structures which could be observed under the microscope using viability stains (Figure 3-2).

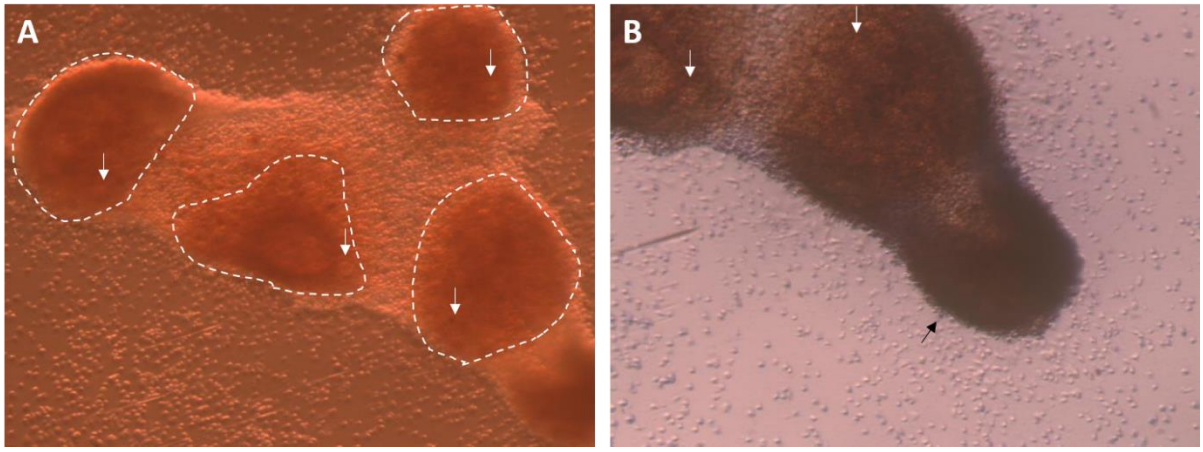

Figure 3-2. Viability staining of cultured mouse ovary fragments. Mouse ovary fragments were cultured as described in Section 3.2.1. At day 6 of the culture period, fragments were stained with neutral red and trypan blue to visualise viable or dead cells, respectively. (**A**) Neutral red staining demonstrated tissue viability. Distinct follicle clusters (marked by dashed lines) could be observed, each containing several follicles (white arrows). (**B**) Same sample as (A) with added trypan blue staining, showing dead cells at the sample border (black arrow).

3.3.2 Human fragmented ovary culture

In planning these experiments, three elements were identified for optimisation to allow successful adaptation of the mFROC method to human tissue: (a) tissue processing, (b) attachment of tissue during culture and (c) viability staining and visualisation. These will be discussed in the following sections.

3.3.2.1 Patient samples

A total of seven experiments were performed in order to adapt this method, using both fresh and frozen-thawed samples from three patients in total (Table 3-1). When this work was first carried out, our group was limited to access to cryopreserved ovarian tissue from the OCTB or fresh donated ovaries from older patients. In order to reduce patient variability, we elected to use samples from a single patient, a 13-year-old with Ewing's sarcoma, for the initial optimisation experiments, with plans to include additional patient samples if the method could be successfully adapted.

Table 3-1. Patient samples used to develop the human fragmented ovary culture method.

Patient	Age	Diagnosis	Fresh or frozen	Type of donation
A	13 years	Ewing's sarcoma	Frozen	Cortical strips
B	53 years	Benign gynaecological indication	Fresh	Whole ovary
C	13 weeks	Type 1 spinal muscular atrophy	Fresh	Whole ovary

3.3.2.2 Tissue processing

To adapt the mFrOC method for human, the size of the tissue fragments needs to be considered. For the mFROC method, neonatal ovaries are first cut into very small fragments. Ovaries of P4 mice are approximately 1 mm across, and as each ovary is cut into eight pieces, each fragment is approximately 100-150 μm. Therefore, the first step in adapting the method for human tissue was to process human ovarian tissue into fragments of a similar size. To achieve this, we tested a range of different tools in Experiments 1 and 4 (Table 3-2), including insulin and acupuncture needles that are used to fragment mouse ovaries. Needles were found to be ineffective, due to the dense nature of the human ovarian cortex. Scalpel blades were more successful, particularly small scalpel blades (no. 15).

One of the hallmarks of the mFROC method is that the mouse ovarian fragments round up during culture, forming spheroids with follicles located on the edge of the structure. We had previously observed in our group that human ovarian tissue does not remodel in this way and therefore tried using short enzymatic digestion to partially break down the cortex to test whether this had any effect on the tissue's ability to round up during culture. However, we found this method to be ineffective, as the tissue fragments became stringy and difficult to manipulate and were unchanged after six days of culture. Processing of neonatal mouse ovaries was performed in glass embryo-dishes (square glass dishes with a rounded cavity), however we found that the rounded bottom made processing with scalpels more difficult. More success was had with glass petri dishes where the dissection medium had been pipetted in the centre to form a dome.

Table 3-2. Overview of different tissue processing methods used to obtain small human ovarian tissue fragments.

Experiment	Patient	Processing variable	Outcome
Experiment 1	A	Insulin and acupuncture needles	Ineffective, human tissue was too dense and did not tear like mouse
Experiment 1	A	Enzymatic digestion (1 mg/mL collagenase or 0.5 mg/mL and trypsin)	Ineffective, tissue became stringy and difficult to manipulate
Experiment 4	A	Scalpel size	No. 15 scalpels were found to be superior than no. 24 allowing smaller pieces to be obtained
Experiment 4	A	Processing dish	Large petri dishes with a central dome of medium allowed easier processing than glass cavity dishes (embryo-dishes)

3.3.2.3 Tissue attachment during culture

To determine whether tissue attachment could be promoted, culture plates were coated with various attachment factors (collagen IV, gelatin, extracellular matrix solution and poly-L-lysine). However, no tissue attachment was observed in any experimental group (Table 3-3). Attachment was not observed in fresh ovarian samples, and while ovaries from the 13-week-old donor were easier to manipulate and more pliant than samples from the older patient and more similar to mouse ovaries, no attachment or reshaping was observed. While culture on top of a polycarbonate membrane did not promote tissue attachment, tissue fragments did remain stationary during the culture period, facilitating real-time imaging. However, membrane pores made visualisation and detailed imaging of the tissue impossible.

Table 3-3. Overview of different tissue processing methods used to promote attachment of human ovarian tissue during *in vitro* culture.

Experiment	Patient	Intervention	Outcome
Experiment 1	A	Culture in standard 24-well plates	No attachment after six days
Experiment 2	A	Culture in standard 24-well plates	No attachment after eight days
Experiment 3	A	Culture in wells coated with collagen IV (0.1 or 0.2 mg/mL)	No attachment after six days
Experiment 3	A	Culture in wells coated with gelatine (1 or 5 mg/mL)	No attachment after six days
Experiment 3	A	Culture in wells coated with extracellular matrix gel (4-6 mg/mL)	No attachment after six days
Experiment 5	A	Culture in wells coated with poly-L-lysine (0.1 mg/mL)	No attachment after six days
Experiment 5	A	Culture on polycarbonate membrane	Tissue kept in place by membrane, but no attachment observed. Visualisation difficult due to membrane pores
Experiment 6	B	Culture in standard 24-well plates (1 mL or 500 µL medium)	No attachment after seven days
Experiment 7	C	Culture in standard 24-well plates	No attachment after seven days

3.3.2.4 Viability staining and visualisation

Trypan blue and neutral red were used to assess tissue viability during culture. Neutral red could be used to identify follicles within the tissue (Figure 3-3A). Trypan blue staining resulted in total tissue staining (Figure 3-3B).

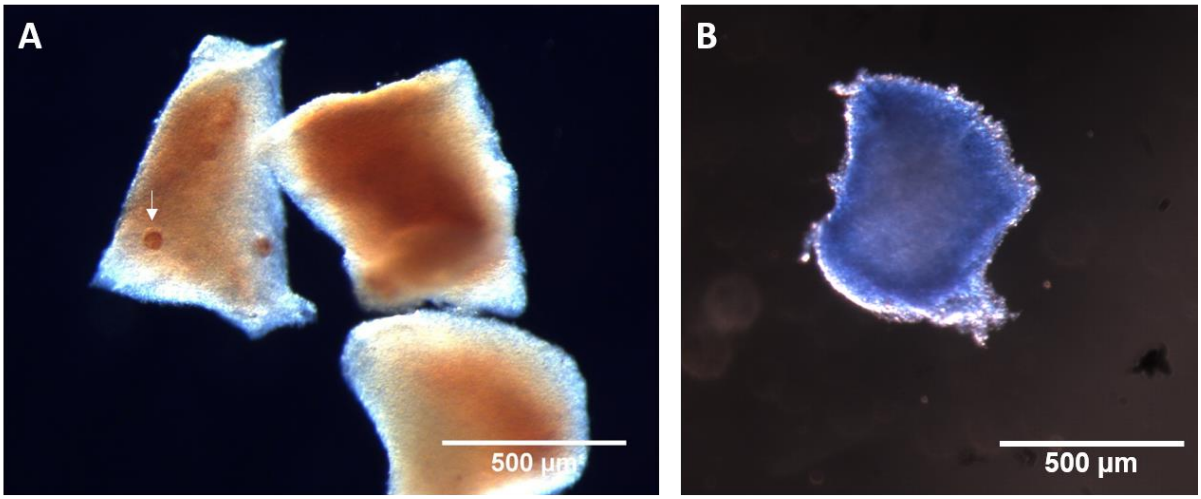

Figure 3-3. Viability staining of human ovarian tissue fragments. (**A**) Representative image of fresh human ovarian tissue stained with neutral red. Viable follicles were observed as round red structures (white arrow). (**B**) Cryopreserved human ovarian tissue stained with trypan blue with the aim of visualising dead cells. Universal blue staining was observed in the tissue.

3.4 Discussion

The aim of this chapter was to adapt the mouse fragmented ovary culture method for human ovarian tissue. Mouse ovaries could be successfully cultured according to the protocol developed by Maiani *et al.* (2012) and adapted by Prof Spears. However, several challenges were faced when it came to adapting the method for human tissue. Firstly, the human ovarian cortex, which contains the immature follicles to be cultured, is extremely dense and rigid, with a greater amount of stromal tissue and extracellular matrix compared to mouse ovaries. While mouse ovaries can reshape into mushroom-like structures during culture, the same phenomenon was not observed in human ovarian tissue from patients ranging from 13 weeks to 53 years, and tissue preparation (fresh or cryopreserved) was not found to affect this. Processing methods including dissection tools and enzymatic digestion did not promote tissue reshaping.

We have previously observed in our group that unlike mouse ovaries, human ovarian tissue does not attach to the culture surface during culture. As this was a key component of the mFROC method, several attachment factors were tested but none were found to promote tissue attachment within the culture period. To determine whether this lack of attachment was due to cryopreservation, culture using fresh ovaries was also performed, but no attachment was

observed. We used ovarian tissue from patients ranging from 13 weeks to 53 years, however no difference in tissue attachment was observed. Ovaries from the 13-week-old donor were observed to be more pliant and easier to manipulate, similar to mouse ovaries, however no attachment or reshaping of the tissue was observed during culture.

Neutral red could be used to identify follicles in the tissue. Neutral red is a water-soluble dye that has been used as a marker of cell viability and has previously been used to detect viable follicles within ovine and human ovarian tissue (Chambers *et al.*, 2010; Kristensen *et al.*, 2018; Bjarkadottir *et al.*, 2021; Walker *et al.*, 2021). While neutral red could be used to identify follicles, trypan blue staining resulted in staining of entire tissue fragments. Trypan blue is a water-soluble dye that permeates cells with compromised membranes and can therefore be used to identify dead cells. Live cells or tissues with intact cell membranes do not take up the dye and remain unstained. Trypan blue has been used to assess viability of follicles isolated from cryopreserved human ovarian tissue (Fauque *et al.*, 2007). The large degree of tissue staining observed may be due to damage sustained by the ovarian stroma during cryopreservation and thawing (explored further in Chapter 5) or may be due to incompatibility of the stain with tissue fragments (Sigma representative, personal correspondence). Follicles could not be visualised in human ovarian tissue stained with trypan blue.

In the present study, human ovarian tissue fragments were cultured for up to eight days, however no tissue attachment or remodelling was observed. Mouse ovarian tissue was observed to attach and form mushroom-like shapes after four days. It is possible that human ovarian tissue requires a longer culture period until the fragments begin to remodel. Others have demonstrated that the edges of fresh human ovarian tissue fragments round up within 2-3 weeks of *in vitro* culture (Laronda *et al.*, 2014; Xu *et al.*, 2021). Laronda *et al.* used alginate-encapsulation of human ovarian tissue fragments while Xu *et al.* cultured tissue fragments on ultra-low attachment plates (Laronda *et al.*, 2014; Xu *et al.*, 2021). Extending the culture period for hFrOCs could be explored in future experiments.

In conclusion, we determined that the mFROC method could not be successfully adapted for human ovarian tissue. The most successful culture preparation protocol was found to involve processing of ovarian tissue using small scalpel blades in a large petri dish containing a central dome of medium, followed by culture using a polycarbonate membrane floating on top of the well, to keep the tissue fragments stationary. However, the membrane pores interfered significantly with visualisation and imaging and real-time observation of follicles could not be achieved. Therefore, this line of research was abandoned and the remaining culture work in this thesis used our group's previously established culture method for human ovarian tissue culture.

Chapter 4

Effect of culture condition on follicle health and development of cryopreserved human ovarian tissue

4.1 Background

Despite recent advances in fertility preservation, limited options exist for certain patient groups, particularly young patients with haematological malignancies who are too young to undergo oocyte retrieval and for whom transplantation of cryopreserved-thawed ovarian tissue is contraindicated (Bastings *et al.*, 2013; Rosendahl *et al.*, 2013). *In vitro* follicle growth (IVFG), followed by *in vitro* maturation (IVM) of oocytes has been suggested as a fertility preservation method for these patients (Hovatta *et al.*, 1997; McLaughlin *et al.*, 2018). The technique involves culture of ovarian tissue to obtain large pre-antral follicles which can be isolated and cultured further, followed by oocyte isolation and IVM resulting in a mature, fertilisable oocyte. This technique has been demonstrated using fresh ovarian tissue, however patients who already have cryopreserved ovarian tissue in storage could also benefit.

Currently there have been two reports of successful human IVFG using fresh ovarian tissue, resulting in mature oocytes (McLaughlin *et al.*, 2018; Xu *et al.*, 2021). The study by McLaughlin *et al.* utilised a four-step culture system, wherein fresh ovarian cortical tissue was cultured *in vitro* for eight days (step 1), after which visible pre-antral follicles were isolated and cultured individually for a further eight days (step 2). Cumulus-oocyte-complexes (COCs) were then isolated from healthy antral follicles and cultured for a further four days (step 3) and IVM of oocytes was performed (step 4). Only a relatively small proportion of follicles were able to continue through each of these steps, with 40-60% of follicles being lost between steps, due to

atresia or insufficient development. In particular, the first step of this method (ovarian tissue culture) is the most limiting as it governs the number of follicles that can be carried on to the next stages. Therefore, it is critical to improve ovarian tissue culture techniques to increase the yield of healthy pre-antral follicles and ensure the success and eventual clinical application of this method.

In vitro culture of human cortical tissue began in the 1990s and since then research groups have adapted their own culture protocols (see Section 1.3.2). The most commonly used culture media are αMEM, often used for cryopreserved tissue (Isachenko *et al.*, 2012; Lerer-Serfaty *et al.*, 2013; Asadi-Azarbaijani *et al.*, 2016; Ramezani *et al.*, 2017; Talevi *et al.*, 2018), and McCoy's 5A (Telfer *et al.*, 2008; McLaughlin *et al.*, 2018; Lopes *et al.*, 2020; Walker *et al.*, 2021). The choice of culture plates, volume of medium, and use of supportive scaffolds such as polycarbonate membranes or extracellular matrices also varies between groups.

Considering these differences in culture methods, we sought to determine whether we could improve the development and health of *in vitro* cultured follicles by altering our group's own culture system for cryopreserved ovarian tissue, in particular the culture medium and medium volume. Another variable we sought to investigate was the use of gas-permeable culture plates, as these had recently been suggested to improve follicle health and development of fresh human ovarian tissue (Talevi *et al.*, 2018). Prior to this study, our group used a culture method based on Lopes *et al.* (2019), wherein tissue pieces are cultured on a polycarbonate membrane floating in 1 mL of McCoy's 5A-based medium (Walker *et al.*, 2021).

4.1.1 Chapter aims

The aim of this study was to determine whether different culture conditions led to (i) increased follicle development and (ii) improved follicle health. We hypothesised that follicle development and health could be improved by culturing tissue in a low medium volume compared to our group's culture method. We compared culture conditions most commonly used in ovarian tissue

culture, investigating two different types of media and three different physical culture conditions (Figure 4-1). The objectives of this chapter were:

- to determine whether any of the six culture conditions tested led to a higher number of proportion of developing (transitional, primary and multilayer) follicles; and
- to determine whether any of the six culture conditions tested resulted in a higher proportion of morphologically healthy follicles.

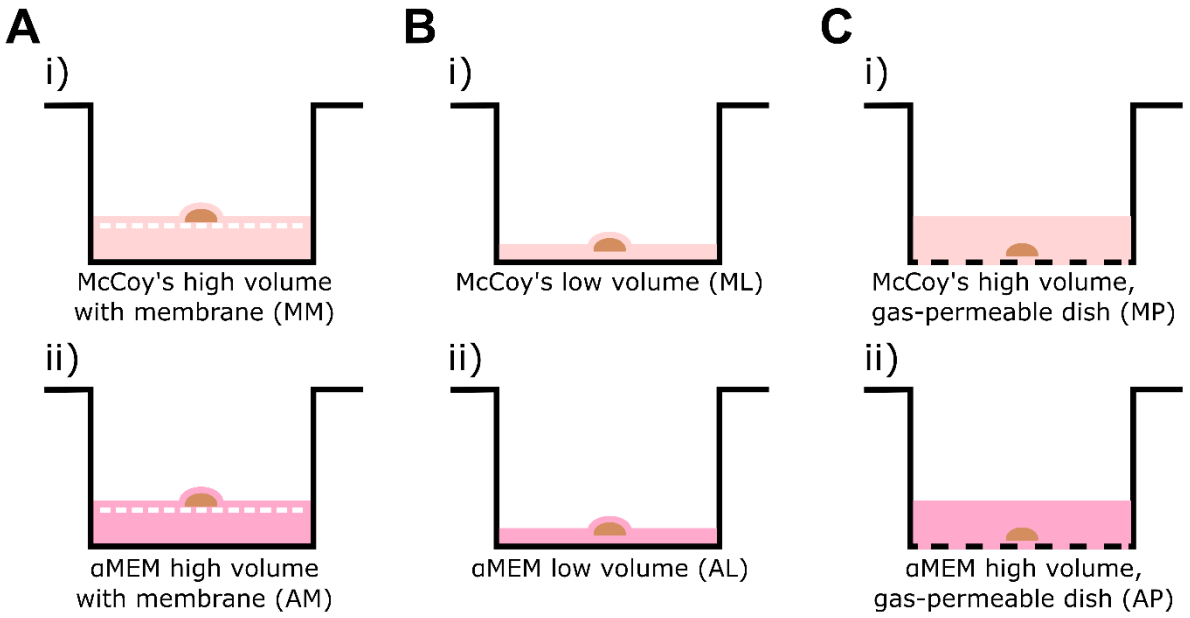

Figure 4-1 Overview of culture conditions used to investigate follicle development and health of cryopreserved human ovarian tissue. Cryopreserved human cortical strips were thawed and processed for culture as described in the methods section. Three plate conditions were tested along with two culture media, resulting in a total of six culture conditions. **(A)** Polycarbonate membrane floating in a high volume (1 mL) of McCoy's 5A (MM, Ai) or αMEM (AM, Aii) medium in a conventional 24-well plate. **(B)** Low volume (300 µL) of McCoy's 5A (ML, Bi) or αMEM (AL, Bii) medium in a conventional 24-well plate. **(C)** High volume (1 mL) of McCoy's 5A (MP, Ci) or αMEM (AP, Cii) medium in a gas-permeable Lumox® 24-well plate. Adapted from Bjarkadottir *et al.* (2021), licenced under a Creative Commons Attribution 4.0 International License.

4.2 Materials and methods

4.2.1 Patient selection

The use of human tissue was approved by the Health Research Authority South Central – Oxford B Research Ethics Committee (REC reference 14/SC/0041). Patient selection criteria were post-

pubertal patients without haematological or gynaecological malignancies, who had not undergone chemotherapy prior to ovarian tissue cryopreservation.

4.2.2 Chemicals and consumables

Leibovitz L-15 medium (11415049), αMEM (22561021), McCoy's 5A (modified) HEPES buffered medium (22330021), L-glutamine (25030024) and ascorbic acid (10012011) were purchased from Thermo Fisher (Paisley, UK). Human serum albumin (AI653), ITS liquid media supplement (100x; I3145), sucrose (S7903), ethylene glycol (324558), sodium pyruvate (S8636), neutral red (N2889), Bouin's solution (HT10132), DPX mountant (06522) and Whatman Nucleopore membranes (WHA110414) were purchased from Sigma Aldrich (Poole, UK). Recombinant human follicle stimulating hormone (FSH; Gonal-F; Z1540) was purchased from Merck Serono (Feltham, UK). Corning Costart tissue culture treated 24-well plates were purchased from Scientific Laboratory Supplies (Nottingham, UK). Lumox® 24-well plates were generously provided by Sarstedt (Nümbrecht, Germany).

4.2.3 Cortical strip culture

Cortical strips were thawed as described in Section 2.2.2. Thawed cortical strips were processed on a heated stage at 37°C into small pieces (approximately 0.25 x 0.5 x 0.5 mm) using a combination of mechanical and manual dissection. Mechanical dissection was performed with the aid of a tissue chopper (McIlwain Tissue Chopper, The Mickle Laboratory Engineering Co., Surrey, UK). A single cortical strip was placed on sheets of round filter paper, moistened with dissection medium, with the long edge perpendicular to the chopper. The tissue was chopped at 0.25 mm intervals and fragments were immediately transferred back to a petri dish containing dissection medium. Tissue fragments were further cut using scalpels into approximately 0.5 x 0.5 x 0.25 mm pieces. Fragments were incubated in neutral red (25 μg/mL in dissection medium) for a minimum of 1 hour, to enable visualisation of follicles under a dissection microscope (Chambers *et al.*, 2010; Walker *et al.*, 2021). NR-positive tissue pieces were preferentially selected for culture.

NR-positive tissue pieces were distributed randomly and evenly between the different culture conditions. This was performed without viewing the pieces under a dissection microscope, so that the researcher was blinded to the degree of NR staining for each tissue piece. Any remaining NR-negative tissue pieces were evenly distributed between the culture conditions in case these contained follicles that could not be visualised with NR. A portion of tissue was fixed as a non-cultured control in Bouin's fixative overnight at RT. Cortical tissue pieces were cultured for 6 days at 37°C under 5% CO_2 in air, with medium changes every other day (half the medium removed and fresh medium added). Following the culture period all tissue pieces were fixed overnight in Bouin's solution at RT and stored in 70% ethanol at 4°C until processing.

Three different plate conditions were tested: a polycarbonate membrane (13 mm diameter, 8 µm pore size) floating in 1 mL of medium in a conventional 24-well culture plate, 300 µL of medium in a conventional 24-well plate, and 1 mL of medium in a gas-permeable Lumox® 24-well plate (Figure 4-1). For each plate condition, two different media were compared, McCoy's 5A and αMEM, each supplemented with 1 mg/mL HSA, 100 U/mL penicillin, 100 µg/mL streptomycin, 2 mM L-glutamine, 10 µg/mL insulin, 5.5 µg/mL transferrin, 5 ng/mL selenium, 50 µg/mL ascorbic acid and 12.5 IU/L recombinant human FSH.

4.2.4 Histological analysis

Fixed ovarian tissue was processed and stained with haematoxylin and eosin as described in Sections 2.5-2.6. Tissue pieces within the same culture condition were embedded in groups of 3-4 pieces per paraffin block. All samples were serially sectioned to completion. The area of every 12th tissue section was measured using ImageJ 1.46r (National Institutes of Health, Bethesda, MD, USA; Rueden *et al.*, 2017; Schneider *et al.*, 2012). Area measurements were used to calculate the volume of each tissue piece (Section 2.6.3.3). Follicle density was determined by dividing the total number of follicles counted in a tissue sample by the tissue volume (Section 2.6.3.3)

Follicles were staged according to Gougeon (1999) as primordial (single layer of flattened pre-granulosa cells), transitional (single layer with at least one cuboidal granulosa cell), primary

(complete layer of cuboidal granulosa cells) and multilayer (two or more complete layers of cuboidal granulosa cells (Section 2.6.3). Follicles were graded according to health based on the presence of pyknotic granulosa cells or oocyte and shrinkage of the ooplasm (Section 2.6.3). Healthy follicles were defined as having a non-pyknotic non-shrunken oocyte with non-pyknotic granulosa cells, degenerating follicles had one of the above factors, while follicles were classified as atretic if they had both an oocyte with a pyknotic nucleus and pyknotic granulosa cells. Every tissue section was analysed and each follicle was followed through neighbouring sections to avoid double counting. Only follicles with a visible nucleolus or a clearly defined nuclear membrane were assessed.

4.2.5 Statistical analysis

All statistical analyses were performed using R statistical software, version 3.5.0. A generalised linear mixed model following a negative binomial distribution (glmmPQL; Venables and Ripley, 2002) was used to determine the effect of culture condition on follicle development, adjusted for patient and tissue volume. A proportional odds model (clmm2; Christensen, 2015) was used to determine whether follicle health was affected by culture condition, again adjusting for tissue volume and patient. Data are presented as mean (± SEM) or as odds ratios with 95% confidence intervals (CI), unless otherwise stated, and statistical significance was defined as $P < 0.05$.

4.3 Results

4.3.1 Patient characteristics

Ovarian tissue samples from three post-pubertal patients (aged 17-25 years at the time of OTC, mean 21.3 ± 3.3 years) were included in this study. None of the patients had received chemotherapy prior to ovarian tissue cryopreservation A total of 5,797 follicles from three patients were analysed for this study, with up to a tenfold difference in follicle numbers between patients (Table 4-1).

Table 4-1. Patient characteristics and follicle numbers. Ovarian tissue samples from three post-pubertal patients were used in this study. Shown here is patient age at the time of ovarian tissue cryopreservation (OTC), patient diagnosis and the total number of follicles analysed in the study.

Patient	Age at OTC (years)	Diagnosis	Total follicles analysed
D	25	Cervical cancer	303
E	17	Ewing's sarcoma (left pelvis)	3,198
F	22	Atypical teratoid rhabdoid tumour	2,295

4.3.2 Human ovarian tissue is characterised by a high level of intra- and inter-patient variability

Follicles were classified based on histology as primordial, transitional, primary or multilayer and each follicle was further graded as healthy, degenerating or atretic based on oocyte and granulosa cell morphology (see Figures 2-1 and 2-2 for representative images).

When visualising the data prior to statistical analysis, we noticed a high level of variability between and within patient samples when comparing non-cultured control samples to samples that had been cultured in McCoy's 5A on a polycarbonate membrane; our group's established culture method based on Lopes *et al.* (2019) prior to this study (Walker *et al.*, 2021; Figure 4-2).

There was variation in follicle density both between patients and with individuals between different tissue pieces, with density ranging from 20.4 to 431.9 follicles/mm^3 in non-cultured tissue and 1.8 to 741.8 follicles/mm^3 in cultured tissue (Figure 4-2A-B).

There were also differences in the distribution of follicle stage between patients in both non-cultured and cultured tissue (Figure 4-2C-D). The proportion of primordial follicles ranged from 30.9% to 80.7% between patients in non-cultured tissue, while the proportion of transitional, primary and multilayer follicles ranged from 18.5-54.7%, 0.7-12.9% and 0.1-1.4%, respectively. These observations precluded the use of commonly used statistical tests, namely Fisher's exact test and chi-squared test, as these are not able to account for inter- and intra-patient variability.

We therefore developed statistical models to enable this variability to be taken into account (Walker *et al.*, 2021).

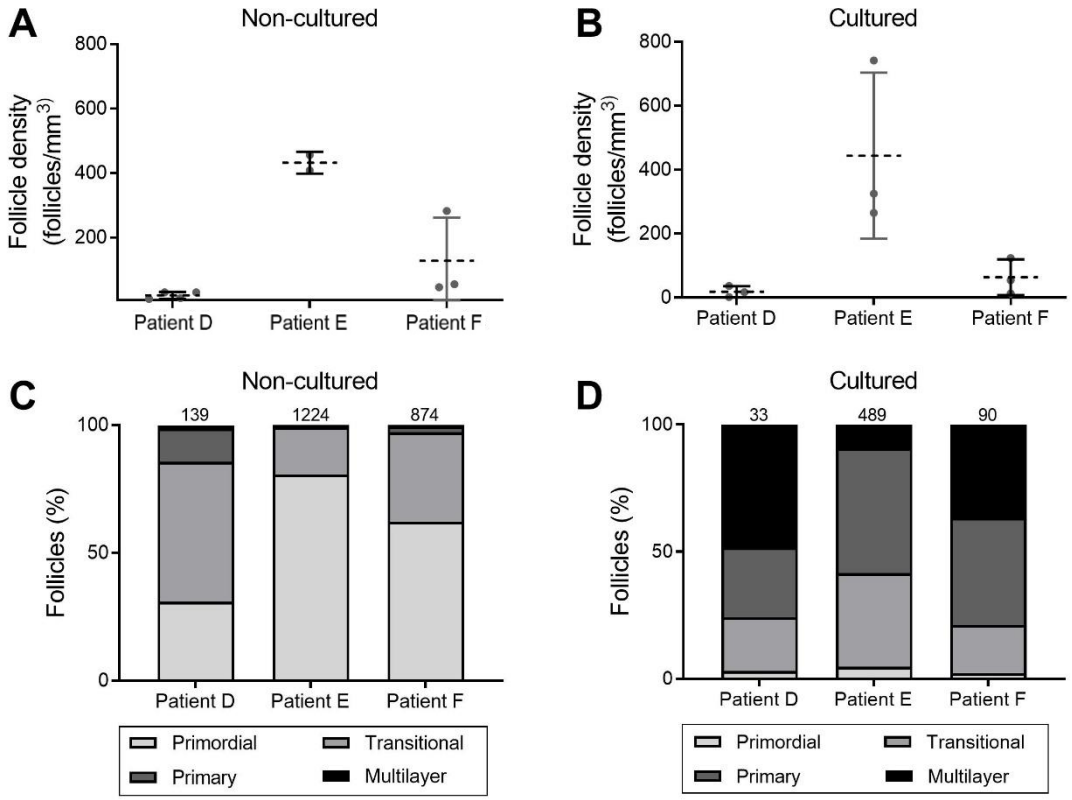

Figure 4-2. Follicle variation between patients in non-cultured and cultured ovarian tissue. Cortical tissue from three patients aged 17-25 years was processed into pieces <1 mm^3 which were fixed for analysis immediately after processing (non-cultured) or after 6 days of culture in a high volume of McCoy's medium on a polycarbonate membrane (cultured). **(A-B)** Follicle density was calculated for each tissue piece based on tissue volume. Data is represented as mean follicles density with error bars representing SEM. Variation in follicle density was observed both between and within individuals in non-cultured (A) and cultured tissue (B). Each data point represents 3-4 pieces of tissue, which were processed and analysed together. **(C-D)** Follicles were staged as primordial, transitional, primary or multilayer. Total follicle numbers are indicated at the bottom of each bar. The proportion of follicles at each developmental stage varied between patients both in non-cultured (C) and cultured tissue (D), though within each patient there was an increased proportion of primary and multilayer follicles after culture.

4.3.3 Follicle development is largely unaffected by culture condition

Follicles grew during the culture period, with the majority of follicles being classified as primordial (70.4%) or transitional (27.2%) in non-cultured tissue, whereas after six days of culture 39.4-79.7% of follicles were at the primary or multilayer stages, depending on the culture condition (Figure 4-3A). This observation was confirmed using a generalised linear mixed model,

which demonstrated that non-cultured tissue contained significantly more primordial and transitional follicles compared to primary or multilayer (P<0.0001, Figure 4-3B). In contrast, tissue cultured in McCoy's 5A on a polycarbonate membrane contained significantly fewer primordial follicles compared to transitional, primary and multilayer (P<0.01, Figure 4-3C).

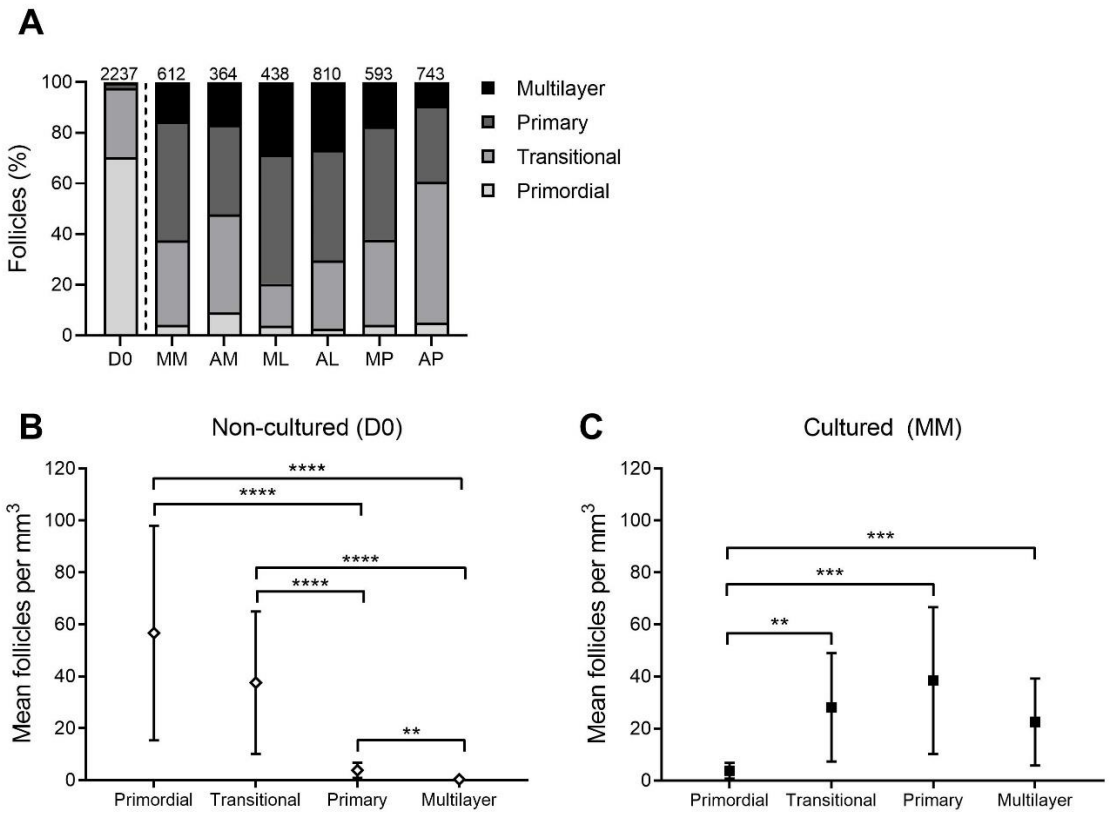

Figure 4-3. Follicle development during culture across six different culture conditions. Cryopreserved ovarian tissue from three patients aged 17-25 was either fixed for analysis immediately after processing (non-cultured, D0) or fixed after six days of culture using one of six different culture conditions. Follicles were staged as primordial, transitional, primary and multilayer based on morphology. **(A)** Follicle development was observed across all culture conditions compared to non-cultured control (D0, separated by dashed line), with a high proportion of primary and multilayer follicles being observed in cultured samples. The numbers across the top of the columns represent the number of follicles analysed in each group, combined from three patients. **(B)** In non-cultured tissue there were significantly more primordial and transitional follicles compared to primary and multilayer follicles. **(C)** In tissue cultured in a high volume of McCoy's medium on a polycarbonate membrane (cultured, MM) there were significantly more follicles at the transitional, primary and multilayer stage compared to primordial stage. Data was analysed using a generalised linear mixed model. Data is represented as mean follicles/mm^3 with error bars representing SEM. * P ≤ 0.05, ** P ≤ 0.01, *** P ≤ 0.001, **** P ≤ 0.0001. D0: non-cultured control; MM: McCoy's high volume with membrane, AM: αMEM high volume with membrane; ML: McCoy's low volume; AL: αMEM low volume, MP: McCoy's high volume, gas permeable plate; AP: αMEM high volume, gas-permeable plate.

Follicle development was compared across the different culture conditions, with all conditions being compared to culture in a high volume of McCoy's 5A on a polycarbonate membrane (MM), as this was our group's established culture method prior to this study (Figure 4-4). There were significantly fewer transitional follicles in tissue cultured in a low volume of McCoy's 5A medium (ML) compared to membrane culture (MM; 7.8 ± 6.0 follicles/mm^3 versus 28.2 ± 20.8 follicles/mm^3 respectively, P<0.05, Figure 4-4B). There was no difference between the conditions for follicles at other stages.

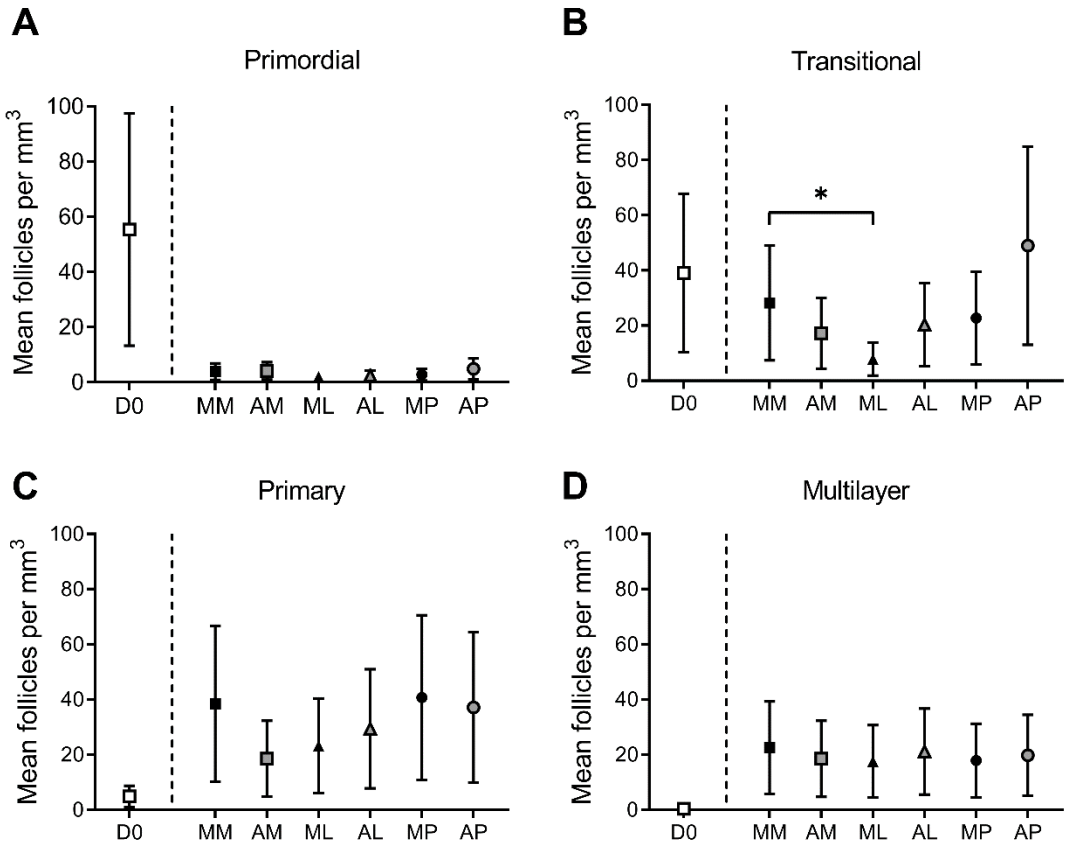

Figure 4-4. Follicle development is largely unaffected by culture condition. Ovarian tissue from three patients aged 17-25 was cultured for six days under six different conditions: in a high volume of McCoy's 5A (M) or αMEM (A) medium on a polycarbonate membrane (MM or AM, respectively), in a low volume of McCoy's 5A or αMEM medium (ML or AL), or in a high volume of McCoy's 5A or αMEM in a gas-permeable plate (MP or AP). After six days of culture, follicles were staged by the appearance and number of granulosa cell layers as primordial, transitional, primary or multilayer. Mean transitional follicle count per mm^3 was significantly lower in ML compared to MM ($p < 0.05$). There was no difference in the mean number of follicles per mm^3 at the primordial, primary or multilayer stages between the different conditions tested and MM. Data was analysed using a generalised linear mixed model. Data is represented as mean follicles/mm^3 with error bars representing SEM. * $P < 0.05$. From Bjarkadottir *et al.* (2021), licenced under a Creative Commons Attribution 4.0 International License.

4.3.4 Culture in low volume conditions improved follicle health

Follicles were classified as healthy, degenerating or atretic based on morphology. Non-cultured tissue contained mostly healthy follicles at all stages, however after six days of culture the proportion of degenerating or atretic follicles had increased considerably across all culture conditions (Figure 4-5). Condition AL was observed to have the highest proportion of healthy follicles at all stages.

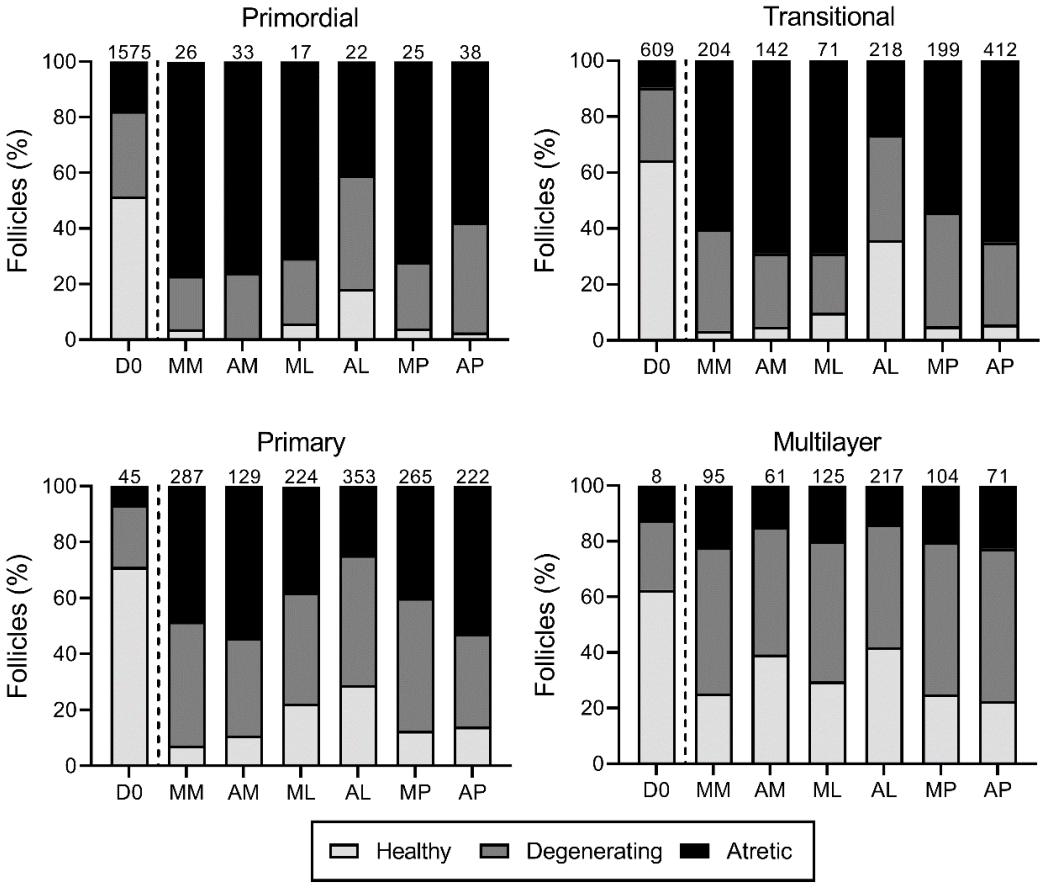

Figure 4-5. Comparison of follicle health across different culture conditions. Ovarian tissue from three patients aged 17-25 was cultured for six days under six different conditions: in a high volume of McCoy's 5A (M) or αMEM (A) medium on a polycarbonate membrane (MM or AM, respectively), in a low volume of McCoy's 5A or αMEM medium (ML or AL), or in a high volume of McCoy's 5A or αMEM in a gas-permeable plate (MP or AP). After six days of culture, follicles were staged as primordial, transitional, primary or multilayer. Follicles were graded by health as healthy, degenerating or atretic, based on the presence or absence of granulosa or oocyte pyknosis and ooplasm shrinkage. Total follicle numbers (combined for three patients) are indicated by the number above each column. Follicle health was lower in all culture conditions compared to the non-cultured control (D0). AL was observed to have the highest proportion of healthy follicles at all stages.

A proportional odds model was used to determine whether a follicle was more likely to be healthy compared to degenerating or atretic after six days in a particular culture condition. Each culture condition was compared to our group's current culture method (MM). Compared to MM, tissue cultured in low volume conditions (McCoy's, ML or αMEM, AL) or permeable dish conditions (MP or AP) had greater odds of healthy multilayer follicles being observed compared to degenerating or atretic (Figure 4-6). The most marked difference in the health of multilayer follicles was seen in the low volume conditions, particularly AL where the odds of observing a healthy follicle were 5 times greater than MM (OR=0.2; 95% CI 0.13-0.32 P<0.001, Figure 4-6D). Tissue cultured in ML had 2.6 times greater odds of multilayer follicles being classified as "healthy" versus "degenerating" or "atretic" compared to MM (OR=0.38; 95% CI 0.23-0.64; P<0.001). Furthermore, tissue cultured in AL was more likely to contain healthy primordial and transitional follicles compared to MM (Figure 4-6A-B). Culture in a high volume of McCoy's 5A medium in a gas-permeable plate (MP) and culture in a high volume of αMEM medium on a membrane (AM) also had a positive impact on follicle health, with the MP group having healthier transitional, primary and multilayer follicles, while the AM group had healthier multilayer follicles.

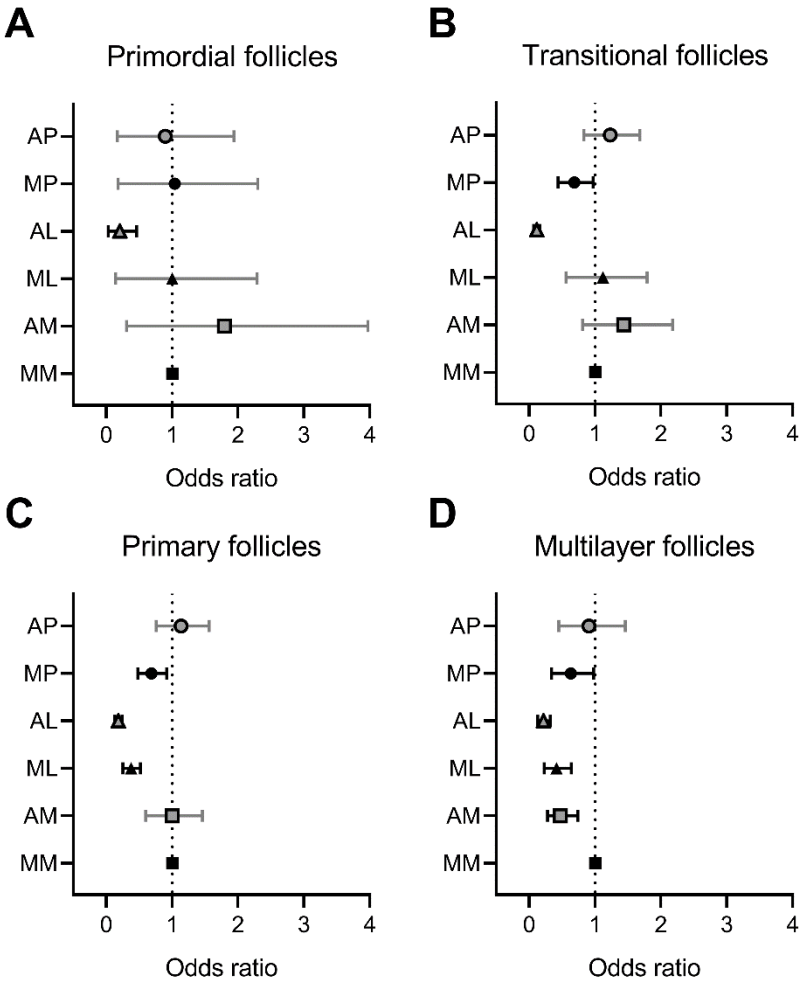

Figure 4-6. Effect of culture condition on follicle health. Ovarian tissue from three patients aged 17-25 was cultured for six days under six different conditions: in a high volume of McCoy's 5A (M) or αMEM (A) medium on a polycarbonate membrane (MM or AM, respectively), in a low volume of McCoy's 5A or αMEM medium (ML or AL), or in a high volume of McCoy's 5A or αMEM in a gas-permeable plate (MP or AP). After six days of culture, follicles were staged by the appearance and number of granulosa cell layers as primordial, transitional, primary or multilayer. Follicles were graded by health as healthy, degenerating or atretic, based on the presence or absence of granulosa or oocyte pyknosis and ooplasm shrinkage. A proportional odds ratio model was used to determine whether any of the conditions tested was more likely to lead to healthier follicles at each stage compared to our current culture method (MM). Data is represented as odds ratio with upper and lower 95% confidence intervals (displayed as error bars). Odds ratio < 1 indicates decreased odds of a follicle being degenerating or atretic compared to MM. Odds ratio > 1 indicates increased odds of a follicle being degenerating or atretic compared to MM. Those conditions where confidence intervals do not cross 1 (black error bars) were significantly less likely to have degenerating or atretic follicles compared to the baseline (MM, $P<0.05$).

As culture in AL resulted in healthier follicles at all stages compared to MM, AL was set as the baseline level of comparison in the proportional odds model, to ascertain whether medium affected follicle health within the low volume condition. Compared to AL, multilayer follicles cultured in ML had 1.9 times greater odds of being classified as degenerating or atretic than healthy (OR=1.92; 95% CI 1.24-2.97; P<0.001) demonstrating that AL yielded superior follicle health compared to ML and indeed all the other culture conditions (Figure 4-7). The superiority of AL was further highlighted by the fact that over 20% of follicles cultured in AL were at the primary or multilayer stage and morphologically healthy – more than any other culture condition (Figure 4-8).

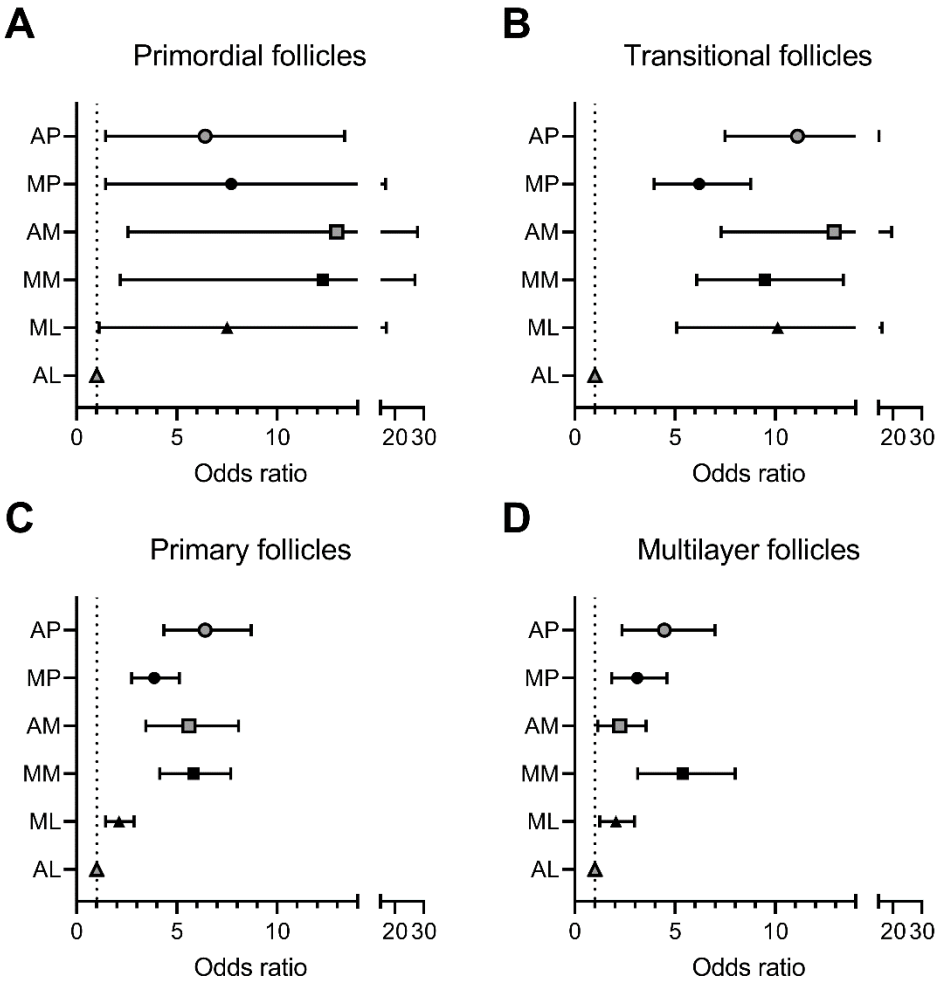

Figure 4-7. Culture in low volume αMEM results in healthier follicle development. Ovarian tissue from three patients aged 17-25 was cultured for six days under six different conditions: in a high volume (H) of McCoy's 5A (M) or αMEM (A) medium on a polycarbonate membrane (MM or AH, respectively), in a low volume (L) of McCoy's 5A or αMEM medium (ML or AL), or in a high volume of McCoy's 5A or αMEM in a gas-permeable plate (MP or AP). After six days of culture, follicles were staged by the appearance and number of granulosa cell layers as primordial, transitional, primary or multilayer. Follicles were graded by health as healthy, degenerating or atretic, based on the presence or absence of granulosa or oocyte pyknosis and ooplasm shrinkage. A proportional odds ratio model was used to determine whether any of the conditions tested was more likely to lead to healthier follicles at each stage compared to the culture method that performed best compared to MM (AL). Data is represented as odds ratio with upper and lower 95% confidence intervals (displayed as error bars). Odds ratio < 1 indicates decreased odds of a follicle being degenerating or atretic compared to AL. Odds ratio > 1 indicates increased odds of a follicle being degenerating or atretic compared to AL. Those conditions where confidence intervals do not cross 1 (black error bars) were significantly more likely to have degenerating or atretic follicles compared to the baseline (AL).

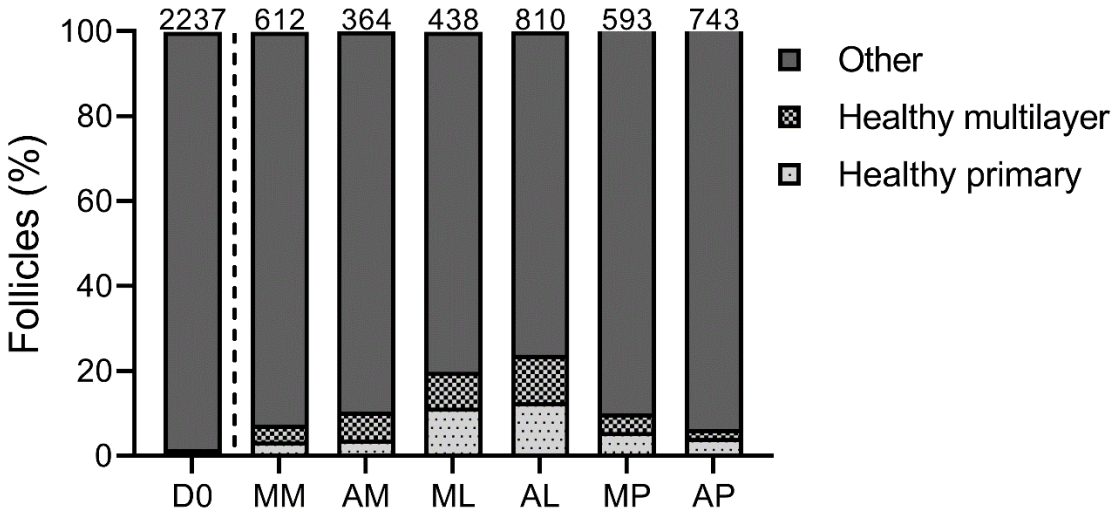

Figure 4-8. Culture in low volume conditions yields healthier growing follicles. The proportion of healthy primary (dotted) and multilayer (checkerboard) follicles were compared across culture conditions. Culture in low volume conditions resulted in the highest proportion of healthy primary and multilayer follicles. Values represent combined values from three post-pubertal patients. The numbers across the top of the columns represent the number of follicles analysed in each group, combined from three patients. D0: non-cultured control; MM: McCoy's high volume with membrane, AM: αMEM high volume with membrane; ML McCoy's low volume; AL: αMEM low volume, MP: McCoy's high volume, gas permeable plate; AP: αMEM high volume, gas-permeable plate.

4.4 Discussion

This study aimed to determine whether the health and development of *in vitro* grown follicles could be improved by altering culture conditions. Cryopreserved-thawed ovarian tissue from three post-pubertal patients was cultured under a total of six different conditions. Two culture media were compared in addition to three physical conditions (medium volumes and plate types; Figure 4-1). At the end of the six-day culture period the morphology of the tissue was assessed using haematoxylin and eosin staining to determine follicle stage and health. Due to considerable inter- and intra-patient variability statistical models were developed for data analysis. Follicle development was found to be largely unaffected by the culture conditions tested. In contrast, follicle health was greatly improved by culturing in a low volume of either McCoy's 5A or αMEM medium. Overall, culture in this low volume αMEM condition (AL) improved follicle health at all stages of development when compared to each of the other conditions tested.

The results of this chapter demonstrate that culture in a low volume of medium led to improved follicle health compared to an approximately three-fold higher medium volume. As follicles develop they release paracrine factors such as growth factors into their surroundings (Albertini *et al.*, 2001; Gilchrist *et al.*, 2004; Skinner, 2005). When tissue is cultured in a low volume of medium, the concentration of these growth factors is increased compared to culture in a higher volume of medium, which may have contributed to decreased follicle atresia observed in the present study. Conversely, this could potentially also have a detrimental effect as any waste products would be present in an increased concentration as well. However, as culture medium was replenished every two days (half of medium removed and replaced with fresh), build-up of harmful waste products may have been prevented.

Oxygen availability is also a contributing factor to follicle health (Morimoto *et al.*, 2007; Talevi *et al.*, 2018). While three different plate conditions were compared in the current study (polycarbonate membrane, low volume and gas-permeable dish), all provided similar access to the air as the ovarian tissue was located close to the medium-gas interface (Figure 4-1). By culturing cryopreserved ovarian tissue in AL we observed a high level of follicle progression: out of 810 follicles from three patients, 26.8% of follicles developed to the multilayer stage and 34.0% of these were morphologically healthy follicles. Talevi *et al.,* (2018) reported that culture of fresh human ovarian tissue in 5 mL of αMEM medium (column height 1.4 mm) in a gas-permeable petri dish led to improved follicle development and health, reporting that out of 287 follicles from six patients, 19.5% were multilayer and 41.7% healthy after six days of culture. This culture method is similar to that of AL described in the current study (AL column height 1.6 mm), however the medium volume used by Talevi *et al.* was 15 times greater. Taking into account the beneficial effects of low volume conditions identified in this study, culturing tissue in a low volume of αMEM in gas-permeable plates may lead to even greater follicle health and should be further explored.

Culture in a low medium volume (ML and AL) yielded the highest proportion of healthy primary and multilayer follicles out of the six conditions tested, with AL resulting in superior follicle health

at all stages. In the present study, tissue pieces were cultured for a total of six days, however a longer culture period may have resulted in more developed follicles. Xu *et al.* recently reported the generation of mature human oocytes grown from fresh human ovarian tissue using a multi-step culture system (Xu *et al.*, 2021). Interestingly, ovarian tissue was cultured for three weeks before secondary follicles were isolated for further culture. This is considerably longer than in the present study, and longer than the 8-day culture period reported by McLaughlin *et al.* (2018) – the only other group to have achieved full follicle development *in vitro*. In addition, Xu *et al.* were able to isolate a total of 103 secondary follicles (125-223 μm in diameter) from 40 tissue pieces (2.6 follicles per piece) compared to 87 follicles (100-150 μm in diameter) isolated from 136 tissue pieces (0.6 follicles per piece) by McLaughlin *et al.* This would suggest that a longer culture period might increase the number of follicles that could be isolated for subsequent culture. It is also noteworthy that Xu et al. were able to obtain morphologically normal MII oocytes, while those produced by McLaughlin et al. were abnormal with large polar bodies and abnormal spindle formation (McLaughlin *et al.*, 2018; Xu *et al.*, 2021).

Studies describing culture of controlled-rate cryopreserved human ovarian tissue, as we used in this study, are limited, as the majority of studies use fresh ovarian tissue (Telfer *et al.*, 2008; McLaughlin *et al.*, 2018; Talevi *et al.*, 2018; Lopes *et al.*, 2020; Xu *et al.*, 2021). Fresh and cryopreserved human ovarian tissue may have different requirements *in vitro*, as has been demonstrated using animal models (Castro *et al.*, 2014), highlighting the need to optimise ovarian tissue culture for both fresh and cryopreserved tissue. This is indeed critical since there are many patients who already have tissue cryopreserved and may require IVFG to generate eggs.

When comparing culture media, follicles at all stages were more likely to be graded as healthy when cultured in a low volume of αMEM (AL) compared to the same volume of McCoy's 5A medium (ML). αMEM contains both sodium pyruvate and a physiological concentration of glucose (5.6 mM), whereas McCoy's 5A contains no pyruvate and a three-times higher concentration of glucose (16.7 mM) and therefore αMEM may provide a more suitable environment for follicle

metabolism. Previous studies have indeed demonstrated pyruvate to be the main energy source during early follicle development in mice (Harris *et al.*, 2007, 2009). Under normal conditions the oocyte is supplied with pyruvate by its supporting somatic cells and it has been demonstrated that pyruvate is taken up from the culture medium during murine *in vitro* follicle culture (Harris *et al.*, 2009). Therefore, αMEM may provide a more suitable energy source for early human follicle metabolism compared to McCoy's, thereby better supporting follicle health.

The rate of follicle progression reported in the present study are in line with those reported in similar studies, noting that they use fresh ovarian tissue (McLaughlin *et al.*, 2018; Talevi *et al.*, 2018). While the present study used ovarian tissue from only three patients, the total number of follicles analysed was four to seven-fold higher than in studies using larger patient numbers (Table 4-2). This may also be because the present study used a younger cohort of patients (21.3 ± 3.3 years compared to 27.1 ± 6.9 years in Talevi *et al.* and 30.7 ± 1.7 years in McLaughlin *et al.*), since it is well established that follicle numbers, and by extension follicle density, decreases with age (Te Velde *et al.*, 1998). We observed that in cryopreserved culture tissue, up to 30.1% of follicles progressed to the multilayer stage after six days in culture, which is higher than that reported by both Talevi *et al.* and McLaughlin *et al* (Table 4-2). While follicle health was not an outcome measure in the study by McLaughlin *et al.*, the proportion of healthy follicles reported by Talevi *et al.* is only slightly higher than the present study (Table 4-2). It should be noted that Talevi *et al.* used fresh ovarian tissue, while the tissue used in the current study had been cryopreserved, which is known to reduce follicle health (Gook *et al.*, 1999; Hreinsson *et al.*, 2003; Zemyarska *et al.*, 2020).

Table 4-2 Comparison of *in vitro* follicle development and health between the current and published studies. Culture medium volume is reflected in the column height, which is the average height of culture medium from the bottom of the culture plate. 'Follicle progression' refers to the proportion of follicles reaching multilayer or secondary stages while 'healthy follicles' refers to the proportion of follicles classified as morphologically healthy (referred to as Grade I in Talevi *et al.* (2018)). Follicle numbers represent combined numbers for all patients (see text body).

Study	Patient details	Fresh or frozen	Culture condition	Column height	Follicle progression	Healthy follicles
Present study	N=3, 21.3 ± 3.3 years	Frozen	Control (n=2237)	N/A	D0: 0.4%	D0: 55.5%
			McCoy's 5A, membrane (n=612)	5.2 mm	D6: 16.2%	D6: 8.7%
			αMEM (n=810)	1.6 mm	D6: 30.1%	D6: 34.0%
			McCoy's 5A (n=438)	1.6 mm	D6: 27.7%	D6: 21.7%
Talevi *et al.* (2018)	N=6, 27.1 ± 6.9 years	Fresh	Control (n=273)	N/A	D0: 2.8%	D0: 50.4%
			αMEM, conventional plate (D6 n=213, D9 n=199)	1.4 mm	D6: 3.6% D9: 4.5%	D6: 12.3% D9: 19%
			αMEM, gas-permeable plate (D6 n=287, D9 n=271)	1.4 mm	D6: 19.5% D9: 19.2%	D6: 41.7% D9: 42.9%
McLaughlin *et al.* (2018)	N=10, 30.7 ± 1.7 years	Fresh	Control (n=385)	N/A	D0: 2.9%	Not reported
			McCoy's 5A (n=355)	1.6 mm	D8: 10.8%	Not reported

4.4.1 Future work

A major outcome measure of this study was follicle health as assessed by morphology, therefore all samples were fixed in Bouin's solution as this fixative preserves follicle morphology better than neutral buffered formalin. In addition, all samples were sectioned to completion to allow accurate determination of follicle numbers and density. Therefore, no additional samples are available for analysis such as molecular analysis. Our group has since developed a novel fixative, Form-Acetic, which preserves follicle morphology while also allowing for molecular analysis such as immunohistochemistry (Adeniran *et al.*, 2021). Future experiments could be performed using

this new fixative in addition to collecting spent culture medium for measurement of steroid hormones and/or markers for cell/tissue health such as lactate dehydrogenase. Although this study did not include stromal cell health as an outcome measure, during our analysis we observed that the stromal cells appeared pyknotic, particularly when compared to available images of fresh samples or cryopreserved xenotransplanted samples, which would have had time to recover and/or regenerate *in vivo*. We therefore developed an experiment to investigate whether the health of cryopreserved-thawed ovarian stroma could be improved. This experiment is described in the next chapter.

4.4.2 Conclusions

In conclusion, this work demonstrates that culture medium volume and composition can have a significant impact on follicle health. Culture in a low volume of αMEM resulted in significantly healthier follicles at all stages of development compared to our current culture method and all other conditions tested. This highlights the need to further optimise culture systems for ovarian tissue culture, particularly culture of cryopreserved ovarian tissue. Improving the health and early development of follicles *in vitro* is a key aspect of developing culture systems capable of supporting follicle development from the earliest stages to result in mature fertilisable eggs. Once developed, these methods could offer a significant number of individuals a chance of achieving pregnancy following cancer treatment. As culture in a low volume of αMEM resulted in the healthiest follicle population, our group's method of culture was changed accordingly and this culture method is used in the subsequent chapters.

Chapter 5

Effect of thawing and processing conditions on ovarian stromal cell death

5.1 Background

During the analysis described in the Chapter 4, we observed a considerable number of pyknotic stromal cells in both cultured and non-cultured tissue, indicating that the stromal cells of cryopreserved-thawed human ovarian tissue were unhealthy. Therefore, we questioned whether the health of the ovarian stroma was compromised during cryopreservation and thawing and what effect this might have on subsequent follicle development. While the effects of cryopreservation on the health and development of *in vitro* cultured follicles has been extensively studied, the ovarian stroma is seldom investigated, with only two studies including stromal cell morphology or density as an outcome measure in sheep (Faustino *et al.*, 2010; Oskam *et al.*, 2010) and goats (Faustino *et al.*, 2010).

The ovarian stroma consists of a variety of cell types and extracellular matrix, and follicle development is dependent upon bi-directional signalling between the follicles and surrounding stroma (Knight and Glister, 2006; Kinnear *et al.*, 2020). In addition, the theca cell layer originates, at least in part, from stromal cells and the ovarian stroma is therefore fundamental for follicle growth (Young and McNeilly, 2010; Rotgers *et al.*, 2018). The ovarian stroma can be damaged by processes such as cryopreservation and chemotherapy treatment, both of which have been shown to cause increased fibrosis in the tissue (Nisolle *et al.*, 2000; Meirow *et al.*, 2007; Gallardo *et al.*, 2018; Pampanini *et al.*, 2019). Fibrosis is characterised by the formation and deposition of excess fibrous connective tissue and matrix proteins such as collagen (Weiskirchen *et al.*, 2019).

The viability and functionality of cryopreserved-thawed human ovarian tissue has already been demonstrated through reports of live births following tissue transplantation (Jadoul *et al.*, 2017; Jensen *et al.*, 2017) and through xenotransplantation experiments, both by our group (Wei, 2018; unpublished) and others (Camboni *et al.*, 2008; Nottola *et al.*, 2008; David *et al.*, 2012). However, there is some evidence that the functionality of the tissue may be affected, such as the formation of theca cells (Amorim *et al.*, 2011). While the recovery and/or proliferation of stromal cells *in vivo* can be inferred from xenotransplantation and transplantation studies, the possibility remains that these cells may recover poorly *in vitro* due to the lack of blood supply and immune cells, however this has not yet been studied in humans.

Where the aim is to develop an *in vitro* system capable of supporting follicle growth from the earliest stages to result in a fully mature oocyte, the health of stromal cells is likely to be an important factor. Currently, the only studies that have achieved full follicle development *in vitro* used fresh human ovarian tissue (McLaughlin *et al.*, 2018; Xu *et al.*, 2021). However, if this method is to be used clinically for fertility preservation, it should be developed for both fresh and cryopreserved tissue to benefit those who have undergone ovarian tissue cryopreservation but are not able to have the tissue transplanted due to risk of malignancy. As follicle development is reliant on follicle-stromal interactions, a high proportion of compromised stromal cells may affect follicle development and health.

Several studies have utilised controlled-rate cryopreserved human ovarian tissue for research purposes, each with slightly varying thawing protocols (Hovatta *et al.*, 1996; Kim *et al.*, 2002; Schmidt *et al.*, 2005; Isachenko *et al.*, 2008; Fabbri *et al.*, 2010; Kedem *et al.*, 2011a; Anderson *et al.*, 2014). Thawing of controlled-rate cryopreserved tissue involves the removal of cryoprotectants, commonly using thawing solutions with a gradual reduction in concentration of the cryoprotectant. However, when reviewing the literature, we noted variation in the temperature of thawing solutions and workbench (ranging from 4°C to 37°C) and in the concentration of serum albumin agents (serum, serum substitute supplement or HSA). In some

cases the full details of the thawing protocol were lacking (Kim *et al.*, 2002; Kedem *et al.*, 2011a). Based on these observations, we sought to determine whether a change in medium and workbench temperature or HSA concentration in thawing and processing media could reduce the level of dead stromal cells. This was judged to be particularly relevant to future planned work investigating the effects of chemotherapy on human ovarian tissue *in vitro*, as starting with a baseline of healthy ovarian cells would be important to reduce the signal-to-noise ratio.

5.1.1 Chapter aims

The aim of this chapter was to determine whether different thawing protocols affected the health of cryopreserved human ovarian stromal cells. In particular, we investigated the effects of temperature of thawing and processing solutions and the concentration of albumin. We hypothesised that by keeping thawed tissue at a low temperature (a state of reduced metabolic activity) until it could be placed in a more supportive environment (i.e. *in vitro* culture) we could improve the health of cryopreserved-thawed ovarian stromal cells. The objectives of this chapter were:

- to determine whether processing temperature or albumin concentration affected collagen deposition (a measure of stromal fibrosis) within 24 h of thawing; and
- to determine whether processing temperature or albumin concentration affected stromal cell death (measured using the TUNEL assay) within 24 h of thawing.

Tissue was fixed at three different timepoints (after thawing, after processing and after 24 h culture) to assess whether the observed levels of damage to the tissue changed over this period and to ensure that any cells triggered to undergo apoptosis during thawing could be detected using the TUNEL assay.

5.2 Materials and methods

5.2.1 Patient details

The use of human tissue was approved by the Health Research Authority South Central – Oxford B Research Ethics Committee (REC reference 14/SC/0041). Samples from three patients were used in this study. Patient selection criteria included post-pubertal patients with no chromosomal abnormalities (e.g. Turners syndrome), haematological or gynaecological cancer and who had not received chemotherapy prior to OTC. Ovarian tissue was cryopreserved by the OCTB as described in Section 2.2.1.

5.2.2 Experimental design

A schematic overview of the experiment is presented in Figure 5-1. Four cortical strips from each patient were used in this study. Once the contents of the cryovial was thawed (see Section 5.2.4), each strip was placed in different experimental conditions as outlined in the figure. After thawing, each strip was processed into small pieces and cultured for up to 24 h. Prior to this experiment, our group performed thawing using pre-warmed solutions with 3 mg/mL HSA (Figure 5-1, grey box).

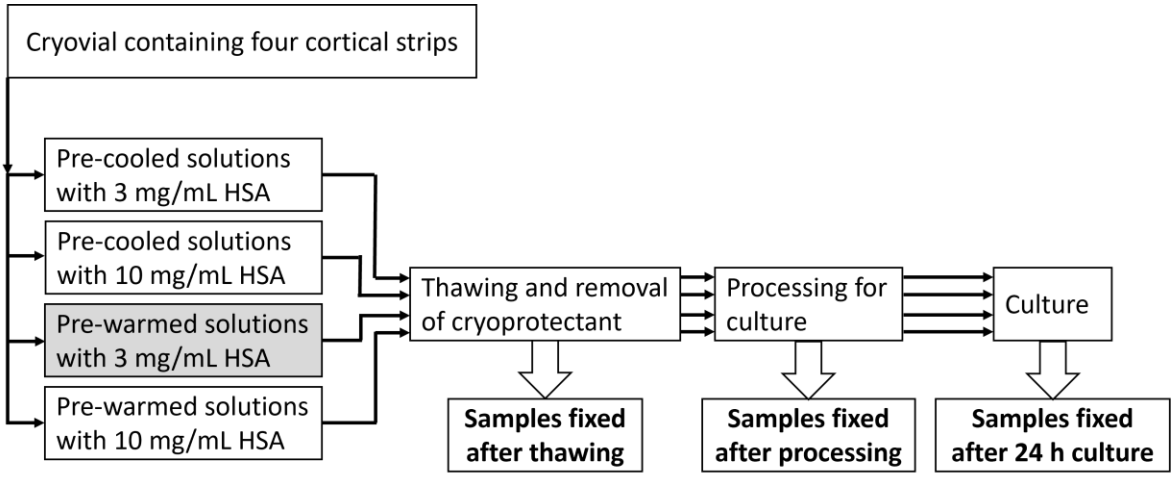

Figure 5-1. Diagram of experimental design investigating the effects of thawing and processing conditions on human ovarian stromal health. For each experimental repeat (one patient per repeat), a cryovial containing four cryopreserved cortical strips was used. Each strip was thawed according to one of four protocols: using pre-cooled (4°C) thawing and processing solutions on an ice block with either 3 or 10 mg/mL HSA or using pre-warmed (37°C) thawing and processing solution on a heated stage with either 3 or 10 mg/mL HSA. Strips were thawed in a reverse ethylene glycol gradient (see materials and methods). A portion of tissue from each group was fixed in Form-Acetic immediately after thawing. The remaining tissue was processed into small fragments for culture. A portion of tissue was fixed after processing and before culture and the remaining tissue was fixed after 24 h culture. The thawing protocol used by our group prior to this experiment is indicated in grey.

5.2.3 Chemicals and consumables

αMEM medium (22561021), L-glutamine (25030024) and ascorbic acid (10012011) were purchased from Thermo Fisher. Leibovitz L-15 medium (L5520), human serum albumin (AI653), ITS liquid media supplement (100x; I3145), sodium pyruvate (S8636), sucrose (S7903) and ethylene glycol (324558) were purchased from Sigma Aldrich.

5.2.4 Ovarian tissue thawing and processing

Cryovials containing four cortical strips were removed from liquid nitrogen, held at room temperature for one minute and immersed in a 37°C water bath for 3 minutes or until the cryoprotectant had just melted. Strips were immediately divided among the four experimental groups (Figure 5-1). Thawing solutions contained a reversed ethylene glycol gradient (1 M, 0.5 M and 0 M), 0.1 M sucrose and HSA (either 3 or 10 mg/mL, see Figure 5-1), in L-15 medium. Cryoprotectant was removed by washing the strips in each of the three thawing solutions for 5 min. Strips were then placed into dissection medium according to their experimental group and

cut into small pieces using scalpels. A portion of tissue was collected at this point and fixed in Form-Acetic (neutral buffered formalin with 5% acetic acid) for 24 h or snap-frozen in liquid nitrogen.

The remaining tissue in each of the four groups was processed into pieces <1 mm^3 in size for culture. Two individuals worked on the tissue processing (myself and fellow DPhil student Babatomisin Adeniran), each processing two experimental groups simultaneously (pre-cooled or pre-warmed groups). To control for individual variation, these groups were alternated during experimental repeats. Once all tissue had been processed into small pieces (2 h after thawing), tissue was either collected and fixed or snap-frozen as above or placed in culture. Tissue was cultured using the protocol optimised in Chapter 4 (see Section 2.4). Culture media consisted of αMEM supplemented with 1 mg/mL HSA, 100 U/mL penicillin, 100 µg/mL streptomycin, 2 mM L-glutamine, 10 µg/mL insulin, 5.5 µg/mL transferrin, 5 ng/mL selenium, 50 µg/mL ascorbic acid and 12.5 IU/L recombinant human FSH. Tissue pieces were cultured individually in 300 µl of culture medium in standard 24-well plates in a humidified environment at 37°C with 5% CO_2 in air. After 24 hours of culture tissue pieces were either fixed or snap-frozen as above. Culture media was collected and frozen at -80°C.

5.2.5 Histological processing and analysis

Fixed tissue samples were embedded in paraffin and sectioned at 5 µm (see Section 2.5). To ensure uniform assessment of each sample, every 9^{th} section was collected and stained with haematoxylin and eosin to assess tissue morphology, while every 10^{th} section was collected and stained using Masson's trichrome staining to visualise collagen and assess tissue fibrosis. See Sections 2.6.1-2.6.2 for details on staining protocols. Quantification of Masson's trichrome staining was performed as described in Section 2.6.4. For Masson's trichrome staining, the first, middle and last collected sections for each sample were analysed. Slides were imaged using a Leica DM2500 microscope and Micropublisher 6 camera.

5.2.6 TUNEL assay

TUNEL assay was performed using the ApopTag® *In Situ* Apoptosis Detection Kit (S7100, Millipore, UK) as described in Section 2.7.1. Samples with no TdT enzyme were used as a negative control, while formalin-fixed 3-week-old mouse ovarian sections (which will contain some atretic follicles) were used as a positive control. Slides were imaged using a Leica DM2500 microscope and Micropublisher 6 camera.

TUNEL signal was assessed as described in Section 2.9.4. Several high-power fields of view were obtained for each section (3-12 fields of view depending on section area). Each field was manually selected to encompass the region underneath the tunica albuginea where follicles are normally located. Follicles were excluded from the analysis and only stromal tissue was analysed.

5.2.7 Statistical analysis

All statistical analyses were performed using GraphPad Prism software (version 8). Data was first tested for normality using the Shaprio-Wilk test. A nested one-way ANOVA was used to investigate the difference between group means for both trichrome staining and TUNEL analysis. This considers the intra-patient variability by treating patient as a random effect. Tukey *post hoc* testing was used to correct for multiple comparisons. Data are presented as mean (± SD) and statistical significance was defined as $P < 0.05$.

5.3 Results

5.3.1 Patient characteristics

Ovarian tissue from four patients was collected for this study, however one patient sample was thawed incorrectly and therefore only samples from three patients could be analysed. These three patients were aged 23 ± 6.2 years (range 18-30) at the time of OTC. Patient diagnosis is presented in Table 5-1; none of the patients received chemotherapy prior to OTC. Ovarian tissue was cryopreserved within 4 h of procurement (2 h 15 min ± 55 min).

Table 5-1. Patient characteristics, including age at OCT, diagnosis and time from ovarian tissue procurement to cryopreservation.

Patient no.	Age at OTC	Diagnosis	Time from procurement to cryopreservation (h:m)
G	18	Hilar cholangiocarcinoma	2:05
H	21	Small round blue cell tumour of distal fibula	1:25
I	30	Medulloblastoma	3:15

5.3.2 Stromal fibrosis is not affected by thawing/processing conditions

Thawed tissue sections were stained using Masson's trichrome staining to assess stromal fibrosis. This resulted in staining of cell nuclei (blue-black), cytoplasm and smooth muscle (red) and collagen (blue; Figure 5-2A). The blue collagen-rich area was measured and all samples were found to have a large area of collagen, with 72.5% ± 6.5% to 78.6% ± 7.6% collagen area in tissue fixed immediately after thawing, depending on the thawing protocol used (Figure 5-2B). Thawing and processing conditions (solution temperature and HSA concentrations) did not affect collagen area as assessed after thawing, processing or after 24 h culture (Figure 5-2B-D).

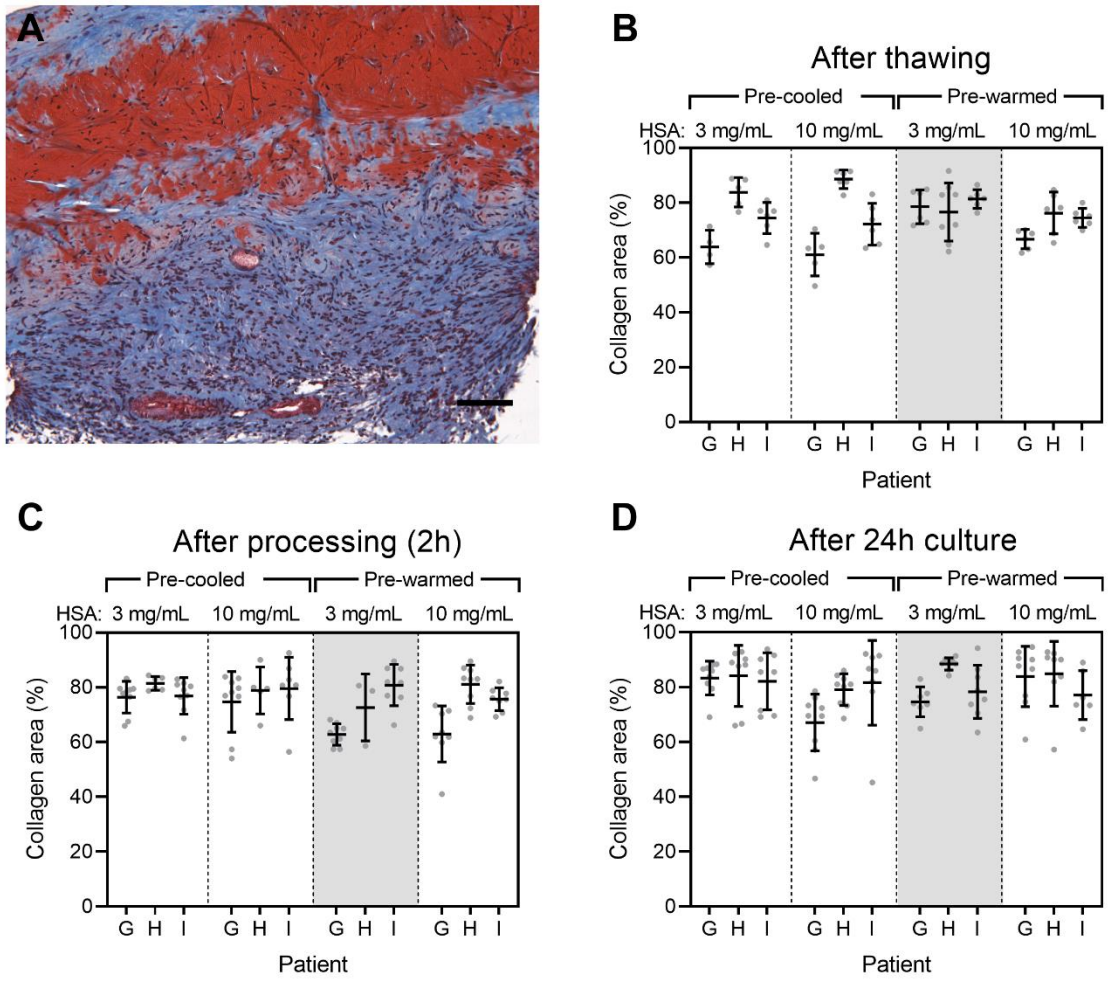

Figure 5-2. Effect of thawing protocol on ovarian stromal fibrosis. (A) Representative image of cryopreserved-thawed ovarian tissue following Masson's trichrome staining. Collagen area is stained blue, cytoplasm or smooth muscle red and nuclei black. Scale bar: 100 µm. **(B-D)** Cryopreserved ovarian tissue from three patients was thawed using either pre-cooled or pre-warmed thawing and dissection solutions, each supplemented with either 3 or 10 mg/mL HSA. Proportion of collagen area was measured in tissue fixed immediately after thawing (B), after processing (C) and after 24 h culture (D). Each data point (grey dot) represents the measurement of a single section evenly distributed through the tissue. The thawing protocol used by our group prior to this experiment is indicated in grey. There was no difference in collagen area between the different thawing protocols tested at any of the three time points.

5.3.3 Stromal cell death cannot be reduced by altering medium temperature or HSA concentration

Stromal cell viability was measured using TUNEL labelling to detect double-stranded DNA breaks, indicated by brown nuclei and indicative of irreparable damage and cell death (Figure 5-3A).

TUNEL-positive stromal cells were detected both at the edges and within the tissue, however there appeared to be more TUNEL-positive cells at the tissue edge.

Immediately following thawing, over one-third of ovarian stromal cells were TUNEL-positive (33.1% ± 10.8% to 41.1% ± 11.6% depending on thawing condition; Figure 5-3B). After processing, there was a significantly lower proportion of TUNEL-positive cells in tissue thawed in pre-warmed solutions with 3 mg/mL HSA (23.1% ± 6.7%, our groups current protocol) compared to tissue thawed in pre-cooled solutions with 3 mg/mL (40.0% ± 12.6%, $P<0.05$) or 10 mg/mL HSA (37.2% ± 11.6%, $P<0.05$, Figure 5-3C).

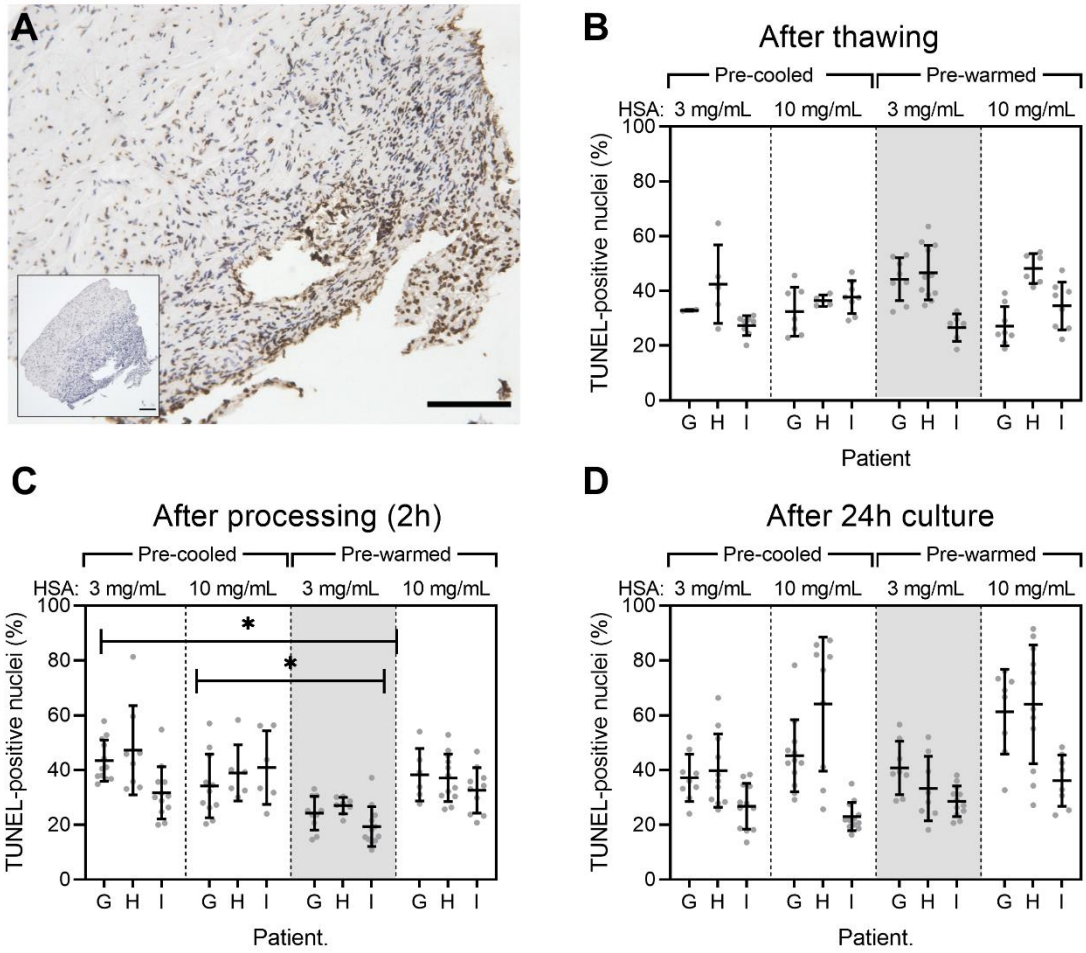

Figure 5-3. Effect of thawing protocol on ovarian stromal cell death. (A) Representative image of TUNEL-labelled cryopreserved-thawed human ovarian tissue. TUNEL-positive cells were visualised using DAB (brown nuclei) while negative cells were stained blue following haematoxylin counterstaining. Small inset shows representative negative control. Scale bar: 100 µm. **(B-D)** Cryopreserved ovarian tissue from three patients was thawed using either pre-cooled or pre-warmed thawing and dissection solutions, each supplemented with either 3 or 10 mg/mL HSA. Proportion of TUNEL-positive cells was measured in tissue fixed immediately after thawing (B), after processing (C) and after 24 h culture (D). Each dot represents the proportion of TUNEL-positive cells in each high-power field (40x magnification). The thawing protocol used by our group prior to this experiment is indicated in grey. There was a significantly lower proportion of TUNEL positive cells in tissue thawed using pre-warmed solutions with 3 mg/mL HSA compared to pre-cooled solutions with either 3 or 10 mg/mL HSA after processing (*: $P<0.05$).

5.4 Discussion

After observing a high level of stromal cell death in cryopreserved-thawed ovarian tissue, we sought to investigate whether this could be reduced by altering our group's thawing protocol. We hypothesised that keeping tissue at a low temperature prior to placing it in culture would reduce stromal cell damage. We thawed cortical strips from four patients in pre-cooled or pre-warmed solutions with either 3 or 10 mg/mL HSA, however only data from three patients was analysed owing to an experimental error with the fourth patient. Tissue was fixed immediately after thawing, after processing for culture and after 24 h culture. Stromal fibrosis was assessed using Masson's trichrome staining to measure collagen area and cell death was measured using the TUNEL assay. We found no difference in stromal fibrosis (collagen area) between any of the conditions tested at any of the three time points. Similarly, cell death was largely unaffected by thawing and processing conditions. There was a 14-17% lower proportion of dead stromal cells in tissue thawed in pre-warmed medium with 3 mg/mL HSA (our current protocol) compared to pre-cooled solutions after 2 h of processing, however this difference was not observed after 24 h culture.

Follicle health was not an outcome measure for this study, as we focused on ovarian stromal health. Interactions between the oocyte and follicular somatic cells (granulosa and theca) during follicle development are well recognised (Gilchrist *et al.*, 2004), but the role of ovarian stromal cells is no less important (Knight and Glister, 2006). Ovarian stromal cells have been demonstrated to be damaged by ovarian tissue cryopreservation, with increased oedema and reduced cellular density (Oskam *et al.*, 2010). Damage to the ovarian stroma caused by cryopreservation may also compromise subsequent theca cell development, indicated by reports of decreased theca layer thickness following grafting of cryopreserved tissue (Amorim *et al.*, 2011). Theca cells provide androgens to the developing follicle for conversion into oestrogens by the granulosa cells and are therefore critical for follicle development (Young and McNeilly, 2010).

We did not observe any differences in collagen area between the four thawing protocols after thawing, processing or 24 h culture. Stromal fibrosis, characterised by increased collagen deposits and decreased cell density, has previously been shown to be increased in cryopreserved human ovarian tissue (Nisolle *et al.*, 2000; Gallardo *et al.*, 2018). Our results indicate that thawing does not cause additional collagen deposits and that fibrosis is likely a result of the cryopreservation itself, rather than thawing. However, this cannot be confirmed from our data as patient-matched fresh tissue was not available. It is also possible that the thawing conditions tested in this chapter were not sufficient to induce a change in fibrosis in the tissue. Vitrification has been demonstrated to better preserve the ovarian stroma, maintaining cell and membrane integrity, whereas after controlled-rate cryopreservation, stromal cells showed signs of pyknosis and ruptured cell membranes (Keros *et al.*, 2009). While controlled-rate freezing remains the gold standard cryopreservation method for ovarian tissue, vitrification may in time become more common once optimal protocols are developed, as has proven to be the case for oocyte and embryo cryopreservation.

We observed reduced levels of TUNEL-positive ovarian stromal cells after processing tissue for culture using pre-warmed thawing and dissection solutions with 3 mg/mL HSA. Reassuringly, this is the protocol used by our group prior to this study. This difference did not translate to reduced TUNEL-positive cells after 24 h culture, therefore we conclude that stromal cell death could not be reduced by the thawing protocols tested here. Interestingly, tissue thawed in solutions with 10 mg/mL HSA had the highest proportion of dead stromal cells after 24 h culture (42.3 ± 22.3% and 55.5 ± 20.7% for pre-cooled and pre-warmed respectively) compared to 3 mg/mL (34.2 ± 11.7% and 33.4 ± 10.0% for pre-cooled and pre-warmed respectively), although this difference was not significant, perhaps due to the low sample number.

Albumin is an essential component of culture media due to its protein-stabilising and antioxidant properties. However, there are some indications that high concentrations of albumin may cause cell death in certain cell types such as renal cells (Ohse *et al.*, 2006; Okamura *et al.*, 2013), although

there are no studies reporting this effect in ovarian stromal cells. Ten mg/mL HSA is commonly used for thawing human ovarian tissue in the literature (Hovatta *et al.*, 1996; Fabbri *et al.*, 2010; Sheikhi *et al.*, 2013), however during culture, ovarian tissue is supplemented with only 1 mg/mL HSA, as in the present study (McLaughlin *et al.*, 2018; Lopes *et al.*, 2020; Bjarkadottir *et al.*, 2021).

A major limiting factor to this study is the low sample number. Ovarian tissue is a limited resource and therefore samples from only four patients were used in this study, though unfortunately only three could be analysed. We planned to increase the sample size if the results suggested that stromal cell health could be altered by thawing. We also collected culture medium for potential steroidal assays as well as snap-freezing a portion of tissue for gene expression or protein analysis. However, considering the results reported above, we did not feel this avenue was worth further investigation, as there was no indication that stromal cell death could be reduced in any of the different regimens tested.

In conclusion, we found that our existing thawing protocol performed best overall and that we were unable to reduce the level of ovarian stromal cell death by altering temperature or albumin concentrations during thawing and processing for culture. As future experiments were planned to assess damage caused by chemotherapeutic agents, it is necessary to have a low baseline of damaged cells at the start of culture, to reduce the signal-to-noise ratio. Based on the results of this chapter I therefore decided to use fresh ovarian tissue instead of cryopreserved for my remaining experiments.

Chapter 6

Development of a whole-mount immunolabelling and tissue clearing method for three-dimensional visualisation of follicles in human ovarian tissue

6.1 Background

As discussed in Chapter 1.2, the ovary is a heterogeneous organ consisting of several different elements including follicles, blood vessels and stroma. Furthermore, follicles themselves are dynamic structures that contain an oocyte surrounded by somatic cells and are often considered as individual units. Therefore, methods that do not destroy the follicle's structure, such as histology or laser-capture microdissection, may be more appropriate for analysing follicles compared to methods that analyse cell digests or tissue lysates (see Section 1.3.3 for further details).

Histology and immunohistochemistry (IHC) are commonly used to analyse ovarian tissue. These methods routinely involve preparing thin tissue sections, usually 5 μm thickness, which can be stained or immunolabelled and visualised under a microscope. However, as follicles are three-dimensional structures ranging in size in humans from ~40 μm (primordial follicles) to over 18 mm (pre-ovulatory follicles; Griffin *et al.*, 2006), a single 5-μm thick section cannot contain an entire follicle. Despite this limitation, it is standard practice to analyse only a single cross-section of each follicle in which the oocyte nucleus is clearly visible, this is also generally the largest follicle cross-section. Although this approach is less time-consuming than analysing every section for each follicle it can lead to two types of errors (Figure 6-1). First, although the oocyte is included in the analysis of a single cross section, any granulosa cells not contained within the section are left out from analysis (Figure 6-1A). This may lead to follicles being incorrectly

classified as, for example, atretic or growing based on the presence or absence of pyknotic or mitotic granulosa cells (Uslu *et al.*, 2017). Second, follicles may be staged incorrectly due to the angle at which the tissue was sectioned and the orientation of the follicle within the piece of tissue, which cannot be controlled for. This is particularly important where the aim is to distinguish primordial follicles from transitional follicles as theoretically, a follicle that is surrounded by flattened pre-granulosa cells in the analysed cross-section (and is therefore classified as primordial) may in fact contain cuboidal cells at the opposite poles that would have been visible if the follicle had been sectioned at a different angle (Figure 6-1B). Accurate distinction between primordial and transitional follicles is particularly important with regards to understanding the effects of chemotherapy drugs on follicles to know whether primordial (quiescent) and transitional (activated) follicles are affected at the same rate or by the same mechanisms.

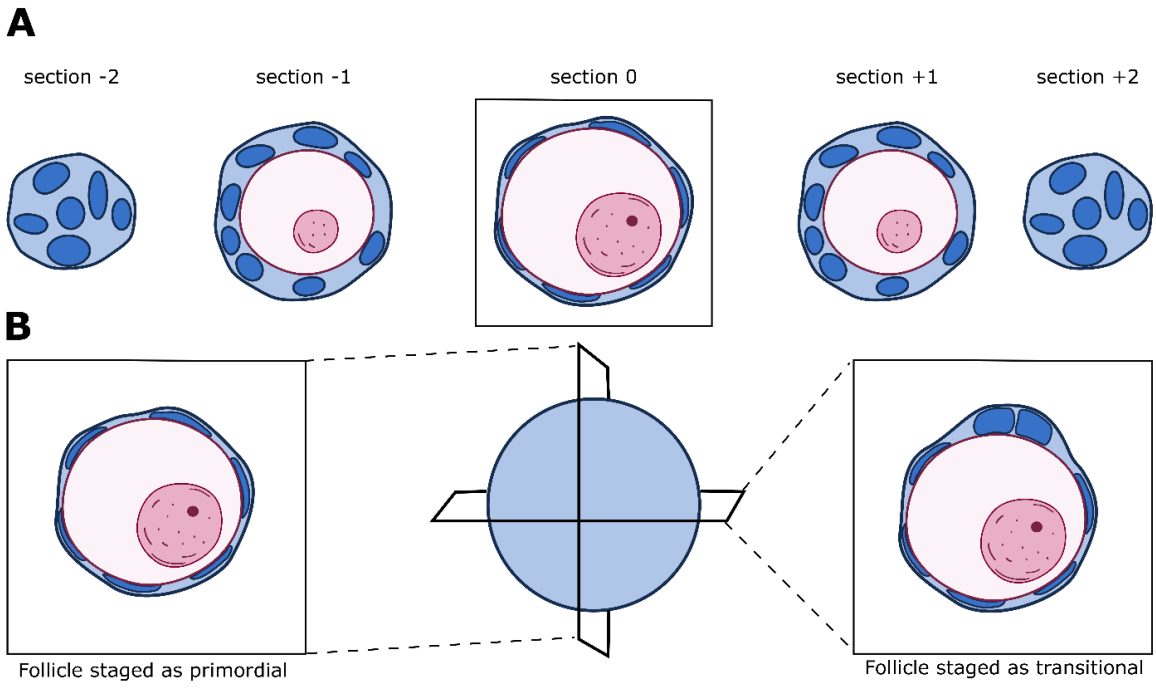

Figure 6-1 Limitations of standard histological follicle analysis. Traditionally, follicles are analysed using histology where the largest cross-section of a follicle is analysed. This can lead to two types of errors. **(A)** Diagram of serial sections through a primordial follicle. Only the largest cross-section containing the oocyte nucleus (outlined) is analysed, leading to loss of information as the pre-granulosa cells contained in the neighbouring sections are disregarded. **(B)** When embedded ovarian tissue is sectioned it is not possible to control at which angle the follicle is sectioned. When distinguishing between primordial and transitional follicles this could lead to a follicle being misclassified.

Being able to image follicles within ovarian tissue fragments while keeping the sample intact would allow for more detailed and accurate follicle analysis. This can be achieved using 'optical sectioning', which enables imaging at different focal planes in the z-plane and can be achieved using confocal microscopy (Conchello and Lichtman, 2005). This would also reduce workload as sectioning of paraffin-embedded tissue would not be required and imaging would be more rapid as sections would not have to be imaged individually. However, imaging of whole tissue samples is limited by factors such as light scattering within the tissue, which occurs as light is repeatedly reflected off cells and cellular structures and is also what gives tissue its milky translucent appearance (Richardson and Lichtman, 2015). This scattering is partly due to the mismatch in refractive index between the sample and the immersion medium. The refractive index describes how fast light travels through a material. For example, air has a refractive index of 1.00, water 1.33 and typical immersion oil used for imaging 1.51. A mismatch in refractive index between two samples causes light to bend as it passes through the material, as can be observed when light gets refracted when moving through a glass of water, causing an object (such as a straw) to appear bent.

Tissue clearing techniques have been developed to allow imaging at greater z-depths. Tissue clearing works by altering the sample's refractive index to match with that of the immersion medium and can be broadly classified as solvent-based clearing and aqueous-based clearing (by simple immersion, hyperhydration or hydrogel embedding; Richardson and Lichtman, 2015). These methods each have their own benefits and shortfalls, and the appropriate method should be selected based on the tissue type and applications, for example whether immunolabelling is required or if the tissue expresses fluorescent proteins (for example using transgenic mice). Solvent-based tissue clearing involves tissue dehydration to remove water and some lipids, followed by immersion in a clearing agent such as benzyl benzoate, which alters the sample's refractive index to match that of the immersion medium (Richardson and Lichtman, 2015).

Tissue clearing methods have been used on mammalian reproductive organs such as placenta (human and non-human primate; Merz *et al.*, 2018; Sargent *et al.*, 2018) and ovary (mouse; Faire

et al., 2015; Feng *et al.*, 2017; Kagami *et al.*, 2018; Rinaldi *et al.*, 2018; McKey *et al.*, 2020; Tong *et al.*, 2020). At the time of writing there have been no reports of tissue clearing of human ovarian tissue or ovarian tissue from non-rodent mammals.

6.1.1 Chapter aims

The aim of this chapter was to develop a technique to analyse human ovarian tissue that would enable accurate distinction between primordial and transitional follicles and allow visualisation of intact pre-antral follicles. The main purpose of developing this technique was to determine whether primordial follicles are damaged by chemotherapy agents. Thus, this method would need to fulfil three criteria. First, it needed to support analysis of intact follicles, including all granulosa cells; second it needed to allow primordial follicles to be accurately distinguished from transitional; and finally it needed to allow for detection of damage to follicles and ovarian tissue. Therefore, the development of this method could be broken down into three aims:

(i) Identify and validate a strategy to label follicles using molecular markers to allow identification of primordial follicles;

(ii) Develop a method of whole-mount immunolabelling and imaging of human ovarian tissue fragments to allow visualisation of intact pre-antral follicles;

(iii) Determine whether the developed technique is compatible with techniques to detect follicle damage.

The objective for each of the aims is as follows:

For Aim i:

- to perform a literature search to identify known molecular markers of follicle activation and/or early development that could be visualised using immunohistochemistry to distinguish between primordial and activated follicles, and
- to perform immunohistochemistry on the selected markers to validate their localisation in human primordial follicles.

For Aim ii:

- to determine whether the Visikol® HISTO™ tissue clearing kit could be used to optically clear human ovarian tissue and allow imaging of intact primordial follicles; and
- to determine the optimal protocol for whole-mount immunolabelling of human ovarian tissue prior to tissue clearing, by comparing different incubation times, temperatures and antibody concentrations.

For Aim iii:

- to investigate whether whole-mount TUNEL-labelling and tissue clearing could be performed using a commercially available TUNEL kit with fluorescent detection

6.2 Materials and methods

6.2.1 Tissue samples

Mouse ovaries were used as positive controls when validating some antibodies for human ovarian tissue. Formalin-fixed mouse ovarian tissue from three-week-old *T-syn*$^{F/F}$:ZP3*Cre* females with a C57BL/6 background were used as positive controls for detection of Smad proteins and FOXO3. These mice have an oocyte-specific deletion of core 1 β1,3-galactosyltransferase 1 (T-synthase), which initiates the synthesis of core-1-derived O-glycans. These mice were considered to be suitable controls as oocyte-specific deletion of *T-syn* does not negatively affect fertility (Williams *et al.*, 2007).

Human ovarian tissue was used to validate and optimise immunohistochemistry protocols and to develop a whole-mount immunolabelling and tissue clearing protocol. These human ovarian tissue samples were either surplus fresh or cryopreserved non-cultured tissue fragments also used in prior experiments. Cryopreserved samples were thawed as described in Section 2.2.2. When these experiments took place our group was developing a new fixative (see Adeniran *et al.*, 2021) and therefore IHC was performed on samples fixed either in neutral buffered formalin or form-acetic (0.1-5% acetic acid in formalin). Fixed tissue fragments were used for whole-mount

immunolabelling and tissue clearing, while paraffin-embedded tissue sections were used for immunohistochemistry. See Chapter 2.5 for details on histological processing. Patient details are presented in Table 6-1.

Table 6-1 Details on patient samples used for immunohistochemistry experiments.

Patient	Age	Diagnosis	Type	Fixative
A	13 years	Ewing's sarcoma	Frozen	Formalin, 0.1-5% Form-acetic
C	13 weeks	Type 1 spinal muscular atrophy	Fresh	Formalin, 5% form-acetic
G	18 years	Hilar cholangiocarcinoma	Frozen	Formalin, 5% form-acetic
L	15 years	Bone tumour	Frozen	Formalin
M	10 years	Severe congenital neutropenia	Frozen	Formalin
N	6 years	Sickle cell disease	Frozen	Formalin
O	12 years	Aplastic anaemia	Frozen	Formalin

6.2.2 Immunohistochemistry

Immunohistochemistry was performed as described in Section 2.7.2. Each antibody was tested on multiple human patient samples and immunohistochemistry was performed at least twice for each antibody. During optimisation of monoclonal mouse anti-FOXO3 (#12829, Cell Signaling Technology) the supplier's recommended protocol (protocol A) was tested and compared to the group's standard protocol (protocol B). These protocols differed with regards to the washing buffer, blocking solution and antibody dilutant (see Table 6-2).

Table 6-2 Comparison between different immunohistochemistry protocols. Protocol A was recommended by an antibody supplier (Cell Signaling Technology), while Protocol B was the group's standard IHC protocol. TBS: Tris-buffered saline, PBS: phosphate-buffered saline, NGS: normal goat serum.

	Protocol A	Protocol B
Washing	TBS with 0.1% Tween-20 (TBST)	PBS with 0.1% Triton-X100 (PBST)
Blocking solution	5% NGS in TBST	20% NGS in PBST
Antibody dilutant	5% NGS in TBST	10% NGS in PBST

Details of primary antibodies used in this chapter are presented in Table 6-3. Negative controls were prepared by either omitting the primary antibody or by using immunoglobulins (IgG or IgM) matching the primary antibody at the same concentration (isotype control). Alexa Fluor 488

Phalloidin (A12379, Life Technologies, UK) was used to detect F-actin. Secondary antibodies targeted the host species for the primary antibody (or isotype control); information on secondary antibodies is presented in Table 6-4. Signal detection was achieved by using either colorimetric or fluorescence detection with signal amplification where appropriate (Section 2.7.2). Nuclear counterstaining was performed with either haematoxylin (colorimetric detection) or 5 µg/mL DAPI (fluorescent detection).

Table 6-3 Information on primary antibodies used in this chapter. Information on primary antibodies, including clone information where available, is present along with host species and whether the antibody is monoclonal (mAb) or polyclonal (pAb). The stock concentration is provided, along with the dilution range tested and patient samples that were labelled.

Target	Cat no.	Supplier	Host	Stock conc.	Dilution	Patient[fixative]
Beta-catenin, clone 12F7	Ab22656	Abcam	Mouse mAb	1 mg/mL	1:200-1:1000	$A^{NBF,FA}$, G^{FA}, L^{NBF}, O^{NBF}
DDX4	Ab13840	Abcam	Rabbit pAb	1 mg/mL	1:100-1:500	$A^{NBF,FA}$, $C^{NBF,FA}$, G^{FA}, L^{NBF}
DDX4, clone 2F9H5	SAB5300115	Sigma	Mouse mAb	Not available	1:200	A^{NBF}, G^{FA}, L^{NBF}
FOXO3	#2497	Cell Signaling Technology	Rabbit mAb	15 µg/mL	1:100	N^{NBF}, O^{NBF}
FOXO3	#12829	Cell Signaling Technology	Rabbit mAb	131.0 µg/mL	1:50-1:3000	$A^{NBF,FA}$, G^{FA}, L^{NBF}, M^{NBF}, N^{NBF}, O^{NBF}
Laminin-alpha	Ab11575	Abcam	Rabbit pAb	0.7 mg/mL	1:100-1:200	$A^{NBF,FA}$, G^{FA}, L^{NBF}, $C^{NBF,FA}$
Laminin-alpha	L9393	Sigma	Rabbit pAb	0.5 mg/mL	1:50-1:100	G^{FA}, L^{NBF}
Laminin gamma-1, clone A5	MA514649	Life Technologies	Rat mAb	0.2 mg/mL	1:100	A^{FA}, C^{FA}, G^{FA}, L^{NBF}
Smad1, clone A4	Sc-7965	Santa Cruz	Mouse mAb	0.2 mg/mL	1:50-1:200	A^{FA}, M^{NBF},
Smad1/5/8	Ab66737[a]	Abcam	Rabbit mAb	1 mg/mL	1:100-1:1000	A^{FA}, C^{FA}, M^{NBF}
Smad2/3	Sc-133098	Santa Cruz	Mouse mAb	0.2 mg/mL	1:50-1:1600	A^{FA}, C^{FA}, G^{FA}, M^{NBF}, N^{NBF}, O^{NBF}

[a]: Antibody is now discontinued but was available when experiments were performed.
NBF: sample fixed in neutral buffered formalin.
FA: sample fixed in form-acetic.

Table 6-4 Information on secondary antibodies used in this chapter.

Antibody	Supplier	Catalogue no.	Conjugate	Detection
Anti-rabbit IgG, raised in goat	Vector Laboratories	BA-1000	Biotin	Colorimetric[a] Fluorescence[b]
Anti-mouse IgG, raised in goat	Life Technologies	A11001	Alexa Fluor 488	Fluorescence
Anti-mouse IgG, raised in goat or donkey	Life Technologies	A11004 and A10037	Alexa Fluor 568	Fluorescence
Anti-rabbit IgG, raised in goat or donkey	Life Technologies	A11008 and A32790	Alexa Fluor 488	Fluorescence
Anti-rat IgG, raised in goat	Life Technologies	A11006	Alexa Fluor 488	Fluorescence

[a]: Signal amplification performed using avidin-peroxidase complex. Detection performed using DAB.
[b]: Signal amplification and detection performed using Streptavidin Alexa Fluor 568 conjugate (S11226, Life Technologies).

6.2.3 Whole-mount immunolabelling and tissue clearing

Whole-mount immunolabelling and tissue clearing was performed using a commercially available tissue clearing kit using Visikol® HISTO™ tissue clearing technology (Tissue Clearing Kit, ab243298, Abcam). The final optimised protocol for whole-mount immunolabelling and tissue clearing of human ovarian tissue fragments is described in Section 2.8. For initial trials, immunolabelling and tissue clearing were performed according to the supplier's protocol for 500 µm-thick samples, with slight modification. Washing and permeabilization was performed in 2 mL microcentrifuge tubes with 1.8 mL solution. All incubation steps were performed at RT with gentle agitation unless otherwise indicated. Fixed tissue fragments were first washed in PBS and then permeabilised in DMSO and methanol (Table 6-5). Samples were then incubated in a penetration buffer (PBS with 0.2% TritonX-100, 0.3 M glycine and 20% DMSO) for 1 h. Samples were transferred to 400 µL blocking solution (PBS with 0.2% TritonX-100, 6% donkey serum and 10% DMSO) and incubated for 3 h at 37°C with gentle agitation. Following blocking, samples were

transferred to the required primary antibody, diluted in antibody buffer (PBS with 0.2% Tween, heparin, 3% donkey serum and 5% DMSO, total volume 400 µL) and incubated for 3 h at 37°C with gentle agitation. This was followed by washing five times for 40 min in washing buffer (PBS with 0.2% Tween and heparin), after which samples were transferred to 400 µL secondary antibody solution (secondary antibody at 1:200 with 5 µg/mL DAPI in antibody buffer). Samples were incubated for 3 h at 37°C with gentle agitation, protected from light.

Immunolabelled samples were washed 10 times for 10 min each, at 37°C with gentle agitation, protected from light. Samples were then dehydrated by washing in 50% methanol/PBS, 80% methanol and 100% methanol for 16 min each. Samples were removed from methanol and carefully dried (using lens paper and allowing the methanol to evaporate) before being transferred to a glass embryodish containing 1 mL Tissue Clearing Reagent 1 (refractive index of 1.50) and incubated for one hour at RT with gentle agitation. Samples were mounted in a prepared silicone isolator (approx. 20 mm diameter, 0.5 mm deep, see Figure 6-12 in results) on a glass slide filled with Tissue Clearing Reagent 2 (refractive index 1.50). Samples were placed in the middle of the well and sealed with a square coverslip (22 x 22 mm, #1.5). Samples were stored at 4°C away from light before imaging. Samples were imaged using a confocal microscope to obtain z-stacks spanning the entire depth of the tissue, see Section 2.9.3 for confocal imaging information. Tissue clearing could be reversed by incubating cleared samples in 100% ethanol at RT until sample opacity was restored. Samples could then be processed for histology as described in Section 2.5.

Table 6-5 Washing and permeabilization protocol for initial testing of whole-mount immunohistochemistry and tissue clearing, following the supplier's protocol.

Step	Chemical	Duration
Dehydration	PBS	16 min
	PBS	16 min
	50% methanol/PBS	16 min
	80% methanol	16 min
	100% methanol	16 min
Permeabilisation	20% DMSO/methanol	16 min
Rehydration	80% methanol	16 min
	50% methanol/PBS	16 min
	PBS	16 min
	0.2% TritonX-100 in PBS	16 min

Several aspects of this protocol were optimised, in particular antibody incubation duration. The ideal incubation temperature for antibody incubation was determined by comparing incubation at 4°C, RT or 37°C, all with gentle agitation. Additional incubation in permeabilization buffer (supplied in tissue clearing kit) overnight at RT prior to immunolabelling was tested. Different antibody incubation times were also tested for both primary and secondary antibodies, ranging from 3 h (suggested by supplier) to seven days. Primary antibody concentration had to be optimised for each antibody. Secondary antibody concentration was increased from 1:200 dilution to 1:100 dilution to improve signal detection.

Optimisation was also required following immunolabelling to improve signal detection. Two additional washes in 100% methanol were added to ensure complete dehydration of the sample prior to clearing. After clearing, samples were mounted onto glass coverslips (22 x 50 mm, #1.5), instead of glass slides, to enable imaging from both sides. In addition, samples were mounted in a thinner imaging chamber (0.25 mm instead of 0.5 mm) to ensure that the working distance of

the objectives was not exceeded. Finally, correction factors were used during imaging by increasing gain with increased z-depth, except in experiments where signal strength across the z plane was being assessed.

6.2.4 Whole-mount TUNEL assay

The potential use of the TUNEL assay for whole fixed human ovarian tissue fragments was explored as no current protocol for this application exists. TUNEL was performed using the Click-iT Plus TUNEL Assay 594 (C10618, Life Technologies). For the first trial, the supplier's standard protocol was followed, though reagent volumes were increased to adapt the protocol for whole-mount labelling. Samples were first washed and permeabilised using the same protocol as for whole-mount immunolabelling as described above. Antigen retrieval was performed by heating samples to 90°C in 10 mM sodium citrate, pH 6 for 20 min. Samples were washed in PBS and incubated in TdT reaction buffer for 10 min at 37°C before incubation in TdT reaction mixture for 1 h at 37°C, with gentle agitation. Samples were washed with 3% BSA and 0.1% TritonX-100 in PBS for 15 min and rinsed in PBS before being transferred to the Click-iT Plus TUNEL reaction cocktail, with 5 μg/mL DAPI. Samples were incubated in the Click-iT solution for 30 min at 37°C. Samples were washed in 3% BSA in PBS for 15 min and rinsed in PBS before being dehydrated and cleared as described above.

Positive controls were generated to assess penetration of the TUNEL kit components. Samples were incubated in 1 unit DNase I diluted into 1x DNase reaction buffer (18068-016, Thermo Fisher) overnight at RT. Samples were then washed three times in PBST for 15 min each before the TUNEL assay was performed as described above.

Optimisation of the TUNEL protocol for whole-mount labelling involved increasing incubation times in the reaction buffers. TdT incubation was increased from 1 h to 2 h, 4 h or 24 h, all at 37°C with gentle agitation. Similarly, Click-iT reaction times were increased from 30 min to 1 h, 2 h or 20 h. Incubation in 5 μg/mL DAPI was increased from 30 min to overnight.

The effect of sample permeabilization was also investigated by incubating samples in a permeabilization solution (0.2%, 2% or 10% TritonX-100 with 20% DMSO) overnight at RT before TUNEL labelling. In addition, 10% DMSO was added to TdT and Click-iT solutions in an effort to improve reagent penetration. Incubation in the TdT solution was increased to 24 h or six days and incubation in the Click-iT solution performed overnight or for seven days. In addition, DAPI concentration was increased to 10 μg/mL. Other efforts to improve tissue permeabilization and reagent penetration included incubation in permeabilization buffer (tissue clearing kit component) and sonication (twice for 20s) with the DNase I and TdT solution.

6.2.5 Imaging and analysis

Imaging and post-processing were performed as described in Chapter 2.9. FOXO3 signal was quantified as described in Section 2.9.5. Briefly, intensity measurements were performed using ImageJ Fiji using the freehand selection tool to select the areas of interest (oocyte nucleus and oocyte cytoplasm). The nuclear/cytoplasmic FOXO3 signal ration was then calculated for each follicle.

Three-dimensional modelling of follicles was performed in Imaris using the Surface function. Areas of interest (follicle basement membrane, oocyte and (pre-)granulosa cell nuclei) were outlined manually for each z-layer and a three-dimensional surface model constructed.

6.2.6 Statistical analysis

To assess the relationship between nuclear/cytoplasmic FOXO3 signal and follicle stage, a non-parametric Kruskal-Wallis test with Dunn's post-hoc testing was used. The mean nuclear/cytoplasmic FOXO3 signal for primordial follicles was compared to the mean signal for other follicle stages and negative controls. A non-linear regression following a one phase decay curve was fitted to the data to determine whether nuclear FOXO3 signal decreased with an increased proportion of cuboidal granulosa cells. Data are presented as mean (± SD or 95% CI), unless otherwise stated, and statistical significance was defined as $P < 0.05$.

6.3 Results

6.3.1 Identification of primordial follicles using molecular markers

The first aim of this chapter was to develop a method that would allow both identification of primordial follicles and differentiation between primordial and transitional follicles. I planned to label human ovarian tissue with FOXO3 and Smad2/3, using the localisation pattern of FOXO3 in oocytes to first rule out activated follicles from analysis and then using Smad2/3 localisation in (pre-)granulosa cells in the remaining follicles to identify primordial follicles. However, as these proteins had been predominantly studied in murine models, with no published reports of Smad2/3 detection in human ovarian follicles, I first set out to validate the presence of these markers in human ovarian tissue and determine their suitability to identify primordial follicles.

6.3.1.1 FOXO3

FOXO3 is a transcription factor involved in maintaining primordial follicle quiescence (see Section 1.4.1). During follicle activation, FOXO3 is translocated from the oocyte nucleus into the cytoplasm, a process that has been demonstrated in mouse, bovine and human ovaries (Liu *et al.*, 2007; Bao *et al.*, 2011; McLaughlin *et al.*, 2014). In order to detect FOXO3 in human ovarian tissue I first tested a monoclonal rabbit anti-FOXO3 antibody (#2497, Cell Signaling Technology), which has previously been used to detect FOXO3 in mouse ovaries (Hardy *et al.*, 2018). A faint positive FOXO3 signal was observed in mouse ovaries (used as a positive control), while no signal was observed in human ovarian tissue (Figure 6-2A). Different antigen retrieval protocols did not improve the signal (data not shown). According to the supplier, this antibody is not recommended for IHC and therefore no further attempts were made to optimise labelling using this particular antibody.

An alternative antibody, monoclonal rabbit anti-FOXO3 (#12829, Cell Signaling Technology) was tested on mouse ovaries (formalin-fixed) and human ovarian tissue (formalin and form-acetic-fixed, patient-matched), following the supplier's recommended protocol (protocol A). Signal was observed in mouse and formalin-fixed human ovarian tissue, but not in form-acetic-fixed human

ovarian tissue (Figure 6-2B). I repeated the experiment using a modified protocol (protocol B, see Table 6-2 for comparison), however these changes had no effect on FOXO3 labelling (Figure 6-2C), and form-acetic-fixed samples remained negative for FOXO3. As form-acetic better preserves follicle morphology compared to formalin, I tried to further optimise FOXO3 labelling for form-acetic fixed samples by comparing different antigen retrieval protocols (Figure 6-3). Twenty-minute heat-induced retrieval in 10 mM sodium citrate was the only condition that resulted in FOXO3 signal, compared to the isotype control. However, this signal was low compared to that observed in formalin-fixed samples.

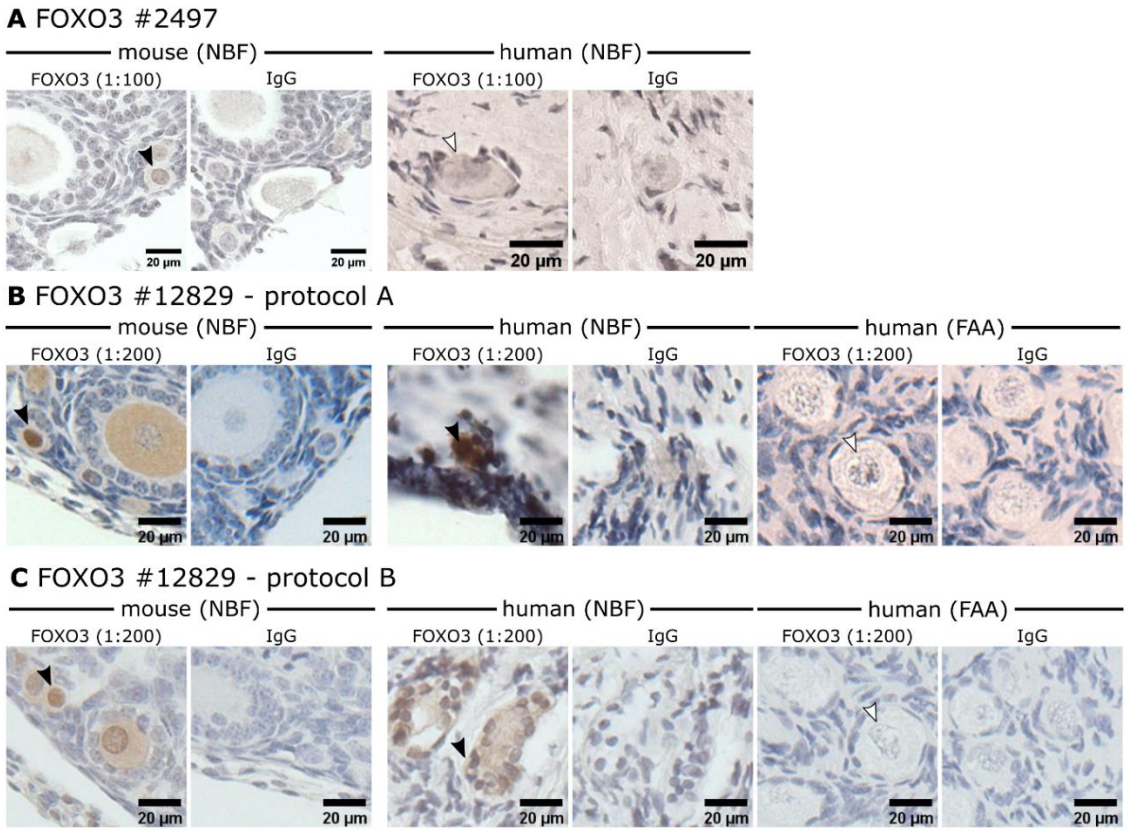

Figure 6-2. FOXO3 antibody validation for mouse and human ovarian tissue. (A) Mouse and human ovarian tissue fixed in neutral buffered formalin (NBF) was labelled with monoclonal rabbit anti-FOXO3 antibody (1:100, #2497, CST) or the same concentration of rabbit IgG. Scale bar represents 20 µm. **(B)** Mouse ovaries (fixed in NBF) and human ovarian tissue (fixed in NBF or form-acetic (FAA)) were labelled with rabbit anti-FOXO3 antibody (1:200, #12829, CST) or the same concentration of rabbit IgG. Immunohistochemistry was performed following the supplier's protocol (protocol A). Scale bar represents 20 µm. **(C)** Mouse ovaries (fixed in NBF) and human ovarian tissue (fixed in NBF or FAA) were labelled with rabbit anti-FOXO3 antibody (1:200, #12829, CST) or the same concentration of rabbit IgG. IHC was performed following a modified protocol (protocol B). Scale bar represents 20 µm. Examples of positive FOXO3 labelling is indicated with black arrowheads, while lack of labelling is indicated with unfilled arrowheads.

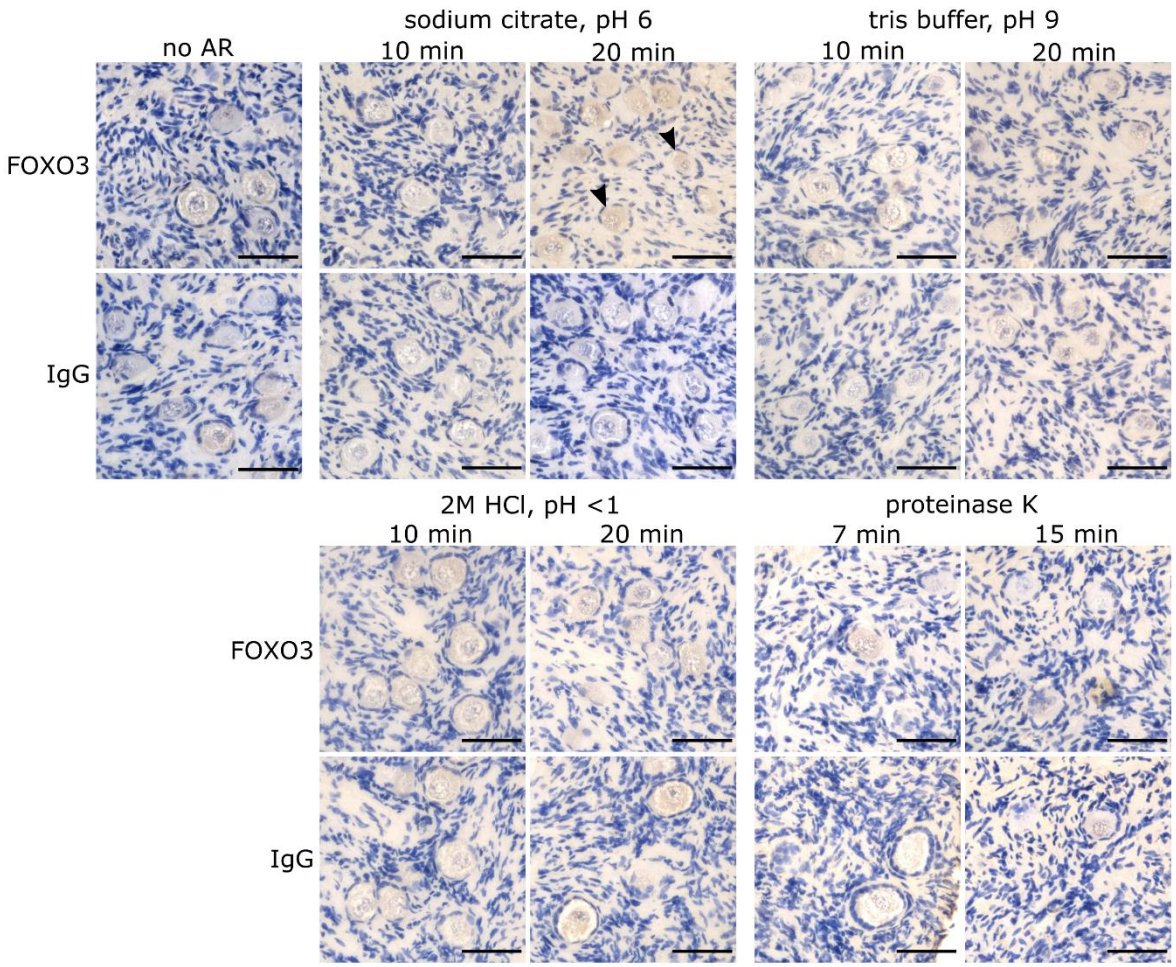

Figure 6-3. Optimising antigen retrieval for FOXO3 detection in form-acetic-fixed human ovarian tissue. Human ovarian tissue fixed in form-acetic was treated with different antigen retrieval (AR) protocols: no AR, heat-induced retrieval in 10 mM sodium citrate (10 or 20 min heating), heat-induced retrieval in tris buffer (10 or 20 min heating), retrieval in 2 M HCl at RT (10 or 20 min) or enzymatic retrieval in 20 µg/mL proteinase K at RT (7 min or 15 min). Sections were then labelled with anti-FOXO3 antibody (1:500, #12829, CST) or the same concentration of rabbit IgG. Sodium citrate retrieval with 20 min heating was the only condition that resulted in positive FOXO3 signal (black arrowheads). Scale bar represents 50 µm.

As I ultimately planned to use fluorescent detection to visualise intact follicles, I next adapted the IHC protocol to use fluorescent secondary antibodies. Streptavidin-based signal amplification was required to detect FOXO3 using fluorescent detection in formalin-fixed samples (Figure 6-4). Despite using the previously optimised antigen-retrieval protocol for samples fixed in form-acetic, FOXO3 was not detected in form-acetic-fixed samples using fluorescent detection (Figure 6-4). I therefore focussed on formalin-fixed tissue for the subsequent FOXO3 experiments.

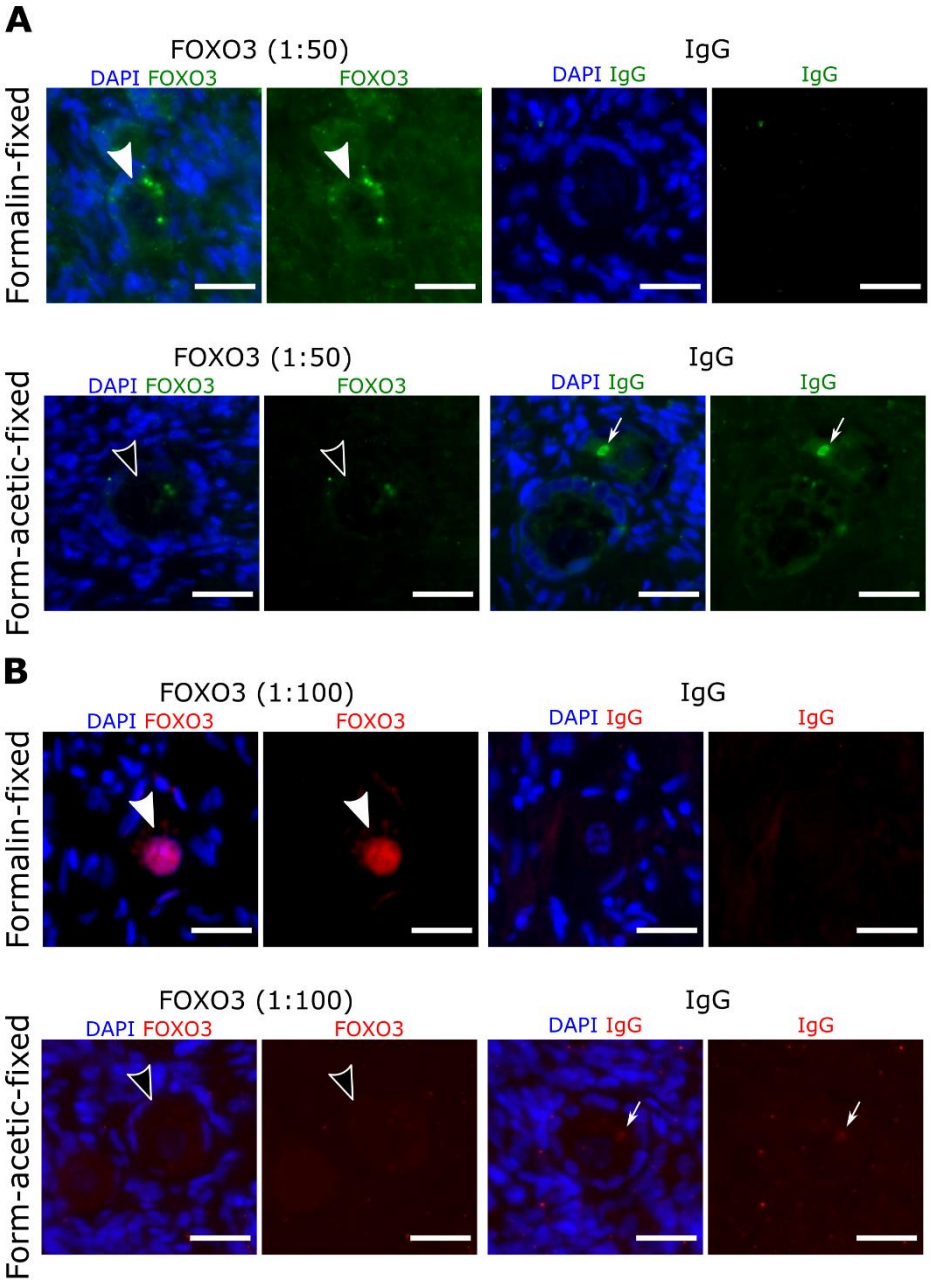

Figure 6-4. FOXO3 labelling using fluorescent detection in formalin and form-acetic-fixed tissue. (A) Human ovarian tissue fixed in either neutral buffered formalin or form-acetic was labelled with anti-FOXO3 antibody (1:50), or the same concentration of IgG, and goat anti-rabbit Alexa Fluor 488 (1:200) and counterstained with 5 µg/mL DAPI. FOXO3 was detected in formalin-fixed samples but not form-acetic fixed samples. **(B)** Human ovarian tissue fixed in either neutral buffered formalin or form-acetic was labelled with anti-FOXO3 antibody (1:100), or the same concentration of IgG, biotinylated goat anti-rabbit (1:200) and streptavidin-conjugated Alexa Fluor 568 (1:50) and counterstained with 5 µg/mL DAPI. FOXO3 was detected in formalin-fixed samples but not form-acetic fixed samples. Filled arrowheads indicate FOXO3 signal, while unfilled arrowheads indicate no signal. White arrows indicate lipofuscin autofluorescence. Scale bar: 20 µm.

In order to determine whether FOXO3 could be used to stage follicles, I analysed the ratio of nuclear to cytoplasmic FOXO3 signal (Figure 6-5). Forty-three FOXO3-labelled follicles from three patients were staged as primordial, transitional or primary based on morphology. Nuclear and cytoplasmic FOXO3 signal was measured using ImageJ Fiji and the ratio of nuclear to cytoplasmic signal was calculated. There was a significant difference in nuclear/cytoplasmic FOXO3 signal between primordial and transitional follicles (primordial: 18.0 ± 10.1 intensity/μm^2, transitional: 5.0 ± 3.6 intensity/μm^2, $P<0.01$; Figure 6-5A) and between primordial and primary follicles (primary: 2.9 ± 3.1 intensity/μm^2, $P<0.01$; Figure 6-5A) but not between transitional and primary follicles.

The relationship between FOXO3 signal and follicle activation was further investigated by counting the number of flattened and cuboidal granulosa cells for each follicle using the largest cross-section of the follicle, containing the oocyte nucleus. Nuclear/cytoplasmic FOXO3 was plotted against the proportion of cuboidal granulosa cells, to determine whether a relationship existed between the two variables (Figure 6-5B). The data was fitted to two models: a horizonal line representing the mean nuclear/cytoplasmic FOXO3 for all follicles, and a one-phase decay curve. Comparison of fits revealed that the one-phase decay model was the preferred model ($P<0.0001$), indicating that nuclear/cytoplasmic FOXO3 decreases as the proportion of cuboidal granulosa cells increases. However, there were a considerable number of outliers.

Although there was a difference in mean nuclear/cytoplasmic FOXO3 signal between primordial and transitional follicles, the difference was not great enough to be useful to identify individual primordial follicles without also relying on morphological assessment. I therefore concluded that FOXO3 was not suitable to identify primordial follicles.

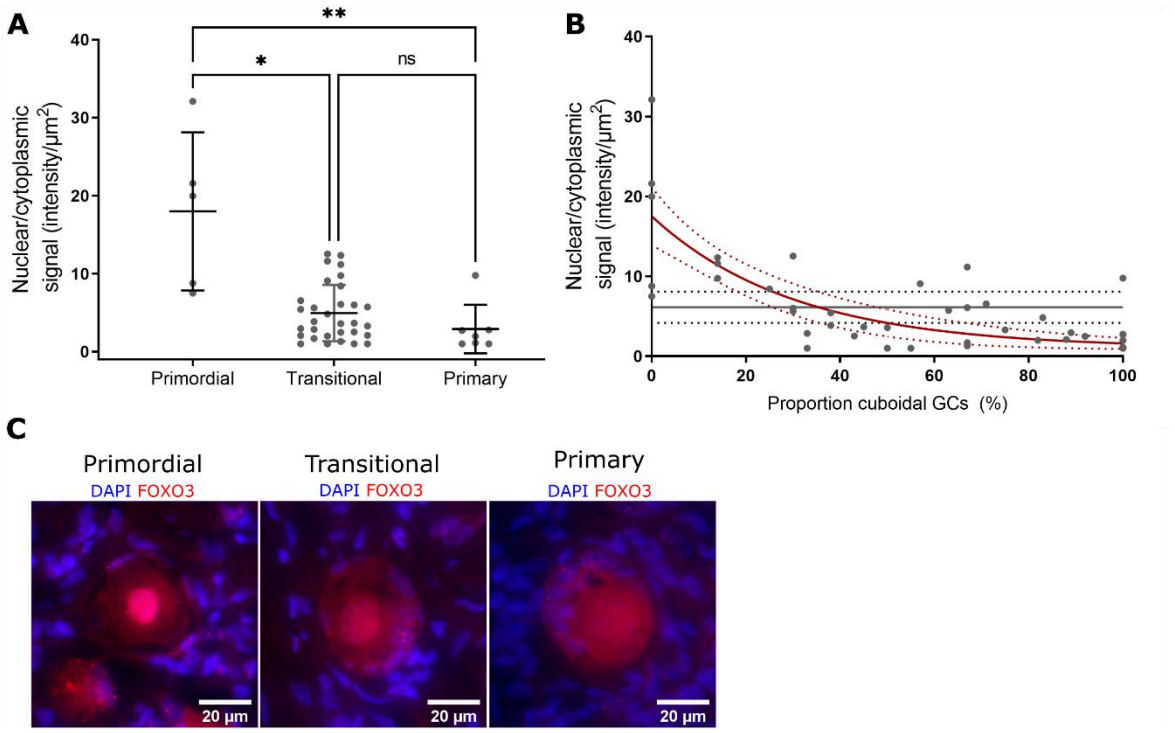

Figure 6-5. Quantification of nuclear to cytoplasmic FOXO3 in human follicles. Formalin-fixed human ovarian tissue from three patients (aged 10, 13 and 15 years) was labelled with anti-FOXO3 antibody or rabbit IgG and counterstained with DAPI. FOXO3-labelled follicles (n=43) were staged based on nuclear counterstaining as primordial (single layer of flattened pre-granulosa cells), transitional (mixture of flattened and cuboidal granulosa cells) and primary (single layer of cuboidal granulosa cells). The number of flattened and cuboidal granulosa cells in each follicle was counted. Nuclear and cytoplasmic FOXO3 signal per area was measured and the ratio of nuclear to cytoplasmic signal was calculated (intensity/µm^2). **(A)** Relationship between follicle stage and nuclear/cytoplasmic FOXO3 signal. There was a significant difference between nuclear/cytoplasmic FOXO3 signal in primordial follicles compared to transitional and primary follicles. **(B)** Nuclear/cytoplasmic FOXO3 signal was plotted against the proportion of cuboidal granulosa cells (GCs; with primordial follicles having 0% cuboidal GCs and primary follicles having 100%). The relationship between nuclear/cytoplasmic FOXO3 signal and proportion of cuboidal GCs appeared to follow a one phase decay curve, with decreased nuclear/cytoplasmic FOXO3 signal with an increased proportion of cuboidal GCs. Red unbroken curve shows average fit, red dotted curves show 95% confidence intervals. Grey unbroken horizonal represents the mean value of all follicles with grey dotted lines indicating 95% confidence intervals. **(C)** Representative images of primordial, transitional and primary follicles labelled with anti-FOXO3 antibody and counterstained with DAPI. Scale bar represents 20 µm. *:P<0.05, **: P<0.01.

6.3.1.2 Smad proteins

Nuclear exclusion of Smad2/3 in pre-granulosa cells has been shown to be an early event in murine follicle activation (Hardy *et al.*, 2018; Granados-Aparici *et al.*, 2019). Smad2/3 are expressed in the nuclei of primordial murine pre-granulosa cells but are excluded from the nucleus during follicle activation, likely in response to binding of an as-yet-unknown member of

the TGFβ superfamily. This is currently the earliest molecular event in follicle activation that has been described. Based on this information I sought to determine whether the same localisation pattern of Smad2/3 could be observed in human follicles and whether this marker could be used to identify primordial follicles.

The Smad2/3 antibody was validated using mouse ovarian tissue and was detected in (pre-)granulosa cells of primordial to secondary stage follicles (Figure 6-6A). In human follicles, Smad2/3 was present in both oocytes and granulosa cells (Figure 6-6B). A total of 60 follicles from three patients (aged 13 weeks to 12 years) were examined for the presence of Smad2/3. Smad2/3 was detected in the cytoplasm of all observed flattened pre-granulosa cells (Figure 6-6Bii), while in cuboidal granulosa cells Smad2/3 was either cytoplasmic or both nuclear and cytoplasmic (Figure 6-6Biii-iv). As no difference in Smad2/3 protein localisation in pre-granulosa cells was observed, it was determined that Smad2/3 was not suitable to identify primordial follicles.

The presence of Smad1/5/8 was also investigated in mouse and human ovarian tissue. Mouse sections were fixed in either formalin or paraformaldehyde while human ovarian tissue was fixed in either formalin or 5% form-acetic. No signal was detected in any sample for either species (data not shown). The presence of Smad1 was similarly investigated in human ovarian tissue fixed in formalin or 5% form-acetic, however no signal was detected (data not shown).

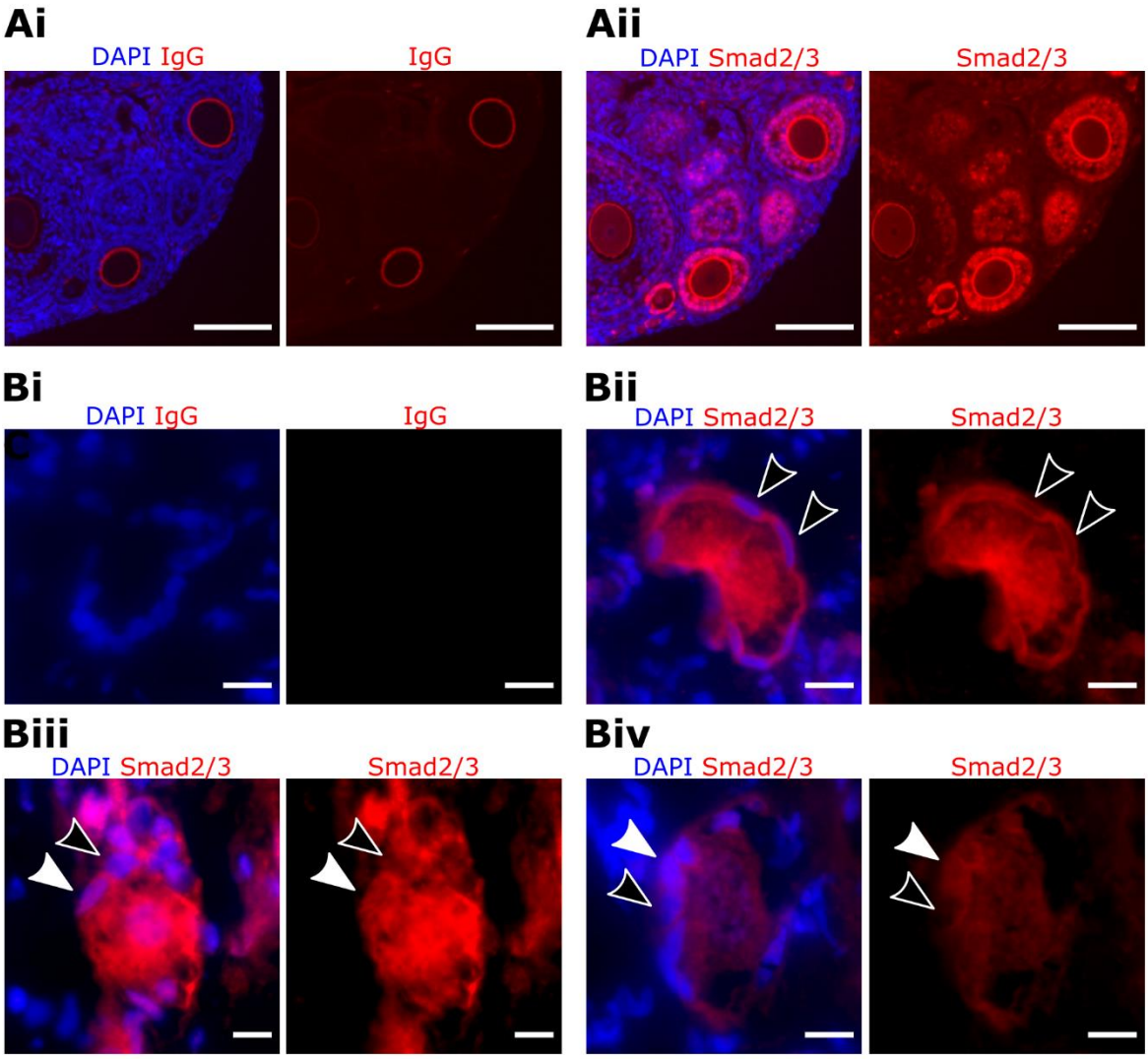

Figure 6-6. Smad2/3 localisation in formalin-fixed mouse and human ovarian follicles. **(A)** Mouse ovaries were labelled with **(i)** IgG or **(ii)** anti-Smad2/3 antibody (1:100) and counterstained with DAPI. Smad2/3 was observed in (pre-)granulosa cells in primordial and growing follicles. Note the positive signal in the zona pellucida in both the antibody-labelled and negative control; this may be a non-specific interaction between the mouse tissue and the secondary antibody (polyclonal goat anti-mouse antibody) and was not of consequence to this research. **(B)** Formalin-fixed human ovarian tissue was labelled with **(i)** IgG or **(ii-iv)** anti-Smad2/3 antibody (1:50) and counterstained with DAPI. Smad2/3 was observed in oocytes and (pre-)granulosa cells. In pre-granulosa cells (ii) and some granulosa cells (iii-iv) Smad2/3 was localised to the cytoplasm (black arrows), while in some granulosa cells it was present in both cytoplasm and nucleus (white arrows). Scale bar represents 50 μm (A) or 10 μm (B).

6.3.1.3 Markers for granulosa cell visualisation

As I had been unable to identify as suitable functional marker to detect primordial follicles, I decided to use follicle morphology to distinguish between primordial (only flattened pre-granulosa cells) and transitional (mixture of flattened and cuboidal (pre-)granulosa cells). I therefore investigated markers that could be used to visualise granulosa cells and allow detection and measurement of these cells.

6.3.1.4 Phalloidin staining

Phalloidin is a peptide that binds to actin filaments and can therefore be used to identify cell borders. I performed phalloidin staining on formalin- and form-acetic-fixed human ovarian tissue samples, however no signal was observed (data not shown).

6.3.1.5 Beta-catenin

Beta-catenin is a cytoplasmic protein involved in cell-cell adhesion (Wheelock and Johnson, 2003). I performed immunolabelling to detect β-catenin in formalin and form-acetic-fixed human ovarian tissue samples. Beta-catenin was detected in granulosa cells and oocytes in formalin-fixed samples, but not form-acetic fixed tissue (Figure 6-7). However, β-catenin detection was inconsistent and low signal was observed in pre-granulosa cells. Therefore, it was determined to be unsuitable for the identification of primordial follicles.

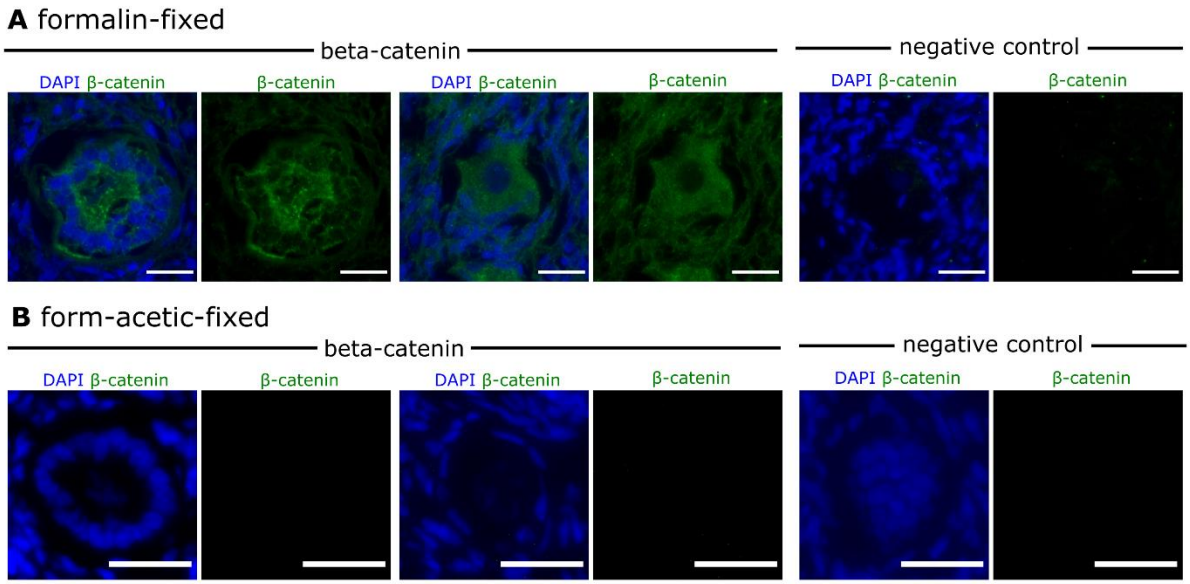

Figure 6-7. Detection of β-catenin in formalin and form-acetic-fixed human ovarian tissue. Human ovarian tissue was labelled with anti-β-catenin antibody (1:1000) to visualise β-catenin (green) and counterstained with DAPI. Primary antibody was omitted for the negative control. **(A)** Beta-catenin was detected in granulosa cells and oocytes in formalin-fixed tissue. **(B)** Beta-catenin was not detected in form-acetic-fixed samples. Scale bar represents 25 μm.

6.3.1.6 Laminin

As I had not been able to identify a marker to label the borders of granulosa cells, I decided to visualise granulosa cells indirectly by labelling the follicle basement membrane and oocyte. I selected laminin as a marker for the basal lamina and DDX4 as an oocyte-specific marker. Three different anti-laminin antibodies were tested to identify an antibody suitable for detecting laminin in primordial follicles. All the antibodies detected laminin in formalin-fixed human ovarian tissue but only one detected laminin in primordial follicles (ab11575, rabbit polyclonal against laminin-α; Figure 6-8). However, the same antibody was not able to detect laminin in primordial follicles in samples fixed in 5% form-acetic, and laminin signal was overall lower in samples fixed in 5% form-acetic compared to neutral buffered formalin (Figure 6-9).

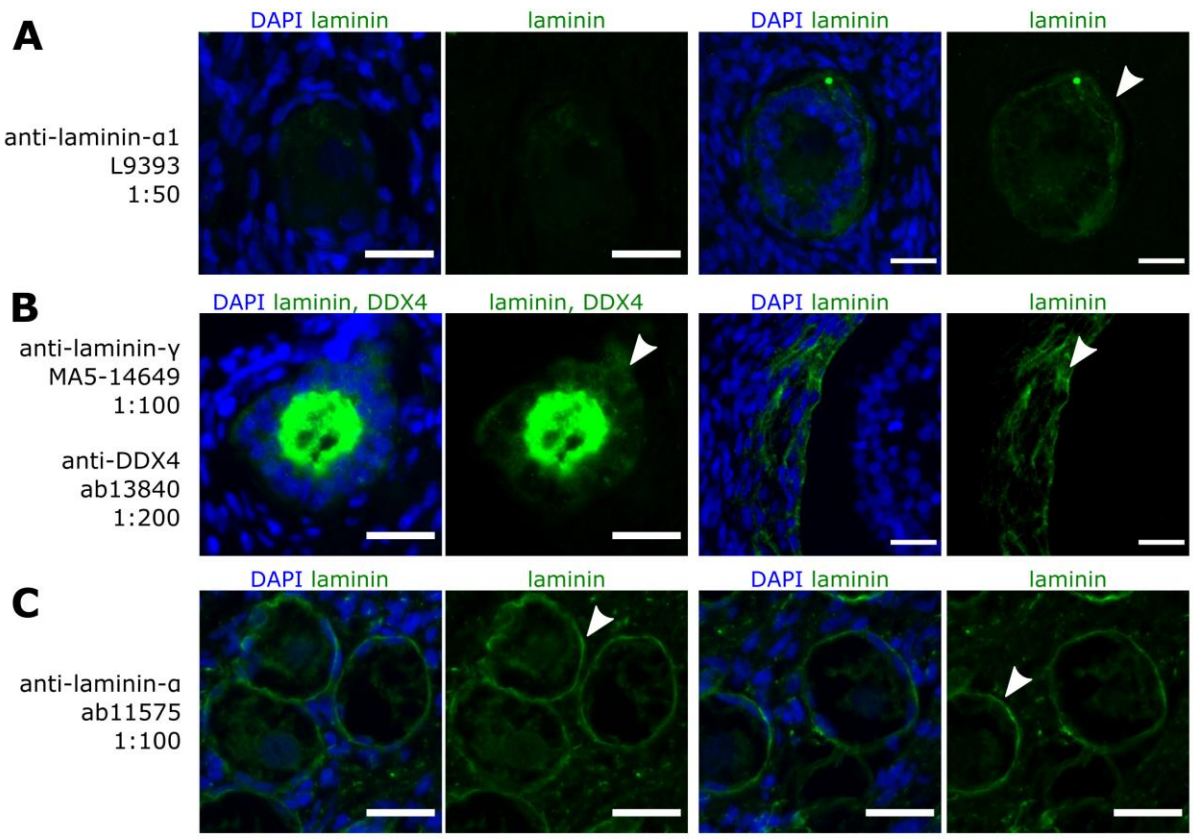

Figure 6-8. Laminin detection in formalin-fixed human ovarian tissue. Human ovarian tissue fixed in neutral-buffered formalin was labelled to detect laminin (green) and counterstained with DAPI (blue). Three different antibodies were tested. Examples of positive laminin signal are indicated by white arrowheads. **(A)** Anti-laminin-α1 (Sigma L9393, rabbit polyclonal). Laminin was not detected in early stage follicles (left) but was detected in growing follicles (right). **(B)** anti-laminin-γ (Thermo Fisher MA5-14649, rat monoclonal), samples were also labelled with DDX4 (Abcam ab13840, rabbit polyclonal). Laminin was detected in growing follicles, no primordial follicles were present in the sample. **(C)** Anti-laminin-α (Abcam ab11575, rabbit polyclonal). Laminin was detected in primordial follicles. Scale bar: 25 μm.

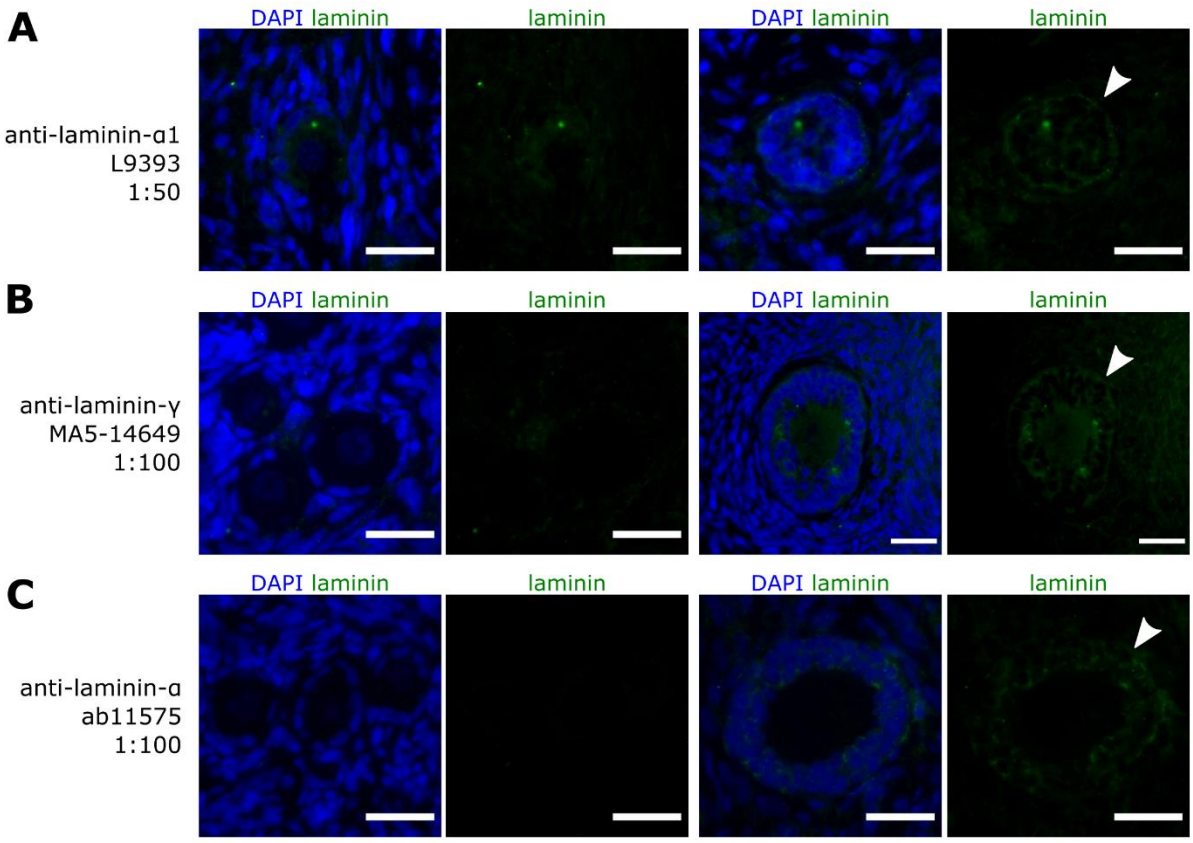

Figure 6-9. Laminin detection in 5% form-acetic-fixed human ovarian tissue. Human ovarian tissue fixed in 5% form-acetic was labelled to detect laminin (green) and counterstained with DAPI (blue). Three different antibodies were tested. Examples of positive laminin signal are indicated by white arrowheads. **(A)** Anti-laminin-α1 (Sigma L9393, rabbit polyclonal). Laminin was not detected in early stage follicles (left) but was detected in growing follicles (right). **(B)** Anti-laminin-γ (Thermo Fisher MA5-14649, rat monoclonal). Laminin was not detected in early stage follicles (left) but was detected in growing follicles (right). **(C)** Anti-laminin-α (Abcam ab11575, rabbit polyclonal). Laminin was not detected in early stage follicles (left) but was detected in growing follicles (right). Scale bar: 25 μm.

In order to investigate whether acetic acid affected detection of laminin, I fixed human ovarian tissue in a range of form-acetic concentrations (0.1-5%) and labelled with laminin-α antibody (ab11575). There was a visible decrease in laminin signal with increased concentration of acetic acid, suggesting that fixation in high concentrations (2.5% or 5%) of acetic acid caused degradation of laminin protein, particularly in primordial follicles (Figure 6-10). One of the negative effects of formalin-fixation is that formalin causes oocyte shrinkage, which is counteracted by the addition of acetic acid (Adeniran *et al.*, 2021).

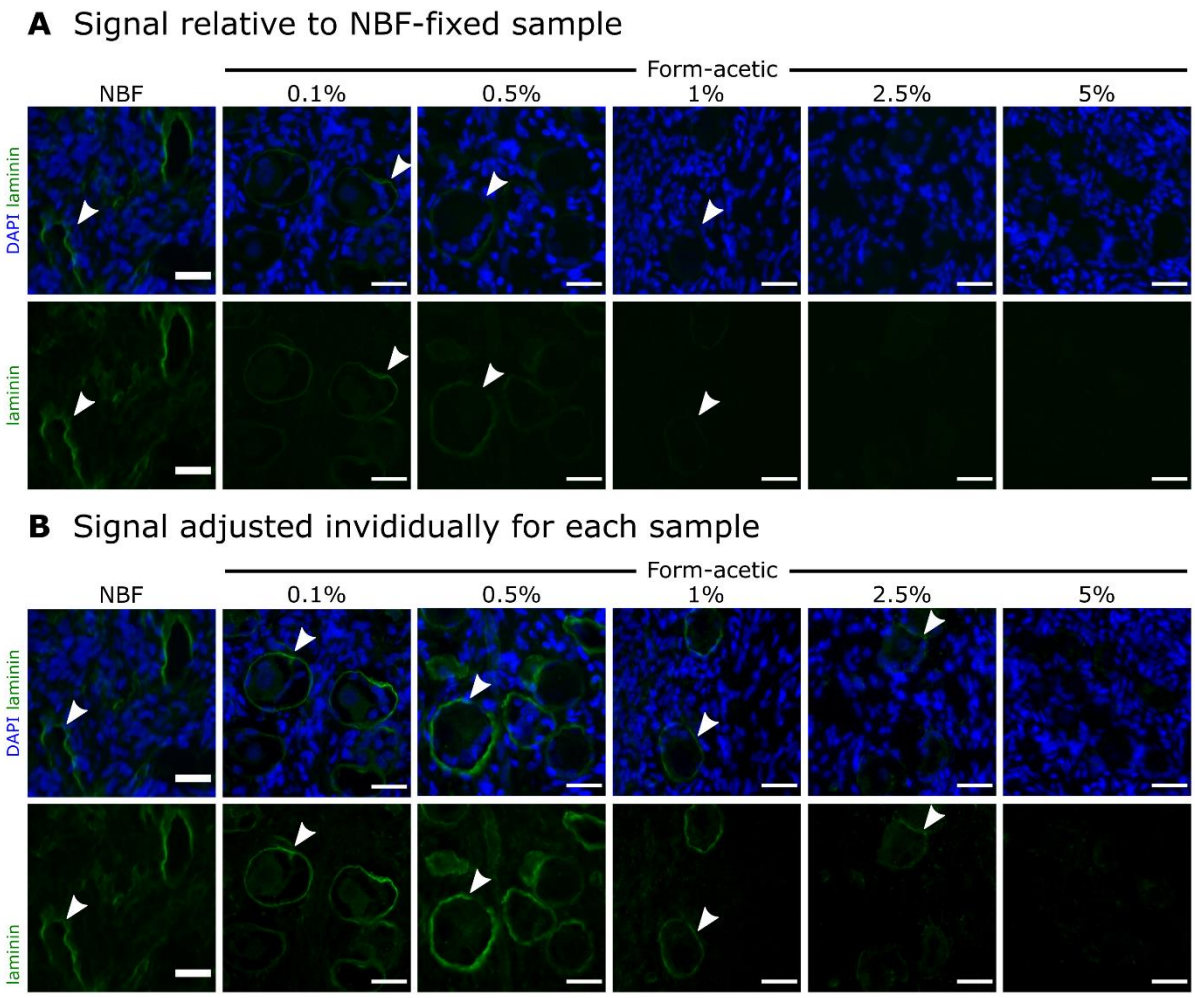

Figure 6-10. Laminin detection in a gradient of 0-5% form-acetic-fixed human ovarian tissue. Human ovarian tissue was fixed in 0% (neutral buffered formalin, NBF), 0.1%, 0.5%, 1%, 2.5% and 5% form-acetic and labelled with anti-laminin antibody (1:100) to detect laminin (green) and counterstained with DAPI (blue). Examples of positive laminin signal are indicated by white arrowheads. **(A)** Signal intensity was adjusted based on the NBF-fixed sample to compare signal between samples. Laminin signal was visible reduced with increased acetic-acid concentration, with no visible laminin in primordial follicles in tissue fixed in 2.5% or 5% form-acetic. **(B)** Signal intensity was adjusted for each sample individually, in order to visualise optimal signal intensity. Laminin positive follicles were visible in all samples, except those fixed in 5% form-acetic. Scale bar: 25 µm.

I next sought to determine the minimum concentration of acetic acid required to preserve laminin signal while also preserving oocyte morphology, by double-immunolabelling samples with laminin and DDX4. Considerable oocyte shrinkage was observed in samples fixed in NBF or 0.1% form-acetic, however 0.5%-1% acetic acid was sufficient to preserve oocyte morphology (Figure 6-11). Based on these experiments I determined that 1% form-acetic was best suited to preserve

follicle structure while allowing for detection of laminin. Furthermore, I found that double-labelling with DDX4 and laminin to visualise the oocyte and follicle boundary, respectively, allowed indirect visualisation of (pre-)granulosa cells, with the help of nuclear counterstaining. As the antibodies I selected for these two markers are both raised in rabbit, the same secondary antibody could be used for detection, as demonstrated in Figure 6-11. Having selected the markers I intended to use for staging follicles, I next set out to develop a whole-mount protocol to label intact follicles, as described in the next section.

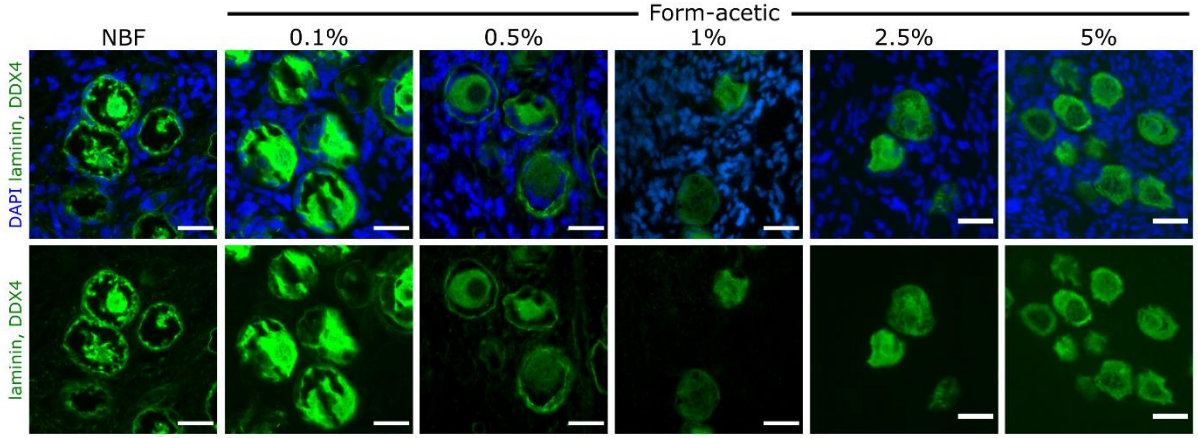

Figure 6-11. DDX4 and laminin detection in a gradient of 0-5% form-acetic-fixed human ovarian tissue. Human ovarian tissue was fixed in 0% (neutral buffered formalin, NBF), 0.1%, 0.5%, 1%, 2.5% and 5% form-acetic and labelled with anti-laminin antibody (1:100) to detect laminin and anti-DDX4 antibody (1:500) to label oocytes (green), and counterstained with DAPI (blue). Oocytes appeared shrunken when fixed in NBF or 0.1% form-acetic, however ≥0.5% form-acetic was sufficient to prevent oocyte shrinkage. It should be noted that due to a lack of follicles in the NBF-fixed sample, a representative image from a different experiment is shown for NBF. Scale bar: 25 µm.

6.3.2 Developing a protocol to optically clear human ovarian tissue

Once I had identified suitable markers to detect primordial follicles (laminin and DDX4), the next aim was to develop a method to visualise intact follicles. I first attempted whole-mount immunolabelling of 50 micron-thick paraffin-embedded tissue sections and confocal imaging, however this did not allow visualisation of intact follicles (data not shown). I instead chose to explore tissue clearing as a method to allow whole-mount immunolabelling and imaging at greater sample thickness than paraffin-embedded tissue sections.

To develop a protocol to optically clear human ovarian tissue, I selected a commercially available tissue clearing kit using Visikol® HISTO™ tissue clearing technology. In order to test the compatibility of this method with human ovarian tissue, I followed the supplier's recommended protocol for immunolabelling and tissue clearing, using small fragments of formalin-fixed human ovarian tissue from a 13-year old patient with approximate dimensions of 0.25 x 0.5 x 1 mm.

Samples were visibly more transparent after incubation in tissue clearing reagent 1 and were near-invisible after mounting in tissue clearing reagent 2 (Figure 6-12A). The sample could be imaged at up to ~120 μm depth without loss of resolution, allowing several intact follicles to be visualised in the sample (Figure 6-12B). Imaging depth was later increased by mounting samples onto glass coverslips, instead of glass slides, so that samples could be imaged from both sides. Follicle morphology appeared normal, with no visible shrinkage or swelling of the tissue (Figure 6-12B-C). A benefit of the Visikol® HISTO™ technique is that the tissue clearing can be reversed, allowing for validation of analysis with conventional histology or immunohistochemistry (Figure 6-12D). Having demonstrated that the Visikol® HISTO™ tissue clearing technique was compatible with human ovarian tissue, I next set out to develop and optimise immunolabelling of the samples, to detect the markers that I had selected in the previous section (laminin and DDX4).

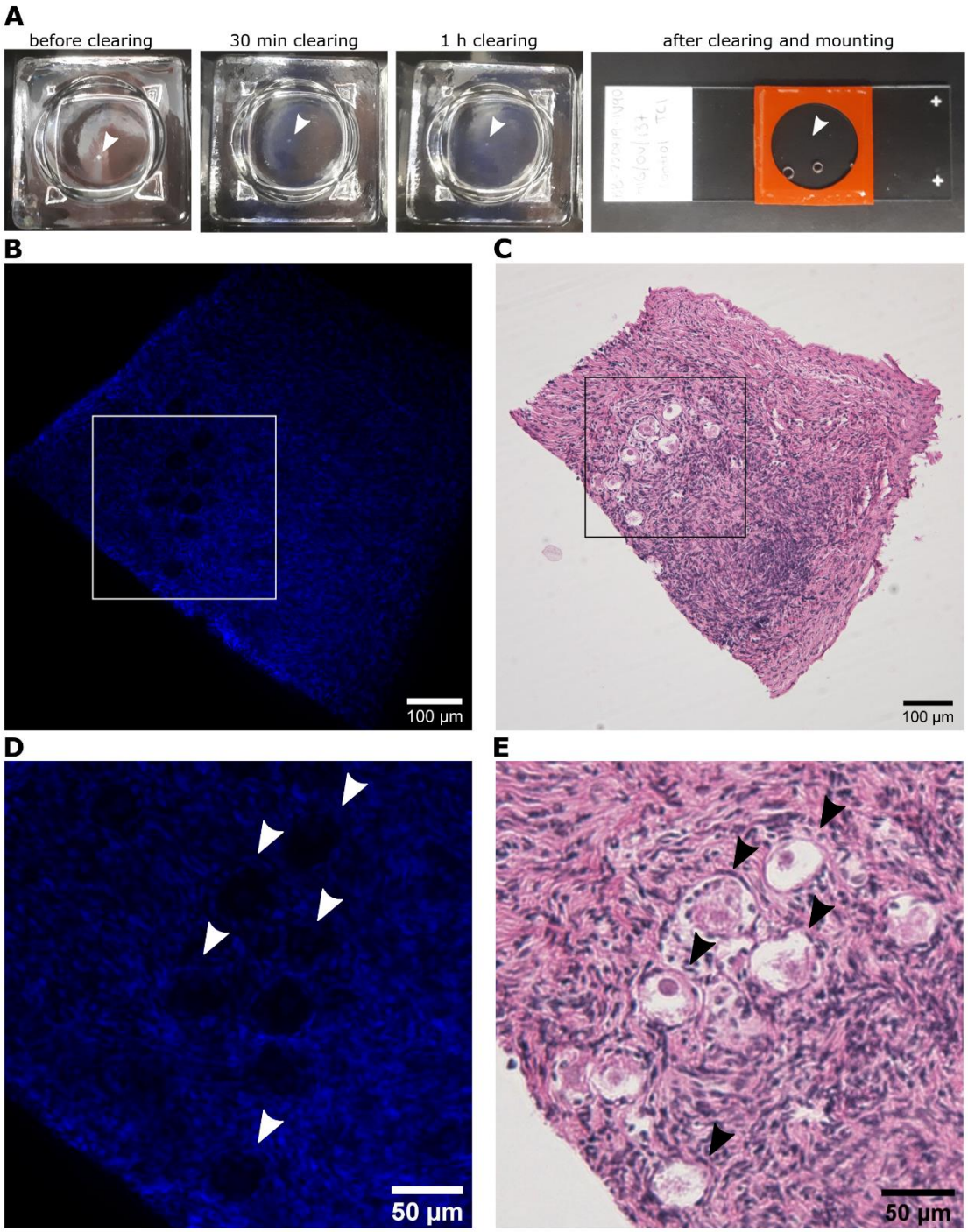

Figure 6-12. Optical clearing and reverse clearing of human ovarian tissue. A fragment of human ovarian tissue from a 13-year-old patient was fixed in NBF stained with 5 µg/mL DAPI nuclear counterstain and optically cleared using Visikol® HISTO™ technology. **(A)** Representative fragment shown (L-R) before clearing, after 30 min in tissue clearing reagent 1, after 1 h in tissue clearing reagent 1 and after mounting in tissue clearing reagent 2. Arrowheads denote the fragment. **(B)** Single slice through the centre of the tissue fragment. Follicles can be visualised, with oocytes appearing as black circles. **(C)** Demonstration of compatibility of tissue clearing with conventional downstream analysis. The sample has been reverse cleared, paraffin-embedded, sectioned and stained with H&E. The section shown is from the same region as in (B). (D-E) Enlarged area from outlined regions in (B) and (C), respectively. Arrows denote corresponding follicles within the sample.

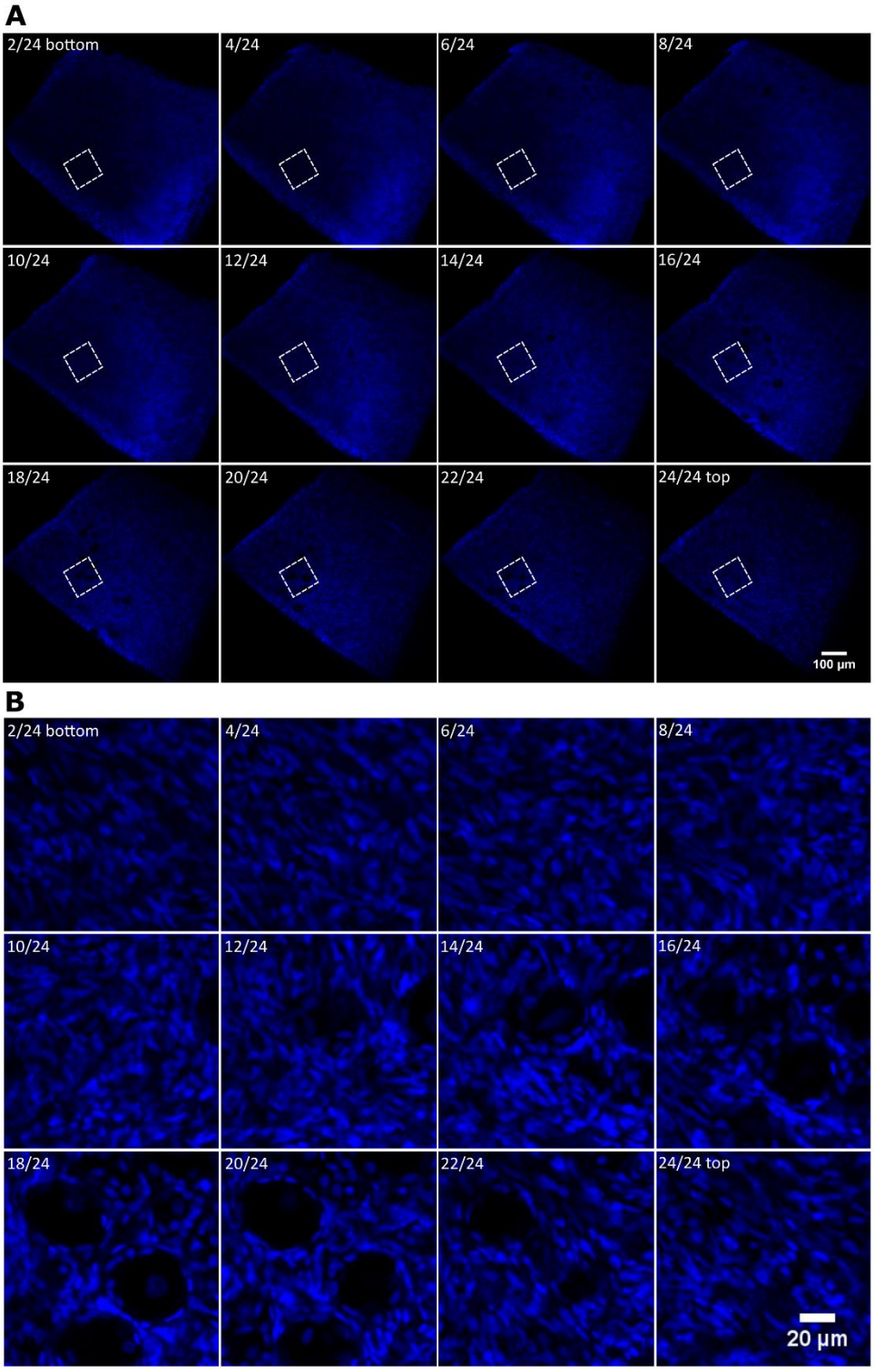

Figure 6-13. Optical sequential sectioning through cleared human ovarian tissue. A fragment of human ovarian tissue from a 13-year-old patient was fixed in NBF, counterstained with 5 µg/mL DAPI and optically cleared using Visikol® HISTO™ technology. Cleared samples were imaged using a confocal microscope to obtain z-stacks imaged at 5 µm intervals. **(A)** Optical sectioning (10 µm intervals) spanning 120 µm of a tissue fragment imaged with a 10x objective. Slices are shown from the bottom to the top of the tissue fragment. Scale bar represents 100 µm. **(B)** Closer view of boxed area from (A), imaged using a 25x oil immersion objective. Follicles can be visualised, with oocytes appearing as black circles with a central nucleus. Scale bar represents 20 µm.

A series of experiments were performed to determine the optimal antibody incubation times and temperatures for immunolabelling human ovarian tissue samples. For the initial test I labelled tissue with a mouse monoclonal DDX4 antibody, to identify oocytes, following the immunolabelling protocol recommended by the supplier of the tissue clearing kit (3 h at 37°C). However, no positive DDX4 signal was observed and furthermore there was a high level of non-specific background (Figure 6-14A). For the second experiment I used FOXO3 antibody to label follicles and extended the incubations, with primary antibody labelling for 24 h at 4°C, followed by overnight incubation with a biotinylated secondary antibody at RT, and overnight incubation with streptavidin-conjugated Alexa Fluor 568 at RT. This resulted in some apparently positive FOXO3 signal, however the non-specific signal remained high (Figure 6-14B-D).

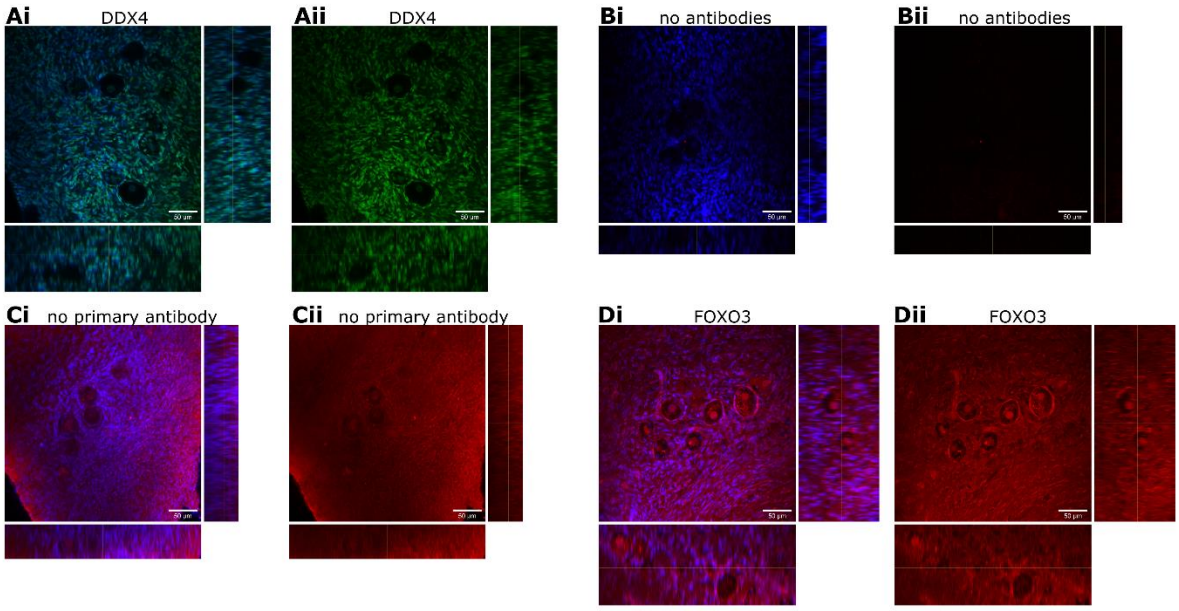

Figure 6-14. Whole-mount immunolabelling with DDX4 or FOXO3 and tissue clearing. Human ovarian tissue fragments (<250 µm thickness) were fixed in NBF and labelled with either DDX4 (1:200, mouse monoclonal) or FOXO3 (1:100, rabbit monoclonal) to label oocytes. Alexa Fluor 488 was used to detect DDX4 labelling (green), while a biotinylated secondary antibody followed by streptavidin-conjugated Alexa Fluor 568 was used to detect FOXO3 (red). DAPI was used as a nuclear counterstain (blue). Samples were optically cleared using VisikolHISTO and imaged using a confocal microscope to obtain z-stacks at 5 µm intervals, spanning a portion of the sample that contained follicles. Each panel shows a central z-slice in addition to orthogonal projections of the y-z (right) and x-z (left) planes. **(A)** DDX4 labelling was performed for 3 h at 37°C, followed by secondary antibody and DAPI for 3 h at 37°C. Follicles were identified in the tissue (Ai, composite blue and green channels), however none were DDX4-positive. A high level of non-specific signal was observed (Aii, green channel only). **(B-D)** FOXO3 labelling was performed for 23 h at 4°C and 6 h at RT, followed by secondary antibody labelling for 16 h at RT and Alexa Fluor 568 conjugate and DAPI for 20 h at RT. Each panel shows a composite of blue and red channels (Bi, Ci, Di) and red channel only (Bii, Cii, Dii). Two negative controls were used, one where no antibodies were added (B) and one where the primary antibody was omitted (C). A high level of non-specific labelling can be seen when these controls are compared. Possible FOXO3-labelling was observed (D), but with a high level of non-specific signal. All scale bars: 50 µm.

For the third experiment, I extended the primary antibody incubation (polyclonal rabbit anti-DDX4) to three days and secondary incubation to one day (approx. 22 h), and compared incubation at 4°C, RT and 37°C in order to determine whether the background signal was related to incubation temperature, as was suggested by the supplier. I also tested additional incubation in the optional Tissue Clearing Permeabilization Buffer supplied in the Tissue Clearing Kit prior to immunolabelling, with overnight incubation at RT. This permeabilization buffer is

recommended for samples that are difficult to clear due to the presence of pigment, collagen or blood, collagen being present in ovarian extracellular matrix. Samples ranged from 140-290 μm in thickness. Immunolabelling at RT or 37°C resulted in considerably higher levels of autofluorescence or non-specific signal compared to incubation at 4°C (Figure 6-15). As the imaging settings (laser power, pinhole size and gain) were set based on the sample that had the highest expected level of signal (37°C incubation with overnight permeabilization), the DDX4 signal in samples incubated at 4°C appeared reduced, however this signal could be increased by post-imaging processing (data not shown). Overnight incubation in Permeabilization Buffer did not appear to improve labelling and was not tested further.

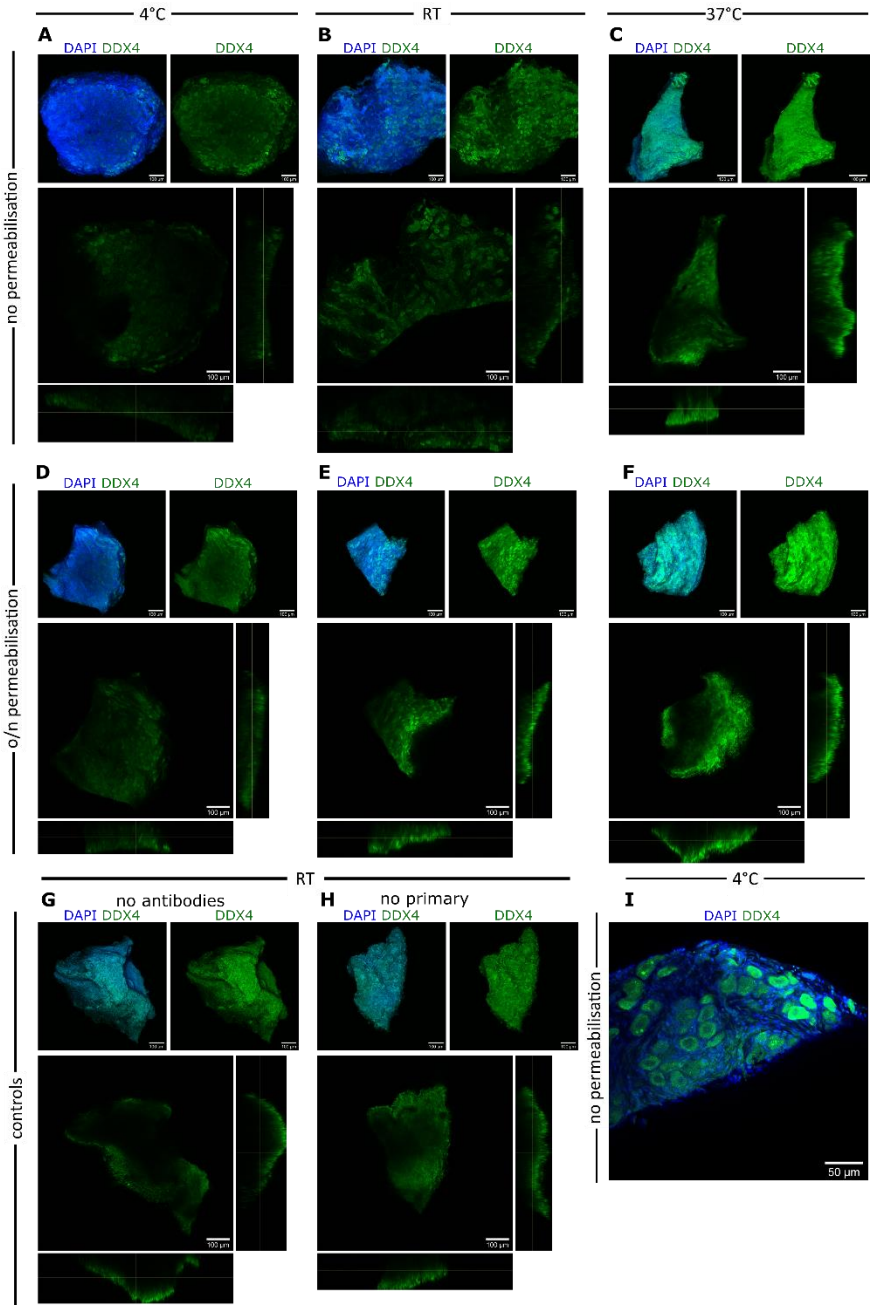

Figure 6-15. Whole-mount immunolabelling at low temperature reduces autofluorescence and non-specific signal. Human ovarian tissue fragments (<250 µm thickness) fixed in 5% form-acetic were labelled with DDX4 (1:200, rabbit polyclonal) to identify oocytes. Alexa Fluor 488 (1:200) was used for antibody detection (green) and DAPI for nuclear counterstaining (blue). Primary antibody incubation was performed for three days, while secondary antibody incubation and counterstaining were performed for one day. (A-F) Antibody incubations were performed at 4°C (A, D), RT (B, E) or 37°C (C, F) with or without overnight incubation at RT in permeabilization buffer. Samples were optically cleared using VisikolHISTO and imaged using a confocal microscope to obtain z-stacks at 5 µm intervals, spanning the entire thickness of the sample. For each panel (A-H) the upper images show maximum intensity projections of z-stacks for composites of DDX4 and DAPI (left) and DDX4 alone (right). The lower images DDX4 labelling in a central section of the tissue fragment with orthogonal projections of the y-z (right) and x-z (bottom) planes. Negative controls were included where either all antibodies were omitted (G) or primary antibody was omitted (H). Scale bar: 100 µm. (I) Magnified view of sample from (A) demonstrating positive labelling of oocytes. Scale bar represents 50 µm.

While performing incubations at 4°C reduced the non-specific background, I observed that there was considerable signal attenuation with increased sample depth, suggesting that the antibodies were not able to fully penetrate the sample. Using ovarian tissue from a 13-week old donor, ensuring that a large number of follicles were present throughout the tissue sample, I investigated extended incubation times using laminin and DDX4 to label the follicle basement membrane and oocytes, respectively (Figure 6-16 and Figure 6-17). Note that this sample was obtained prior to investigating different concentrations of form-acetic, as described in Section 6.3.1, therefore the sample was fixed in 5% form-acetic rather than 1% form-acetic. Extending incubation times of both the primary and secondary antibody to one week each and increasing the secondary antibody concentration resulted in improved signal at increased sample depths (up to 250 μm; Figure 6-16 to Figure 6-17). During these experiments I observed that the DDX4 signal was sometimes poorly visible when co-labelling with laminin (using 1:100 dilution for each antibody). I performed sequential labelling, first labelling with DDX4 (with subsequent secondary antibody labelling for some samples), followed by laminin labelling and secondary antibody incubation. Sequential labelling did not affect signal detection (data not shown), however decreasing the concentration of laminin (1:400 dilution instead of 1:100) while maintaining the same concentration of DDX4 (1:100 dilution) resulted in both markers being clearly visible. These concentrations were used for all subsequent experiments.

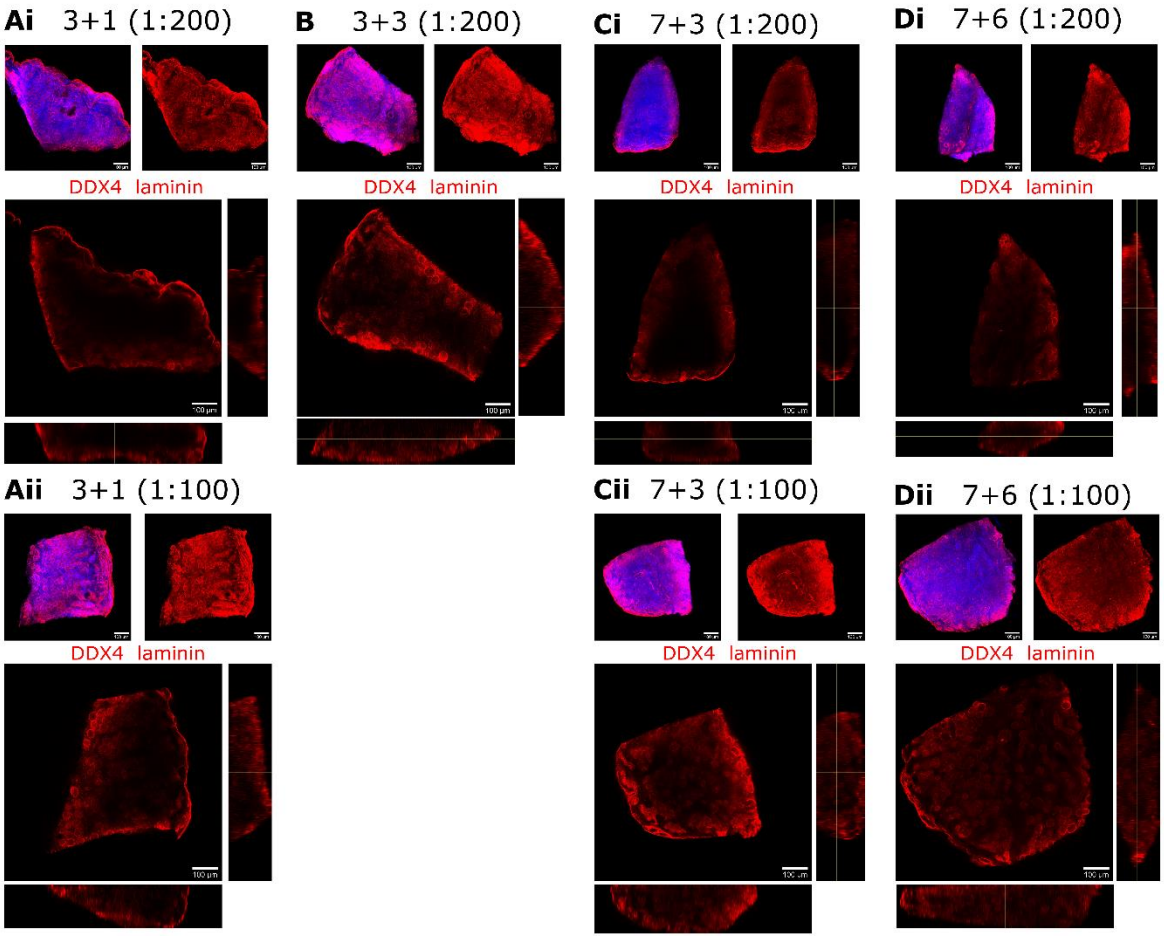

Figure 6-16 Extended whole-mount immunolabelling of DDX and laminin with tissue clearing. Human ovarian tissue fragments (<250 µm thickness) fixed in 5% form-acetic were labelled with DDX4 (1:100, rabbit polyclonal) and laminin (1:400, rabbit polyclonal) to identify oocytes and basal lamina respectively. Alexa Fluor 568 was used to detect both DDX4 and laminin (red) and DAPI for nuclear counterstaining (blue). Primary antibody incubation was performed for three or seven days, while secondary antibody incubation and counterstaining were performed for one, three or six days at two concentrations (1:200 or 1:100). Samples were optically cleared using Visikol® HISTO™ and imaged using a confocal microscope to obtain z-stacks at 10 µm intervals, spanning the entire thickness of the sample. Upper panels show maximum intensity projections of z-stacks for composites of DDX4/laminin and DAPI (left) and DDX4/laminin alone (right). Lower panels show a central section of the tissue fragment with orthogonal projections of the y-z (right) and x-z (bottom) planes. **(A)** Three-day primary antibody incubation followed by one-day incubation with secondary antibody at 1:200 (Ai) or 1:100 (Aii). Signal was observed at the edges of the sample, with considerable drop-off towards the centre of the tissue. **(B)** Three-day primary antibody incubation followed by three-day incubation with secondary antibody at 1:200. Signal was observed at the edges of the sample, with considerable drop-off towards the centre of the tissue. **(C)** Seven-day primary antibody incubation followed by three-day incubation with secondary antibody at 1:200 (Ci) or 1:100 (Cii). Samples incubated in 1:200 secondary antibody had a low signal intensity, while even labelling was observed after incubation in 1:100 secondary antibody. **(D)** Seven-day primary antibody incubation followed by six-day incubation with secondary antibody at 1:200 (Di) or 1:100 (Dii). Signal drop-off was observed when using 1:200 secondary antibody, however signal was evenly distributed when secondary antibody was increased to 1:100. Scale bar: 100 µm.

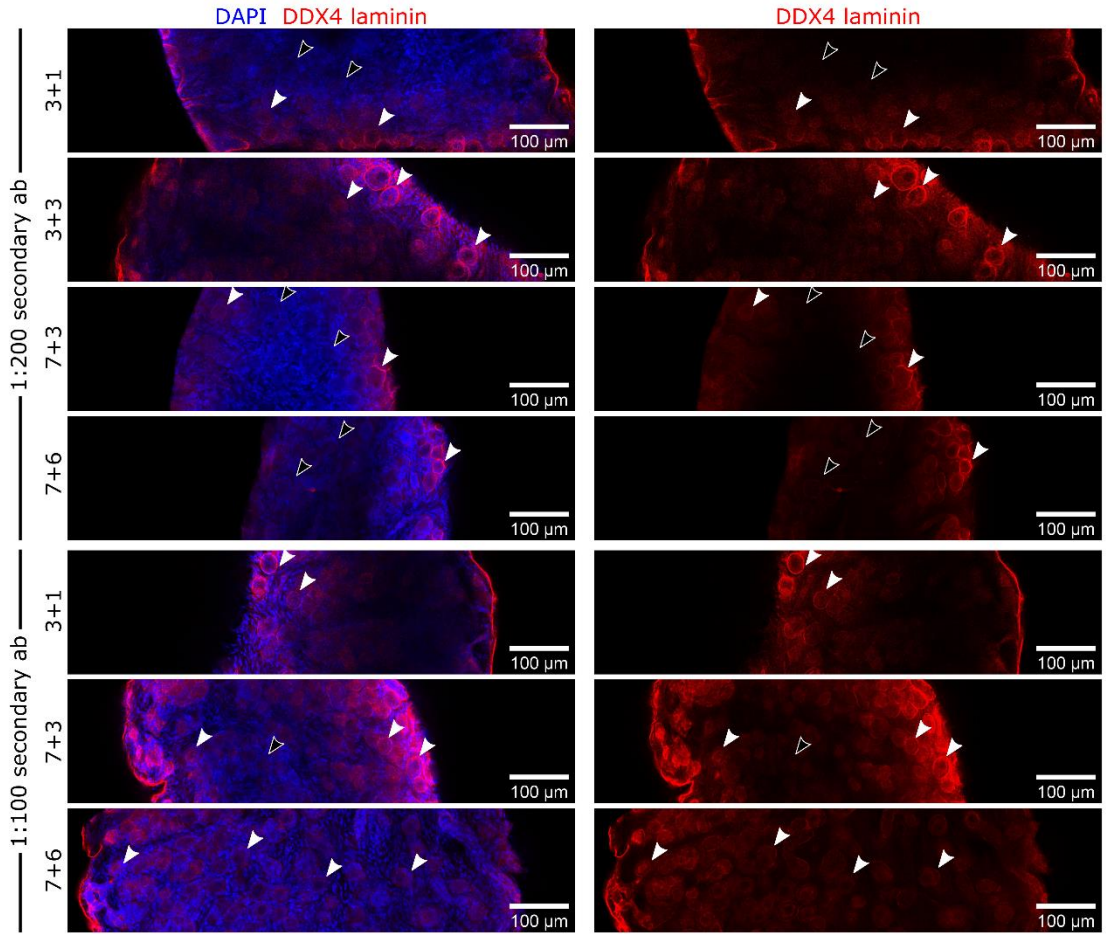

Figure 6-17. Signal evaluation of extended whole-mount immunolabelling of DDX4 and laminin with tissue clearing. Human ovarian tissue fragments (<250 µm thickness) fixed in 5% form-acetic were labelled with DDX4 (1:100, rabbit polyclonal) and laminin (1:400, rabbit polyclonal) to identify oocytes and basal lamina respectively. Alexa Fluor 568 was used for antibody detection (red) and DAPI for nuclear counterstaining (blue). Primary antibody incubation was performed for three or seven days, while secondary antibody incubation and counterstaining were performed for one, three or six days at two concentrations (1:200 or 1:100). Samples were optically cleared using Visikol® HISTO™ and imaged using a confocal microscope to obtain z-stacks at 10 µm intervals, spanning the entire thickness of the sample. A single slice through a central z-slice of each sample is shown for composites of DDX4/laminin (red) and DAPI (blue, left column) and DDX4/laminin alone (right column). White arrows indicate positive DDX4/laminin labelling, while black arrows indicate non-labelled follicles. One-week incubation for both primary and secondary antibodies, with 1:100 secondary antibody dilution was the only condition that allowed visualisation of follicles throughout the entire sample (bottom row).

Loss of signal at increased sample depth could also be caused by insufficient tissue clearing and limitations during imaging. Therefore, three other main adjustments were made to the immunolabelling and tissue clearing protocol. Firstly, during tissue dehydration prior to clearing, two additional wash steps in 100% methanol were added to ensure complete dehydration.

Secondly, samples were mounted in a thinner imaging chamber (0.25 mm instead of 0.5 mm) to ensure that the working distance of the objectives was not exceeded, in addition to mounting the samples onto a coverslip so the sample could be imaged from both sides if needed. Finally, correction factors were employed during imaging by increasing gain with increased sample depth. Together, these changes all led to marked improvement in imaging.

6.3.3 Detection of double-stranded DNA breaks and tissue clearing

Having demonstrated that this novel whole-mount immunolabelling and tissue clearing method was compatible with immunohistochemistry, I next set out to investigate whether it was compatible with other labelling methods such as TUNEL. Using a commercial TUNEL kit with fluorescent detection, I first performed the standard supplier recommended protocol, increasing reagent volumes to adapt the protocol for whole-mount labelling. As TUNEL generally requires pre-treatment with either proteinase K or heating in sodium citrate to reveal double-stranded DNA breaks, I compared TUNEL with no pre-treatment and with 20 min heating at 90°C in 10 mM sodium citrate, pH 6 (Figure 6-18). In both cases, TUNEL-positive nuclei were detected, however these were observed only at the sample surface, with no positive signal within the sample itself, indicating that either the TdT enzyme, the fluorophore, or both did not adequately penetrate the sample.

I next investigated whether extended incubation in these reagents led to improved signal detection. Samples that had been pre-treated with DNase I overnight at RT to induce dsDNA breaks in order to determine the degree of signal penetration. Samples were incubated with the TdT enzyme for 1, 2, 4 or 24 h at 37°C and the Click-IT fluorophore reaction was performed for 30 min, 1 h, 2 h or 20 h, respectively, at 37°C (Figure 6-19). Increased incubation did not increase the signal penetration, TUNEL-positive cells were only detected at the surface of the sample. In the sample incubated in TdT for 24 h and Click-IT for 20 h, I observed that a low-level of background fluorescence within the sample, suggesting that the fluorophore was able to penetrate the tissue but did not react with labelled cells, perhaps due to lack of labelling.

Based on these results I decided to investigate whether increasing sample permeabilization would lead to improved signal, by performing a permeabilization step with 20% DMSO and 0.2%, 2% or 10% Triton X-100 overnight at RT prior to labelling. I also tested the addition of 10% DMSO to the TdT or Click-IT reaction solutions (or both). In addition, I tried extending the incubations in TdT and the Click-IT reaction to six and seven days, respectively (Figure 6-20). Following 24 h incubation in the TdT enzyme, I observed that samples that had been permeabilised in 2% or 10% Triton-X100 were stained purple. All samples that were incubated in the TdT enzyme for 6 days were also purple, irrespective of the permeabilization protocol used, although the staining was stronger with increased Triton-X100 concentration used. No improvement in signal penetration was observed, despite increased incubation and/or permeabilization (Figure 6-20).

In order to determine whether low signal penetration was due to the dense nature of human ovarian cortical tissue, I performed TUNEL using tissue from an 18-year-old patient and from a 13-week-old donor, as the stroma from the latter patient was less dense (Figure 6-21). I also introduced an additional permeabilization step, incubating samples overnight at RT in a permeabilization buffer provided in the tissue clearing kit. In addition, I tried sonicating samples briefly with DNase I and the TdT enzyme solution, in an effort to get the enzymes to penetrate the samples. Samples were permeabilized with 0.2% Triton-X100 and 20% DMSO before commencing with DNase I treatment and TUNEL labelling, with TdT incubation performed for 3 days and the Click-IT fluorophore reaction performed for 24 h. As with the previous experiments, TUNEL-positive cells were only detected on the surface of the sample, with no positive cells detected within the sample itself. Additional permeabilization or sonication did not increase signal penetration, nor was there a difference between the two patients (Figure 6-21).

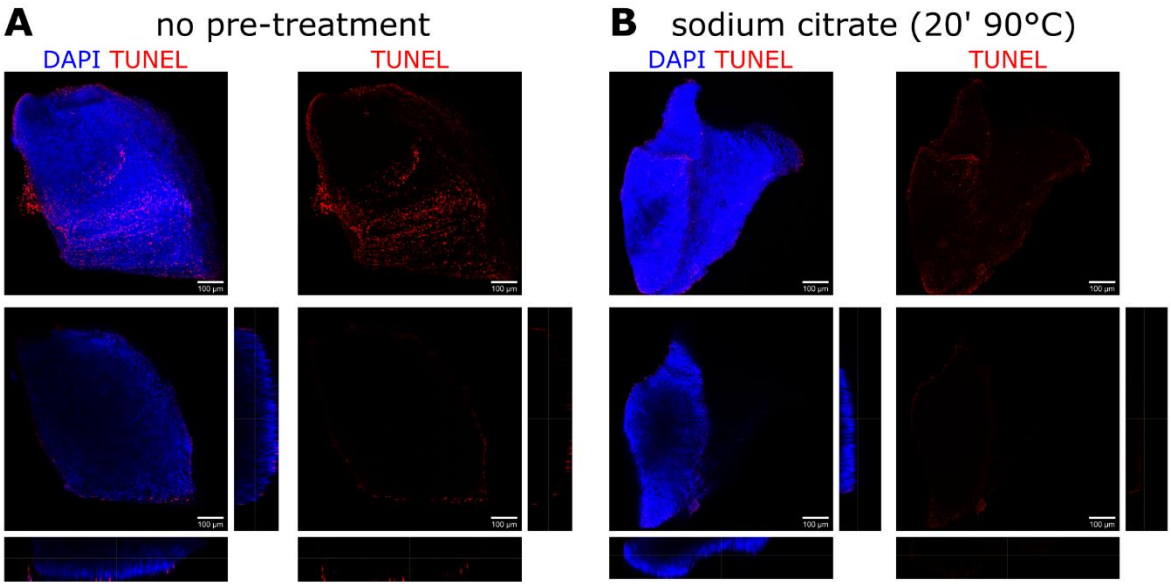

Figure 6-18. Adapting TUNEL to whole-mount labelling and tissue clearing – standard protocol. Whole-mount TUNEL was performed on human ovarian tissue fragments (<250 µm thickness) fixed in NBF, using the protocol provided by the supplier (for use with FFPE tissue sections). Samples were optically cleared using Visikol® HISTO™ and imaged using a confocal microscope to obtain z-stacks at 10 µm intervals, spanning the entire thickness of the sample. Each panel shows maximum intensity projections for the z-stack as well as a central z-slice with orthogonal projections in the y-z (right) and x-z (bottom) planes. The protocol was performed **(A)** without any pre-treatment or **(B)** with 20 min incubation in 10 mM sodium citrate, pH 6 at 90°C. TUNEL-positive nuclei were observed in both samples, however these were only present on the surface of the sample and no TUNEL-positive cells were detected within the sample. Scale bar: 100 µm.

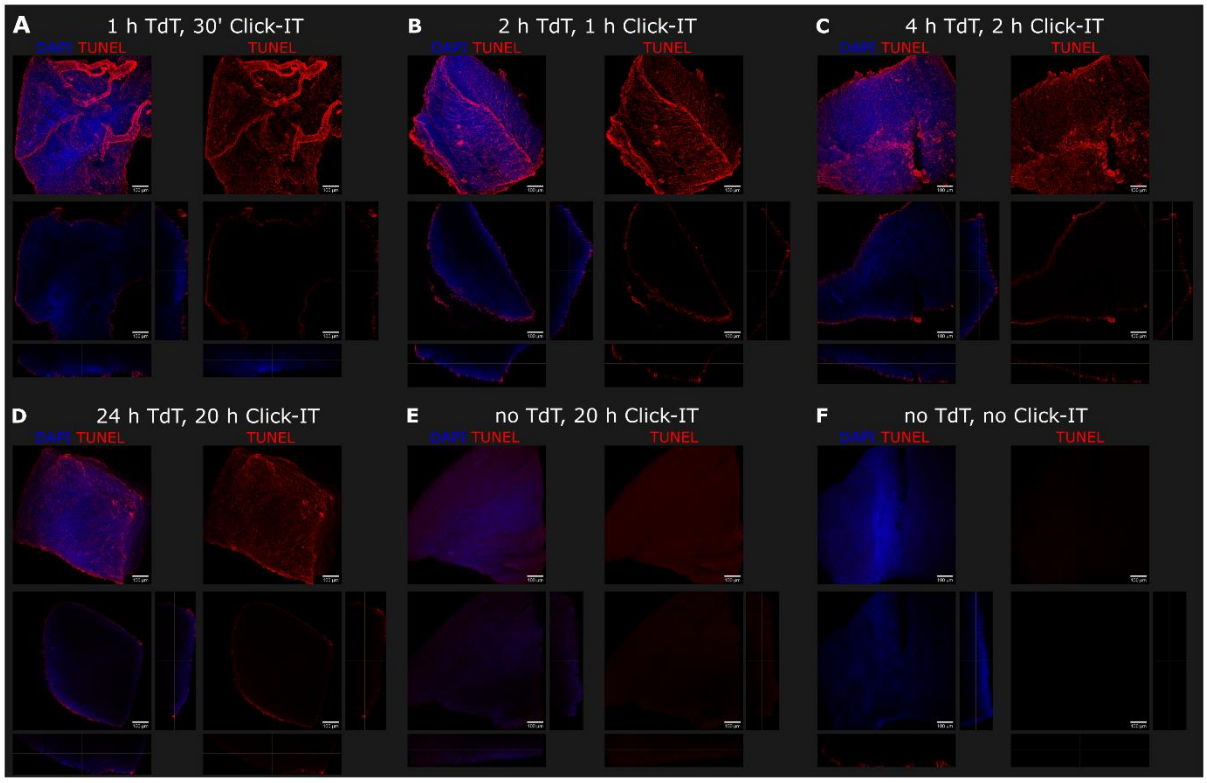

Figure 6-19. Adapting TUNEL to whole-mount labelling and tissue clearing – extended incubation. Whole-mount TUNEL was performed on human ovarian tissue fragments (<250 µm thickness) fixed in NBF, adapting the supplier's recommended protocol by increasing incubations in the TdT enzyme and Click-IT fluorophore reaction (and DAPI nuclear counterstaining). All samples were treated with DNase I overnight prior to labelling. Samples were optically cleared using Visikol® HISTO™ and imaged using a confocal microscope to obtain z-stacks at 5 µm intervals, spanning the entire thickness of the sample. Each panel shows maximum intensity projections for the z-stack as well as a central z-slice with orthogonal projections in the y-z (right) and x-z (bottom) planes. **(A)** 1 h incubation in TdT enzyme, 30 min incubation Click-IT fluorophore reaction (supplier's standard protocol). **(B)** 2 h incubation in TdT enzyme, 1 h incubation Click-IT fluorophore reaction. **(C)** 4 h incubation in TdT enzyme, 2 h incubation Click-IT fluorophore reaction. **(D)** 24 h incubation in TdT enzyme, 20 h incubation Click-IT fluorophore reaction. **(E)** Negative control, with no TdT enzyme, 20 h incubation Click-IT fluorophore reaction. **(F)** Negative control, with no TdT enzyme and no Click-IT fluorophore reaction. TUNEL-positive cells were only detected at the sample surface. Background fluorophore signal was detected within samples after 20 h Click-IT reaction. Scale bar: 100 µm.

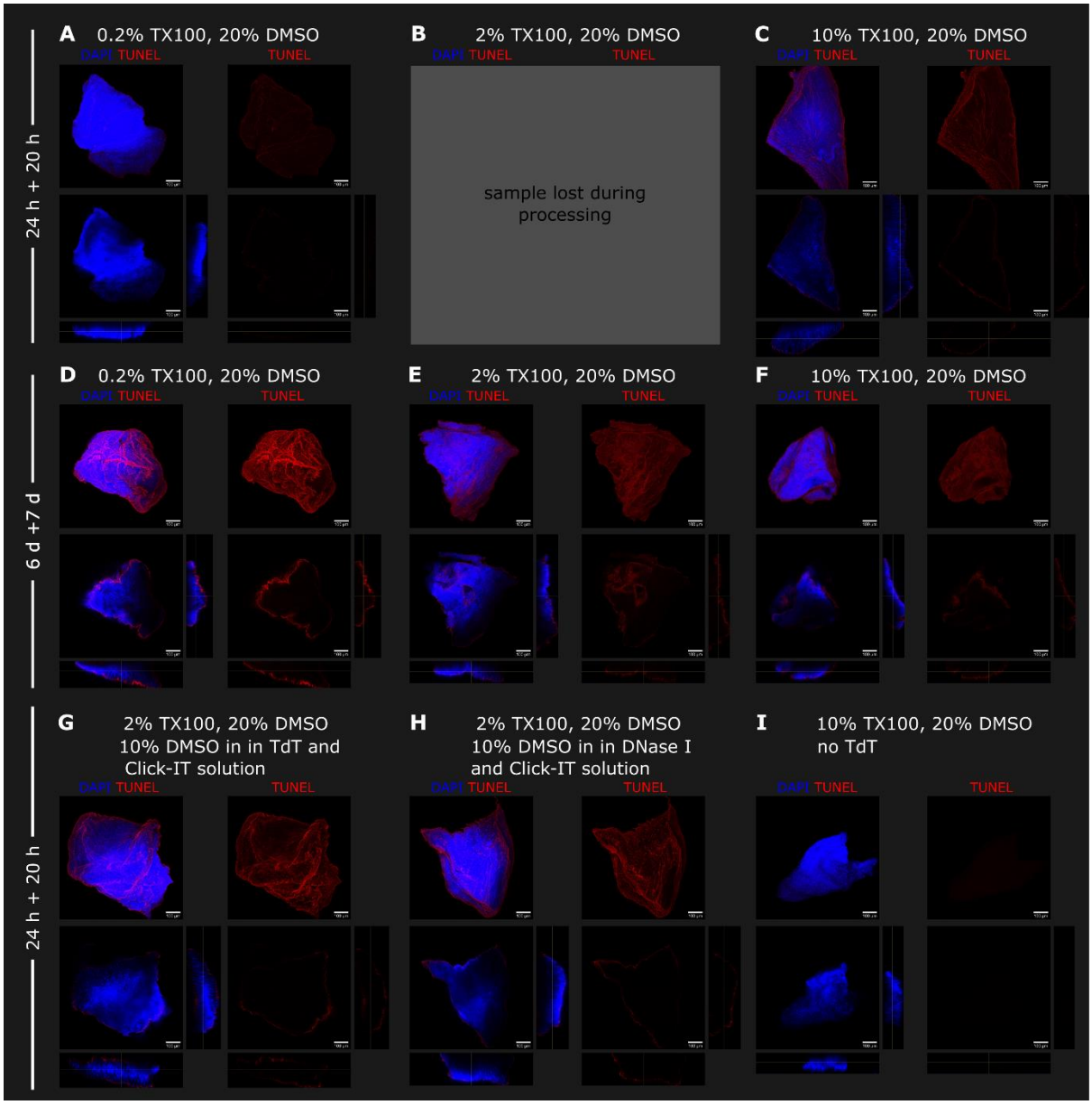

Figure 6-20. Adapting TUNEL to whole-mount labelling and tissue clearing – permeabilization and extended incubation. Whole-mount TUNEL was performed on human ovarian tissue fragments (<250 µm thickness) fixed in 5% form-acetic, adapting the supplier's recommended protocol by permeabilizing samples overnight at RT in 20% DMSO with 0.2, 2 or 10% Triton-X100 (TX100) and by increasing incubations in the TdT enzyme and Click-IT fluorophore reaction (and DAPI nuclear counterstaining). All samples were treated with DNase I overnight prior to labelling. Samples were optically cleared using Visikol® HISTO™ and imaged using a confocal microscope to obtain z-stacks at 5 µm intervals, spanning the entire thickness of the sample. Each panel shows maximum intensity projections for the z-stack as well as a central z-slice with orthogonal projections in the y-z (right) and x-z (bottom) planes. **(A-C)** 24 h incubation in TdT enzyme followed by 20 h Click-IT fluorophore reaction after initial permeabilization in 20% DMSO with 0.2% (A), 2% (B) or 10% (C) TX-100. **(D-F)** 6 day incubation in TdT enzyme followed by 7 day Click-IT fluorophore reaction after initial permeabilization in 20% DMSO with 0.2% (D), 2% (E) or 10% (F) TX-100. **(G)** Same protocol as (B), with 10% DMSO added to TdT and Click-IT solutions. **(H)** Same protocol as (B), with 10% DMSO added to DNase I and Click-IT solutions. **(I)** Negative control, following same protocol as (C), without addition of TdT enzyme. TUNEL-positive cells were only detected at the sample surface. Scale bar: 100 µm.

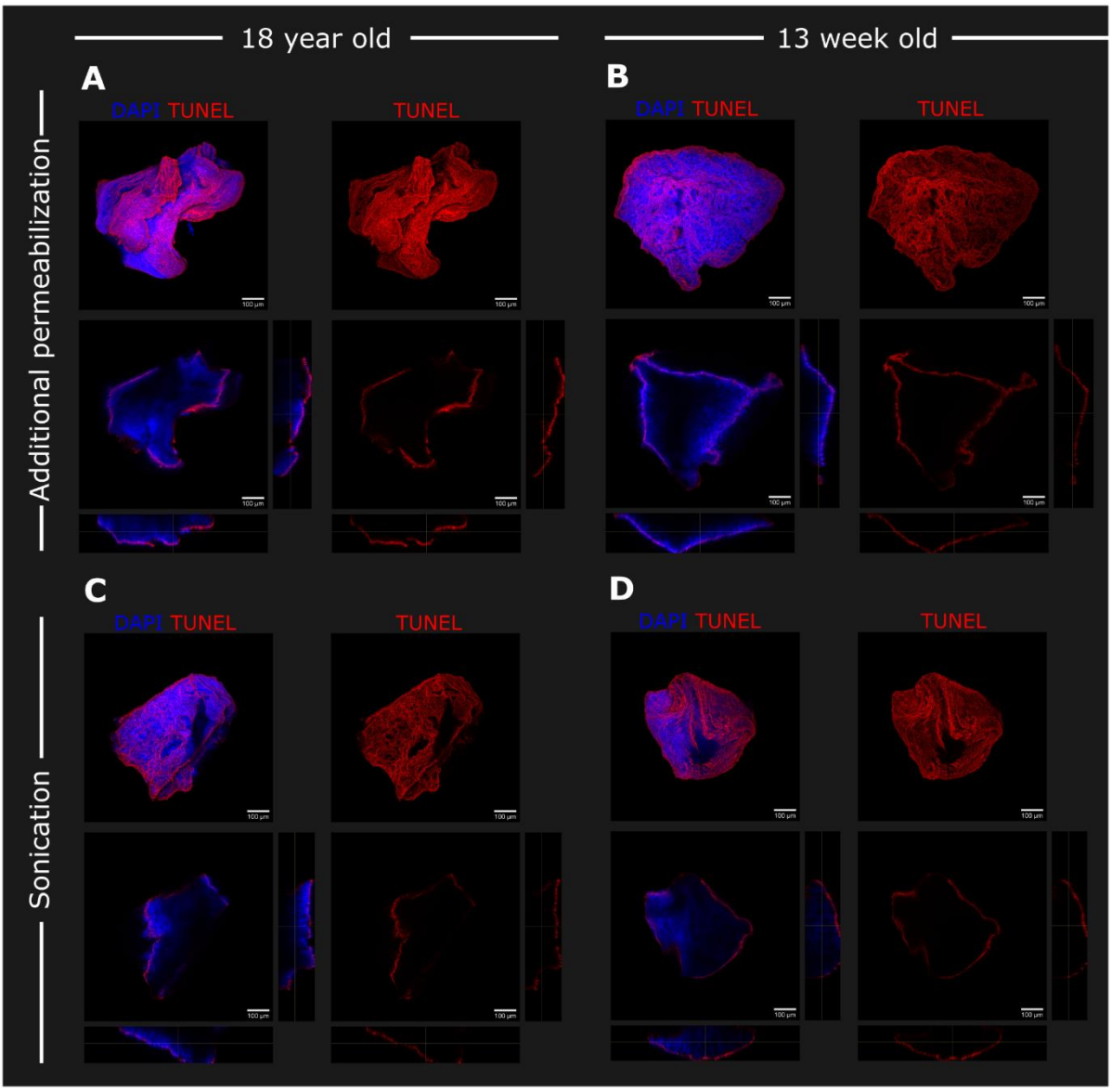

Figure 6-21 Adapting TUNEL to whole-mount labelling and tissue clearing – permeabilization and sonication. Whole-mount TUNEL was performed on human ovarian tissue fragments (<250 µm thickness), fixed in 5% form-acetic. Samples were permeabilised in 0.2% Triton-X100 with 20% DMSO overnight before being treated with DNase I. TdT enzyme incubation was performed for three days, and the Click-IT fluorophore reaction (and DAPI nuclear counterstaining) was performed for 24 h. Samples were optically cleared using Visikol® HISTO™ and imaged using a confocal microscope to obtain z-stacks at 5 µm intervals, spanning the entire thickness of the sample. Each panel shows maximum intensity projections for the z-stack as well as a central z-slice with orthogonal projections in the y-z (right) and x-z (bottom) planes. **(A-B)** Samples from a 18-year-old patient (A) and a 13-week-old donor (B) were incubated overnight at RT in a Tissue Clearing Permeabilization buffer before commencing with TUNEL labelling. **(C-D)** Samples from a 18-year-old patient (C) and a 13-week-old donor (D) were sonicated twice for 10 s with DNase I and twice for 20 s with TdT enzyme solution. TUNEL-positive cells were only detected at the sample surface, with no difference between individuals. Scale bar: 100 µm.

6.3.4 Whole-mount immunolabelling and tissue clearing – the optimised protocol

Following extensive optimisation, intact follicles could be visualised at up to ~120 µm depth using whole-mount labelling with laminin and DDX4, followed by tissue clearing. A diagram of the optimised protocol is presented in Figure 6-22. The resulting images could be viewed in image analysis software such as ImageJ, which allowed visualisation across the xy, xz and yz planes (Figure 6-23A). Laminin could be visualised around the follicle basement membrane, while DDX4 labelled the oocyte cytoplasm (Figure 6-23B). Using advanced image analysis software such as Imaris, 3D reconstructions could be created using built-in software tools (Figure 6-23). This technique would be used to investigate follicle activation *in vitro*, as described in the next chapter.

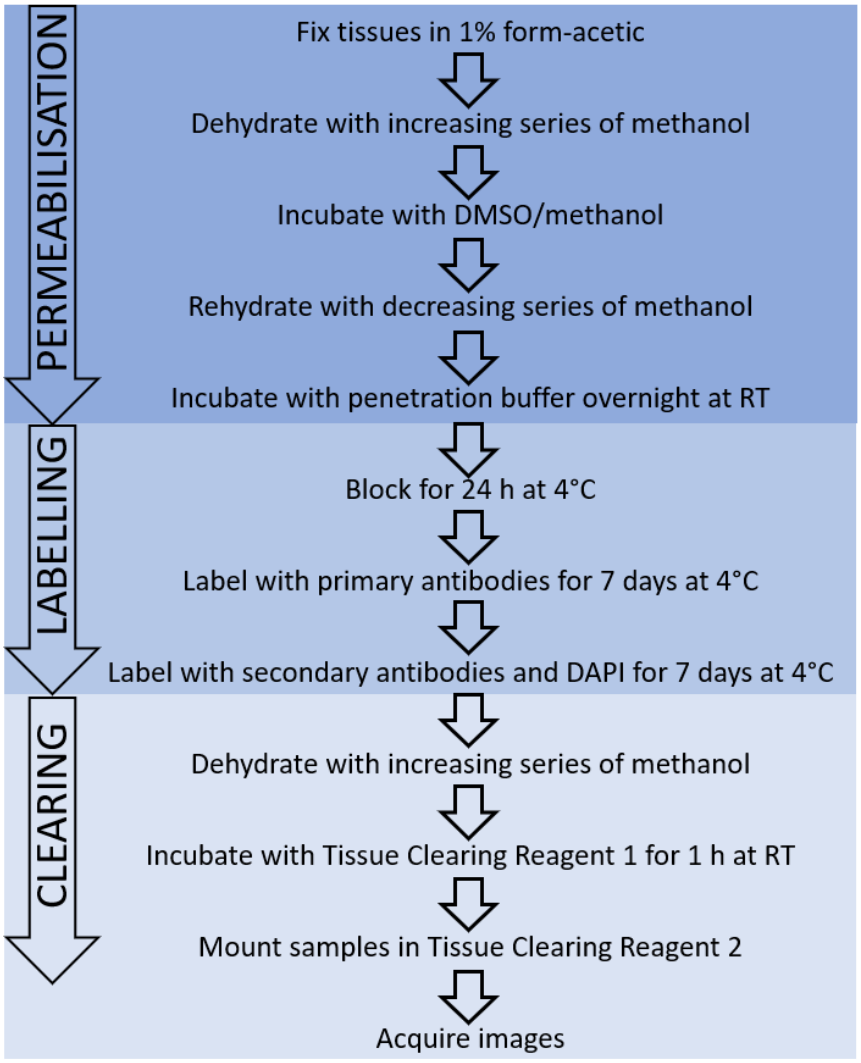

Figure 6-22 Diagram of optimised whole-mount immunolabelling and tissue clearing protocol. For full details of the optimised protocol, see Chapter 2.8.

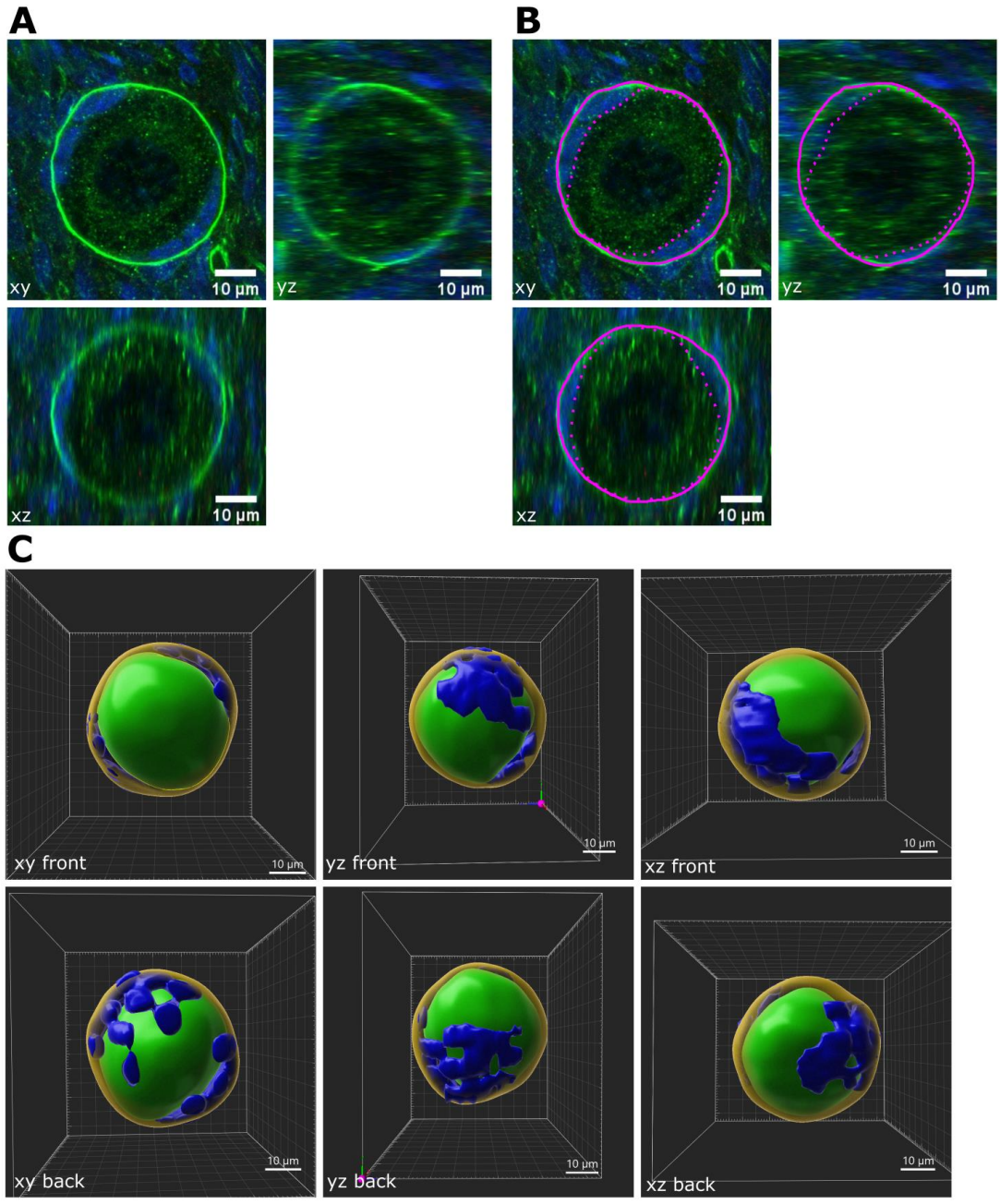

Figure 6-23 Three-dimensional follicle reconstruction using images obtained from cleared human ovarian tissue. Human ovarian tissue fixed in 1% formacetic was labelled with laminin (1:400) and DDX4 (1:100) to detect the follicle basement membrane and oocyte, respectively. Samples were counterstained with DAPI, optically cleared using Visikol® HISTO™ and imaged using a 25x oil immersion objective to obtain z-stacks at 1 µm intervals. **(A)** Representative follicle labelled with laminin and DDX4 (green) and DAPI (blue) demonstrating a central slice through the xy plane and orthogonal views through the xz and yz planes. **(B)** Same image as (A) but highlighting granulosa cell visualisation as the area between the basement membrane (magenta, unbroken line) and the oocyte (magenta, dotted line). **(C)** Three-dimensional reconstruction, using Imaris, of the same follicle as (A). The basal lamina (yellow), oocyte (green) and granulosa cell nuclei (blue) were manually selected, allowing 3D reconstruction. The follicle is shown from different angles as indicated on each panel. Scale bars represent 10 µm.

6.4 Discussion

6.4.1 Identification of primordial follicles using molecular markers

Follicles are currently classified based on morphology: primordial follicles have a single layer of flattened pre-granulosa cells, while transitional (activated) follicles have a mixture of flattened and cuboidal (pre-)granulosa cells. However, it is logical to assume that molecular events within the follicle precede these morphological changes. I therefore sought to determine whether molecular markers could be used to identify primordial follicles. I selected FOXO3 and Smad2/3 as possible candidates to identify primordial follicles.

FOXO3

FOXO3 is a transcription factor that maintains primordial follicle dormancy; it is translocated from the oocyte nucleus to the cytoplasm during follicle activation, as part of the PTEN-Akt-FOXO3 pathway (Section 1.4.1). I investigated the presence of FOXO3 in human ovarian tissue and localisation pattern in primordial, transitional and primary follicles with the aim of using FOXO3 localisation to identify primordial follicles.

FOXO3 was detected in formalin-fixed human ovarian tissue, using both chromogenic and fluorescent detection methods. In contrast, FOXO3 signal was very weak in form-acetic-fixed tissue and could not be detected using fluorescent labelling, despite considerable optimisation including antigen retrieval and signal amplification. As the samples used to compare the two fixatives were from the same patient, this effect was likely due to the difference in fixatives rather than patient variability. Form-acetic contains 5% acetic acid, which is known to cross-link nucleoproteins and may have contributed to the reduction in FOXO3 signal (Baker, 1958; Adeniran *et al.*, 2021). Therefore, I decided to use formalin-fixed samples to investigate FOXO3 in primordial and activated follicles.

In primordial follicles, FOXO3 signal was higher in the nucleus than in the cytoplasm and nuclear FOXO3 decreased in transitional and primary follicles. Furthermore, in transitional follicles, nuclear FOXO3 appeared to decrease with an increased proportion of cuboidal granulosa cells,

however this effect was weak. This may be due to the fact that only the largest cross-section of each follicle was analysed and therefore not all granulosa cells were included in the analysis, potentially skewing the results. This is the first report of quantification of FOXO3 in human transitional follicles, however, others studies have reported this characteristic pattern of nuclear-to-cytoplasmic translocation of FOXO3 as the follicle develops from the primordial to the primary stage (McLaughlin *et al.*, 2014; Takeuchi *et al.*, 2019). In the study by McLaughlin *et al.,* FOXO3 nuclear translocation was not analysed in relation to follicle stage and indeed, primordial and transitional follicles were categorised together as non-growing follicles, while in the present study transitional follicles were analysed separately from primordial follicles (McLaughlin *et al.*, 2014). Takeuchi *et al.* reported that in patients with endometriosis, there was a significantly lower proportion of primordial follicles with nuclear FOXO3 compared to non-affected controls. However, this study is significantly limited by the fact that based on the representative images presented in the study, follicles classified as 'FOXO3 negative' appear not to have any nuclear counterstaining and therefore it may not have been appropriate to characterised nuclear FOXO3 labelling in these follicles, as the section used may not have included the oocyte nucleus. In addition, the authors do not characterise transitional follicles (Takeuchi *et al.*, 2019).

Although there was a significant difference in mean nuclear/cytoplasmic FOXO3 signal between primordial and transitional follicles, this difference was not distinct enough in individual follicles so as to be useful in identifying primordial follicles without also relying on morphological characterisation. I therefore concluded that FOXO3 labelling was not suitable for identifying primordial follicles.

Smad2/3

The Smad proteins are members of the TGFβ superfamily and transmit signals from the cell surface to the cell nucleus. Receptor-regulated Smad2/3 transduce the signal of Activins, TGFβ1-3 and GDF9, while AMH and BMP act via Smad1/5/8 (see Section 1.4.2). Smad2/3 was detected in (pre-)granulosa cells in mouse follicles, and in oocytes and (pre-)granulosa cells in human

follicles. In human pre-granulosa cells, Smad2/3 was detected in the cytoplasm but not in the nucleus, while nuclear Smad2/3 was observed in cuboidal granulosa cells. This is in contrast to studies in immature mice, which have reported Smad2/3 to be localised to the nucleus of pre-granulosa cells in primordial follicles (Hardy *et al.*, 2018). As Smad2/3 localisation has not previously been demonstrated in humans, it is possible that expression of this protein is different in mice to humans.

To explore whether follicle activation occurred via a different group of receptor-regulated Smads, the presence of Smad1/5/8 was investigated in both human and mouse ovarian tissue, however no signal was observed in either species despite attempts at signal amplification. It is unclear why no signal was observed, as localisation of Smad1/5/8 in the mouse ovary has previously been described where it was detected in growing follicles (Fenwick *et al.*, 2013). Based on these results I determined that the Smad proteins would not be useful in identifying primordial follicles.

Markers for granulosa cell visualisation

As I had not been able to identify a molecular marker to identify primordial follicles, I instead determined to identify primordial follicles based on morphology. I therefore investigated markers that would enable visualisation of the follicle, including oocyte and granulosa cells to allow morphological assessment of granulosa cell size and shape.

Phalloidin was not detected in formalin or form-acetic-fixed human ovarian tissue samples. Phalloidin is an actin-binding peptide and can be used to visualise cell borders and has been used to visualise F-actin in mouse ovaries, however this was achieved using paraformaldehyde-fixed cryosections (Da Silva-Buttkus *et al.*, 2008; Mora *et al.*, 2012). Similarly, phalloidin has been used to detect F-actin in isolated human follicles fixed in paraformaldehyde (Xu *et al.*, 2009b). Paraformaldehyde fixation is recommended for actin detection, as 10% neutral buffered formalin contains methanol which stabilises the aqueous formaldehyde but disrupts the structure of actin. Therefore, I explored alternative ways to label granulosa cells.

Beta-catenin was detected in the cytoplasm of granulosa cells and oocytes in formalin-fixed human ovarian tissue, but not form-acetic-fixed samples. Beta-catenin is a cytoplasmic transcription factor involved in cell-cell adhesion and has previously been detected in mouse ovaries where it is mainly localised at the oocyte cytoplasm and interface between oocytes and granulosa cells in primordial follicles, as well as between granulosa cells in growing follicles (Mora *et al.*, 2012; Yan *et al.*, 2019). In adult human ovaries, β-catenin was shown to be localised to the oocyte-pre-granulosa cell interface, the oocyte cytoplasm and nucleus (Bothun and Woods, 2019). As the observed β-catenin signal was low in pre-granulosa cells in human ovarian tissue, I determined that it could not be used to detect pre-granulosa cell borders to enable visualisation and measurements of these cells.

Three different anti-laminin antibodies were tested on formalin-fixed human ovarian tissue, targeting laminin-α, α1 and γ. All antibodies detected laminin, however only the polyclonal antibody against laminin-α detected laminin in primordial follicles and therefore this antibody was selected for the remaining experiments. The expression of laminins in the human ovarian cortex was recently described, the overall most expressed laminins were laminin-α2, α5, β1, β2, and γ1 (Hao *et al.*, 2020). Three laminin-subtypes have been identified in bovine primordial follicles: α1, β2 and γ1 (Rodgers *et al.*, 2003). No laminin signal was observed in primordial follicles from ovarian tissue fixed in form-acetic. To determine whether acetic acid (present in the form-acetic fixative at 5% v/v) poorly preserved or degraded laminin, a range of 0.1-5% form-acetic was tested. Indeed, the intensity of laminin signal appeared to decrease with increased concentrations of acetic acid and laminin was detected in samples fixed in formalin and 0.1-1% form-acetic.

Laminin and DDX4 co-labelling was explored as a way to indirectly visualise granulosa cells as the space between the positively labelled follicle basement membrane (laminin-positive) and oocyte (DDX4-positive). This labelling method has previously been used to measure follicle, granulosa cell and oocyte area in mouse ovaries (Hardy *et al.*, 2018). DDX4 is routinely used to label oocytes in mouse ovaries and has been characterised in human ovarian tissue (Albamonte

et al., 2013). Co-labelling with laminin and DDX4 revealed that 0.5-1% form-acetic was ideal for preserving the laminin signal while also minimising formalin-induced oocyte shrinkage.

Based on these experiments, 1% form-acetic was selected as the preferred fixative to detect both laminin and DDX4 in primordial follicles. This labelling method allowed clear visualisation of the oocyte and follicle basement membrane, allowing pre-granulosa cells to be visualised with the help of nuclear counterstaining, thereby allowing primordial follicles to be identified. These markers were next used to develop a whole-mount immunolabelling and tissue clearing method to allow visualisation of intact follicles.

6.4.2 Development of a whole-mount immunolabelling and tissue clearing technique

I developed a protocol involving whole-mount immunolabelling and tissue clearing to allow visualisation of intact follicles within human ovarian tissue fragments. This was achieved using a commercially available, solvent-based tissue clearing technique. This tissue clearing technique, Visikol® HISTO™, has previously been used to generate 3D renderings of immunolabelled non-human primate and human placental tissue (Merz *et al.*, 2018; Sargent *et al.*, 2018). Other tissue clearing methods have been used to investigate mouse ovaries (Faire *et al.*, 2015; Feng *et al.*, 2017; Kagami *et al.*, 2018; Rinaldi *et al.*, 2018; McKey *et al.*, 2020), however there are no reports of this technology being used on human ovarian tissue.

Human ovarian tissue fragments were sucessfully rendered almost completely transparent and the tissue could be visualised up to approximately 120 μm depth, which was later improved to ~250 μm by imaging each sample from both sides. This limitation in z-depth is likely due to the dense, cellular nature of the human ovarian cortex which causes light scattering and limits resolution (Richardson and Lichtman, 2015). It is possible that clearing could be improved by using alternative tissue clearing techniques, as the Visikol® HISTO™ technique does not fully remove lipids from the tissue, which can be a source of light scattering. However, other tissue clearing methods can cause tissue shrinkage or swelling, which might affect follicle morphology (Richardson and Lichtman, 2015).

Although optical clearing of human ovarian tissue was successful, whole-mount immunolabelling of these samples proved more challenging and required considerable optimisation. For fragments up to 500 μm thick, the supplier suggested antibody incubation at 37°C for up to three hours, however I found that incubation at 4°C was necessary to reduce autofluorescence and non-specific signal. Furthermore, it was necessary to incubate samples in antibody solutions for one week to ensure full antibody penetration. This is likely due to the dense nature of the human ovarian cortex, which may have resulted in slow diffusion of antibodies within the tissue.

6.4.3 Detection of apoptotic cells

I performed a series of experiments in an attempt to determine whether the TUNEL assay was compatible with whole-mount immunolabelling and tissue clearing. While TUNEL labelling proved compatible with tissue clearing and TUNEL-positive cells could be detected, these were isolated at the sample surface. I was unable to improve the signal penetration, despite extensive attempts at optimisation, including extended incubations in the TUNEL reagents and increasing tissue permeabilization. I observed that following permeabilization in high concentrations of Triton-X100 and DMSO the tissue turned purple after incubation in the TdT enzyme solution. This was likely due to precipitation of unchelated cobalt, which is present in the TdT reaction buffer (ThermoFisher representative, personal communication). Furthermore, high concentrations of Triton-X100 may interefere with copper(II) and cobalt, which are present in the Click-IT reaction solution and TdT reaction solutions, respectively (ThermoFisher representative, personal communication).

Antigen retrieval using heat and sodium citrate did not improve TUNEL labelling. Proteinase K pre-treatment is an alternative method of antigen retrieval, commonly used for TUNEL labelling. However, I have previously observed that pre-treatment with proteinase K is incompatible with some antibodies such as AMH, causing off-target labelling (data not shown). Furthermore, excess proteinase K digestion may also cause DNA digestion resulting in diffuse non-specific signal (Dmitrieva and Burg, 2007), we have observed this particularly for tissue fixed in form-acetic (data not shown). As I intended to perform multiplex whole-mount labelling with TUNEL and

immunolabelling, I determined that proteinase K pre-treatment would likely be incompatible with this method, therefore I did not seek to validate it.

Based on the experiments I have described above, I concluded that the Click-iT TUNEL assay was incompatible with whole-mount labelling of human ovarian tissue. It is possible that other commercially available TUNEL kits might be more suitable for whole-mount labelling. For example, the FragEL DNA fragmentation detection kit (QIA39-1EA, Sigma) uses fluorescein-labelled TdT to detect double-stranded DNA breaks. Moreover, as this tissue clearing technique *was* compatible with whole-mount immunolabelling, detection of DNA damage or apoptosis using other markers such as γH2AX or cleaved caspase might be more suitable than the TUNEL assay. Gamma-H2AX is involved in DNA repair and is an early marker for double-stranded DNA breaks. Previous studies have found that detection of double-stranded DNA breaks using TUNEL or γH2AX produce similar results when assessing apoptosis (Natale *et al.*, 2017). Detection of cleaved caspase 3 (CC3) is another method of investigating apoptosis, however this is limited by the fact that the presence of CC3 is transient (Walsh *et al.*, 2011). In addition, detection of CC3 alone may be inappropriate as cleaved caspase 7 (CC7) is also involved in apoptosis (Lamkanfi and Kanneganti, 2010). An alternative way of detecting both CC3 and CC7 is to expose cells to a short peptide during culture, which once cleaved by CC3/7 binds to DNA and becomes fluorescent. The presence of this bound peptide can then be detected using fluorescence microscopy. This method would need to be validated for use with cultured tissue fragments and tissue clearing, however it has been successfully used with cultured brain slices and a different tissue clearing technique (Chang *et al.*, 2014).

Due to the COVID-19 pandemic, it became apparent that I would not be able to perform culture experiments investigating the effects of chemotherapy drugs on primordial follicles. Therefore, I did not seek to further develop a protocol to detect follicle damage and death using whole-mount immunolabelling and tissue clearing and focused on investigating follicle activation *in vitro*, as described in the next chapter.

6.4.4 Summary and future work

In this chapter, I successfully developed a tissue clearing technique that could be used to image human ovarian tissue at up ~120 μm, allowing tissue fragments of up to 250 μm to be visualised. Furthermore, using double-labelling with laminin and DDX4, the follicle basement membrane and oocyte could be visualised, respectively, allowing granulosa cells to be visualised indirectly. Tissue fixation was found to greatly impact antibody labelling and 1% form-acetic was determined to be optimal to preserve laminin while also preventing formalin-induced oocyte shrinkage. While this labelling technique allowed visualisation of (pre-)granulosa cells indirectly with the help of nuclear counterstaining, future work could further investigate additional markers to label individual (pre-)granulosa cells. For the purpose of this investigation it was determined that labelling with laminin and DDX4 using tissue fixed in 1% form-acetic would be used to visualise intact primordial follicles. The use of this technique would be further explored in the next chapter, where it was used to investigate follicle activation *in vitro*.

Chapter 7

Investigation of follicle activation of fresh human ovarian tissue in vitro

7.1. Background

Although early follicle development takes place over several months *in vivo,* the process is considerably expedited *in vitro*, as demonstrated by the fact that human follicle growth has been supported from the unilaminar to the antral stage, resulting in mature oocytes within only three to nine weeks (McLaughlin *et al.*, 2018; Xu *et al.*, 2021). Several studies have highlighted rapid follicle activation of human ovarian tissue *in vitro* (Telfer *et al.*, 2008; Grosbois and Demeestere, 2018; Walker *et al.*, 2021). Foetal bovine and baboon primordial follicles underwent rapid activation within two days of ovarian tissue culture, with primordial follicles decreasing by over 50% coupled with an increase in transitional and primary follicles (Wandji *et al.*, 1996, 1997). Sudden, widespread activation was found to occur between 12-24 h of foetal bovine ovaries being placed into culture, suggesting a specific mechanism acting on all follicles capable of *in vitro* activation (Fortune *et al.*, 2000). One study has demonstrated that human primordial follicles undergo activation within 48 h of *in vitro* culture (De Roo *et al.*, 2020).

The reason for rapid *in vitro* follicle activation is twofold. Firstly, the removal of the ovarian tissue from its native environment is thought to result in the loss of inhibitory factors, such as AMH, which normally keep primordial follicles in a dormant state (Fortune *et al.*, 2000). Secondly, processing of ovarian tissue into small fragments disrupts the Hippo pathway and triggers follicle activation (Scott *et al.*, 2004a; Kawamura *et al.*, 2013; Gavish *et al.*, 2014; Grosbois and Demeestere, 2018). Both the Hippo pathway (Section 1.4.3) and the PI3K pathway (involved in physiological follicle activation and described in detail in Section 1.4.2) have been found to be

activated during *in vitro* processing and culture of human ovarian tissue. Ovarian fragmentation promotes nuclear translocation of YAP, a Hippo effector protein, within granulosa cells (Grosbois and Demeestere, 2018). This leads to upregulation of BIRC1 and CCN2, downstream targets of YAP. In the same study, exposure to PI3K pathway activators triggered follicle activation, while treatment with an mTORC1 inhibitor maintained dormancy (Grosbois and Demeestere, 2018). Furthermore, follicles located near the cut site of the tissue were more developed, however this effect was not quantified. De Roo et *al.* reported a significant decrease in primordial follicles within 48 h of culture, coupled with activation of YAP and upregulation of CCN2, though YAP localisation was not quantified (De Roo *et al.*, 2020). Xenografting of frozen-thawed human ovarian tissue has also been found to trigger follicle activation via the PI3K and Hippo pathways (Masciangelo *et al.*, 2020). There was an increased proportion of primordial follicles with cytoplasmic FOXO1 and a greater proportion of primordial follicles with nuclear YAP in pre-granulosa cells after three days of grafting (Masciangelo *et al.*, 2020).

Although rapid and widespread follicle activation *in vitro* may be useful for culturing a large number of follicles, for example to produce mature oocytes for future fertility preservation, it can present difficulties in other cases, for example when investigating the effects of chemotherapy drugs on primordial follicles. The mechanisms involved in chemotherapy-induced follicle damage remain poorly understood, particularly whether primordial follicles are directly affected or whether they are indirectly lost through accelerated activation (see Section 1.5). The study of chemotherapy-induced follicle damage in humans relies heavily on xenotransplantation and/or *in vitro* culture, however as described above both methods result in mass follicle activation, making the study of primordial follicles difficult. Very few studies have investigated the effects of chemotherapy drugs on human ovarian tissue *in vitro* (Soleimani *et al.*, 2011; Lopes *et al.*, 2020).

Our collaborators at the University of Edinburgh recently studied the effects of doxorubicin and/or cisplatin on human ovarian tissue *in vitro* (Lopes *et al.*, 2020). In this study, ovarian tissue was exposed to chemotherapy drugs for 24 h and then cultured for a further four days. In order to investigate the effects of these drugs on primordial follicles, we planned to conduct a similar

experiment, but collecting the tissue earlier, 12-48 h after drug exposure. In the above study, tissue fragments were allowed to 'recover' from manual handling for 24 h before the chemotherapy drugs were added to the culture system (N. Spears, personal communication; Lopes *et al.*, 2020). However, as follicle activation *in vitro* has been shown to occur within 48 h and perhaps as early as 12 h based on animal models, it is possible that some follicles had activated prior to the chemotherapy drugs being added. We therefore sought to investigate how rapidly follicle activation of human ovarian tissue occurs *in vitro,* to inform the design of the chemotherapy culture experiment. We planned to use the novel whole-mount immunolabelling and tissue clearing method developed in Chapter 6 to accurately identify primordial follicles and allow analysis of intact follicles within the ovarian tissue.

7.1.1. Chapter aims

The aim of this study was to investigate follicle activation of fresh human ovarian tissue *in vitro*. Specifically, I hypothesised that primordial follicles underwent activation as a result of tissue processing and that activation would be observed within 48 h of culture, with the proportion of primordial follicles decreasing over time. This study was devised as a preliminary study to inform the design of subsequent study investigating the effects of chemotherapy drugs on human ovarian tissue *in vitro*. In order to investigate the effects of chemotherapy drugs on primordial follicles, we needed to identify the ideal timepoint for adding chemotherapy drugs, allowing the tissue sufficient time to recover while introducing the drug before mass-activation had occurred. In addition, we were interested in investigating the role of the Hippo pathway on follicle activation *in vitro,* in addition to looking at spatial effects using three-dimensional modelling. Therefore, the aims of this chapter were:

1. To determine whether conventional staging methods (staging at the central cross section on one two-dimensional plane) were sufficient to accurately identify primordial follicles.
2. To determine how rapidly follicle activation occurs *in vitro,* using human ovarian tissue cultured for up to 48 h.

3. To investigate whether the Hippo pathway is altered in primordial follicles due to tissue fragmentation during processing, specifically by localisation of YAP in primordial follicles.
4. To investigate how tissue processing and *in vitro* culture affect follicle activation.

This chapter had the following objectives:

- For Aim 1: to determine whether an equal number of primordial and transitional follicles were identified using both conventional staging (based on central cross section in a single plane) and three-dimensional staging;
- For Aim 2: to compare the proportion of primordial follicles at different timepoints, up to 48 h of culture, to assess whether follicle activation increases over time *in vitro;*
- For Aim 3: to measure YAP localisation in the granulosa cells (nucleus and cytoplasm) of primordial follicles to determine whether YAP signalling is altered following tissue fragmentation and *in vitro* culture
- For Aim 4: to measure the distance of follicles from the cut site(s) of the tissue fragments and from other follicles across three dimensions to determine whether these spatial effects affect follicle activation.

7.2. Materials and methods

7.2.1. Patient samples

Fresh ovarian tissue was collected from patients <20 years with no previous chemotherapy treatment as described in Chapter 2.2. The OCTB handled patient consent, ovary procurement and processing of ovaries into cortical strips. Two fresh cortical strips in chilled L-15 medium were collected from each patient and strips were kept at 4°C until use (within 1 h). Further details, including ethical approval, can be found in Chapters 2.1-2.2.

7.2.2. Tissue culture

Upon arrival in the laboratory, the strips were transferred to dissection medium (3 mg/mL HSA, 100 U/mL penicillin, 100 µg/mL streptomycin, 2 mM L-glutamine and 2 mM sodium pyruvate in

L-15 medium). A small portion of each strip was immediately fixed to act as a non-processed, non-cultured control. The remaining tissue was processed into small pieces (approx. 0.5 x 0.5 x 0.25 mm) using scalpel blades under a dissection microscope. The fragments were incubated in 50 µg/mL neutral red in an αMEM-based dissection medium with the same supplements as above for 2 h at 37°C in a humidified incubator with 5% CO_2. Fragments were visualised under a dissection microscope (dark-field) and fragments containing NR-positive follicles were preferentially selected for culture before those with no staining.

Tissue pieces were cultured individually as described in Chapter 2.4. A portion of tissue was fixed as a post-processing, non-cultured control (0 h). Tissue pieces were cultured for up to 48 h, with a portion being fixed at different timepoints (after 2 h, 4 h, overnight, 24 h or 48 h culture). Samples were fixed in 1% form-acetic for 24 h and stored in 70% ethanol.

7.2.3. Whole-mount immunolabelling and tissue clearing

Whole-mount immunolabelling and tissue clearing was performed as described in Chapter 2.8. For each patient, three to five tissue pieces from each group were labelled, with at least one NR-positive sample included in each sample group. Samples were labelled with rabbit anti-laminin polyclonal antibody (1.75 µg/mL, ab11575, Abcam), rabbit anti-DDX4 polyclonal antibody (10 µg/mL, ab13840, Abcam) and mouse anti-YAP monoclonal antibody (14.2 µg/mL, 12395S, Cell Signaling Technology). Antibody signal was detected using Alexa Fluor 488 donkey anti-rabbit IgG (1:100, 20 µg/mL, A21205, Thermo Fisher Scientific) to detect laminin and DDX4, and Alexa Fluor 568 donkey anti-mouse IgG (1:100, 20 µg/mL, A10037, Thermo Fisher Scientific) to detect YAP. A negative control was prepared using rabbit IgG (10 µg/mL, 3900S, Cell Signaling Technology) and mouse IgG1 (14.2 µg/mL, 401401, BioLegend). Nuclei were counterstained using 5 µg/mL DAPI. Cleared tissue samples were stored at 4°C and protected from light.

7.2.4. Imaging

Images were collected using a Zeiss 780 upright confocal microscope. Images of whole tissue fragments were obtained with a x10/0.45 numerical aperture (NA) objective (working distance

2 mm) at 2.5 µm intervals while follicles were imaged using a x25/0.8 NA oil immersion objective (working distance 570 µm) at 1.5 µm intervals. DAPI was excited using a 405 nm laser detected at 380-480 nm. Alexa Fluor 488 was detected using a 488 nm laser and a 490-555 nm emission. Alexa Fluor 568 and 594 were excited using a 594 nm laser and detected at 580-630 nm. Optimal pinhole size was determined for each channel and kept constant for all samples. Gain settings for DAPI and Alexa Fluor 488 were adjusted invididually for each sample, to allow clear visualisation of cell nuclei (DAPI) and laminin and oocytes (Alexa Fluor 488), as these markers would not be quantified. Gain settings for Alexa Fluor 568 was kept constant for all samples. Z-compensation with extrapolation was used to adjust for decreasing signal brightness at greater z-depths. Z-stacks were obtained by identifying the top and bottom of the sample. Samples were first imaged from one side and then flipped over and imaged from the other side to overcome imaging resolution limitations.

7.2.5. Image analysis

Images of cleared tissue samples were analysed using ImageJ Fiji and Imaris (version 9.7.0). Measurements across the xy, xz or yz planes were performed in ImageJ Fiji using orthogonal views and the measurement tools to measure the size of follicles, oocytes and granulosa cells. Oocyte and follicle volume (V) was calculated based on the oocyte or follicle radius (r) at the x, y and z planes using the following formula for the volume of an ellipsoid:

$$V = \frac{4}{3}\pi r_x r_y r_z$$

7.2.6. Statistical analysis

Data was analysed using GraphPad Prism (version 9.1.). Data was tested for normality using the Shapiro-Wilk test. Ordinary one-way ANOVA with Tukey's *post-hoc* testing was used to compare granulosa cell, oocyte and follicle size measurements of primordial and transitional follicles. Statistical significance was defined as $P<0.05$.

7.3. Results

7.3.1. Patient characteristics

Fresh human ovarian tissue samples were processed and cultured for up to 48 h, with samples collected at the start of processing (Ctrl), before culture (0 h) and after 2 h, 4 h, overnight, 24 h and 48 h culture. We initially set out to collect ovarian tissue samples from six patients, however owing to restrictions caused by the COVID-19 pandemic, only samples from three patients were obtained. Information on these patients, aged 9-12 years, is presented in Table 7-1.

Table 7-1. Characteristics of patients used to investigate follicle activation *in vitro*. OCT: ovarian tissue cryopreservation.

Patient	Age at OTC	Pubertal status	Diagnosis
R	9	Pre-pubertal	Osteosarcoma
S	11	Unknown	Sickle cell disease
T	12	Pubertal	Localised synovial sarcoma

Neutral red (NR) was used during sample processing to visualise containing follicles, appearing as red-stained circles. NR-positive fragments were evenly distributed across the experimental groups, to help ensure that all groups contained samples with follicles. Any remaining NR-negative tissue pieces were also included in the experiment in case these contained follicles that had not been visualised with NR. During processing and culture of tissue from patient T, it was observed that only seven out of over 40 tissue pieces were NR-positive, each with only 1-3 NR-positive structures (Figure 7-1A). One NR-positive piece was fixed separately to determine whether NR-positive structures were indeed follicles, using whole-mount immunolabelling and tissue clearing to detect laminin and DDX4 (Figure 7-1B). NR did not allow visualisation of all follicles, two follicles had been visualised with NR staining, however three follicles were visible after immunolabelling and tissue clearing. The two follicles visible with NR were at the surface of the tissue piece, while the third was located approximately 100 μm within the tissue.

There was considerable variation in follicle numbers both between and within patients, in line with what was characterised in Chapter 4. Although at least one NR-positive piece of tissue was included in all experimental groups, in some of these groups tissue fragments contained no follicles (Table 7-2). In particular, for patient T, four out of seven experimental groups contained no follicles. Due to the low sample number resulting from these observations, it was determined that statistical analysis could not be performed between the different experimental conditions. Therefore, this chapter will instead focus on descriptive analysis and observations.

Table 7-2. Overview of immunolabelled tissue fragments from each experimental group. The number of follicle-containing fragments out of total fragments is shown along with total follicles analysed. Emphasis is placed on groups where none of the fragments contained follicles.

	Fragments containing follicles			**Total follicles analysed**		
Group	**Patient R**	**Patient S**	**Patient T**	**Patient R**	**Patient S**	**Patient T**
Control	1 of 3	2 of 3	2 of 5	11	218	5
0 h culture	2 of 3	4 of 4	1 of 3	15	81	6
2 h culture	2 of 3	4 of 4	**0 of 3**	59	74	**0**
4 h culture	1 of 3	4 of 4	**0 of 3**	55	24	**0**
Overnight culture	1 of 3	3 of 4	1 of 3	44	73	33
24 h culture	2 of 3	2 of 4	**0 of 3**	34	30	**0**
48 h culture	2 of 3	2 of 4	**0 of 3**	82	48	**0**

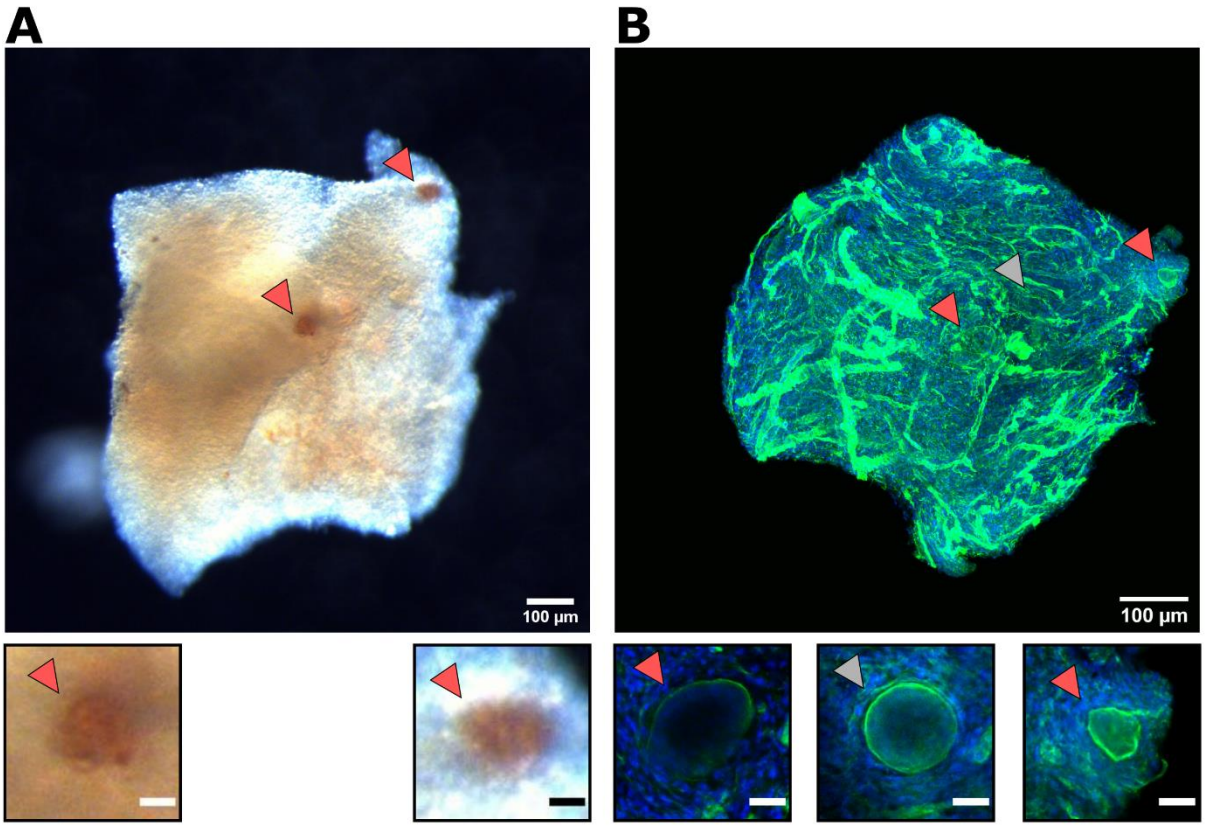

Figure 7-1. Use of neutral red to detect follicles prior to tissue culture. Fresh ovarian tissue from patient T (12 years old) was cut into small pieces and stained with NR for 2 h. **(A)** Two follicles could be visualised as NR-positive (red arrowheads). Lower panels show a magnified view of the follicles. **(B)** Maximum intensity projection of the same piece of tissue as in (A), following immunolabelling and tissue clearing to detect laminin and DDX4 (green) with nuclear counterstaining (DAPI, blue). Z-stacks were obtained at 10 µm intervals. Red arrows indicate the location of the follicles from (A) while the grey arrowhead indicates a follicle approximately 100 µm within the tissue piece that was not visible following NR staining. Note the large number of blood vessels, appearing as green threads. Lower panels show a central slice through each follicle, as they appear from left to right in the tissue piece. Scale bars represent 20 µm unless otherwise indicated in the figure.

7.3.2. Three-dimensional staging of follicles

The first aim of this chapter was to determine whether conventional classification of primordial follicles, namely assessment of morphology at the largest cross-section, was sufficient to accurately distinguish between primordial (oocyte surrounded by flattened pre-granulosa cells) and transitional (oocyte surrounded by a mixture of flattened and cuboidal (pre-)granulosa cells) follicles. Tissue that had been fixed prior to processing and culture (control) and labelled with DDX4 and laminin and was used for this analysis. Staging was performed using the method

developed in Chapter 6 using whole-mount immunolabelling to detect DDX4 and laminin followed by tissue clearing. Granulosa cells could be visualised using this method as the space between the laminin and DDX4 signal, with the help of nuclear counterstaining. Follicles were visualised across three dimensions (xy plane, xz plane and yz plane, Figure 7-2A). At each plane, follicles were classified as having only flattened pre-granulosa cells (F) or a mixture of flattened and cuboidal (pre-)granulosa cells (C, Figure 7-2B). Based on this analysis, follicles were classified as primordial (only flattened pre-granulosa cells across all three planes, FFF) or transitional (cuboidal granulosa cells observed in at least one plane, Figure 7-2C). Transitional follicles were further classified as having cuboidal granulosa cells at one (FFC), two (FCC) or all three planes (CCC). For each follicle and oocyte, the diameter (largest and perpendicular diameter on xy plane) and depth (diameter across the z-axis) was measured, in addition to (pre-)granulosa cell height at each plane.

A total of 52 follicles from patient S were included in the analysis. Control samples from patient T contained only primary follicles and these samples were therefore excluded. Furthermore, control samples from patient R contained only unusual disc-shaped follicles which could not be accurately staged across the xz or yz axis and were therefore not included in this analysis. These disc-shaped follicles are discussed in the next section.

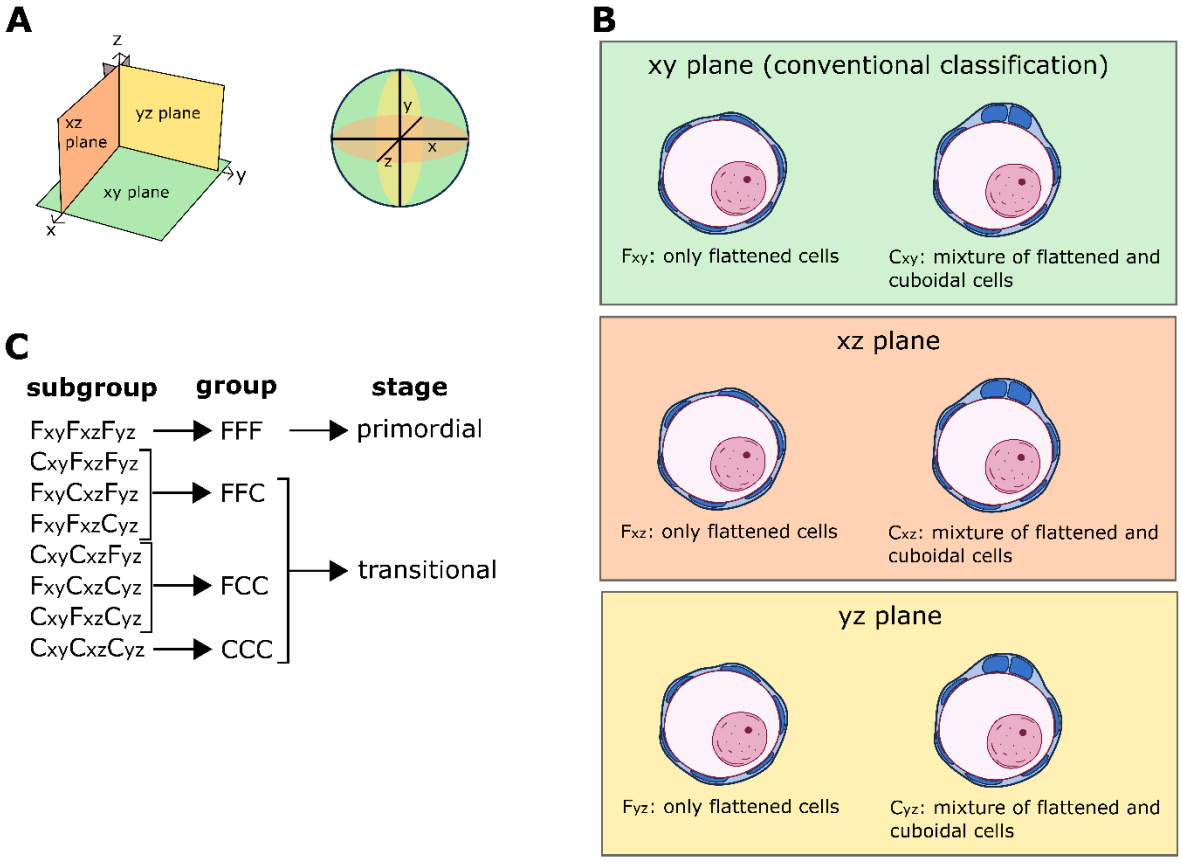

Figure 7-2. Diagram of planned identification of primordial follicles using three-dimensional classification. (A) Diagram of the three coordinate planes: xy (green), yz (yellow) and xz (orange). These planes are also demonstrated across a sphere, as follicles are spherical structures. **(B)** Each follicle was assessed across three planes and categorised based on morphology as having only flattened pre-granulosa cells (F) or a mixture of flattened and cuboidal (pre-)granulosa cells (C). Subscript indicates the relevant plane. **(C)** Each follicle could be classified into one of eight subgroups (left column) based on morphological classification across each of the three planes. Follicles were grouped based on having flattened pre-granulosa cells across all three planes (FFF), or as having cuboidal granulosa cells at one (FFC), two (FCC) or all three planes (CCC). Follicles in the FFF group were classified as primordial, while follicles in the FFC, FCC or CCC groups were considered transitional.

When viewed only across the xy plane (as in conventional analysis), 24 follicles were classified as primordial and 28 as transitional (Figure 7-3). However, when viewed across all three planes, only 10 follicles were found to be primordial and 42 were transitional (Figure 7-3). Therefore, by using the conventional staging method, 58% of follicles classified as primordial contained cuboidal granulosa cells that could not be observed across the xy plane and were therefore actually transitional follicles. Out of the 42 transitional follicles, only 12 follicles contained one or more cuboidal cells at all three planes (Figure 7-3).

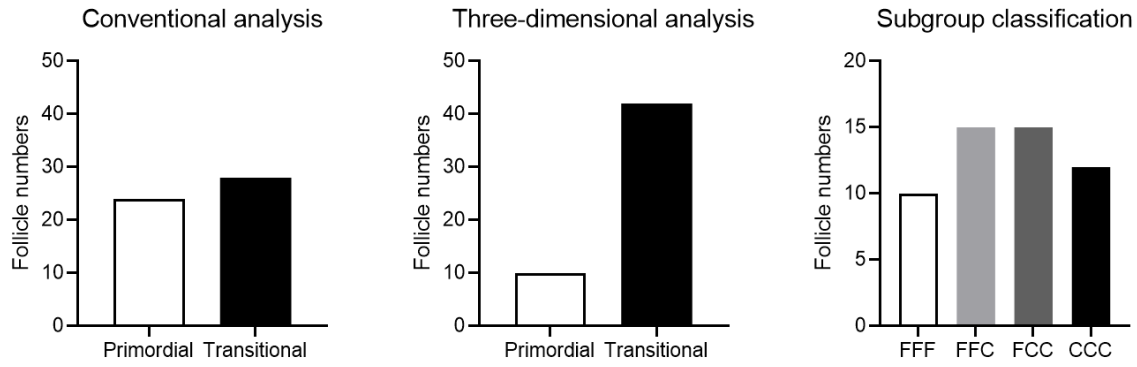

Figure 7-3. Identification of primordial and transitional follicles using conventional and three-dimensional classification. A total of 52 follicles from Patient S (non-processed, non-cultured tissue) were analysed. Follicles were classified as primordial or transitional based on the largest follicle cross-section across the xy plane (conventional analysis) or across three planes (three-dimensional analysis). Follicles were further classified into subgroups based on whether only flattened pre-granulosa cells were observed across all three planes (FFF, primordial) or cuboidal granulosa cells were observed at one (FFC), two (FCC) or all three planes (CCC).

Follicle and oocyte diameters were measured across three axes (x, y and z) and volume calculated (Figure 7-4A). There was no difference in follicle size (diameter across the x, y and z axes) or follicle volume between the four groups, nor in oocyte size or volume (Figure 7-4B-C). However, there was a significant difference in both mean and maximum (pre-)granulosa cell size between the groups (Figure 7-4C). The maximum (pre-)granulosa cell size was significantly smaller for FFF (primordial) follicles (3.5 ± 0.5 μm) compared to transitional follicles (FCC and CCC, 4.6 ± 1.2 μm with $P<0.05$ and 5.4 ± 0.9 μm with $P<0.0001$, respectively). Within transitional follicles, there was also a difference in maximum (pre-)granulosa cell height between FFC and CCC follicles (3.9 ± 0.6 μm vs. 5.4 ± 0.9 μm with $P<0.001$). Furthermore, there was a significant difference in mean (pre-)granulosa cell size between the groups. The mean (pre-)granulosa cell size of FFF follicles was significantly smaller than transitional follicles (CCC group, 2.5 ± 0.4 μm compared to 3.2 ± 0.4 μm with $P<0.001$). Within transitional follicles, there was a significant difference in mean (pre-)granulosa cell size between FFC and CCC ($P<0.0001$) and FCC and CCC ($P<0.05$) follicles (FFC: 2.5 ± 0.4 μm, FCC: 2.8 ± 0.4 μm and CCC: 3.2 ± 0.4 μm).

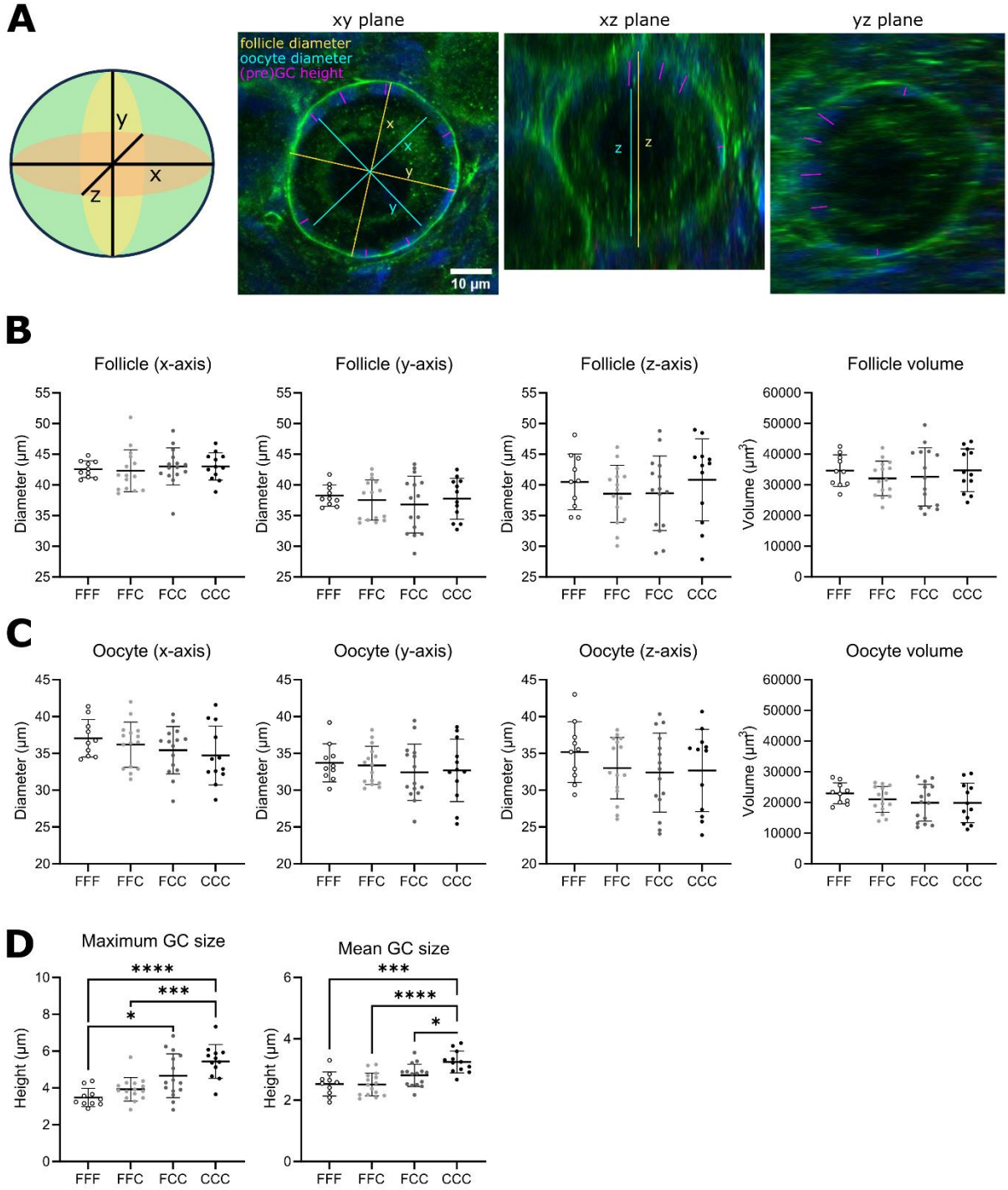

Figure 7-4. Three-dimensional analysis of primordial and transitional follicles. Fifty-two follicles from Patient S (non-processed, non-cultured tissue) were classified across three planes based on morphology as FFF (only flattened pre-granulosa cells, primordial) or FFC, FCC or CCC (mixture of flattened and cuboidal (pre-)granulosa cells, transitional) as described in the text. **(A)** Diagram of an ellipsoid to represent a three-dimensional view of a follicle. Representative image of a follicle (classified as FCC) is shown. For each follicle, the maximum follicle (yellow) and oocyte (blue) diameter was measured (defined as the x-axis) as well as the perpendicular diameter (y-axis). The depth of the follicle was also measured across the z-axis. The height of (pre-)granulosa cells was measured across all three planes (xy, xz and yz). **(B)** Follicle diameter (x- and y-axis), follicle depth and follicle volume. **(C)** Oocyte diameter (x- and y-axis), oocyte depth and oocyte volume. **(D)** Maximum and mean (pre-)GC height. * $P < 0.05$, *** $P < 0.001$, **** $P < 0.0001$.

In summary, this analysis demonstrated the importance of considering the follicle as a three-dimensional structure and viewing follicles across all three dimensions when distinguishing between primordial and transitional follicles. While the size of (pre-)granulosa cell differed between primordial and transitional follicles and within transitional follicle subgroups, there was no difference in follicle or oocyte size.

7.3.3. Follicles are irregularly shaped across three dimensions

Fresh ovarian tissue from three young patients was processed into small fragments and cultured for up to 48 h, with samples fixed before culture (0 h) and after 2 h, 4 h, overnight, 24 h and 48 h culture. Samples were labelled with DDX4 and laminin to visualise the oocyte and follicle basement membrane, respectively. Whole-mount immunolabelling and tissue clearing was used to visualise intact follicles across three dimensions. Follicle diameter was measured along the x, y and z-axes to assess follicle size and shape. Due to limitations with imaging resolution and greater z-depths, only follicles located within ~120 μm from the tissue surface could be measured.

When viewed across three dimensions, it was observed that follicles were irregularly shaped, with some follicles appearing flat or disc shaped. This phenomenon was observed for pre-antral follicles of all stages (primordial, transitional, primary and multilayer) across all three patients. The size and shape of primordial and transitional follicles from patients R and S was further investigated (Figure 7-5). Disc-shaped follicles were observed in both non-cultured (control, 0 h) and cultured tissue (2 h – 48 h; Figure 7-5A); these follicles had a smaller diameter across the z-axis compared to the x or y axes (Figure 7-5B). In some tissue fragments, both disc-shaped and more regular spherical/ellipsoid follicles were observed, however some fragments of tissue contained predominantly spherical/ellipsoid or disc-shaped follicles. There was no relationship between the location of a follicle within the tissue fragment (z-depth) and length across the z-axis (data not shown). Interestingly, the appearance of disc-shaped follicles was only evident across the z-axis, however it was noted that in follicles with a very small z-diameter the oocyte was

poorly visible when viewed across the xy plane (for example see representative follicle from Patient S after 2 h culture, Figure 7-5A).

Some tissue fragments from Patient R contained many follicles that appeared atretic, these were shrunken or irregularly shaped and had a condensed oocyte nucleus (see 2 h, 4 h and 48 h cultured follicles from Patient R, Figure 7-5A). However, follicle health could not be assessed based on laminin and DDX4 labelling, though interestingly these follicles appeared to have a stronger DDX4 signal, thought this was not quantified (Figure 7-5A).

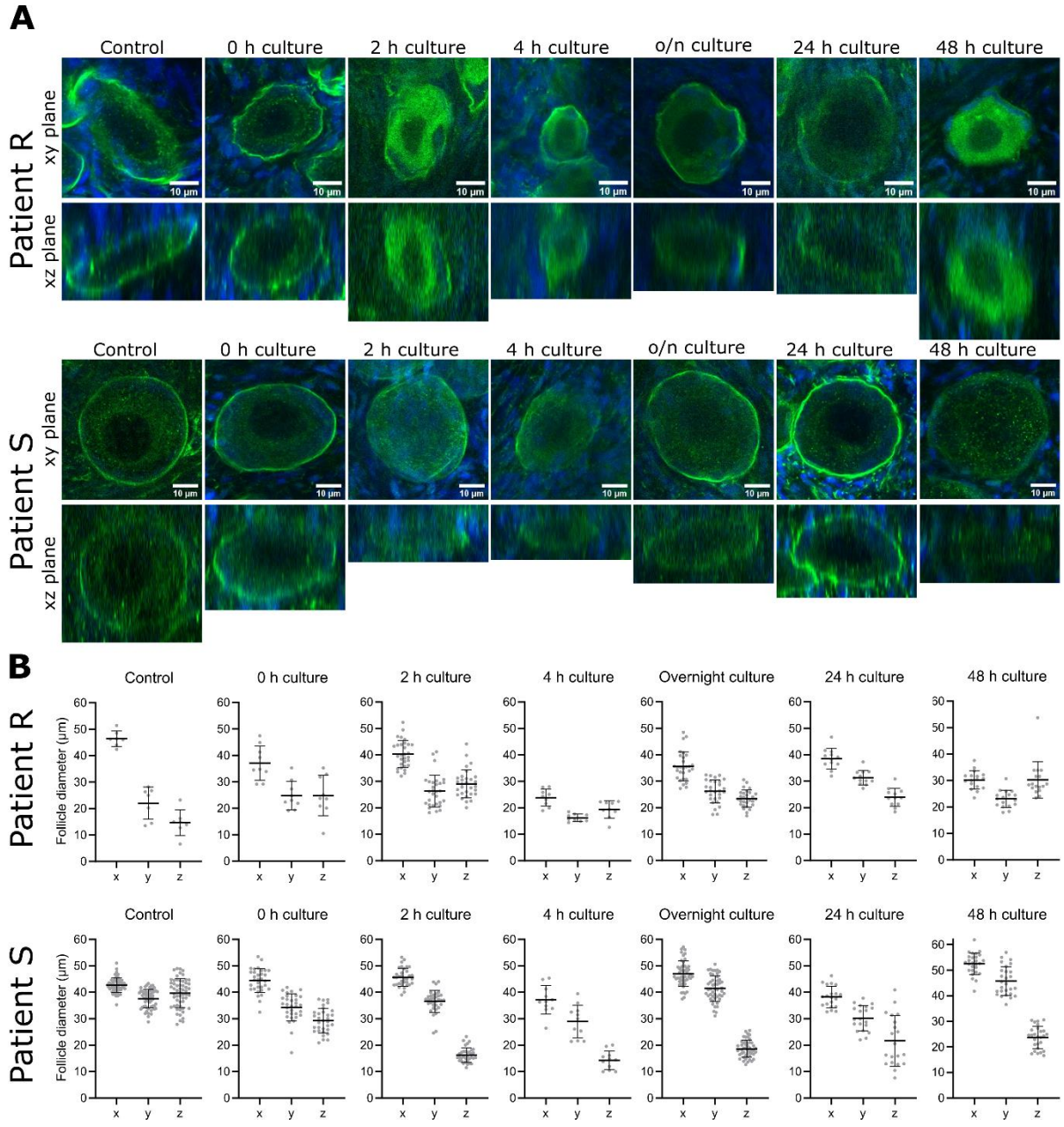

Figure 7-5 Three-dimensional follicle size in tissue cultured *in vitro* for up to 48 h. Fresh ovarian tissue from three young patients was processed into small fragments and cultured for up to 48 h. Tissue fragments were labelled with DDX4 and laminin (green) to detect the oocyte and follicle basement membrane, respectively, and counterstained with DAPI (blue) using whole-mount immunolabelling and tissue clearing. Confocal microscopy was used to obtain z-stacks of the labelled and cleared tissue fragments. **(A)** Representative images of primordial and transitional follicles from patients R (upper images) and S (lower images). Each follicle is shown through a central slice across the xy and xz planes. Note the variable size of follicles between the two patients and between different conditions. Scale bars represent 10 µm. **(B)** Follicle diameter across the x, y and z axes. Each dot represents a single follicle, with bars representing mean ± SD. For spherical follicles, the follicle diameter across the x, y and z planes is approximately equal, however the majority of follicles observed were irregular in shape, commonly appearing flat or disc-shaped, as demonstrated by a low follicle diameter across the z-axis. Statistical analysis was not performed as these data came from individual patients. See Table 7-2 for follicle numbers.

7.3.4. Follicle activation *in vitro*

The second aim of this chapter was to investigate follicle activation of fresh ovarian tissue *in vitro*. Cultured tissue was fixed at different timepoints up to 48 h to assess how rapidly follicle activation occurs *in vitro*. As assessment of follicle activation requires accurate distinction between primordial and transitional follicles, three-dimensional follicle staging (as described in section 7.3.2) was to be used. However, due to the large number of disc-shaped follicles, described in the previous section, a large portion of follicles could not be assessed across the xz or yz planes due to difficulties in visualising the oocyte and granulosa cells. Therefore, follicle staging was performed using conventional classification across the xy plane (Figure 7-6A).

There was considerable variation in follicle stage distribution between and within patients (Figure 7-6B). Unfortunately, Patient T had very few follicles, with four out of seven sample groups having no follicles at all. Therefore, due to the small sample size, statistical analysis could not be performed and follicle stage distribution is therefore presented for each patient individually (Figure 7-6B). *In vitro* culture did not appear to cause increased follicle activation within 48 h, for Patients R and S there appeared to be a random distribution of follicle stage across the different timepoints, however, transitional follicles appeared to be the dominant follicle population. In Patient T, only primary follicles were observed in non-cultured tissue (control and 0 h).

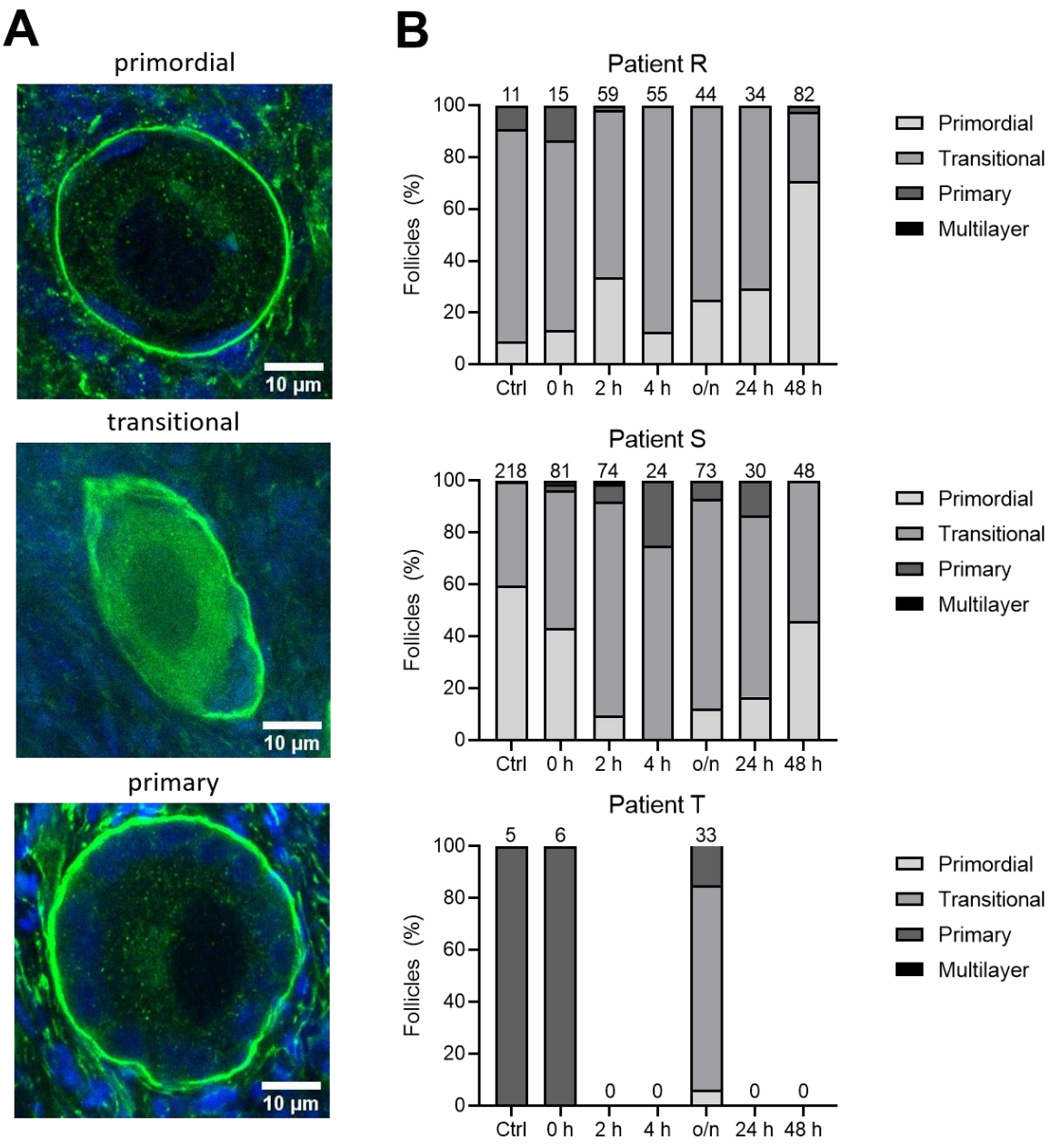

Figure 7-6. Two-dimensional staging of follicles from fresh ovarian tissue cultured for up to 48 h. Fresh ovarian tissue from three young patients was processed into small fragments and cultured for up to 48 h. Tissue fragments were labelled with DDX4 and laminin (green) to detect the oocyte and follicle basement membrane, respectively, and counterstained with DAPI (blue) using whole-mount immunolabelling and tissue clearing. Confocal microscopy was used to obtain z-stacks of the labelled and cleared tissue fragments. **(A)** Representative images of follicles at different stages: primordial (Patient S, control), transitional (Patient R, overnight culture) and primary (Patient S, 24 h culture). **(B)** Distribution of follicle stage (using conventional two-dimensional staging across the xy plane) between groups for each patient. Numbers at the top of each column represents the total number of follicles in that group. Ctrl: non-processed, non-cultured control, o/n: overnight culture.

7.3.5. YAP signalling

The third aim of this chapter was to investigate whether the Hippo pathway was involved in follicle activation of *in vitro* cultured fresh ovarian tissue. Tissue fragments were labelled with DDX4 and laminin (to visualise the follicle) and YAP, a transducer of the Hippo pathway, using whole-mount immunolabelling and tissue clearing. YAP signalling in primordial and transitional follicles was to be analysed to determine whether YAP signalling was involved in follicle activation.

YAP was not detected in primordial, transitional or primary follicles (Figure 7-7A). However, YAP was detected in other structures, particularly in blood vessels and granulosa cells of multilayer follicles (Figure 7-7B). As the YAP signal in primordial and transitional follicles could could not be distinguished from non-specific background signal, YAP signalling could not be investigated.

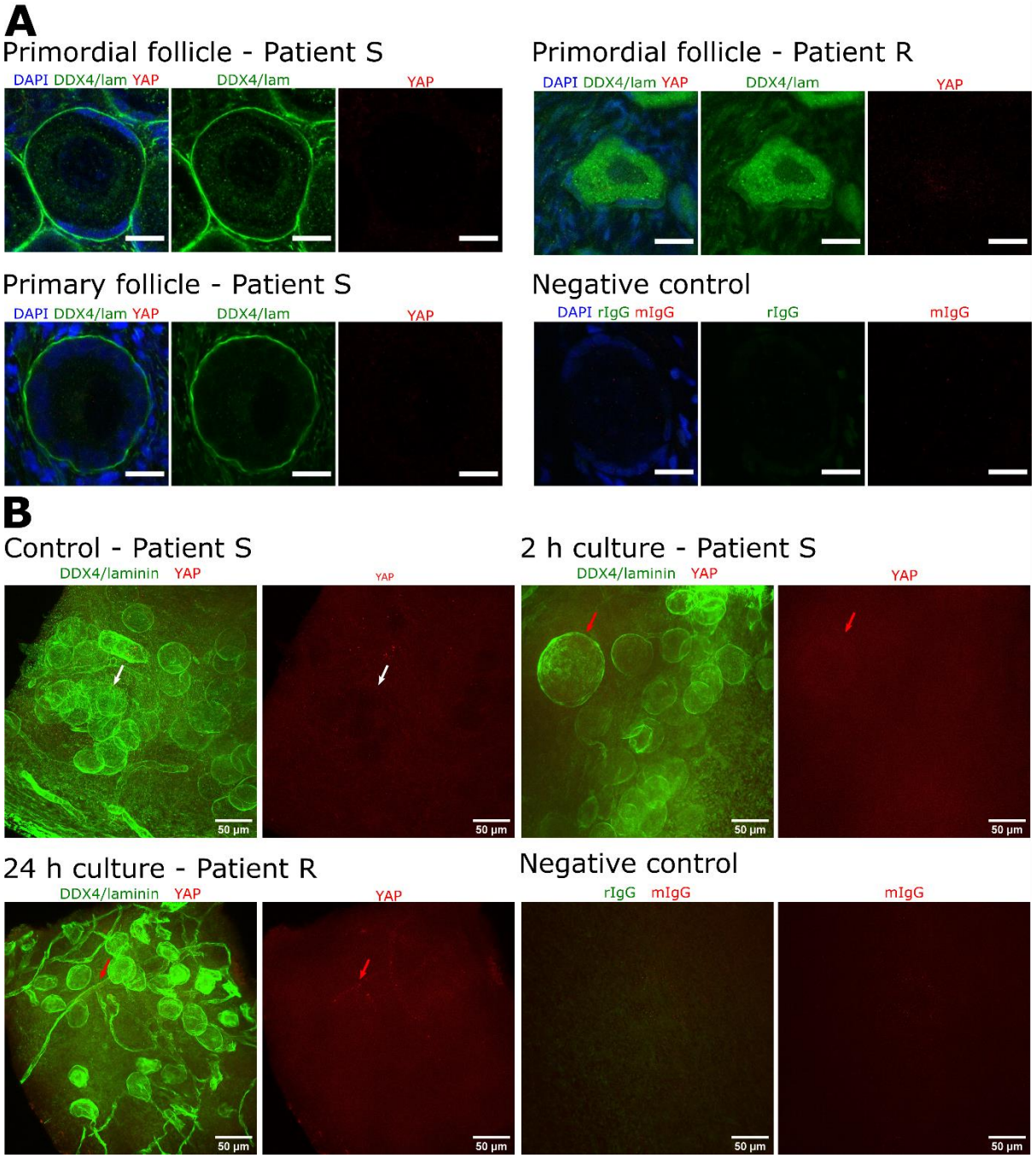

Figure 7-7. Detection of YAP in human ovarian tissue. Fresh ovarian tissue from three young patients was processed into small fragments and cultured for up to 48 h. Tissue fragments were labelled with DDX4 and laminin (green) to detect the oocyte and follicle basement membrane, respectively, YAP (red) and counterstained with DAPI (blue) using whole-mount immunolabelling and tissue clearing. Negative control samples were prepared by adding mouse or rabbit IgG instead of primary antibodies. Confocal microscopy was used to obtain z-stacks of the labelled and cleared tissue fragments at 1.5 µm intervals. **(A)** YAP was not detected in follicles (primordial, transitional or primary) in human ovarian tissue. Scale bar represents 10 µm. **(B)** Representative maximum projection images of human ovarian tissue labelled with DDX4, laminin and YAP. YAP was not detected in primordial follicles (white arrow) but was detected in the granulosa cells of multilayer follicles and blood vessels (red arrows). Note that laminin is present in both follicle basement membranes (green circles) and blood vessels (green strands). Scale bars represent 50 µm.

7.3.6. Spatial effects of follicle activation

The final aim of this chapter was to investigate the spatial effects of tissue processing and *in vitro* culture on follicle activation. For this aim I planned to use three-dimensional reconstruction to label the location of follicles within each tissue fragment and use the information gathered from the previous sections to investigate the relationship between follicle location (within the tissue and distance from other follicles), follicle stage and YAP signalling. However, due to the difficulties described above, namely irregularities in follicle shape and size and lack of YAP signal in primordial follicles, in addition to the limited sample size, it was determined that this analysis could not be performed using the data available.

7.4. Discussion

This chapter aimed to investigate follicle activation *in vitro*, using a novel technique developed in Chapter 6 to allow three-dimensional visualisation and analysis of follicles. Fresh human ovarian tissue was processed into small fragments and cultured for up to 48 h. In designing this study, we planned to collect ovarian tissue from six young patients, however, due to the COVID-19 pandemic, only samples from three patients could be obtained. Furthermore, one of the patient samples had very low follicle numbers and therefore statistical analysis could not be performed. Despite these limitations, some new and interesting observations were made that warrant further investigation.

The main purpose of the novel whole-mount immunolabelling and tissue clearing technique developed in Chapter 6 was to enable accurate classification of primordial follicles and distinction from transitional follicles, which have one or more cuboidal granulosa cells. Using three-dimensional visualisation, 58% of follicles that appeared primordial when viewed across the xy plane (as in conventional analysis) were found to have cuboidal granulosa cells when viewed across the orthogonal planes (xz and yz) and were therefore in fact transitional follicles. Out of the follicles analysed in this study, primordial and transitional follicles did not differ in follicle or oocyte diameter, yet there was a difference in (pre-)granulosa cell size. However, this

investigation was limited by the fact that only 52 follicles from a single patient could be analysed, additional patient samples are therefore needed to confirm these results. This is the first study to describe three-dimensional analysis of human primordial and transitional follicles. Previously, three-dimensional analysis of mouse and bovine follicle size has been reported using either serial histological sections (van Wezel and Rodgers, 1996) or tissue clearing (Feng *et al.*, 2017), however these studies did not involve measurements or detailed assessment of (pre-)granulosa cells.

In the present study, the majority of follicles in tissue fragments (both non-cultured tissue and tissue cultured for up to 48 h) were at the transitional stage, having a mixture of flattened and cuboidal (pre-)granulosa cells. This is in line with reports from both our own group (Bjarkadottir *et al.*, 2021; Walker *et al.*, 2021) and others (de Bruin *et al.*, 2002; Pampanini *et al.*, 2019; Lopes *et al.*, 2020). It is interesting that even though transitional follicles are known to be a large follicle population, equal to if not larger than the primordial follicle population, the ovarian reserve continues to be defined as consisting of *primordial* follicles. This is likely due to a lack of clarity as some studies do include transitional follicles in the ovarian reserve (de Bruin *et al.*, 2002; McLaughlin *et al.*, 2014). Indeed, transitional follicles are often overlooked during analysis or grouped arbitrarily with primordial or primary follicles (Table 7-3). Transitional follicles are commonly considered to be dormant, seemingly based on the fact that the oocyte does not increase in size until the primary stage (Gougeon and Chainy, 1987; de Bruin *et al.*, 2002). However, by definition, the transitional follicle has undergone a shift in (pre-)granulosa cell shape, which is preceded by cell division (Hardy *et al.*, 2018). This would suggest that transitional follicles are active in some way and distinct from primordial follicles, though they may not be in a state of rapid growth as it takes several months for a follicle to reach the primary stage (Gougeon, 1986).

Table 7-3. Variable classification of human transitional follicles in different studies.

Classification of transitional follicles	Papers
Mixture of flattened and cuboidal (pre-)GCs	Gougeon, 1996; Telfer *et al.*, 2008; Asadi Azarbaijani *et al.*, 2015; De Roo *et al.*, 2017, 2020; Grosbois and Demeestere, 2018; McLaughlin *et al.*, 2018; Walker *et al.*, 2021; Pampanini *et al.*, 2019; Lopes *et al.*, 2020; Bjarkadottir *et al.*, 2021
Not classified *Primary follicles classified as having at least one cuboidal GC*	Hreinsson *et al.*, 2002; Takae *et al.*, 2018; Yan *et al.*, 2018
Not classified *Primordial follicles classified as having >50% flattened pre-GCs, primary follicles classified as having >50% cuboidal GCs*	Wright *et al.*, 1999
Not classified *No mention of follicles with a mixture of flattened and cuboidal (pre-)GCs*	Schmidt *et al.*, 2005; Gandolfi *et al.*, 2006; Isachenko *et al.*, 2012; Lerer-Serfaty *et al.*, 2013; Ramezani *et al.*, 2017; Talevi *et al.*, 2018

This study is the first to investigate human pre-antral follicles across three dimensions. Interestingly, some follicles were observed to be disc-shaped rather than spherical as was expected, with a reduced follicle diameter across the z-axis compared to the x and y axes. Follicles appeared to display a range of diameters along the z-axis. Disc-shaped follicles were observed across primordial, transitional and primary stages. These disc-shaped follicles were detected in all three patients and in both cultured and non-cultured tissue, suggesting that this effect was not caused by *in vitro* culture. There was no relationship with follicle diameter across the z-axis and the location (depth) of the follicle within the tissue. It was particularly notable that this reduced follicle diameter was only observed across the z-axis and was only apparent when the follicle was viewed across the xz or yz plane. That would seem to suggest that this phenomenon represents an artefact of tissue clearing, however in that case one would expect all samples to be equally affected. It should also be noted that some tissue fragments contained both spherical and disc-shaped follicles. It is impossible to know how the orientation of the tissue fragment during imaging relates to the original orientation of the fragment within the intact ovary. It may be that

the act of processing the ovary, namely isolation of the ovarian cortex and processing into small fragments, both of which involve manual handling of the tissue with forceps and scalpels, caused compression of some follicles. It may also be that some follicles are naturally compressed within the ovary itself, perhaps due to neighbouring antral follicles that are excised during processing. Further investigation of this phenomenon is warranted to investigate whether these disc-shaped follicles are formed due to physiological conditions or experimental processing.

Unfortunately, follicle activation *in vitro* could not be fully assessed due to low sample numbers and the appearance of disc-shaped follicles, which prevented all follicles from being three-dimensionally staged. However, based on the limited data available there did not appear to be a drastic increase in follicle activation within 48 h of culture*. In vitro* culture is known to trigger follicle activation, however very few studies have investigated activation within the first 48 h of culture. One study reported a reduction in primordial follicle numbers within 2-4 days of culture (De Roo *et al.*, 2020). However, considering that there was no increase in the number of transitional follicles and the importance of three-dimensional analysis when distinguishing between these two classes of follicles, these findings may be limited. The number of primary follicles did not increase until after six days of culture, suggesting that follicle activation may be a relatively slow process, though it is certainly expedited *in vitro* compared to *in vivo*. Follicle activation within 48 h of culture remains to be fully investigated and these experiments should be repeated with more patient samples. If follicle activation is found to occur rapidly, the inclusion of inhibitory drugs such as mTORC1 inhibitor Everolimus could be considered, though this might not inhibit activation via the Hippo pathway (Grosbois and Demeestere, 2018).

We were unable to analyse YAP localisation in primordial follicles, due to lack of signal in primordial and transitional follicles. However, YAP was detected in other structures including granulosa cells of multilayer follicles and blood vessels. The antibody used here has been used to detect YAP in human follicles (Masciangelo *et al.*, 2020) and therefore the lack of signal in primordial follicles was surprising. This may have been due to the imaging technique used; in the present study the thickness of each optical section was 1.5 µm thick to allow detailed imaging of

each follicle, while Masciangelo and colleagues used 5-µm-thick sections and therefore maybe not enough YAP was located within the 1.5-µm-thick optical sections to be detected. However, it should be noted that both laminin and DDX4 were clearly visible in the same optical sections. Patient age may also have been a contributing factor, as other studies investigating YAP in human follicles have used adult samples while the patients in the present study were below the age of 12 (De Roo *et al.*, 2020; Masciangelo *et al.*, 2020). Only one study has quantified YAP signalling in primordial follicles, however in this study follicle classification was not defined and it is therefore not known whether transitional follicles were included with primordial follicles or in the 'growing follicle' category (Masciangelo *et al.*, 2020). Other studies have reported that the Hippo pathway drives follicle activation in response to mechanical tissue manipulation, however while YAP was detected in these studies it was not quantified (De Roo *et al.*, 2020).

Due to the limited sample size, the appearance of disc-shaped follicles which prevented three-dimensional staging of all follicles, and lack of YAP detection in primordial follicles, it was not possible to investigate the spatial effects of follicle activation *in vitro*. Some studies have indicated that the distance of follicles from the cut surface of processed tissue fragments plays a role in follicle activation, however this needs to be further investigated (Grosbois and Demeestere, 2018). Spatial patterns within the mouse ovary have previously been described, however this was limited to analysis across the xy plane (Da Silva-Buttkus *et al.*, 2009). Spatial analysis of growing follicles in the human ovary was recently described, however this was again limited to the xy plane (Quan *et al.*, 2020). Tissue clearing of whole mouse ovaries has enabled characterisation of ovarian structure and follicle dynamics (Faire *et al.*, 2015; Feng *et al.*, 2017; McKey *et al.*, 2020). The whole-mount immunolabelling and tissue clearing technique used in the present study would allow the investigation of spatial effects across three dimensions in human ovarian tissue which would further our understanding on follicle development.

7.4.1 Conclusion

This chapter highlights the need to consider follicles as three-dimensional structures, particularly when investigating follicle activation. Although analysis of ovarian tissue relies on histological

analysis, new methods have been developed that allow three-dimensional visualisation and analysis of tissue, which would greatly benefit the field of ovarian research, as demonstrated in this chapter. Furthermore, there is a need to clearly define follicles of different stages and determine whether follicles that have undergone morphological changes indicative of follicle activation should be considered functionally different to dormant primordial follicles. By addressing these basic issues we can begin to better understand the complexities involved in follicle activation and the role of *in vitro* manipulation on follicle development.

Chapter 8

Discussion

The number of young cancer survivors is growing, as both the incidence and survival rates for cancer increases, particularly among those aged below 24 years. Cancer treatment can cause damage to the ovaries, which can have distressing and long-term effects on the individual, including infertility. Although there are ways of preserving the future fertility of girls and women undergoing cancer treatment, these methods are invasive and some do not restore the patient's ovarian function. In recent years, there has been growing interest in developing non-invasive pharmacological methods of preserving female fertility, which would involve administrating drugs that would protect the ovaries from the damaging effects of chemotherapy. However, the mechanisms of chemotherapy-induced follicle loss remain poorly understood, hampering progress in the field. This is partly due to the numerous challenges faced when working with human ovarian tissue, including limited access of human ovarian tissue for research purposes and heterogeneity in follicle density. In addition, although research using mouse models has begun to elucidate the mechanisms of chemotherapy-induced ovarian damage, there are numerous challenges to be faced when translating this research to human. The aim of this thesis was to address the gaps of knowledge by developing culture and imaging techniques to investigate human follicle development *in vitro*.

8.1. Summary of results

One of the challenges of ovarian tissue research is that follicles are enclosed within the ovarian stroma and are therefore difficult to visualise, particularly due to the small size of early

developing follicles. In Chapter 3 I set out to adapt the mouse fragmented ovary culture method, which allows real-time visualisation of follicles *in vitro*, to culture human ovarian tissue. However, owing to structural differences of human and mouse ovaries, and lack of human ovarian tissue attachment and reshaping during culture, this proved unsuccessful. Therefore, the remainder of this thesis used cortical strip culture to investigate follicle development *in vitro*.

Our group had established a culture method for cryopreserved human ovarian tissue, observing follicle growth within six days of culture. However, a large proportion of atretic follicles was observed in the cultured tissue. In light of this, and recent advancements in the field of human *in vitro* follicle growth, we sought to investigate whether our current culture methods and thawing protocols could be improved. In Chapter 4, we investigated six different culture methods and found that culture in a low volume of αMEM resulted in improved follicle morphological health after six days of culture compared to our previous protocol. We found that there were high levels of both inter- and intra-patient variability in follicle density and development and developed statistical modelling to account for this variability during analysis. During this experiment, we observed that the health of the ovarian stroma, a frequently overlooked component of ovarian tissue, appeared compromised in cryopreserved tissue. Chapter 5 sought to improve cryopreserved human ovarian stromal health by investigating changes in our thawing protocol, however we found that our existing thawing protocol performed best overall. These experiments highlighted that cryopreservation causes some damage to ovarian tissue, both to follicles and stroma. As future experiments were planned involving investigation of chemotherapy-induced ovarian damage *in vitro*, I concluded that fresh ovarian tissue would be more suitable to investigate the effects of chemotherapy drugs and therefore chose to work with fresh ovarian tissue for my remaining experiments.

Analysis of ovarian tissue commonly involves sectioning fixed tissue samples at 5 μm thickness followed by histology and immunohistochemistry. This method conserves the structure of the tissue and enables analysis of follicles as individual units. According to standard practice, only the largest cross-section of each follicle is analysed. However, as follicles are over 40 μm in diameter,

this results in incomplete assessment as only a few granulosa cells of the total population are contained in the largest cross-section. Importantly, this may result in inaccurate classification of primordial follicles. Recent efforts in understanding chemotherapy-induced ovarian damage have focused on determining whether primordial follicles are damaged or unaffected by chemotherapy drugs – therefore accurate classification of primordial follicles is essential. In Chapter 6 I developed a technique to analyse human ovarian tissue to enable accurate distinction between primordial and transitional follicles and allow three-dimensional visualisation of pre-antral follicles. This was achieved using whole-mount immunolabelling with DDX4 and laminin, to visualise the oocyte and follicle basement membrane, respectively, followed by tissue clearing and confocal imaging to allow imaging of tissue samples ~200 μm in thickness.

The technique developed in Chapter 6 was used to investigate follicle activation of fresh ovarian tissue *in vitro* in Chapter 7. Fresh ovarian tissue from young patients was cultured for up to 48 h to determine how rapidly follicle activation occurred and investigate the involvement of the Hippo pathway in non-physiological follicle activation caused by tissue fragmentation using three-dimensional analysis. This experiment revealed that three-dimensional analysis is necessary to accurately distinguish between primordial and transitional follicles. Interestingly, a large proportion of follicles from all patients were disc-shaped rather than spherical, with a small diameter across the z-axis. Unfortunately, this precluded three-dimensional analysis of all follicles and therefore the spatial relationship of follicle activation *in vitro* could not be assessed using three-dimensional analysis. No apparent increase in follicle activation was observed within 48 h of culture, however this could not be fully analysed due to low sample numbers. Finally, YAP signalling was not detected in primordial follicles and therefore the Hippo pathway could not be investigated.

A final set of experiments was planned for this thesis, investigating the effects of chemotherapy drugs on human primordial follicles *in vitro*. However, due to the significant disruptions and restrictions caused by the COVID-19 pandemic, which also negatively impacted Chapter 7, these experiments could unfortunately not be performed.

8.2. Limitations of human follicle analysis

Studies on ovarian function or follicle development are mostly conducted using mice as a model for human. Mouse models have been used to investigate follicle activation, chemotherapy-induced ovarian damage and to recapitulate the full process of follicle development *in vitro*. However, in order for this work to be translated to clinical practice and fertility preservation, namely for developing pharmacological protective agents and developing oocytes from ovarian tissue *in vitro*, studies using human ovarian tissue must be conducted. Human ovarian tissue must be procured surgically which cannot be ethically performed without clinical indication. Therefore, most studies on human ovarian tissue use donated tissue from healthy adults undergoing elective caesarean section or laparoscopy for benign gynaecological disease. However, these patients are often >30 years old and therefore may have low follicle density. This can result in only a small number of follicles per patient being analysed within each experimental group.

In the work presented in this thesis, ovarian tissue was obtained from the Oxford Cell and Tissue Biobank (OCTB). Ovarian tissue obtained from the OCTB was donated to research by patients undergoing unilateral oophorectomy and ovarian tissue cryopreservation due to gonadotoxic treatment, or occasionally by patients undergoing oophorectomy (total or unilateral) for benign disease. One of the benefits of obtaining tissue from the OCTB is the availability of tissue from young patients, as these samples have a higher follicle density. However, ovaries from children and adolescents are known to contain abnormal follicles not observed in adults (Peters *et al.*, 1978; Anderson *et al.*, 2014), which must be taken into account during assessment of follicle health. Furthermore, these are patients with malignant or haematologic disease who may be seriously ill at the time of ovarian tissue procurement. A recent study found no differences in follicle morphology, density or protein expression in ovaries from girls and adolescents with β-thalassemia or sickle cell disease compared to control (Mamsen *et al.*, 2021). However, while the control group was matched in terms of age, most were cancer patients (34 out of 43 patients).

Although the effects of *chemotherapy* on ovarian tissue have been investigated, the effect of cancer itself on the ovary has not been studied.

The density of pre-antral follicles varies throughout the human ovarian cortex, irrespective of age, as was highlighted in Chapter 4 of this thesis and has been well documented in the literature (Qu *et al.*, 2000; Poirot *et al.*, 2002; Schmidt *et al.*, 2003). Furthermore, there is considerable variation in follicle density and developmental distribution between individuals (Schmidt *et al.*, 2003; McLaughlin *et al.*, 2015; Mamsen *et al.*, 2021; Walker *et al.*, 2021). This variability can present two problems. Firstly, when culturing small pieces of human ovarian tissue, some tissue fragments may contain zero follicles, however this is often not evident until after histological processing and therefore results in a loss of time and resources (see Chapter 7 and Anderson *et al.*, 2014; Ikeda *et al.*, 2016). We have found that incubation of tissue fragments in neutral red allows us to visualise tissue pieces containing follicles (Chapter 4), however as demonstrated in Chapter 7, not all follicles can be visualised using this method. Other groups report visualisation of primordial follicles using simple brightfield microscopy of tissue fragments prior to culture (McLaughlin *et al.*, 2018; Xu *et al.*, 2021), however we have not been able to visualise follicles in this way. While these methods are not fully effective, they can be used to increase the likelihood of only tissue pieces containing follicles being cultured, or at least that all experimental conditions contain follicles. The second problem is that although studies may utilise tissue samples of equal volume from multiple patients, follicle numbers may vary by an order of magnitude. A study on whole sheep ovaries concluded that to overcome the impact of natural follicle heterogeneity when performing *in vivo* or *in vitro* treatment comparisons, cortical tissue from a single animal should be used (Fransolet *et al.*, 2014), however this is difficult when using human ovarian tissue as generally only a small number of cortical strips can be obtained from each patient. In Chapter 4, we developed a mixed effects model which accounts for both this inter- and intra-patient variability, which is critical to obtain accurate and meaningful results. Unfortunately, there are many examples of inappropriate statistical analysis being performed, where data from all patients in combined without considering the variability described above. However, reassuringly,

some groups do appear to be employing mixed effects models and hopefully this practice will become standard practice in time (De Roo *et al.*, 2020; Christianson *et al.*, 2021; Shai *et al.*, 2021).

In vitro culture of cryopreserved human ovarian tissue was performed in Chapter 4 to investigate follicle development. IVFG is currently being developed as a possible fertility preservation method for young patients for whom other fertility preservation methods are unavailable, however to date mature MII human oocytes have only been obtained using fresh ovarian tissue (Xiao *et al.*, 2015; McLaughlin *et al.*, 2018; Xu *et al.*, 2021). Some patients who have already undergone ovarian tissue cryopreservation might benefit from IVFG and therefore it is crucial to develop these methods for both fresh and cryopreserved ovarian tissue. However, cryopreservation is known to cause damage to follicles and the ovarian stroma (Isachenko *et al.*, 2009; Keros *et al.*, 2009; Zemyarska *et al.*, 2020) and cryopreserved tissue may therefore not be suitable to study processes such as follicle activation or chemotherapy-induced follicle damage. Therefore, fresh ovarian tissue was used in this thesis to investigate follicle activation *in vitro.* Cryopreservation of ovarian tissue may also affect follicle function, as demonstrated by follicles having thinner theca layers following xenotransplantation of cryopreserved ovarian tissue (Amorim *et al.*, 2011). However, over 130 live births have been achieved following ovarian tissue cryopreservation, demonstrating the functionality of the tissue (Donnez *et al.*, 2015b; Dunlop *et al.*, 2016; Meirow *et al.*, 2016; Rodriguez-Wallberg *et al.*, 2016; Van der Ven *et al.*, 2016; Donnez and Dolmans, 2017; Jensen *et al.*, 2017; Gellert *et al.*, 2018).

8.3. Are primordial and transitional follicles distinct populations?

The mammalian ovarian reserve is classically defined as consisting of primordial follicles (McGee and Hsueh, 2000; Skinner, 2005; Richards and Pangas, 2010; Kim, 2012; Spears *et al.*, 2019; Telfer, 2019; Grosbois *et al.*, 2020) and primordial follicles are often said to be the dominant follicle population in the ovary (Hovatta, 2005; Zhang and Liu, 2015; Telfer, 2019). However, an early study characterising the adult human ovary demonstrated that primordial and transitional follicles represented an equal portion of the total follicle population (approximately 40% each;

Gougeon and Chainy, 1987). In our own group we have observed that primordial follicles represent ~30-80% of the total follicle population (Bjarkadottir *et al.*, 2021; Walker *et al.*, 2021); other studies have reported similar findings (de Bruin *et al.*, 2002; Telfer *et al.*, 2008; Asadi Azarbaijani *et al.*, 2015; De Roo *et al.*, 2017; Grosbois and Demeestere, 2018; Pampanini *et al.*, 2019; Lopes *et al.*, 2020). However, many studies do not classify transitional follicles and instead group them with either primordial or primary follicles (Table 7-3, Chapter 7).

Oocyte size does not increase until the primary stage (Gougeon and Chainy, 1987; de Bruin *et al.*, 2002), and therefore transitional, and sometimes primary, follicles are often classified together as 'resting' or 'non-growing' follicles (Gougeon, 1996; Smitz and Cortvrindt, 2002; Wallace and Kelsey, 2010; McLaughlin *et al.*, 2014). Indeed, in bovine species, primordial follicles are classified as having a mixture of flattened and cuboidal (pre-)granulosa cells (van Wezel and Rodgers, 1996). Although these follicles are not in a state of rapid growth, and therefore the term 'non-growing' may be accurate, there may still be important differences between a dormant primordial follicle, and an activated transitional follicle, whose oocyte has not yet resumed growth. Indeed, studies in mice have demonstrated that the (pre-)granulosa cells undergo molecular changes, followed by proliferation and squamous-to-cuboidal-transformation, prior to changes in the oocyte (Zhang *et al.*, 2014; Hardy *et al.*, 2018). Furthermore, there may be some species-specific differences in follicle activation between mice and large mammalian species, as has been suggested regarding the function of FOXO3 and FOXO1 in oocyte activation (Tarnawa *et al.*, 2013; Ernst *et al.*, 2017; Ting and Zelinski, 2017; De Roo *et al.*, 2020; Masciangelo *et al.*, 2020).

Although the distinction between primordial and transitional follicles may appear pedantic, this distinction may be critical to elucidate the mechanisms of chemotherapy-induced follicle damage. Currently, there is much debate as to whether primordial follicles are directly destroyed by chemotherapy agents or whether they are lost through accelerated activation (see Chapter 1.5). The root to this confusion may lie in the distinction between primordial and transitional follicles as it could be that dormant primordial follicles are unaffected by chemotherapy drugs, while transitional follicles are more susceptible. One research group has reported direct damage to

primordial follicles in human xenografts across multiple studies (Oktem and Oktay, 2007b; Soleimani *et al.*, 2011; Li *et al.*, 2014; Titus *et al.*, 2021). However, it is unclear whether transitional follicles were included among primordial, as this follicle population is not clearly defined in these studies. Indeed, in one study the authors used foetal tissue (at 24 weeks gestation) on the basis that it contains only primordial follicles (Oktem and Oktay, 2007b), however follicle development is known to occur at the foetal stage (Smitz and Cortvrindt, 2002; Cole *et al.*, 2006). It is critical to clearly define which follicle populations are being investigated in order to elucidate whether primordial follicles are directly damaged by chemotherapy drugs.

8.4. Future work investigating the effect of chemotherapy drugs on human ovarian tissue

All experiments in this thesis were leading up to a final chapter to elucidate the effects of chemotherapy drugs on primordial follicles using the methods developed to ensure the results obtained would be reliable and robust. However, this study could not be performed owing to disruptions caused by the COVID-19 pandemic. The experiment would have involved *in vitro* treatment of fresh human ovarian tissue with cisplatin and carboplatin, chemotherapy drugs with a medium risk of gonadotoxicity (Blumenfeld, 2012), with tissue collected after 8-48 h and up to 6 d to assess damage to primordial follicles and growth potential of follicles after treatment. Damage to human 'primordial' follicles from chemotherapy drugs has previously been reported within 24-72 h *in vitro* and within 12 h *in vivo* (Soleimani *et al.*, 2011; Bildik *et al.*, 2018; Titus *et al.*, 2021), while apoptosis of murine primordial follicles *in vivo* is triggered within 8 h of treatment with cisplatin or cyclophosphamide (Nguyen *et al.*, 2019).

Using the techniques developed in Chapters 6 and 7, follicles would have been analysed across three dimensions to allow accurate identification of primordial and transitional follicles to determine whether these follicle populations are equally susceptible to chemotherapy-induced damage. Follicle damage would have been assessed by detecting γH2AX (to detect double-stranded DNA breaks) and cleaved caspase 3 and 7 to detect apoptosis. As cleaved caspases are transiently expressed in the cell, I had planned to explore whether they could be detected using a

fluorogenic substrate for activated caspase 3/7 (CellEvent™) that remains fluorescent even though caspase 3/7 is no longer active. TAp63 has been demonstrated to be a key mediator of oocyte apoptosis in mice (Kerr *et al.*, 2012a; Coutandin *et al.*, 2016), however its role in human follicles has not yet been studied and therefore this would also have been an interesting parameter to investigate. Further experiments exploring the prevalence and relevance of disc-shaped follicles as described in Chapter 7 would also have been conducted.

8.5. Final remarks

This work presented in this thesis has demonstrated the limitations of investigating human ovarian tissue and highlighted the need to consider both the heterogeneity of follicles within the ovarian tissue and the fact that follicles are three-dimensional structures. This needs to be taken into account to allow accurate analysis of human ovarian tissue, particularly in order to elucidate the mechanisms of chemotherapy-induced damage to primordial follicles. Understanding of these mechanisms is critical to pave the way for the development of non-invasive pharmacological fertility preservation methods in the future.

Chapter 9

References

Abercrombie M (1946) Estimation of nuclear population from microtome sections. *The Anatomical Record* **94** 239–247.

Abir R, Moore P, Franks S, Margara R, Mobberley M and Winston RML (1997) Mechanical isolation and *in vitro* growth of preantral and small antral human follicles. *Fertility and Sterility* **68** 682–688.

Abir R, Roizman P, Fisch B, Nitke S, Okon E, Orvieto R and Ben Rafael Z (1999) Pilot study of isolated early human follicles cultured in collagen gels for 24 hours. *Human Reproduction* **14** 1299–1301.

Abir R, Fisch B, Nitke S, Okon E, Raz A and Rafael ZB (2001) Morphological study of fully and partially isolated early human follicles. *Fertility and Sterility* **75** 141–146.

Abir R, Ben-Haroush A, Felz C, Okon E, Raanani H, Orvieto R, Nitke S and Fisch B (2008) Selection of patients before and after anticancer treatment for ovarian cryopreservation. *Human Reproduction* **23** 869–877.

Accili D and Arden KC (2004) FoxOs at the Crossroads of Cellular Metabolism, Differentiation, and Transformation. *Cell* **117** 421–426.

Adeniran B V, Bjarkadottir BD, Appeltant R, Lane S and Williams SA (2021) Improved preservation of ovarian tissue morphology that is compatible with antigen detection using a fixative mixture of formalin and acetic acid. *Human Reproduction* **36** 1871–1890.

Adhikari D and Liu K (2009) Molecular mechanisms underlying the activation of mammalian primordial follicles. *Endocrine Reviews* **30** 438–464.

Adhikari D, Flohr G, Gorre N, Shen Y, Yang H, Lundin E, Lan Z, Gambello MJ and Liu K (2009a) Disruption of Tsc2 in oocytes leads to overactivation of the entire pool of primordial follicles. *Molecular Human Reproduction* **15** 765–770.

Adhikari D, Zheng W, Shen Y, Gorre N, Hämäläinen T, Cooney AJ, Huhtaniemi I, Lan ZJ and Liu K (2009b) Tsc/mTORC1 signaling in oocytes governs the quiescence and activation of primordial follicles. *Human Molecular Genetics* **19** 397–410.

Al-Asari S and Abduljabbar A (2012) Laparoscopic ovarian transposition before pelvic radiation in rectal cancer patient: Safety and feasibility. *Annals of Surgical Innovation and Research* **6** 1–7.

Albamonte MI, Albamonte MS, Stella I, Zuccardi L and Vitullo AD (2013) The infant and pubertal human ovary: Balbiani's body-associated VASA expression, immunohistochemical detection of apoptosis-related BCL2 and BAX proteins, and DNA fragmentation. *Human Reproduction* **28** 698–706.

Albamonte MI, Calabró LY, Albamonte MS, Zuccardi L, Stella I, Halperin J and Vitullo AD (2020) PTEN and FOXO3 expression in the prenatal and postnatal human ovary. *Journal of Assisted Reproduction and Genetics* **37** 1613–1622.

Albertini DF, Combelles CMH, Benecchi E and Carabatsos MJ (2001) Cellular basis for

paracrine regulation of ovarian follicle development. *Reproduction* **121** 647–653.

Alberts B, Johnson A, Lewis J, Morgan D and Raff M (2015) Cell Death. In *Molecular Biology of the Cell*, Sixth Ed., pp 1021–1034. New York: New York: Gardland Science.

Alexandri C, Stamatopoulos B, Rothé F, Bareche Y, Devos M and Demeestere I (2019) MicroRNA profiling and identification of let-7a as a target to prevent chemotherapy-induced primordial follicles apoptosis in mouse ovaries. *Scientific Reports* **9** 1–10.

Amorim CA, Van Langendonckt A, David A, Dolmans MM and Donnez J (2009) Survival of human pre-antral follicles after cryopreservation of ovarian tissue, follicular isolation and *in vitro* culture in a calcium alginate matrix. *Human Reproduction* **24** 92–99.

Amorim CA, David A, Dolmans MM, Camboni A, Donnez J and Van Langendonckt A (2011) Impact of freezing and thawing of human ovarian tissue on follicular growth after long-term xenotransplantation. *Journal of Assisted Reproduction and Genetics* **28** 1157–1165.

Anderson RA, McLaughlin M, Wallace WHB, Albertini DF and Telfer EE (2014) The immature human ovary shows loss of abnormal follicles and increasing follicle developmental competence through childhood and adolescence. *Human Reproduction* **29** 97–106.

Anderson RA, Mitchell RT, Kelsey TW, Spears N, Telfer EE and Wallace WHB (2015) Cancer treatment and gonadal function: Experimental and established strategies for fertility preservation in children and young adults. *The Lancet Diabetes and Endocrinology* **3** 556–567.

Anderson RA, Wallace WHB and Telfer EE (2017) Ovarian tissue cryopreservation for fertility preservation: clinical and research perspectives. *Human Reproduction Open* **2017** 1–9.

Anderson RA, Brewster DH, Wood R, Nowell S, Fischbacher C, Kelsey TW and Wallace WHB (2018) The impact of cancer on subsequent chance of pregnancy: a population-based analysis. *Human Reproduction* **33** 1281–1290.

Arunakumari G, Shanmugasundaram N and Rao VH (2010) Development of morulae from the oocytes of cultured sheep preantral follicles. *Theriogenology* **74** 884–894.

Asadi-Azarbaijani B, Sheikhi M, Nurmio M, Tinkanen H, Juvonen V, Dunkel L, Hovatta O, Oskam IC and Jahnukainen K (2016) Minimal residual disease of leukemia and the quality of cryopreserved human ovarian tissue *in vitro*. *Leukemia and Lymphoma* **57** 700–707.

Asadi Azarbaijani B, Sheikhi M, Oskam IC, Nurmio M, Laine T, Tinkanen H, Mäkinen S, Tanbo TG, Hovatta O and Jahnukainen K (2015) Effect of previous chemotherapy on the quality of cryopreserved human ovarian tissue *in vitro*. *PLoS ONE* **10** 1–13.

Attisano L (2002) Signal Transduction by the TGF-beta Superfamily. *Science* **296** 1646–1647.

Baarends WM, Uilenbroek JT, Kramer P, Hoogerbrugge JW, van Leeuwen EC, Themmen AP and Grootegoed JA (1995) Anti-müllerian hormone and anti-müllerian hormone type II receptor messenger ribonucleic acid expression in rat ovaries during postnatal development, the estrous cycle, and gonadotropin-induced follicle growth. *Endocrinology* **136** 4951–4962.

Baker JR (1958) *Principles of Biological Microtechniques: A Study on Fixation and Dyeing*. Methuen: Wiley.

Bao RM, Hayakawa K, Moniruzzaman M, Taketsuru H and Miyano T (2011) FOXO3 knockdown accelerates development of bovine primordial follicles. *Journal of Reproduction and Development* **57** 475–480.

Bar-Joseph H, Ben-Aharon I, Tzabari M, Tsarfaty G, Stemmer SM and Shalgi R (2011) *In vivo* bioimaging as a novel strategy to detect Doxorubicin-Induced damage to gonadal blood vessels. *PLoS ONE* **6** 2–9.

Barcroft J, Dayoub N and Thong KJ (2013) Fifteen year follow-up of embryos cryopreserved in cancer patients for fertility preservation. *Journal of Assisted Reproduction and Genetics* **30** 1407–1413.

Barton SE, Najita JS, Ginsburg ES, Leisenring WM, Stovall M, Weathers RE, Sklar CA, Robison LL and Diller L (2013) Infertility, infertility treatment, and achievement of pregnancy in female survivors of childhood cancer: A report from the Childhood Cancer Survivor Study cohort. *The Lancet Oncology* **14** 873–881.

Bassett DL (1943) The changes in the vascular pattern of the ovary of the albino rat during the estrous cycle. *American Journal of Anatomy* **73** 251–291.

Bastings L, Beerendonk CCM, Westphal JR, Massuger LF a G, Kaal SEJ, van Leeuwen FE, Braat DDM and Peek R (2013) Autotransplantation of cryopreserved ovarian tissue in cancer survivors and the risk of reintroducing malignancy: A systematic review. *Human Reproduction Update* **19** 483–506.

Bedoschi G, Navarro PA and Oktay K (2016) Chemotherapy-induced damage to ovary: mechanisms and clinical impact. *Future Oncology* **12** 2333–2344.

Bedoschi GM, Navarro PA and Oktay KH (2019) Novel insights into the pathophysiology of chemotherapy-induced damage to the ovary. *Panminerva Medica* **61** 68–75.

Ben-Aharon I, Bar-Joseph H, Tzarfaty G, Kuchinsky L, Rizel S, Stemmer SM and Shalgi R (2010) Doxorubicin-induced ovarian toxicity. *Reproductive Biology and Endocrinology* **8** 1–7.

van den Berg MH, van Dijk M, Byrne J, Berger C, Dirksen U, Winther JF, Fossa SD, Grabow D, Grandage VL, Haupt R *et al.* (2021) Treatment-related fertility impairment in long-term female childhood, adolescent and young adult cancer survivors: investigating dose-effect relationships in a European case-control study (PanCareLIFE). *Human Reproduction* **36** 1561–1573.

Bernabé BP, Woodruff T, Broadbelt LJ and Shea LD (2020) Ligands, receptors and transcription factors that mediate inter-cellular and intra-cellular communication during ovarian follicle development. *Reproductive Sciences* **27** 690–703.

Bertoldo MJ, Bernard J, Duffard N, Tsikis G, Alves S, Calais L, Uzbekova S, Monniaux D, Mermillod P and Locatelli Y (2016) Inhibitors of c-jun phosphorylation impede ovine primordial follicle activation. *Molecular Human Reproduction* **22** 338–349.

Bildik G, Acılan C, Sahin GN, Karahuseyinoglu S and Oktem O (2018) C-Abl is not actıvated in DNA damage-induced and Tap63-mediated oocyte apoptosıs in human ovary. *Cell Death & Disease* **9** 943.

Billiar RB, St. Clair JB, Zachos NC, Burch MG, Albrecht ED and Pepe GJ (2004) Localization and Developmental Expression of the Activin Signal Transduction Proteins Smads 2, 3, and 4 in the Baboon Fetal Ovary1. *Biology of Reproduction* **70** 586–592.

Bjarkadottir BD, Walker CA, Fatum M, Lane S and Williams SA (2021) Analysing culture methods of frozen human ovarian tissue to improve follicle survival. *Reproduction and Fertility* **2** 59–68.

Blaustein A (1982) Anatomy and Histology of the Human Ovary. In *Pathology of the Female Genital Tract*, pp 416–441. Ed A Blaustein. New York: Springer.

Blumenfeld Z (2008) GnRH-agonists in fertility preservation. *Current Opinion in Endocrinology, Diabetes and Obesity* **15** 523–528.

Blumenfeld Z (2012) Chemotherapy and fertility. *Best Practice and Research: Clinical Obstetrics and Gynaecology* **26** 379–390.

Bolcun-Filas E, Rinaldi VD, White ME and Schimenti JC (2014) Reversal of Female Infertility by Chk2 Ablation Reveals the Oocyte DNA Damage Checkpoint Pathway. *Science* **343** 533–536.

Bothun AM and Woods DC (2019) Dynamics of WNT signaling components in the human ovary from development to adulthood. *Histochemistry and Cell Biology* **151** 115–123.

de Bruin JP, Dorland M, Spek ER, Posthuma G, van Haaften M, Looman CWN and te Velde ER (2002) Ultrastructure of the Resting Ovarian Follicle Pool in Healthy Young Women. *Biology of Reproduction* **66** 1151–1160.

Brunet A, Bonni A, Zigmond MJ, Lin MZ, Juo P, Hu LS, Anderson MJ, Arden KC, Blenis J and Greenberg ME (1999) Akt promotes cell survival by phosphorylating and inhibiting a forkhead transcription factor. *Cell* **96** 857–868.

Burgering BMT and Medema RH (2003) Decisions on life and death: FOXO Forkhead transcription factors are in command when PKB/Akt is off duty. *Journal of Leukocyte Biology* **73** 689–701.

Burton GJ, Yung HW, Cindrova-Davies T and Charnock-Jones DS (2009) Placental Endoplasmic Reticulum Stress and Oxidative Stress in the Pathophysiology of Unexplained Intrauterine Growth Restriction and Early Onset Preeclampsia. *Placenta* **30** 43–48.

Camboni A, Martinez-Madrid B, Dolmans MM, Nottola S, Van Langendonckt A and Donnez J (2008) Autotransplantation of frozen-thawed ovarian tissue in a young woman: ultrastructure and viability of grafted tissue. *Fertility and Sterility* **90** 1215–1218.

Cancer Research UK (2014) Cancer survival statistics for all cancers combined.

Cancer Research UK (2020) Cancer incidence statistics.

Carlsson IB, Laitinen MPE, Scott JE, Louhio H, Velentzis L, Tuuri T, Aaltonen J, Ritvos O, Winston RML and Hovatta O (2006a) Kit ligand and c-Kit are expressed during early human ovarian follicular development and their interaction is required for the survival of follicles in long-term culture. *Reproduction* **131** 641–649.

Carlsson IB, Scott JE, Visser JA, Ritvos O, Themmen APN and Hovatta O (2006b) Anti-Mullerian hormone inhibits initiation of growth of human primordial ovarian follicles *in vitro*. *Human Reproduction* **21** 2223–2227.

Castrillon DH, Miao L, Kollipara R, Horner JW and DePinho RA (2003) Suppression of ovarian follicle activation in mice by the Transcription Factor Foxo3a. *Science* **301** 215–218.

Castro SV, Carvalho AA, Silva CMG, Santos FW, Campello CC, de Figueiredo JR and Rodrigues APR (2014) Frozen and fresh ovarian tissue require different culture media to promote *in vitro* development of bovine preantral follicles. *Biopreservation and Biobanking* **12** 317–324.

Chambers EL, Gosden RG, Yap C and Picton HM (2010) In situ identification of follicles in ovarian cortex as a tool for quantifying follicle density, viability and developmental potential in strategies to preserve female fertility. *Human Reproduction* **25** 2559–2568.

Chan BP and Leong KW (2008) Scaffolding in tissue engineering: General approaches and tissue-specific considerations. *European Spine Journal* **17** 467–479.

Chang TC, Mikheev AM, Huynh W, Monnat RJ, Rostomily RC and Folch A (2014) Parallel microfluidic chemosensitivity testing on individual slice cultures. *Lab on a Chip* **14** 4540–4551.

Chang EM, Lim E, Yoon S, Jeong K, Bae S, Lee DR, Yoon TK, Choi Y and Lee W (2015) Cisplatin induces overactivation of the dormant primordial follicle through PTEN/AKT/FOXO3α pathway which leads to loss of ovarian reserve in mice. *PLoS ONE* **10** 1–16.

Chemaitilly W, Mertens AC, Mitby P, Whitton J, Stovall M, Yasui Y, Robison LL and Sklar C a (2006) Acute ovarian failure in the childhood cancer survivor study. *The Journal of Clinical Endocrinology and Metabolism* **91** 1723–1728.

Chemaitilly W, Li Z, Krasin MJ, Brooke RJ, Wilson CL, Green DM, Klosky JL, Barnes N, Clark KL, Farr JB *et al.* (2017) Premature ovarian insufficiency in childhood cancer survivors: A report from the St. Jude lifetime cohort. *Journal of Clinical Endocrinology and Metabolism* **102** 2242–2250.

Chen XY, Xia HX, Guan HY, Li B and Zhang W (2016) Follicle loss and apoptosis in cyclophosphamide-treated mice: What's the matter? *International Journal of Molecular Sciences* **17** 836.

Chen Y, Yu Q and Xu CB (2017) A convenient method for quantifying collagen fibers in atherosclerotic lesions by imagej software. *International Journal of Clinical and Experimental Medicine* **10** 14904–14910.

Chen CY, Chen J, He L and Stiles BL (2018) PTEN: Tumor suppressor and metabolic regulator. *Frontiers in Endocrinology* **9** 1–12.

Cheng Y, Feng Y, Jansson L, Sato Y, Deguchi M, Kawamura K and Hsueh AJ (2015) Actin polymerization-enhancing drugs promote ovarian follicle growth mediated by the Hippo signaling effector YAP. *FASEB Journal* **29** 2423–2430.

Cheng J, Xiangyan R, Qi Z, Yanglu L, Juan D, Fengyu J, Muqing G and Mueck AO (2021) Long-time low-temperature transportation of human ovarian tissue before cryopreservation. *Reproductive BioMedicine Online* **00** 1–12.

Chong-Kopera H, Inoki K, Li Y, Zhu T, Garcia-Gonzalo FR, Rosa JL and Guan KL (2006) TSC1 stabilizes TSC2 by inhibiting the interaction between TSC2 and the HERC1 ubiquitin ligase. *Journal of Biological Chemistry* **281** 8313–8316.

Chow EJ, Stratton KL, Leisenring WM, Oeffinger KC, Sklar CA, Donaldson SS, Ginsberg JP, Kenney LB, Levine JM, Robison LL *et al.* (2016) Pregnancy after chemotherapy in male and female survivors of childhood cancer treated between 1970 and 1999: A report from the Childhood Cancer Survivor Study cohort. *The Lancet Oncology* **17** 567–576.

Christensen RHB (2015) ordinal-Regression Models for Ordinal Data. R package version 2015.6-28. *See Http://Www. Cran. r-Project. Org/Package= Ordinal*.

Christianson MS, Lukish DA, McCarter R, Pryor H and Lukish JR (2021) Ovarian tissue cryopreservation in young females with cancer and its impact on ovarian follicle density. *Journal of Pediatric Surgery*.

Cobo A, García-Velasco JA, Coello A, Domingo J, Pellicer A and Remohí J (2016) Oocyte vitrification as an efficient option for elective fertility preservation. *Fertility and Sterility* **105** 755–764.

Cobo A, García-Velasco J, Domingo J, Pellicer A and Remohí J (2018) Elective and Onco-fertility preservation: Factors related to IVF outcomes. *Human Reproduction* **33** 2222–2231.

Cole B, Hensinger K, Maciel GAR, Chang RJ and Erickson GF (2006) Human fetal ovary development involves the spatiotemporal expression of P450c17 protein. *Journal of Clinical Endocrinology and Metabolism* **91** 3654–3661.

Colvin M (2003) Alkylating Agents and Platinum Antitumor Compounds. In *Holland-Frei Cancer*

Medicine, Sixth Ed. Eds DW Kufe, RE Pollock, RR Weichselbaum, RC Bast Jr, TS Gansler, JF Holland and E Frei. Hamilton (ON): BC Decker.

Conchello JA and Lichtman JW (2005) Optical sectioning microscopy. *Nature Methods* **2** 920–931.

Cortvrindt RG and Smitz JEJ (2002) Follicle culture in reproductive toxicolgy: A tool for in-vitro testing of ovarian function? *Human Reproduction Update* **8** 243–254.

Cortvrindt R, Smitz J and Van Steirteghem AC (1996) In-vitro maturation, fertilization and embryo development of immature oocytes from early preantral follicles from prepuberal mice in a simplified culture system. *Human Reproduction (Oxford, England)* **11** 2656–2666.

Coutandin D, Osterburg C, Srivastav RK, Sumyk M, Kehrloesser S, Gebel J, Tuppi M, Hannewald J, Schäfer B, Salah E *et al.* (2016) Quality control in oocytes by p63 is based on a spring-loaded activation mechanism on the molecular and cellular level. *ELife* **5** 1–22.

Creux H, Monnier P, Son WY and Buckett W (2018) Thirteen years' experience in fertility preservation for cancer patients after *in vitro* fertilization and *in vitro* maturation treatments. *Journal of Assisted Reproduction and Genetics* **35** 583–592.

Crisponi L, Deiana M, Loi A, Chiappe F, Uda M, Amati P, Bisceglia L, Zelante L, Nagaraja R, Porcu S *et al.* (2001) The putative forkhead transcription factor FOXL2 is mutated in blepharophimosis/ptosis/epicanthus inversus syndrome. *Nature Genetics* **27** 159–166.

Critchley HOD and Wallace WHB (2005) Impact of cancer treatment on uterine function. *Journal of the National Cancer Institute. Monographs* 64–68.

Dath C, Van Eyck AS, Dolmans MM, Romeu L, Delle Vigne L, Donnez J and Van Langendonckt A (2010) Xenotransplantation of human ovarian tissue to nude mice: Comparison between four grafting sites. *Human Reproduction* **25** 1734–1743.

David A, Dolmans MM, Van Langendonckt A, Donnez J and Amorim CA (2011) Immunohistochemical localization of growth factors after cryopreservation and 3 weeks' xenotransplantation of human ovarian tissue. *Fertility and Sterility* **95** 1241–1246.

David A, Van Langendonckt A, Gilliaux S, Dolmans MM, Donnez J and Amorim CA (2012) Effect of cryopreservation and transplantation on the expression of kit ligand and anti-Mllerian hormone in human ovarian tissue. *Human Reproduction* **27** 1088–1095.

Delgado M and Ganea D (2013) Vasoactive intestinal peptide: A neuropeptide with pleiotropic immune functions. *Amino Acids* **45** 25–39.

Demeestere I, Delbaere A, Gervy C, Van Den Bergh M, Devreker F and Englert Y (2002) Effect of preantral follicle isolation technique on in-vitro follicular growth, oocyte maturation and embryo development in mice. *Human Reproduction* **17** 2152–2159.

Demeestere I, Simon P, Dedeken L, Moffa F, Tsépélidis S, Brachet C, Delbaere A, Devreker F and Ferster A (2015) Live birth after autograft of ovarian tissue cryopreserved during childhood. *Human Reproduction* **30** 2107–2109.

Desmeules P and Devine PJ (2006) Characterizing the ovotoxicity of cyclophosphamide metabolites on cultured mouse ovaries. *Toxicological Sciences* **90** 500–509.

Devos M, Grosbois J and Demeestere I (2020) Interaction between PI3K/AKT and Hippo pathways during *in vitro* follicular activation and response to fragmentation and chemotherapy exposure using a mouse immature ovary model. *Biology of Reproduction* **102** 717–729.

Dijkers PF, Medema RH, Pals C, Banerji L, Thomas NSB, Lam EW-F, Burgering BMT, Raaijmakers JAM, Lammers J-WJ, Koenderman L *et al.* (2000) Forkhead Transcription Factor FKHR-L1 Modulates Cytokine-Dependent Transcriptional Regulation of p27KIP1.

Molecular and Cellular Biology **20** 9138–9148.

Dikic I and Elazar Z (2018) Mechanism and medical implications of mammalian autophagy. *Nature Reviews Molecular Cell Biology* **19** 349–364.

Ding CC, Thong KJ, Krishna A and Telfer EE (2010) Activin A inhibits activation of human primordial follicles *in vitro*. *Journal of Assisted Reproduction and Genetics* **27** 141–147.

Dmitrieva NI and Burg MB (2007) Osmotic Stress and DNA Damage. In *Methods in Enzymology*, pp 241–252. Elsevier Masson SAS.

Dolci S, Williams DE, Ernst MK, Resnick JL, Brannan CI, Lock LF, Lyman SD, Boswell HS and Donovan PJ (1991) Requirement for mast cell growth factor for primordial germ cell survival in culture. *Nature* **352** 809–811.

Dolmans MM, Michaux N, Camboni A, Martinez-Madrid B, Van Langendonckt A, Nottola SA and Donnez J (2006) Evaluation of Liberase, a purified enzyme blend, for the isolation of human primordial and primary ovarian follicles. *Human Reproduction* **21** 413–420.

Dolmans MM, Hollanders de Ouderaen S, Demylle D and Pirard C (2015) Utilization rates and results of long-term embryo cryopreservation before gonadotoxic treatment. *Journal of Assisted Reproduction and Genetics* **32** 1233–1237.

Donehower LA, Harvey M, Slagle BL, Mcarthurt MJ, Jrt CAM, Butel JS and Bradley A (1991) Donehower et al 1992 gemms. 215–221.

Donnez J (2006) Ovarian tissue cryopreservation and transplantation: a review. *Human Reproduction Update* **12** 519–535.

Donnez J and Dolmans M-M (2013) Fertility preservation in women. *Nature Reviews Endocrinology* **9** 735–749.

Donnez J and Dolmans MM (2015) Ovarian cortex transplantation: 60 reported live births brings the success and worldwide expansion of the technique towards routine clinical practice. *Journal of Assisted Reproduction and Genetics* **32** 1167–1170.

Donnez J and Dolmans M-M (2017) Fertility Preservation in Women. *New England Journal of Medicine* **377** 1657–1665.

Donnez J, Dolmans MM, Diaz C and Pellicer A (2015a) Ovarian cortex transplantation: Time to move on from experimental studies to open clinical application. *Fertility and Sterility* **104** 1097–1098.

Donnez J, Dolmans MM, Pellicer A, Diaz-Garcia C, Ernst E, Macklon KT and Andersen CY (2015b) Fertility preservation for age-related fertility decline. *The Lancet* **385** 506–507.

Van Dorp W, Haupt R, Anderson RA, Mulder RL, Van den Heuvel-Eibrink MM, Van Dulmen-den Broeder E, Su HI, Winther JF, Hudson MM, Levine JM *et al.* (2018) Reproductive function and outcomes in female survivors of childhood, adolescent, and young adult cancer: A review. *Journal of Clinical Oncology* **36** 2169–2180.

Druckenmiller S, Goldman KN, Labella PA, Fino ME, Bazzocchi A and Noyes N (2016) Successful Oocyte Cryopreservation in Reproductive-Aged Cancer Survivors. *Obstetrics and Gynecology* **127** 474–480.

Drury JL and Mooney DJ (2003) Hydrogels for tissue engineering: Scaffold design variables and applications. *Biomaterials* **24** 4337–4351.

Dunlop CE, Brady BM, McLaughlin M, Telfer EE, White J, Cowie F, Zahra S, Wallace WHB and Anderson RA (2016) Re-implantation of cryopreserved ovarian cortex resulting in restoration of ovarian function, natural conception and successful pregnancy after haematopoietic stem cell transplantation for Wilms tumour. *Journal of Assisted Reproduction and Genetics* **33** 1615–1620.

Durlinger ALL (1999) Control of Primordial Follicle Recruitment by Anti-Mullerian Hormone in the Mouse Ovary. *Endocrinology* **140** 5789–5796.

Durlinger ALL, Gruijters MJG, Kramer P, Karels B, Ingraham HA, Nachtigal MW, Uilenbroek JTJ, Grootegoed JA and Themmen APN (2002) Anti-Mullerian Hormone Inhibits Initiation of Primordial Follicle Growth in the Mouse Ovary. *Endocrinology* **143** 1076–1084.

Eastman A (1987) The formation, isolation and characterization of DNA adducts produced by anticancer platinum complexes. *Pharmacology and Therapeutics* **34** 155–166.

Eldani M, Luan Y, Xu PC, Bargar T and Kim SY (2020) Continuous treatment with cisplatin induces the oocyte death of primordial follicles without activation. *FASEB Journal* **34** 13885–13889.

Di Emidio G, Rossi G, Bonomo I, Alonso GL, Sferra R, Vetuschi A, Artini PG, Provenzani A, Falone S, Carta G *et al.* (2017) The natural carotenoid crocetin and the synthetic tellurium compound as101 protect the ovary against cyclophosphamide by modulating sirt1 and mitochondrial markers. *Oxidative Medicine and Cellular Longevity* **2017**.

Di Emidio G, Santini SJ, D'Alessandro AM, Vetuschi A, Sferra R, Artini PG, Carta G, Falone S, Amicarelli F and Tatone C (2019) SIRT1 participates in the response to methylglyoxal-dependent glycative stress in mouse oocytes and ovary. *Biochimica et Biophysica Acta - Molecular Basis of Disease* **1865** 1389–1401.

Engelman JA, Luo J and Cantley LC (2006) The evolution of phosphatidylinositol 3-kinases as regulators of growth and metabolism. *Nature Reviews Genetics* **7** 606–619.

Eppig JJ (1977) Mouse oocyte development *in vitro* with various culture systems. *Developmental Biology* **60** 371–388.

Eppig JJ and O'Brien MJ (1996) Development *in vitro* of mouse oocytes from primordial follicles. *Biology of Reproduction* **54** 197–207.

Eppig JJ and O'Brien MJ (1998) Comparison of preimplantation developmental competence after mouse oocyte growth and development *in vitro* and *in vivo*. *Theriogenology* **49** 415–422.

Eppig JJ and Schroeder a C (1989) Capacity of mouse oocytes from preantral follicles to undergo embryogenesis and development to live young after growth, maturation, and fertilization *in vitro*. *Biology of Reproduction* **41** 268–276.

Erickson GF, Magoffin DA, Cragun JR and Chang RJ (1990) The effects of insulin and insulin-like growth factors-I and -II on estradiol production by granulosa cells of polycystic ovaries. *Journal of Clinical Endocrinology and Metabolism* **70** 894–902.

Ernst EH, Grøndahl ML, Grund S, Hardy K, Heuck A, Sunde L, Franks S, Andersen CY, Villesen P and Lykke-Hartmann K (2017) Dormancy and activation of human oocytes from primordial and primary follicles: Molecular clues to oocyte regulation. *Human Reproduction* **32** 1684–1700.

Ernst EH, Franks S, Hardy K, Villesen P and Lykke-Hartmann K (2018) Granulosa cells from human primordial and primary follicles show differential global gene expression profiles. *Human Reproduction* **33** 666–679.

Fabbri R, Pasquinelli G, Montanaro L, Mozzanega B, Magnani V, Tamburini F, Venturoli S and Keane D (2007) Healthy early preantral follicle can be obtained in a culture of frozen-thawed human ovarian tissue of 32 weeks. *Ultrastructural Pathology* **31** 257–262.

Fabbri R, Pasquinelli G, Keane D, Magnani V, Paradisi R and Venturoli S (2010) Optimization of protocols for human ovarian tissue cryopreservation with sucrose, 1,2-propanediol and human serum. *Reproductive BioMedicine Online* **21** 819–828.

Faddy MJ, Gosden RG, Gougeon A, Richardson SJ and Nelson JF (1992) Accelerated disappearance of ovarian follicles in mid-life: implications for forecasting menopause. *Human Reproduction (Oxford, England)* **7** 1342–1346.

Faire M, Skillern A, Arora R, Nguyen DH, Wang J, Chamberlain C, German MS, Fung JC and Laird DJ (2015) Follicle dynamics and global organization in the intact mouse ovary. *Developmental Biology* **403** 69–79.

Familiari G, Caggiati A, Nottola SA, Ermini M, Benedetto MR Di and Motta PM (1993) Ultrastructure of human ovarian primordial follicles after combination chemotherapy for hodgkin's disease. *Human Reproduction* **8** 2080–2087.

Fan X, Bialecka M, Moustakas I, Lam E, Torrens-Juaneda V, Borggreven N V., Trouw L, Louwe LA, Pilgram GSK, Mei H *et al.* (2019) Single-cell reconstruction of follicular remodeling in the human adult ovary. *Nature Communications* **10** 1–13.

Faubion SS, Kuhle CL, Shuster LT and Rocca WA (2015) Long-term health consequences of premature or early menopause and considerations for management. *Climacteric* **18** 483–491.

Fauque P, Ben Amor A, Joanne C, Agnani G, Bresson JL and Roux C (2007) Use of trypan blue staining to assess the quality of ovarian cryopreservation. *Fertility and Sterility* **87** 1200–1207.

Fauser BCJM and Van Heusden AM (1997) Manipulation of human ovarian function: Physiological concepts and clinical consequences. *Endocrine Reviews* **18** 71–106.

Faustino LR, Santos RR, Silva CMG, Pinto LC, Celestino JJH, Campello CC, Figueiredo JR and Rodrigues APR (2010) Goat and sheep ovarian tissue cryopreservation: Effects on the morphology and development of primordial follicles and density of stromal cell. *Animal Reproduction Science* **122** 90–97.

Fawcett SL, Gomez AC, Barter SJ, Ditchfield M and Set P (2012) More harm than good? The anatomy of misguided shielding of the ovaries. *British Journal of Radiology* **85** 442–447.

De Felici M, Scaldaferri ML, Lobascio M, Iona S, Nazzicone V, Klinger FG and Farini D (2004) Experimental approaches to the study of primordial germ cell lineage and proliferation. *Human Reproduction Update* **10** 197–206.

Feng Y, Cui P, Lu X, Hsueh B, Möller Billig F, Zarnescu Yanez L, Tomer R, Boerboom D, Carmeliet P, Deisseroth K *et al.* (2017) CLARITY reveals dynamics of ovarian follicular architecture and vasculature in three-dimensions. *Scientific Reports* **7** 1–13.

Fenwick MA, Mora JM, Mansour YT, Baithun C, Franks S and Hardy K (2013) Investigations of TGF-β signaling in preantral follicles of female mice reveal differential roles for bone morphogenetic protein 15. *Endocrinology* **154** 3423–3436.

Fortune JE, Cushman RA, Wahl CM and Kito S (2000) The primordial to primary follicle transition. *Molecular and Cellular Endocrinology* **163** 53–60.

Frand AR, Cuozzo JW and Kaiser CA (2000) Pathways for protein disulphide bond formation. *Trends in Cell Biology* **10** 203–210.

Fransolet M, Labied S, Henry L, Masereel MC, Rozet E, Kirschvink N, Nisolle M and Munaut C (2014) Strategies for using the sheep ovarian cortex as a model in reproductive medicine. *PLoS ONE* **9** 1–7.

Fries JF, Sharp GC, Mcdevitt HO and Holman HR (1973) Cyclophosphamide therapy in systemic lupus erythematosus and polymyositis. *Arthritis & Rheumatism* **16** 154–162.

Gallardo TD, John GB, Bradshaw K, Welt C, Reijo-Pera R, Vogt PH, Touraine P, Bione S, Toniolo D, Nelson LM *et al.* (2008) Sequence variation at the human FOXO3 locus: A

study of premature ovarian failure and primary amenorrhea. *Human Reproduction* **23** 216–221.

Gallardo M, Paulini F, Corral A, Balcerzyk M, Lucci CM, Ambroise J, Merola M, Fernandez-maza L, Risco R, Dolmans MM *et al.* (2018) Evaluation of a new freezing protocol containing 20% dimethyl sulphoxide concentration to cryopreserve human ovarian tissue. *Reproductive BioMedicine Online* **37** 653–665.

Gandolfi F, Paffoni A, Papasso Brambilla E, Bonetti S, Brevini TAL and Ragni G (2006) Efficiency of equilibrium cooling and vitrification procedures for the cryopreservation of ovarian tissue: comparative analysis between human and animal models. *Fertility and Sterility* **85** 1150–1156.

Gao J, Huang Y, Li M, Zhao H, Zhao Y, Li R, Yan J, Yu Y and Qiao J (2015) Effect of local basic fibroblast growth factor and vascular endothelial growth factor on subcutaneously allotransplanted ovarian tissue in ovariectomized mice. *PLoS ONE* **10** 1–11.

Garor R, Abir R, Erman A, Felz C, Nitke S and Fisch B (2009) Effects of basic fibroblast growth factor on *in vitro* development of human ovarian primordial follicles. *Fertility and Sterility* **91** 1967–1975.

Gavish Z, Peer G, Hadassa R, Yoram C and Meirow D (2014) Follicle activation and 'burn-out' contribute to post-transplantation follicle loss in ovarian tissue grafts: The effect of graft thickness. *Human Reproduction* **29** 989–996.

Gebel J, Tuppi M, Krauskopf K, Coutandin D, Pitzius S, Kehrloesser S, Osterburg C and Dötsch V (2017) Control mechanisms in germ cells mediated by p53 family proteins. *Journal of Cell Science* **130** 2663–2671.

Gellert SE, Pors SE, Kristensen SG, Bay-Bjørn AM, Ernst E and Yding Andersen C (2018) Transplantation of frozen-thawed ovarian tissue: an update on worldwide activity published in peer-reviewed papers and on the Danish cohort. *Journal of Assisted Reproduction and Genetics* **35** 561–570.

Ghezelayagh Z, Abtahi NS, Rezazadeh Valojerdi M, Mehdizadeh A and Ebrahimi B (2020) The combination of basic fibroblast growth factor and kit ligand promotes the proliferation, activity and steroidogenesis of granulosa cells during human ovarian cortical culture. *Cryobiology* **96** 30–36.

Ghezelayagh Z, Abtahi NS, Khodaverdi S, Rezazadeh Valojerdi M, Mehdizadeh A and Ebrahimi B (2021) The effect of agar substrate on growth and development of cryopreserved-thawed human ovarian cortical follicles in organ culture. *European Journal of Obstetrics and Gynecology and Reproductive Biology* **258** 139–145.

Gigli I, Cushman RA, Wahl CM and Fortune JE (2005) Evidence for a role for anti-Müllerian hormone in the suppression of follicle activation in mouse ovaries and bovine ovarian cortex grafted beneath the chick chorioallantoic membrane. *Molecular Reproduction and Development* **71** 480–488.

Gilchrist RB, Ritter LJ and Armstrong DT (2004) Oocyte-somatic cell interactions during follicle development in mammals. *Animal Reproduction Science* **82–83** 431–446.

Glick D, Barth S and Macleod KF (2010) Autophagy: Cellular and molecular mechanisms. *Journal of Pathology* **221** 3–12.

Godin I, Deed R, Cooke J, Zsebo K, Dexter M and Wylie CC (1991) Effects of the steel gene product on mouse primordial germ cells in culture. *Nature* **352** 807–809.

Goldman KN, Chenette D, Arju R, Duncan FE, Keefe DL, Grifo JA, Schneiderb RJ and Schneider RJ (2017) mTORC1/2 inhibition preserves ovarian function and fertility during genotoxic chemotherapy. *Proceedings of the National Academy of Sciences* **114** 3186–3191.

Gonfloni S, Di Tella L, Caldarola S, Cannata SM, Klinger FG, Di Bartolomeo C, Mattei M, Candi E, De Felici M, Melino G *et al.* (2009) Inhibition of the c-Abl-TAp63 pathway protects mouse oocytes from chemotherapy-induced death. *Nature Medicine* **15** 1179–1185.

Gook DA, Edgar DH and Stern C (1999) Effect of cooling rate and dehydration regimen on the histological appearance of human ovarian cortex following cryopreservation in 1,2-propanediol. *Human Reproduction* **14** 2061–2068.

Gook DA, McCully BA, Edgar DH and McBain JC (2001) Development of antral follicles in human cryopreserved ovarian tissue following xenografting. *Human Reproduction* **16** 417–422.

Gook DA, Edgar DH, Borg J, Archer J, Lutjen PJ and McBain JC (2003) Oocyte maturation, follicle rupture and luteinization in human cryopreserved ovarian tissue following xenografting. *Human Reproduction* **18** 1772–1781.

Gosden RG, Boulton MI, Grant K and Webb R (1994a) Follicular development from ovarian xenografts in SCID mice. *Journal of Reproduction and Fertility* **101** 619–623.

Gosden RG, Baird DT, Wade JC and Webb R (1994b) Restoration of fertility to oophorectomized sheep by ovarian autografts stored at-196°c. *Human Reproduction* **9** 597–603.

Gougeon A (1986) Dynamics of follicular growth in the human: a model from preliminary results. *Hum. Reprod.* **1** 81–87.

Gougeon A (1996) Regulation of ovarian follicular development in primates: facts and hypotheses. *Endocrine Reviews* **17** 121–155.

Gougeon A and Chainy GBN (1987) Morphometric studies of small follicles in ovaries of women at different ages. *Journal of Reproduction and Fertility* **81** 433–442.

Gougeon A and Lefevre B (1983) Evolution of the diameters of the largest healthy and atretic follicles during the human menstrual cycle. *Journal of Reproduction and Fertility* **69** 497–502.

Gougeon A, Ecochard R and Thalabard JC (1994) Age-related changes of the population of human ovarian follicles: Increase in the disappearance rate of non-growing and early-growing follicles in aging women. *Biology of Reproduction* **50** 653–663.

Granados-Aparici S, Hardy K, Franks S, Sharum IB, Waite SL and Fenwick MA (2019) SMAD3 directly regulates cell cycle genes to maintain arrest in granulosa cells of mouse primordial follicles. *Scientific Reports* **9** 6513.

Green DM, Sklar CA, Boice JD, Mulvihill JJ, Whitton JA, Stovall M and Yasui Y (2009) Ovarian failure and reproductive outcomes after childhood cancer treatment: Results from the childhood cancer survivor study. *Journal of Clinical Oncology* **27** 2374–2381.

Griffin J, Emery BR, Huang I, Peterson CM and Carrell DT (2006) Comparative analysis of follicle morphology and oocyte diameter in four mammalian species (mouse, hamster, pig, and human). *Journal of Experimental and Clinical Assisted Reproduction* **3** 1–9.

Grosbois J and Demeestere I (2018) Dynamics of PI3K and Hippo signaling pathways during *in vitro* human follicle activation. *Human Reproduction* **33** 1–10.

Grosbois J, Vermeersch M, Devos M, Clarke HJ and Demeestere I (2019) Ultrastructure and intercellular contact-mediated communication in cultured human early stage follicles exposed to mTORC1 inhibitor. *Molecular Human Reproduction* **25** 706–716.

Grosbois J, Devos M and Demeestere I (2020) Implications of non-physiological ovarian primordial follicle activation for fertility preservation. *Endocrine Reviews* **26** 1–15.

Guzel Y, Bildik G and Oktem O (2018a) Sphingosine-1-phosphate protects human ovarian follicles from apoptosis *in vitro*. *European Journal of Obstetrics & Gynecology and Reproductive Biology* **222** 19–24.

Guzel Y, Bildik G, Dilege E and Oktem O (2018b) Sphingosine-1-phosphate reduces atresia of primordial follicles occurring during slow-freezing and thawing of human ovarian cortical strips. *Molecular Reproduction and Development* **85** 858–864.

Guzman L, Ortega-Hrepich C, Albuz FK, Verheyen G, Devroey P, Smitz J and De Vos M (2012) Developmental capacity of *in vitro*-matured human oocytes retrieved from polycystic ovary syndrome ovaries containing no follicles larger than 6 mm. *Fertility and Sterility* **98** 503–507.

Hamoda H and British Menopause Society and Women's Health Concern (2017) The British Menopause Society and Women's Health Concern recommendations on the management of women with premature ovarian insufficiency. *Post Reproductive Health* **23** 22–35.

Hansen M, Chandra A, Mitic LL, Onken B, Driscoll M and Kenyon C (2008) A role for autophagy in the extension of lifespan by dietary restriction in C. elegans. *PLoS Genetics* **4** e25.

Hao J, Tuck AR, Sjödin MOD, Lindberg J, Sand A, Niklasson B, Argyraki M, Hovatta O and Damdimopoulou P (2017) Resveratrol supports and alpha-naphthoflavone disrupts growth of human ovarian follicles in an *in vitro* tissue culture model. *Toxicology and Applied Pharmacology* **338** 73–82.

Hao J, Tuck AR, Prakash CR, Damdimopoulos A, Sjödin MOD, Lindberg J, Niklasson B, Pettersson K, Hovatta O and Damdimopoulou P (2020) Culture of human ovarian tissue in xeno-free conditions using laminin components of the human ovarian extracellular matrix. *Journal of Assisted Reproduction and Genetics* **37** 2137–2150.

Harada M, Nose E, Takahashi N, Hirota Y, Hirata T, Yoshino O, Koga K, Fujii T and Osuga Y (2015) Evidence of the activation of unfolded protein response in granulosa and cumulus cells during follicular growth and maturation. *Gynecological Endocrinology* **31** 783–787.

Harding HP, Zhang Y and Ron D (1999) Protein translation and folding are coupled by an endoplasmic-reticulum-resident kinase. *Nature* **397** 271–274.

Hardy K, Mora JM, Dunlop C, Carzaniga R, Franks S and Fenwick MA (2018) Nuclear exclusion of SMAD2/3 in granulosa cells is associated with primordial follicle activation in the mouse ovary. *Journal of Cell Science* **131** jcs218123.

Harris SE, Adriaens I, Leese HJ, Gosden RG and Picton HM (2007) Carbohydrate metabolism by murine ovarian follicles and oocytes grown *in vitro*. *Reproduction* **134** 415–424.

Harris SE, Leese HJ, Gosden RG and Picton HM (2009) Pyruvate and oxygen consumption throughout the growth and development of murine oocytes. *Molecular Reproduction and Development* **76** 231–238.

Hemmings BA and Restuccia DF (2012) PI3K-PKB/Akt Pathway. *Cold Spring Harbor Perspectives in Biology* **4** a011189–a011189.

Henderson KM, McNatty KP, Smith P, Gibb M, O'Keeffe LE, Lun S, Heath DA and Prisk MD (1987) Influence of follicular health on the steroidogenic and morphological characteristics of bovine granulosa cells *in vitro*. *Journal of Reproduction and Fertility* **79** 185–193.

Hernandez-Fonseca H, Bosch P, Sirisathien S, Wininger JD, Massey JB and Brackett BG (2004) Effect of site of transplantation on follicular development of human ovarian tissue transplanted into intact or castrated immunodeficient mice. *Fertility and Sterility* **81** 888–

892.

Hirashima Y, Moniruzzaman M and Miyano T (2011) P27KIP1 negatively regulates the activation of murine primordial oocytes. *Journal of Reproduction and Development* **57** 217–222.

Hirobe S, He WW, Lee MM and Donahoe PK (1992) Mullerian inhibiting substance messenger ribonucleic acid expression in granulosa and Sertoli cells coincides with their mitotic activity. *Endocrinology* **131** 854–862.

Hirshfield AN (1991) Development of follicles in the mammalian ovary. *International Review of Cytology* **124** 43–101.

Horie K, Takakura K, Taii S, Narimoto K, Noda Y, Nishikawa S, Nakayama H, Fujita J and Mori T (1991) The Expression of c-kit Protein during Oogenesis and Early Embryonic Development1. *Biology of Reproduction* **45** 547–552.

Horie K, Fujita J, Takakura K, Kanzaki H, Suginami H, Iwai M, Nakayama H and Mori T (1993) Pregnancy: The expression of c-kit protein in human adult and fetal tissues. *Human Reproduction* **8** 1955–1962.

Hornick JE, Duncan FE, Shea LD and Woodruff TK (2013) Multiple follicle culture supports primary follicle growth through paracrine-acting signals. *Reproduction* **145** 19–32.

Hosaka T, Biggs WH, Tieu D, Boyer AD, Varki NM, Cavenee WK and Arden KC (2004) Disruption of forkhead transcription factor (FOXO) family members in mice reveals their functional diversification. *Proceedings of the National Academy of Sciences of the United States of America* **101** 2975–2980.

Hossain Z, Ali SM, Hui LK, Xu J, Chee PN, Guo K, Qi Z, Ponniah S, Hong W and Hunziker W (2007) Glomerulocystic kidney disease in mice with a targeted inactivation of Wwtr1. *Proceedings of the National Academy of Sciences of the United States of America* **104** 1631–1636.

Hovatta O (2005) Methods for cryopreservation of human ovarian tissue. *Reproductive BioMedicine Online* **10** 729–734.

Hovatta O, Silye R, Krausz T, Abir R, Margara R, Trew G, Lass A and Winston RM (1996) Cryopreservation of human ovarian tissue using dimethylsulphoxide and propanediol-sucrose as cryoprotectants. *Human Reproduction* **11** 1268–1272.

Hovatta O, Silye R, Abir R, Krausz T and Winston RM (1997) Extracellular matrix improves survival of both stored and fresh human primordial and primary ovarian follicles in long-term culture. *Human Reproduction* **12** 1032–1036.

Hovatta O, Wright C, Krausz T, Hardy K and Winston RML (1999) Human primordial, primary and secondary ovarian follicles in long-term culture: Effect of partial isolation. *Human Reproduction* **14** 2519–2524.

Høyer PE, Byskov AG and Møllgård K (2005) Stem cell factor and c-Kit in human primordial germ cells and fetal ovaries. *Molecular and Cellular Endocrinology* **234** 1–10.

Hreinsson JG, Scott JE, Rasmussen C, Swahn ML, Hsueh AJW and Hovatta O (2002) Growth Differentiation Factor-9 Promotes the Growth, Development, and Survival of Human Ovarian Follicles in Organ Culture. *The Journal of Clinical Endocrinology & Metabolism* **87** 316–321.

Hreinsson J, Zhang P, Swahn ML, Hultenby K and Hovatta O (2003) Cryopreservation of follicles in human ovarian cortical tissue. Comparison of serum and human serum albumin in the cryoprotectant solutions. *Human Reproduction* **18** 2420–2428.

Huang EJ, Manova K, Packer AI, Sanchez S, Bachvarova RF and Besmer P (1993) The

murine Steel Panda mutation affects kit ligand expression and growth of early ovarian follicles. *Developmental Biology* **157** 100–109.

Huang N, Yu Y and Qiao J (2017) Dual role for the unfolded protein response in the ovary: adaption and apoptosis. *Protein and Cell* **8** 14–24.

Hułas-Stasiak M and Gawron A (2011) Follicular atresia in the prepubertal spiny mouse (Acomys cahirinus) ovary. *Apoptosis* **16** 967–975.

Ikeda Y, Hasegawa A, Tsubamoto H, Wakimoto Y, Kumamoto K and Shibahara H (2016) Effects of gremlin-2 on the transition of primordial follicles during early folliculogenesis in the human ovary. *European Journal of Obstetrics Gynecology and Reproductive Biology* **203** 72–77.

Isachenko V, Isachenko E, Reinsberg J, Montag M, Braun F and van der Ven H (2008) Cryopreservation of human ovarian tissue: Effect of spontaneous and initiated ice formation. *Reproductive BioMedicine Online* **16** 336–345.

Isachenko V, Lapidus I, Isachenko E, Krivokharchenko A, Kreienberg R, Woriedh M, Bader M and Weiss JM (2009) Human ovarian tissue vitrification versus conventional freezing: Morphological, endocrinological, and molecular biological evaluation. *Reproduction* **138** 319–327.

Isachenko V, Mallmann P, Petrunkina AM, Rahimi G, Nawroth F, Hancke K, Felberbaum R, Genze F, Damjanoski I and Isachenko E (2012) Comparison of *in vitro*- and chorioallantoic membrane (CAM)-culture systems for cryopreserved medulla-contained human ovarian tissue. *PLoS ONE* **7** 1–9.

El Issaoui M, Giorgione V, Mamsen LS, Rechnitzer C, Birkebæk N, Clausen N, Kelsey TW and Andersen CY (2016) Effect of first line cancer treatment on the ovarian reserve and follicular density in girls under the age of 18 years. *Fertility and Sterility* **106** 1757-1762.e1.

Jacks T, Remington L, Williams BO, Schmitt EM, Halachmi S, Bronson RT and Weinberg RA (1994) Tumor spectrum analysis in p53-mutant mice. *Current Biology* **4** 1–7.

Jadoul P, Dolmans MM and Donnez J (2010) Fertility preservation in girls during childhood: Is it feasible, efficient and safe and to whom should it be proposed? *Human Reproduction Update* **16** 617–630.

Jadoul P, Guilmain A, Squifflet J, Luyckx M, Votino R, Wyns C and Dolmans MM (2017) Efficacy of ovarian tissue cryopreservation for fertility preservation: Lessons learned from 545 cases. *Human Reproduction* **32** 1046–1054.

Jensen AK, Macklon KT, Fedder J, Ernst E, Humaidan P and Andersen CY (2017) 86 successful births and 9 ongoing pregnancies worldwide in women transplanted with frozen-thawed ovarian tissue: focus on birth and perinatal outcome in 40 of these children. *Journal of Assisted Reproduction and Genetics* **34** 337.

Jiao ZX and Woodruff TK (2013) Follicle microenvironment-associated alterations in gene expression in the mouse oocyte and its polar body. *Fertility and Sterility* **99** 1453-1459.e1.

Jin X, Han CS, Yu FQ, Wei P, Hu ZY and Liu YX (2005) Anti-apoptotic action of stem cell factor on oocytes in primordial follicles and its signal transduction. *Molecular Reproduction and Development* **70** 82–90.

John GB, Gallardo TD, Shirley LJ and Castrillon DH (2008) Foxo3 is a PI3K-dependent molecular switch controlling the initiation of oocyte growth. *Developmental Biology* **321** 197–204.

Kagami K, Shinmyo Y, Ono M, Kawasaki H and Fujiwara H (2018) Three-dimensional evaluation of murine ovarian follicles using a modified CUBIC tissue clearing method.

Reproductive Biology and Endocrinology **16** 1–7.

Kaghad M, Bonnet H, Yang A, Creancier L, Biscan JC, Valent A, Minty A, Chalon P, Lelias JM, Dumont X *et al.* (1997) Monoallelically expressed gene related to p53 at 1p36, a region frequently deleted in neuroblastoma and other human cancers. *Cell* **90** 809–819.

Kaipia A and Hsueh AJW (1997) Regulation of Ovarian. *Regulation of Ovarian Follicle Atresia* **59** 349–363.

Kaivo-Oja N, Jeffery LA, Ritvos O and Mottershead DG (2006) Smad signalling in the ovary. *Reproductive Biology and Endocrinology* **4** 1–13.

Kaldis P (2007) Another Piece of the p27Kip1 Puzzle. *Cell* **128** 241–244.

Kalich-Philosoph L, Roness H, Carmely A, Fishel-Bartal M, Ligumsky H, Paglin S, Wolf I, Kanety H, Sredni B and Meirow D (2013) Cyclophosphamide triggers follicle activation and 'burnout'; AS101 prevents follicle loss and preserves fertility. *Science Translational Medicine* **5** 185ra62.

Kamen BA, Cole PD and Bertino JR (2003) Folate antagonists. In *Holland-Frei Cancer Medicine*, Sixth Ed. Eds DW Kufe, RE Pollock, RR Weichselbaum, RC Bast Jr, TS Gansler, JF Holland and E Frei. Hamilton (ON): BC Decker.

Karavani G, Schachter-Safrai N, Revel A, Mordechai-Daniel T, Bauman D and Imbar T (2019) *In vitro* maturation rates in young premenarche patients. *Fertility and Sterility* **112** 315–322.

Kawamura K, Cheng Y, Suzuki N, Deguchi M, Sato Y, Takae S, Ho C -h., Kawamura N, Tamura M, Hashimoto S *et al.* (2013) Hippo signaling disruption and Akt stimulation of ovarian follicles for infertility treatment. *Proceedings of the National Academy of Sciences* **110** 17474–17479.

Kawashima I and Kawamura K (2018) Regulation of follicle growth through hormonal factors and mechanical cues mediated by Hippo signaling pathway. *Systems Biology in Reproductive Medicine* **64** 3–11.

Kedem A, Hourvitz A, Fisch B, Shachar M, Cohen S, Ben-Haroush A, Dor J, Freud E, Felz C and Abir R (2011a) Alginate scaffold for organ culture of cryopreserved-thawed human ovarian cortical follicles. *Journal of Assisted Reproduction and Genetics* **28** 761–769.

Kedem A, Fisch B, Garor R, Ben-Zaken A, Gizunterman T, Felz C, Ben-Haroush A, Kravarusic D and Abir R (2011b) Growth Differentiating Factor 9 (GDF9) and bone morphogenetic protein 15 both activate development of human primordial follicles *in vitro*, with seemingly more beneficial effects of GDF9. *Journal of Clinical Endocrinology and Metabolism* **96** 1246–1254.

Keros V, Xella S, Hultenby K, Pettersson K, Sheikhi M, Volpe A, Hreinsson J and Hovatta O (2009) Vitrification versus controlled-rate freezing in cryopreservation of human ovarian tissue. *Human Reproduction* **24** 1670–1683.

Kerr JB, Hutt KJ, Cook M, Speed TP, Strasser A, Findlay JK and Scott CL (2012a) Cisplatin-induced primordial follicle oocyte killing and loss of fertility are not prevented by imatinib. *Nature Medicine* **18** 1170–1172.

Kerr JB, Hutt KJ, Michalak EM, Cook M, Vandenberg CJ, Liew SH, Bouillet P, Mills A, Scott CL, Findlay JK *et al.* (2012b) DNA Damage-Induced Primordial Follicle Oocyte Apoptosis and Loss of Fertility Require TAp63-Mediated Induction of Puma and Noxa. *Molecular Cell* **48** 343–352.

Keshet E, Lyman SD, Williams DE, Anderson DM, Jenkins NA and Copeland Parada NGLF (1991) Embryonic RNA expression patterns of the c-kit receptor and its cognate ligand suggest multiple functional roles in mouse development. *EMBO Journal* **10** 2425–2435.

Kierzenbaum AL (2007) *Histology and Cell Biology: An Introduction to Pathology*. Philadelphia, PA: Mosby Elsevier.

Kim JY (2012) Control of ovarian primordial follicle activation. *Clinical and Experimental Reproductive Medicine* **39** 10–14.

Kim S-Y and Kurita T (2018) New Insights into the Role of Phosphoinositide 3-Kinase Activity in the Physiology of Immature Oocytes: Lessons from Recent Mouse Model Studies. *European Medical Journal. Reproductive Health* **3** 119–125.

Kim SS, Soules MR and Battaglia DE (2002) Follicular development, ovulation, and corpus luteum formation in cryopreserved human ovarian tissue after xenotransplantation. *Fertility and Sterility* **78** 77–82.

Kim SS, Kang HG, Kim NH, Lee HC and Lee HH (2005) Assessment of the integrity of human oocytes retrieved from cryopreserved ovarian tissue after xenotransplantation. *Human Reproduction* **20** 2502–2508.

Kim SY, Nair DM, Romero M, Serna VA, Koleske AJ, Woodruff TK and Kurita T (2018) Transient inhibition of p53 homologs protects ovarian function from two distinct apoptotic pathways triggered by anticancer therapies. *Cell Death and Differentiation* **26** 502–515.

Kinnear HM, Tomaszewski CE, Chang FL, Moravek MB, Xu M, Padmanabhan V and Shikanov A (2020) The ovarian stroma as a new frontier. *Reproduction* **160** R25–R39.

Knight PG and Glister C (2006) TGF-β superfamily members and ovarian follicle development. *Reproduction* **132** 191–206.

Komatsu K and Masubuchi S (2020) Increased supply from blood vessels promotes the activation of dormant primordial follicles in mouse ovaries. *Journal of Reproduction and Development* **66** 105–113.

Koyama H, Wada T, Nishizawa Y, Iwanaga T, Aoki Y, Terasawa T, Kosaki G, Yamamoto T and Wada A (1977) Cyclophosphamide-induced ovarian failure and its therapeutic significance in patients with breast cancer. *Cancer* **39** 1403–1409.

Kristensen SG, Rasmussen A, Byskov AG and Andersen CY (2011) Isolation of pre-antral follicles from human ovarian medulla tissue. *Human Reproduction* **26** 157–166.

Kristensen SG, Liu Q, Mamsen LS, Greve T, Pors SE, Bjørn AB, Ernst E, Macklon KT and Andersen CY (2018) A simple method to quantify follicle survival in cryopreserved human ovarian tissue. *Human Reproduction* **5** 2276–2284.

Kumar S (2007) Caspase function in programmed cell death. *Cell Death and Differentiation* **14** 32–43.

Kurita T, Cunha GR, Robboy SJ, Mills AA and Medina RT (2005) Differential expression of p63 isoforms in female reproductive organs. *Mechanisms of Development* **122** 1043–1055.

Kuwana T, Bouchier-Hayes L, Chipuk JE, Bonzon C, Sullivan BA, Green DR and Newmeyer DD (2005) BH3 Domains of BH3-Only Proteins Differentially Regulate Bax-Mediated Mitochondrial Membrane Permeabilization Both Directly and Indirectly. *Molecular Cell* **17** 525–535.

Lambertini M, Ceppi M, Poggio F, Peccatori FA, Azim HA, Ugolini D, Pronzato P, Loibl S, Moore HCF, Partridge AH *et al.* (2015) Ovarian suppression using luteinizing hormonereleasing hormone agonists during chemotherapy to preserve ovarian function and fertility of breast cancer patients: A meta-analysis of randomized studies. *Annals of Oncology* **26** 2408–2419.

Lamkanfi M and Kanneganti TD (2010) Caspase-7: A protease involved in apoptosis and inflammation. *International Journal of Biochemistry and Cell Biology* **42** 21–24.

Lande Y, Fisch B, Tsur A, Farhi J, Prag-Rosenberg R, Ben-Haroush A, Kessler-Icekson G, Zahalka MA, Ludeman SM and Abir R (2017) Short-term exposure of human ovarian follicles to cyclophosphamide metabolites seems to promote follicular activation *in vitro*. *Reproductive BioMedicine Online* **34** 104–114.

Laronda MM, Duncan FE, Hornick JE, Xu M, Pahnke JE, Whelan K a., Shea LD and Woodruff TK (2014) Alginate encapsulation supports the growth and differentiation of human primordial follicles within ovarian cortical tissue. *Journal of Assisted Reproduction and Genetics* **31** 1013–1028.

Laronda MM, Rutz AL, Xiao S, Whelan KA, Duncan FE, Roth EW, Woodruff TK and Shah RN (2017) A bioprosthetic ovary created using 3D printed microporous scaffolds restores ovarian function in sterilized mice. *Nature Communications* **8** 15261.

Lee JY and Kitaoka M (2018) A beginner's guide to rigor and reproducibility in fluorescence imaging experiments. *Molecular Biology of the Cell* **29** 1519–1525.

Lee KP, Lee JH, Kim TS, Kim TH, Park HD, Byun JS, Kim MC, Jeong W Il, Calvisi DF, Kim JM *et al.* (2010) The Hippo-Salvador pathway restrains hepatic oval cell proliferation, liver size, and liver tumorigenesis. *Proceedings of the National Academy of Sciences of the United States of America* **107** 8248–8253.

Lerer-Serfaty G, Samara N, Fisch B, Shachar M, Kossover O, Seliktar D, Ben-Haroush A and Abir R (2013) Attempted application of bioengineered/biosynthetic supporting matrices with phosphatidylinositol-trisphosphate-enhancing substances to organ culture of human primordial follicles. *Journal of Assisted Reproduction and Genetics* **30** 1279–1288.

Li Q, Pangas SA, Jorgez CJ, Graff JM, Weinstein M and Matzuk MM (2008) Redundant roles of SMAD2 and SMAD3 in ovarian granulosa cells *in vivo*. *Molecular and Cellular Biology* **28** 7001–7011.

Li F, Turan V, Lierman S, Cuvelier C, De Sutter P and Oktay K (2014) Sphingosine-1-phosphate prevents chemotherapy-induced human primordial follicle death. *Human Reproduction* **29** 107–113.

Li S, Fan Q, Xie Y, Lin H, Qiu Q, Liang Y and Zhang Q (2019) VIP activates primordial follicles of rat through ERK-mTOR pathway in tissue culture. *Reproduction* **157** 475–484.

Li J, Zhang Y, Zheng N, Li B, Yang J, Zhang C, Xia G and Zhang M (2020) CREB activity is required for mTORC1 signaling-induced primordial follicle activation in mice. *Histochemistry and Cell Biology* **154** 287–299.

Liang J, Wu YL, Chen BJ, Zhang W, Tanaka Y and Sugiyama H (2013) The C-Kit receptor-mediated signal transduction and tumor-related diseases. *International Journal of Biological Sciences* **9** 435–443.

Liebenthron J, Köster M, Drengner C, Reinsberg J, Van Der Ven H and Montag M (2013) The impact of culture conditions on early follicle recruitment and growth from human ovarian cortex biopsies *in vitro*. *Fertility and Sterility* **100** 483-91.e5.

Lin P, Yang Y, Li X, Chen F, Cui C, Hu L, Li Q, Liu W and Jin Y (2012) Endoplasmic reticulum stress is involved in granulosa cell apoptosis during follicular atresia in goat ovaries. *Molecular Reproduction and Development* **79** 423–432.

Ling YH, El-Naggar AK, Priebe W and Perez-Soler R (1996) Cell cycle-dependent cytotoxicity, G2/M phase arrest, and disruption of p34cdc2/cyclin B1 activity induced by doxorubicin in synchronized P388 cells. *Molecular Pharmacology* **49** 832–841.

Lintern-Moore S and Moore GPM (1979) The initiation of oocyte growth in the mouse ovary. *Annales de Biologie Animale, Biochimie, Biophysique* **19** 1399–1407.

Liu L, Rajareddy S, Reddy P, Du C, Jagarlamudi K, Shen Y, Gunnarsson D, Selstam G, Boman

K and Liu K (2007) Infertility caused by retardation of follicular development in mice with oocyte-specific expression of Foxo3a. *Development (Cambridge, England)* **134** 199–209.

Liu ZQ, Shen M, Wu WJ, Li BJ, Weng QN, Li M and Liu HL (2015) Expression of PUMA in Follicular Granulosa Cells Regulated by FoxO1 Activation During Oxidative Stress. *Reproductive Sciences* **22** 696–705.

Livera G, Petre-Lazar B, Guerquin M-J, Trautmann E, Coffigny H and Habert R (2008) p63 null mutation protects mouse oocytes from radio-induced apoptosis. *Reproduction* **135** 3–12.

Lo BKM, Sheikh S and Williams SA (2019) *In vitro* and *in vivo* mouse follicle development in ovaries and reaggregated ovaries. *Reproduction* **5** 135–148.

Loos B, Engelbrecht AM, Lockshin RA, Klionsky DJ and Zakeri Z (2013) The variability of autophagy and cell death susceptibility: Unanswered questions. *Autophagy* **9** 1270–1285.

Lopes F, Smith R, Anderson RA and Spears N (2014) Docetaxel induces moderate ovarian toxicity in mice, primarily affecting granulosa cells of early growing follicles. *Molecular Human Reproduction* **20** 948–959.

Lopes F, Liu J, Morgan S, Matthews R, Nevin L, Anderson RA and Spears N (2020) Single and combined effects of cisplatin and doxorubicin on the human and mouse ovary *in vitro*. *Reproduction* **159** 193–204.

Lotz L, Liebenthron J, Nichols-Burns SM, Montag M, Hoffmann I, Beckmann MW, van der Ven H, Töpfer D and Dittrich R (2014) Spontaneous antral follicle formation and metaphase II oocyte from a non-stimulated prepubertal ovarian tissue xenotransplant. *Reproductive Biology and Endocrinology* **12** 1–5.

Louhio H, Hovatta O, Sjöberg J and Tuuri T (2000) The effects of insulin, and insulin-like growth factors I and II on human ovarian follicles in long-term culture. *Molecular Human Reproduction* **6** 694–698.

Luan Y, Edmonds ME, Woodruff TK and Kim SY (2019) Inhibitors of apoptosis protect the ovarian reserve from cyclophosphamide. *Journal of Endocrinology* **240** 243–256.

Luyckx V, Scalercio S, Jadoul P, Amorim CA, Soares M, Donnez J and Dolmans MM (2013a) Evaluation of cryopreserved ovarian tissue from prepubertal patients after long-term xenografting and exogenous stimulation. *Fertility and Sterility* **100** 1350–1357.

Luyckx V, Dolmans MM, Vanacker J, Scalercio SR, Donnez J and Amorim CA (2013b) First step in developing a 3D biodegradable fibrin scaffold for an artificial ovary. *Journal of Ovarian Research* **6** 83.

Maas K, Mirabal S, Penzias A, Sweetnam PM, Eggan KC and Sakkas D (2018) Hippo signaling in the ovary and polycystic ovarian syndrome. *Journal of Assisted Reproduction and Genetics* **35** 1763–1771.

Maiani E, Di Bartolomeo C, Klinger FG, Cannata SM, Bernardini S, Chateauvieux S, Mack F, Mattei M, De Felici M, Diederich M *et al.* (2012) Reply to: Cisplatin-induced primordial follicle oocyte killing and loss of fertility are not prevented by imatinib. *Nature Medicine* **18** 1172–1174.

Maidarti M, Clarkson YL, McLaughlin M, Anderson RA and Telfer EE (2018) Inhibition of PTEN activates bovine non-growing follicles *in vitro* but increases DNA damage and reduces DNA repair response. *Human Reproduction* **34** 297–307.

Mamsen LS, Kristensen SG, Pors SE, Bøtkjær JA, Ernst E, Macklon KT, Gook D, Kumar A, Kalra B and Andersen CY (2021) Consequences of β-thalassemia or sickle cell disease for ovarian follicle number and morphology in girls who had ovarian tissue cryopreserved. *Frontiers in Endocrinology* **11** 1–9.

Man L, Lustgarten-Guahmich N, Kallinos E, Redhead-Laconte Z, Liu S, Schattman B, Redmond D, Hancock K, Zaninovic N, Schattman G *et al.* (2020) Comparison of human antral follicles of xenograft versus ovarian origin reveals disparate molecular signatures. *Cell Reports* **32** 108027.

Manavella DD, Cacciottola L, Pommé S, Desmet CM, Jordan BF, Donnez J, Amorim CA and Dolmans MM (2018) Two-step transplantation with adipose tissue-derived stem cells increases follicle survival by enhancing vascularization in xenografted frozen-thawed human ovarian tissue. *Human Reproduction* **33** 1107–1116.

Manova K, Nocka K, Besmer P and Bachvarova RF (1990) Gonadal expression of c-kit encoded at the W locus of the mouse. *Development* **110** 1057–1069.

Manova K, Huang EJ, Angeles M, De Leon V, Sanchez S, Pronovost SM, Besmer P and Bachvarova RF (1993) The expression pattern of the c-kit ligand in gonads of mice supports a role for the c-kit receptor in oocyte growth and in proliferation of spermatogonia. *Developmental Biology* **157** 85–99.

Marcello MF, Nuciforo G, Romeo R, Di Dino G, Russo I, Russo A, Palumbo G and Schilirò G (1990) Structural and ultrastructural study of the ovary in childhood leukemia after successful treatment. *Cancer* **66** 2099–2104.

Mariño G, Niso-Santano M, Baehrecke EH and Kroemer G (2014) Self-consumption: The interplay of autophagy and apoptosis. *Nature Reviews Molecular Cell Biology* **15** 81–94.

Masciangelo R, Hossay C, Chiti MC, Manavella DD, Amorim CA, Donnez J and Dolmans M-M (2020) Role of the PI3K and Hippo pathways in follicle activation after grafting of human ovarian tissue. *Journal of Assisted Reproduction and Genetics* **37** 101–108.

Mason AJ, Hayflick JS, Zoeller RT, Young WS, Phillips HS, Nikolics K and Seeburg PH (1986) A deletion truncating the gonadotropin-releasing hormone gene is responsible for hypogonadism in the hpg mouse. *Science* **234** 1366–1371.

Matsui Y, Toksoz D, Nishikawa S, Nishikawa S-I, Williams D, Zsebo K and Hogan BLM (1991) Effect of Steel factor and leukaemia inhibitory factor on murine primordial germ cells in culture. *Nature* **353** 750–752.

Matthews SJ, Picton H, Ernst E and Andersen CY (2018) Successful pregnancy in a woman previously suffering from β-thalassemia following transplantation of ovarian tissue cryopreserved before puberty. *Minerva Ginecologica* **70** 432–435.

McCall ML, Keaty EC and Thompson JD (1958) Conservation of ovarian tissue in the treatment of carcinoma of the cervix with radical surgery. *American Journal of Obstetrics and Gynecology* **75** 590–600.

McGee EA and Hsueh AJW (2000) Initial and Cyclic Recruitment of Ovarian Follicles. *Endocrine Reviews* **21** 200–214.

McGee EA and Raj RS (2015) Regulators of ovarian preantral follicle development. *Seminars in Reproductive Medicine* **33** 179–184.

McGee EA, Smith R, Spears N, Nachtigal MW, Ingraham H and Hsueh AJW (2001) Müllerian inhibitory substance induces growth of rat preantral ovarian follicles. *Biology of Reproduction* **64** 293–298.

McKey J, Cameron LA, Lewis D, Batchvarov IS and Capel B (2020) Combined iDISCO and CUBIC tissue clearing and lightsheet microscopy for in toto analysis of the adult mouse ovary. *Biology of Reproduction*.

McLaughlin M, Innell HL, Anderson RA and Telfer EE (2014) Inhibition of phosphatase and tensin homologue (PTEN) in human ovary *in vitro* results in increased activation of primordial follicles but compromises development of growing follicles. *Molecular Human*

Reproduction **20** 736–744.

McLaughlin M, Kelsey TW, Wallace WHB, Anderson RA and Telfer EE (2015) An externally validated age-related model of mean follicle density in the cortex of the human ovary. *Journal of Assisted Reproduction and Genetics* **32** 1089–1095.

McLaughlin M, Kelsey TW, Wallace WHB, Anderson RA and Telfer EE (2017) Non-growing follicle density is increased following adriamycin, bleomycin, vinblastine and dacarbazine (ABVD) chemotherapy in the adult human ovary. *Human Reproduction* **32** 165–174.

McLaughlin M, Albertini DF, Wallace WHB, Anderson RA and Telfer EE (2018) Metaphase II oocytes from human unilaminar follicles grown in a multi-step culture system. *Molecular Human Reproduction* **24** 1–8.

McNatty KP, Hillier SG, van den Boogaard AMJ, Trimbos-Kemper TCM, Reichert LE and van Hall E V. (1983) Follicular development during the luteal phase of the human menstrual cycle. *The Journal of Clinical Endocrinology & Metabolism* **56** 1022–1031.

Meirow D and Nugent D (2001) The effects of radiotherapy and chemotherapy on female reproduction. *Human Reproduction Update* **7** 535–543.

Meirow D, Dor J, Kaufman B, Shrim A, Rabinovici J, Schiff E, Raanani H, Levron J and Fridman E (2007) Cortical fibrosis and blood-vessels damage in human ovaries exposed to chemotherapy. Potential mechanisms of ovarian injury. *Human Reproduction* **22** 1626–1633.

Meirow D, Biederman H, Anderson R a and Wallace WHB (2010) Toxicity of chemotherapy and radiation on female reproduction. *Clinical Obstetrics and Gynecology* **53** 727–739.

Meirow D, Ra'anani H, Shapira M, Brenghausen M, Derech Chaim S, Aviel-Ronen S, Amariglio N, Schiff E, Orvieto R and Dor J (2016) Transplantations of frozen-thawed ovarian tissue demonstrate high reproductive performance and the need to revise restrictive criteria. *Fertility and Sterility* **106** 467–474.

Meng L, Jan SZ, Hamer G, Van Pelt AM, Van Der Stelt I, Keijer J and Teerds KJ (2018) Preantral follicular atresia occurs mainly through autophagy, while antral follicles degenerate mostly through apoptosis. *Biology of Reproduction* **99** 853–863.

Merz G, Schwenk V, Shah R, Salafia C, Necaise P, Joyce M, Villani T, Johnson M and Crider N (2018) Three-dimensional Rendering and Analysis of Immunolabeled, Clarified Human Placental Villous Vascular Networks. *Journal of Visualized Experiments* 1–10.

Miller JJ, Williams GF and Leissring JC (1971) Multiple late complications of therapy with cyclophosphamide, including ovarian destruction. *The American Journal of Medicine* **50** 530–535.

Mora JM, Fenwick MA, Castle L, Baithun M, Ryder TA, Mobberley M, Carzaniga R, Franks S and Hardy K (2012) Characterization and Significance of Adhesion and Junction-Related Proteins in Mouse Ovarian Follicles. *Biology of Reproduction* **86** 1–14.

Morgan S, Lopes F, Gourley C, Anderson RA and Spears N (2013) Cisplatin and Doxorubicin Induce Distinct Mechanisms of Ovarian Follicle Loss; Imatinib Provides Selective Protection Only against Cisplatin. *PLoS ONE* **8**.

Morimoto Y, Oku Y, Sonoda M, Haruki A, Ito K, Hashimoto S and Fukuda A (2007) High oxygen atmosphere improves human follicle development in organ cultures of ovarian cortical tissues *in vitro*. *Human Reproduction* **22** 3170–3177.

Morita Y, Manganaro TF, Tao XJ, Martimbeau S, Donahoe PK and Tilly JL (1999) Requirement for phosphatildylinositol-3'-kinase in cytokine-mediated germ cell survival during fetal oogenesis in the mouse. *Endocrinology* **140** 941–949.

Motro B and Bernstein A (1993) Dynamic changes in ovarian c-kit and Steel expression during the estrous reproductive cycle. *Developmental Dynamics* **197** 69–79.

Motro B, Van Der Kooy D, Rossant J, Reith A and Bernstein A (1991) Contiguous patterns of c-kit and steel expression: Analysis of mutations at the W and Sl loci. *Development* **113** 1207–1221.

Moustakas A, Souchelnytskyi S and Heldin CH (2001) Smad regulation in TGF-beta signal transduction. *Journal of Cell Science* **114** 4359–4369.

Muruvi W, Picton HM, Rodway RG and Joyce IM (2005) *In vitro* growth of oocytes from primordial follicles isolated from frozen-thawed lamb ovaries. *Theriogenology* **64** 1357–1370.

Nagamatsu G, Shimamoto S, Hamazaki N, Nishimura Y and Hayashi K (2019) Mechanical stress accompanied with nuclear rotation is involved in the dormant state of mouse oocytes. *Science Advances* **5** 1–13.

Nagashima T, Kim J, Li Q, Lydon JP, de Mayo FJ, Lyons KM and Matzuk MM (2011) Connective tissue growth factor is required for normal follicle development and ovulation. *Molecular Endocrinology* **25** 1740–1759.

Natale F, Rapp A, Yu W, Maiser A, Harz H, Scholl A, Grulich S, Anton T, Hörl D, Chen W *et al.* (2017) Identification of the elementary structural units of the DNA damage response. *Nature Communications* **8**.

Nguyen QN, Zerafa N, Liew SH, Morgan FH, Strasser A, Scott CL, Findlay JK, Hickey M and Hutt KJ (2018) Loss of PUMA protects the ovarian reserve during DNA-damaging chemotherapy and preserves fertility. *Cell Death and Disease* **9** 618.

Nguyen QN, Zerafa N, Liew SH, Findlay JK, Hickey M and Hutt KJ (2019) Cisplatin- and cyclophosphamide-induced primordial follicle depletion is caused by direct damage to oocytes. *Molecular Human Reproduction* **25** 433–444.

Nisolle M, Casanas-Roux F, Qu J, Motta P and Donnez J (2000) Histologic and ultrastructural evaluation of fresh and frozen-thawed human ovarian xenografts in nude mice. *Fertility and Sterility* **74** 122–129.

Nottola SA, Camboni A, Van Langendonckt A, Demylle D, Macchiarelli G, Dolmans MM, Martinez-Madrid B, Correr S and Donnez J (2008) Cryopreservation and xenotransplantation of human ovarian tissue: an ultrastructural study. *Fertility and Sterility* **90** 23–32.

O'Brien MJ, Pendola JK and Eppig JJ (2003) A revised protocol for *in vitro* development of mouse oocytes from primordial follicles dramatically improves their developmental competence. *Biology of Reproduction* **68** 1682–1686.

Office For National Statistics (2020a) *Cancer Registration Statistics, England: 2017*.

Office For National Statistics (2020b) *Birth Characteristics in England and Wales: 2019*.

Ohse T, Inagi R, Tanaka T, Ota T, Miyata T, Kojima I, Ingelfinger JR, Ogawa S, Fujita T and Nangaku M (2006) Albumin induces endoplasmic reticulum stress and apoptosis in renal proximal tubular cells. *Kidney International* **70** 1447–1455.

Okamura K, Dummer P, Kopp J, Qiu L, Levi M, Faubel S and Blaine J (2013) Endocytosis of Albumin by Podocytes Elicits an Inflammatory Response and Induces Apoptotic Cell Death. *PLoS ONE* **8**.

Oktay K, Newton H, Mullan J and Gosden RG (1998) Development of human primordial follicles to antral stages in SCID/hpg mice stimulated with follicle stimulating hormone. *Human Reproduction* **13** 1133–1138.

Oktem O and Oktay K (2007a) Quantitative assessment of the impact of chemotherapy on ovarian follicle reserve and stromal function. *Cancer* **110** 2222–2229.

Oktem O and Oktay K (2007b) A novel ovarian xenografting model to characterize the impact of chemotherapy agents on human primordial follicle reserve. *Cancer Research* **67** 10159–10162.

Oktem O, Alper E, Balaban B, Palaoglu E, Peker K, Karakaya C and Urman B (2011) Vitrified human ovaries have fewer primordial follicles and produce less antimüllerian hormone than slow-frozen ovaries. *Fertility and Sterility* **95** 2661-2664.e1.

Olesen HØ, Pors SE, Jensen LB, Grønning AP, Lemser CE, Nguyen Heimbürger MTH, Mamsen LS, Getreu N, Christensen ST, Andersen CY *et al.* (2021) N-acetylcysteine protects ovarian follicles from ischemia-reperfusion injury in xenotransplanted human ovarian tissue. *Human Reproduction* **36** 429–443.

Oskam IC, Asadi BA and Santos RR (2010) Histologic and ultrastructural features of cryopreserved ovine ovarian tissue: deleterious effect of 1,2-propanediol applying different thawing protocols. *Fertility and Sterility* **93** 2764–2766.

Oslowski CM and Urano F (2011) Measuring ER stress and the unfolded protein response using mammalian tissue culture system. In *Methods in Enzymology*, 1st ed, pp 71–92. Elsevier Inc.

Otala M, Erkkilä K, Tuuri T, Sjöberg J, Suomalainen L, Suikkari A-M, Pentikäinen V and Dunkel L (2002) Cell death and its suppression in human ovarian tissue culture. *Molecular Human Reproduction* **8** 228–236.

Otala M, Mäkinen S, Tuuri T, Sjöberg J, Pentikäinen V, Matikainen T and Dunkel L (2004) Effects of testosterone, dihydrotestosterone, and 17β-estradiol on human ovarian tissue survival in culture. *Fertility and Sterility* **82** 1077–1085.

Pampanini V, Wagner M, Asadi-Azarbaijani B, Oskam IC, Sheikhi M, Sjödin MOD, Lindberg J, Hovatta O, Sahlin L, Björvang RD *et al.* (2019) Impact of first-line cancer treatment on the follicle quality in cryopreserved ovarian samples from girls and young women. *Human Reproduction* **34** 1674–1685.

Pangas SA, Rademaker AW, Fishman DA and Woodruff TK (2002) Localization of the activin signal transduction components in normal human ovarian follicles: Implications for autocrine and paracrine signaling in the ovary. *Journal of Clinical Endocrinology and Metabolism* **87** 2644–2657.

Pangas SA, Li X, Umans L, Zwijsen A, Huylebroeck D, Gutierrez C, Wang D, Martin JF, Jamin SP, Behringer RR *et al.* (2008) Conditional Deletion of Smad1 and Smad5 in Somatic Cells of Male and Female Gonads Leads to Metastatic Tumor Development in Mice. *Molecular and Cellular Biology* **28** 248–257.

Pascuali N, Scotti L, Di Pietro M, Oubiña G, Bas D, May M, Gómez Muñoz A, Cuasnicú PS, Cohen DJ, Tesone M *et al.* (2018) Ceramide-1-phosphate has protective properties against cyclophosphamide-induced ovarian damage in a mice model of premature ovarian failure. *Human Reproduction* **33** 1–16.

Peluffo MC, Ting AY, Zamah AM, Conti M, Stouffer RL, Zelinski MB and Hennebold JD (2012) Amphiregulin promotes the maturation of oocytes isolated from the small antral follicles of the rhesus macaque. *Human Reproduction* **27** 2430–2437.

Pesce M, Farrace MG, Piacentini M, Dolci S and De Felici M (1993) Stem cell factor and leukemia inhibitory factor promote primordial germ cell survival by suppressing programmed cell death (apoptosis). *Development* **118** 1089–1094.

Peters H, Byskov AG and Grinsted J (1978) Follicular growth in fetal and prepubertal ovaries

of humans and other primates. *Clinics in Endocrinology and Metabolism* **7** 469–485.

Pizzorno G, Diasio RB and Cheng Y-C (2003) Pyrimidine and Purine Antimetabolites. In *Holland-Frei Cancer Medicine*, Sixth Ed. Eds DW Kufe, RE Pollock, RR Weichselbaum, RC Bast Jr, TS Gansler, JF Holland and E Frei. Hamilton (ON): BC Decker.

Poirot C, Vacher-Lavenu MC, Helardot P, Guibert J, Brugières L and Jouannet P (2002) Human ovarian tissue cryopreservation: Indications and feasibility. *Human Reproduction* **17** 1447–1452.

Poirot C, Fortin A, Lacorte JM, Akakpo JP, Genestie C, Vernant JP, Brice P, Morice P, Leblanc T, Gabarre J *et al.* (2019) Impact of cancer chemotherapy before ovarian cortex cryopreservation on ovarian tissue transplantation. *Human Reproduction* **34** 1083–1094.

Public Health England (2021) *Children, Teenagers and Young Adults UK Cancer Statistics Report 2021*.

Qu J, Godin PA, Nisolle M and Donnez J (2000) Distribution and epidermal growth factor receptor expression of primordial follicles in human ovarian tissue before and after cryopreservation. *Human Reproduction* **15** 302–310.

Quan N, Mara JN, Grover AR, Pavone ME and Duncan FE (2020) Spatial Analysis of Growing Follicles in the Human Ovary to Inform Tissue Engineering Strategies. *Tissue Engineering - Part A* **26** 733–746.

Raffel N, Lotz L, Hoffmann I, Liebenthron J, Söder S, Beckmann MW and Dittrich R (2017) Repetitive Maturation of Oocytes from Non-Stimulated Xenografted Ovarian Tissue from a Prepubertal Patient Indicating the Independence of Human Ovarian Tissue. *Geburtshilfe Und Frauenheilkunde* **77** 1304–1311.

Rahimi G, Isachenko E, Sauer H, Wartenberg M, Isachenko V, Hescheler J, Mallmann P and Nawroth F (2001) Measurement of apoptosis in long-term cultures of human ovarian tissue. *Reproduction* **122** 657–663.

Rajareddy S, Reddy P, Du C, Liu L, Jagarlamudi K, Tang W, Shen Y, Berthet C, Peng SL, Kaldis P *et al.* (2007) p27kip1 (cyclin-dependent kinase inhibitor 1B) controls ovarian development by suppressing follicle endowment and activation and promoting follicle atresia in mice. *Molecular Endocrinology* **21** 2189–2202.

Ramezani M, Salehnia M and Jafarabadi M (2017) Short term culture of vitrified human ovarian cortical tissue to assess the cryopreservation outcome: Molecular and morphological analysis. *Journal of Reproduction and Infertility* **18** 162–171.

Reddy P, Liu L, Adhikari D, Jagarlamudi K, Rajareddy S, Shen Y, Du C, Tang W, Hämäläinen T, Peng SL *et al.* (2008) Oocyte-specific deletion of pten causes premature activation of the primordial follicle pool. *Science* **319** 611–613.

Reddy P, Adhikari D, Zheng W, Liang S, Hämäläinen T, Tohonen V, Ogawa W, Noda T, Volarevic S, Huhtaniemi I *et al.* (2009) PDK1 signaling in oocytes controls reproductive aging and lifespan by manipulating the survival of primordial follicles. *Human Molecular Genetics* **18** 2813–2824.

Richards J and Pangas SA (2010) The ovary : basic biology and clinical implications. *The Journal of Clinicas Investigation* **120** 963–972.

Richardson DS and Lichtman JW (2015) Clarifying Tissue Clearing. *Cell* **162** 246–257.

Rinaldi VD, Bloom JC and Schimenti JC (2018) Whole Mount Immunofluorescence and Follicle Quantification of Cultured Mouse Ovaries. *Journal of Visualized Experiments* **2018** 1–8.

Robertson GP (2005) Functional and therapeutic significance of Akt deregulation in malignant melanoma. *Cancer and Metastasis Reviews* **24** 273–285.

Robinson LLL, Gaskell TL, Saunders PTK and Anderson RA (2001) Germ cell specific expression of c-kit in the human fetal gonad. *Molecular Human Reproduction* **7** 845–852.

Rodgers R, Irving-Rodgers H and Russell D (2003) Extracellular matrix of the developing ovarian follicle. *Reproduction* **126** 415–424.

Rodriguez-Wallberg KA, Tanbo T, Tinkanen H, Thurin-Kjellberg A, Nedstrand E, Kitlinski ML, Macklon KT, Ernst E, Fedder J, Tiitinen A *et al.* (2016) Ovarian tissue cryopreservation and transplantation among alternatives for fertility preservation in the Nordic countries – compilation of 20 years of multicenter experience. *Acta Obstetricia et Gynecologica Scandinavica* **95** 1015–1026.

De Roo C, Lierman S, Tilleman K, Peynshaert K, Braeckmans K, Caanen M, Lambalk CB, Weyers S, T'Sjoen G, Cornelissen R *et al.* (2017) Ovarian tissue cryopreservation in female-to-male transgender people: insights into ovarian histology and physiology after prolonged androgen treatment. *Reproductive BioMedicine Online* **34** 557–566.

De Roo C, Lierman S, Tilleman K and De Sutter P (2020) In-vitro fragmentation of ovarian tissue activates primordial follicles through the Hippo pathway. *Human Reproduction Open* **2020** 1–16.

Rosendahl M, Greve T and Andersen CY (2013) The safety of transplanting cryopreserved ovarian tissue in cancer patients: A review of the literature. *Journal of Assisted Reproduction and Genetics* **30** 11–24.

Rossi V, Lispi M, Longobardi S, Mattei M, Rella F Di, Salustri A, De Felici M and Klinger FG (2017) LH prevents cisplatin-induced apoptosis in oocytes and preserves female fertility in mouse. *Cell Death and Differentiation* **24** 72–82.

Rotgers E, Jørgensen A and Yao HHC (2018) At the crossroads of fate-Somatic cell lineage specification in the fetal gonad. *Endocrine Reviews* **39** 739–759.

Roti Roti EC, Leisman SK, Abbott DH and Salih SM (2012) Acute doxorubicin insult in the mouse ovary is cell- and follicle-type dependent. *PLoS ONE* **7**.

Rowghani NM, Heise MK, McKeel D, McGee EA, Koepsel RR and Russell AJ (2004) Maintenance of Morphology and Growth of Ovarian Follicles in Suspension Culture. *Tissue Engineering* **10** 545–552.

Rowinsky E (2003) Microtubule-Targeting Natural Products. In *Holland-Frei Cancer Medicine*, Sixth Ed. Eds DW Kufe, RE Pollock, RR Weichselbaum, RC Bast Jr, TS Gansler, JF Holland and E Frei. Hamilton (ON): BC Decker.

Roy SK and Treacy BJ (1993) Isolation and long-term culture of human preantral follicles. *Fertility and Sterility* **59** 783–790.

Rubin EH and Hait WN (2003) Anthracyclines and DNA Intercalators/Epipodophyllotoxins/ Camptothecins/DNA Topoisomerases. In *Holland-Frei Cancer Medicine*, 6th editio. Eds DW Kufe, RE Pollock, RR Weichselbaum, RC Bast Jr, TS Gansler, JF Holland and E Frei. Hamilton (ON): BC Decker.

Rueden CT, Schindelin J, Hiner MC, DeZonia BE, Walter AE, Arena ET and Eliceiri KW (2017) ImageJ2: ImageJ for the next generation of scientific image data. *BMC Bioinformatics* **18** 1–26.

Ruifrok A and Johnston DA (2001) Quantification of histochemical staining by color deconvolution. *Analytical and Quantitative Cytology and Histology* 291–299.

Saatcioglu HD, Cuevas I and Castrillon DH (2016) Control of Oocyte Reawakening by Kit. *PLoS Genetics* **12** e1006215.

Sadeu JC and Smitz J (2008) Growth differentiation factor-9 and anti-Müllerian hormone

expression in cultured human follicles from frozen-thawed ovarian tissue. *Reproductive BioMedicine Online* **17** 537–548.

Salama M and Woodruff TK (2019) From bench to bedside: Current developments and future possibilities of artificial human ovary to restore fertility. *Acta Obstetricia et Gynecologica Scandinavica* **98** 659–664.

Salama M, Anazodo A and Woodruff TK (2019) Preserving fertility in female patients with hematological malignancies: the key points. *Expert Review of Hematology* **12** 375–377.

Salmena L, Carracedo A and Pandolfi PP (2008) Tenets of PTEN Tumor Suppression. *Cell* **133** 403–414.

Sanfilippo S, Canis M, Romero S, Sion B, Déchelotte P, Pouly JL, Janny L, Smitz J and Brugnon F (2013) Quality and functionality of human ovarian tissue after cryopreservation using an original slow freezing procedure. *Journal of Assisted Reproduction and Genetics* **30** 25–34.

Sargent J, Roberts V, Gaffney J and Frias A (2018) Clarification and confocal imaging of the nonhuman primate placental micro-anatomy. *BioTechniques* **66** 79–84.

Sarraj MA and Drummond AE (2012) Mammalian foetal ovarian development: consequences for health and disease. *Reproduction* **143** 151–163.

Schindelin J, Arganda-Carreras I, Frise E, Kaynig V, Longair M, Pietzsch T, Preibisch S, Rueden C, Saalfeld S, Schmid B *et al.* (2012) Fiji: an open-source platform for biological-image analysis. *Nature Methods* **9** 676–682.

Schmidt KLTT, Byskov AG, Andersen AN, Müller J and Andersen CY (2003) Density and distribution of primordial follicles in single pieces of cortex from 21 patients and in individual pieces of cortex from three entire human ovaries. *Human Reproduction* **18** 1158–1164.

Schmidt D, Ovitt CE, Anlag K, Fehsenfeld S, Gredsted L, Treier A-C and Treier M (2004) The murine winged-helix transcription factor Foxl2 is required for granulosa cell differentiation and ovary maintenance. *Development* **131** 933–942.

Schmidt KLT, Kryger-Baggesen N, Byskov AG and Andersen CY (2005) Anti-Müllerian hormone initiates growth of human primordial follicles *in vitro*. *Molecular and Cellular Endocrinology* **234** 87–93.

Schmidt VM, Isachenko E, Rappl G, Rahimi G, Hanstein B, Morgenstern B, Mallmann P and Isachenko V (2018) Construction of human artificial ovary from cryopreserved ovarian tissue: Appearance of apoptosis and necrosis after enzymatic isolation of follicles. *Cryobiology* **84** 10–14.

Schneider CA, Rasband WS and Eliceiri KW (2012) NIH Image to ImageJ: 25 years of image analysis. *Nature Methods* **9** 671–675.

Scott JE, Carlsson IB, Bavister BD and Hovatta O (2004a) Human ovarian tissue cultures: Extracellular matrix composition, coating density and tissue dimensions. *Reproductive BioMedicine Online* **9** 287–293.

Scott JE, Zhang P and Hovatta O (2004b) Benefits of 8-bromo-guanosine 3′,5′-cyclic monophosphate (8-br-cGMP) in human ovarian cortical tissue culture. *Reproductive BioMedicine Online* **8** 319–324.

Seli E, Babayev E, Collins SC, Nemeth G and Horvath TL (2014) Minireview: Metabolism of female reproduction: Regulatory mechanisms and clinical implications. *Molecular Endocrinology* **28** 790–804.

Shai D, Aviel-Ronen S, Spector I, Raanani H, Shapira M, Gat I, Roness H and Meirow D

(2021) Ovaries of patients recently treated with alkylating agent chemotherapy indicate the presence of acute follicle activation, elucidating its role among other proposed mechanisms of follicle loss. *Fertility and Sterility* **115** 1239–1249.

Shalet SM, Beardwell CG, Jones PHM, Pearson D and Orrell DH (1976) Ovarian failure following abdominal irradiation in childhood. *British Journal of Cancer* **33** 655–658.

Shapira M, Dolmans MM, Silber S and Meirow D (2020) Evaluation of ovarian tissue transplantation: results from three clinical centers. *Fertility and Sterility* **114** 388–397.

Shea LD, Woodruff TK and Shikanov A (2014) Bioengineering the ovarian follicle microenvironment. *Annual Review of Biomedical Engineering* **16** 29–52.

Sheikhi M, Hultenby K, Niklasson B, Lundqvist M and Hovatta O (2013) Preservation of human ovarian follicles within tissue frozen by vitrification in a xeno-free closed system using only ethylene glycol as a permeating cryoprotectant. *Fertility and Sterility* **100** 170–177.

Shi Y and Massagué J (2003) Mechanisms of TGF-β signaling from cell membrane to the nucleus. *Cell* **113** 685–700.

Da Silva-Buttkus P, Jayasooriya GS, Mora JM, Mobberley M, Ryder TA, Baithun M, Stark J, Franks S and Hardy K (2008) Effect of cell shape and packing density on granulosa cell proliferation and formation of multiple layers during early follicle development in the ovary. *Journal of Cell Science* **121** 3890–3900.

Da Silva-Buttkus P, Marcelli G, Franks S, Stark J and Hardy K (2009) Inferring biological mechanisms from spatial analysis: Prediction of a local inhibitor in the ovary. *Proceedings of the National Academy of Sciences* **106** 456–461.

Silva JRV, Tharasanit T, Taverne MAM, van der Weijden GC, Santos RR, Figueiredo JR and van den Hurk R (2006) The activin-follistatin system and *in vitro* early follicle development in goats. *Journal of Endocrinology* **189** 113–125.

Silva GM, Rossetto R, Chaves RN, Duarte ABG, Araújo VR, Feltrin C, Bernuci MP, Anselmo-Franci JA, Xu M, Woodruff TK *et al.* (2015) *In vitro* development of secondary follicles from pre-pubertal and adult goats cultured in two-dimensional or three-dimensional systems. *Zygote* **23** 475–484.

Simon LE, Kumar TR and Duncan FE (2020) *In vitro* ovarian follicle growth: a comprehensive analysis of key protocol variables. *Biology of Reproduction* **103** 455–470.

Skinner MK (2005) Regulation of primordial follicle assembly and development. *Human Reproduction Update* **11** 461–471.

Smitz JEJ and Cortvrindt RG (2002) The earliest stages of folliculogenesis *in vitro*. *Reproduction* **123** 185–202.

Soleimani R, Heytens E, Van Den Broecke R, Rottiers I, Dhont M, Cuvelier CA and De Sutter P (2010) Xenotransplantation of cryopreserved human ovarian tissue into murine back muscle. *Human Reproduction* **25** 1458–1470.

Soleimani R, Heytens E, Darzynkiewicz Z and Oktay K (2011) Mechanisms of chemotherapy-induced human ovarian aging: double strand DNA breaks and microvascular compromise. *Aging* **3** 782–793.

Sonmezer M and Oktay K (2004) Fertility preservation in female patients. *Human Reproduction Update* **10** 251–266.

Spanel-Borowski K (1981) Morphological investigations on follicular atresia in canine ovaries. *Cell and Tissue Research* **214** 155–168.

Spears N, Lopes F, Stefansdottir A, Rossi V, De Felici M, Anderson RA and Klinger FG

(2019) Ovarian damage from chemotherapy and current approaches to its protection. *Human Reproduction Update* **25** 1–21.

St John MAR, Tao W, Fei X, Fukumoto R, Carcangiu ML, Brownstein DG, Parlow AF, McGrath J and Xu T (1999) Mice deficient of Lats1 develop soft-tissue sarcomas, ovarian tumours and pituitary dysfunction. *Nature Genetics* **21** 182–186.

Stoop H, Honecker F, Cools M, de Krijger R, Bokemeyer C and Looijenga LHJ (2005) Differentiation and development of human female germ cells during prenatal gonadogenesis: An immunohistochemical study. *Human Reproduction* **20** 1466–1476.

Stubbs SA, Webber LJ, Stark J, Rice S, Margara R, Lavery S, Trew GH, Hardy K and Franks S (2013) Role of insulin-like growth factors in initiation of follicle growth in normal and polycystic human ovaries. *Journal of Clinical Endocrinology and Metabolism* **98** 3298–3305.

Suh EK, Yang A, Kettenbach A, Bamberger C, Michaelis AH, Zhu Z, Elvin JA, Bronson RT, Crum CP and McKeon F (2006) P63 Protects the Female Germ Line During Meiotic Arrest. *Nature* **444** 624–628.

Suzuki N, Yoshioka N, Takae S, Sugishita Y, Tamura M, Hashimoto S, Morimoto Y and Kawamura K (2015) Successful fertility preservation following ovarian tissue vitrification in patients with primary ovarian insufficiency. *Human Reproduction* **30** 608–615.

Takae S, Tsukada K, Maeda I, Okamoto N, Sato Y, Kondo H and Shinya K (2018) Preliminary human application of optical coherence tomography for quantification and localization of primordial follicles aimed at effective ovarian tissue transplantation. *Journal of Assited Reproduction and Genetics* **35** 627–636.

Takahashi M, Hayashi M, Manganaro TF and Donahoe PK (1986) The ontogeny of mullerian inhibiting substance in granulosa cells of the bovine ovarian follicle. *Biology of Reproduction* **35** 447–453.

Takeuchi A, Koga K, Satake E, Makabe T, Taguchi A, Miyashita M, Takamura M, Harada M, Hirata T, Hirota Y *et al.* (2019) Endometriosis Triggers Excessive Activation of Primordial Follicles via PI3K-PTEN-Akt-Foxo3 Pathway. *Journal of Clinical Endocrinology and Metabolism* **104** 5547–5554.

Talevi R, Sudhakaran S, Barbato V, Merolla A, Braun S, Nardo M Di, Costanzo V, Ferraro R, Iannantuoni N, Catapano G *et al.* (2018) Is oxygen availability a limiting factor for *in vitro* folliculogenesis? *PLoS ONE* **13** e0192501.

Tanikawa M, Harada T, Mitsunari M, Onohara Y, Iwabe T and Terakawa N (1998) Expression of c-kit messenger ribonucleic acid in human oocyte and presence of soluble c-kit in follicular fluid. *Journal of Clinical Endocrinology and Metabolism* **83** 1239–1242.

Tarnawa ED, Baker MD, Aloisio GM, Carr BR and Castrillon DH (2013) Gonadal Expression of Foxo1, but Not Foxo3, Is Conserved in Diverse Mammalian Species. *Biology of Reproduction* **88** 103.

Tavana S, Valojerdi MR, Azarnia M and Shahverdi A (2016) Restoration of ovarian tissue function and estrous cycle in rat after autotransplantation using hyaluronic acid hydrogel scaffold containing VEGF and bFGF. *Growth Factors* **34** 97–106.

Taylan E and Oktay KH (2017) Current state and controversies in fertility preservation in women with breast cancer. *World Journal of Clinical Oncology* **8** 241–248.

Teerds KJ and Dorrington JH (1993) Immunohistochemical localization of 3β-hydroxysteroid dehydrogenase in the rat ovary during follicular development and atresia. *Biology of Reproduction* **49** 989–996.

Telfer EE (2019) Future developments: *In vitro* growth (IVG) of human ovarian follicles. *Acta Obstetricia et Gynecologica Scandinavica* **98** 653–658.

Telfer EE, McLaughlin M, Ding C and Thong KJ (2008) A two-step serum-free culture system supports development of human oocytes from primordial follicles in the presence of activin. *Human Reproduction* **23** 1151–1158.

Terada Y, Terunuma-Sato Y, Kakoi-yoshimoto T, Hasegawa H, Ugajin T, Koyanagi Y, Ito M, Murakami T, Sasano H, Yaegashi N *et al.* (2008) Development of human graafian follicles following transplantation of human ovarian tissue into NOD/SCID/γcnull mice. *American Journal of Reproductive Immunology* **60** 534–540.

Thanatsis N, Kaponis A, Koika V, Georgopoulos NA and Decavalas GO (2019) Reduced Foxo3a, FoxL2, and p27 mRNA expression in human ovarian tissue in premature ovarian insufficiency. *Hormones* **18** 409–415.

Thien A, Prentzell MT, Holzwarth B, Kläsener K, Kuper I, Boehlke C, Sonntag AG, Ruf S, Maerz L, Nitschke R *et al.* (2015) TSC1 Activates TGF-β-Smad2/3 Signaling in Growth Arrest and Epithelial-to-Mesenchymal Transition. *Developmental Cell* **32** 617–630.

Thomas FH, Armstrong DG and Telfer EE (2003) Activin promotes oocyte development in ovine preantral follicles *in vitro*. *Reproductive Biology and Endocrinology* **1** 76.

Ting AY and Zelinski MB (2017) Characterization of FOXO1,3 and 4 transcription factors in ovaries of fetal, prepubertal and adult rhesus macaques. *Biology of Reproduction* **96** 1052–1059.

Ting AY, Yeoman RR, Lawson MS and Zelinski MB (2011) *In vitro* development of secondary follicles from cryopreserved rhesus macaque ovarian tissue after slow-rate freeze or vitrification. *Human Reproduction* **26** 2461–2472.

Titus S, Szymanska KJ, Musul B, Turan V, Taylan E, Garcia- Milian R, Mehta S and Oktay K (2021) Individual-oocyte transcriptomic analysis shows that genotoxic chemotherapy depletes human primordial follicle reserve *in vivo* by triggering proapoptotic pathways without growth activation. *Scientific Reports* **11** 407.

Tomic D, Brodie SG, Deng C, Hickey RJ, Babus JK, Malkas LH and Flaws JA (2002) Smad 3 May Regulate Follicular Growth in the Mouse Ovary. *Biology of Reproduction* **66** 917–923.

Tong X, Liu Y, Xu X, Shi J, Hu W, Ma T, Cui P, Lu W, Pei Z, Xu M *et al.* (2020) Ovarian innervation coupling with vascularity: the role of electro-acupuncture in follicular maturation in a rat model of polycystic ovary syndrome. *Frontiers in Physiology* **11** 1474.

Torrance C, Telfer E and Gosden RG (1989) Quantitative study of the development of isolated mouse pre-antral follicles in collagen gel culture. *Journal of Reproduction and Fertility* **87** 367–374.

Tuck AR, Robker RL, Norman RJ, Tilley WD and Hickey TE (2015) Expression and localisation of c-kit and KITL in the adult human ovary. *Journal of Ovarian Research* **8** 31.

Tuominen VJ, Ruotoistenmäki S, Viitanen A, Jumppanen M and Isola J (2010) ImmunoRatio: A publicly available web application for quantitative image analysis of estrogen receptor (ER), progesterone receptor (PR), and Ki-67. *Breast Cancer Research* **12** R56.

Tuppi M, Kehrloesser S, Coutandin DW, Rossi V, Luh LM, Strubel A, Hötte K, Hoffmeister M, Schäfer B, De Oliveira T *et al.* (2018) Oocyte DNA damage quality control requires consecutive interplay of CHK2 and CK1 to activate p63. *Nature Structural and Molecular Biology* **25** 261–269.

Uda M, Ottolenghi C, Crisponi L, Garcia JE, Deiana M, Kimber W, Forabosco A, Cao A, Schlessinger D and Pilia G (2004) Foxl2 disruption causes mouse ovarian failure by pervasive blockage of follicle development. *Human Molecular Genetics* **13** 1171–1181.

Uslu B, Dioguardi CC, Haynes M, Miao DQ, Kurus M, Hoffman G and Johnson J (2017)

Quantifying growing versus non-growing ovarian follicles in the mouse. *Journal of Ovarian Research* **10** 1–11.

Vanacker J and Amorim CA (2017) Alginate: A Versatile Biomaterial to Encapsulate Isolated Ovarian Follicles. *Annals of Biomedical Engineering* **45** 1633–1649.

Vanacker J, Camboni A, Dath C, Van Langendonckt A, Dolmans MM, Donnez J and Amorim CA (2011) Enzymatic isolation of human primordial and primary ovarian follicles with Liberase DH: Protocol for application in a clinical setting. *Fertility and Sterility* **96** 379-383.e3.

Vatansever D, İncir S, Bildik G, Taskiran C and Oktem O (2020) *In vitro* AMH production of ovarian tissue samples in culture correlates with their primordial follicle pool. *European Journal of Obstetrics and Gynecology and Reproductive Biology* **254** 138–140.

Te Velde ER, Scheffer GJ, Dorland M, Broekmans FJ and Fauser BCJM (1998) Developmental and endocrine aspects of normal ovarian aging. *Molecular and Cellular Endocrinology* **145** 67–73.

Van der Ven H, Liebenthron J, Beckmann M, Toth B, Korell M, Krüssel J, Frambach T, Kupka M, Hohl MK, Winkler-Crepaz K *et al.* (2016) Ninety-five orthotopic transplantations in 74 women of ovarian tissue after cytotoxic treatment in a fertility preservation network: Tissue activity, pregnancy and delivery rates. *Human Reproduction* **31** 2031–2041.

Venables WN and Ripley BD (2002) *Modern Applied Statistics with S*. Springer.

Vigier B, Picard JY, Tran D, Legeai L and Josso N (1984) Production of anti-müllerian hormone: Another homology between sertoli and granulosa cells. *Endocrinology* **114** 1315–1320.

De Vos M, Smitz J and Woodruff TK (2014) Fertility preservation in women with cancer. *The Lancet* **384** 1302–1310.

Wagner M, Yoshihara M, Douagi I, Damdimopoulos A, Panula S, Petropoulos S, Lu H, Pettersson K, Palm K, Katayama S *et al.* (2020) Single-cell analysis of human ovarian cortex identifies distinct cell populations but no oogonial stem cells. *Nature Communications* **11** 1–15.

Walker CA, Bjarkadottir BD, Fatum M, Lane S and Williams SA (2021) Variation in follicle health and development in cultured cryopreserved ovarian cortical tissue: a study of ovarian tissue from patients undergoing fertility preservation. *Human Fertility* **24** 188–198.

Wallace WHB and Kelsey TW (2010) Human ovarian reserve from conception to the menopause. *PLoS ONE* **5** 1–9.

Wallace WHB, Thomson AB and Kelsey TW (2003) The radiosensitivity of the human oocyte. *Human Reproduction* **18** 117–121.

Wallace WHB, Anderson RA and Irvine DS (2005) Fertility preservation for young patients with cancer: who is at risk and what can be offered? *The Lancet Oncology* **6** 209–218.

Wallace WHB, Kelsey TW and Anderson RA (2016) Fertility preservation in pre-pubertal girls with cancer: The role of ovarian tissue cryopreservation. *Fertility and Sterility* **105** 6–12.

Walsh JG, Logue SE, Lüthi AU and Martin SJ (2011) Caspase-1 promiscuity is counterbalanced by rapid inactivation of processed enzyme. *Journal of Biological Chemistry* **286** 32513–32524.

Wandji S-A, Sršeň V, Voss AK, Eppig JJ and Fortune JE (1996) Initiation *in vitro* of growth of

bovine primordial follicles. *Biology of Reproduction* **55** 942–948.

Wandji SA, Sŕseň V, Nathanielsz PW, Eppig JJ and Fortune JE (1997) Initiation of growth of baboon primordial follicles *in vitro*. *Human Reproduction* **12** 1993–2001.

Wang B, Mu Y, Ni F, Zhou S, Wang J, Cao Y and Ma X (2010) Analysis of FOXO3 mutation in 114 Chinese women with premature ovarian failure. *Reproductive BioMedicine Online* **20** 499–503.

Wang N, Luo LL, Xu JJ, Xu MY, Zhang XM, Zhou XL, Liu WJ and Fu YC (2014) Obesity accelerates ovarian follicle development and follicle loss in rats. *Metabolism: Clinical and Experimental* **63** 94–103.

Wang Y, Liu M, Johnson SB, Yuan G, Arriba AK, Zubizarreta ME, Chatterjee S, Nagarkatti M, Nagarkatti P and Xiao S (2019) Doxorubicin obliterates mouse ovarian reserve through both primordial follicle atresia and overactivation. *Toxicology and Applied Pharmacology* **381** 114714.

Watkins WJ, Umbers AJ, Woad KJ, Harris SE, Winship IM, Gersak K and Shelling AN (2006) Mutational screening of FOXO3A and FOXO1A in women with premature ovarian failure. *Fertility and Sterility* **86** 1518–1521.

Webber LJ, Stubbs SA, Stark J, Margara RA, Trew GH, Lavery SA, Hardy K and Franks S (2007) Brief report: Prolonged survival in culture of preantral follicles from polycystic ovaries. *Journal of Clinical Endocrinology and Metabolism* **92** 1975–1978.

Weenen C, Laven JSE, von Bergh ARM, Cranfield M, Groome NP, Visser JA, Kramer P, Fauser BCJM and Themmen APN (2004) Anti-Müllerian hormone expression pattern in the human ovary: Potential implications for initial and cyclic follicle recruitment. *Molecular Human Reproduction* **10** 77–83.

Wei X (2018) Investigation of the effects of Anti-Mullerian Hormone on preventing Doxorubicin-induced primordial follicle loss. University of Oxford.

Weiskirchen R, Weiskirchen S and Tacke F (2019) Organ and tissue fibrosis: Molecular signals, cellular mechanisms and translational implications. *Molecular Aspects of Medicine* **65** 2–15.

West E, Shea L and Woodruff T (2007) Engineering the Follicle Microenvironment. *Seminars in Reproductive Medicine* **25** 287–299.

van Wezel IL and Rodgers RJ (1996) Morphological characterization of bovine primordial follicles and their environment *in vivo*. *Biology of Reproduction* **55** 1003–1011.

Wheelock MJ and Johnson KR (2003) Cadherins as Modulators of Cellular Phenotype. *Annual Review of Cell and Developmental Biology* **19** 207–235.

Williams SA, Xia L, Cummings RD, McEver RP and Stanley P (2007) Fertilization in mouse does not require terminal galactose or N-acetylglucosamine on the zona pellucida glycans. *Journal of Cell Science* **120** 1341–1349.

Woodruff TK and Shea LD (2007) The role of the extracellular matrix in ovarian follicle development. *Reproductive Sciences (Thousand Oaks, Calif.)* **14** 6–10.

Wright CS, Hovatta O, Margara R, Trew G, Winslon RML, Franks and Hardy K (1999) Effects of follicle-stimulating hormone and serum substitution on the in-vitro growth of human ovarian follicles. *Human Reproduction* **14** 1555–1562.

Wycherley G, Downey D, Kane MT and Hynes AC (2004) A novel follicle culture system markedly increases follicle volume, cell number and oestradiol secretion. *Reproduction* **127** 669–677.

Xia X, Yin T, Yan J, Yan L, Jin C, Lu C, Wang T, Zhu X, Zhi X, Wang J *et al.* (2015) Mesenchymal

stem cells enhance angiogenesis and follicle survival in human cryopreserved ovarian cortex transplantation. *Cell Transplantation* **24** 1999–2010.

Xiao S, Zhang J, Romero MM, Smith KN, Shea LD and Woodruff TK (2015) *In vitro* follicle growth supports human oocyte meiotic maturation. *Scientific Reports* **5** 17323.

Xie Y, Li S, Zhou L, Lin H, Jiao X, Qiu Q, Liang Y and Zhang Q (2020) Rapamycin preserves the primordial follicle pool during cisplatin treatment *in vitro* and *in vivo*. *Molecular Reproduction and Development* **87** 442–453.

Xin M, Kim Y, Sutherland LB, Murakami M, Qi X, McAnally J, Porrello ER, Mahmoud AI, Tan W, Shelton JM *et al.* (2013) Hippo pathway effector Yap promotes cardiac regeneration. *Proceedings of the National Academy of Sciences of the United States of America* **110** 13839–13844.

Xu J, Oakley J and McGee EA (2002) Stage-Specific Expression of Smad2 and Smad3 During Folliculogenesis. *Biology of Reproduction* **66** 1571–1578.

Xu M, West E, Shea LD and Woodruff TK (2006a) Identification of a stage-specific permissive *in vitro* culture environment for follicle growth and oocyte development. *Biology of Reproduction* **75** 916–923.

Xu M, Ph D, Kreeger PK, Shea LD and Teresa K (2006b) Tissue-engineered follicles produce live, fertile offspring. *Tissue Engineering* **12** 2739–2746.

Xu M, Banc A, Woodruff TK and Shea LD (2009a) Secondary follicle growth and oocyte maturation by culture in alginate hydrogel following cryopreservation of the ovary or individual follicles. *Biotechnology and Bioengineering* **103** 378–386.

Xu M, Barrett SL, West-Farrell E, Kondapalli LA, Kiesewetter SE, Shea LD and Woodruff TK (2009b) *In vitro* grown human ovarian follicles from cancer patients support oocyte growth. *Human Reproduction* **24** 2531–2540.

Xu M, Sun J, Wang Q, Zhang Q, Wei C and Lai D (2018) Chronic restraint stress induces excessive activation of primordial follicles in mice ovaries. *PLoS ONE* **13** 1–17.

Xu F, Lawson MS, Bean Y, Ting AY, Pejovic T, De Geest K, Moffitt M, Mitalipov SM and Xu J (2021) Matrix-free 3D culture supports human follicular development from the unilaminar to the antral stage in vitro yielding morphologically normal metaphase II oocytes. *Human Reproduction* **36** 1326–1338.

Yadav AK, Yadav PK, Chaudhary GR, Tiwari M, Gupta A, Sharma A, Pandey AN, Pandey AK and Chaube SK (2019) Autophagy in hypoxic ovary. *Cellular and Molecular Life Sciences* **76** 3311–3322.

Yan H, Zhang J, Wen J, Wang Y, Niu W, Teng Z, Zhao T, Dai Y, Zhang Y, Wang C *et al.* (2018) CDC42 controls the activation of primordial follicles by regulating PI3K signaling in mouse oocytes. *BMC Biology* **16** 1–16.

Yan H, Wen J, Zhang T, Zheng W, He M, Huang K, Guo Q, Chen Q, Yang Y, Deng G *et al.* (2019) Oocyte-derived E-cadherin acts as a multiple functional factor maintaining the primordial follicle pool in mice. *Cell Death and Disease* **10** 160.

Yang Q and Guan KL (2007) Expanding mTOR signaling. *Cell Research* **17** 666–681.

Yang A, Kaghad M, Wang Y, Gillett E, Fleming MD, Dötsch V, Andrews NC, Caput D and McKeon F (1998) P63, a P53 Homolog At 3Q27-29, Encodes Multiple Products With Transactivating, Death-Inducing, and Dominant-Negative Activities. *Molecular Cell* **2** 305–316.

Yang A, Schweitzer R, Sun D, Kaghad M, Walker N, Bronson RT, Tabin C, Sharpe A, Caput D, Crum C *et al.* (1999) P63 Is Essential for Regenerative Proliferation in Limb, Craniofacial

and Epithelial Development. *Nature* **398** 714–718.

Yang A, Walker N, Bronson R, Kaghad M, Oosterwegel M, Bonnin J, Vagner C, Bonnet H, Dikkes P, Sharpe A *et al.* (2000) p73-deficient mice have neurological, pheromonal and inflammatory defects but lack spontaneous tumours. *Nature* **404** 99–103.

Yang Y, Lin P, Chen F, Wang A, Lan X, Song Y and Jin Y (2013) Luman recruiting factor regulates endoplasmic reticulum stress in mouse ovarian granulosa cell apoptosis. *Theriogenology* **79** 633-639.e3.

Yang D, Jiang T, Lin P, Chen H, Wang L, Wang N, Zhao F, Wang A and Jin Y (2017) Knock-down of apoptosis inducing factor gene protects endoplasmic reticulum stress-mediated goat granulosa cell apoptosis. *Theriogenology* **88** 89–97.

Yasmin E, Balachandren N, Davies MC, Jones GL, Lane S, Mathur R, Webber L and Anderson RA (2018) Fertility preservation for medical reasons in girls and women: British fertility society policy and practice guideline. *Human Fertility* **21** 3–26.

Yefimova MG, Lefevre C, Bashamboo A, Eozenou C, Burel A, Lavault MT, Meunier AC, Pimentel C, Veau S, Neyroud AS *et al.* (2020) Granulosa cells provide elimination of apoptotic oocytes through unconventional autophagy-assisted phagocytosis. *Human Reproduction* **35** 1346–1362.

Yin H, Kristensen SG, Jiang H, Rasmussen A and Andersen CY (2016) Survival and growth of isolated pre-antral follicles from human ovarian medulla tissue during long-term 3D culture. *Human Reproduction* **31** 1531–1539.

Yoshida H, Takakura N, Kataoka H, Kunisada T, Okamura H and Nishikawa SI (1997) Stepwise requirement of c-kit tyrosine kinase in mouse ovarian follicle development. *Developmental Biology* **184** 122–137.

Yoshida H, Matsui T, Yamamoto A, Okada T and Mori K (2001) XBP1 mRNA is induced by ATF6 and spliced by IRE1 in response to ER stress to produce a highly active transcription factor. *Cell* **107** 881–891.

Young JM and McNeilly AS (2010) Theca: The forgotten cell of the ovarian follicle. *Reproduction* **140** 489–504.

Zemyarska MS, Bjarkadottir BD, Wei X, Walker CA, Lane SM, Davies J and Williams SA (2020) The Effect of Delayed Processing on Ovarian Tissue Stored for Fertility Preservation. *Journal of Fertility Preservation* **1** 1–10.

Zhang H and Liu K (2015) Cellular and molecular regulation of the activation of mammalian primordial follicles: Somatic cells initiate follicle activation in adulthood. *Human Reproduction Update* **21** 779–786.

Zhang P, Louhio H, Tuuri T, Sjoberg J, Hreinsson J, Telfer EE and Hovatta O (2004) *In vitro* effect of cyclic adenosine 3', 5'-monophosphate (cAMP) on early human ovarian follicles. *J Assist Reprod Genet* **21** 301–306.

Zhang H, Risal S, Gorre N, Busayavalasa K, Li X, Shen Y, Bosbach B, Brännström M and Liu K (2014) Somatic cells initiate primordial follicle activation and govern the development of dormant oocytes in mice. *Current Biology* **24** 2501–2508.

Zhang J, Yan L, Wang Y, Zhang S, Xu X, Dai Y, Zhao S, Li Z, Zhang Y, Xia G *et al.* (2020) in vivo and *in vitro* activation of dormant primordial follicles by EGF treatment in mouse and human. *Clinical and Translational Medicine* **10** 1–15.

Zhao Y, Zhang Y, Li J, Zheng N, Xu X, Yang J, Xia G and Zhang M (2018) MAPK3/1 participates in the activation of primordial follicles through mTORC1-KITL signaling. *Journal of Cellular Physiology* **233** 226–237.

Zheng W, Zhang H and Liu K (2014a) The two classes of primordial follicles in the mouse ovary: Their development, physiological functions and implications for future research. *Molecular Human Reproduction* **20** 286–292.

Zheng W, Zhang H, Gorre N, Risal S, Shen Y and Liu K (2014b) Two classes of ovarian primordial follicles exhibit distinct developmental dynamics and physiological functions. *Human Molecular Genetics* **23** 920–928.

Zhou J, Peng X and Mei S (2019) Autophagy in ovarian follicular development and Atresia. *International Journal of Biological Sciences* **15** 726–737.

Zhuo Y, Hua L, Feng B, Jiang X, Li J, Jiang D, Huang X, Zhu Y, Li Z, Yan L *et al.* (2019) Fibroblast growth factor 21 coordinates adiponectin to mediate the beneficial effects of low-protein diet on primordial follicle reserve. *EBioMedicine* **41** 623–635.

Appendix A – other publications and awards

Publications during DPhil not directly arising from thesis

Walker CA, Bjarkadottir BD, Fatum M, Lane S, Williams SA.
Variation in follicle health and development in cultured cryopreserved ovarian cortical tissue: a study of ovarian tissue from patients undergoing fertility preservation.
Human Fertility. 2021. 24(3):188-198. Published online May 2019 doi: 10.1080/14647273.2019.1616118
See Appendix C

Zemyarska MS*, Bjarkadottir BD*, Wei X, Walker CA, Lane SM, Davies J, Williams SA
The Effect of Delayed Processing on Ovarian Tissue Stored for Fertility Preservation
Journal of Fertility Preservation. 2020. 1. doi:10.32371/jfp/246108
*equal contribution to work
See Appendix D

Adeniran BV, Bjarkadottir BD, Appeltant R, Lane S, Williams SA
Improved preservation of ovarian tissue morphology that is compatible with antigen detection using a fixative mixture of formalin and acetic acid
Human Reproduction. 2021. 36(7):1871-1890. doi: 10.1093/humrep/deab075
See Appendix E

Awards and grants during DPhil

Icelandic National Bank Student Award (2020)
[Námsstyrkur Landsbankans]
Award of 500,000 ISK (£3,500) to support students pursuing a graduate degree.

Icelandic Chamber of Commerce Education Award (2020)
[Námsstyrkur Viðskiptaráðs Íslands]
Award of 1,000,000 ISK (approx. £7,000) to support Icelandic students pursing a graduate degree abroad.

Icelandic Cancer Research Scientific Fund (2019)
[Vísindasjóður krabbameinsfélags Íslands]
Grant of 2,493,889 ISK (£14,500) for the project titled: Towards non-invasive female fertility preservation for cancer patients: Mechanism of chemotherapy-induced follicle damage and identification of fertoprotective agents.

Max Perutz Science Writing Award (2018)
Runner-up in essay competition held by the Medical Research Council. Essay title: *Stopping the conveyor belt – cancer and fertility.* Available at https://mrc.ukri.org/news/blog/stopping-the-conveyor-belt-cancer-and-fertility/

RESEARCH

Analysing culture methods of frozen human ovarian tissue to improve follicle survival

Briet D Bjarkadottir[1,*], Charlotte A Walker[1,*], Muhammad Fatum[1,2], Sheila Lane[3] and Suzannah A Williams[1]

[1]Nuffield Department of Women's and Reproductive Health, University of Oxford, Oxford, UK
[2]Oxford Fertility, Institute of Reproductive Sciences, Oxford, UK
[3]Department of Paediatric Oncology and Haematology, Oxford University Hospitals NHS Foundation Trust, Oxford, UK

Correspondence should be addressed to S A Williams: suzannah.williams@wrh.ox.ac.uk

*(B D Bjarkadottir and C A Walker contributed equally to this work)

Abstract

In vitro follicle growth is a potential fertility preservation method for patients for whom current methods are contraindicated. Currently, this method has only been successful using fresh ovarian tissue. Since many patients who may benefit from this treatment currently have cryopreserved ovarian tissue in storage, optimising *in vitro* follicle growth (IVG) for cryopreserved-thawed tissue is critical. This study sought to improve the first step of IVG by comparing different short-term culture systems for cryopreserved-thawed human ovarian tissue, in order to yield a higher number of healthy multilayer follicles. We compared two commonly used culture media (αMEM and McCoy's 5A), and three plate conditions (300 µL, 1 mL on a polycarbonate membrane and 1 mL in a gas-permeable plate) on the health and development of follicles after 6 days of culture. A total of 5797 follicles from three post-pubertal patients (aged 21.3 ± 2.3 years) were analysed across six different culture conditions and non-cultured control. All culture systems supported follicle development and there was no difference in developmental progression between the different conditions tested. Differences in follicle morphology were evident with follicles cultured in low volume conditions having significantly greater odds of being graded as morphologically normal compared to other conditions. Furthermore, culture in a low volume of αMEM resulted in the highest proportion of morphologically normal primary and multilayer follicles (23.8% compared to 6.3-19.9% depending on condition). We, therefore, recommend culturing cryopreserved human ovarian tissue in a low volume of αMEM to support follicle health and development.

Lay summary

Ovaries contain a large number of follicles, each containing an immature egg and other important cells. Cancer treatments can lead to long-lasting negative side effects to the ovaries including the destruction of follicles, resulting in infertility. One strategy to preserve fertility is freezing of ovaries or ovarian tissue in girls and women undergoing cancer treatment. The long-term aim is to thaw and grow their ovarian tissue in the laboratory to obtain mature eggs, which can then be fertilised. In this study, we compared six different methods of growing previously frozen human ovarian tissue in order to best support follicle growth and health. We found that using the lowest amount of αMEM medium (a specific type of nutrient-rich growth solution) resulted in the highest proportion of healthy follicles. Improving the methods used to grow ovarian tissue, particularly frozen tissue, is important for future fertility preservation.

Key Words: ▸ cryopreservation ▸ ovary ▸ follicle ▸ human ▸ in vitro growth ▸ fertility preservation

Reproduction and Fertility (2021) **2** 59–68

https://raf.bioscientifica.com
https://doi.org/10.1530/RAF-20-0058

Introduction

Advances in cancer treatment have led to increased survival rates, particularly among young children and adolescents. The increased number of young cancer survivors highlights the need for effective fertility preservation methods for these individuals. Current methods of female fertility preservation include cryopreservation of eggs, embryos and ovarian tissue (Wallace 2011, Yasmin *et al.* 2018). However, pre-pubertal girls are unable to undergo egg or embryo cryopreservation and for some of these patients, reimplantation of ovarian tissue is contraindicated due to the risk of reintroducing malignant cells (Bastings *et al.* 2013, Rosendahl *et al.* 2013). There is therefore a need to develop alternative fertility preservation methods for these patients (Salama *et al.* 2019).

One potential method of fertility preservation is *in vitro* growth (IVG) of follicles by culturing fresh or frozen ovarian tissue followed by *in vitro* maturation (IVM) of immature oocytes resulting in mature developmentally competent eggs (Salama & Woodruff 2019, Telfer 2019). This was recently achieved using fresh ovarian tissue and a four-step culture protocol (McLaughlin *et al.* 2018). In the first step, small pieces of ovarian cortical tissue, each containing primordial follicles, are cultured for 6–8 days to allow for the development of multilayer follicles which can then be isolated for subsequent culture (Telfer *et al.* 2008, McLaughlin *et al.* 2018). This is a limiting step for IVG as it governs the number of follicles that can be carried on to the next stages. Thus, optimisation of the initial step of ovarian tissue culture to increase the yield of healthy multilayer follicles is critical for the success and subsequent clinical application of this method. Furthermore, since many patients who would benefit from IVG have already undergone ovarian tissue cryopreservation, it is important that IVG techniques are established for both fresh and cryopreserved tissue samples.

Since the first report of human ovarian cortical tissue culture in the 1990s (Hovatta *et al.* 1997), a number of different culture systems have been developed. These methods range from culturing tissue pieces in a low volume of medium (Telfer *et al.* 2008, McLaughlin *et al.* 2018) to culture on hydrophobic membranes (Walker *et al.* 2019, Lopes *et al.* 2020) and membrane inserts (Scott *et al.* 2004, Garor *et al.* 2009). The most commonly used basic media are McCoy's 5A (McLaughlin *et al.* 2018, Walker *et al.* 2019, Lopes *et al.* 2020) and αMEM (Scott *et al* 2004, Huang *et al.* 2008, Garor *et al.* 2009, Isachenko *et al.* 2012, Lerer-Serfaty *et al.* 2013, Asadi-Azarbaijani *et al.* 2016, Ramezani *et al.* 2017), with the latter frequently being used for cryopreserved-thawed tissue. Although animal models have suggested that fresh and frozen ovarian tissue may have different metabolic requirements and require different media (Castro *et al.* 2014), there has been no reported comparison between these two commonly used culture media for the culture of cryopreserved human ovarian tissue. In addition, it has been reported that increased oxygen availability through culture of fresh human ovarian tissue in gas-permeable culture plates had a positive impact on follicle health and development (Talevi *et al.* 2018) and thus this is an important variable that needs to be further investigated.

In this study we sought to compare different methods of culturing cryopreserved-thawed human ovarian tissue in order to maximise follicle development and health during the initial step of IVG. Based on existing methods in the published literature, we selected six culture conditions, comparing the effects of two types of culture media and three plate conditions with similar oxygen availability. We report here the effect of each of these conditions on follicle progression and morphology after 6 days of culture, using statistical modelling to account for intra- and inter-patient variability.

Materials and methods

Ovarian tissue collection

The use of human tissue was approved by Health Research Authority South Central – Oxford B Research Ethics Committee (REC reference: 14/SC/0041). Cryopreserved ovarian tissue was obtained from the Oxford Cell and Tissue Biobank. Patient selection criteria included post-pubertal patients undergoing unilateral oophorectomy and subsequent ovarian tissue cryopreservation due to malignancy or blood disorder. Exclusion criteria included ovarian cancer and prior chemotherapy or radiation treatment. As part of the consent process, permission to use tissue in research had been obtained. Cortical strips were cryopreserved using slow freezing by the Oxford Cell and Tissue Biobank in 1.5 M ethylene glycol, 0.1 M sucrose and 10% serum substitute supplement in Leibovitz L-15 medium and stored in vapour phase liquid nitrogen.

Chemicals and consumables

Leibovitz L-15 medium (11415049), minimum essential medium alpha (αMEM) (22561021), McCoy's 5A (modified) HEPES buffered medium (22330021), L-glutamine (25030024) and ascorbic acid (10012011) were purchased

https://raf.bioscientifica.com
https://doi.org/10.1530/RAF-20-0058

from Thermo Fisher. Human serum albumin (AI653), ITS liquid media supplement (100×; I3145), Penicillin and streptomycin (P0781) sodium pyruvate (S8636), neutral red (N2889), sucrose (S7903), ethylene glycol (324558), Whatman Nucleopore membranes (WHA110414), Bouin's solution (HT10132), Gill no 2 haematoxylin (GHS232), Eosin Y solution (HT110332) and DPX mountant (06522) were purchased from Sigma Aldrich. Recombinant human follicle-stimulating hormone (FSH; Gonal-F; Z1540) was purchased from Merck Serono (Feltham, UK). Corning Costart tissue culture treated 24-well plates were purchased from Scientific Laboratory Supplies (Nottingham, UK). Lumox® 24-well plates were generously provided by Sarstedt (Nümbrecht, Germany).

Tissue thawing and cortical strip culture

Cortical strips were thawed and processed for culture as described previously (Walker *et al.* 2019). Briefly, following thawing in a water bath (30°C for 3 min), cortical strips were washed through thawing solutions for 5 min each at room temperature to remove cryoprotectants. The thawing solutions contained a reversed ethylene glycol gradient (1.0, 0.5 and 0 M), 0.1 M sucrose and 3 mg/mL human serum albumin (HSA) in L-15 medium. Thawed strips were transferred to dissection medium (3 mg/mL HSA, 100 U/mL penicillin, 100 µg/mL streptomycin, 2 mM L-glutamine and 2 mM sodium pyruvate in L-15 medium) and mechanically chopped using a McIlwain tissue chopper (Campden Instruments Ltd, UK), after which the fragments were further cut manually using scalpels and forceps into approximately 0.5 × 0.5 × 0.25 mm pieces. Tissue fragments were incubated in 25 µg/mL neutral red for 1 h to visualise fragments with viable follicles (Chambers *et al.* 2010, Walker *et al.* 2019).

Tissue pieces were distributed randomly and evenly between six different culture conditions (9–12 pieces per condition per patient), fragments, where red staining was observed, were allocated before non-stained fragments. One piece of tissue was placed in each culture well. A portion of tissue was fixed overnight in Bouin's solution as a non-cultured control. Three different plate conditions were tested: a polycarbonate membrane (13 mm diameter, 8 µm pore size) floating in 1 mL of medium in a conventional 24-well culture plate, 300 µL of medium in a conventional 24-well plate, and 1 mL of medium in a gas-permeable Lumox® 24-well plate (Fig. 1). The well size and diameter were the same for both types of culture plates and in all conditions the ovarian tissue was located at the medium-gas interface. Two different media were compared for each plate condition (i.e. six experimental conditions in total): McCoy's 5A and αMEM, both supplemented with 1 mg/mL HSA, 100 U/mL penicillin, 100 µg/mL streptomycin, 2 mM L-glutamine, 10 µg/mL insulin, 5.5 µg/mL transferrin, 5 ng/mL selenium, 50 µg/mL ascorbic acid and 12.5 IU/L recombinant human FSH. Cortical tissue pieces were cultured for 6 days at 37°C under 5% CO_2 in air, with medium changes every other day (half the medium removed and fresh medium added). For tissue cultured on a polycarbonate membrane, care was taken to visually confirm that the tissue pieces were covered by a thin layer of medium during the entire culture period. Following the culture period, all tissue pieces were fixed in Bouin's solution overnight before storage in 70% ethanol at 4°C.

Histological analysis

Fixed ovarian tissue was dehydrated in a graded series of ethanol, cleared in xylene and embedded in paraffin wax. The wax-embedded tissue was entirely serially sectioned

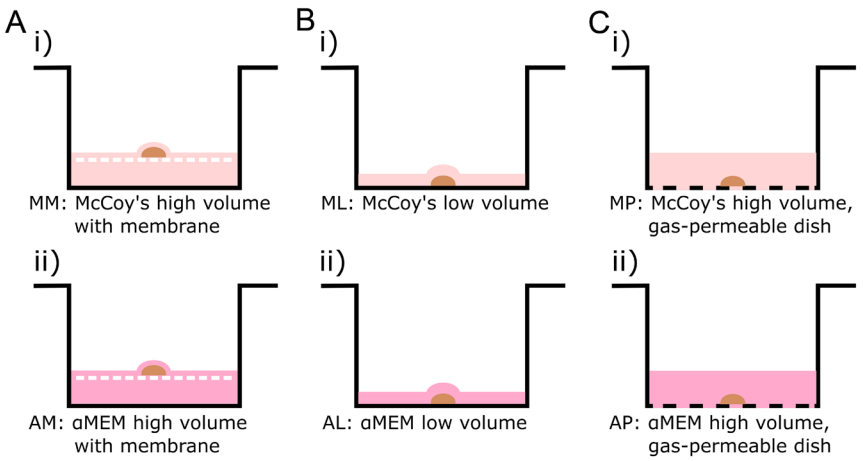

Figure 1 Overview of culture conditions. Cryopreserved human ovarian tissue (represented by a brown half-moon shape, not to scale) was cultured under different culture conditions. Three plate conditions were tested along with two culture media, resulting in a total of six culture conditions. (A) Polycarbonate membrane floating in a high volume (1 mL) of McCoy's 5A (MM; Ai) or αMEM (AM; Aii) medium in a conventional 24-well plate. (B) Low volume (300 µL) of McCoy's 5A (ML; Bi) or αMEM (AL; Bii) medium in a conventional 24-well plate; (C) High volume (1 mL) of McCoy's 5A (MP; Ci) or αMEM (AP; Cii) medium in a gas-permeable Lumox® 24-well plate.

https://raf.bioscientifica.com
https://doi.org/10.1530/RAF-20-0058

at 5 µm, mounted on glass slides and stained with haematoxylin and eosin.

Follicles were staged as previously described (Gougeon 1996, Walker *et al.* 2019) as primordial (single layer of flattened pre-granulosa cells), transitional (single layer with at least one cuboidal granulosa cell), primary (complete layer of cuboidal granulosa cells) and multilayer (at least one complete layer of granulosa cells plus one or more partial or complete layers). Follicles were graded according to morphology based on the presence of pyknotic granulosa cells or oocyte and shrinkage of the ooplasm as previously described (Walker *et al.* 2019). Morphologically normal follicles were defined as having a non-pyknotic non-shrunken oocyte with non-pyknotic granulosa cells, degenerating follicles had one of the above factors, while follicles were classified as atretic if they had both an oocyte with a pyknotic nucleus and pyknotic granulosa cells. Every tissue section was analysed and each follicle was followed through neighbouring sections to avoid double counting. Only follicles with a visible nucleolus or a clearly defined nuclear membrane were assessed. Follicles were analysed by two independent researchers with at least 10% overlap to ensure consistency in staging and health grading.

Every 12th section of each piece of tissue was imaged at a low magnification and the area measured using the freehand measuring tool in ImageJ 1.46r (National Institutes of Health, USA; Schneider *et al.* 2012, Rueden *et al.* 2017). Average area measurements were used to calculate the volume of each tissue piece. Follicle density was determined by dividing the total number of follicles counted in a tissue sample by the tissue volume. All imaging was performed using a Leica DM2500 microscope (Leica Microsystems, Germany), fitted with a QImaging Micropublisher 5.0 RTV camera running the QCapture Pro 7 software (QImaging, Canada).

Statistical analysis and modelling

All statistical analyses were performed using R statistical software, version 3.5.0. A generalised linear mixed model following a negative binomial distribution (glmmPQL; Venables & Ripley 2002) was used to determine the effect of culture condition on follicle development, adjusted for patient and tissue volume. A proportional odds model (clmm2; Christensen 2015) was used to determine whether follicle morphology was affected by culture condition, again adjusting for tissue volume and patient. Data are presented as mean (±S.E.M.), combined proportions (%) from all patients or as odds ratios (OR) with 95% CIs, unless otherwise stated, and statistical significance was defined as $P < 0.05$.

Results

Patient characteristics

Samples from three post-pubertal patients (aged 17–25 years, mean 21.3 ± 2.3 years) were used in this study. Table 1 shows patient age, diagnosis and non-cultured follicle density. The total number of follicles analysed from all three patients across all conditions was 5797. There was great variation in follicle density in both cultured and non-cultured tissue between patients, ranging from 20.4 ± 5.5 to 431.9 ± 23.8 follicles/mm^3 for non-cultured tissue (Table 1). This, coupled with our group's previous work (Walker *et al.* 2019), highlighted the need for statistical modelling to account for this intra-patient variability.

Follicle development was predominantly unaffected by culture condition

Follicles were classified based on histology as primordial, transitional, primary or multilayer (Fig. 2). There was no difference in follicle density between the different culture conditions (Fig. 3A). Follicles grew during the culture period, with the majority of follicles being classified as primordial (70.4%) or transitional (27.2%) in non-cultured tissue, whereas after 6 days of culture 39.4–79.7% of follicles were at the primary or multilayer stages, depending on the culture condition (Figs 2, 3B and Table 2). Tissue cultured in a low medium volume contained the highest proportion of multilayer follicles, 26.8% for McCoy's (ML) and 28.5% for αMEM (AL). Follicle development was compared across the different culture conditions using a generalised linear mixed model, with all conditions being compared to culture in a high volume of McCoy's 5A medium on a polycarbonate membrane

Table 1 Patient characteristics and non-cultured follicle density.

Patient	**Age** (years)	**Diagnosis**	**Total follicles analysed**	**Non-cultured follicle density** (follicles/mm^3)
1	25	Cervical cancer	303	20.4 ± 5.5
2	17	Ewing's sarcoma	3198	431.9 ± 23.8
3	22	Atypical teratoid rhabdoid tumour	2295	127.7 ± 77.3

https://raf.bioscientifica.com
https://doi.org/10.1530/RAF-20-0058

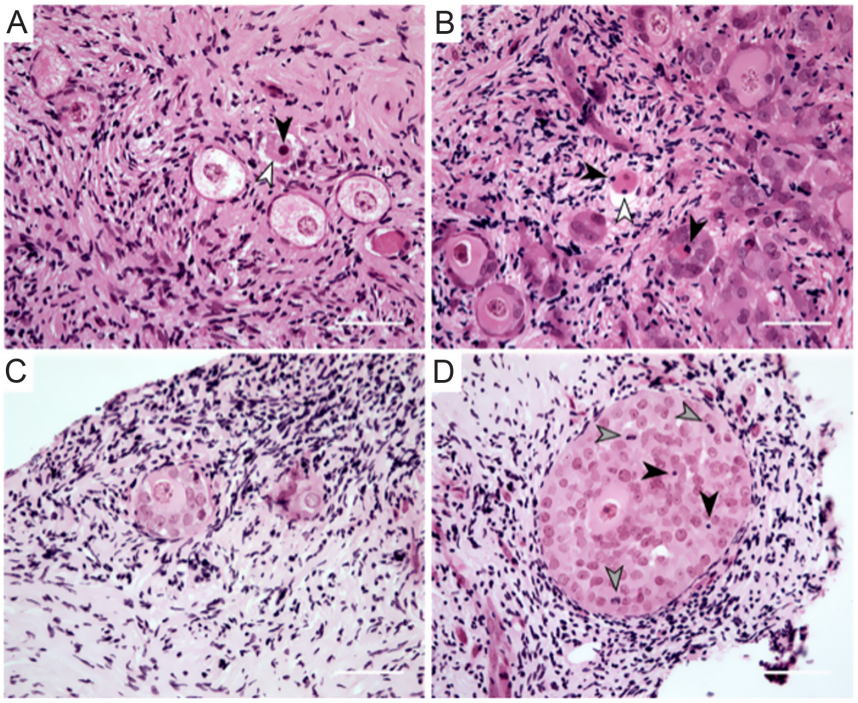

Figure 2 Representative images of non-cultured and cultured cryopreserved human ovarian tissue. Follicles were staged as primordial (P0; single layer of flattened pre-granulosa cells), transitional (T; single layer with at least one cuboidal granulosa cell), primary (P1; single layer of cuboidal granulosa cells) and multilayer (at least one complete layer of granulosa cells plus one or more partial or complete layers). Follicle health was assessed based on the presence or absence of pyknotic granulosa cells or oocyte (black arrowhead) and shrunken ooplasm (white arrowhead). (A) Representative image of non-cultured cryopreserved ovarian tissue from a 22-year-old patient. (B) Representative image of cryopreserved ovarian tissue from a 17-year-old patient cultured for 6 days in a low volume of αMEM medium (AL). (C and D) Examples of normal multilayer follicles after 6 days of culture in AL, same patient as (A). Three granulosa cells undergoing mitosis can be seen in panel D (grey arrowhead). Scale bar = 50 μm.

(MM) as this was our group's established culture method based on Lopes *et al*. (2020) prior to this study (Walker *et al*. 2019; Fig. 4). There were significantly fewer transitional follicles in tissue cultured in a low volume of McCoy's 5A medium (ML) compared to membrane culture (MM; 7.8 ± 6.0 follicles/mm^3 vs 28.2 ± 20.8 follicles/mm^3 respectively, $P<0.05$, Fig. 4B). There was no difference between the conditions for follicles at other stages. Follicle density did not affect follicle development (data not shown). Within the multilayer follicle group, only culture in low-volume conditions resulted in follicles with >3 layers of granulosa cells (Table 2). However, there were not enough follicles with ≥3 granulosa cell layers to allow for statistical analysis.

Culture in low volume conditions improved follicle morphology

Follicles were classified as morphologically normal, degenerating or atretic. Non-cultured tissue contained mostly normal follicles at all stages, however, after 6 days of culture the proportion of degenerating or atretic follicles had increased considerably for all culture conditions (Figs 2 and 5). As with development, follicle morphological health was not affected by follicle density (data not shown). A proportional odds model was used to determine whether a follicle was more likely to be normal compared to degenerating or atretic after 6 days in a particular culture condition (Fig. 6). Compared to MM, tissue cultured in low volume conditions (McCoy's, ML or αMEM, AL) or permeable dish conditions (MP or AP) had greater odds of normal multilayer follicles being observed compared to degenerating or atretic (Fig. 6D). The most marked improvement in the morphology of multilayer follicles was seen in the low volume conditions, particularly AL where the odds of observing a normal follicle were five times greater than MM (OR = 0.2; 95% CI 0.13–0.32; $P< 0.001$). Tissue cultured in ML had 2.6 times greater odds of multi-layered follicles being classified as 'normal' follicles vs 'degenerating' or 'atretic' compared to MM (OR = 0.38; 95% CI 0.23–0.64; $P< 0.001$).

As culture in AL resulted in morphologically healthier follicles of all stages compared to MM, AL was set as the baseline level of comparison in the proportional odds model, to ascertain whether medium affected follicle health within the low volume condition. Compared to AL, multilayer follicles cultured in ML had 1.9 times greater odds of being classified as degenerating or atretic than normal (OR = 1.92; 95% CI 1.24–2.97; $P< 0.001$) showing that AL yielded superior follicle morphology compared to the other conditions tested (Fig. 2). When the proportion of normal primary or multilayer follicles was compared between culture conditions, we observed that culture in AL yielded over 20% normal primary or multilayer follicles, more than the other culture conditions.

https://raf.bioscientifica.com
https://doi.org/10.1530/RAF-20-0058

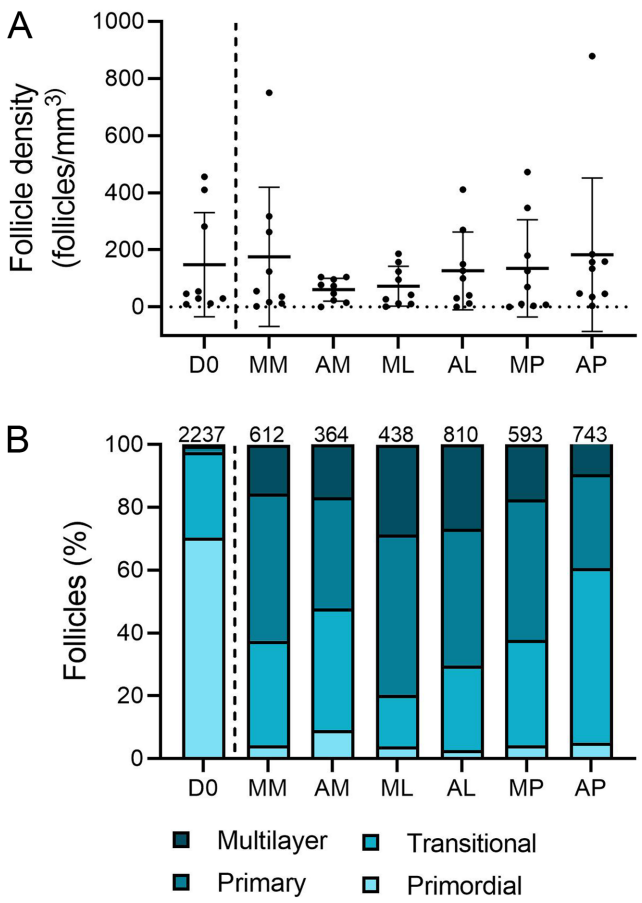

Figure 3 Follicle density and development after 6-day culture of cryopreserved human ovarian tissue. (A) There was no difference in follicle density between any of the culture conditions or non-cultured control. (B) Follicles were staged as primordial (single layer of flattened pre-granulosa cells), transitional (single layer with at least one cuboidal granulosa cell), primary (single layer of cuboidal granulosa cells) and multilayer (at least one complete layer of granulosa cells plus one or more partial or complete layers). Follicle development was observed across all culture conditions compared to non-cultured control (D0, separated by dashed line), with a high proportion of primary and multilayer follicles being observed in cultured samples. The numbers across the top of the columns represent the number of follicles analysed in each group, combined from three patients. D0: non-cultured control; MM: McCoy's high volume with membrane, AM: αMEM high volume with membrane; ML: McCoy's low volume; AL: αMEM low volume, MP: McCoy's high volume, gas permeable plate; AP: αMEM high volume, gas-permeable plate.

Discussion

Here we report that culture medium and plate conditions significantly impact the morphology of follicles generated from 6-day *in vitro* culture of cryopreserved human ovarian tissue. We found that culture in a low volume of αMEM resulted in morphologically healthier follicles at all stages of development compared to the same volume of McCoy's 5A medium, and culture using polycarbonate membranes or gas-permeable plates with a higher medium volume.

Our results demonstrate that culture in a low medium volume led to improved follicle morphology compared to an approximately three-fold higher medium volume with a polycarbonate membrane or a gas-permeable dish. It should be noted that all three plate conditions (polycarbonate membrane, low volume and gas-permeable dish), all provided equal access to the air as the ovarian tissue was located close to the medium-gas interface (Fig. 1). Improved follicle morphology in low volume culture may have been due to higher concentrations of soluble secreted factors released by follicles or their surrounding cells which may have contributed to decreased follicle atresia. By culturing cryopreserved ovarian tissue in a low volume of αMEM we observed a high level of follicle progression, with 26.8% multilayer follicles (two or more partial or complete granulosa cell layers) out of 810 follicles from three patients, with 34.0% morphologically normal follicles. Oxygen availability has previously been demonstrated to be a contributing factor to follicle health (Morimoto *et al.* 2007, Talevi *et al.* 2018). Talevi *et al.* (2018) reported that culture of fresh human ovarian tissue in 5 mL of αMEM medium (column height 1.4 mm) in a gas-permeable petri dish led to improved follicle development and health, reporting that out of 287 follicles from six patients, 19.5% were multilayer and 41.7% normal after 6 days of culture. This culture method is similar to that of a low volume of αMEM (AL) described in the current study (AL column height 1.6 mm), however the medium volume used by Talevi *et al.* (2018) was 15 times greater. Taking into account the potential benefits of low volume conditions mentioned above, culturing tissue in a low volume of αMEM in gas-permeable plates may lead to even greater follicle health and should be further investigated.

Culture in a low medium volume (ML and AL) yielded the highest proportion of normal primary and multilayer follicles out of the six conditions tested. Our culture in a low volume of McCoy's 5A is similar to the first of a four-step culture method used by McLaughlin *et al.* (2014), the only successful generation of mature human oocytes grown from ovarian tissue (McLaughlin *et al.* 2018), however, we found that culture in a low volume of αMEM resulted in superior follicle morphological health at all stages of development. Here, ovarian tissue was cultured for 6 days, which has previously been reported to support follicle development (Telfer *et al.* 2008), with a similar proportion of secondary follicles being reported after 6 and 9 days of culture (Talevi *et al.* 2018). This short-term culture is the initial step for IVG and the most limiting since it determines the number of follicles available for subsequent culture. Therefore, improving the health and

https://raf.bioscientifica.com
https://doi.org/10.1530/RAF-20-0058

Table 2 Proportion of follicles at each developmental stage for non-cultured control (D0) and different culture conditions for human ovarian tissue. Details of the multilayer follicle group are provided, showing the number of follicles with two, three or over three granulosa cell (GC) layers. Data are presented as *n* (%).

Stage	D0	MM	AM	ML	AL	MP	AP
Primordial	1575 (70.4%)	26 (4.2%)	33 (9.1%)	17 (3.9%)	22 (2.7%)	25 (4.2%)	38 (5.1%)
Transitional	609 (27.2%)	204 (33.3%)	141 (38.7%)	72 (16.4%)	218 (26.9%)	199 (33.6%)	412 (55.5%)
Primary	45 (2.0%)	283 (46.2%)	126 (34.6%)	217 (49.5%)	346 (42.7%)	261 (44.0%)	219 (29.5%)
Multilayer	8 (0.4%)	99 (16.2%)	64 (17.6%)	132 (30.1%)	224 (27.7%)	108 (18.2%)	74 (10.0%)
2 GC layers	6 (0.3%)	78 (12.7%)	50 (13.7%)	109 (24.9%)	196 (24.2%)	93 (15.7%)	64 (8.6%)
3 GC layers	2 (0.1%)	21 (3.4%)	14 (3.8%)	21 (4.8%)	27 (3.3%)	15 (2.5%)	10 (1.3%)
≥3 GC layers	0 (0.0%)	0 (0.0%)	0 (0.0%)	2 (0.5%)	1 (0.1%)	0 (0.0%)	0 (0.0%)
Total	2237	612	364	438	810	593	743

AH, αMEM high volume with membrane; AL, αMEM low volume; AP, αMEM high volume, gas-permeable plate; ML McCoy's low volume; MM, McCoy's high volume with membrane; MP, McCoy's high volume, gas permeable plate.

development of early growing follicles could improve the yield of isolated follicles for IVG.

Studies describing culture of controlled-rate cryopreserved human ovarian tissue, as we have used in the present study, are limited, and the majority of studies use fresh ovarian tissue (Telfer *et al.* 2008, McLaughlin *et al.* 2018, Talevi *et al.* 2018, Lopes *et al.* 2020). Follicle growth *in vitro* may be compromised by cryopreservation and cryopreserved ovarian tissue may have different requirements *in vitro*, as has been demonstrated using animal models (Ting *et al.* 2011, Castro *et al.* 2014). Interestingly, Castro *et al.* (2014) reported improved follicle viability in cryopreserved bovine ovarian tissue after culture in McCoy's 5A medium compared to αMEM and M199, which is in contrast with the results presented here where αMEM was found to be superior. However, the culture systems cannot be directly compared, as Castro *et al.* (2014) cultured samples under 1 mL of medium in conventional 24-well plates, therefore oxygen availability was different to the culture systems described here, where all tissue was at the medium-gas interface. αMEM has also found to be superior for culture of fresh bovine and human ovarian

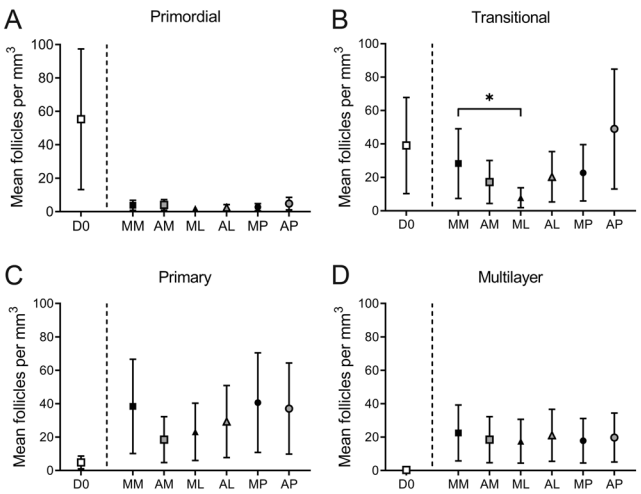

Figure 4 Follicle development is largely unaffected by culture condition. Follicles were classified as (A) primordial, (B) transitional, (C) primary or (D) multilayer based on histology in non-cultured tissue and tissue cultured for 6 days in different conditions. Transitional follicle density was significantly lower in ML compared to MM ($P < 0.05$). There was no difference in the density of primordial, primary or multilayer follicles between the different conditions tested and MM. Data were analysed using a generalised linear mixed model. *$P < 0.05$. D0: non-cultured control; MM: McCoy's high volume, with membrane AM: αMEM high volume with membrane; ML: McCoy's low volume; AL: αMEM low volume, MP: McCoy's high volume, gas-permeable plate; AP: αMEM high volume, gas-permeable plate.

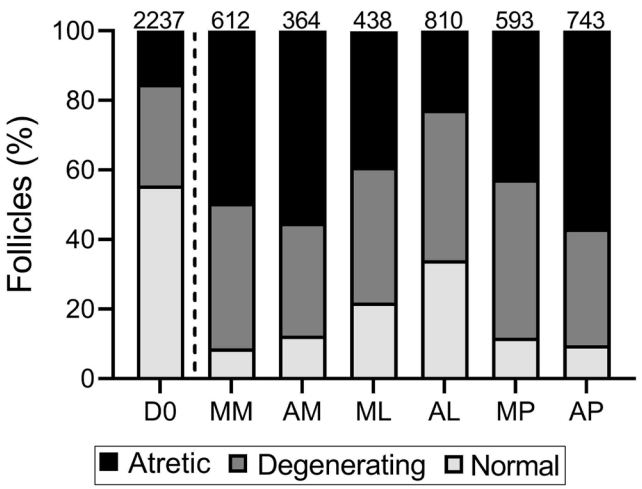

Figure 5 Follicle morphological health after 6-day culture of cryopreserved human ovarian tissue. Follicles were classified as morphologically normal (no evidence of degeneration), degenerating (presence of either a pyknotic oocyte, pyknotic granulosa cells or shrunken ooplasm), and atretic (presence of both pyknotic oocyte and pyknotic granulosa cells). The proportion of atretic follicles was increased in cultured tissue compared to non-cultured control. The numbers across the top of the columns represent the number of follicles analysed in each group, combined from three patients. D0: non-cultured control; MM: McCoy's high volume with membrane, AM: αMEM high volume with membrane; ML McCoy's low volume; AL: αMEM low volume, MP: McCoy's high volume, gas permeable plate; AP: αMEM high volume, gas-permeable plate.

https://raf.bioscientifica.com
https://doi.org/10.1530/RAF-20-0058

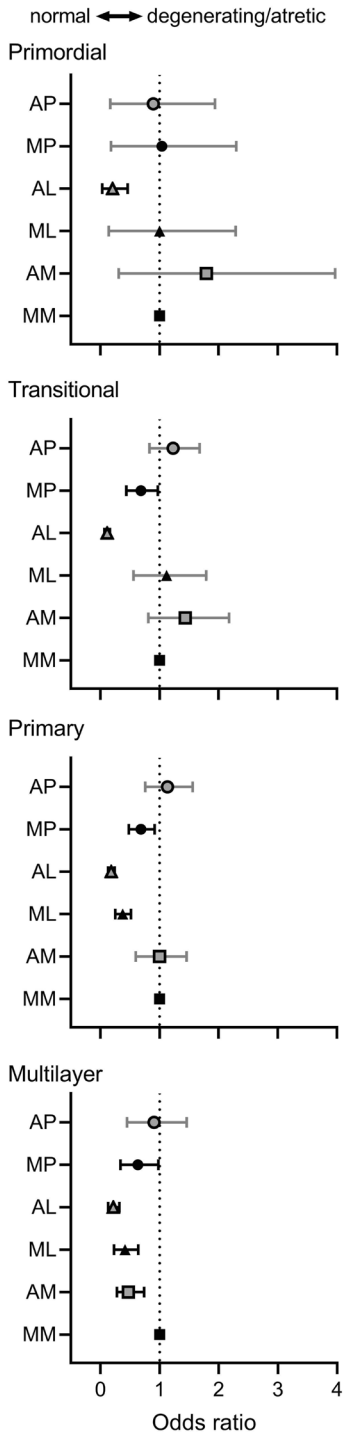

Figure 6 Effect of culture condition on follicle morphological health. A proportional odds ratio model was used to determine whether any of the conditions tested was more likely to lead to morphologically healthier follicles at each stage compared to MM. Data are represented as odds ratio with upper and lower confidence intervals (displayed as error bars). Odds ratio < 1 indicates decreased odds of a follicle being degenerating or atretic compared to MM. Odds ratio > 1 indicates increased odds of a follicle being degenerating or atretic compared to MM. Those conditions where confidence intervals do not cross 1 (black lines) were significantly less likely to have degenerating or atretic follicles compared to the baseline (MM, $P < 0.05$). MM: McCoy's high volume with membrane, AH: αMEM high volume with membrane; ML McCoy's low volume; AL: αMEM low volume, MP: McCoy's high volume, gas permeable plate; AP: αMEM high volume, gas-permeable plate.

tissue (Wright *et al.* 1999, Jimenez *et al.* 2016), highlighting the need to optimise ovarian tissue culture for both fresh and cryopreserved tissue. This is indeed critical since there are many patients who already have tissue cryopreserved and may require IVG to generate eggs.

Chemotherapy treatment prior to ovarian tissue cryopreservation may also compromise the development of these follicles *in vitro*, however only two studies exist and data are confounded by differences in the age between control and treated groups (Asadi Azarbaijani *et al.* 2015, Pampanini *et al.* 2019). Clearly, if we are to progress to a clinical treatment, the effect of prior chemotherapy on subsequent follicle development *in vitro* needs to be explored.

Follicles at all stages were more likely to be graded as normal when cultured in a low volume of αMEM (AL) compared to the same volume of McCoy's 5A medium (ML). αMEM contains both sodium pyruvate and a physiological concentration of glucose (5.6 mM), whereas McCoy's 5A contains no pyruvate and three times higher concentration of glucose (16.7 mM) and therefore αMEM may provide a more suitable environment for follicle metabolism. Previous studies have indeed demonstrated pyruvate to be the main energy source during early follicle development in mice (Harris *et al.* 2007, 2009). Under normal conditions, the oocyte is supplied with pyruvate by its supporting somatic cells however it has been demonstrated that pyruvate is taken up from the culture medium during *in vitro* follicle culture (Harris *et al.* 2009). Therefore, αMEM may provide a more suitable energy source for early follicle metabolism compared to McCoy's, thereby better supporting follicle health although it is unknown at this time if cryopreservation has any effect on subsequent tissue requirements in culture.

The analysis presented in the present study was performed based on clearly defined and detailed morphological criteria, as previously described (Walker *et al.* 2019). While morphology is a widely used and generally accepted measure of follicle health and survival (McLaughlin *et al.* 2014, Talevi *et al.* 2018, Pampanini *et al.* 2019, Walker *et al.* 2019, Lopes *et al.* 2020), there are some limitations in using morphological parameters alone to evaluate follicle health. Namely, fixatives such as neutral buffered formalin cause tissue-dependant shrinkage, which we have observed can obscure the morphology of human ovarian follicles

https://raf.bioscientifica.com
https://doi.org/10.1530/RAF-20-0058

in particular, and may result in misinterpretation of data (Adeniran *et al.* 2021). In the present study, tissue was fixed in Bouin's solution, which prevents tissue shrinkage and better preserves morphology, however, this fixative is incompatible with molecular analysis such as immunohistochemistry. Due to the limited availability of cryopreserved ovarian tissue and the heterogeneity of follicles within the tissue, we focussed solely on well-defined morphological outcome measures for the present study. In studies using a combination of morphological and molecular analyses, the two methods are generally in agreement (Talevi *et al.* 2018). Indeed, molecular analysis may present its own set of limitations, including challenges in selecting an appropriate marker in addition to the transience of some marker expression (Pampanini *et al.* 2019).

In conclusion, we report that culture in a low volume of αMEM in conventional 24-well plates led to improved follicle health after 6 days of culture compared to other conditions with similar oxygen availability. This highlights the need to further optimise culture systems for ovarian tissue culture, particularly culture of cryopreserved ovarian tissue. Improving the health and early development of follicles *in vitro* is a key aspect of developing culture systems capable of supporting follicle development from the earliest stages to result in mature fertilisable eggs. Once developed, these methods could offer a significant number of individuals a chance of achieving pregnancy following cancer treatment.

Declaration of interest

Suzannah Williams is a Lay Editor of Reproduction and Fertility. Suzannah Williams was not involved in the review or editorial process for this paper, on which he/she is listed as an author

Funding

This work was supported by the Oxford Medical Research Council Doctoral Training Programme (Oxford MRC-DTP) grant awarded to B D B (grant number MR/N013468/1) and by a joint scholarship to C A W from the Clarendon fund and NDWRH.

Author contribution statement

S A W, C A W and B D B designed the study. M F obtained the original ethical approval which was modified by S A W and approved by M F. S L was instrumental in obtaining the tissues used in the study and is a supervisor of B D B. C A W and B D B carried out all cultures and data analysis. C A W, B D B and S A W wrote and prepared the manuscript. All authors critically read and approved the final manuscript.

Acknowledgements

The authors would like to thank all staff and the Oxford Cell and Tissue Biobank for their assistance in obtaining patient samples, in addition to the patients themselves for donating tissue to research. Thanks go to Prof Norah Spears for assistance in establishing culture techniques. The authors are also grateful to Sarstedt for providing the Lumox® culture plates.

References

Adeniran BV, Bjarkadottir BD, Appeltant R, Lane S & Williams SA 2021 Improved preservation of ovarian tissue morphology that is compatible with antigen detection using a fixative mixture of formalin and acetic acid. *Human Reproduction* In press. (https://doi.org/10.1093/humrep/deab075)

Asadi-Azarbaijani B, Sheikhi M, Nurmio M, Tinkanen H, Juvonen V, Dunkel L, Hovatta O, Oskam IC & Jahnukainen K 2016 Minimal residual disease of leukemia and the quality of cryopreserved human ovarian tissue in vitro. *Leukemia and Lymphoma* **57** 700–707. (https://doi.org/10.3109/10428194.2015.1065980)

Asadi Azarbaijani B, Sheikhi M, Oskam IC, Nurmio M, Laine T, Tinkanen H, Mäkinen S, Tanbo TG, Hovatta O & Jahnukainen K 2015 Effect of previous chemotherapy on the quality of cryopreserved human ovarian tissue in vitro. *PLoS ONE* **10** e0133985. (https://doi.org/10.1371/journal.pone.0133985)

Bastings L, Beerendonk CCM, Westphal JR, Massuger LFAG, Kaal SEJ, van Leeuwen FE, Braat DDM & Peek R 2013 Autotransplantation of cryopreserved ovarian tissue in cancer survivors and the risk of reintroducing malignancy: a systematic review. *Human Reproduction Update* **19** 483–506. (https://doi.org/10.1093/humupd/dmt020)

Castro SV, Carvalho AA, Silva CMG, Santos FW, Campello CC, de Figueiredo JR & Rodrigues APR 2014 Frozen and fresh ovarian tissue require different culture media to promote in vitro development of bovine preantral follicles. *Biopreservation and Biobanking* **12** 317–324. (https://doi.org/10.1089/bio.2014.0020)

Chambers EL, Gosden RG, Yap C & Picton HM 2010 In situ identification of follicles in ovarian cortex as a tool for quantifying follicle density, viability and developmental potential in strategies to preserve female fertility. *Human Reproduction* **25** 2559–2568. (https://doi.org/10.1093/humrep/deq192)

Christensen RHB 2015 Ordinal-regression models for ordinal data. R package version 2015.6-28. (available at: http://www.cran.r-project.org/package=ordinal)

Garor R, Abir R, Erman A, Felz C, Nitke S & Fisch B 2009 Effects of basic fibroblast growth factor on in vitro development of human ovarian primordial follicles. *Fertility and Sterility* **91** (Supplement 5) 1967–1975. (https://doi.org/10.1016/j.fertnstert.2008.04.075)

Gougeon A 1996 Regulation of ovarian follicular development in primates: facts and hypotheses. *Endocrine Reviews* **17** 121–155. (https://doi.org/10.1210/edrv-17-2-121)

Harris SE, Adriaens I, Leese HJ, Gosden RG & Picton HM 2007 Carbohydrate metabolism by murine ovarian follicles and oocytes grown in vitro. *Reproduction* **134** 415–424. (https://doi.org/10.1530/REP-07-0061)

Harris SE, Leese HJ, Gosden RG & Picton HM 2009 Pyruvate and oxygen consumption throughout the growth and development of murine oocytes. *Molecular Reproduction and Development* **76** 231–238. (https://doi.org/10.1002/mrd.20945)

Hovatta O, Silye R, Abir R, Krausz T & Winston RM 1997 Extracellular matrix improves survival of both stored and fresh human primordial and primary ovarian follicles in long-term culture. *Human Reproduction* **12** 1032–1036. (https://doi.org/10.1093/humrep/12.5.1032)

Huang L, Mo Y, Wang W, Li Y, Zhang Q & Yang D 2008 Cryopreservation of human ovarian tissue by solid-surface vitrification. *European Journal of Obstetrics, Gynecology, and Reproductive Biology* **139** 193–198. (https://doi.org/10.1016/j.ejogrb.2008.03.002)

Isachenko V, Mallmann P, Petrunkina AM, Rahimi G, Nawroth F, Hancke K, Felberbaum R, Genze F, Damjanoski I & Isachenko E 2012 Comparison of in vitro- and chorioallantoic membrane (CAM)-culture systems for cryopreserved medulla-contained human ovarian tissue. *PLoS ONE* **7** e32549. (https://doi.org/10.1371/journal.pone.0032549)

Jimenez CR, Araújo VR, Penitente-Filho JM, de Azevedo JL, Silveira RG & Torres CAA 2016 The base medium affects ultrastructure and survival of bovine preantral follicles cultured in vitro. *Theriogenology* **85** 1019–1029. (https://doi.org/10.1016/j.theriogenology.2015.11.007)

Lerer-Serfaty G, Samara N, Fisch B, Shachar M, Kossover O, Seliktar D, Ben-Haroush A & Abir R 2013 Attempted application of bioengineered/biosynthetic supporting matrices with phosphatidylinositol-trisphosphate-enhancing substances to organ culture of human primordial follicles. *Journal of Assisted Reproduction and Genetics* **30** 1279–1288. (https://doi.org/10.1007/s10815-013-0052-8)

Lopes F, Liu J, Morgan S, Matthews R, Nevin L, Anderson RA & Spears N 2020 Single and combined effects of cisplatin and doxorubicin on the human and mouse ovary in vitro. *Reproduction* **159** 193–204. (https://doi.org/10.1530/REP-19-0279)

McLaughlin M, Innell HL, Anderson RA & Telfer EE 2014 Inhibition of phosphatase and tensin homologue (PTEN) in human ovary in vitro results in increased activation of primordial follicles but compromises development of growing follicles. *Molecular Human Reproduction* **20** 736–744. (https://doi.org/10.1093/molehr/gau037).

McLaughlin M, Albertini DF, Wallace WHB, Anderson RA & Telfer EE 2018 Metaphase II oocytes from human unilaminar follicles grown in a multi-step culture system. *Molecular Human Reproduction* **24** 135–142. (https://doi.org/10.1093/molehr/gay002)

Morimoto Y, Oku Y, Sonoda M, Haruki A, Ito K, Hashimoto S & Fukuda A 2007 High oxygen atmosphere improves human follicle development in organ cultures of ovarian cortical tissues in vitro. *Human Reproduction* **22** 3170–3177 (https://doi.org/10.1093/humrep/dem314).

Pampanini V, Wagner M, Asadi-Azarbaijani B, Oskam IC, Sheikhi M, Sjödin MOD, Lindberg J, Hovatta O, Sahlin L, Björvang RD, *et al.* 2019 Impact of first-line cancer treatment on the follicle quality in cryopreserved ovarian samples from girls and young women. *Human Reproduction* **34** 1674–1685. (https://doi.org/10.1093/humrep/dez125)

Ramezani M, Salehnia M & Jafarabadi M 2017 Short term culture of vitrified human ovarian cortical tissue to assess the cryopreservation outcome: molecular and morphological analysis. *Journal of Reproduction and Infertility* **18** 162–171.

Rosendahl M, Greve T & Andersen CY 2013 The safety of transplanting cryopreserved ovarian tissue in cancer patients: a review of the literature. *Journal of Assisted Reproduction and Genetics* **30** 11–24. (https://doi.org/10.1007/s10815-012-9912-x)

Rueden CT, Schindelin J, Hiner MC, DeZonia BE, Walter AE, Arena ET & Eliceiri KW 2017 ImageJ2: ImageJ for the next generation of scientific image data. *BMC Bioinformatics* **18** 529. (https://doi.org/10.1186/s12859-017-1934-z)

Salama M & Woodruff TK 2019 From bench to bedside: current developments and future possibilities of artificial human ovary to restore fertility. *Acta Obstetricia et Gynecologica Scandinavica* **98** 659–664. (https://doi.org/10.1111/aogs.13552)

Salama M, Anazodo A & Woodruff TK 2019 Preserving fertility in female patients with hematological malignancies: a multidisciplinary oncofertility approach. *Annals of Oncology* **30** 1760–1775. (https://doi.org/10.1093/annonc/mdz284)

Schneider CA, Rasband WS & Eliceiri KW 2012 NIH Image to ImageJ: 25 years of image analysis. *Nature Methods* **9** 671–675. (https://doi.org/10.1038/nmeth.2089)

Scott JE, Carlsson IB, Bavister BD & Hovatta O 2004 Human ovarian tissue cultures: extracellular matrix composition, coating density and tissue dimensions. *Reproductive Biomedicine Online* **9** 287–293. (https://doi.org/10.1016/s1472-6483(10)62143-8)

Talevi R, Sudhakaran S, Barbato V, Merolla A, Braun S, Nardo M Di, Costanzo V, Ferraro R, Iannantuoni N, Catapano G, *et al.* 2018 Is oxygen availability a limiting factor for in vitro folliculogenesis? *PLoS ONE* **13** e0192501. (https://doi.org/10.1371/journal.pone.0192501)

Telfer EE 2019 Future developments: in vitro growth (IVG) of human ovarian follicles. *Acta Obstetricia et Gynecologica Scandinavica* **98** 653–658. (https://doi.org/10.1111/aogs.13592)

Telfer EE, McLaughlin M, Ding C & Thong KJ 2008 A two-step serum-free culture system supports development of human oocytes from primordial follicles in the presence of activin. *Human Reproduction* **23** 1151–1158. (https://doi.org/10.1093/humrep/den070)

Ting AY, Yeoman RR, Lawson MS & Zelinski MB 2011 In vitro development of secondary follicles from cryopreserved rhesus macaque ovarian tissue after slow-rate freeze or vitrification. *Human Reproduction* **26** 2461–2472. (https://doi.org/10.1093/humrep/der196)

Venables WN & Ripley BD 2002 *Modern Applied Statistics with S*. Springer.

Walker CA, Bjarkadottir BD, Fatum M, Lane S & Williams SA 2019 Variation in follicle health and development in cultured cryopreserved ovarian cortical tissue: a study of ovarian tissue from patients undergoing fertility preservation. *Human Fertility* In press. (https://doi.org/10.1080/14647273.2019.1616118)

Wallace WHB 2011 Oncofertility and preservation of reproductive capacity in children and young adults. *Cancer* **117** (Supplement 10) 2301–2310. (https://doi.org/10.1002/cncr.26045)

Wright CS, Hovatta O, Margara R, Trew G, Winslon RML, Franks S & Hardy K 1999 Effects of follicle-stimulating hormone and serum substitution on the in-vitro growth of human ovarian follicles. *Human Reproduction* **14** 1555–1562. (https://doi.org/10.1093/humrep/14.6.1555)

Yasmin E, Balachandren N, Davies MC, Jones GL, Lane S, Mathur R, Webber L & Anderson 2018 Fertility preservation for medical reasons in girls and women: British Fertility Society Policy and Practice Guideline. *Human Fertility* **21** 3–26. (https://doi.org/10.1080/14647273.2017.1422297)

Received in final form 8 February 2021
Accepted 25 February 2021
Accepted Manuscript published online 26 February 2021

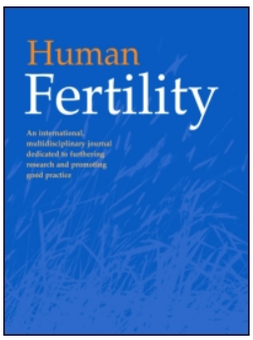

Taylor & Francis
Taylor & Francis Group

Human Fertility

an international, multidisciplinary journal dedicated to furthering research and promoting good practice

ISSN: 1464-7273 (Print) 1742-8149 (Online) Journal homepage: https://www.tandfonline.com/loi/ihuf20

Variation in follicle health and development in cultured cryopreserved ovarian cortical tissue: a study of ovarian tissue from patients undergoing fertility preservation

Charlotte A. Walker, Briet D. Bjarkadottir, Muhammad Fatum, Sheila Lane & Suzannah A. Williams

To cite this article: Charlotte A. Walker, Briet D. Bjarkadottir, Muhammad Fatum, Sheila Lane & Suzannah A. Williams (2019): Variation in follicle health and development in cultured cryopreserved ovarian cortical tissue: a study of ovarian tissue from patients undergoing fertility preservation, Human Fertility, DOI: 10.1080/14647273.2019.1616118

To link to this article: https://doi.org/10.1080/14647273.2019.1616118

Published online: 23 May 2019.

HUMAN FERTILITY
https://doi.org/10.1080/14647273.2019.1616118

Taylor & Francis
Taylor & Francis Group

ORIGINAL ARTICLE

Variation in follicle health and development in cultured cryopreserved ovarian cortical tissue: a study of ovarian tissue from patients undergoing fertility preservation

Charlotte A. Walker[a], Briet D. Bjarkadottir[a], Muhammad Fatum[a,b], Sheila Lane[c] and Suzannah A. Williams[a]

[a]Nuffield Department of Women's and Reproductive Health, University of Oxford, Oxford, UK; [b]Oxford Fertility, Institute of Reproductive Sciences, Oxford, UK; [c]Department of Paediatric Oncology and Haematology, Oxford University Hospitals NHS Foundation Trust, Oxford, UK

ABSTRACT

This study investigated how follicle health and development in human ovarian tissue cryopreserved for fertility preservation varied between patients before and after 6 d of *in vitro* culture. Ovarian tissue from 12 patients (9–25 years) was used. In 3 patients, a 1hr neutral red (NR) incubation was used to identify tissues with viable follicles. Tissues were fixed, sectioned and follicles staged and graded for health. Inter-patient differences were observed in the non-cultured tissue in the number of both healthy follicles ($p = 0.005$) and growing follicles ($p = 0.005$). After culture there was significant variation in the number of transitional, primary and secondary follicles between patients ($p < 0.001$). Asymmetric primary follicles with a single complete layer of granulosa cells plus two or more additional partial layers were 5.5 times more likely to be observed in cultured compared to non-cultured tissue ($p = 0.0063$). Non-cultured ($p = 0.0125$) and cultured ($p < 0.001$) tissue selected using NR had more healthy follicles compared to tissue not selected using NR. Non-cultured and cultured tissue selected using NR had more healthy follicles compared to tissue not selected using NR ($p = 0.0125$; $p < 0.001$). We demonstrate that inter-patient variation exists in the health and development of follicles before and after culture. Culture systems need to be optimized to support cryopreserved ovarian tissue and these findings should prompt researchers to consider patient variation when evaluating culture systems.

ARTICLE HISTORY
Received 26 November 2018
Accepted 7 March 2019

KEYWORDS
Cryopreservation; ovary; follicle; human; *in vitro* growth; cancer

Introduction

Cryopreservation of ovarian cortical tissue has been established as a successful method for preserving fertility in patients for whom traditional approaches, such as storage of mature eggs or embryos, are not possible. This includes pre-pubertal girls and women for whom cancer treatment cannot be delayed (Anderson, Wallace, & Telfer, 2017). Growth of follicles from this tissue *in vitro* is emerging as an alternative method to circumvent some of the limitations associated with transplantation (Nisolle, Casanas-Roux, Qu, Motta, & Donnez, 2000).

The overall goal of *in vitro* follicle growth is to generate systems that support development and maturation of a competent human egg for use by women at risk of premature ovarian insufficiency (De Vos, Smitz, & Woodruff, 2014; McLaughlin, Albertini, Wallace, Anderson, & Telfer, 2018; Xiao et al., 2015). For humans, an *in vitro* system capable of generating metaphase II oocytes from fresh cortical tissue has recently been described using a three-step culture method prior to *in vitro* maturation (McLaughlin et al., 2018). However, culture systems aiming to support the initiation of follicle growth and early development have predominantly used fresh tissue from healthy women undergoing gynaecological operations whose biology may differ from those who may benefit from fertility preservation. To date, there is no data regarding the variation in health and development of follicles *in vitro* from tissue cryopreserved for fertility preservation in women undergoing gonadotoxic treatments, despite the high importance of this for developing techniques for fertility restoration.

Follicle distribution in the cortex of human ovaries is extremely heterogeneous. The density of primordial follicles between different pieces of cortex from the same ovary can vary by greater than two orders of magnitude (Schmidt, Byskov, Nyboe Andersen, Muller,

CONTACT Suzannah A Williams suzannah.williams@wrh.ox.ac.uk Nuffield Department of Women's and Reproductive Health, University of Oxford, Level 3, Women's Centre, John Radcliffe Hospital, Oxford OX3 9DU, UK

& Yding Andersen, 2003). This creates challenges in identifying cortical tissue fragments with follicles for culture. Neutral Red (NR) is a weak cationic supravital dye that is soluble in water and has been used in cytotoxicity studies as a marker of cell viability (Allison & Young, 1964; Borenfreund & Puerner, 1985). It has been demonstrated to effectively label viable follicles within ovine cortical tissue and has subsequently been used to determine follicular density of fresh human cortical tissue or medulla by incubating the tissue for 4 h before visualization (Chambers, Gosden, Yap, & Picton, 2010; Kristensen et al., 2018). It remains to be investigated whether this dye can be incorporated into the workflow of human cortical strip culture without the use of a 4-h incubation to allow visualization of follicles in fresh tissue before culture.

The aims of this study were to determine: (i) how the health and developmental stage of follicles differs between women who have cryopreserved cortical tissue for fertility preservation; (ii) whether the *in vitro* developmental capacity of follicles from cryopreserved tissue varies between them; and (iii) whether incubating cortical tissue with NR for a short period of time to identify tissue with viable follicles could improve the number of viable follicles after 6 d of culture.

Materials and methods

Ethical approval

The use of human tissue was approved by Health Research Authority South Central – Oxford B Research Ethics Committee (REC reference: 14/SC/0041).

Ovarian tissue collection

Cryopreserved ovarian tissue was obtained from twelve patients aged 9–25 years. All were undergoing ovarian tissue cryopreservation, as a fertility preservation measure due to malignancy or blood disorder. None had received chemotherapy or radiation treatment prior to ovarian tissue cryopreservation. As part of the consent process, permission to use tissue in research had been obtained.

Chemicals and consumables

Leibovitz L-15 medium, McCoy's 5A (modified) HEPES buffered medium, L-glutamine and ascorbic acid were obtained from Thermo Fisher (Paisley, UK). Human serum albumin (HSA), ITS liquid media supplement (100×), sucrose, ethylene glycol, sodium pyruvate, NR, Bouin's solution and Whatman Nuclepore membranes were obtained from Sigma Aldrich (Poole, UK). Recombinant human follicle stimulating hormone (FSH; Gonal-F) was obtained from Merck Serono (Feltham, UK). Corning Costar tissue culture treated 24-well plates were obtained from Scientific Laboratory Supplies (Nottingham, UK).

Cryoprotection and cryopreservation

Ovarian tissue cryopreservation was performed by the Oxford Cell and Tissue Biobank. Cortical tissue cut into cortical strips (~2 × 1 × 5 mm) were placed into cryovials containing 1 mL of cryoprotectant medium (1.5 M ethylene glycol, 0.1 M sucrose, 10% (v/v) serum substitute supplement in L-15 medium) and incubated for 1 h at 4 °C before being frozen using a controlled rate slow freezer (IceCube 15M; SY-LAB, Norcross, GA). Following cryopreservation, the vials were stored in vapour phase liquid nitrogen.

Tissue thawing and cortical strip culture

Cryovials were held at room temperature for approximately 1 min before being immersed in a 30 °C water bath for 3 min. Cortical strips were washed through three thawing solutions containing a reversed ethylene glycol gradient (1, 0.5 and 0 M), 0.1 M sucrose and 3 mg/mL HSA in Leibovitz L-15 medium for 5 min and transferred to a petri dish containing Dissection Medium (3 mg/mL HSA, 100 U/mL penicillin, 100 μg/mL streptomycin, 2 mM L-glutamine and 2 mM sodium pyruvate in L-15 medium). Tissue was mechanically chopped using the McIlwain tissue chopper, and further cut manually using a scalpel and forceps into ~0.5 × 0.5 × 0.25 mm pieces.

Tissue pieces of uniform size were distributed randomly and evenly between wells of a 24-well plate with excess remnant tissue discarded. A portion of tissue fragments was fixed overnight in Bouin's fixative as a non-cultured control. Tissue was cultured on a polycarbonate membrane (13 mm diameter, 8 μm pore size) floating on 1 mL of culture medium in a 24-well culture plate; culture medium contained McCoy's 5A supplemented with 1 mg/mL HSA, 100 U/mL penicillin, 100 μg/mL streptomycin, 2 mM L-glutamine, 10 μg/mL insulin, 5.5 μg/mL transferrin, 5 ng/mL selenium, 50 μg/mL ascorbic acid and 12.5 IU/L recombinant human FSH. Cortical tissue was cultured for 6 d at 37 °C under 5% CO_2 in air, with half the medium being replaced with fresh medium every other day. Following the culture period, the tissue pieces were fixed overnight in

Table 1. Characteristics of patients diagnosed with malignant disease or blood disorder who underwent ovarian tissue cryopreservation for fertility preservation.

Patient	Age (years)	Post-pubertal	Regular periods	Diagnosis	Prior treatment	Time from surgery to cryopreservation
A	9	No	N/A	Medulloblastoma	None	3 h 16 min
B	11	No	N/A	Sickle cell	None	4 h 19 min
C	16	No	N/A	Osteosarcoma	None	5 h 20 min
D	16	Yes	Unknown	Ewing's sarcoma	None	5 h 10 min
E	17	Yes	Yes	Ewing's sarcoma	None	2 h 05 min
F	18	Yes	Unknown	Sickle cell	None	3 h 57 min
G	19	Yes	Unknown	Low-grade serous adenocarcinoma	None	6 h 15 min
H	22	Yes	Unknown[a]	Burkitt lymphoma stage 1A	None	4 h 18 min
I	22	Yes	Unknown	Atypical teratoid Rhabdoid tumour (Grade IV)	None	5 h 00 min
J	23	Yes	Yes	Breast cancer, grade 3, oestrogen positive, non-metastatic	None	3 h 05 min
K	23	Yes	Unknown[a]	Hodgkin lymphoma	None	4 h 20 min
L	25	Yes	Yes	Cervical cancer	None	3 h 32 min

[a]Patient taking the oral contraceptive pill.

Bouin's solution and stored in 70% ethanol until they were processed.

Neutral red (NR) visualization

To identify fragments containing follicles, after processing cortical tissue with the tissue chopper, fragments from patients E, I and L (Table 1) were incubated in NR (25 μg/mL in dissection medium) at room temperature for 1 h while the tissue was cut (as in the standard protocol). Allocation of tissue between groups was performed without a microscope to blind the researcher to the degree of staining and detail of the tissue pieces.

Histological analysis

The fixed ovarian tissue was dehydrated through a graded series of ethanol (70, 80, 95, 3 × 100%), cleared in xylene and embedded in paraffin wax at 64 °C for three hours. The wax-embedded tissue was serially sectioned at 5 μm and stained with haematoxylin and eosin.

Follicles were staged based on criteria described by Gougeon (1986); primordial (single layer of flattened pre-granulosa cells), transitional (single layer with at least one cuboidal granulosa cell), primary (complete layer of cuboidal granulosa cells) and secondary, two or more complete layers of cuboidal granulosa cells (Figure 1). Where follicles had a single complete layer of cuboidal cells, the number of any additional partial layers of granulosa cells was recorded. Non-growing follicles were those at the primordial stage. Transitional, primary and secondary follicles were classed as growing. Granulosa cell and oocyte pyknosis, and shrinkage of ooplasm were selected as markers for follicle health based on the existing literature and the ease of assessing health factors in a non-biased manner (Gougeon, 1986). Healthy follicles had a non-pyknotic non-shrunken oocyte with non-pyknotic granulosa cells, degenerating follicles had one of the above factors, while follicles were classified as atretic if they had both an oocyte with a pyknotic nucleus and pyknotic granulosa cells (Figure 2). All tissue sections were analysed for the presence of follicles, and only follicles with a visible nucleolus or a clearly defined nuclear membrane were assessed, to avoid double-counting. A blinded researcher performed follicle counts and assessment; a second blinded researcher confirmed repeatability.

Calculation of follicle density

To determine the volume of the tissue, the area of every 12th tissue section was measured using ImageJ 1.46r (National Institutes of Health, Bethesda, MD). Follicle density was determined by dividing the total number of follicles counted in a tissue sample by the tissue volume.

Statistical analysis and modelling

All statistical analyses were performed using R statistical software version 3.5.0 (R Foundation for Statistical Computing, Vienna, Austria). Statistical analysis was performed using Fisher's Exact Test. Tests adjusting for patient variation used the lme4 package in R (Bates, Mächler, Bolker, & Walker, 2015). All logistic regressions were offset for tissue volume and included patient as a random effect. Data are presented as mean or as odds ratio with 95% confidence intervals where available and statistical significance was defined

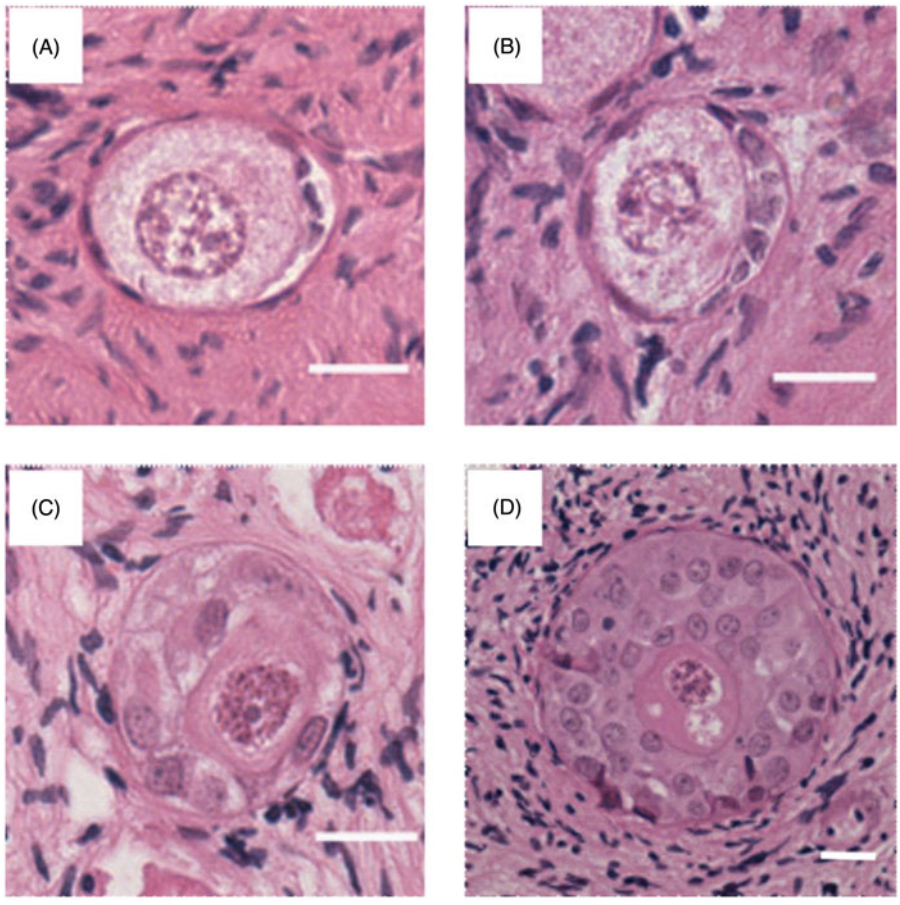

Figure 1. Developmental staging of human follicles from cryopreserved ovarian tissue from patients diagnosed with malignant disease or blood disorder. Representative images of follicles in cryopreserved-thawed ovarian tissue. Tissue was fixed in Bouin's, embedded and stained with haematoxylin and eosin. Follicles were staged as: (A) primordial with a single layer of flattened pre-granulosa cells; (B) transitional with a single layer of at least one cuboidal granulosa cell; (C) primary with a complete layer of cuboidal granulosa cells; or (D) secondary with two or more complete layers of cuboidal granulosa cells. Scale bar = 20 μm.

as $p < 0.05$. Due to the small number of secondary follicles observed, no statistical analysis was performed on this cohort.

Results

Patient characteristics

Nine of the twelve patients were confirmed as having gone through puberty, the remaining three had not. Of the nine post-pubertal patients, information about menstrual cycle was available for three who were reported as having regular cycles (Table 1). Two patients, where information about their menstrual cycle was unavailable, were taking the oral contraceptive pill. The mean age (±SEM) of patients who had gone through puberty was significantly higher than for those who had not (20.56 ± 1.04 *vs.* 12 ± 2.08 years, respectively; $p < 0.01$).

There was no difference in the time from tissue procurement to cryopreservation between the pre- and post-pubertal groups. The mean time from completion of surgery to start of cryopreservation was 4 h 13 ± 19 min (Table 1).

Follicular density of tissue post-cryopreservation from the 12 patients varied from 18.10 to 448.43 follicles/mm^3 between patient samples (Figure 3) and all cortical strips contained follicles. Despite the small sample of tissue and the known heterogeneity of follicle distribution in the ovary, there was a significant inverse correlation between follicular density and age ($r = -0.62$, $p < 0.05$).

Number of growing follicles in non-cultured cryopreserved tissue varies between patients

Follicles were observed in non-cultured tissue from 11 of the 12 patient samples. Non-growing follicles were

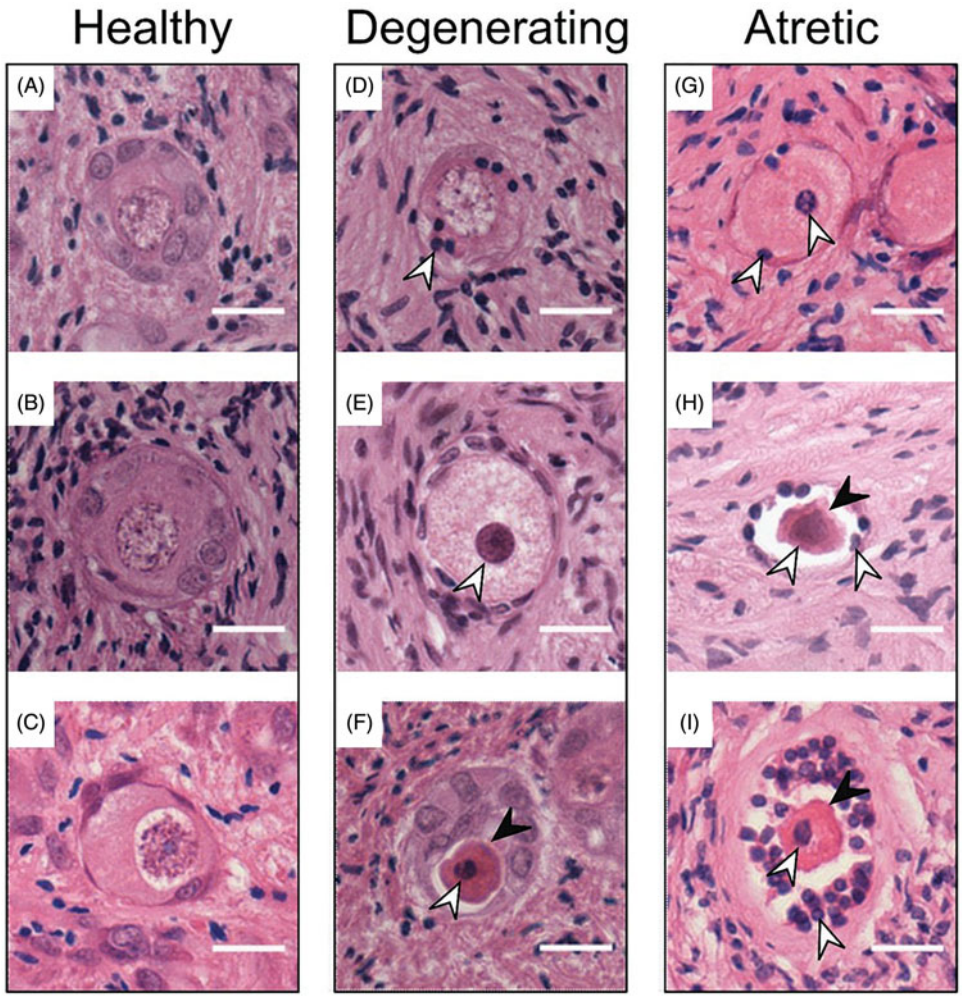

Figure 2. Classification of follicle health in human follicles from cryopreserved ovarian tissue from patients diagnosed with malignant disease or blood disorder. Follicle health was assessed based on the presence or absence of pyknotic granulosa cells, a pyknotic oocyte and a shrunken ooplasm: Images A–C show healthy follicles with healthy granulosa cells, a non-pyknotic and non-shrunken oocyte whereas degenerating follicles had either (D) pyknotic granulosa cells (white arrowhead), (E) a pyknotic oocyte (white arrowhead) with normal ooplasm or (F) a pyknotic oocyte (white arrowhead) with a shrunken ooplasm (black arrowhead) and normal granulosa cells. Atretic follicles had both pyknotic granulosa cells and a pyknotic oocyte (white arrowheads), without shrunken ooplasm (G), or with shrunken ooplasm (black arrowheads, H,I). Scale bar = 20 μm.

those classified as primordial based on morphology (Figure 1(A)), growing follicles were those classified as transitional, primary, or secondary (Figure 1(B–D)). The number of growing compared to non-growing follicles in uncultured tissue varied significantly based on patient and can be seen in Figure 4(A) ($p < 0.001$). Non-growing follicles were the dominant population in non-cultured tissue for five patient samples (patients A, B, E, H and I), an equal percentage of growing and non-growing were seen in two patient samples (patients C and D), and the percentage of growing follicles dominated in four patient samples (patients G, J, K and L). Interestingly, only growing follicles were observed in non-cultured tissue from patient K, however, as only three follicles were seen in this tissue (Table 2) it may be due to the small sample size.

Follicle health in non-cultured cryopreserved tissue varies between patients

Follicles were graded as being healthy, degenerating or atretic based on the presence or absence of pyknotic granulosa cells, a pyknotic oocyte and shrunken ooplasm (Figure 2). There was significant variation between patient samples in the percentage of healthy follicles in non-cultured tissue (Figure 4(B); $p < 0.001$).

In three patient samples, tissue fragments were preferentially selected for non-culture or culture based on visualization of follicles using the vital dye NR.

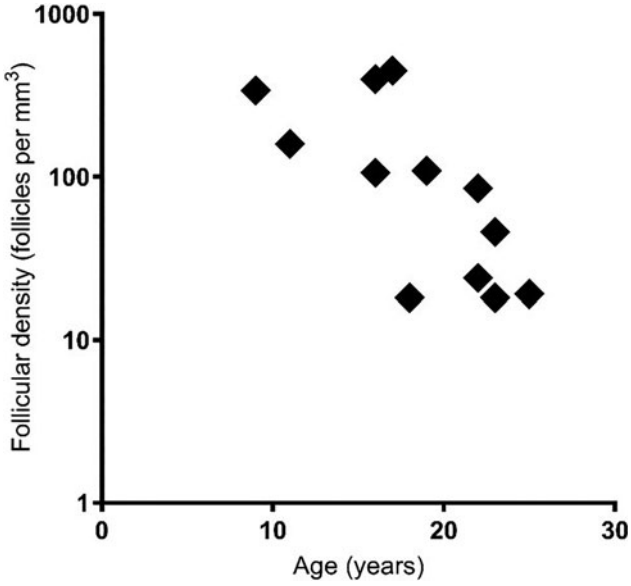

Figure 3. The density of follicles in relation to age in cryopreserved ovarian cortical tissue from 12 patients diagnosed with a malignant disease or blood disorder.

Tissues from these samples (patients E, I and J) showed a similar percentage of healthy follicles in the primordial and growing follicle populations. This was in contrast to the nine patient samples in which NR was not used as in five of these, the percentage of healthy follicles was greater in the primordial population compared to the growing population (Figure 4(C,D)).

The probability of a follicle being healthy in non-cultured tissue did not differ between pre- and post-pubertal patients and was unaffected by the time from surgery to cryopreservation.

Follicle health, but not development is greater in non-cultured tissue selected by neutral red staining

An example of a follicle with NR staining can be seen in Figure 5(A). In non-cultured tissue where NR was used to select tissue fragments as described above, the odds of a follicle being healthy was over 11 times that for follicles from tissue where NR was not used (Figure 5(B); OR = 11.4, 95% CI (1.7–77.4); $p = 0.0125$). There was a smaller percentage of growing follicles in tissue selected using NR though this was not significant (Figure 5(B)).

Cultured cryopreserved tissue has a dominant population of growing follicles in all patients

Overall, culture resulted in a significant change in the non-growing and growing follicle populations, with the odds of observing a growing follicle in cultured tissue being 52 times that of non-cultured tissue (OR = 52.44, 95% CI (37.05–76.41), $p < 0.0001$).

The health and development of follicles in tissue from each patient samples are detailed in Figure 6. There was no difference in the percentage of follicles growing following culture (Figure 6(A)), however, there was variation within the growing population in the proportion of follicles at the transitional, primary and secondary stages (Figure 6(B)). Primary follicles were the dominant growing follicles in all patient samples except for patient K and patient B where 50% of follicles were transitional and 50% were primary. The number of secondary follicles observed after 6 d of culture was low compared to transitional and primary follicles and represented at most 9% of the total follicles in cultured tissue (Figure 6(B); Patient C). Between 8 and 80% of follicles were multi-laminar follicles with more than one layer of granulosa cells (Figure 6(C)). The percentage of growing follicles in tissue after 6 d of culture was not different between fragments that had been selected based on NR staining and those that had not been selected based on NR (Figure 6(F)).

Neutral red selected tissue has superior follicle health post-culture

Despite significant activation and development of follicles in cultured tissue, overall follicle survival in cultured tissue was low. Following 6 d of culture, all follicles from tissue not selected using NR showed some sign of degeneration (Figure 6(E)), however, this is not surprising as 78.08% of follicles in this cohort showed some sign of degeneration in non-cultured cryopreserved tissue (Figure 5). In tissue selected by NR staining, 18.14% ($n = 612$; 3 patients) of follicles were healthy after 6 d of culture (Figure 6(E)). Since 60.39% of follicles were healthy in non-cultured tissue selected using NR (Figure 5), this meant that follicles in these tissues were over 13 times more likely to be healthy in non-cultured compared to cultured tissue (OR= 13.67, 95% CI (10.04–18.91), $p < 0.0001$). The odds of a follicle from NR selected tissue being healthy after 6 d in culture were 26 times that of a follicle from tissue where NR was not used to select fragments for culture (Figure 6(E); OR = 108.9, 95% CI (12.3–962.8), $p < 0.001$).

Follicles grown in culture have asymmetric granulosa cell distribution

In cultured tissue, primary follicles were 3.2 times more likely to have at least one additional partial

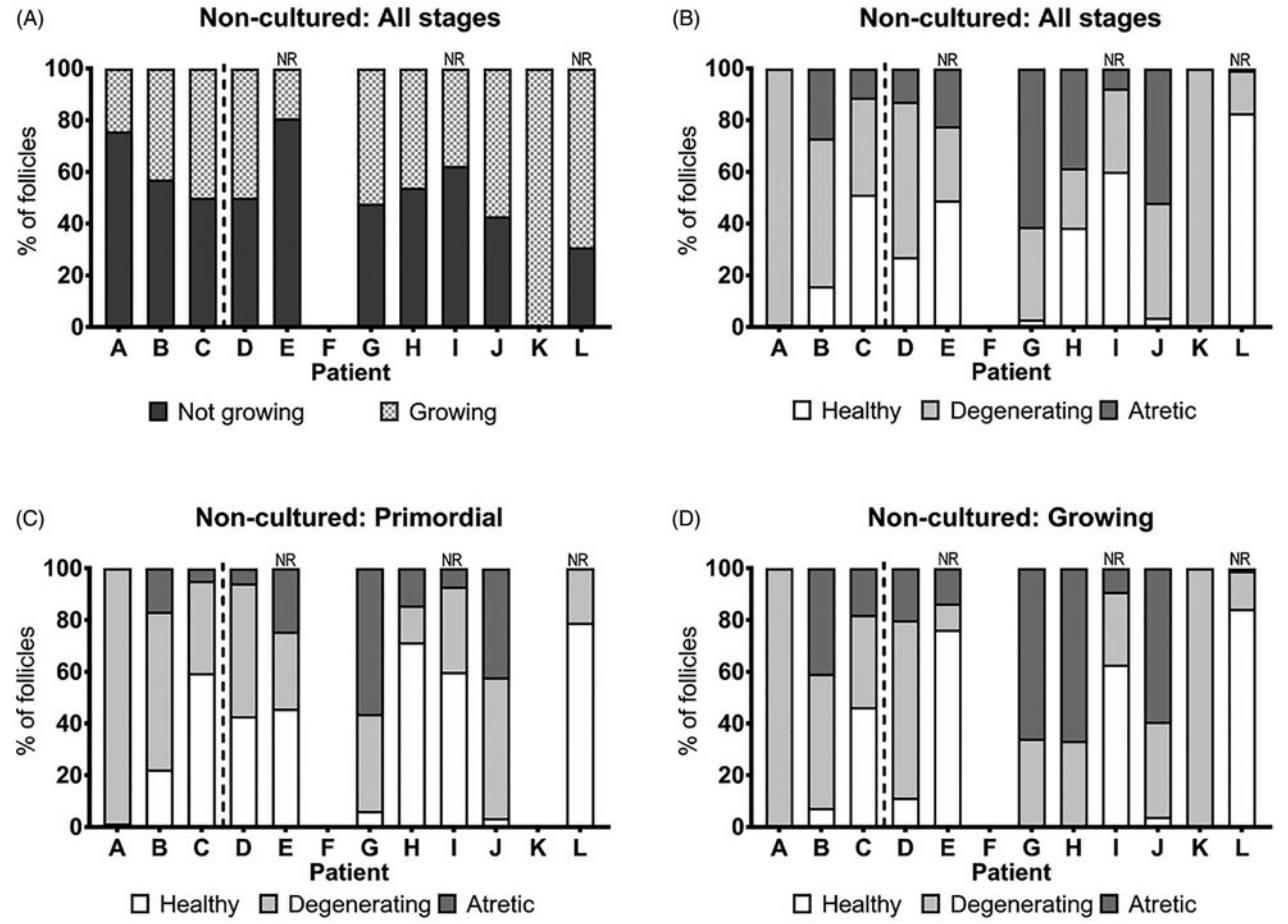

Figure 4. Variation between patients in the percentage of growing and healthy follicles in non-cultured cryopreserved human ovarian tissue from patients diagnosed with malignant disease or blood disorder. Patients are listed by ascending age with the dashed line indicating the split between those who were not post-pubertal (patients A–C) and those who were post-pubertal (patients D–L). Significant variation in the number of growing follicles was observed in non-cultured cryopreserved ovarian cortical tissue from all patients with follicles (A) ($p < 0.001$, Fisher's Exact Test); no follicles were observed in non-cultured tissue from patient F. The number of healthy (no morphological evidence of degeneration), degenerating (presence of either a pyknotic oocyte, pyknotic granulosa cells or shrunken ooplasm), and atretic (presence of both pyknotic oocyte and pyknotic granulosa cells) varied significantly between patients (B) ($p < 0.001$, Fisher's Exact Test). Images (C,D) show the percentage of healthy primordial follicles was greater than that of the growing follicle population in non-cultured tissue, with the exception of those follicles stained with neutral red (NR; patients E, I and L) which showed a similar percentage of healthy follicles in the primordial and growing follicle populations. NR: neutral red staining used to select tissue.

Table 2. Number of follicles observed in cultured and non-cultured cryopreserved human ovarian tissue.

Patient	Non-cultured	Cultured	Total	Selected using neutral red
A	99	27	126	–
B	63[a]	85	148	–
C	168[a]	67[a]	235	–
D	70	58	128	–
E	1224	489[a]	1713	Yes
F	0	14	14	–
G	67[a]	68	135	–
H	13	14[a]	27	–
I	874	90	964	Yes
J	133[a]	15[a]	148	–
K	3[a]	12	15	–
L	139	33[a]	172	Yes

[a]Secondary follicles present.

granulosa cell layer compared to non-cultured primary follicles (OR = 3.17, 95% CI (1.83–5.80), $p < 0.001$; Figure 7(A)). Asymmetric follicles, primary follicles with two or more partial layers of granulosa cells and only one complete layer of granulosa cells, were observed in eight of the cultured patient samples (Figure 7(C,D)). By contrast in non-cultured tissue, only two asymmetric primary follicles were observed, each in fragments of tissue from different patients (Figure 7(A)). The odds of a primary follicle being asymmetric in cultured tissue was 5.5 times that of non-cultured tissue (OR = 5.46, 95% CI (1.40–46.92), $p = 0.0063$).

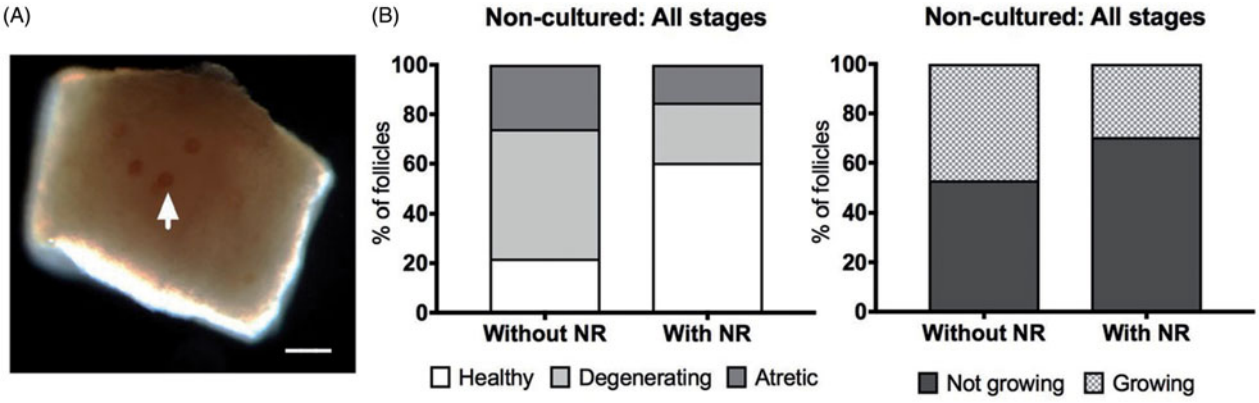

Figure 5. Use of neutral red facilitates selection of tissue fragments containing viable follicles in cryopreserved ovarian tissue from patients diagnosed with malignant disease or blood disorder. Cortical tissue incubated in neutral red NR for 1 h revealed viable follicles stained red shown in image (A) (white arrowhead). Thawed cryopreserved tissue fragments with follicles identified by NR staining for 1 h ($n = 3$ patients) contained significantly more healthy follicles compared to tissue where NR was not used (B) ($n = 9$ patients) ($p < 0.02$, OR = 11.4, 95% CI (1.7–77.4), logistic regression adjusted for tissue volume with patient as a random effect). There was no difference in the number of growing follicles in non-cultured tissue selected by NR staining compared to tissue where NR was not used. Scale bar = 100 μm.

Discussion

This study is, to our knowledge, the first to evaluate the patient-specific health and development of follicles following *in vitro* culture of cortical tissue cryopreserved for fertility preservation. Furthermore, we describe a protocol for human cortical strip culture utilizing NR to identify fragments with viable follicles for culture.

Our results highlight wide variation between patients in the health and developmental stage of follicles in cryopreserved ovarian cortical tissue. Early studies looking at the viability of ovarian cortical tissue cryopreserved in humans focused on success of xenotransplantation studies to demonstrate function without accompanying histological assessment. Variation and lack of clarity in morphological criteria for atresia between studies, as well as differing methods of cryoprotection, has made it challenging to define a baseline for cryopreservation-derived follicle degeneration. Here, we describe the morphological criteria assessed, providing images of each variation of follicle health we observed. Variation in follicle health post-thaw may be tied to follicle health in fresh tissue as despite finding no difference between fresh and frozen-thawed follicles, 27% of follicles in fresh tissue showed multiple signs of atresia; eosinophilia of the ooplasm, contraction and clumping of the chromatin material, and wrinkling of the nuclear membrane (Hovatta et al., 1996).

We found the use of just 1 h of NR incubation effective and easy to implement within the culture workflow with follicles identified in thin cortical fragments by their red staining. When tissue with viable follicles was selected by NR-staining, a significantly greater number of follicles in non-cultured tissue had a healthy morphology (60% compared to 22%, respectively). Our findings support those from Kristensen et al. (2018) who used a 4 h NR incubation to demonstrate the specificity of NR for viable follicles in cortical tissue from women undergoing fertility preservation before gonadotoxic treatment. Additionally, our results demonstrate that a shorter NR incubation period is adequate to identify tissue fragments with viable follicles, enhancing the value of such a technique in selecting tissue for culture with the aim of optimizing the proportion of healthy follicles.

In several patients, the percentage of multi-layered follicles present after 6 d of culture was equal to or greater than that published by McLaughlin, Kinnell, Anderson, and Telfer (2014) indicating both methods support equivalent follicle development. Interestingly, a significant proportion of primary follicles in cultured tissue were asymmetric, with two or more partial granulosa cell layers in addition to a single complete layer. This finding is significant as current multi-step *in vitro* protocols involve the excision of secondary follicles based on size following cortical strip culture (McLaughlin et al., 2018; Telfer, McLaughlin, Ding, & Thong, 2008). However, based on size asymmetric follicles would be indistinguishable from non-asymmetric follicles when using a dissecting, brightfield microscope. It is unclear whether the asymmetry is a result of the physical culture environment or whether it is a result of accelerated growth due to culture conditions. Furthermore, it is important to ascertain the impact of

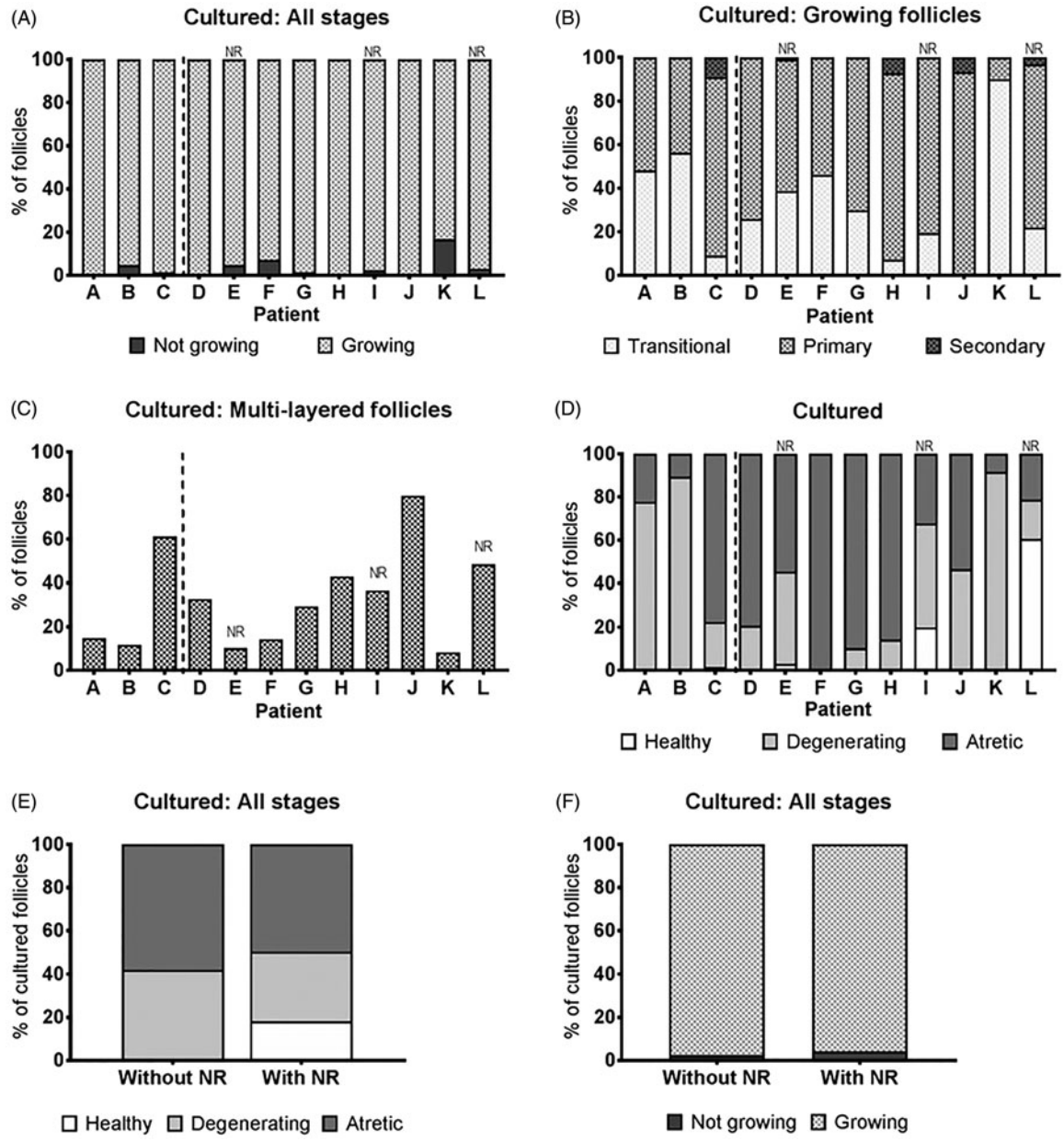

Figure 6. Variation between patients in percentage of growing and healthy follicles and the effect of tissue selection using neutral red in cultured cryopreserved ovarian tissue from patients diagnosed with malignant disease or blood disorder. There was no variation in the overall number of growing follicles in cultured cryopreserved ovarian cortical tissue (A) ($p = 0.289$, Fisher's Exact Test), however, within the growing population of follicles in cultured tissue (B), the relative number of transitional, primary and secondary follicles varied between patients ($p < 0.001$, Fisher's Exact Test), as did the percentage of multi-layered follicles, multilaminar follicles with more than one layer of granulosa cells (C). There was significant variation in the number of healthy, degenerating and atretic follicles between patients (D) ($p < 0.001$, Fisher's Exact Test). Tissue selection using neutral red had a significant impact on the proportion of healthy follicles present (E) ($p < 0.001$, OR = 108.9, 95% CI (12.3–962.8), logistic regression adjusted for tissue volume with patient as a random effect) but did not impact the number of growing follicles (F) ($p > 0.05$, Fisher's Exact Test). NR: neutral red staining used to select tissue.

asymmetry on subsequent follicle growth and developmental competence of the enclosed oocytes, particularly since current follicle selection for further development would not differentiate between them and non-asymmetric follicles.

Follicle health declines over the course of culture and there is evidence to suggest that this decline is more marked in cryopreserved tissue (Hovatta, Silye, Abir, Krausz, & Winston, 1997). We assessed if tissue selection using NR-staining would lead to better follicle development after culture. When NR was not used, nearly all follicles showed some sign of degeneration after 6 d of culture which was unsurprising given that only 22% were healthy in the non-cultured tissue.

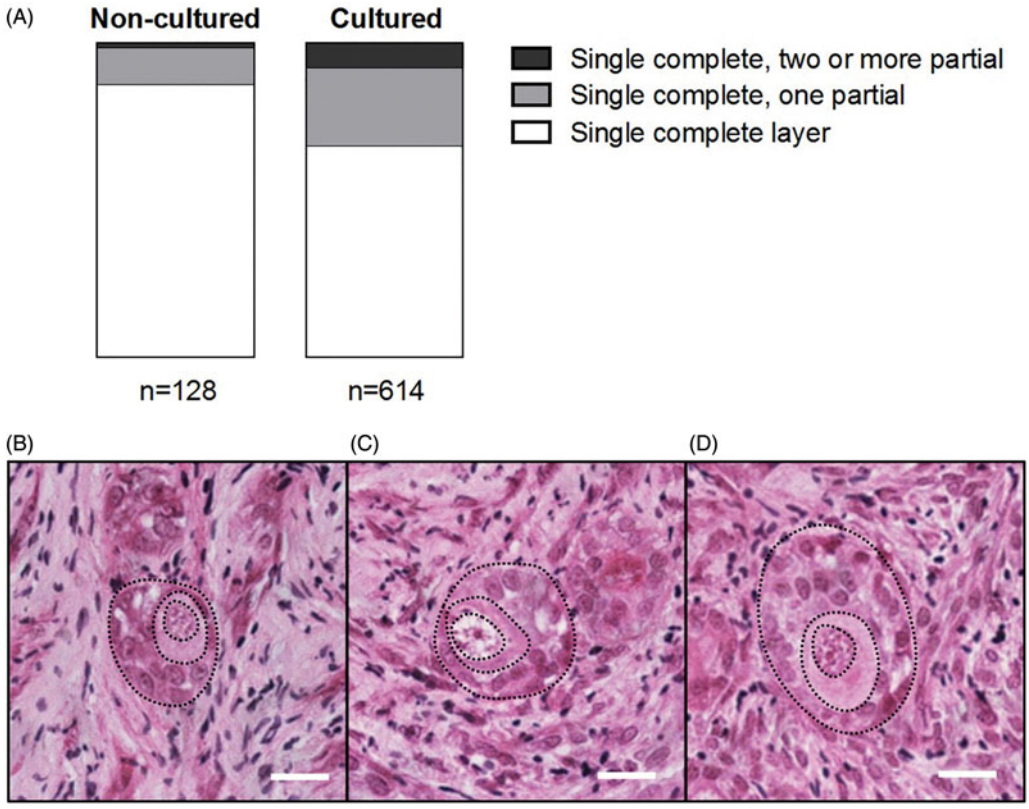

Figure 7. Asymmetric granulosa cell layers were more common in primary follicles in cultured cryopreserved tissue from patients diagnosed with malignant disease or blood disorder. Asymmetric primary follicles with variable numbers of partial granulosa cell layers were observed in non-cultured and cultured tissue. Primary follicles were significantly more likely to be asymmetric (those with a single complete layer of granulosa cells and two or more partial layers) with culture (A) (OR = 1117.3, 95% CI (250.2–4990.7), $p < 0.0001$, logistic regression adjusted for tissue volume with patient as a random effect). A follicle with a single complete granulosa cell layer and one partial layer is shown in image (B). Asymmetric primary follicles with a single complete granulosa cell layer and two or three partial layers are shown in images (C,D), respectively. Scale bar = 20 μm.

By contrast from 60% healthy follicles present in NR-selected non-cultured tissue, 18% of follicles retained a healthy morphology. These results are consistent with the 2.5-to-3-fold decrease in the proportion of healthy follicles reported by other groups culturing cryopreserved tissue over a similar timeframe, despite differences in culture systems (Asadi-Azarbaijani et al., 2016; Azarbaijani et al., 2015; Hovatta et al., 1997; Sanfilippo et al., 2013).

Although this analysis was based on a small volume of tissue per patient, an inverse correlation between age and follicle density was observed, confirming and extending that reported by Schmidt et al. (2003) with a sample of tissue from 21 women. The heterogeneity in follicle distribution within the human cortex is well described (Poirot et al., 2002; Qu, Godin, Nisolle, & Donnez, 2000; Schmidt et al., 2003), and has been cited as a strong reason that multiple pieces of ovarian cortex should be replaced upon re-implantation. It is possible that this heterogeneity extends to the response of follicles within a single ovary to the effects of cryopreservation, culture, or transplantation and the variation between patients reported in this study lends support to this idea.

In conclusion, *in vitro* development of eggs remains an exciting option for fertility restoration, but variation between patients may necessitate a more individual approach to downstream treatment options. We demonstrated here for the first time that there is variation between patients both in the health of non-cultured tissue post-cryopreservation as well as the health and development after 6 d in culture. The culture system described was effective in initiating follicle activation and growth in this tissue, but optimization is required to improve the survival of follicles across the culture period. Given the heterogeneity of tissue and clear variation in follicle health post-thaw in these patients, demonstrating that using the non-toxic viability marker NR in the existing culture workflow as described here to select tissue is an important advance in improving the efficiency and effectiveness of *in vitro* follicle development as an alternative method of fertility restoration.

Acknowledgements

The authors would like to thank all staff and the Oxford Cell and Tissue Biobank for their assistance in obtaining patient samples. Thanks go to Prof. Norah Spears for assistance in establishing culture techniques.

Disclosure statement

No potential conflict of interest was reported by the authors.

Funding

The study was supported by a joint scholarship to C.A.W from the Clarendon fund and NDWRH, and by an Oxford-MRC Doctoral Training Partnership (Oxford-MRC DTP) to B.D.B.

References

Allison, A., & Young, M. (1964). Uptake of dyes and drugs by living cells in culture. *Life Sciences*, *3*, 1407–1414. doi: 10.1016/0024-3205(64)90082-7.

Anderson, R.A., Wallace, W.H.B., & Telfer, E.E. (2017). Ovarian tissue cryopreservation for fertility preservation: Clinical and research perspectives. *Human Reproduction Open*, *2017*, hox001. doi: 10.1093/hropen/hox001.

Asadi-Azarbaijani, B., Sheikhi, M., Nurmio, M., Tinkanen, H., Juvonen, V., Dunkel, L., … Jahnukainen, K. (2016). Minimal residual disease of leukemia and the quality of cryopreserved human ovarian tissue *in vitro*. *Leukemia and Lymphoma*, *57*, 700–707. doi: 10.3109/10428194.2015.1065980.

Azarbaijani, B.A., Sheikhi, M., Oskam, I.C., Nurmio, M., Laine, T., Tinkanen, H., … Jahnukainen, K. (2015). Effect of previous chemotherapy on the quality of cryopreserved human ovarian tissue in vitro. *PLoS One*, *10*, e0133985. doi: 10.1371/journal.pone.0133985.

Bates, D., Mächler, M., Bolker, B., & Walker, S. (2015). Fitting linear mixed-effects models using lme4. *Journal of Statistical Software*, *67*, 1–48. doi: 10.18637/jss.v067.i01.

Borenfreund, E., & Puerner, J.A. (1985). Toxicity determined in vitro by morphological alterations and neutral red absorption. *Toxicology Letters*, *24*, 119–124. doi: 10.1016/0378-4274(85)90046-3.

Chambers, E., Gosden, R., Yap, C., & Picton, H. (2010). In situ identification of follicles in ovarian cortex as a tool for quantifying follicle density, viability and developmental potential in strategies to preserve female fertility. *Human Reproduction*, *25*, 2559–2568. doi: 10.1093/humrep/deq192.

De Vos, M., Smitz, J., & Woodruff, T.K. (2014). Fertility preservation in women with cancer. *The Lancet*, *384*, 1302–1310. doi: 10.1016/S0140-6736(14)60834-5.

Gougeon, A. (1986). Dynamics of follicular growth in the human: A model from preliminary results. *Human Reproduction*, *1*, 81–87. doi: 10.1093/oxfordjournals.humrep.a136365.

Hovatta, O., Silye, R., Abir, R., Krausz, T., & Winston, R. (1997). Extracellular matrix improves survival of both stored and fresh human primordial and primary ovarian follicles in long-term culture. *Human Reproduction*, *12*, 1032–1036. doi: 10.1093/humrep/12.5.1032.

Hovatta, O., Silye, R., Krausz, T., Abir, R., Margara, R., Trew, G., … Winston, R.M.L. (1996). Cryopreservation of human ovarian tissue using dimethylsulphoxide and propanediol-sucrose as cryoprotectants. *Human Reproduction*, *11*, 1268–1272. doi: 10.1093/oxfordjournals.humrep.a019370.

Kristensen, S.G., Liu, Q., Mamsen, L.S., Greve, T., Pors, S.E., Bjørn, A.B., … Andersen, C.Y. (2018). A simple method to quantify follicle survival in cryopreserved human ovarian tissue. *Human Reproduction*, 33, 2276–2284. doi: 10.1093/humrep/dey318.

McLaughlin, M., Albertini, D.F., Wallace, W.H.B., Anderson, R.A., & Telfer, E.E. (2018). Metaphase II oocytes from human unilaminar follicles grown in a multi-step culture system. *MHR: Basic Science of Reproductive Medicine*, *24*, 135–142. doi: 10.1093/molehr/gay002.

McLaughlin, M., Kinnell, H.L., Anderson, R.A., & Telfer, E.E. (2014). Inhibition of phosphatase and tensin homologue (PTEN) in human ovary *in vitro* results in increased activation of primordial follicles but compromises development of growing follicles. *Molecular Human Reproduction*, *20*, 736–744. doi: 10.1093/molehr/gau037.

Nisolle, M., Casanas-Roux, F., Qu, J., Motta, P., & Donnez, J. (2000). Histologic and ultrastructural evaluation of fresh and frozen-thawed human ovarian xenografts in nude mice. *Fertility and Sterility*, *74*, 122–129. doi: 10.1016/S0015-0282(00)00548-3.

Poirot, C., Vacher-Lavenu, M.C., Helardot, P., Guibert, J., Brugières, L., & Jouannet, P. (2002). Human ovarian tissue cryopreservation: Indications and feasibility. *Human Reproduction*, *17*, 1447–1452. doi: 10.1093/humrep/17.6.1447.

Qu, J., Godin, P.A., Nisolle, M., & Donnez, J. (2000). Distribution and epidermal growth factor receptor expression of primordial follicles in human ovarian tissue before and after cryopreservation. *Human Reproduction*, *15*, 302–310. doi: 10.1093/humrep/15.2.302.

Sanfilippo, S., Canis, M., Romero, S., Sion, B., Déchelotte, P., Pouly, J.L., … Brugnon, F. (2013). Quality and functionality of human ovarian tissue after cryopreservation using an original slow freezing procedure. *Journal of Assisted Reproduction and Genetics*, *30*, 25–34. doi: 10.1007/s10815-012-9917-5.

Schmidt, K.L., Byskov, A.G., Nyboe Andersen, A., Muller, J., & Yding Andersen, C. (2003). Density and distribution of primordial follicles in single pieces of cortex from 21 patients and in individual pieces of cortex from three entire human ovaries. *Human Reproduction*, *18*, 1158–1164. doi: 10.1093/humrep/deg246.

Telfer, E.E., McLaughlin, M., Ding, C., & Thong, K.J. (2008). A two-step serum-free culture system supports development of human oocytes from primordial follicles in the presence of active in. *Human Reproduction*, *23*, 1151–1158. doi: 10.1093/humrep/den070.

Xiao, S., Zhang, J., Romero, M.M., Smith, K.N., Shea, L.D., & Woodruff, T.K. (2015). *In vitro* follicle growth supports human oocyte meiotic maturation. *Scientific Reports*, *5*, 17323. doi: 10.1038/srep17323.

Bendola Publishing
Journal of Fertility Preservation
Vol. 1 (2020), Article ID 246108, 10 pages
doi:10.32371/jfp/246108

Research Article

The Effect of Delayed Processing on Ovarian Tissue Stored for Fertility Preservation

M. S. Zemyarska,[1] B. D. Bjarkadottir,[1] X. Wei,[1] C. A. Walker,[1] S. M. Lane,[2] J. Davies,[3] and S. A. Williams[1]

[1]*Nuffield Department of Women's and Reproductive Health, Women's Centre, John Radcliffe Hospital, University of Oxford, Oxford OX3 9DU, UK*
[2]*Department of Paediatric Oncology and Haematology, Children's Hospital Oxford, Oxford University Hospitals NHS Foundation Trust, Oxford OX3 9DU, UK*
[3]*Oxford Cell and Tissue Biobank, Children's Hospital Oxford, Oxford University Hospitals NHS Foundation Trust, Oxford OX3 9DU, UK*
Address correspondence to S. A. Williams, suzannah.williams@wrh.ox.ac.uk

Received 7 July 2020; Revised 11 October 2020; Accepted 12 October 2020

Abstract *Background.* Ovarian tissue cryopreservation (OTC) is important for fertility preservation and conservation. Delay in OTC can occur for transport or workflow management, yet little is understood about the effect of this on the tissue. *Objective.* To determine if a delay of 24–48 h to OTC affects primordial follicle (PF) health. *Methods.* Ovaries ($n = 6$ sheep) were processed immediately or after storage at 4 °C (24 h, 48 h). Tissue was fixed fresh, after cryopreservation or 10-day xenotransplantation. Morphological assessment of follicle health and development was performed. *Findings.* A total of 1,541 follicles were analysed. A 24 h processing delay did not impact PF health in fresh or cryopreserved tissue. In fresh tissue, a 48 h delay had an adverse effect on PF health (OR = 2.47, 95% CI 1.29–4.71). Interestingly, a 48 h delay resulted in cryopreserved tissue being less likely to be graded as abnormal compared to control (OR = 0.56, 95% CI 0.36–0.87). There was no difference in PF health or development across groups following xenotransplantation. *Conclusion.* Ovarian tissue can be stored for up to 48 h prior to cryopreservation with no net impact on PF morphology which is indicative of health.

Keywords fertility preservation; delayed processing; ovarian cryopreservation; follicle; human; sheep; conservation

1. Introduction

At present, over 80% of children and adolescents diagnosed with cancer will survive the disease and reach adulthood [1]. Furthermore, as of 2011, there are an estimated 388,000 childhood cancer survivors in the US [2] and over 30,000 in the UK [3]. Childhood cancer treatment can, however, often be associated with a significant negative impact on the growth, development and, commonly, the fertility of young patients [4]. Thus, fertility preservation is of importance to young oncology patients, in order to prevent further emotional distress at the time of cancer diagnosis and long-term negative impact on the recovery and future wellbeing of childhood cancer survivors [5].

Ovarian tissue cryopreservation (OTC) is a method of fertility preservation that is becoming increasingly well-established world-wide. This involves dissection, cryoprotection and freezing of the ovarian cortex with the aim of preserving the primordial pool of follicles contained within. Importantly, although the intervention is still considered experimental in several countries, as of 2017, an estimated 130 pregnancies have been achieved after ovarian tissue transplantation globally [6]. However, OTC remains a specialised procedure, which requires practical experience, specialist equipment and dedicated facilities, which comply with EU and/or national regulations. As a result, although individual experimental cases have been reported from 21 countries [7], the availability of the technique as a modality of fertility preservation is limited [8], while the need for it may continue to rise.

One suitable approach to improve accessibility to OTC involves ovarian tissue being procured at various satellite clinics and transported to a central cryopreservation facility; this has been termed the "Danish model" [8,9]. However, the Danish model may require overnight storage of the tissue to allow for long-distance transportation of the samples and co-ordination and workload management at the cryopreservation facility. This may create a delay between ovarian tissue retrieval and processing for cryopreservation, during which the ovary is in a state of ischaemia, which can cause nutrient deprivation, hypoxia and, as a result, cell death [10]. The process of tissue cryopreservation and thawing is further associated with great physiological stress to living cells and tissues due to the dramatic changes in osmolarity and temperature experienced by the tissue, as well as the formation of structurally disruptive ice crystals [11]. Hence, it is of concern that pre-exposure of the ovarian tissue to challenging conditions such as prolonged cold ischaemia has the potential to exacerbate the damaging effects of freeze-thaw on tissue health and integrity, even if no direct effects were observed in fresh tissue.

At present, two case reports of cryopreservation delay for up to 20 h at 4 °C with one subsequent live birth have provided proof of principle that follicles can survive freeze-delay and that ovarian cortical tissue can retain graft functionality [8,12]. However, the impact of cryopreservation delay on the health of the primordial pool remains controversial, with studies reporting either no effect on follicle density and health [13] or a negative effect on both [14].

In this context, the present study set out to examine the effect of delayed processing and cryopreservation on ovarian tissue stored for fertility preservation using tissue processed in a clinically relevant manner. The sheep was used as a model organism for three reasons: (1) its structural similarity with human ovaries [15]; (2) human OTC has been largely optimised using the sheep as a model; and (3) it is the only species, aside from rodents and primates, in which a live birth has been achieved after transplantation of frozen-thawed ovarian tissue [16]. As the clinical value of cryopreserved ovarian tissue is largely determined by its potential to restore fertility following autologous grafting, xenotransplantation into immunodeficient mice was employed to examine the effect of delayed processing on in vivo development after cryopreservation and thawing. The aim of the study was to establish if processing delay of 24 h or 48 h had an effect on primordial follicle morphology in fresh, frozen-thawed and xenotransplanted ovine ovarian cortical tissue.

2. Materials and methods

2.1. Tissue collection

Pairs of ovaries from six female lambs (*Ovis aries*, breed unknown) were collected from a local abattoir and transported on ice in 100 mL of transport medium (Leibovitz's L-15 medium [Thermo Fisher, UK] supplemented with 100 U/mL penicillin and 100 μg/mL streptomycin [Sigma, UK] and 2.5 μg/mL amphotericin B [Sigma]). Upon arrival at the laboratory, one ovary from each pair was immediately processed for cryopreservation (no delay), while the other ovary was stored at 4 °C in transport medium for 24 h or 48 h.

2.2. Ovarian tissue processing and cryopreservation

Ovaries were processed for cryopreservation using procedures aligned with the relevant standard operating procedures (SOPs) applied at the Oxford Cell and Tissue Biobank (Oxford, UK) [17,18], with some modification. Each ovary was bivalved and the ovarian medulla was gently dissected away using curved scissors under aseptic conditions. The outermost 1 mm of the ovarian cortex was cut to strips of approximately $5 \times 2 \times 1$ mm using a surgical scalpel blade. All tissue handling was carried out in transport media on a *Medicool* ice block. Cortical strips were either fixed directly after processing (fresh samples) or cryopreserved. For cryopreservation, individual cortical strips were transferred to Nunc cryotubes and equilibrated in 1 mL of cryoprotectant medium containing L-15 supplemented with 1.5 M ethylene glycol (Sigma), 0.1 M sucrose (Sigma), and 3 mg/mL bovine serum albumin (BSA, Fisher Scientific, UK) for 1 h on ice. Cryopreservation was carried out in a controlled-rate freezer (IceCube 14S, SY-LAB, Sweden) using the following cooling programme: start temperature: 4 °C; cooling rate I: −2 °C/min to −9 °C; cooling rate II: −0.3 °C/min to −40 °C; cooling rate III: −10 °C/min to −140 °C. Manual seeding was performed at −9 °C and after freezing samples were stored in vapour phase liquid nitrogen.

2.3. Tissue thawing

Cryotubes were thawed in a water bath at 30 °C for 3 min, after which cortical strips were washed through three thawing solutions, containing a decreasing gradient of ethylene glycol (1 M, 0.5 M and 0 M), 0.1 M sucrose and 3 mg/mL BSA in L-15 medium, for 5 min each at room temperature. For samples that were to be xenotransplanted, 2.5 μg/mL amphotericin B, 100 U/mL penicillin, and 100 μg/mL streptomycin were added to the thawing solutions. Tissue was transplanted within 1 h of thawing.

2.4. Mice

Immunodeficient female mice (SCID; CB17/Icr-Prkdc^{SCID}/IcrIcoCrl) were obtained from Charles River Laboratories (Kent, UK) and housed together in a cage with filtered air supply under a 12:12 h light-dark cycle with ad libitum access to sterile food and water. The animals were acclimatised for two weeks prior to surgery and xenotransplantation was carried out at 8 weeks of age.

2.5. Ethics approval

Animal work was carried out in accordance with project license number 30/3352 granted to Dr Suzannah Williams under The Animals (Scientific Procedures) Act 1986.

2.6. Xenotransplantation

Thawed cortical strips ($1 \times 1 \times 3$ mm) were transplanted subcutaneously to the left flank of immunocompromised mice (Supplementary Figure 1). Four strips were transplanted to each mouse via two incisions each leading to two separate pockets. For each mouse, strips from one ovarian pair (no delay and 24 h delay) were transplanted into two pockets created from the first incision and strips from another ovarian pair (no delay and 48 h delay) were transplanted into two pockets created from the second incision. Each graft's position was secured in the pocket before the incision was closed. Mice were housed individually for the first 24 h after surgery. Recovery was monitored by observation and measuring body weight post-transplant; mice were weighed twice daily in the first 48 h and once daily thereafter. After

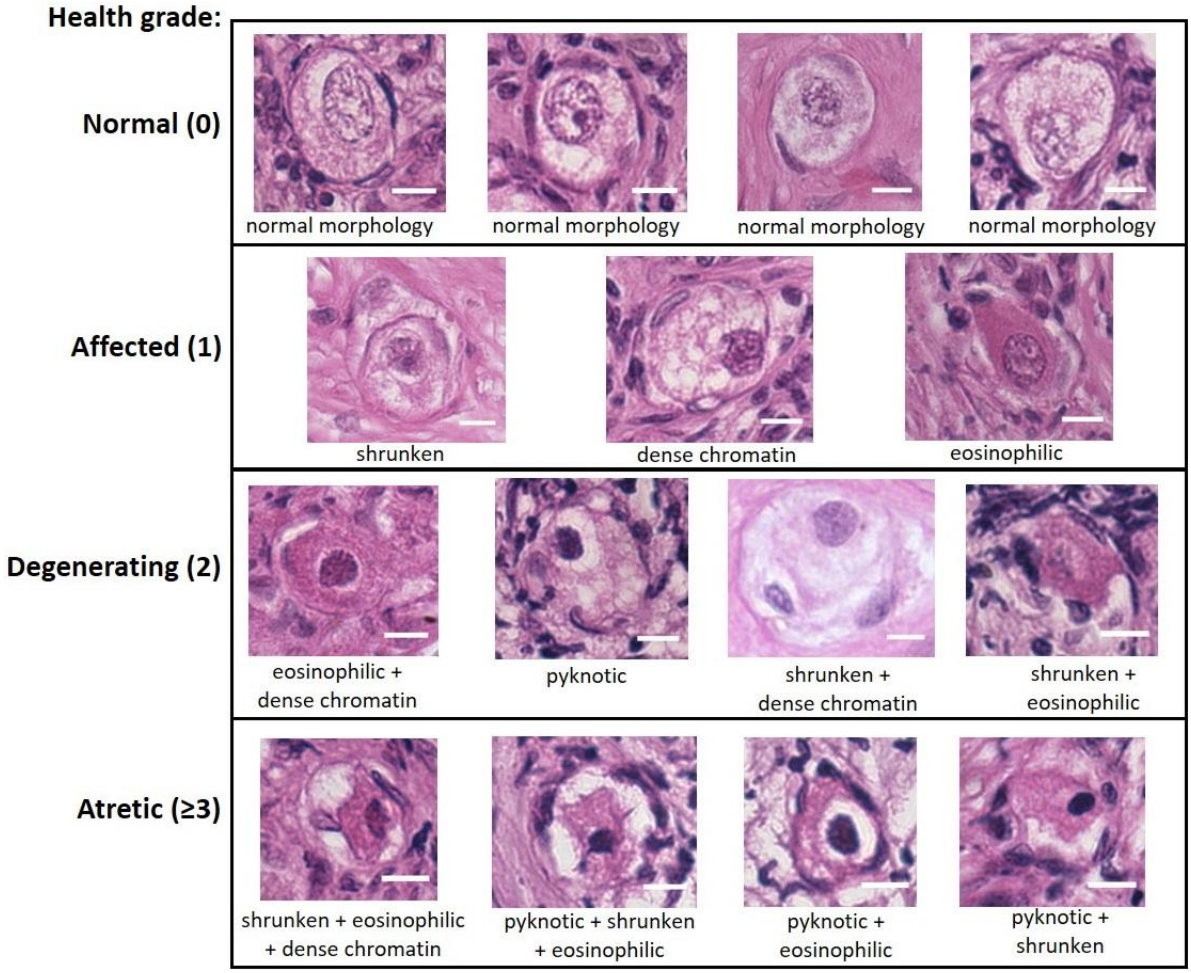

Figure 1: *Health grading of primordial follicles based on morphological appearance.* Bouin's-fixed ovine ovarian tissue was analysed for the presence of primordial follicles (oocyte surrounded by a single layer of flattened pregranulosa cells) using haematoxylin and eosin (H&E) staining. Follicles were scored based on the presence of morphological markers (dense chromatin, eosinophilia, shrunken ooplasm [one point each] or pyknosis [two points]) as normal (0), affected (1), degenerating (2) or atretic (≥ 3). Scale bar: 10 μm.

a period of 10 days, the animals were sacrificed by cervical dislocation and all grafts were retrieved.

2.7. Histological analysis

Cortical strips were fixed in Bouin's solution overnight at room temperature and embedded in paraffin wax. Serial sections were obtained at 5 μm thickness and slides were stained with haematoxylin and eosin (H&E). Samples were imaged at $\times$400 magnification using a Leica DM2500 microscope. Images were captured using QCapture Pro 7 software. Follicles were graded in a blinded manner by two independent researchers, with a concordance rate of over 90%.

Primordial follicles were identified based on morphology defined by a single layer of flattened granulosa cells [19]. Oocyte health was assessed as described previously [18], with slight modification. Oocytes were graded as normal (grade 0) if they had no morphological markers, affected (grade 1) if they had either dense chromatin, eosinophilia or shrinkage of the ooplasm (one point each), degenerating (grade 2) if they had two of the above or nuclear pyknosis (two points), and atretic (grade $\geq$ 3) if they had more than two of the above markers (Figure 1). Up to 50 primordial follicles were analysed within each tissue fragment, except for xenotransplants, where all primordial follicles were included in the analysis.

2.8. Data analysis

All statistical analyses were performed using R statistical software, version 3.5.0. A proportional odds model (clmm2; [20]) was used to determine whether delay before processing affected follicle health, adjusting for individual sheep (random effect). A logistic regression model (glmer; [21]) was used to determine the odds of follicles being classified as

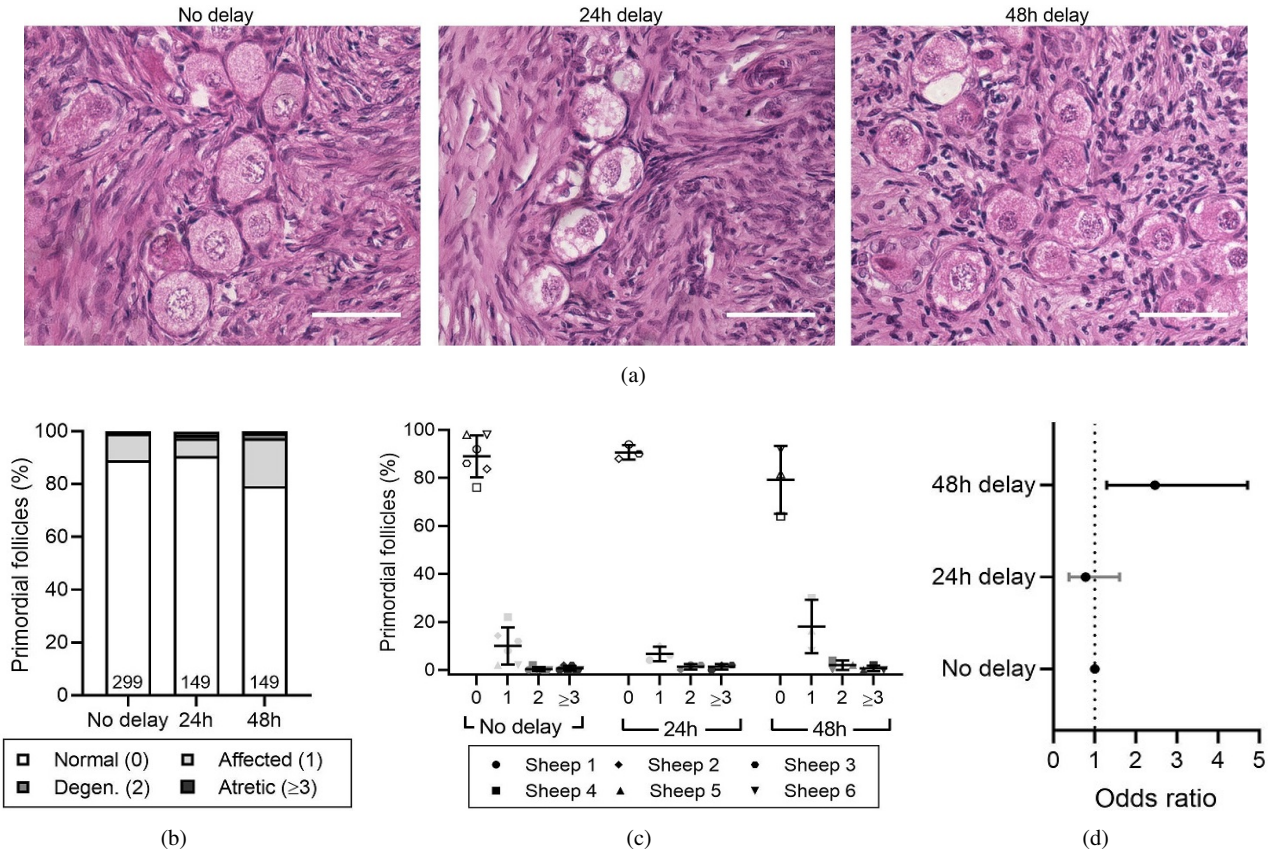

Figure 2: *Effect of delayed processing on primordial follicle morphology in fresh ovarian tissue.* Ovine ovarian tissue was either processed immediately (no delay; $n = 6$), 24 h ($n = 3$) or 48 h ($n = 3$) after collection and fixed in Bouin's solution. (a) Representative images of fresh ovine ovarian tissue. Scale bar: 50 μm. (b) Health distribution of primordial follicles in fresh ovine ovarian tissue. Numbers at the base of columns refer to the total number of follicles analysed. Primordial follicles (oocyte surrounded by a single layer of flattened pregranulosa cells) were analysed using H&E staining and scored based on the presence of morphological markers (dense chromatin, eosinophilia, shrunken ooplasm [one point each] or pyknosis [two points]) as normal (0), affected (1), degenerating (2) or atretic (≥ 3). (c) Same data as in (b), showing the distribution of health grades between animals (mean $\pm$ SD). (d) Proportional ORs and 95% CIs of follicles being graded as ≥ 1 when processed after 24 h or 48 h compared to the no delay group.

growing after xenotransplantation, again adjusting for individual sheep. The total number of follicles per group (n) is indicated for each analysis. Statistical significance was defined as $P < .05$. Data are presented as mean $\pm$ SD or as odds ratios (ORs) with 95% confidence intervals (CI).

3. Results

3.1. The effect of processing delay on fresh ovarian tissue

The vast majority of follicles in all fresh tissues were morphologically normal; $89.0 \pm 8.7\%$ for the immediately processed (no delay) group, $90.6 \pm 3.0\%$ for the 24 h-delay group, and $79.2 \pm 14.2\%$ for the 48 h-delay group (Figures 2(a)–2(c), Table 1). Compared to immediately processed samples, a 24 h delay did not result in an increased likelihood of primordial follicles being graded as morphologically abnormal (OR = 0.78, 95% CI 0.38–1.60, $P > .05$). In contrast, primordial follicles from samples processed 48 h after procurement were 2.5 times more likely to be graded as abnormal compared to no delay samples (OR = 2.47, 95% CI 1.29–4.71, $P < .01$; Figure 2(d)).

3.2. The effect of processing delay on cryopreserved and thawed ovarian tissue

As expected, the process of cryopreservation caused damage to primordial follicles, with follicles in cryopreserved-thawed samples being over 28 times more likely to be graded as abnormal compared to fresh tissue (OR = 28.60, 95% CI 17.91–45.65, $P < .0001$, Figure 3). Thus, the proportion of normal primordial follicles was lower in cryopreserved-thawed tissue compared to fresh tissue, irrespective of processing time (Figures 4(a)–4(c), Table 1). The mean proportion of normal follicles in cryopreserved-thawed tissue was $26.6 \pm 17.0\%$ for the no-delay group and

Table 1: Summary of proportion of follicles per health grade (% ± SD) across conditions (no delay, 24 h delay, 48 h delay) in fresh, cryopreserved-thawed, and xenotransplanted ovarian tissue.

Tissue type	Follicle health (grade)	No delay	24 h delay	48 h delay
Fresh	**Normal (0)**	**89.0 ± 8.7**	**90.6 ± 3.0**	**79.2 ± 14.2**
	Affected (1)	10.1 ± 7.7	6.7 ± 3.0	18.1 ± 11.1
	Grades 0 and 1	99.0 ± 1.1	97.3 ± 1.2	97.3 ± 3.1
	Degenerating (2)	0.3 ± 0.8	1.3 ± 1.2	2.0 ± 2.0
	Atretic (≥ 3)	0.7 ± 1.0	1.3 ± 1.2	0.7 ± 1.2
Cryopreserved-thawed	**Normal (0)**	**26.6 ± 17.0**	**20.4 ± 2.1**	**45.7 ± 31.3**
	Affected (1)	41.6 ± 10.5	50.0 ± 8.5	27.5 ± 4.8
	Grades 0 and 1	68.2 ± 15.3	70.5 ± 10.2	73.2 ± 28.0
	Degenerating (2)	19.0 ± 9.4	23.5 ± 10.5	18.8 ± 19.4
	Atretic (≥ 3)	12.8 ± 9.1	6.0 ± 3.4	8.0 ± 8.7
Xenotransplanted	**Normal (0)**	**55.7 ± 9.8**	**81.5 ± 3.5**	**43.0 ± 28.8**
	Affected (1)	16.7 ± 16.5	8.5 ± 2.1	29.3 ± 13.5
	Grades 0 and 1	70.1 ± 17.7	91.1 ± 7.6	72.3 ± 39.6
	Degenerating (2)	28.0 ± 19.1	8.5 ± 7.8	4.7 ± 5.0
	Atretic (≥ 3)	0.0 ± 0.0	1.0 ± 1.4	23.0 ± 39.8

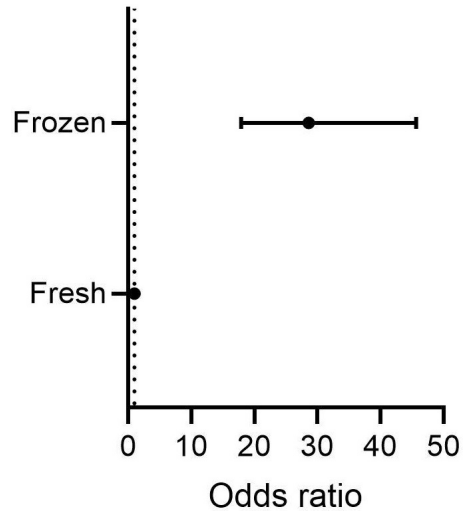

Figure 3: *Effect of cryopreservation of ovarian tissue on primordial follicle morphology.* Proportional ORs and 95% CIs of follicles being graded as ≥ 1 in fresh tissue compared to cryopreserved-thawed tissue. Ovine ovarian tissue was processed immediately and either fixed or cryopreserved-thawed, and fixed ($n = 6$) in Bouin's solution. Primordial follicles (oocyte surrounded by a single layer of flattened pregranulosa cells) were analysed using H&E staining and scored based on the presence of molecular markers (dense chromatin, eosinophilia, shrunken ooplasm [one point each] or pyknosis [two points]) as normal (0), affected (1), degenerating (2) or atretic (≥ 3). Black CI bars indicate $P < .05$.

20.4 ± 2.1% for the 24 h-delay group. Interestingly, tissue processed 48 h after collection had a higher proportion of normal primordial follicles, 45.7 ± 31.3%, though with considerable deviation between individuals (Figure 4(c)). This translated to a 44% decrease in the odds of a follicle being graded as abnormal compared to immediately processed tissue (OR = 0.56, 95% CI 0.36–0.87, $P < .01$; Figure 4(d)). There was no difference in the health of primordial follicles after a 24 h delay before processing compared to immediately processed tissue (OR = 0.93, 95% CI 0.61–1.41, $P > .05$).

3.3. The effect of processing delay on ovarian tissue xenotransplanted after cryopreservation

Cryopreserved-thawed ovine ovarian tissue from 0 h, 24 h, and 48 h groups was xenografted subcutaneously into SCID mice for 10 days. The number of follicles found in each graft differed substantially across conditions; out of the six control grafts (immediately processed samples) only three contained follicles, with the remaining grafts containing potential degenerating follicle remnants (follicle-like structures with no oocyte; Table 2). Conversely, follicles were observed in two out of three grafts for the 24 h-delay group and all three grafts for the 48 h-delay group. Many primordial follicles were normal after 10-day xenografting, however, considerable variation was observed between grafts, particularly for the 48 h-delay group. The proportion of normal primordial follicles was 55.7 ± 9.8% for the immediately processed group, 81.5 ± 3.5% for the 24 h-delay group, and 43.0 ± 28.8% for the 48 h-delay group (Figures 5(a)–5(c), Table 1). There was no difference in the likelihood of a primordial follicle being graded as abnormal for the 24 h-delay (OR = 0.36, 95% CI 0.081–1.59, $P > .05$) or 48 h-delay groups (OR = 5.0, 95% CI 0.80–30.83, $P > .05$) compared to the no delay group (Figure 5(d)).

Of the eight grafts containing follicles, six contained both primordial and growing follicles indicating that follicle activation occurred during the xenografting period (Table 2; Figure 6). The other two grafts that contained follicles

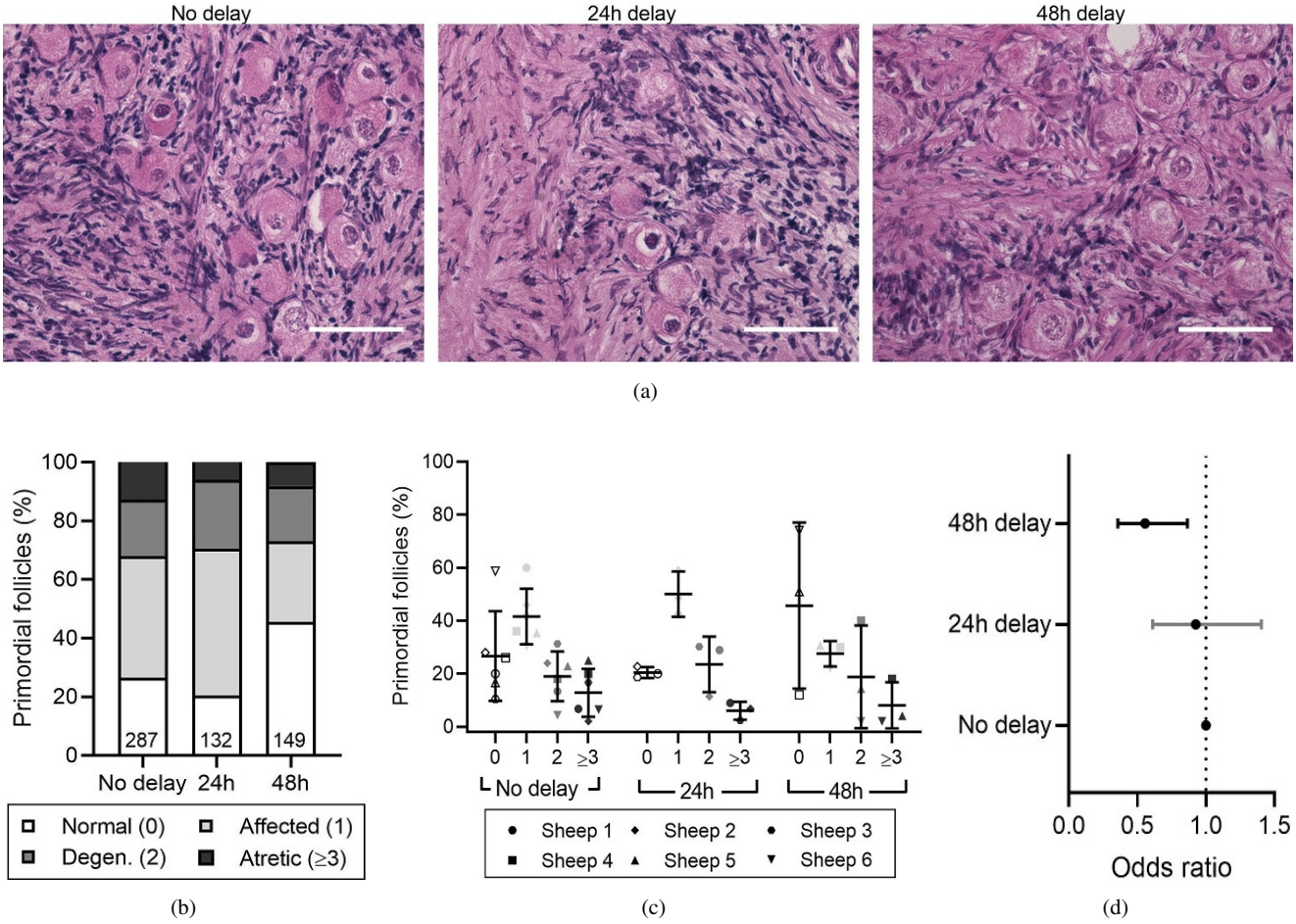

Figure 4: *Effect of delayed processing on primordial follicle morphology in cryopreserved-thawed ovarian tissue.* Ovine ovarian tissue was either processed immediately (no delay; $n = 6$), 24 h ($n = 3$) or 48 h ($n = 3$) after collection, cryopreserved by slow freezing, thawed and fixed in Bouin's solution. (a) Representative images of cryopreserved-thawed ovine ovarian tissue. Scale bar: 50 μm. (b) Health distribution of primordial follicles in cryopreserved-thawed ovine ovarian tissue. Numbers at the base of columns refer to the total number of follicles analysed. Primordial follicles (oocyte surrounded by a single layer of flattened pregranulosa cells) were analysed using H&E staining and scored based on the presence of morphological markers (dense chromatin, eosinophilia, shrunken ooplasm [one point each] or pyknosis [two points]) as normal (0), affected (1), degenerating (2) or atretic (≥ 3). (c) Same data as in (b), showing the distribution of health grades between animals (mean $\pm$ SD). (d) Proportional ORs and 95% CIs of follicles being graded as ≥ 1 when processed after 24 h or 48 h compared to the no delay group. Black CI bars indicate $P < .05$.

Table 2: Number of follicles per graft following 10-day xenotransplantation of cryopreserved-thawed ovine ovarian tissue with delayed processing.

Animal	No delay	24 h delay	48 h delay
Sheep 1	25 follicles (14 primordial, 56%)	27 follicles (14 primordial, 52%)	N/A
Sheep 2	No follicles	154 follicles (86 primordial, 56%)	N/A
Sheep 3	6 follicles (6 primordial, 100%)	No follicles	N/A
Sheep 4	No follicles	N/A	75 follicles (50 primordial, 67%)
Sheep 5	No follicles	N/A	32 follicles (16 primordial, 50%)
Sheep 6	2 follicles (2 primordial, 100%)	N/A	55 follicles (26 primordial, 47%)
Total	**33 (22 primordial)**	**181 (100 primordial)**	**162 (92 primordial)**

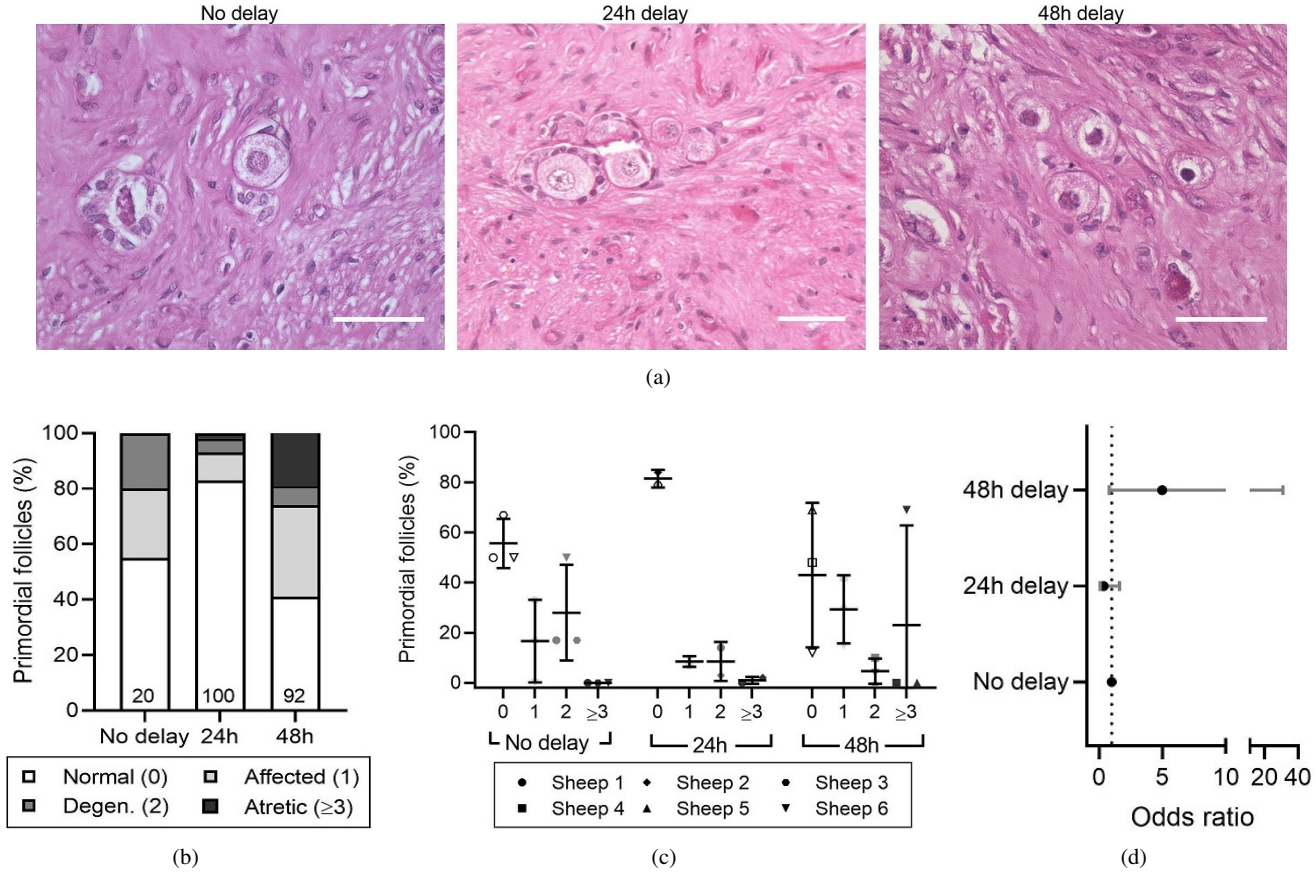

Figure 5: *Effect of delayed processing on primordial follicle morphology in cryopreserved-thawed xenotransplanted ovarian tissue.* Ovine ovarian tissue was either processed immediately (no delay; $n = 6$), 24 h ($n = 3$) or 48 h ($n = 3$) after collection and cryopreserved. Samples were thawed and xenotransplanted subcutaneously for 10 days, after which they were fixed in Bouin's solution. (a) Representative images of cryopreserved-thawed ovine ovarian tissue. Scale bar: 50 μm. (b) Health distribution of primordial follicles in cryopreserved-thawed ovine ovarian tissue. Numbers at the base of columns refer to the total number of follicles analysed. Primordial follicles (oocyte surrounded by a single layer of flattened pregranulosa cells) were analysed using H&E staining and scored based on the presence of morphological markers (dense chromatin, eosinophilia, shrunken ooplasm [one point each] or pyknosis [two points]) as normal (0), affected (1), degenerating (2) or atretic (≥ 3). (c) Same data as in (b), showing the distribution of health grades between animals (mean $\pm$ SD). (d) Proportional ORs and 95% CIs of follicles being graded as ≥ 1 when processed after 24 h or 48 h compared to the no delay group.

contained only primordial follicles and in very low numbers; 2 and 6 follicles (Table 2). The proportion of growing follicles was $17.3 \pm 30.0\%$ for tissue processed immediately after collection, $46.0 \pm 2.8\%$ for tissue processed after 24 h and $45.3 \pm 10.8\%$ for tissue processed after 48 h (Figure 6(a)), with the highest variability between animals in the no delay group (Figure 6(b)). There was no difference in the likelihood of a follicle being classified as "growing" between the groups (24 h-delay OR = 1.30, 95% CI 0.59–3.22, $P > .05$; 48 h-delay OR = 1.26, 95% CI 0.55–3.96, $P > .05$; Figure 6(c)).

4. Discussion

This study demonstrates that a processing delay of 24 h at 4 °C did not impact the morphology of the primordial follicles which is indicative of health in fresh or cryopreserved ovine ovarian tissue. In contrast, a processing delay of 48 h resulted in primordial follicles being more likely to be graded as abnormal compared to immediately-processed tissue, while tissue cryopreserved after 48 h was more likely to contain morphologically normal follicles compared to the immediately-processed control. Xenografting of cryopreserved ovarian strips indicated the tissue can support follicle health and development in all experimental groups, with the delay in processing resulting in no difference in the health of primordial follicles, nor in the proportion of growing follicles.

Here we reported that cryopreservation had a significant negative impact on primordial follicle health, with only 20–40% of follicles being classified as normal. Health

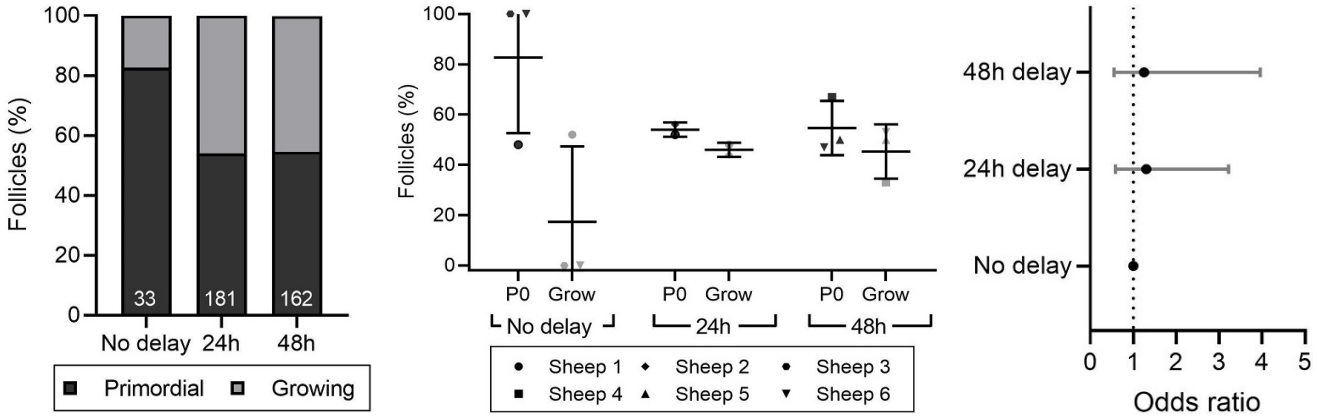

Figure 6: *Follicle development after xenotransplantation of ovarian tissue with or without delayed processing.* Ovine ovarian tissue was either processed immediately (no delay; $n = 6$), 24 h ($n = 3$) or 48 h ($n = 3$) after collection and cryopreserved. Samples were thawed and xenotransplanted subcutaneously for 10 days, after which they were fixed in Bouin's solution. (a) Proportion of primordial and growing follicles in cryopreserved-thawed ovine ovarian tissue following 10-day xenotransplantation. Follicles were classified as primordial (P0; oocyte surrounded by a single layer of flattened pregranulosa cells) or growing (Grow; oocyte surrounded by one or more layers of either a mixture of flattened and cuboidal granulosa cells or a complete layer of cuboidal cells. (b) Same data as in (a), showing the distribution of follicle developmental stages between animals (mean ± SD). (c) Proportional ORs and 95% CIs of follicles being classified as growing when processed after 24 h or 48 h compared to the no delay group.

classification criteria vary considerably between studies, and the criteria used in the present study were deliberately strict, in order to detect any discrete morphological changes within the follicles. Others have reported 50–80% normal follicles following cryopreservation, which is consistent with our report if the classification criteria to judge the health of the follicles in this study are adjusted to match [22, 23]. We acknowledge that the results of the present study are somewhat limited by the use of morphology alone to assess primordial follicle health. However, the criteria used were well-defined and, in studies using a combination of morphological and molecular analyses, the two methods are generally in agreement [24]. While the use of molecular markers may have complemented the results presented here, they present their own limitations including challenges in selecting an appropriate marker for the damage mechanism in question, in addition to the transience of some marker expression [25].

A 24 h processing delay had no significant effect on primordial follicle health post-cryopreservation and thawing. This finding is consistent with the presence of morphologically normal primordial follicles after a 20 h processing delay at 4 °C of human ovarian cortical tissue as reported by Rosendahl et al. [12]. Isachenko et al. also provided evidence that a 24 h cryopreservation delay at 4 °C does not affect the proportion of morphologically normal follicles or follicle density in frozen-thawed ovarian cortical tissue [13]. Conversely, another study described a decrease in the proportion of morphologically normal follicles induced by a 24 h freeze-delay prior to thawing and in vitro culture of human ovarian tissue [14], however, this study used vitrification, which relies on very high concentrations of cryoprotectants, while the present study employed slow freezing which is the currently accepted gold-standard method of OTC [26].

Remarkably, a processing delay of 48 h resulted in a 44% decrease in the probability of follicles being graded as affected, degenerating or atretic after cryopreservation, despite showing the opposite effect in fresh tissue. This is consistent with findings from Isachenko et al. who explored a 24 h delay at 4 °C suggesting a role for pre-cooling of human ovarian tissue before cryopreservation [13]. It is possible that acclimatisation of the ovarian tissue at 4 °C for 48 h provides a more gradual temperature transition, which primes the tissue to better respond to the challenges of cryopreservation and, thus, experience a reduced insult on the health of the primordial follicle pool. However, as there was significant variability in morphological follicle health distribution between the three biological replicates in response to a 48 h delay, confirming this result with human ovarian tissue is required before such delays can be used for fertility preservation.

At present, the only way to utilise cryopreserved ovarian cortical strips for fertility restoration is autologous transplantation of the tissue either orthotopically or heterotopically. Although morphological analysis after

cryopreservation and thawing granted important insight into the effects of processing delay on primordial follicle health, the role of the tissue in fertility restoration is ultimately defined by its potential to sustain follicle health and growth after transplantation. Therefore, in this study we used xenotransplantation to determine if the delay in OTC had modified functional potential. Importantly, all treatment groups contained grafts that supported follicle development. Nevertheless, there was significant variation in follicle numbers between grafts, with some grafts containing no follicles at all. The variable number of follicles in the grafts was accounted for in the statistical model used. Total absence of follicles was observed in 3 out of 6 grafts that were processed immediately and 1 out of 3 24 h-delay grafts, but all contained degenerating follicle remnants. Most surprisingly, statistical analysis revealed that delayed processing of up to 48 h did not adversely affect follicle development in cryopreserved-transplanted tissue, as primordial and growing follicles were observed in all three of the 48 h-delay grafts. Thus, the presence of follicles in 5 out of 6 grafts confirms that such a delay does not render the tissue deficient in follicles capable of growth, nor does it hinder revascularisation of the tissue, a key component to the success of transplantation. By extension, this data also suggests that a processing delay of 24 h or 48 h did not cause complete loss of function of the vasculature and the supporting stromal cells. This finding is consistent with insight from other studies that also identified follicles in ovarian tissue xenotransplanted after a 24 h delay in cryopreservation [12, 13]. Moreover, these results demonstrate that a processing delay of either 24 h or 48 h had no significant impact on primordial follicle health, nor on the proportion of growing follicles after xenotransplantation indicating that delayed processing does not affect the potential for follicle development following transplantation. To the best knowledge of the authors, the work presented here is the first report of normal morphology and follicle growth and development in ovarian tissue grafts after a 48 h delay in cryopreservation.

Although cryopreservation of ovarian tissue with as little delay as possible seems obvious and is considered the gold standard in most countries [27], it is possible that transient cold ischaemia during delayed processing induces a metabolic adjustment which enables quiescent primordial follicles to better withstand ischaemia prior to revascularisation. Energetic adjustment to ischaemia is well-documented in muscle tissue [28] and it is possible that the oocyte is also equipped with the capacity to adjust to metabolism in avascular conditions. Furthermore, there is some evidence to suggest that ischaemic preconditioning can improve the outcomes of organ transplantation [29] and, in this context, our findings might suggest that the benefits of ischaemic preconditioning are not lost after cryopreservation and thawing of the tissue. This, taken together with studies using human tissue, which demonstrated that follicles can survive a processing delay of up to 20 h at 4 °C and lead to a live birth [8, 12, 13], indicates that ovarian tissue responds to delayed cryopreservation favourably without a statistically significant negative impact on the primordial pool.

The results we present here have provided strong evidence to support the idea that ovarian tissue can be chilled for 24 or even 48 h prior to cryopreservation with no statistically significant net negative impact on the health of the primordial pool of follicles after transplantation and in vivo development of the tissue. This lends strength to an emerging body of evidence suggesting that the delayed processing is safe, or even beneficial, for cryopreserved ovarian tissue. Validation of these findings using human ovarian tissue or other endangered species of interest would thereby present a new, feasible approach to increasing access to ovarian tissue freezing for fertility preservation. It should be noted that in the present study ovaries were left intact until the time of processing, therefore, it cannot be concluded that ovarian biopsies would have a similar response. Nevertheless, these findings are of high relevance to fertility preservation and, in particular, the way OTC is organised on a local and national level for humans and endangered species. An update of the current guidelines to reflect an extended window for tissue processing will ensure that the modality is more widely available to patients without the need to create new facilities. Fundamentally, such an advancement is a great step towards ensuring that every cancer patient who has a need, has an option.

Authors' contributions M. S. Zemyarska, B. D. Bjarkadottir, X. Wei, C. A. Walker, S. M. Lane, J. Davies, and S. A. Williams were involved in the conception and design of the study, data interpretation and analysis, and manuscript generation. M. S. Zemyarska, B. D. Bjarkadottir, X. Wei, and C. A. Walker were involved in data acquisition, with M. S. Zemyarska and B. D. Bjarkadottir generating the bulk of the data, performing most of the data analysis and drafting the article. M. S. Zemyarska and B. D. Bjarkadottir contributed equally to this work. All authors critically read and approved the final manuscript.

Funding This work was supported by the Oxford Medical Research Council Doctoral Training Programme (Oxford MRC-DTP) grant awarded to B. D. Bjarkadottir (grant number MR/N013468/1) and by a joint scholarship to C. A. Walker from the Clarendon fund and NDWRH and partially funded by the NDWRH.

Acknowledgments The authors wish to thank all staff of the Oxford Cell and Tissue Biobank (OCTB) for their assistance with training in tissue processing and cryopreservation, Prof. David Bennett for use of the surgery facilities, and all staff of Biomedical Sciences John Radcliffe for assistance with the mice used in this study.

Conflict of interest The authors declare that they have no conflict of interest.

References

[1] K. D. Miller, R. L. Siegel, C. C. Lin, A. B. Mariotto, J. L. Kramer, J. H. Rowland, et al., *Cancer treatment and survivorship statistics, 2016*, CA Cancer J Clin, 66 (2016), 271–289.

[2] S. M. Phillips, L. S. Padgett, W. M. Leisenring, K. K. Stratton, K. Bishop, K. R. Krull, et al., *Survivors of childhood cancer in the United States: prevalence and burden of morbidity*, Cancer Epidemiol Biomarkers Prev, 24 (2015), 653–663.

[3] G. T. Armstrong, Y. Chen, Y. Yasui, W. Leisenring, T. M. Gibson, A. Mertens, et al., *Reduction in late mortality among 5-year survivors of childhood cancer*, N Engl J Med, 374 (2016), 833–842.

[4] H. A. Spoudeas, *Growth and endocrine function after chemotherapy and radiotherapy in childhood*, Eur J Cancer, 38 (2002), 1748–1759.

[5] C. Duffy and S. Allen, *Medical and psychosocial aspects of fertility after cancer*, Cancer J, 15 (2009), 27–33.

[6] J. Donnez and M. M. Dolmans, *Fertility preservation in women*, N Engl J Med, 377 (2017), 1657–1665.

[7] S. E. Gellert, S. E. Pors, S. G. Kristensen, A. M. Bay-Bjørn, E. Ernst, and C. Yding Andersen, *Transplantation of frozen-thawed ovarian tissue: an update on worldwide activity published in peer-reviewed papers and on the Danish cohort*, J Assist Reprod Genet, 35 (2018), 561–570.

[8] R. Dittrich, L. Lotz, G. Keck, I. Hoffmann, A. Mueller, M. W. Beckmann, et al., *Live birth after ovarian tissue autotransplantation following overnight transportation before cryopreservation*, Fertil Steril, 97 (2012), 387–390.

[9] A. K. Jensen, K. T. Macklon, J. Fedder, E. Ernst, P. Humaidan, and C. Y. Andersen, *86 successful births and 9 ongoing pregnancies worldwide in women transplanted with frozen-thawed ovarian tissue: focus on birth and perinatal outcome in 40 of these children*, J Assist Reprod Genet, 34 (2017), 325–336. Erratum in J Assist Reprod Genet, 34 (2017), 337.

[10] G. Majno and I. Joris, *Apoptosis, oncosis, and necrosis. An overview of cell death*, Am J Pathol, 146 (1995), 3–15.

[11] S. S. Kim, D. E. Battaglia, and M. R. Soules, *The future of human ovarian cryopreservation and transplantation: fertility and beyond*, Fertil Steril, 75 (2001), 1049–1056.

[12] M. Rosendahl, K. T. Schmidt, E. Ernst, P. E. Rasmussen, A. Loft, A. G. Byskov, et al., *Cryopreservation of ovarian tissue for a decade in Denmark: a view of the technique*, Reprod Biomed Online, 22 (2011), 162–171.

[13] V. Isachenko, P. Todorov, E. Isachenko, G. Rahimi, A. Tchorbanov, N. Mihaylova, et al., *Long-time cooling before cryopreservation decreased translocation of phosphatidylserine (Ptd-L-Ser) in human ovarian tissue*, PLoS One, 10 (2015), e0129108. Erratum in PLoS One, 14 (2019), e0212961.

[14] S. Klocke, C. Tappehorn, and G. Griesinger, *Effects of supra-zero storage on human ovarian cortex prior to vitrification-warming*, Reprod Biomed Online, 29 (2014), 251–258.

[15] K. Oktay, *Ovarian tissue cryopreservation and transplantation: preliminary findings and implications for cancer patients*, Hum Reprod Update, 7 (2001), 526–534.

[16] R. G. Gosden, D. T. Baird, J. C. Wade, and R. Webb, *Restoration of fertility to oophorectomized sheep by ovarian autografts stored at −196 °C*, Hum Reprod, 9 (1994), 597–603.

[17] K. Lakhoo, J. Davies, S. Chakraborty, S. Berg, R. Tennyson, D. Fowler, et al., *Development of a new reproductive tissue cryopreservation clinical service for children: the Oxford programme*, Pediatr Surg Int, 35 (2019), 1271–1278. Erratum in Pediatr Surg Int, 36 (2020), 537.

[18] C. Walker, B. Bjarkadottir, M. Fatum, S. Lane, and S. Williams, *Variation in follicle health and development in cultured cryopreserved ovarian cortical tissue: a study of ovarian tissue from patients undergoing fertility preservation*, Hum Fertil, (2019), 11.

[19] T. Lundy, P. Smith, A. O'Connell, N. L. Hudson, and K. P. McNatty, *Populations of granulosa cells in small follicles of the sheep ovary*, J Reprod Fertil, 115 (1999), 251–262.

[20] R. H. Christensen, *ordinal: Regression Models for Ordinal Data*, R package version 2019.12-10. See https://cran.r-project.org/web/packages/ordinal/, 2019.

[21] D. Bates, M. Mächler, B. Bolker, and S. Walker, *Fitting linear mixed-effects models using lme4*, J Stat Softw, 67 (2015), 1–48.

[22] L. R. Faustino, R. R. Santos, C. M. Silva, L. C. Pinto, J. J. Celestino, C. C. Campello, et al., *Goat and sheep ovarian tissue cryopreservation: Effects on the morphology and development of primordial follicles and density of stromal cell*, Anim Reprod Sci, 122 (2010), 90–97.

[23] S. Cecconi, G. Capacchietti, V. Russo, P. Berardinelli, M. Mattioli, and B. Barboni, *In vitro growth of preantral follicles isolated from cryopreserved ovine ovarian tissue*, Biol Reprod, 70 (2004), 12–17.

[24] R. Talevi, S. Sudhakaran, V. Barbato, A. Merolla, S. Braun, M. Di Nardo, et al., *Is oxygen availability a limiting factor for in vitro folliculogenesis?*, PLoS One, 13 (2018), e0192501.

[25] V. Pampanini, M. Wagner, B. Asadi-Azarbaijani, I. C. Oskam, M. Sheikhi, M. O. D. Sjödin, et al., *Impact of first-line cancer treatment on the follicle quality in cryopreserved ovarian samples from girls and young women*, Hum Reprod, 34 (2019), 1674–1685.

[26] M. M. Dolmans and D. D. Manavella, *Recent advances in fertility preservation*, J Obstet Gynaecol Res, 45 (2019), 266–279.

[27] J. Donnez, M. M. Dolmans, A. Pellicer, C. Diaz-Garcia, M. Sanchez Serrano, K. T. Schmidt, et al., *Restoration of ovarian activity and pregnancy after transplantation of cryopreserved ovarian tissue: a review of 60 cases of reimplantation*, Fertil Steril, 99 (2013), 1503–1513.

[28] I. R. Lanza, D. M. Wigmore, D. E. Befroy, and J. A. Kent-Braun, *In vivo ATP production during free-flow and ischaemic muscle contractions in humans*, J Physiol, 577 (2006), 353–367.

[29] J. T. Ambros, I. Herrero-Fresneda, O. G. Borau, and J. M. Boira, *Ischemic preconditioning in solid organ transplantation: from experimental to clinics*, Transpl Int, 20 (2007), 219–229.

Human Reproduction, Vol.00, No.0, pp. 1–20, 2021
doi:10.1093/humrep/deab075

human reproduction

ORIGINAL ARTICLE ***Reproductive biology***

Improved preservation of ovarian tissue morphology that is compatible with antigen detection using a fixative mixture of formalin and acetic acid

B.V. Adeniran[1], B.D. Bjarkadottir[1], R. Appeltant [1], S. Lane[2,3], and S.A. Williams [1,2,*]

[1]Nuffield Department of Women's and Reproductive Health, Women's Centre, John Radcliffe Hospital, University of Oxford, Oxford, UK [2]Future Fertility Programme Oxford, Oxford, UK [3]Department of Paediatric Oncology and Haematology, Children's Hospital Oxford, Oxford University Hospitals NHS Foundation Trust, Oxford, UK

*Correspondence address. Nuffield Department of Women's and Reproductive Health, Women's Centre, John Radcliffe Hospital, University of Oxford, Oxford OX3 9DU, UK. Tel: +44-0-1865 221014; E-mail: suzannah.williams@wrh.ox.ac.uk
https://orcid.org/0000-0003-1798-976X

Submitted on December 13, 2019; resubmitted on February 13, 2021; editorial decision on March 8, 2021

STUDY QUESTION: Can ovarian tissue morphology be better preserved whilst enabling histological molecular analyses following fixation with a novel fixative, neutral buffered formalin (NBF) with 5% acetic acid (referred to hereafter as Form-Acetic)?

SUMMARY ANSWER: Fixation with Form-Acetic improved ovarian tissue histology compared to NBF in multiple species while still enabling histological molecular analyses.

WHAT IS KNOWN ALREADY: NBF fixation results in tissue shrinkage in various tissue types including the ovary. Components of ovarian tissue, notably follicles, are particularly susceptible to NBF-induced morphological alterations and can lead to data misrepresentation. Bouin's solution (which contains 5% acetic acid) better preserves tissue architecture compared to NBF but is limited for immunohistochemical analyses.

STUDY DESIGN, SIZE, DURATION: A comparison of routinely used fixatives, NBF and Bouin's, and a new fixative, Form-Acetic was carried out. Ovarian tissue was used from three different species: human (n = 5 patients), sheep (n = 3; 6 ovaries; 3 animals per condition) and mouse (n = 14 mice; 3 ovaries from 3 different animals per condition).

PARTICIPANTS/MATERIALS, SETTING, METHODS: Ovarian tissue from humans (aged 13 weeks to 32 years), sheep (reproductively young i.e. 3–6 months) and mice (10 weeks old) were obtained and fixed in 2 ml NBF, Bouin's or Form-Acetic for 4, 8, and 24 h at room temperature. Tissues were embedded and sectioned. Five-micron sections were stained with haemotoxylin and eosin (H&E) and the percentage of artefact (clear space as a result of shrinkage) between ovarian structures was calculated. Additional histological staining using Periodic acid-Schiff and Masson's trichrome were performed on 8 and 24 h NBF, Bouin's and Form-Acetic fixed samples to assess the compatibility of the new fixative with stains. On ovarian tissue fixed for both 8 and 24 h in NBF and Form-Acetic, immunohistochemistry (IHC) studies to detect FOXO3a, FoxL2, collagen IV, laminin and anti-Müllerian hormone (AMH) proteins were performed in addition to the terminal deoxynucleotidyl transferase nick end labelling (TUNEL) assay to determine the compatibility of Form-Acetic fixation with types of histological molecular analyses.

MAIN RESULTS AND THE ROLE OF CHANCE: Fixation in Form-Acetic improved ovarian tissue morphology compared to NBF from all three species and either slightly improved or was comparable to Bouin's for human, mouse and sheep tissues. Form-Acetic was compatible with H&E, Periodic acid-Schiff and Masson's trichrome staining and all proteins (FOXO3a, FoxL2, collagen IV and laminin and AMH) could be detected via IHC. Furthermore, Form-Acetic, unlike NBF, enabled antigen recognition for most of the proteins tested without the need for antigen retrieval. Form-Acetic also enabled the detection of damaged DNA via the TUNEL assay using fluorescence.

LARGE SCALE DATA: N/A

LIMITATIONS, REASONS FOR CAUTION: In this study, IHC analysis was performed on a select number of protein types in ovarian tissue thus encouraging further studies to confirm the use of Form-Acetic in enabling the detection of a wider range of protein forms in addition to other tissue types.

WIDER IMPLICATIONS OF THE FINDINGS: The simplicity in preparation of Form-Acetic and its superior preservative properties whilst enabling forms of histological molecular analyses make it a highly valuable tool for studying ovarian tissue. We, therefore, recommend that Form-Acetic replaces currently used fixatives and encourage others to introduce it into their research workflow.

STUDY FUNDING/COMPETING INTEREST(S): This work was supported by the Oxford Medical Research Council Doctoral Training Programme (Oxford MRC-DTP) grant awarded to B.D.B. (Grant no. MR/N013468/1), the Fondation Hoffmann supporting R.A. and the Petroleum Technology Development Fund (PTDF) awarded to B.V.A.

Key words: fixation / histology / immunohistochemistry / form-acetic / neutral buffered formalin / Bouin's / ovary / human / mouse / sheep

Introduction

Fixation is the cornerstone of histopathology as it enables tissue preservation in an archival form thereby enabling the long-term study of cellular architecture and tissue composition. A number of different fixatives are commercially available, with the aldehyde group of fixatives serving as the most common for tissue fixation. Formaldehyde, which belongs to the aldehyde group, is the most widely used fixative and acts by forming covalent chemical bonds (commonly referred to as cross-links) between and within certain regions of protein structures thereby preserving the tissue (Fraenkel-Conrat and Olcott, 1948; Gustavson. 1956). It is commonly supplied as 10% (v/v) neutral buffered formalin (NBF) and comprises approximately 4% formaldehyde in PBS. Twenty-four hours fixation in NBF is the accepted standard for pathologists for most tissue types although fixation times may vary depending on tissue size in research use (Howat and Wilson, 2014).

The pitfall to using NBF is tissue-type-dependent shrinkage (Siu *et al.*, 1986; Pritt *et al.*, 2005; Jonmarker *et al.*, 2006; Chen *et al.*, 2012). Shrinkage has been reported in many tissue types including the prostate (Jonmarker *et al.*, 2006), oesophagus (Siu *et al.*, 1986), head and neck tissue (Chen *et al.*, 2012). NBF-induced shrinkage has regularly been observed in ovarian tissue but rarely acknowledged as it is considered an unavoidable issue. Marked shrinkage can adversely result in a misrepresentation of data for analytical purposes. In cancer studies, NBF-induced shrinkage resulted in decreased tumour size measurements and a misdiagnosis by underestimating the stage of the tumour (Hsu *et al.*, 2007; Tran *et al.*, 2015). In our laboratory, we have observed shrinkage in NBF fixed ovarian tissue, with follicles being particularly susceptible, and observed that NBF-induced shrinkage could affect ovarian tissue analysis (unpublished data).

The ovary is a dynamic organ with a high level of heterogeneity in terms of cell types, follicle stages, and structure. Morphological analyses of ovarian tissue before and after experimental manipulation provide an insight into follicle development and, hence, ovarian function and these rely heavily on observations of ovarian tissue histology following fixation. Therefore, accurate histological evaluation of ovarian tissue is critical. Ovarian tissue analysis involves classifying follicles according to their developmental stage in addition to assessing follicle health on fixed sections, both of which are employed by many research groups studying ovarian function (Fenwick and Hurst, 2002; Pangas *et al.*, 2007; Chambers *et al.*, 2010; Fenwick *et al.*, 2013; Kim *et al.*, 2015; Fabbri *et al.*, 2016; Stefansdottir *et al.*, 2016; Chiti *et al.*, 2017; McLaughlin *et al.*, 2018; Lee *et al.*, 2019; Winship *et al.*, 2019).

Shrinkage induced by NBF affects ovarian tissue architecture at the level of individual cells. It can be morphologically characterised as shrunken ooplasm within oocytes, condensed nuclei, shrunken stromal, and granulosa cells with 'clear space' seen in between the various cell types. NBF-induced morphological alterations also form part of the criteria involved in assessing follicle health, such as assessing whether there is contact between the oocyte and granulosa cells (Pampanini *et al.*, 2019; Walker *et al.*, 2019). This results in a dilemma wherein follicle death may be histologically presumed where, in fact, the fixative is the primary cause of the morphological appearance. Downstream molecular assays of cell death may be utilised to affirm or disprove observations, but this can be time-consuming and expensive when not required.

NBF is widely used in ovarian tissue fixation and is considered superior to other commercially available fixatives because it enables both routine histology and the detection of numerous protein molecules using immuno-labelling (Howat and Wilson, 2014). However, as outlined above, NBF can cause tissue shrinkage, particularly in ovarian tissue and, therefore, alternative solutions have been sought. Bouin's solution (formaldehyde, picric acid, and acetic acid in an aqueous solution) has been demonstrated to preserve ovarian tissue morphology better than NBF and is, therefore, often used for the fixation of ovarian tissue for histological analyses. Its use is, however, limited to histology owing to its protein coagulative properties which make it poorly suited to immuno-labelling (Howat and Wilson, 2014). Thus, the search for the perfect fixative carries on.

The optimal fixative should allow for good morphological detailing, unbiased diagnosis of disease and evaluation of developmental stages amongst other histological criteria. The fixative should also allow for most if not all protein types to be easily recognisable/identified on fixed tissue, as is the case for NBF. In addition to these, the fixative should enable the preservation of DNA/RNA to enable sequencing/detection. Our aim was, therefore, to develop a fixative that was capable of preserving tissue as the 'ideal' fixative outlined above, focussing on the most commonly used applications for the study of ovarian tissue, namely histological and immunohistochemical (IHC) staining.

In this study, we compare a new fixative comprising NBF with 5% acetic acid (termed Form-Acetic) with two routinely used fixatives, NBF and Bouin's solution, by analysis of tissue morphology and antigen

availability for IHC in ovarian tissue from human, sheep, and mouse. We tested 5% acetic acid in NBF since this is the concentration present in Bouin's solution. We demonstrate that fixation with Form-Acetic resulted in improved morphological preservation in addition to also supporting downstream assays, such as IHC and terminal deoxynucleotidyl transferase nick end labelling (TUNEL), in ovarian tissue from multiple species.

Materials and methods

Ethics and tissue collection

Human

The use of human tissue was approved by the Health Research Authority South Central—Oxford B Research Ethics Committee (REC reference 14/SC/0041). Fresh whole ovaries (n = 3 patients) and frozen ovarian cortical tissue (n = 2 patients) were obtained from the Oxford Cell and Tissue Biobank (OCTB) (Table I); OCTB obtained consent from the patients to donate this tissue for research. None of the patients had previously received chemotherapy or radiotherapy. The ovaries/ovarian tissue were removed as part of surgical procedures and donated for research.

The fresh ovaries were transported and dissected in cold (4°C) Leibovitz L-15 media (Sigma, Gillingham, UK, L5520) to isolate the ovarian cortex. The frozen cortical tissue was thawed in solutions of decreasing concentrations of ethylene glycol (1.0, 0.5, and 0 M) (Sigma, 324558), 0.1 M sucrose (Sigma, S7903), and 3 mg/mL human serum albumin (HSA; Sigma, A1653) for 5 min each at room temperature, using a rocking motion. All cortical tissue was further dissected in fresh L-15 into pieces approximately ≤ 1 mm^3. Processing time between tissue collection from the OCTB and fixation was approximately 1 h.

Table I Characteristics of human samples and assays performed.

	Patient	1	2	3	4	5
	Age	<1 year	32 years	29 years	9 years	13 years
	Fresh/frozen	Fresh	Fresh	Fresh	Frozen	Frozen
Assays	H&E		Y	Y		Y
	PAS		Y	Y		
	Trichrome		Y	Y		
	FOXO3a	Y	Y	Y	Y	Y
	FoxL2		Y	Y	Y	Y
	Laminin	Y	Y		Y	
	Collagen IV	Y	Y		Y	
	AMH (DAB)	Y	Y	Y	Y	Y
	AMH (IF)	Y	Y		Y	
	TUNEL	Y			Y	

Y = analysis performed, yr = years of age, DAB = 3'-diaminobenzidine, IF = immunofluorescence, greyed out = not tested H&E: haemotoxylin and eosin, PAS: Periodic acid-Schiff, FOXO3a: fork-head box O3 (transcription factor), FoxL2: fork-head box protein L2 (transcription factor), anti-Müllerian hormone (AMH; hormone), laminin α1 and collagen IV (extracellular matrix proteins).

Sheep

Female reproductive tracts were obtained shortly after death at a local abattoir. Tracts were assessed visually and based on the size of the ovaries and uterus, appeared to be from young animals (3-6 months). Pairs of visually normal sheep ovaries (n = 3) were collected and transported in L-15 (Gibco, Loughborough, UK, 11415049) supplemented with 2.5 μg/mL Amphotericin B (Gibco, 15290-018), 100 IU/mL penicillin and 100 mg/mL streptomycin (Sigma, P0781) on ice to the laboratory (approximately 1 h). In fresh L-15, the ovarian cortex was isolated from pairs of ovaries and dissected into pieces approximately ≤ 1 mm^3. Processing time between dissection and fixation was approximately 1 h.

Mouse

Pairs of ovaries were obtained from euthanised wild-type C57BL/10 mice (27 ovaries from 14 mice) at 10 weeks of age. Each ovary was dissected out and rinsed in Dulbecco's PBS (DPBS, Sigma, D8662) prior to fixation. Time between ovary collection and fixation was approximately 1 h.

Tissue allocation, fixation, embedding and sectioning

Samples from each species were fixed by immersion in 2 ml of 10% NBF (VWR, Poole, UK, 11699408), Bouin's (Sigma, HT10132) and Form-Acetic (5% acetic acid in NBF) (acetic acid, Merck, Feltham, UK, 1.00063.1011) solution for 4, 8, and 24 h at room temperature with gentle rocking. The volume of fixative was at least 10× the volume of the sample. For human and sheep fixation, three pieces of ovarian cortical tissue from each individual were fixed in each condition. Samples from individual patients and each sheep were randomly allocated to each fixative condition at the same time and could be traced to particular individuals. For mice, ovaries were fixed whole with one ovary from three different mice in each condition. Post fixation, the ovarian tissue/ovaries were washed in 70% ethanol twice for 5 min and stored in 70% ethanol for a minimum of 1 h and a maximum of 6 months before embedding; all samples fixed at the same time (i.e. in all conditions) were embedded at the same time to control for duration in 70% ethanol. For embedding, fixed ovarian samples were dehydrated in increasing concentrations of ethanol (70%, 80%, 95%, 100% ×3), cleared in xylene (×3) and embedded in paraffin wax. All samples were serially sectioned at 5 μm.

Histological staining

Sections from the fixed human, sheep, and mouse specimen were stained with haemotoxylin and eosin (H&E; Haemotoxylin, Gill no 2, Sigma, GHS232; Eosin Y, Sigma, HT110332), Periodic acid-Schiff (PAS; Periodic acid solution, Sigma, 3951; Schiff's reagent, Merck, 1.09033.0500) and Masson's trichrome (Abcam, Cambridge, UK, ab150686) stain. In brief, 5 μm sections were dewaxed (×3) in xylene and rehydrated in decreasing concentrations of ethanol (×3 100%, 90%, 70%, 50%) before proceeding with further staining. For H&E, sections were incubated in haemotoxylin for 2 min, de-stained (1% hydrochloric acid in 70% ethanol) for 5 s, washed in 80% ethanol for 1 min, followed by a brief incubation (1 s) in eosin before dehydrating in ethanol (95% and 100% ×3) and clearing in xylene (×3). For PAS, sections were incubated in periodic acid for 5 min, Schiff's reagent for 15 min and haemotoxylin for 90 s before dehydrating in ethanol (95% and 100% ×3) and clearing in xylene (×3). For Masson's trichrome,

sections were incubated in pre-heated (60°C) Bouin's solution for 1 h, followed by Weigert's iron haematoxylin for 5 min, Biebrich scarlet/acid fuchsin solution for 15 min, phosphomolybdic/phosphotungstic acid solution for 14 min, aniline blue for 9 min and acetic acid for 5 min before dehydrating in ethanol (95% ×2 and 100% ×2) and clearing in xylene (×2). Stained slides were mounted using DPX mountant (Sigma, 06522), examined under a light microscope (Leica DM2500) and images captured using the QImaging Micropublisher 6 camera and accompanying Ocular imaging software (QImaging, Surrey, Canada).

Histological artefact assessment

Three histological assessments were performed on H&E-stained sections to determine the morphological integrity of ovarian tissue after fixation and these involved assessing follicle integrity (the amount of clear space, as a result of cellular shrinkage due to fixation, observed within the follicle), follicle-stroma integrity (space between the follicle and the surrounding stroma) and stroma integrity (space between stromal cells). Follicles at the primordial to secondary stage were assessed for the follicle and follicle-stroma integrity categories, and regions considered as artefact (clear space) for each category were measured using ImageJ (National Institutes of Health, Bethesda, MD, USA) (Supplementary Fig. S1). In assessing follicle integrity, regions of artefact were identified and the total area of these measurements within the follicle was calculated as a percentage of the total follicular area. Only follicles with a visible oocyte nucleus or nuclear membrane were included in this assessment. Follicle-stroma integrity was determined by measuring the total perimeter of non-interaction between the follicle and the stroma and calculated as a percentage of the total follicular perimeter. Stroma integrity was determined by measuring the total area of artefact within the stroma as a percentage of the total stroma area for each section analysed, using thresholding. Thresholding involved the conversion of images to 8 bits, which changed the coloured image to black and white; carried out for all sections. Threshold values were adjusted using the original colour image as a reference to discriminate artefact from stained regions of tissue. Spaces due to blood vessels and previously assessed categories (follicle and follicle-stroma integrity) were excluded from the stroma integrity analysis. To avoid double counting of follicles, analysed sections of human and sheep ovaries were at least 25 µm apart while mouse ovary sections were at least 100 µm apart. Sections selected for analysis were distributed throughout the tissue. All sections were assessed blindly.

Ovarian follicle classification

Follicles were classified according to established criteria (Pedersen and Peters, 1968; Gougeon, 1996; Lundy *et al.*, 1999; Grasa *et al.*, 2015; Walker *et al.*, 2019); primordial (oocyte is surrounded by a single layer of flattened pre-granulosa cells), transitional (a mixed layer of flattened and cuboidal granulosa cells surrounding the oocyte), primary (minimum of a complete layer of cuboidal cells surrounding the oocyte), and secondary (two layers of cuboidal granulosa cells surrounding the oocyte). Mouse pre-antral follicles were defined as having many granulosa cell layers with interspersed fluid filled areas and antral follicles were those that contained many layers of granulosa cells and a large antral cavity (Pedersen and Peters, 1968).

Immunohistochemistry using diaminobenzidine and immunofluorescence

All IHC/immunofluorescence (IF) experiments were performed at least twice for each individual sample tested. Sections containing follicles of appropriate developmental stage were selected for IHC/IF, but not all patient samples were used for IHC/IF analyses owing to the limited numbers of follicles on sections (Table I).

Immunohistochemical evaluation was performed on sections fixed in NBF and Form-Acetic for 8 h and 24 h for the following antibody targets: fork-head box O3 (FOXO3a; transcription factor), fork-head box protein L2 (FoxL2; transcription factor), anti-Müllerian hormone (AMH; hormone), laminin α1 and collagen IV (extracellular matrix proteins). Following dewaxing and rehydration, sections were subject to no antigen retrieval (No AR) or heat-induced antigen retrieval (AR) by microwave heating for 10 min with a further 20 min cool-down period using either sodium citrate (pH 6.0) (for FOXO3a and collagen IV) or 1× antigen unmasking solution, Tris-based (Vector Laboratories, Peterborough, UK, H-3301) (for FoxL2, laminin and AMH). Sections (for DAB staining only) were then treated with 3% hydrogen peroxide for 5 min and washed in PBS (20 mM phosphate, 150 mM NaCl, pH 7.4) for 5 min two times to block endogenous peroxidase activity.

To detect AMH, FOXO3a, collagen IV and laminin proteins, sections were blocked in 5% normal goat serum (NGS; Vector) in PBS with 0.05% Tween 20 (Fisher Scientific, Loughborough, UK) (PBS-T) to prevent non-specific binding for 1 h at room temperature. Sections were incubated in 5% NGS in PBS-T overnight at 4°C with mouse monoclonal anti-AMH (1:100; Biorad, Dalkeith, UK, MCA2246), rabbit monoclonal anti-FOXO3a (1:100; Cell Signaling Technology, UK, 12829S), rabbit polyclonal anti-collagen IV (1:100; Millipore, Hertfordshire, UK, AB8201), or rabbit polyclonal anti-laminin α1 (1:30; Sigma, L9393). For FoxL2 detection, sections were blocked with 5% rabbit serum (Sigma, R9133) in PBS-T for 1 h at room temperature followed by goat polyclonal anti-FoxL2 (1:500; Novus Biologicals, Oxon, UK, NB100-127755) overnight at 4°C. The sections were washed three times for 5 min in PBS-T and incubated in the following secondary antibodies: biotinylated goat anti-mouse IgG (Vector Laboratories, UK, BA-9200, 1:100 dilution) for AMH, goat anti-rabbit IgG (Vector Laboratories, BA-1000, 1:200 dilution) for FOXO3a, collagen IV and laminin, and rabbit anti-goat (Vector Laboratories, BA-5000, 1:300 dilution) for FoxL2 for 1 h at room temperature. Negative control sections were treated with the following appropriate IgG antibodies: purified mouse IgG κ isotype (Biolegend, London, UK, 401401), rabbit mAb IgG XP isotype control (Cell Signaling Technology, DA1E) and for FoxL2, the negative control section had the primary antibody omitted. Following secondary antibody incubation, sections were washed in PBS-T for 3 min, three times.

Staining was achieved using the Vectastain ABC Elite kit (Vector Laboratories) for 30 min at room temperature followed by a final development with a DAB peroxidase substrate kit (Vector Laboratories). Slides were counterstained in Gills 2 haemotoxylin, mounted and images were captured using the QImaging Micropublisher 6 camera and accompanying Ocular imaging software (QImaging, Canada) and the Lumenera Infinity 5 camera and accompanying Infinity Analyze software (Teledyne Lumenera, Nepean, Canada).

A portion of slides labelled to detect AMH (after AR) were visualised using fluorescence. Following secondary antibody incubation as

described above, sections were incubated with streptavidin Alexa Fluor 568 conjugate (1:200; Thermo Fisher, S11226) for 30 min at room temperature. Slides were washed in PBS-T and counterstained with 5 µg/mL DAPI (Sigma, D9542) before being mounted with Vectashield® Hardset™ Antifade mounting medium (Vector Laboratories, H-1400).

Fluorescent-labelled sections were imaged under a fluorescent microscope (Leica DMRBE) with LED illumination and DAPI-FITC-TRITC filters. Images were captured using the QImaging Retiga R3 camera and Velocity software. All sections were imaged using the same acquisition settings (laser power, gain, and exposure). Post-imaging processing was performed using ImageJ to enhance qualitative aspects (brightness and contrast) of the red channel (fluorescent AMH labelling) to allow for increased visibility of figures in print. All adjustments were made following best-practice guidelines (Lee and Kitaoka, 2018), with all images (control and experimental across all groups) treated and adjusted identically with adjustments applied uniformly to whole images. Imaging processing steps involved adjusting the upper and lower limits of the display range by modifying the minimum and maximum settings of the image (16-bit). The optimal range was first determined using the sample with the lowest level of observed signal (24 h Form-Acetic) and the corresponding IgG negative control to ensure high signal visibility with minimal background. The same settings were then applied to all other sample groups. The blue channel (DAPI counterstain) was not altered.

TUNEL assay

Detection of double-stranded DNA breaks was performed using the Click-IT™ Plus TUNEL assay (Invitrogen, UK, C10618) according to the manufacturers' instructions on 8 h and 24 h NBF and Form-Acetic fixed human and mouse sections. Slides were counterstained with 5 µg/mL DAPI, mounted with Vectashield Hardset Antifade mounting medium and imaged under a fluorescent microscope with LED illumination and DAPI-FITC-TRITC filters. Positive control sections were treated with 1 IU/ml DNase I (Invitrogen, 18047019).

Statistical analyses

All statistical analyses were performed using R statistical software version 4.0.2. (R Foundation for Statistical Computing, Vienna, Austria). Linear mixed effects regressions (lm4e package; Bates *et al.* 2015) were used to detect the effect of fixative and duration on histological scores (follicle integrity, follicle-stroma integrity, and stroma integrity), where individual was included as a random effect to adjust for individual variation. Data are presented as mean ± SEM and statistical significance was defined as $P < 0.05$.

Results

Form-Acetic preserves and improves ovarian tissue morphology

Ovarian tissue from human, sheep, and mouse were fixed in NBF, Bouin's, and Form-Acetic for 4, 8, and 24 h (Figs 1, 2, and 3). The fixed tissue was processed and stained with H&E. Within the stroma of NBF fixed tissue, artefact was often seen. NBF also introduced artefact that affected follicle-stroma integrity wherein intact follicles receded away from the stroma. NBF also caused shrunken ooplasms within oocytes and granulosa cell nuclei condensation, thereby affecting the follicle integrity (Figs 1, 2, and 3). In Bouin's fixation, all three categories (follicle integrity, follicle-stroma integrity, stroma integrity) were affected in human and sheep tissues while in mouse, the stroma integrity was mainly affected. Infrequently seen in Form-Acetic fixed sections was artefact that affected all three categories (Figs 1, 2, and 3).

The percentage of tissue shrinkage after fixation was measured using ImageJ. Table I provides details on patient samples involved in the histological analyses. Following histological assessments, fixation in Form-Acetic or Bouin's resulted in lower levels of artefact in human and mouse ovarian samples compared to NBF for all three categorical measures at all three-time points: 4, 8, and 24 h. For sheep ovarian samples, the level of artefact was reduced at all three time points for two of the three categories (follicle-stroma integrity and stroma integrity) whereas follicle integrity was improved by Form-Acetic compared to NBF at 24 h, but not 4 or 8 h (Fig. 4).

When comparing Form-Acetic to Bouin's for mouse ovarian sections, the level of artefact in sections was equivalent for all three artefact categories for the same duration of fixation. When comparing Bouin's and Form-Acetic for both the human and sheep samples, where there was a significant difference between the fixatives the level of artefact in Form-Acetic was always lower (Fig. 4).

When comparing the duration of fixation (4, 8, and 24 h) within a category and a species, the level of artefact in NBF fixed tissues differed significantly in five of the nine comparisons (Fig. 4) as compared to two of nine for Bouin's and one of nine for Form-Acetic. Moreover, for some measures, integrity improved with duration in NBF (human stroma and sheep follicle integrity), but for others, integrity decreased with time (sheep follicle-stroma) or increased from 4 to 8 h then decreased at 24 h (stroma integrity). This indicated that NBF-induced artefact is less predictable and more variable with duration of fixation than Bouin's and Form-Acetic.

In ovine samples, 4 h fixation in Form-Acetic was more comparable to Bouin's fixed samples (Fig. 4) and resulted in increased artefact compared to 8 and 24 h fixation. Based on these data, we focussed on 8 and 24 h for further analyses.

The above describes comparisons made between the different fixatives for each time point, and for each fixative solution for different fixation durations. Further comparisons were performed between the groups and the results can be found in Supplementary Tables SI, SII, and SIII.

Form-Acetic fixation is compatible with histological staining

To determine the compatibility of Form-Acetic with other histological stains, PAS and Masson's trichrome stains were performed on 8 and 24 h NBF, Bouin's and Form-Acetic fixed sections.

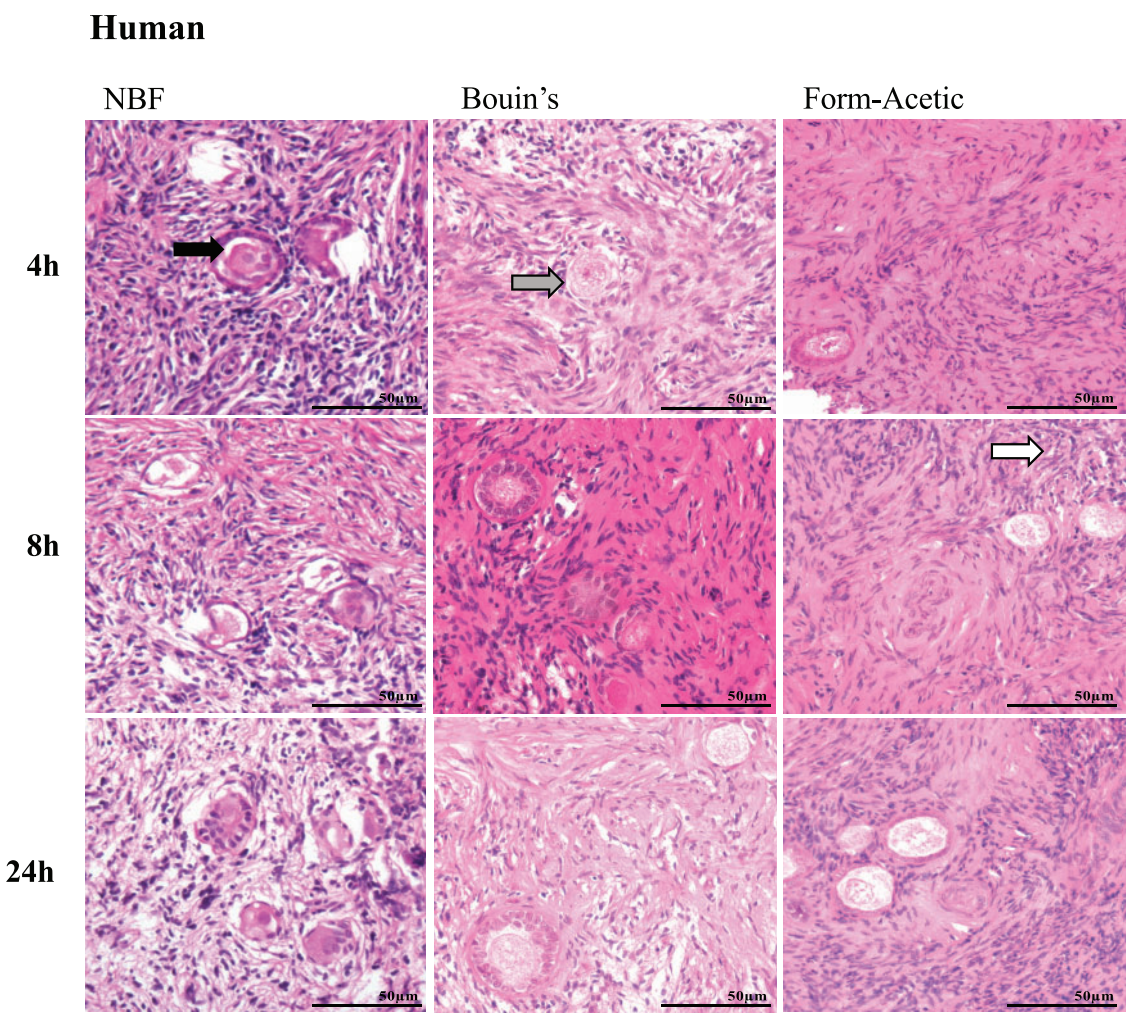

Figure 1. Representative images of haemotoxylin & eosin stained human ovarian sections prepared with different fixatives. Prior to haemotoxylin & eosin (H&E) staining, human ovarian tissue sections were fixed in neutral buffered formalin (NBF), Bouin's and Form-Acetic (NBF with 5% acetic acid) solution for 4 h, 8 h, and 24 h. Arrows highlight regions of artefact including: intact follicles receding away from the stroma (follicle-stroma integrity; grey arrow), shrunken ooplasms within oocytes (follicle integrity; black arrow), granulosa cell nuclei condensation, and space within the stroma (stroma integrity; white arrow). Images are representative of human ovarian cortex samples, n=3 patients per condition (fresh n=2, frozen n=1).

Periodic acid-Schiff

In human ovarian tissue, carbohydrate moieties in the basement membrane and zona pellucida of follicles were distinctly stained magenta by the PAS (Fig. 5A) irrespective of which fixative was used. In mouse sections, the zona pellucida was distinctly magenta in all conditions (Fig. 5B). In sheep sections, the basement membrane was also faintly magenta in all conditions but much less compared to the mouse and human samples (Fig. 5C).

Masson's trichrome Masson's trichrome is an extracellular matrix dye, which stains collagen blue, nuclei blue-black, and muscles/cytoplasm red. Staining was performed on human and sheep samples only as mouse ovarian tissue contains very little collagen-enriched stroma (Berkholtz *et al.*, 2006). All fixatives were compatible with the Masson's trichome stain, revealing a similar staining pattern of the various cellular structures between conditions (Fig. 6A and B). The stain also revealed the clear spaces introduced by the fixation of ovarian tissues.

Form-Acetic is compatible with immunohistochemical studies

To determine whether Form-Acetic was compatible with immunolabelling, NBF and Form-Acetic fixed human, mouse, and sheep samples (8 and 24 h) were subject to IHC, with and without AR. In human and mouse, a range of antibodies, encompassing different antigen categories, were tested: FOXO3a, FoxL2, collagen IV, laminin, and AMH, using DAB for visualisation. Compatibility of Form-Acetic with fluorescent detection was also

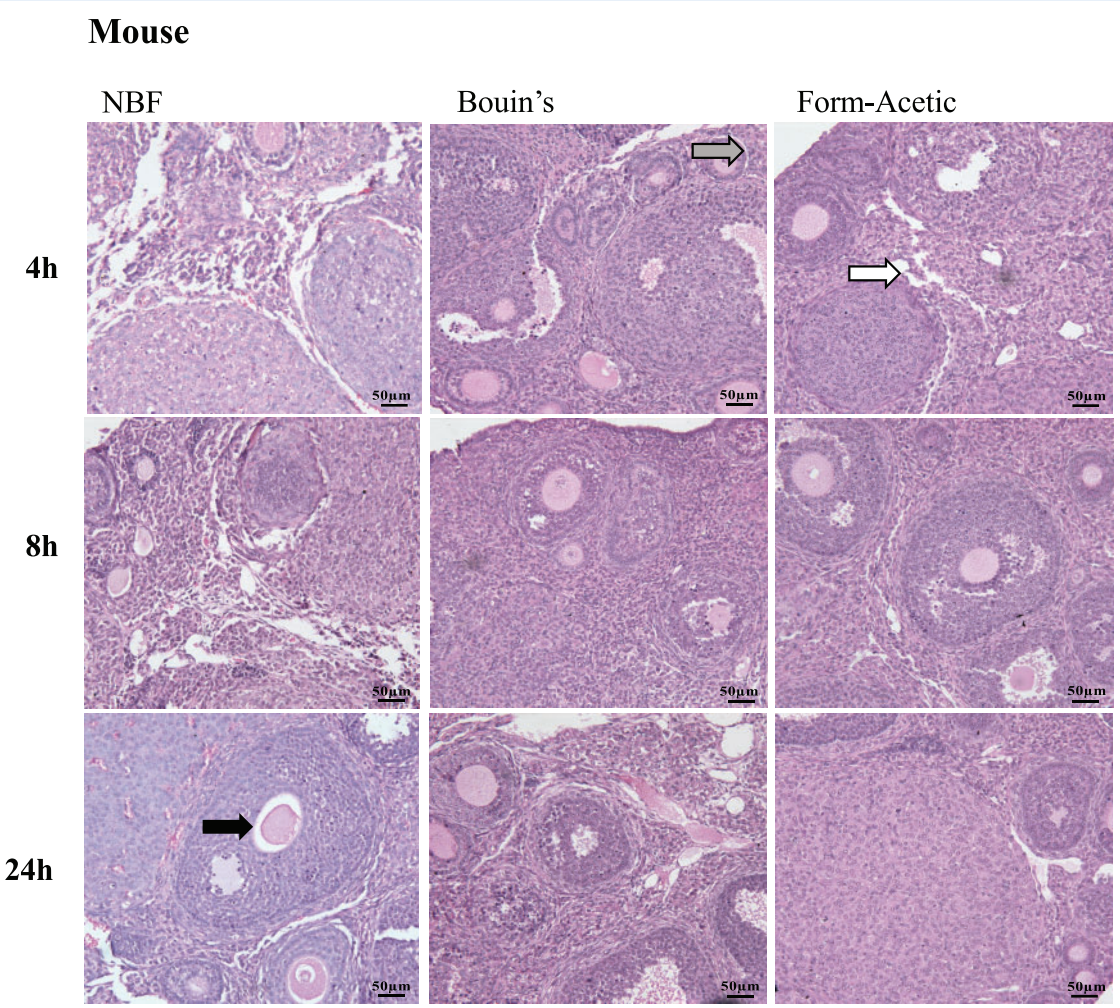

Figure 2. Representative images of H&E stained mouse ovarian sections prepared with different fixatives. Prior to H&E staining, mouse ovarian tissue sections were fixed in NBF, Bouin's and Form-Acetic (NBF with 5% acetic acid) solution for 4 h, 8 h, and 24 h. Arrows highlight regions of artefact including: intact follicles receding away from the stroma (follicle-stroma integrity; grey arrow), shrunken ooplasms within oocytes (follicle integrity; black arrow), granulosa cell nuclei condensation and space within the stroma (stroma integrity; white arrow). Images are representative of mouse ovaries, n=3 animals per condition.

validated in human tissue using AMH labelling with AR. Labelling for sheep samples was carried out for AMH, collagen IV, and laminin proteins only owing to poor antigenicity of FoxL2 and FOXO3a antibodies to sheep antigens. Table I provides details on patient samples involved in IHC analyses. Experiments using NBF and Form-Acetic fixed sections for each species were carried out in the same assay (for each antigen) and subjected to the same DAB exposure time; DAB exposure times varied depending on antibody used.

Form-Acetic allows detection of a nuclear/cytoplasmic transcription suppressor—FOXO3a

FOXO3a was detected in the oocytes and granulosa cells of primordial and primary follicles of AR-treated human and murine sections fixed for 8 and 24 h in NBF and Form-Acetic (Fig. 7). However, when AR was not performed, FOXO3a was not detected in human ovarian sections irrespective of fixation (Fig. 7). In mouse samples without AR, however, FOXO3a was detected faintly in both Form-Acetic and NBF fixed sections at both time points (Fig. 7).

Form-Acetic allows nuclear detection of a transcription factor—FoxL2

FoxL2 was detected in the granulosa cells of transitional to pre-antral stage follicles of NBF and Form-Acetic fixed human and murine samples that had been subject to AR (Fig. 8). Staining was also observed in the ooplasm of follicles in human sections (Fig. 8). Without AR, FoxL2 was only detected in Form-Acetic fixed human and mouse samples but not NBF fixed (Fig. 8).

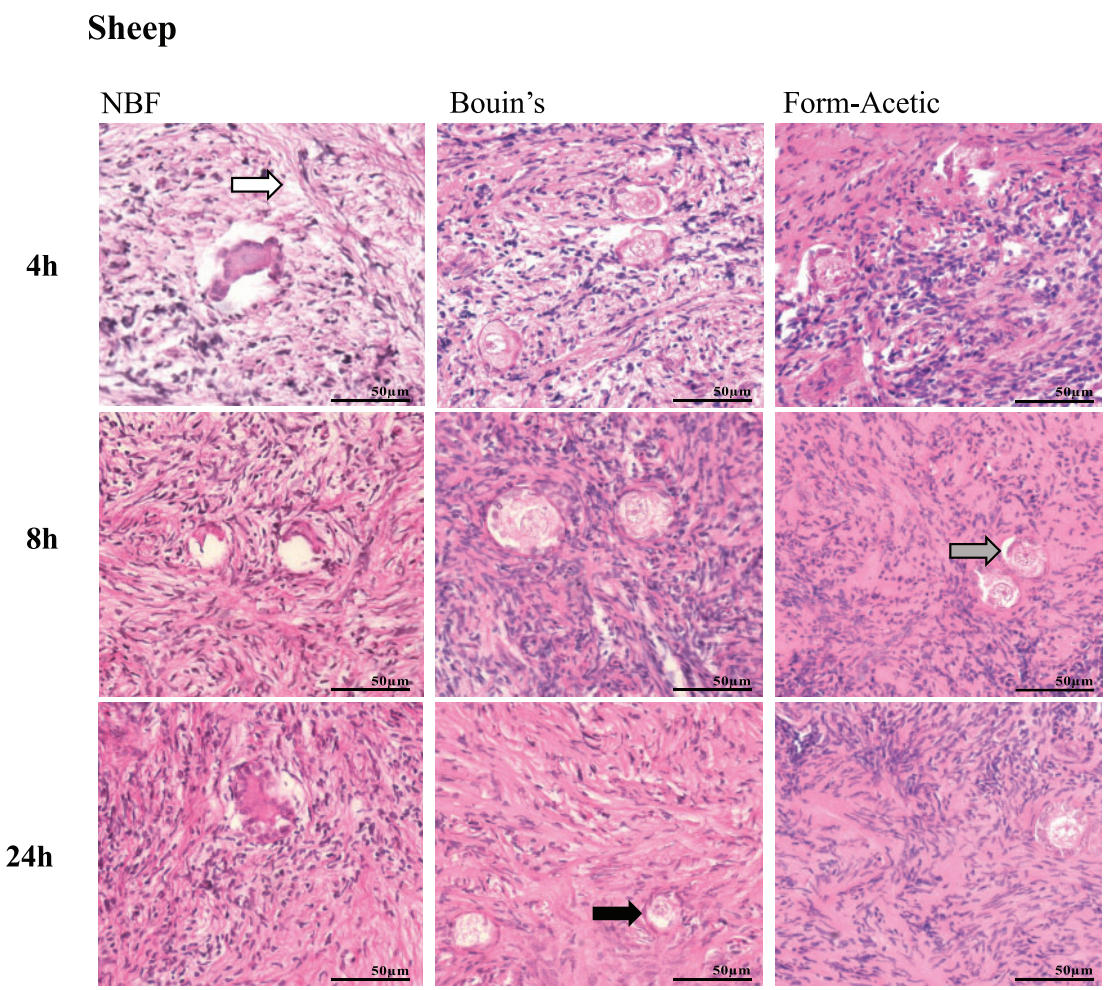

Figure 3. Representative images of H&E stained sheep ovarian sections prepared with different fixatives. Prior to H&E staining sheep ovarian tissue sections were fixed in NBF, Bouin's and Form-Acetic (NBF with 5% acetic acid) solution for 4 h, 8 h, and 24 h. Arrows highlight regions of artefact including: intact follicles receding away from the stroma (follicle-stroma integrity; grey arrow), shrunken ooplasms within oocytes (follicle integrity; black arrow), granulosa cell nuclei condensation, and space within the stroma (stroma integrity; white arrow). Images are representative of sheep ovarian cortex samples, n=3 animals per condition.

Form-Acetic allows detection of extracellular matrix components

Following AR, both laminin and collagen IV were detected in follicular cells, basement membranes, blood vessels and within the stroma for both NBF and Form-Acetic fixed human, mouse and sheep ovarian sections after 8 and 24 h fixation (Figs 9 and 10). Without AR, laminin was detected in both NBF and Form-Acetic fixed sections from human, mouse and sheep ovaries (Fig. 9). However, without AR, collagen IV was robustly detected only in Form-Acetic fixed human ovarian sections and not NBF fixed human tissue and not in mice or sheep tissue prepared in either fixative (Fig. 10).

Form-Acetic facilitates detection of a soluble glycoprotein hormone—AMH

For AMH, a robust signal was observed following AR treatment in and around the granulosa cells of human primary follicles and mouse pre-antral stage follicles after Form-Acetic and NBF fixation (Fig. 11). AMH was also strongly detected after AR in sheep tissues fixed for 8 h in Form-Acetic, but less so for those fixed in NBF; images are from the same experiment. For 24 h sheep samples, a robust signal was observed in granulosa cells of Form-Acetic fixed follicles, however owing to the lack of a comparable follicle in the NBF fixed sheep ovaries, a direct comparison cannot be made between NBF and Form-Acetic fixed tissues. When AR was not performed, AMH was robustly detected in Form-Acetic fixed mouse and sheep sections but more weakly in human sections, whereas after NBF fixation, a weak signal was observed only in mouse tissues and not in human or sheep tissues (Fig. 11).

Form-Acetic also proved compatible with IF, as AMH was detected in the granulosa cells of both NBF and Form-Acetic fixed human sections after 8 and 24 h fixation (Fig. 12). Autofluorescence caused by lipofuscin was present in oocytes and stroma in both NBF (8 h) and Form-Acetic (8 and 24 h) fixed tissues but appeared more abundant in Form-Acetic fixed samples (Fig. 12).

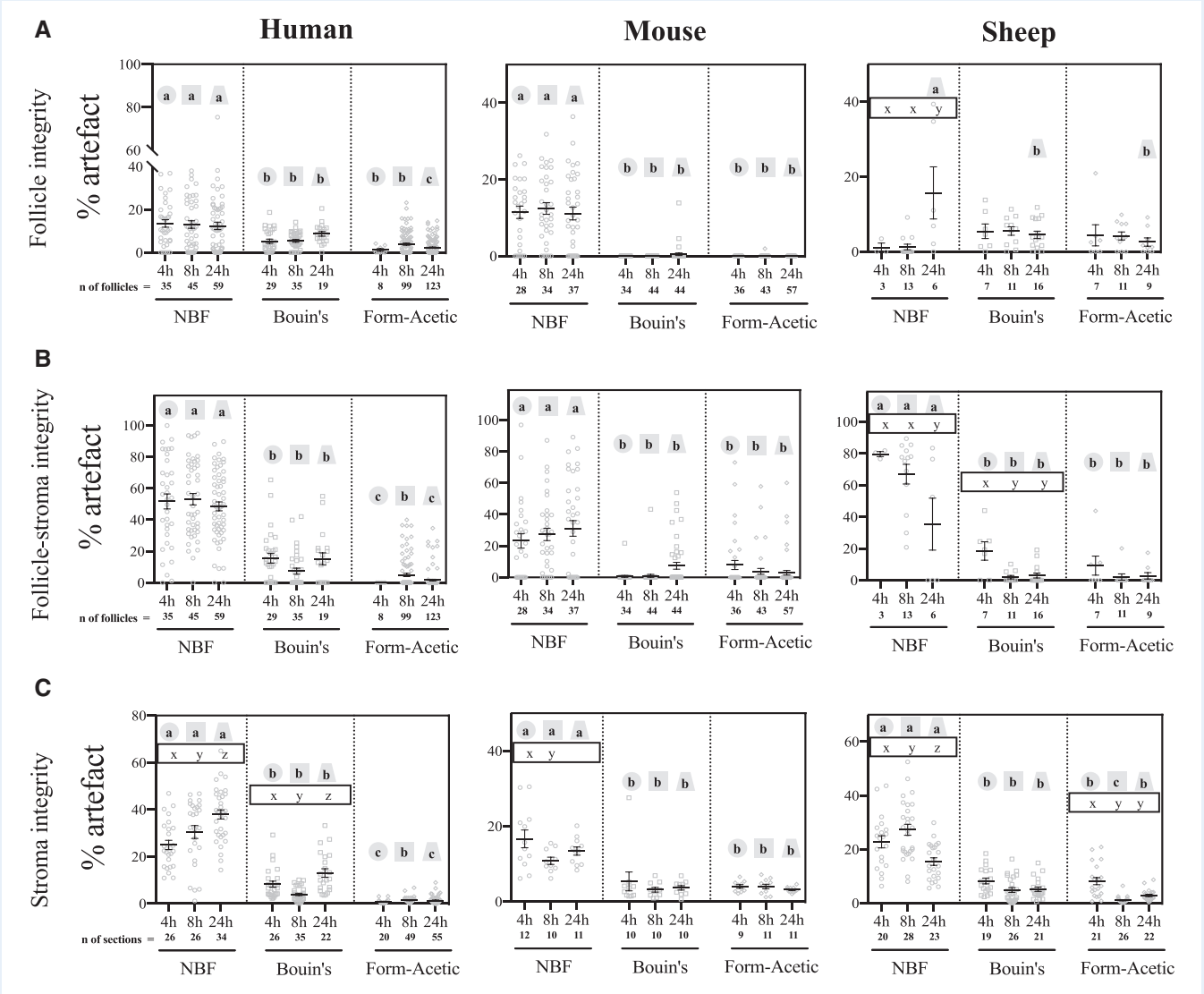

Figure 4. Histological assessments of fixative conditions using H&E stained human, mouse and sheep ovarian sections. Ovarian sections of human, mouse and sheep were fixed in NBF, Bouin's and Form-Acetic (NBF with 5% acetic acid) for 4 h, 8 h, and 24 h. Histological assessments were performed to determine the morphological integrity of follicles, the follicle and stroma interaction, and the stroma. The percentage of 'clear space' (referred to as artefact) was measured to determine follicle integrity (A, top panel), follicle-stroma integrity (B, middle panel) and stroma integrity (C, bottom panel) after fixation in different fixatives. Percentages are represented as grey symbols with the mean ± SEM (in black) also shown. Calculations were performed to determine the degree of artefact associated with each condition. Significance between any two variables was determined with linear mixed effects regressions (lm4e package; Bates *et al.* 2015) using R statistical software version 4.0.2. A significant difference between variables is indicated by different letters on the graph ($P<0.05$). The letters a/b/c are used to denote significance between the different fixatives at a specific time-point. Each time-point, independent of the fixative, has the same shape around letters of significance to indicate that comparisons are between the fixative groups at that particular time. In contrast, the letters *x*/*y*/*z* denote significance within a fixative group only. The letters are within the same shape outline to show that comparisons are within the fixative group between the different times. Where no letter is seen to represent significance between or within groups, this suggests that no significant difference was seen between conditions. Further information on significance levels is provided in Supplementary Table SI. Images used for analysis were from n=3 different individuals per condition.

Form-Acetic fixation does not inhibit the TUNEL assay

To validate the compatibility of Form-Acetic fixation in detecting double-stranded DNA breaks, the TUNEL assay was performed. Fragmented DNA was distinctly labelled after both 8 and 24 h of fixation in both NBF and Form-Acetic mouse and human ovarian tissue (Fig. 13). The TUNEL assay was also performed multiple times using DAB as the means of detecting fragmented DNA and, again, we observed TUNEL-positive cells at both time points for both NBF and Form-Acetic fixed mouse ovarian sections (data not shown).

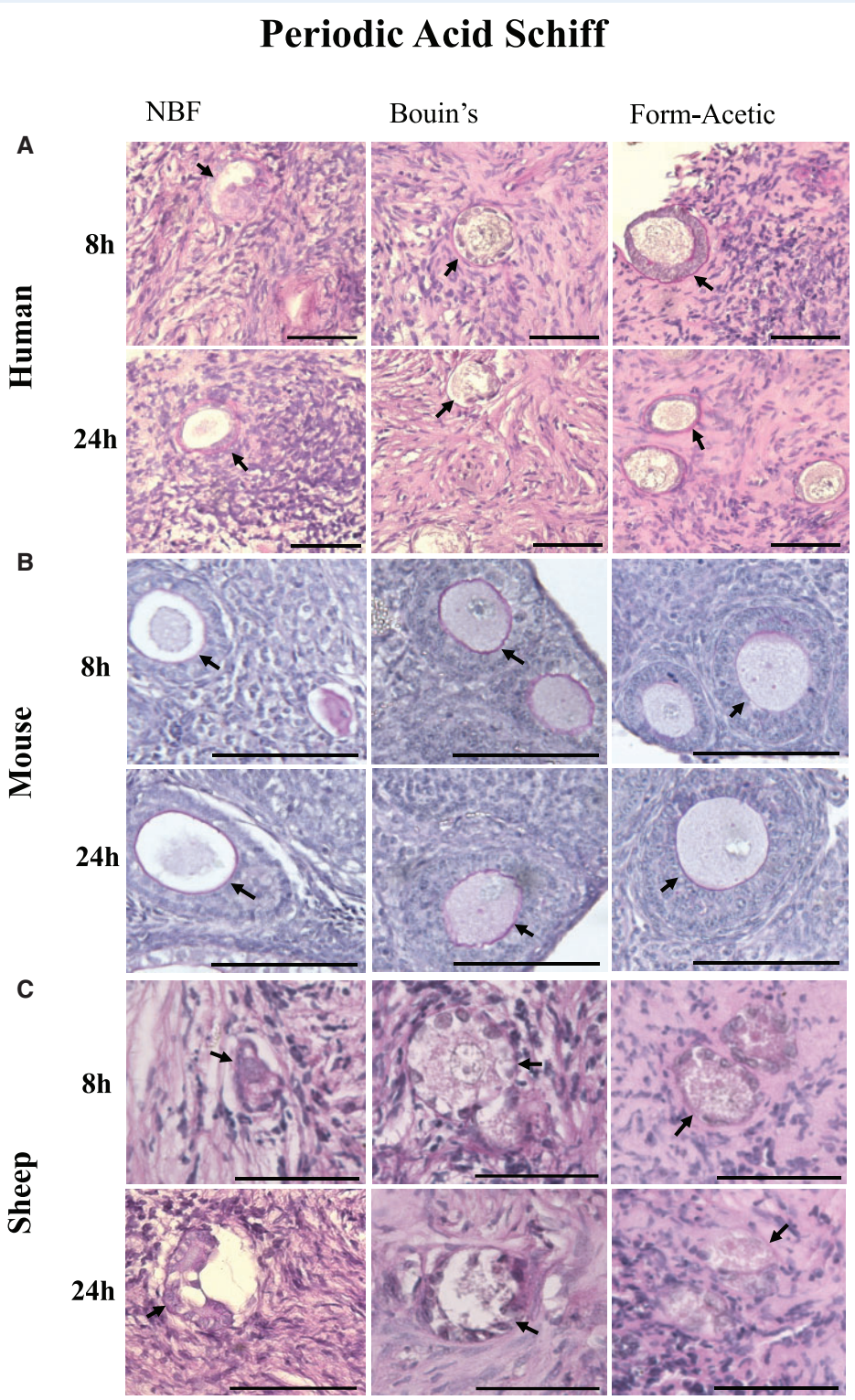

Figure 5. Periodic acid Schiff stain of human, mouse and sheep ovarian tissue prepared with different fixatives. Periodic acid Schiff (PAS) staining was performed on (A) human, (B) mouse and (C) sheep ovarian sections fixed in NBF, Bouin's, and Form-Acetic (NBF with 5% acetic acid) for 8 h and 24 h. Images are representative of human ovarian cortex samples, n=2 patients per condition (fresh n=2), sheep ovarian cortex samples, n=3 animals per condition, and mouse ovaries, n=3 animals per condition. Scale bar represents 50 μm.

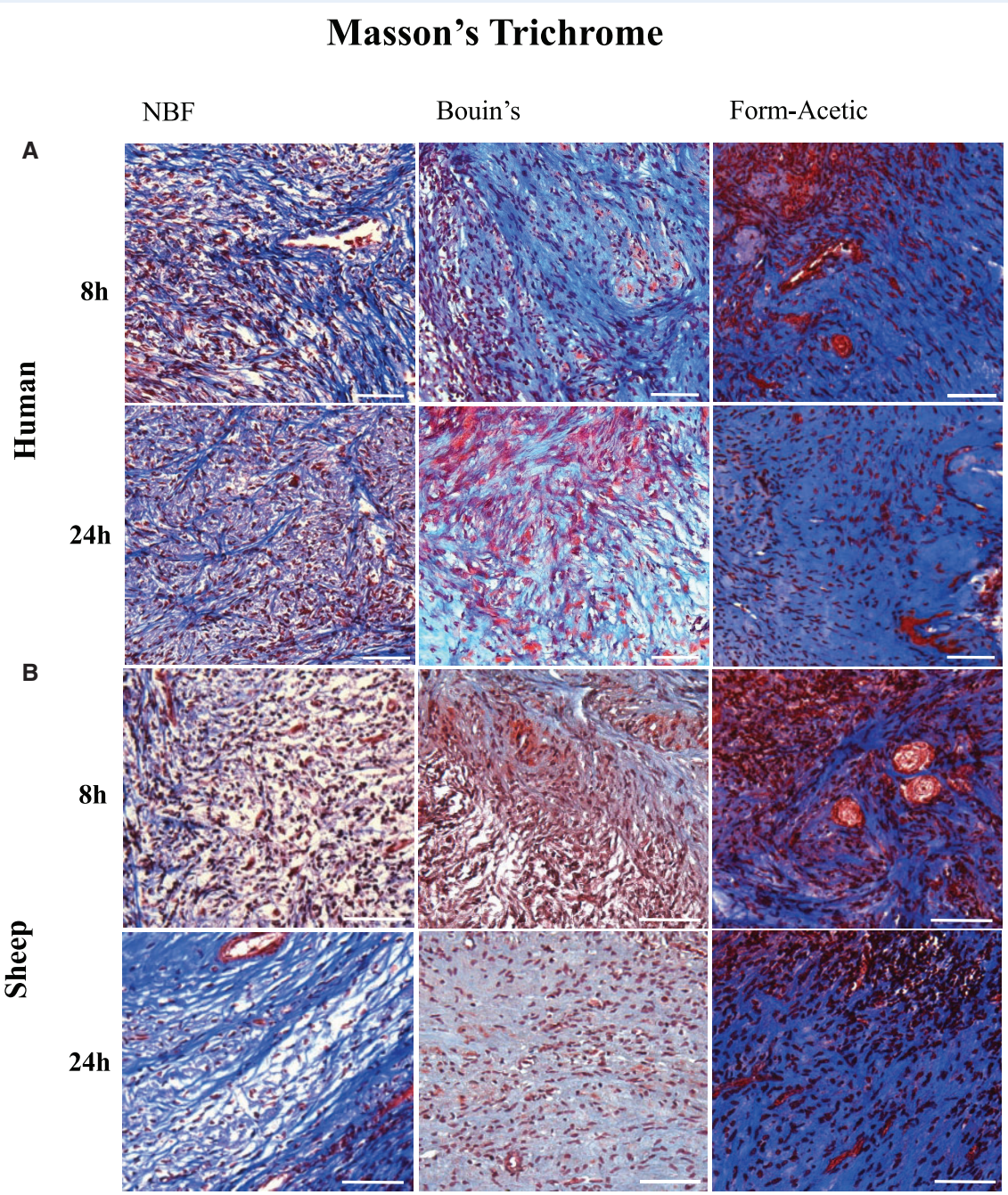

Figure 6. Masson's trichrome stain of human and sheep ovarian tissue prepared with different fixatives. Masson's trichrome staining was performed on (A) human and (B) sheep ovarian sections fixed in NBF, Bouin's, and Form-Acetic (NBF with 5% acetic acid) for 8 h and 24 h. Images are representative of human ovarian cortex samples, n=2 patients per condition (fresh n=2) and sheep ovarian cortex samples, n=3 animals per condition. Scale bar represents 50μm.

Discussion

The study aimed to develop a fixative that not only preserved ovarian tissue morphology without introducing artefact but also could enable downstream histological molecular assays involving protein and nuclear material detection. We identified that fixation with Form-Acetic preserved ovarian tissue morphology and in most cases was capable of reducing artefact in three different species. We also demonstrated that Form-Acetic showed compatibility with multiple histological stains, including H&E, PAS and Masson's trichrome, allowing for clear detailing of microstructures within fixed sections. Critically, tissues from the three species proved to be suitable for IHC and a wide range of

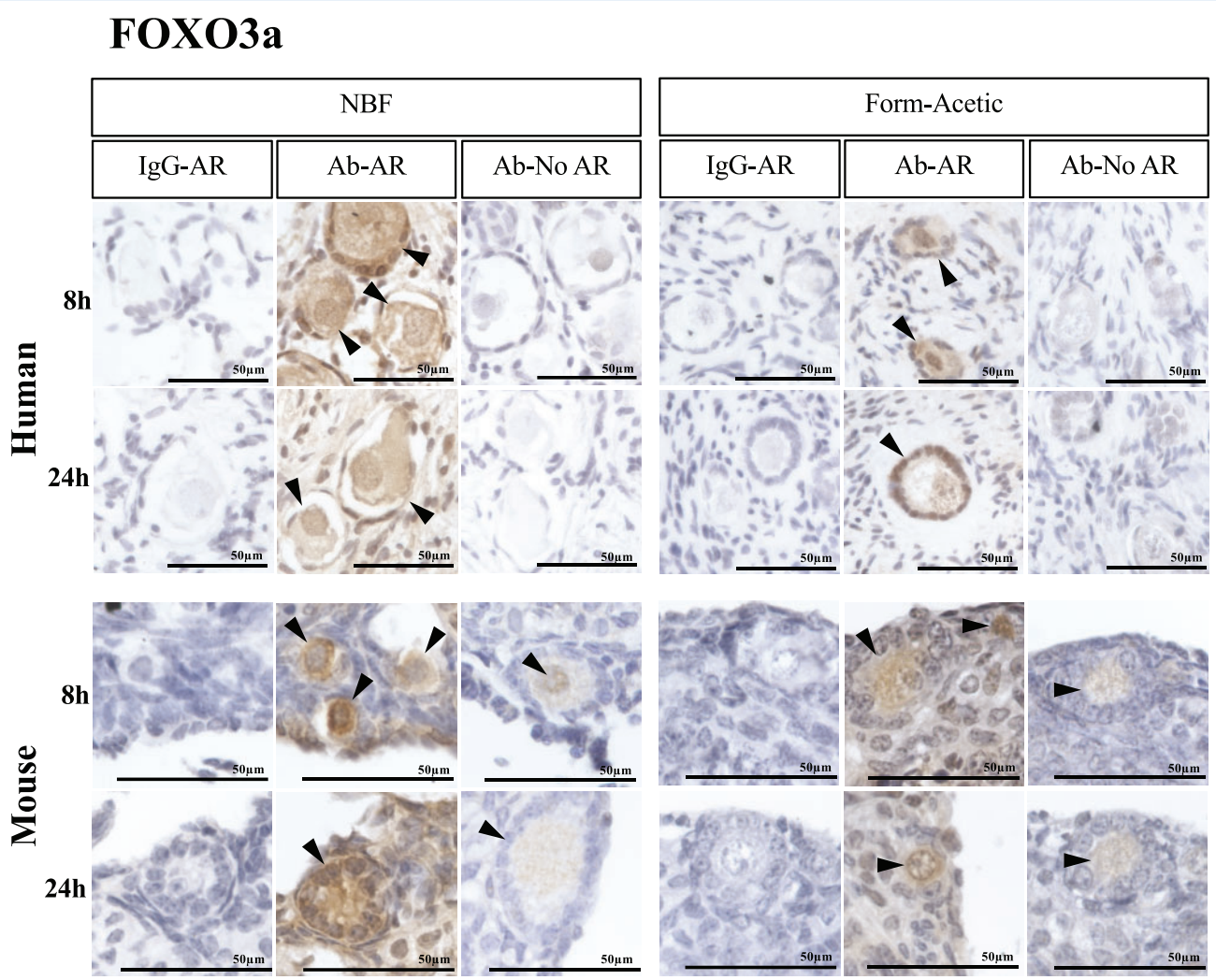

Figure 7. Detection of FOXO3a using immunohistochemistry in human and mouse ovarian tissue preserved with different fixatives. Following the fixation of ovarian tissue in NBF and Form-Acetic (NBF with 5% acetic acid) solutions for 8 h and 24 h, immunohistochemistry (IHC) was performed on human and mouse ovarian sections. Fork-head box O3 (FOXO3a) (a transcription factor), was detected in the oocytes of primordial to primary follicles. Follicles/cells positively stained are indicated by the arrowheads. IgG-AR: isotype IgG control was applied on the section treated with antigen retrieval (AR), Ab-AR: antibody was applied, and an AR step was performed, Ab-No AR: antibody was applied, and no AR step was performed. Images are representative of experiments using human ovarian cortex samples, n=5 patients per condition (fresh n=3, frozen n=2), and mouse ovaries, n=3 animals per condition. IHC experiments were performed at least twice for each sample. NB: The 12 images in each panel for a single species were all from the same experiment with the same DAB exposure enabling direct comparison between the samples.

proteins (FOXO3a, FoxL2, collagen IV, laminin, and AMH) were detected in tissue fixed with Form-Acetic, consistent with NBF in this study and studies by other groups using NBF (Yamada *et al.*, 1999; Berkholtz *et al.*, 2006; John *et al.*, 2008; Pisarska *et al.*, 2010; Campbell *et al.*, 2012; Kallio *et al.*, 2012; Heeren *et al.*, 2015; Saatcioglu *et al.*, 2016; Fujisawa *et al.*, 2018; Eivazkhani *et al.*, 2019; Ouni *et al.*, 2019). It was also noted that proteins were detected similarly in both frozen-thawed and fresh human tissue fixed in Form-Acetic. Lastly, we established that AMH detection was equivalent in Form-Acetic fixed sheep and human ovarian sections prepared 14 months earlier compared to those freshly prepared. Based on our results, we, therefore, recommend the use of Form-Acetic as a fixative in ovarian research.

Shrinkage introduced by NBF poses a concern, occurring in diverse tissue types ranging from 50% in oesophageal tissue (Siu *et al.*, 1986) to 34% in breast tissue (Yeap *et al.*, 2007). In this study, we did not measure loss in tissue volume following NBF fixation but compared artefact levels in NBF fixed tissue to Form-Acetic fixed tissue, which presented minimal artefact. It has been proposed by Jones (1972) that the shrinkage seen in NBF-fixed tissue, especially breast and fatty tissue, may be a consequence of lipid degradation by formaldehyde into its water-soluble components and explains that subsequent cellular dehydration presents the shrinkage that we observe during histology. With Form-Acetic, however, this shrinkage does not occur owing to the properties of acetic acid. Acetic acid is a frequent component of

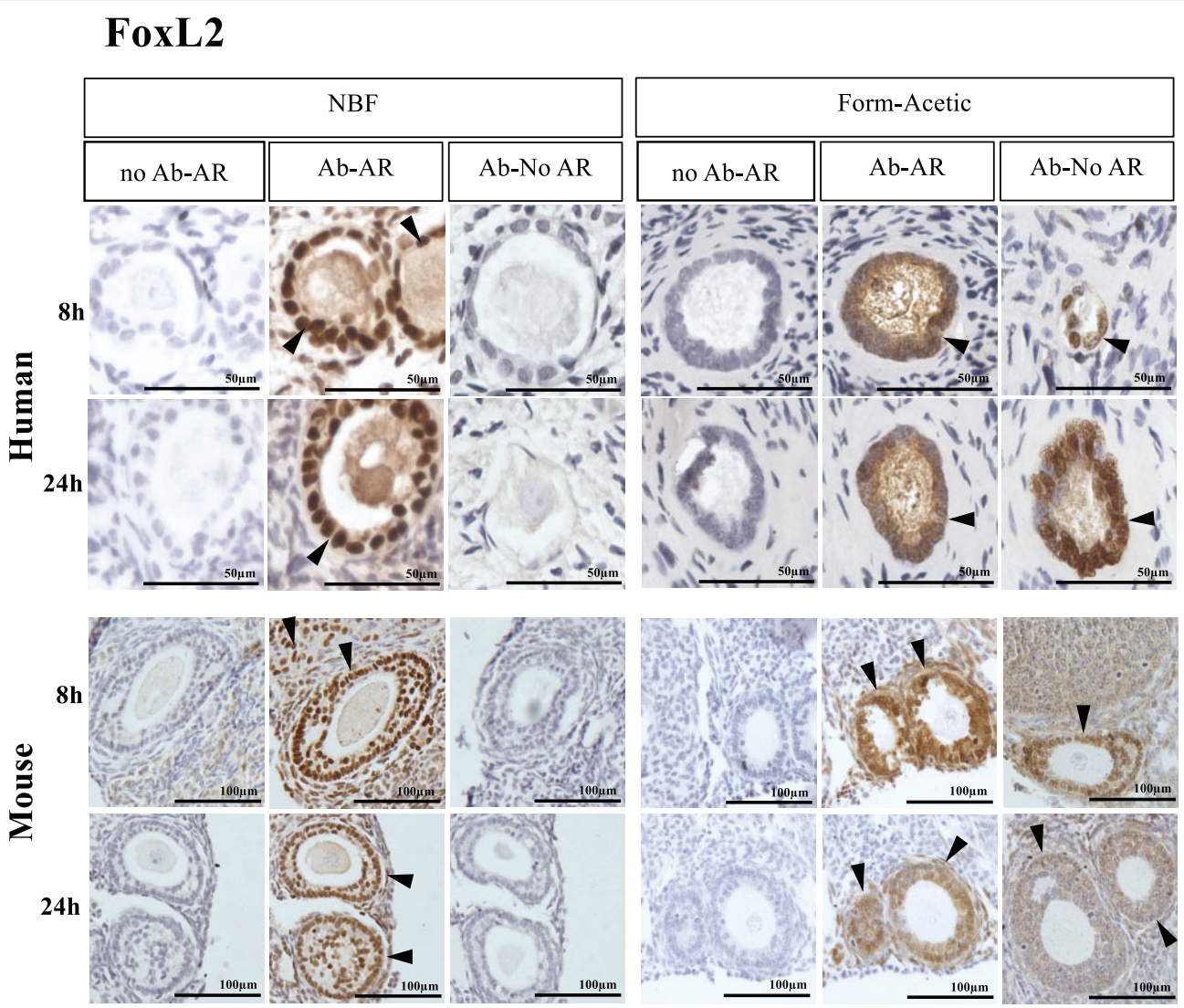

Figure 8. Detection of FoxL2 using IHC in human and mouse ovarian tissue preserved with different fixatives. Following the fixation of ovarian tissue in NBF and Form-Acetic (NBF with 5% acetic acid) solutions for 8 h and 24 h, IHC was performed on human and mouse ovarian sections. Fork-head box protein L2 (FoxL2, a transcription factor) was detected in the granulosa cells of follicles. Follicles/cells positively stained are indicated by the arrowheads. No Ab-AR: no antibody was applied on the section treated with AR (control), Ab-AR: antibody was applied, and an AR step was performed, Ab-No AR: antibody was applied, and no AR step was performed. FoxL2 images are representative of experiments using human ovarian cortex samples, n=4 patients per condition (fresh n=2, frozen n=2), and mouse ovaries, n=3 animals per condition. IHC experiments were performed at least twice for each sample. NB: The 12 images in each panel for a single species were all from the same experiment with the same DAB exposure enabling direct comparison between the samples.

fixative solutions, including Bouin's, and is known to counteract the shrinkage introduced by picric acid in Bouin's solution (Howat and Wilson, 2014). It is likely that this enriching property of the acid is responsible for the reduced proportion of artefact in Form-Acetic fixed tissue as observed in this study. It is also possible that the acetic acid might be protecting the tissue during the post-fixation processing events that can also cause shrinkage (Baker, 1958).

Acetic acid is a weak acid and its presence in Form-Acetic rendered AR redundant for some IHC analyses, potentially related to the ability of acetic acid to break down cross-linkages between protein molecules (Baker, 1958). Borkar *et al.* (2011) detailed the denaturing property of 9 M glacial acetic acid in the presence of the HIV protease, showing a direct interaction between certain regions of the protein and acetic acid molecules. In our study, 0.874 M acetic acid was used; therefore, it is possible that the concentration and quick penetration rate of acetic acid within the fixative is sufficient to preserve epitopes that would otherwise be altered by formaldehyde fixation but not denature the protein thereby enabling protein detection without AR.

Acetic acid cross-links nucleoproteins but not cytoplasmic proteins and is also known not to preserve the Golgi apparatus or

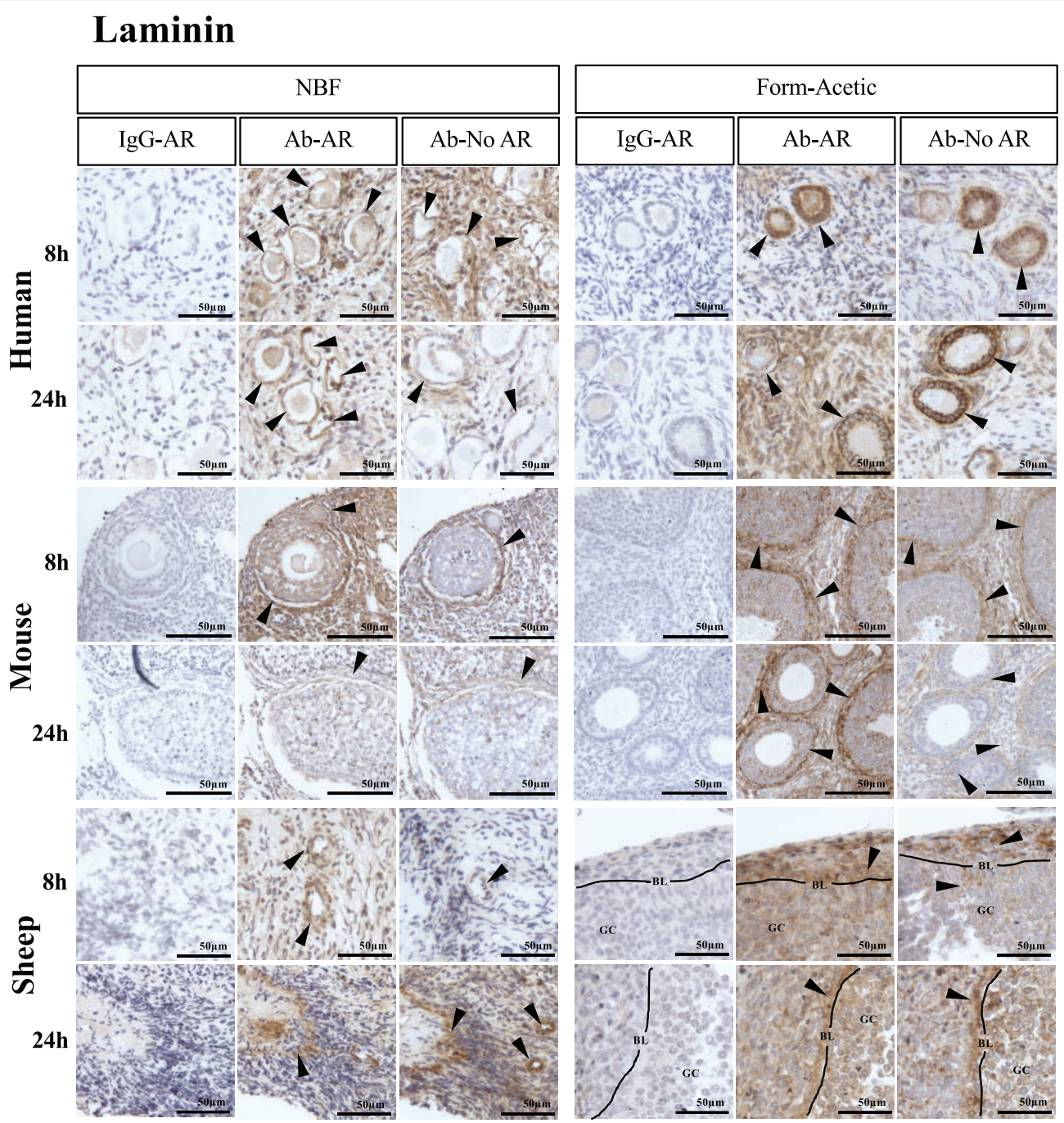

Figure 9. Detection of laminin using IHC in human, mouse, and sheep ovarian tissue preserved with different fixatives. Following the fixation of ovarian tissue in NBF and Form-Acetic (NBF with 5% acetic acid) solutions for 8 h and 24 h, IHC was performed on human, mouse and sheep ovarian sections to detect laminin in follicles of all developmental stages, blood vessels and the stroma. Follicles/cells/regions positively stained are indicated by the arrowheads (GC, granulosa cell; BL, basal lamina). IgG-AR: isotype IgG antibody control was applied on the section treated with AR, Ab-AR: antibody was applied, and an AR step was performed, Ab-No AR: antibody was applied, and no AR step was performed. Images are representative of experiments using human ovarian cortex samples, n=3 patients per condition (fresh n=2, frozen n=1), sheep ovarian cortex, n=3 animals per condition, and mouse ovaries, n=3 animals per condition. IHC experiments were performed at least twice for each sample. NB: The 12 images in each panel for a single species were all from the same experiment with the same DAB exposure enabling direct comparison between the samples.

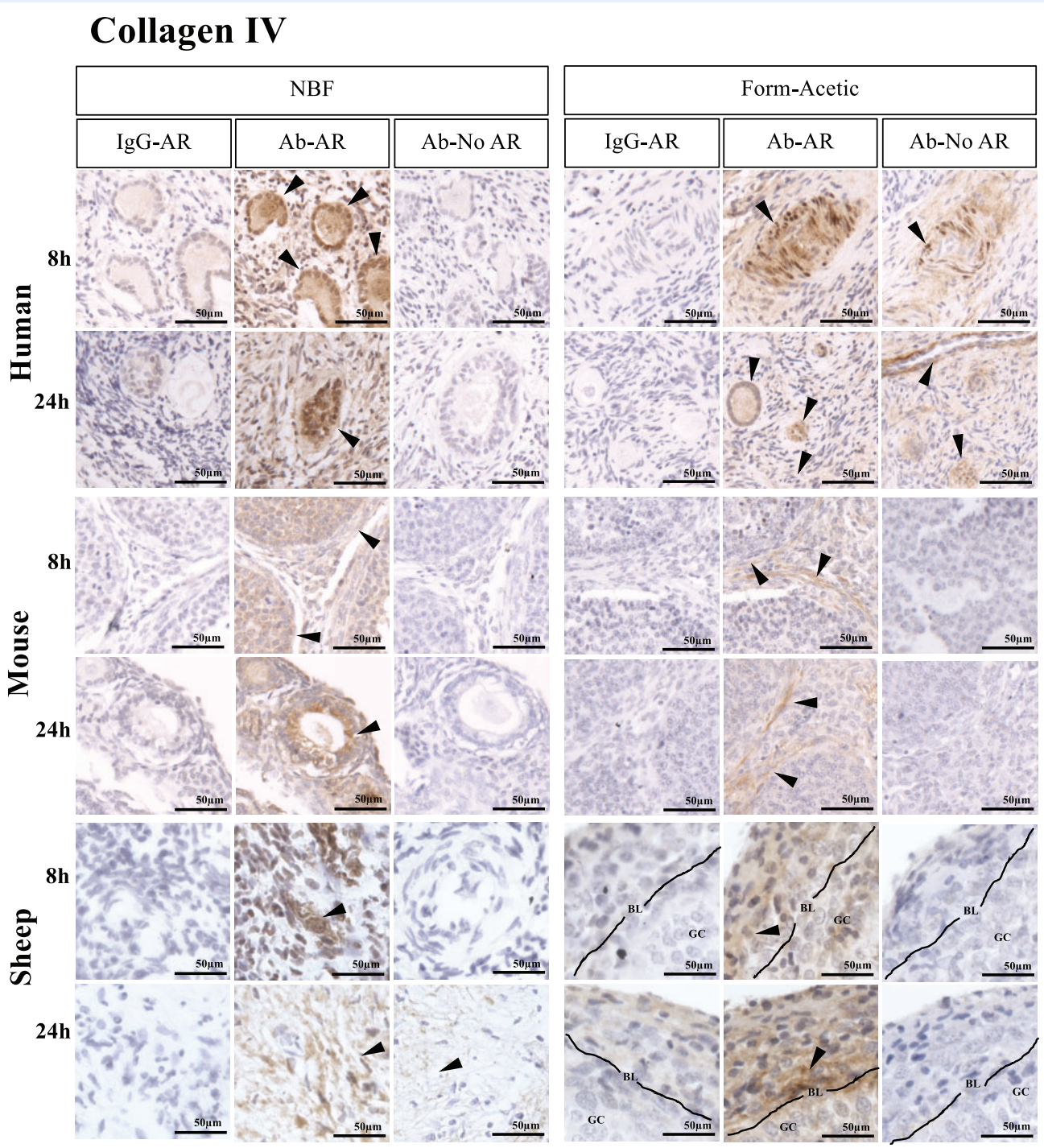

Figure 10. Detection of Collagen IV using IHC in human, mouse and sheep ovarian tissue preserved with different fixatives. Following the fixation of ovarian tissue in NBF and Form-Acetic (NBF with 5% acetic acid) solutions for 8 h and 24 h, IHC was performed on human, mouse and sheep ovarian sections to detect collagen IV in follicles of all developmental stages, blood vessels and the stroma. Follicles/cells/regions positively stained are indicated by the arrowheads. IgG-AR: isotype IgG antibody control was applied on the section treated with AR, Ab-AR: antibody was applied, and an AR step was performed, Ab-No AR: antibody was applied, and no AR step was performed. Images are representative of experiments using human ovarian cortex samples, n=3 patients per condition (fresh n=2, frozen n=1), sheep ovarian cortex, n=3 animals per condition, and mouse ovaries, n=3 animals per condition. IHC experiments were performed at least twice for each sample. NB: The 12 images in each panel for a single species were all from the same experiment with the same DAB exposure enabling direct comparison between the samples.

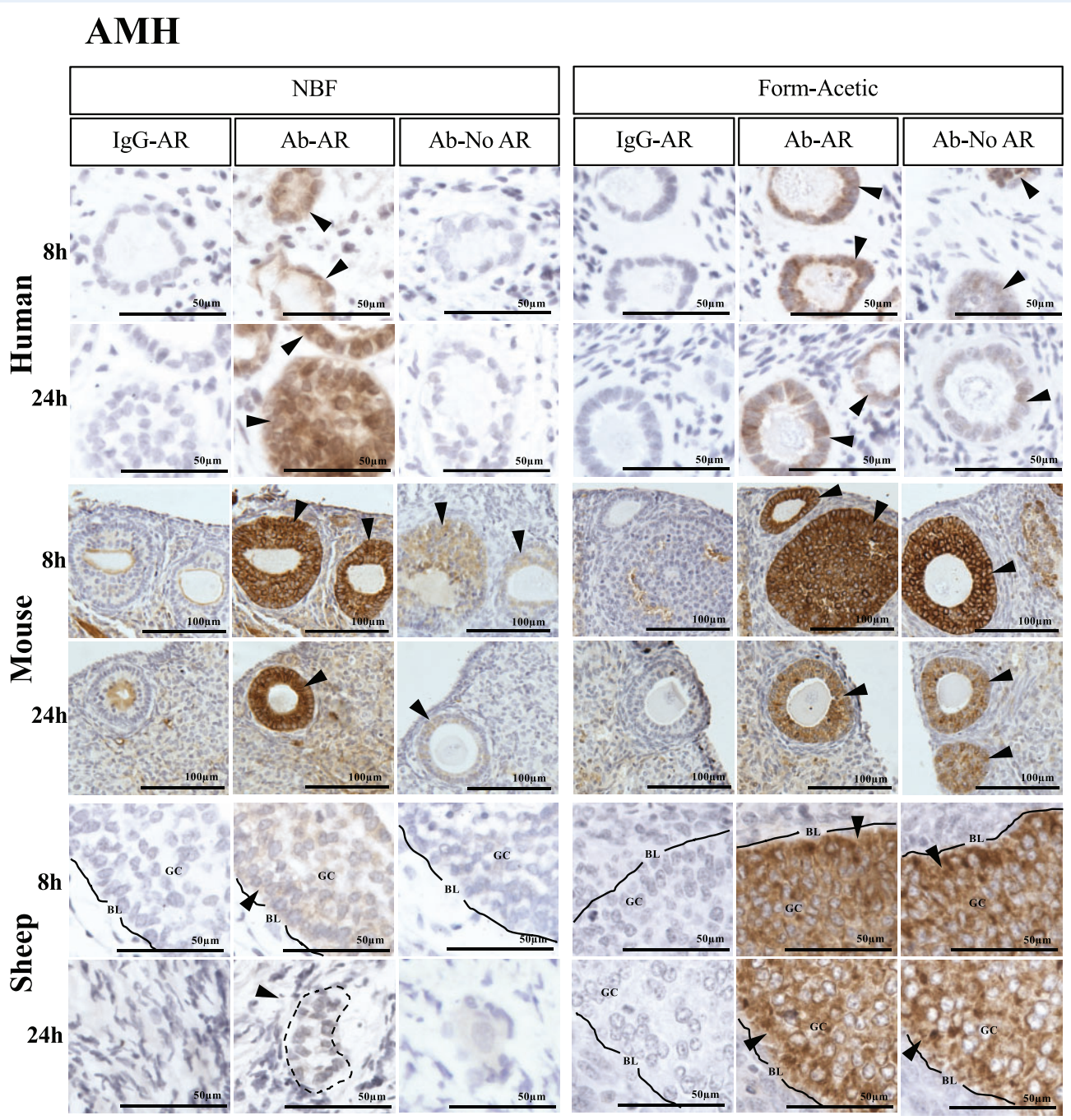

Figure 11. Detection of anti-Müllerian hormone using IHC in human, mouse and sheep ovarian tissue preserved with different fixatives. Following the fixation of ovarian tissue in NBF and Form-Acetic (NBF with 5% acetic acid) solutions for 8 h and 24 h, IHC was performed on human, mouse, and sheep ovarian sections to detect anti-Müllerian hormone (AMH) in the granulosa cells of growing follicles. Follicles/cells positively stained are indicated by the arrowheads (GC, granulosa cell; BL, basal lamina). IgG-AR: isotype IgG antibody control was applied on the section treated with AR, Ab-AR: antibody was applied, and an AR step was performed, Ab-No AR: antibody was applied, and no AR step was performed. Images are representative of experiments using human ovarian cortex samples, n=5 patients per condition (fresh n=3, frozen n=2), sheep ovarian cortex, n=3 animals per condition, and mouse ovaries, n=3 animals per condition. IHC experiments were performed at least twice for each sample. NB: The 12 images in each panel for a single species were all from the same experiment with the same DAB exposure enabling direct comparison between the samples with the exception of sheep Form-Acetic 24 h Ab-No AR.

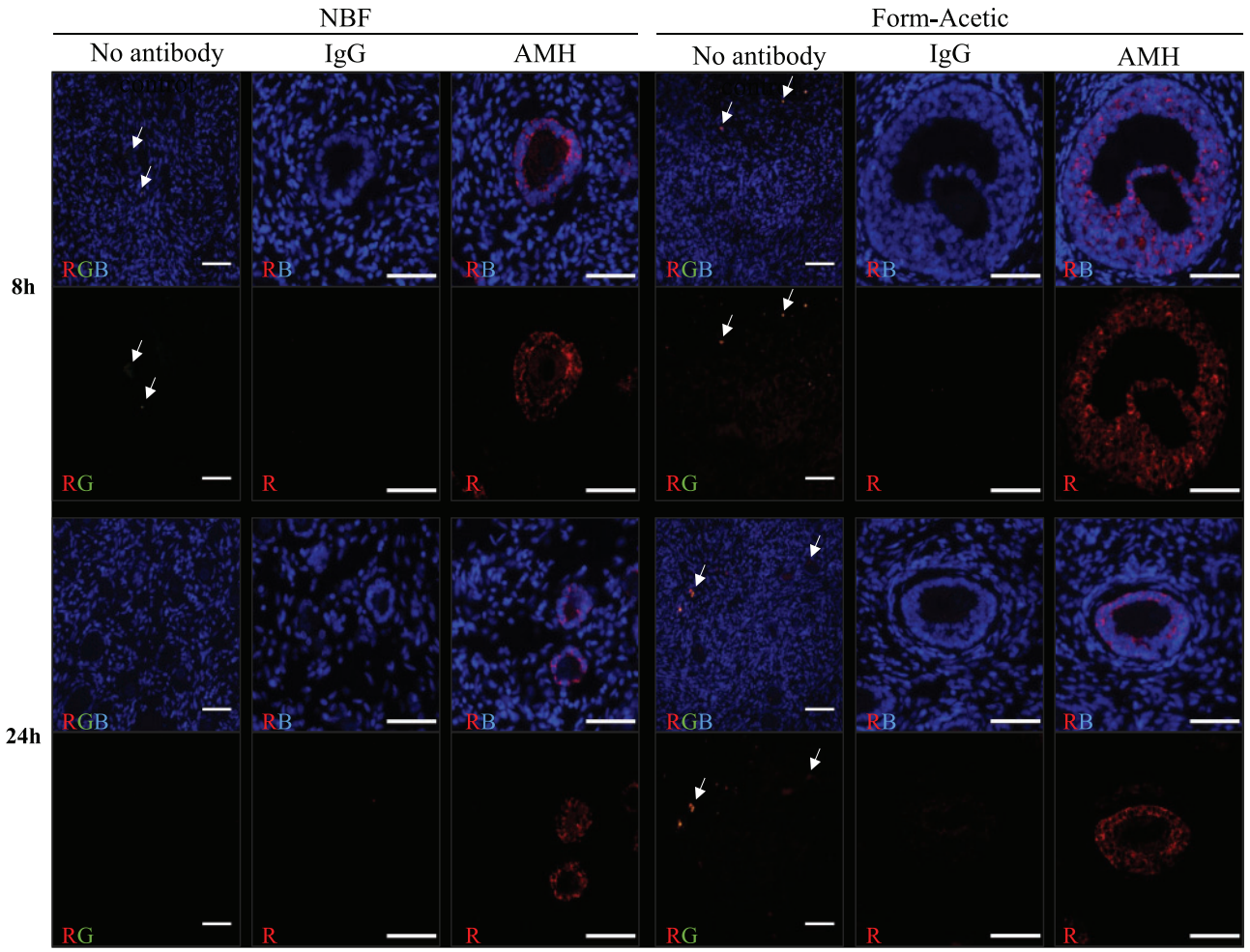

Figure 12. Detection of AMH using IHC with fluorescent detection in human ovarian tissue preserved with different fixatives. Following the fixation of human ovarian tissue in NBF and Form-Acetic (NBF with 5% acetic acid) solutions for 8 h and 24 h, IHC using antigen retrieval to detect AMH was performed to detect the glycoprotein in the granulosa cells of follicles. AMH (red) was detected using streptavidin conjugated Alexa Fluor 568 and nuclei (blue) were counterstained with DAPI. Images were processed identically in ImageJ to adjust qualitative aspects (brightness/contrast) to ensure high signal visibility according to best-practice guidelines (see methods section for details). AMH was detected in granulosa cells of growing follicles, while no signal was observed in the negative control (not treated with antibodies) and IgG control (rabbit IgG instead of primary antibody). Autofluorescence caused by lipofuscin (arrows) was visible across the green-red spectrum in oocytes and stroma in both NBF (8 h) and Form-Acetic (8 h and 24 h) fixed tissues (R = red, G = green, B = blue). Images are representative of experiments using human ovarian cortex samples, n=3 (n=2, fresh and n=1, frozen). Each scale bar is 50 μm.

mitochondria (Baker, 1958); presumably equivalently in Bouin's and Form-Acetic. It is thereby important to conduct further studies to observe and detail the interaction of the fixative with these cellular structures using Form-Acetic with different acetic acid concentrations. Interestingly, Form-Acetic appeared to better preserve lysosomes as lipofuscin autofluorescence was more abundant in oocytes and the stroma of the Form-Acetic fixed tissues. To determine if the lipofuscin signal could be removed to enable other molecules in the oocyte to be investigated using fluorescence, we used commercially available quenching products and successfully removed the autofluorescence signal of lipofuscin (data not shown).

As previously stated, the ideal fixative should enable DNA/RNA preservation for sequencing. NBF directly interacts with nuclear material and results in poor detection (Bresters *et al.*, 1994), sequence alterations (Williams *et al.*, 1999), and even degradation (Srinivasan *et al.*, 2002) of the genetic content. The molecular interaction that Form-Acetic may have with nuclear material is not completely known as we only examined whether fixation with Form-Acetic enabled the detection of fragmented DNA. However, Baker and Silverton (1976) reported on the ability of acetic acid to precipitate nuclear-material and identified it as a useful tool for studying DNA/RNA content. It is thereby probable that Form-Acetic may preserve nuclear material

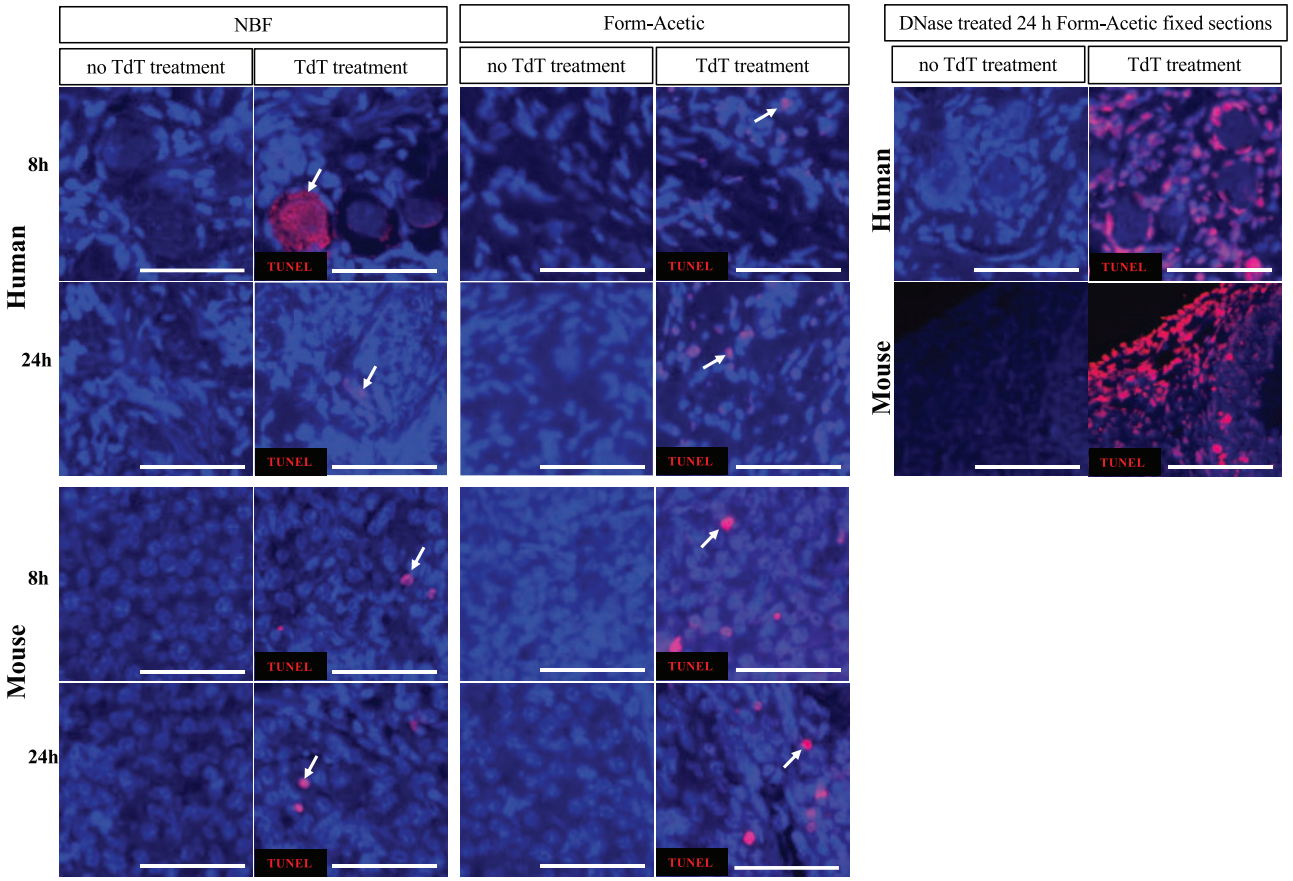

Figure 13. Representative images of human and mouse ovarian tissue preserved with different fixatives and subjected to the TUNEL assay. TUNEL was performed on 8 h and 24 h NBF and Form-Acetic (NBF with 5% acetic acid) fixed human and mouse ovarian sections. TUNEL-positive cells (red) were detected using Alexa Fluor 594 and are denoted with white arrows while cellular nuclei (blue) were counterstained with DAPI (TdT, terminal deoxynucleotidyl transferase). Positive control sections were treated with 1 IU/mL DNase I. Images are representative of experiments using human ovarian cortex samples, n=2 (n=1, fresh and n=1, frozen) and for mouse, n=2 per condition. Each scale bar is 100 µm.

composition and organisation for molecular studies including DNA/RNA extraction, amplification, and sequencing to generate quality sequences or detection.

In addition to the primary objectives, we also observed that Form-Acetic benefited the tissue preparation and the embedding process. Hardening of NBF fixed tissues, particularly for the human and sheep samples, meant that these samples sometimes 'fell out' of the paraffin wax during sectioning, leaving empty areas in the wax ribbons. When a tissue was behaving like this, blocks containing fixed samples had to be hydrated in ice water in-between sectioning to counteract this event. Sectioning difficulty such as this was not encountered with Form-Acetic and Bouin's fixed samples, because of the properties of acetic acid which prevent hardening of fixed tissues caused by alcohol treatment during sample processing (Baker, 1958).

Based on our observations and the data presented here, we propose that Form-Acetic becomes the fixative of choice for histo-morphological analyses. From the results, we recommend fixation of whole mouse ovaries, or ovarian tissue pieces from large mammals (approximately 1 mm^3) for 8–24 h for both routine histology and histological molecular analysis. However, 24 h fixation in Form-Acetic is a highly convenient duration for subsequent collection and does not inhibit antigen availability. Fixation times and volumes may need to be optimised for larger tissue pieces or different tissue types. Penetration of acetic acid is rapid and, therefore, diffusion of NBF is likely to be the limiting factor when estimating fixation time. Finally, as is currently the case for NBF, determining IHC protocols for different antigens will likely require optimisation.

In summary, we have defined the use of a fixative known as Form-Acetic, that is able to preserve ovarian tissue morphology in a manner superior to the most commonly used fixatives for multiple species. The fixative is simple to prepare, requiring only two commonly available reagents; NBF and acetic acid. We have demonstrated that the fixative is compatible with common histological staining methods in human, mouse and sheep tissues. Critically, the fixative is also compatible with the detection of a range of proteins using IHC and, for some proteins, AR steps are unnecessary unlike NBF. In addition, we have confirmed that the fixative allows for detection of fragmented DNA using the TUNEL assay. We, therefore, recommend that Form-Acetic

replaces currently used fixatives and encourage others to introduce it into their research workflows.

Supplementary data

Supplementary data are available at *Human Reproduction* online.

Data availability

The data underlying this research article can be made available upon reasonable request to the corresponding author.

Acknowledgements

Authors wish to thank staff of the Oxford Cell and Tissue Biobank (OCTB) for their assistance in providing samples.

Authors' roles

B.V. Adeniran, B.D. Bjarkadottir, and S.A. Williams were all involved in the conception and design of the study, data interpretation and analysis, and manuscript generation. B.V. Adeniran and B.D. Bjarkadottir were both involved in data acquisition, with B.V. Adeniran generating the bulk of the data, performing most of the data analysis and drafting the article. B.D. Bjarkadottir carried out the statistical analysis. R. Appeltant was involved in data acquisition and manuscript generation. S. Lane was essential for all aspects of obtaining the human samples and was involved in manuscript generation. All authors contributed to and agreed the final draft of the manuscript.

Funding

This work was supported by the Oxford Medical Research Council Doctoral Training Programme (Oxford MRC-DTP) grant awarded to B.D.B. (Grant no. MR/N013468/1), Fondation Hoffmann supporting R.A and the Petroleum Technology Development Fund (PTDF) awarded to B.V.A.

Conflict of interest

No potential conflict of interest was reported by the authors.

References

Baker FJ, Silverton RE. 13 – Fixation. In F. J. Baker and R. E. Silverton (eds), *Introduction to Medical Laboratory Technology* (5th ed.). Oxford: Butterworth-Heinemann, 1976, 312–327.

Baker JR. *Principles of Biological Microtechnique; A Study of Fixation and Dyeing*. Methuen: Wiley, 1958.

Bates D, Machler M, Bolker B, Walker S. Fitting linear mixed-effects models using lme4. *J Stat Soft* 2015;**67**:1–48. 10.18637/jss.v067.i01.

Berkholtz CB, Lai BE, Woodruff TK, Shea LD. Distribution of extracellular matrix proteins type I collagen, type IV collagen, fibronectin, and laminin in mouse folliculogenesis. *Histochem Cell Biol* 2006;**126**:583–592.

Borkar AN, Rout MK, Hosur RV. Visualization of early events in acetic acid denaturation of HIV-1 protease: a molecular dynamics study. *PLoS One* 2011;**6**:e19830.

Bresters D, Schipper MEI, Reesink HW, Boeser-Nunnink BDM, Cuypers HTM. The duration of fixation influences the yield of HCV cDNA-PCR products from formalin-fixed, paraffin-embedded liver tissue. *J Virol Methods* 1994;**48**:267–272.

Campbell BK, Clinton M, Webb R. The role of anti-Müllerian hormone (AMH) during follicle development in a monovulatory species (Sheep). *Endocrinology* 2012;**153**:4533–4543.

Chambers EL, Gosden RG, Yap C, Picton HM. In situ identification of follicles in ovarian cortex as a tool for quantifying follicle density, viability and developmental potential in strategies to preserve female fertility. *Hum Reprod* 2010;**25**:2559–2568.

Chen CH, Hsu MY, Jiang RS, Wu SH, Chen FJ, Liu SA. Shrinkage of head and neck cancer specimens after formalin fixation. *J Chin Med Assoc* 2012;**75**:109–113.

Chiti MC, Dolmans MM, Hobeika M, Cernogoraz A, Donnez J, Amorim CA. A modified and tailored human follicle isolation procedure improves follicle recovery and survival. *J Ovarian Res* 2017;**10**:71.

Eivazkhani F, Abtahi NS, Tavana S, Mirzaeian L, Abedi F, Ebrahimi B, Montazeri L, Valojerdi MR, Fathi R. Evaluating two ovarian decellularization methods in three species. *Mater Sci Eng C* 2019;**102**:670–682.

Fabbri R, Macciocca M, Vicenti R, Pasquinelli G, Caprara G, Valente S, Seracchioli R, Paradisi R. Long-term storage does not impact the quality of cryopreserved human ovarian tissue. *J Ovarian Res* 2016;**9**:50.

Fenwick MA, Hurst PR. Immunohistochemical localization of active caspase-3 in the mouse ovary: growth and atresia of small follicles. *Reproduction* 2002;**5**:659–665.

Fenwick MA, Mora JM, Mansour YT, Baithun C, Franks S, Hardy K. Investigations of TGF-beta signaling in preantral follicles of female mice reveal differential roles for bone morphogenetic protein 15. *Endocrinology* 2013;**154**:3423–3436.

Fraenkel-Conrat H, Olcott HS. The reaction of formaldehyde with proteins. V. Cross-linking between amino and primary amide or guanidyl groups. *J Am Chem Soc* 1948;**70**:2673–2684.

Fujisawa M, Moh-Moh-Aung A, Zeng Z, Yoshimura T, Wani Y, Matsukawa A. Ovarian stromal cells as a source of cancer-associated fibroblasts in human epithelial ovarian cancer: a histopathological study. *PLoS One* 2018;**13**:e0205494.

Gougeon A. Regulation of ovarian follicular development in primates: facts and hypotheses. *Endocr Rev* 1996;**17**:121–155.

Grasa P, Ploutarchou P, Williams SA. Oocytes lacking O-glycans alter follicle development and increase fertility by increasing follicle FSH sensitivity, decreasing apoptosis, and modifying GDF9:BMP15 expression. *FASEB J* 2015;**29**:525–539.

Gustavson KH. *The Chemistry and Reactivity of Collagen*. New York, NY: Academic Press, 1956.

Heeren AM, Van Iperen L, Klootwijk DB, De Melo Bernardo A, Roost MS, Fernandes MMG, Louwe LA, Hilders CG, Helmerhorst FM, Van Der Westerlaken LAJ. *et al.* Development of the follicular

basement membrane during human gametogenesis and early folliculogenesis. *BMC Dev Biol* 2015;**15**:4–13.

Howat WJ, Wilson BA. Tissue fixation and the effect of molecular fixatives on downstream staining procedures. *Methods* 2014;**1**: 12–19.

Hsu PK, Huang HC, Hsieh CC, Hsu HS, Wu YC, Huang MH, Hsu WH. Effect of formalin fixation on tumor size determination in stage I non-small cell lung cancer. *Ann Thorac Surg* 2007;**84**: 1825–1829.

John GB, Gallardo TD, Shirley LJ, Castrillon DH. Foxo3 is a PI3K-dependent molecular switch controlling the initiation of oocyte growth. *Dev Biol* 2008;**321**:197–204.

Jones D. Reactions of aldehydes with unsaturated fatty acids during histological fixation. *Histochem J* 1972;**4**:421–465.

Jonmarker S, Valdman A, Lindberg A, Hellstrom M, Egevad L. Tissue shrinkage after fixation with formalin injection of prostatectomy specimens. *Virchows Arch* 2006;**449**:297–301.

Kallio S, Aittomaki K, Piltonen T, Veijola R, Liakka A, Vaskivuo TE, Dunkel L, Tapanainen JS. Anti-Müllerian hormone as a predictor of follicular reserve in ovarian insufficiency: special emphasis on FSH-resistant ovaries. *Hum Reprod* 2012;**27**:854–860.

Kim J, Coffey DM, Ma L, Matzuk MM. The ovary is an alternative site of origin for high-grade serous ovarian cancer in mice. *Endocrinology* 2015;**156**:1975–1981.

Lee J, Lee HC, Kim SY, Cho GJ, Woodruff TK. Poorly-controlled type I diabetes mellitus impairs LH-LHCGR signaling in the ovaries and decreases female fertility in mice. *Yonsei Med J* 2019;**60**: 667–678.

Lee JY, Kitaoka M. A beginner's guide to rigor and reproducibility in fluorescence imaging experiments. *Mol Biol Cell* 2018;**29**: 1519–1525.

Lundy T, Smith P, O'Connell A, Hudson NL, McNatty KP. Populations of granulosa cells in small follicles of the sheep ovary. *J Reprod Fertil* 1999;**115**:251–262.

McLaughlin M, Albertini DF, Wallace WHB, Anderson RA, Telfer EE. Metaphase II oocytes from human unilaminar follicles grown in a multi-step culture system. *Mol Hum Reprod* 2018;**24**:135–142.

Pampanini V, Wagner M, Asadi-Azarbaijani B, Oskam IC, Sheikhi M, Sjödin MOD, Lindberg J, Hovatta O, Sahlin L, Björvang RD. *et al.* Impact of first-line cancer treatment on the follicle quality in cryopreserved ovarian samples from girls and young women. *Hum Reprod* 2019;**34**:1674–1685.

Ouni E, Vertommen D, Chiti MC, Dolmans MM, Amorim CA. A draft map of the human ovarian proteome for tissue engineering and clinical applications. *Mol Cell Proteomics* 2019;**18**:S159–S173.

Pangas SA, Jorgez CJ, Tran M, Agno J, Li X, Brown CW, Kumar TR, Matzuk MM. Intraovarian activins are required for female fertility. *Mol Endocrinol* 2007;**21**:2458–2471.

Pedersen T, Peters H. Proposal for a classification of oocytes and follicles in the mouse ovary. *J Reprod Fertil* 1968;**17**:555–557.

Pisarska MD, Kuo FT, Bentsi-Barnes IK, Khan S, Barlow GM. LATS1 phosphorylates forkhead L2 and regulates its transcriptional activity. *Am J Physiol – Endocrinol Metab* 2010;**299**:101–109.

Pritt B, Tessitore JJ, Weaver DL, Blaszyk H. The effect of tissue fixation and processing on breast cancer size. *Hum Pathol* 2005;**36**: 756–760.

Saatcioglu HD, Cuevas I, Castrillon DH. Control of oocyte reawakening by kit. *PLoS Genet* 2016;**12**:e1006215.

Siu KF, Cheung HC, Wong J. Shrinkage of the esophagus after resection for carcinoma. *Ann Surg* 1986;**2**:173–176.

Srinivasan M, Sedmak D, Jewell S. Effect of fixatives and tissue processing on the content and integrity of nucleic acids. *Am J Pathol* 2002;**161**:1961–1971.

Stefansdottir A, Johnston ZC, Powles-Glover N, Anderson RA, Adams IR, Spears N. Etoposide damages female germ cells in the developing ovary. *BMC Cancer* 2016;**16**:482.

Tran T, Sundaram CP, Bahler CD, Eble JN, Grignon DJ, Monn MF, Simper NB, Cheng L. Correcting the shrinkage effects of formalin fixation and tissue processing for renal tumors: toward standardization of pathological reporting of tumor size. *J Cancer* 2015;**6**: 759–766.

Walker CA, Bjarkadottir BD, Fatum M, Lane S, Williams SA. Variation in follicle health and development in cultured cryopreserved ovarian cortical tissue: a study of ovarian tissue from patients undergoing fertility preservation. *Hum Fertil (Camb)* 2019; **0**:1–11.

Williams C, Pontén F, Moberg C, Söderkvist P, Uhlén M, Pontén J, Sitbon G, Lundeberg J. A high frequency of sequence alterations is due to formalin fixation of archival specimens. *Am J Pathol* 1999; **155**:1467–1471.

Winship AL, Carpenter M, Griffiths M, Hutt KJ. Vincristine chemotherapy induces atresia of growing ovarian follicles in mice. *Toxicol Sci* 2019;**169**:43–53.

Yamada S, Fujiwara H, Honda T, Higuchi T, Nakayama T, Inoue T, Maeda M, Fujii S. Human granulosa cells express integrin α2 and collagen type IV: possible involvement of collagen type IV in granulosa cell luteinization. *Mol Hum Reprod* 1999;**5**:607–617.

Yeap BH, Muniandy S, Lee SK, Sabaratnam S, Singh M. Specimen shrinkage and its influence on margin assessment in breast cancer. *Asian J Surg* 2007;**30**:183–187.